

# Transactions of the ASME

Some Experiments on the Influence of Various Factors on Drill Performance . . .	<i>D. F. Galloway</i>	191
Seal Leakage in the Rotary Regenerator and Its Effect on Rotary-Regenerator Design for Gas Turbines. . . . .	<i>D. B. Harper</i>	233
Mass-Transfer Cooling in a Laminar Boundary Layer With Constant Fluid Properties. . . . .	<i>J. P. Hartnett and E. R. G. Eckert</i>	247
The New Zealand Thermal Area and Its Development for Power Production . . .	<i>C. J. Banwell</i>	255
Flow Sampling and Discharge Measurement in Geothermal Bores . . . . .	<i>C. J. Banwell</i>	269
Temperature and Velocity Distribution and Transfer of Heat in a Liquid Metal . . . . .	<i>H. E. Brown, B. H. Amstead, and B. E. Short</i>	279
Mean-Temperature Difference in One, Two, and Three-Pass Crossflow Heat Exchangers . . . . .	<i>R. A. Stevens, J. Fernandez, and J. R. Woolf</i>	287
Convection Phenomena in Fluids Heated From Below . . . . .	<i>Simon Ostrach</i>	299
Experimental Superheater for Steam at 2000 Psi and 1250 F—Report After 14,281 Hours of Operation . . . . .	<i>J. H. Hoke and F. Eberle</i>	307
High-Temperature Corrosion of Alloys Exposed in the Superheater of an Oil-Fired Boiler. . . . .	<i>D. W. McDowell, Jr., R. J. Randebaugh, and W. E. Somers</i>	319
Use of Nonlinear Valve Characteristics in the Control of a Simple Blending Process . . .	<i>J. L. Shearer</i>	329
The Maximum Temperature Profile in Journal Bearings. . . . .	<i>O. Pinkus and B. Sternlicht</i>	337
Temperature Distribution in the Journal-Bearing Lubricant Film . . . . .	<i>M. B. Purvis, W. E. Meyer, and T. C. Benton</i>	343
The Spring-Supported Thrust Bearing . . . . .	<i>Fletcher Osterle and Edward Saibel</i>	351
Instrumentation for Steam-Consumption Tests on Medium Steam Turbine-Generator Sets . . . . .	<i>D. E. Kimball</i>	357
Procedures for Testing Large Steam Turbine-Generators in Central Stations . . . . .	<i>E. M. Kratz and J. C. Westcott</i>	365
A Practical Application of Uncertainty Calculations to Measured Data . . . . .	<i>L. W. Thrasher and R. C. Binder</i>	373
Investigation of Causes of Low Wheel-to-Rail Adhesion and Possible Methods of Improving It . . . . .	<i>F. G. Fisher and R. K. Allen</i>	377
First Commercial Supercritical-Pressure Steam-Electric Generating Unit for Philo Plant. . . . .	<i>S. N. Fiala</i>	389
First Commercial Supercritical-Pressure Steam Generator for Philo Plant . . . . .	<i>W. H. Rowand and A. M. Frendberg</i>	409
First Commercial Supercritical-Pressure Steam Turbine—Built for the Philo Plant . . . . .	<i>C. W. Elston and R. Sheppard</i>	417
Contributions to Hydraulic Control—7, Analysis of the Effects of Nonlinearity in a Valve-Controlled Hydraulic Drive . . . . .	<i>E. I. Reeves</i>	427
Integration of Steam and Hydro Power in Northern California . . . . .	<i>Walter Dreyer</i>	433

TRANSACTIONS OF THE AMERICAN SOCIETY OF MECHANICAL ENGINEERS

VOLUME 79

FEBRUARY 1957

NUMBER 2

# Transactions

of The American Society of Mechanical Engineers

---

Published on the tenth of every month, except March, June, September, and December

---

## OFFICERS OF THE SOCIETY:

W. F. RYAN, *President*

JOSEPH L. KOFF, *Treasurer*

C. E. DAVIS, *Secretary*

EDGAR J. KATZ, *Asst. Treasurer*

## COMMITTEE ON PUBLICATIONS:

W. E. REASER, *Chairman*

KERR ATKINSON

D. G. A. SKROTECKI

JOHN DE S. COUTINHO

HENDLEY N. BLACKMON

H. N. WEINBERG } *Junior Advisory Members*  
J. N. VIERMANN }

GEORGE A. SYTHSON, *Editor Emeritus*

J. A. NORTH, *Production*

J. J. JAKLITSCH, Jr., *Editor*

## REGIONAL ADVISORY BOARD OF THE PUBLICATIONS COMMITTEE:

ROY L. PARRELL—I

H. M. CATER—V

GLEN R. FRYLING—II

C. R. EARLE—VI

F. J. HEINZ—III

M. B. HOGAN—VII

FRANCIS C. SMITH—IV

LINN HELANDER—VIII

---

Published monthly by The American Society of Mechanical Engineers. Publication office at 20th and Northampton Streets, Easton, Pa. The editorial department is located at the headquarters of the Society, 29 West Thirty-Ninth Street, New York 18, N. Y. Cable address, "Mechanics," New York. Price \$1.50 a copy, \$12.00 annually for Transactions and the *Journal of Applied Mechanics*; to members, \$1.00 a copy, \$6.00 annually. Add \$1.50 for postage to all countries outside the United States, Canada, and Pan American Union. Changes of address must be received at Society headquarters seven weeks before they are to be effective on the mailing list. Please send old as well as new address. . . . By-Law: The Society shall not be responsible for statements or opinions advanced in papers or . . . printed in its publications (B13, Par. 4). . . . Entered as second-class matter March 2, 1928, at the Post Office at Easton, Pa., under the Act of August 24, 1912. . . . Copyrighted, 1957, by The American Society of Mechanical Engineers. Reprints from this publication may be made on condition that full credit be given the Transactions of the ASME and the author, and that date of publication be stated.

# Some Experiments on the Influence of Various Factors on Drill Performance

By D. F. GALLOWAY,<sup>1</sup> LEICESTERSHIRE, ENGLAND

The experiments described in this paper are part of a series of investigations to obtain basic data needed for improving drilling techniques in a number of engineering factories. The main criteria of drill performance and some of the principal factors which influence performance are discussed. Special attention is given to drill shape, and particularly to those elements, such as relief angle, point angle, relative lip height, and so on, which can be controlled by the drill user. The theory of self-regenerative vibration in drilling is discussed, and theories are developed to explain inaccuracies in hole size and alignment. The paper includes test results which tend to support these theories. Reference is made to those considerations of drill geometry and specification which entered into the investigations. The influence of the drilling machine on drill performance was discussed in a previous paper by the author.

## INTRODUCTION

THE extensive use of drilling in the engineering industry, involving in Britain alone the consumption of millions of drills per annum and a correspondingly high expenditure of man-hours and machine-hours, has given rise in recent years to an increasing volume of research to improve the efficiency of drilling. Because of the vast scale on which drilling operations are carried out, even a slight increase in the general level of drill performance would yield important practical and economic benefits to individual firms and the engineering industries as a whole. This research is not only leading to substantial improvements in tool performance, but also to more accurate prediction of tool performance, which is a basic requirement in the development of automation.

The experiments described were concerned particularly with drill shape, and were part of a general program of research aimed at improving both the level and consistency of drill performance by studies of the effects of factors associated with the drill, machine, cutting fluid, and work material. In these investigations about 1,000,000 holes were drilled.

## GENERAL EXPERIMENTAL PROCEDURE

Drilling operations in a number of plants were studied to determine the main criteria and factors involved; these criteria and the main factors affecting them are given in Fig. 1. Preliminary tests were then carried out to determine the range of the main variables, and to facilitate the construction of suitable apparatus.

<sup>1</sup> Director of Research, Production Engineering Research Association of Great Britain, Melton Mowbray.

Contributed by the Production Engineering Division and presented at a joint session of the Production Engineering Division and Research Committee on Metal Processing at the Semi-Annual Meeting, Cleveland, Ohio, June 17-21, 1956, of THE AMERICAN SOCIETY OF MECHANICAL ENGINEERS.

NOTE: Statements and opinions advanced in papers are to be understood as individual expressions of their authors and not those of the Society. Manuscript received at ASME Headquarters, April 25, 1956. Paper No. 56-SA-18.

The general experimental procedure involved close control of the drill, drilling machine, cutting fluid, material machined, etc., while the selected variables such as relief angle, relative lip height, etc., were varied, and drill life, quality of holes, etc., were measured. A wide range of experimental conditions was used to facilitate application of the test results to the solution of specific drilling problems. The drills used were prepared by one maker under the strictest practicable control of material, heat-treatment, and manufacturing conditions, but in spite of the precautions taken there were often significant variations between drills and in individual drills. Consequently, it was necessary to employ statistical experimental designs such as the Latin and Youden squares to separate the main effects of these unavoidable variations from the effects of the deliberately varied factors.

The materials drilled included mild steel, alloy steels, cast iron, and titanium alloy. The properties, analyses, and specifications of these materials are given in Appendix 1.

The consistency of the cutting fluids was checked by analysis, and the temperature, rate of flow, and method of application of the fluid were kept sensibly constant using heaters, thermostats, and a ring distributor.

The spindle speed, feed rate, machine alignment, and machine settings such as hole depth, were checked at intervals throughout the tests.

In the drill-life tests, the general procedure was to drill blind holes to a depth of about two diameters in test blocks clamped to the table of a dynamometer; torque and thrust were automatically recorded throughout the tests.

## PREPARATION AND CALIBRATION OF APPARATUS

**Drilling Machines.** The results of preliminary tests confirmed that the deflections and vibrations of the portal frame-drill testing machines illustrated in Fig. 2 were considerably less than those of conventional radial and vertical drilling machines. The portal-frame construction has the advantages of rigidity and symmetry indicated in a previous paper.<sup>2</sup>

**Dynamometers.** The large dynamometer is shown in Fig. 3(a). The table is free to rotate and move downwards under the torque and thrust of the drill within limits imposed by two steel diaphragms which actuate electrical micrometer units connected to a torque-and-thrust recorder. The records show either torque and thrust variations when drilling one hole, or in effect, a series of maximum torque and thrust values for a number of holes.

The torque system was calibrated using levers and dead weights, and the thrust system using the spring device shown in Fig. 3(b). Hysteresis effects were small and the interaction of the torque and thrust movement did not exceed 4 per cent. Full-scale torque and thrust readings were obtained with table rotations of less than 40 sec of arc and vertical movements of less than 0.004 in.

The small dynamometer shown in Fig. 3(c) was designed for tests with drills below  $\frac{1}{8}$ -in. diam. The torque and thrust elements were calibrated by the use of levers and dead weights.

<sup>2</sup> "Some Experiments on the Deflections and Vibrations of Drilling Machines," by D. F. Galloway, paper presented at a general meeting of The Institution of Mechanical Engineers, December 9, 1955.

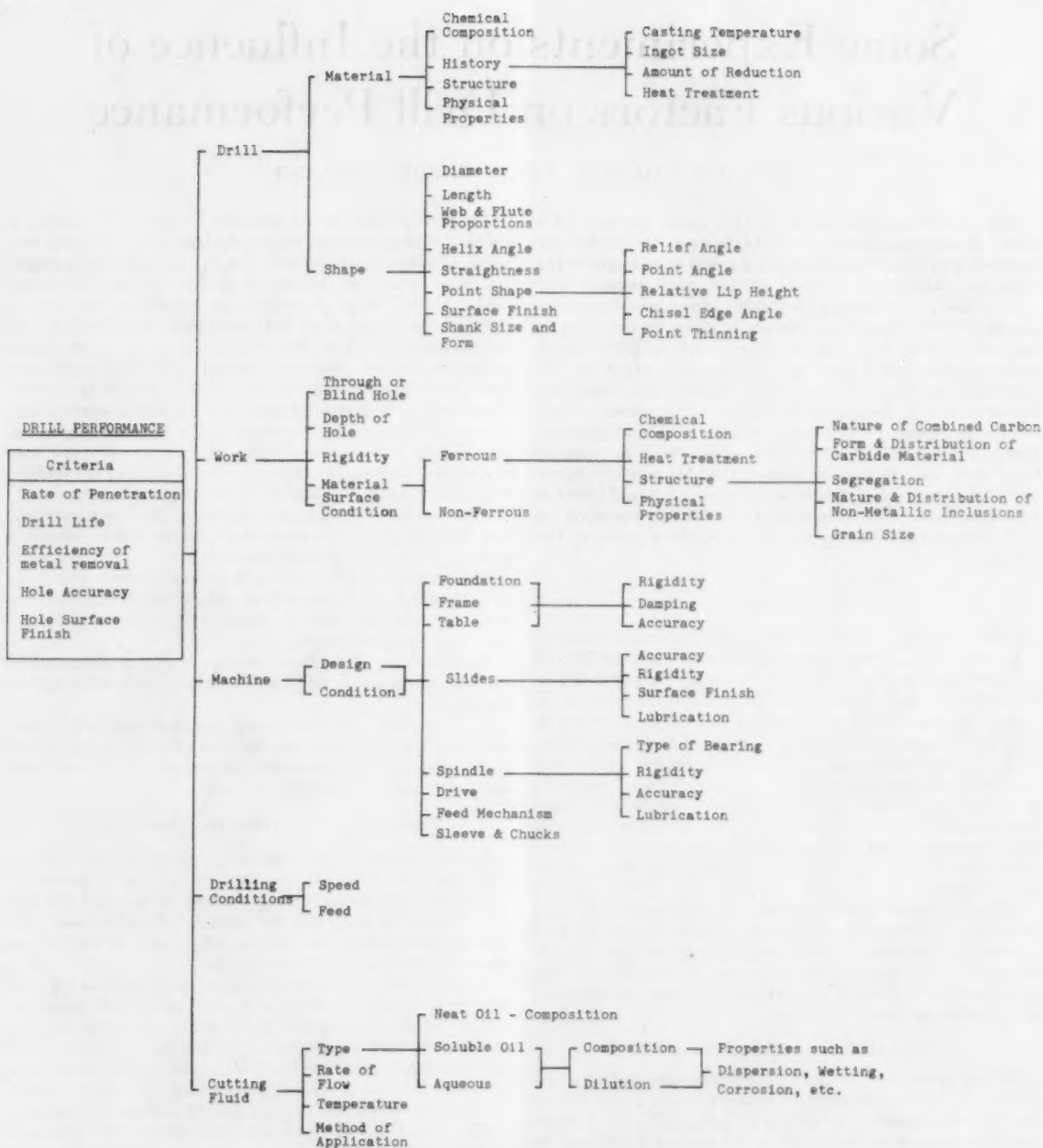


FIG. 1 PRINCIPAL TECHNICAL CRITERIA AND FACTORS INVOLVED IN DRILLING

Typical torque and thrust calibration curves are shown in Fig. 3(d). The calibration curve of the capacitance measuring system of the dynamometer was not quite linear, and was also rather susceptible to variations in zero setting with changes in the supply voltage; this was not a serious disadvantage, however, as the zero reading was automatically marked along the record at fre-

quent intervals in all tests. The mechanical hysteresis was negligible, and the interaction of the torque and thrust movements was not more than 2 per cent. Full-scale torque and thrust readings could be obtained with table rotations of less than 2 min of arc and vertical movements of less than 0.002 in.

*Drill-Point Inspection Apparatus.* The large drill-point in-

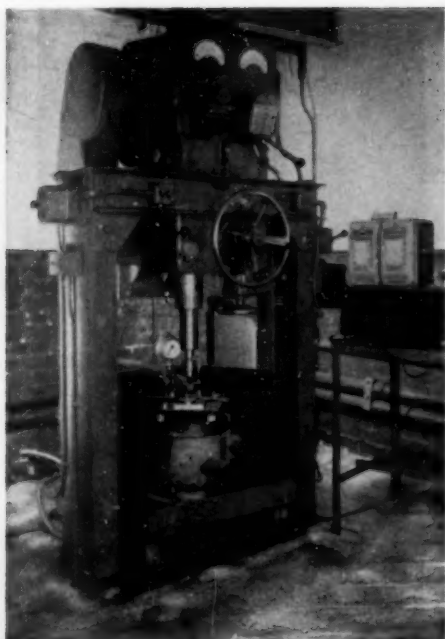
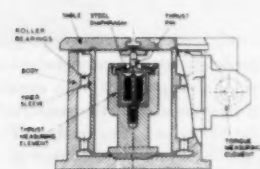


Fig. 2(a) Portal frame drill-testing machine

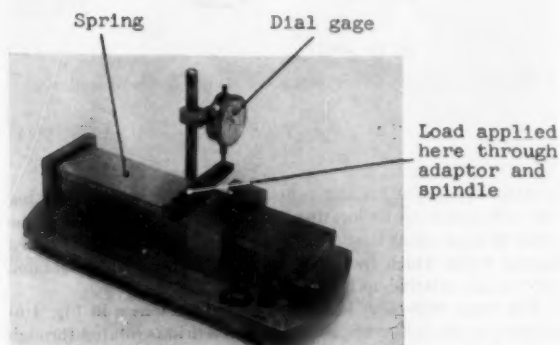


Fig. 2(b) Small drill-testing machine

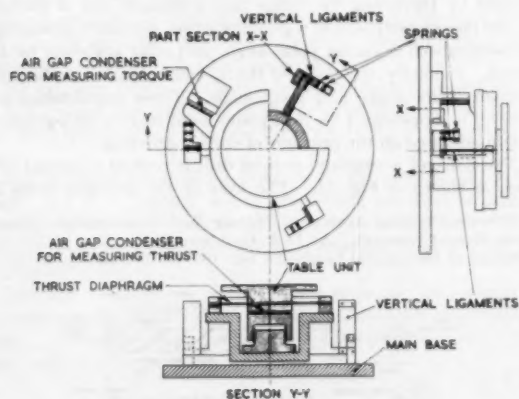
FIG. 2 SPECIAL MACHINES FOR INVESTIGATIONS INTO DRILLING



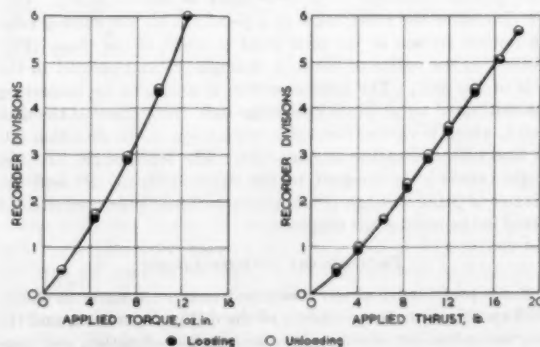
(a) Large drilling dynamometer



(b) Spring calibration device for thrust element of large dynamometer



(c) Small drilling dynamometer

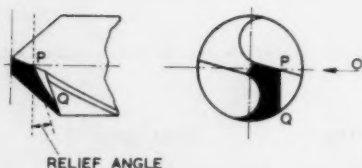


(d) Calibration curves for small dynamometer

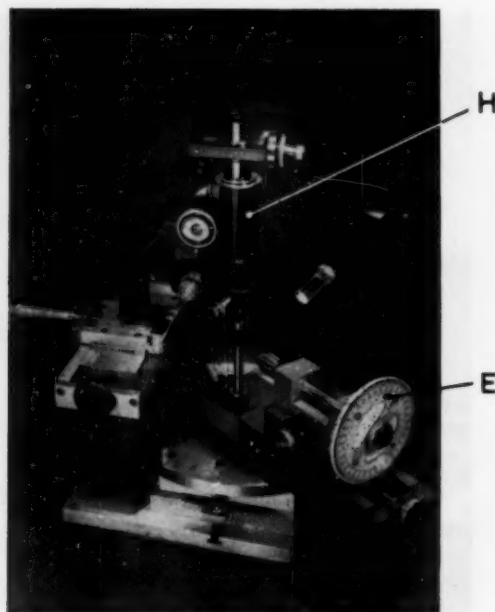
FIG. 3 DYNAMOMETERS FOR INVESTIGATIONS INTO DRILLING



(a) Large drill-point tester



(c) Measurement of nominal relief angle by optical sectioning



(b) Small drill-point tester

FIG. 4 DRILL-POINT INSPECTION APPARATUS

spection apparatus, Fig. 4(a), comprises a V-block (A) supporting the drill, a back center locating it, a protractor (B) indicating the angle through which the drill is rotated, and a dial gage (C) with a special stylus which traverses the drill flank when determining relief angle, relative lip height, and the like.

The small drill-point inspection apparatus shown in Fig. 4(b) is based on similar principles. The small drill is rotated through angles indicated by a protractor scale (E) and the drill point is explored optically with a microscope (H).

An instrument based on the principle of optical sectioning also was developed for directly observing nominal relief angle. The general principle of measurement is shown in Fig. 4(c). To determine the relief angle at a point (P) on the cutting edge an optical section of the drill point is made in the plane (PQ) normal to the radius of the drill through (P) and parallel to the axis of the drill. The optical section is produced by projecting the outline of an accurate knife edge onto the surface of the drill point, which is viewed through a microscope in the direction (O) in line with the radius through (P). The relief angle, i.e., the angle between the tangent to the curve (PQ) at (P) and the diametral plane through (P), is then read directly on a protractor fitted in the microscope eyepiece.

#### PRELIMINARY INVESTIGATIONS

Some preliminary observations and tests were made to clarify drill specification, the geometry of the drilling operation, and the relative suitability of short-duration, medium-duration, and long-duration life tests.

**Drill Specification.** Preliminary tests showed that there were considerable variations between drills supplied for the same purpose by different makers. Typical ranges of variation of shape and hardness are given in Appendix 2; all drills used in the main series of experiments conformed to the drill specification given in that Appendix.

To facilitate accurate control and precise specification of drill shape, a comprehensive twist-drill nomenclature was developed following an analysis of drill geometry, an examination of applicable drill-grinding machines, and the construction of the drill-inspection apparatus described previously. This nomenclature was published in a previous paper<sup>3</sup>; the main elements and angles are illustrated in Fig. 5, and the principal definitions are given in Appendix 3.

**Drill Geometry.** If, as is usually the case, the point of a drill is ground by traversing the flanks past a straight line of contact on the face or periphery of a grinding wheel, certain relationships connecting web thickness, point angle, and relief angle can be deduced. Similarly, the shape of the lip can be related to the flute contour, helix angle, and point angle. These relationships are derived in Appendix 4 for drill points produced by drill-grinding machines based on the principle of conical grinding.

The flank of a conically ground drill is part of a conical surface, as shown in Fig. 28. The axes of the grinding cones lie

<sup>3</sup> "Some Practical Aspects of Cutting Tool Nomenclature Arising From Recent Research," by D. F. Galloway, Proceedings of The Institution of Mechanical Engineers, vol. 168, no. 1, 1954, pp. 67-88.

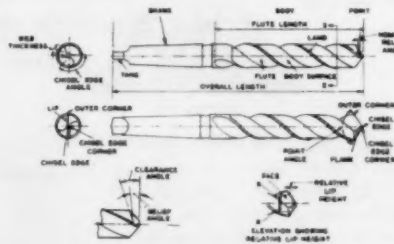


FIG. 5 DRILL NOMENCLATURE

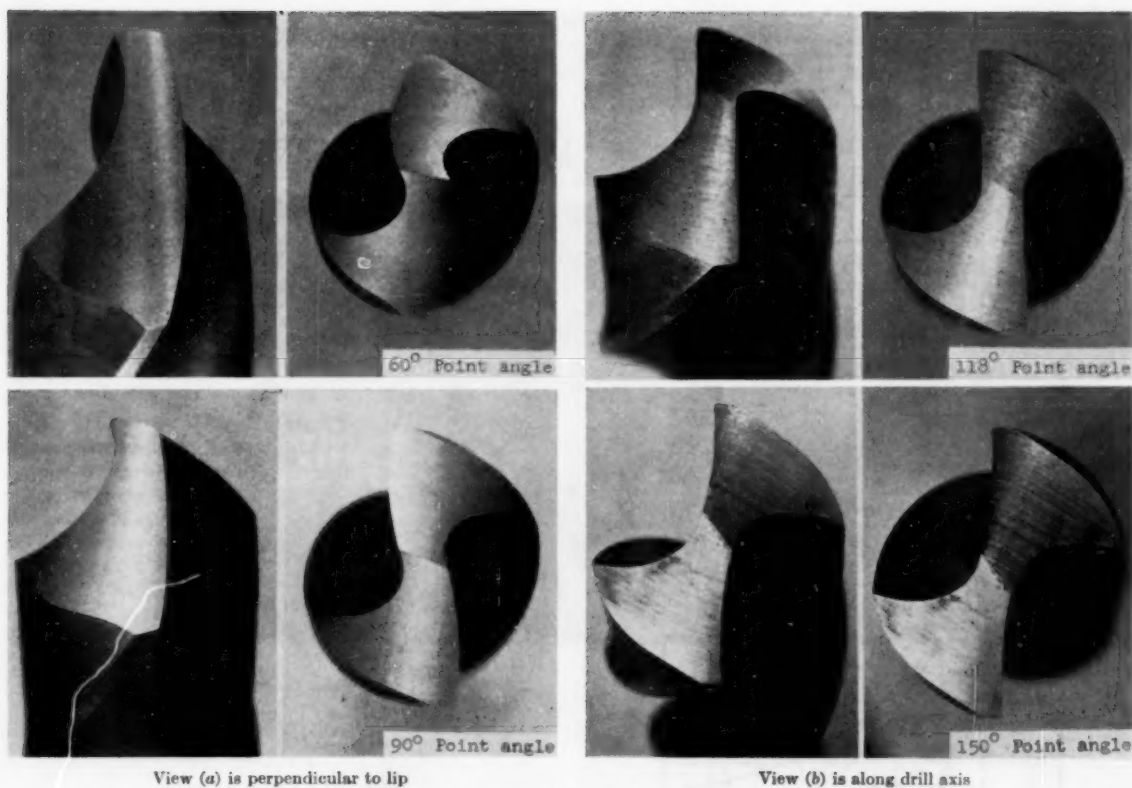


FIG. 6 VARIATION IN LIP SHAPE WITH POINT ANGLE

in planes parallel to and at distances  $f$  from the plane containing the axis of the drill, and are inclined to each other at an angle  $2\chi$ . The chisel edge is produced at the intersection of the two grinding cones. The concept of conical grinding can be extended to cam-controlled drill-grinding machines by considering the grinding action to be composed of a series of instantaneous conical grinding motions. Only expressions for the curvature of the flank and the chisel-edge angle are affected by this generalization of the grinding action; the relationships between the relief angle at the lip and the other angles at the point remain unchanged provided the lip shape does not depart very far from a straight line.

The shape of the drill lip depends on the point angle, helix angle, and flute contour, which are usually arranged to give a straight lip at the conventional point angle of 118 deg. Any departures from this angle result in a concave or convex lip, as illustrated in Fig. 6.

The rake is closely related to the helix angle and decreases progressively with the helix angle from the outer corner to the chisel edge. It is shown in Appendix 4 that the rake is related to the helix angle by the following equation

$$\cot \gamma_s = \frac{1}{(\rho^2 - \tau^2)^{1/2}} (\rho \cot \gamma \sin \kappa - \tau \cos \kappa)$$

where  $\gamma_s$  = rake at any point  $P$  on lips;  $\gamma$  = helix angle at  $P$ ;  $\kappa = 1/2$  point angle

$$\rho = \frac{\text{radius } r \text{ at } P}{\text{radius } R \text{ at outer corners}}$$

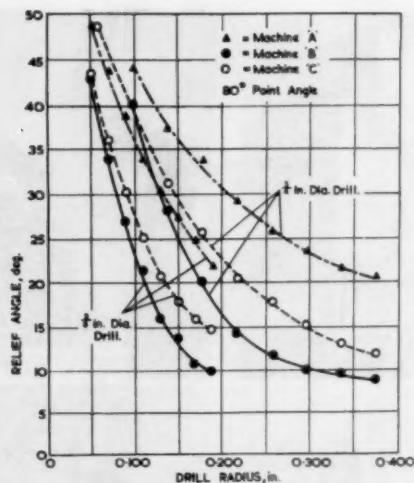
$$\tau = \frac{\text{web thickness } 2t}{\text{radius } R \text{ at outer corners}}$$

The nominal relief angle increases rapidly from the outer corners of the drill to the chisel edge. For drills ground by traversing the flanks past a straight line of contact on the grinding wheel, the following equation from Appendix 4 may be used to calculate the variation in nominal relief angle along the lips

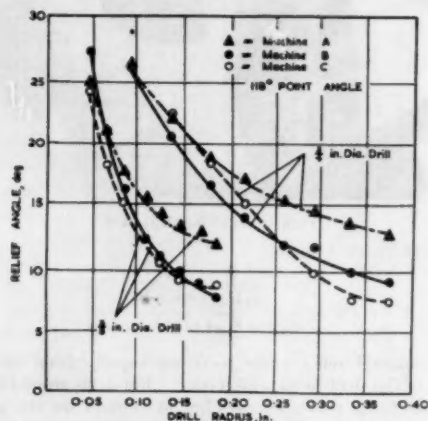
$$\tan \alpha = \frac{\tau}{\rho} \left[ 1 - \left( \frac{\rho^2 - \tau^2}{1 - \tau^2} \right)^{1/2} \right] \cot \kappa + \frac{1}{\rho} \left( \frac{\rho^2 - \tau^2}{1 - \tau^2} \right)^{1/2} \tan \alpha_s$$

where  $\alpha$  = nominal relief angle at any point  $P$  on lips;  $\alpha_s$  = nominal relief angle at outer corners;  $\kappa = 1/2$  point angle;  $\rho$  and  $\tau$  are as given in the rake formula.

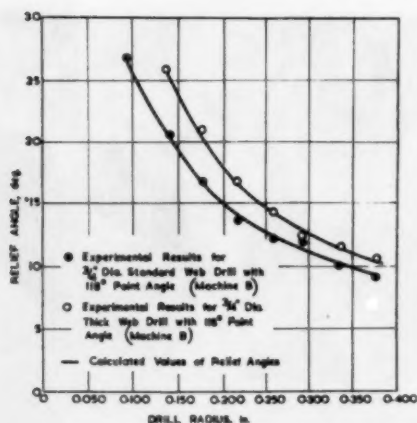
The variation in nominal relief angle along the lips of  $3/8$ -in. and  $1/4$ -in.-diam drills ground to point angles of 80 and 118 deg on three different drill-grinding machines is shown in Figs. 7(a) and 7(b), respectively. Theoretical curves for standard and thick-web drills with a point angle of 118 deg were calculated for machine (B) from the relief-angle equation and are shown in Fig. 7(c) together with measured values of relief angle. The measured values are in good agreement with the calculated values. The measured values for machine (A) were also in good agreement with the calculated values, but for drills ground on machine (C) there was some deviation from the theoretical curve, possibly due to misalignment of the drill lips with respect to the generator of the grinding cone.



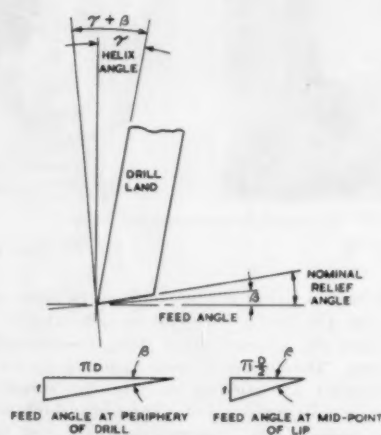
(a) Measured values of relief angle for 80-deg point angle drills ground on three machines



(b) Measured values of relief angle for 118-deg point angle drills ground on three machines



(c) Calculated and measured values of relief angle for standard and thick-web drills



(d) Effect of feed on angles at drill point

FIG. 7 RELIEF AND FEED ANGLES ALONG DRILL LIPS

The curves in Fig. 7(c) for the  $3/4$ -in.-diam standard and thick-web drills show that web thickness has only a slight effect on the variation of nominal relief angle along the lips. Figs. 7(a) and 7(b) show, however, that reducing the point angle results in a substantial increase in nominal relief angle, moving from the outer corners to the chisel edge.

During drilling the rake and relief angles are modified by the feed angle  $\beta$  shown in Fig. 7(d). The feed angle at any radius  $r$  from the drill axis is equal to

$$\tan^{-1} \left( \frac{f}{2\pi r} \right)$$

where  $f$  is the feed in inches per revolution (ipr). The effect of the feed angle is to increase the rake and reduce the relief angle, but in practice the effect is usually very small.

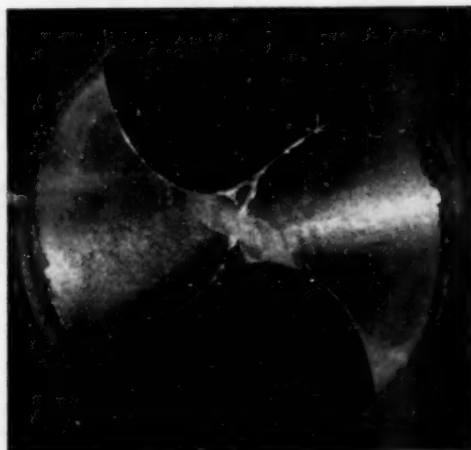
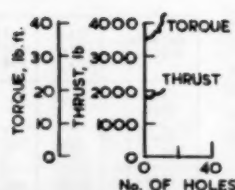
**Test Duration and Criteria in Drill-Life Tests.** The effects of factors such as drill shape, drill material, cutting fluid, and so on, must be considered in relation to the penetration rate, which,

together with drill life, forms the basis of workshop decisions concerning production rates and drilling costs. Depending on the choice of penetration rate the influence of drill-point shape on drill life can be determined in tests of short, medium, or long duration. The shorter the tests, the lower the cost and the consumption of material, but as the tests are progressively shortened by raising the penetration rate, the relationships between drill life and the various factors (relief angle, and so on) determined in the investigations may become less applicable to normal workshop conditions. Ideally, the test conditions should be accelerated as much as possible while still providing a reliable basis for the selection of workshop drilling conditions.

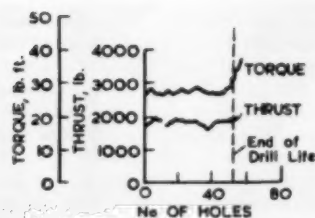
For a given penetration rate an infinite number of combinations of speed and feed can be chosen, but only a narrow range of combinations is of practical interest. This is the range in which drill life is near the optimum for the required penetration rate, and the conditions are usually such that the pattern of drill failure is characterized by an even distribution of wear along the cutting

edges for the greater part of drill life, followed either by accelerated wear of the outer corners or rapid blunting of the chisel edge as the end of drill life approaches. At abnormally high penetration rates giving a very short drill life there appears to be no well-defined optimum range of speed/feed combinations, and the pattern of drill failure may differ substantially from that obtained at lower rates of penetration. Under these extreme conditions a proper analogy between the tests and practice is no longer preserved, and the results of the tests are of very limited value.

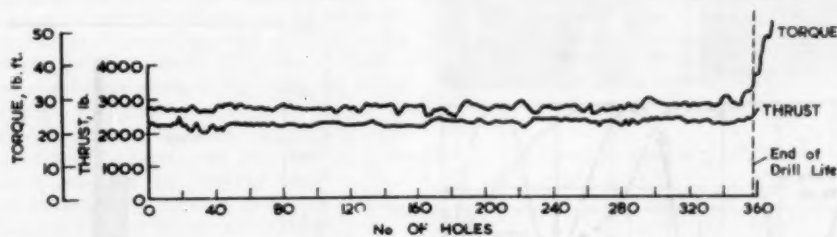
To determine a satisfactory range of test conditions for the main investigation, preliminary tests were carried out in steel and cast iron with



(a) Short-duration test in steel En 12



(b) Medium-duration test in steel En 12



(c) Long-duration test in steel En 12

$\frac{1}{8}$ -in.-diam drills. The tests fell into three groups:

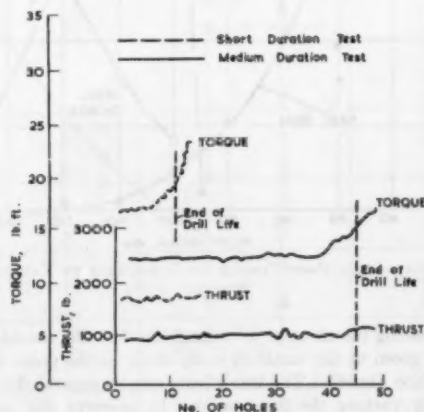
(a) Long-duration tests at normal workshop rates of penetration giving drill lives about 200-in. total depth drilled.

(b) Medium-duration tests at higher rates of penetration giving drill lives between about 50 and 200-in. total depth drilled.

(c) Short-duration tests at very high rates of penetration giving drill lives of approximately 40-in. total depth drilled.

Torque and thrust were plotted continuously for every hole drilled, and observations were made of drill wear and cutting noise throughout the tests.

Typical results obtained in the short, medium, and long-duration life tests are shown together with examples of drill wear in Fig. 8. At high penetration rates, torque and thrust rose sharply and the test was stopped after about 10 holes when the outer corners had reached the badly worn condition shown in Fig. 8(a). In the medium and long-duration tests, Fig. 8(b) and 8(c), the end of drill life was preceded by a slight increase in thrust, a rapid increase in torque, wear at the outer corners, and sometimes by a high-pitched noise or "cry." Long-duration tests gave wear patterns similar to those in medium-duration tests, and if continued beyond the commencement of the



(d) Short and medium-duration tests in cast iron

FIG. 8 TORQUE, THRUST, AND DRILL WEAR DURING SHORT, MEDIUM, AND LONG-DURATION DRILL-LIFE TESTS

rise in torque the outer corners collapsed after only a few holes. In some tests the chisel edge failed and thrust rose rapidly.

The foregoing tests showed that a suitable criterion of imminent drill failure in steel was the rise in torque or thrust, and the appearance of wear on the lips and/or chisel edge, and that the results of medium-duration life tests could be applied in normal workshop practice.

The patterns of drill failure in cast iron varied with the iron, some being similar to those in steel, and some giving gradual wear and a continuous rise in torque and thrust as shown in Fig. 8(d). In cast irons causing this gradual type of drill wear the tests were discontinued when torque had increased 20 per cent.

#### RESULTS OF INVESTIGATIONS INTO DRILL LIFE IN RELATION TO POINT SHAPE

Although drills are commonly ground with a point angle of 118 deg, Fig. 9 shows that for each material there was a different range of point angle which gave longest drill life. Drill life in cast iron was a maximum with a point angle of 60 deg at high speeds and moderate feeds, and with a point angle of 80 deg at lower feeds and speeds and in tough iron.

Material Drilled	Drill Dia. in.	Helix angle Deg.	Relief Angle Deg.	Speed r.p.m.	Feed in./rev.	Cutting Fluid
Cast Iron	5/8	28	10.1/2	940	0.010	None
Steel En 10	5/8	28	10.1/2	1,380	0.010	Soluble Oil
Steel En 3A	5/8	28	10.1/2	1,210	0.010	Soluble Oil
Steel En 30B	5/8	28	10.1/2	387	0.010	Soluble Oil
Ti 150A	0.323	25	12	760	0.0014	Soluble Oil

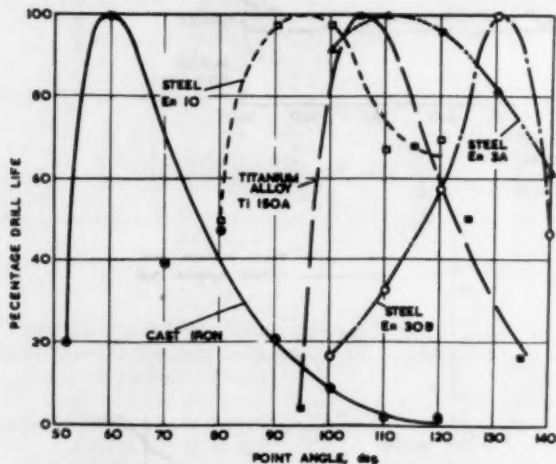


FIG. 9 EFFECT OF POINT ANGLE ON DRILL LIFE IN VARIOUS MATERIALS

In assessing the effect of point angle on drill life, consideration must be given to the variation in lip shape as the point angle is altered (see Fig. 6). The two effects can be separated to some extent by varying the flute contour to preserve the same lip shape at each point angle, avoiding as far as possible alterations to chip flow, rake, and the like.

Fig. 10 indicates that the optimum nominal relief angle was between 9 and 15 deg for the materials tested.

Material Drilled	Drill Dia. in.	Helix Angle Deg.	Point Angle Deg.	Speed r.p.m.	Feed in./rev.	Cutting Fluid
Cast Iron	5/8	28	60	940	0.010	None
Steel En 10	5/8	28	100	1,380	0.010	Soluble Oil
Steel En 30B	5/8	28	130	387	0.010	Soluble Oil

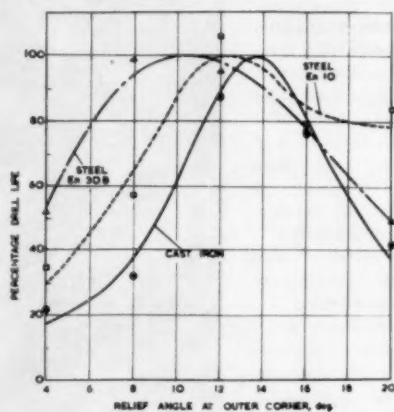
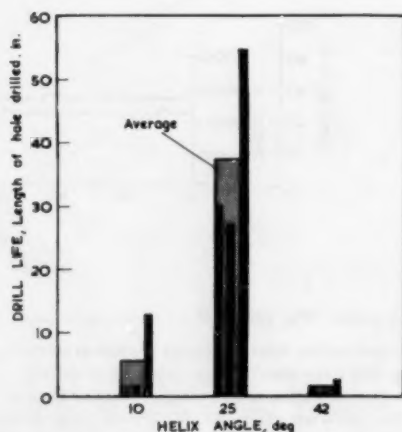


FIG. 10 EFFECT OF RELIEF ANGLE ON DRILL LIFE IN VARIOUS MATERIALS

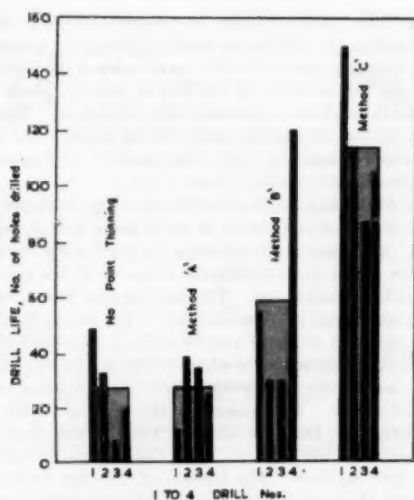


Drilling conditions:  
 Point angle 105°  
 Relief angle 10°  
 Spindle speed 760 rpm  
 Feed 0.0014 in./rev  
 Cutting fluid soluble oil

FIG. 11 RESULTS OF LIMITED TESTS INDICATING EFFECT OF HELIX ANGLE ON DRILL LIFE WHEN DRILLING Ti 150A WITH 0.323-IN. DIAM DRILLS

The effects of helix angle on drill life were not generally investigated, but the results of a few tests on titanium alloy Ti 150A (Fig. 11) indicated that a 25-deg helix angle gave longer life than 10 or 42 deg.

Various methods of point thinning are commonly used in attempts to improve drill life and reduce cutting forces. With drills having a tapered web the web thickness increases as the drill is ground back, and drill life is reduced unless the drill point



(a) Results of drill-life tests

Drill diam.  $\frac{3}{8}$  in. Spindle speed 945 rpm  
 Helix angle  $28^\circ$  Feed 0.0135 in./rev  
 Point angle  $118^\circ$  Cutting fluid soluble oil  
 Relief angle  $10\frac{1}{2}^\circ$

FIG. 12 EFFECT OF VARIOUS METHODS OF POINT THINNING ON DRILL LIFE WHEN DRILLING STEEL EN 10

is thinned to approximately the original section. Even when the web thickness has not become excessive, careful point thinning can improve drill life, as shown by the test results in Fig. 12(a) for thinned and unthinned drills. The three methods of point thinning investigated are shown in Fig. 12(b); in method A the chisel-edge length is reduced by notching the point at the ends of the chisel wheel; in method B is similar to method A except that the notches are just confined to the trailing edges and consequently the chisel-edge length remains the same; in method C metal is ground off part of the trailing edges to provide greater clearance near the corners of the chisel edge.

The effects of relative lip height on drill life and hole accuracy have been referred to in a previous paper by the author.<sup>3</sup> It was pointed out that relative lip height is one of the commonest faults in drill grinding, and that excessive relative lip height can substantially reduce drilling efficiency. As shown later in the present paper, the unbalanced forces acting on a drill with a large relative lip height tend to displace the general axis of the drill from the axis of rotation towards a position where the resultant forces on the lips are in balance, but even so the cutting conditions at the two lips are different and premature failure of the drill occurs. The results in Fig. 13, for example, show that drill life was increased nearly three times by reducing the relative lip height for  $\frac{3}{8}$ -in.-diam drills from 0.015 in. to 0.001 in.

The outer corners of a drill are sometimes chamfered or rounded in an attempt to increase drill life and im-

Drill diameter  $\frac{3}{8}$  in.  
 Spindle speed 760 rpm  
 Feed 0.018 in./rev  
 Cutting fluid soluble oil

FIG. 13 (right) EFFECT OF RELATIVE LIP HEIGHT ON DRILL LIFE IN STEEL EN 12

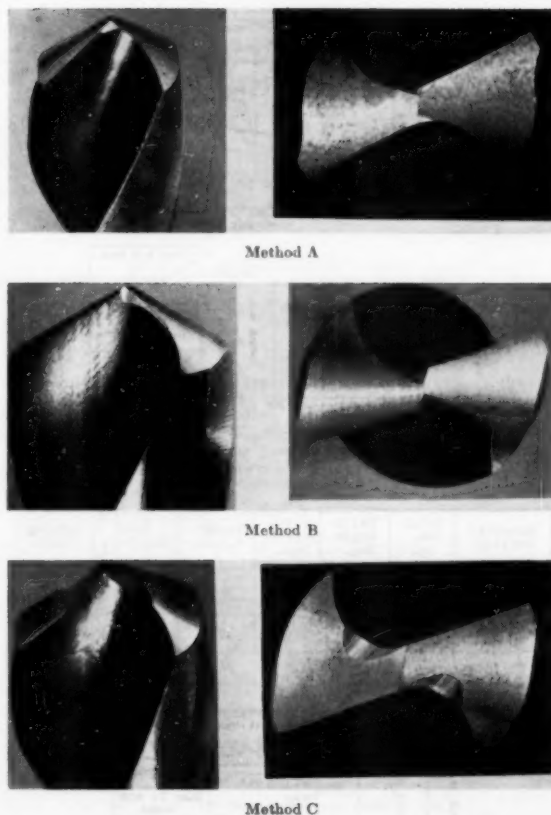
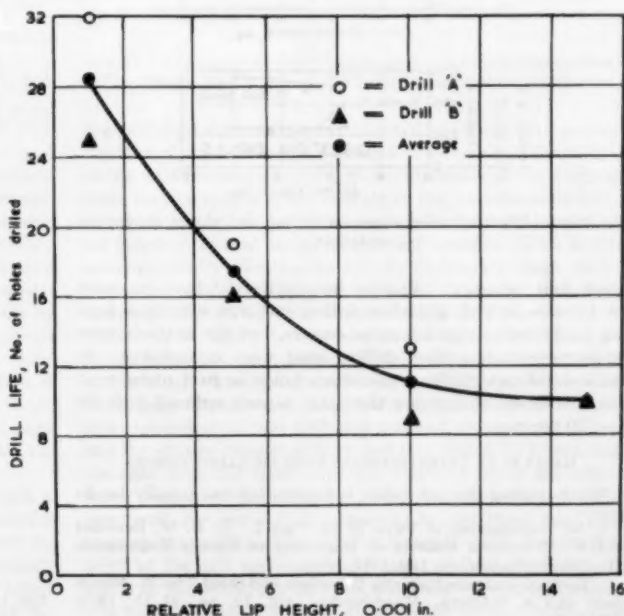


Fig. 12(b) Methods of point thinning investigated



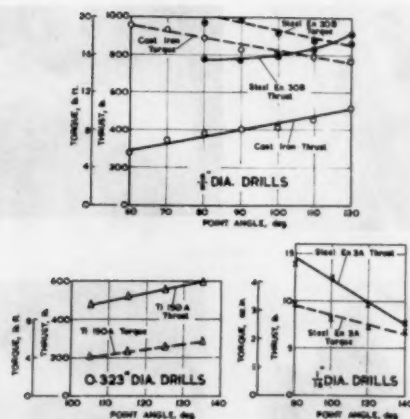


FIG. 14 EFFECT OF POINT ANGLE ON TORQUE AND THRUST IN VARIOUS MATERIALS

Material Drilled	Drill Dia. in.	Helix Angle Deg.	Point Angle Deg.	Speed r.p.m.	Feed in./rev.	Cutting Fluid
Cast Iron	5/8	28	60	940	0.010	None
Steel En 30B	5/8	28	130	387	0.010	Soluble Oil
Ti 150A	0.323	25	115	760	0.0014	Soluble Oil

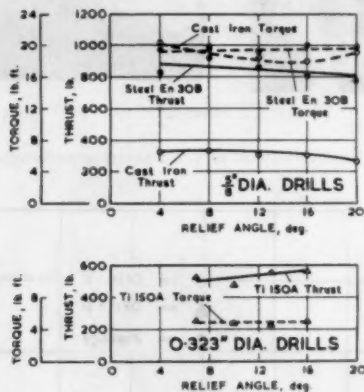


Fig. 15(a) Effect of relief angle on torque and thrust in various materials

prove hole accuracy. Various investigators<sup>4,5</sup> have reported an increase in drill life when drilling cast iron with drills having chamfered or rounded outer corners, but the author's tests on corner rounding when drilling steel were inconclusive. In two series of tests, drilling 5/8-in.-diam holes in steel under various conditions, chamfering the outer corners reduced drill life over 30 per cent.

#### RESULTS OF INVESTIGATIONS INTO DRILLING FORCES

When drilling through holes, the operation can usually be di-

<sup>4</sup> "An Investigation of Twist Drills, Part I," by B. W. Benedict and W. P. Lukens, Bulletin of University of Illinois Engineering Experiment Station, no. 159, 1917.

<sup>5</sup> "Zerspanungsprüfung von Gusseisen und Stahl," by W. Mendelson and A. Wallich, *Maschinenbau*, vol. 12, no. 14-15, 1933, p. 402.

vided into three distinct phases as follows: Phase 1—the drill point penetrates the workpiece surface (this phase is completed when the outer corners of the drill have entered the workpiece); phase 2—the full diameter of the hole is drilled; phase 3—the drill breaks through the underside of the workpiece. The effects of various factors on drilling forces during phase 2 will be considered; observations also have been made of drill movements, torques, thrusts, etc., during phases 1 and 3.

**Effect of Drill Shape on Drilling Forces.** Fig. 14 shows typical variations of torque and thrust as point angle was varied. Except with 1/16-in.-diam drills, reducing the point angle lowered the thrust; the reason for the different behavior of the small drills has not yet been established. Torque increased with a reduction in point angle except in titanium alloy. The rise in torque with cast iron and steel probably can be explained partly by the increase in specific cutting force which occurs as the chip thickness decreases, and partly by the curvature of the cutting edges at small point angles. The reason for the reversal of the torque characteristic with titanium alloy is not clear, but it may be related to the tendency of Ti 150A chips to weld to the drill and hole surfaces. The friction of the chip over surfaces remote from the cutting edge therefore may possibly contribute more to the cutting force than is the case with other materials, and consequently the torque may be influenced to a larger extent

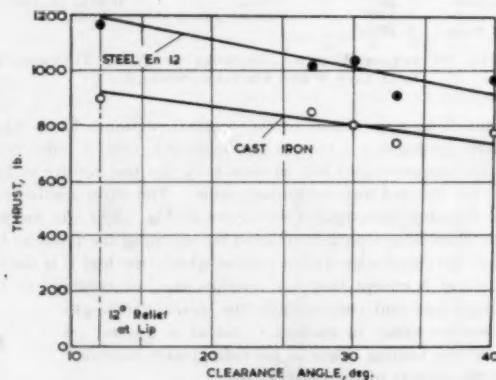


Fig. 15(b) Effect of clearance angle on thrust when drilling steel En 12 and cast iron with 5/8-in.-diam drills

FIG. 15 EFFECT OF RELIEF AND CLEARANCE ANGLES ON DRILLING FORCES

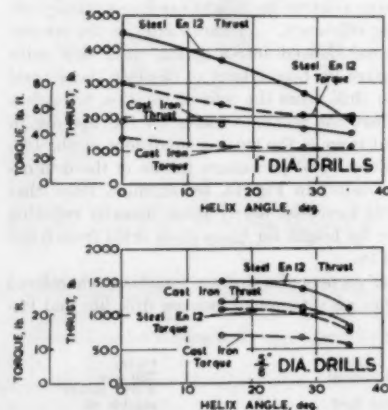


FIG. 16 EFFECT OF HELIX ANGLE ON TORQUE AND THRUST IN STEEL EN 12 AND CAST IRON

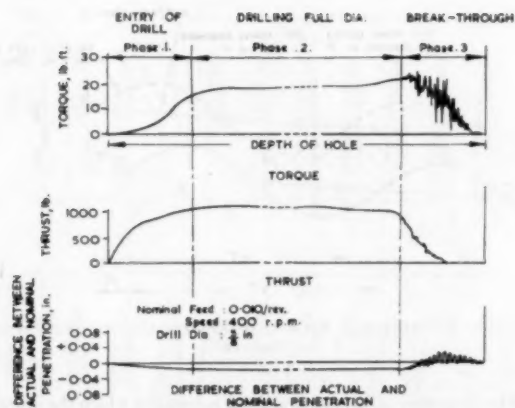


Fig. 17(a) Dynamometer records of torque and thrust and difference between actual and nominal penetration of drill

than usual by the direction of chip flow rather than by the shape of the chip section. A different mode of behavior for Ti 150A is also suggested by its high thrust/torque ratio in relation to steel and cast iron.

Results in Fig. 15(a) show that when relief angle was varied from 4 to 20 deg it had little effect on the cutting forces, but results in Fig. 15(b) show that the addition of 30-40-deg clearance behind a 12-deg relief on the first 5 deg of flank reduced thrust by about 10 per cent. The amount of clearance should be limited to maintain the strength of the chisel edge.

Fig. 16 shows that torque and thrust decreased as helix angle increased. Although lower torque and thrust reduce power consumption and machine and workpiece deflections, the helix angle frequently must be determined by other considerations. For example, increasing the helix angle reduces the amount of metal supporting the lips, which may then chip especially at heavy feeds. When tough materials such as high-manganese steel are drilled a helix angle of about 15 deg is commonly used; the web thickness is also usually increased.

The webs of commercial drills are normally increased in thickness toward the shank to stiffen the drill, but this has the disadvantage that thrust increases as the drill is reduced in length by successive grinding operations.<sup>3</sup> Three methods of point thinning sometimes used in attempts to reduce thrust are illustrated in Fig. 12(b). Investigations of seven variations of these methods showed that none of them reduced thrust sufficiently in cast iron and steel En 12 to justify thinning the points of thin web drills (web thickness/diameter ratio—0.11) for this reason alone, and some methods actually tended to increase the thrust. Carried far enough, method B reduced the thrust on shortened drills having a thick web at the point (web thickness/diameter ratio—0.21) by 40 to 60 per cent, but this was achieved only by weakening the point seriously. Method C, which provides greater trailing-edge clearance near the corners of the chisel edge, appeared to be the most satisfactory general method of thinning drills for cast iron and steel En 12 as it reduced thrust by 25 to 40 per cent and did not weaken the lips or chisel edge. As shown in Fig. 12(a), this method of point thinning also improved drill life.

**Forces at Drill Break-Through.** As the drill enters the work in phase 1, the cutting forces rapidly increase and the machine is deflected from its unloaded position, causing a reduction in the feed. Throughout phase 2, the torque, thrust, and feed remain sensibly constant. During phase 3 in a blind hole the actual feed of the drill continues after the feed mechanism has been dis-

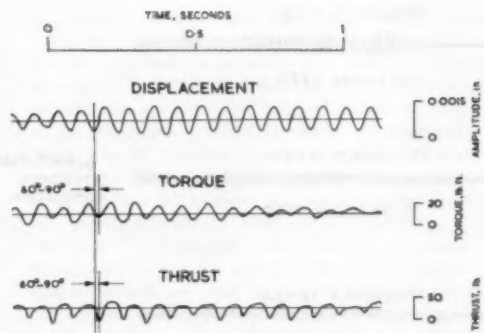


Fig. 17(b) Records of periodic fluctuations in torque and thrust and difference between actual and nominal penetration of drill

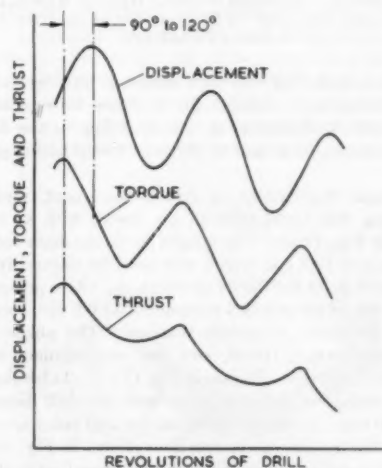


Fig. 17(c) Phase relationships between drill displacement and force on drill point

FIG. 17 VARIATION OF DRILLING FORCES AND DRILL DISPLACEMENT WHEN DRILLING A 1/2-IN.-DIAM HOLE IN MILD STEEL

engaged until the machine has returned to its unloaded position, but in a through hole rapid changes in torque and thrust occur as the drill point breaks through the underside of the work, and there may be a substantial increase in the instantaneous feed as the elastic energy stored in the machine structure is released and the machine returns to its undeflected position. This is often accompanied by vibration, so that during break-through the cutting edges of the drill may be subjected to specific loads far in excess of those set up under steady drilling conditions.

Records of thrust, torque, and axial displacement of the drill during break-through tests on a radial drilling machine are shown in Fig. 17(a). The displacement record, which was obtained with strain-gage displacement meters, shows differences between the axial movement of the drill and nominal penetration. Torque and thrust rose steadily at first, and then remained substantially constant until the chisel edge was about to break through the lower surface of the workpiece, when thrust decreased, torque rose, and the actual feed increased. As the chisel edge broke through the machine began to vibrate and continued until the point of the drill had completely emerged from the hole. The vibration of the machine and drill was reflected in both the torque and thrust records, but particularly in the torque record, where

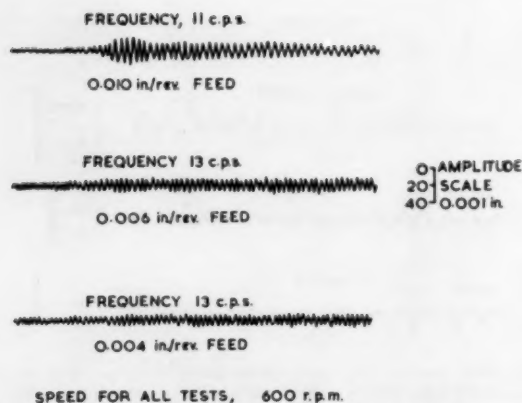


FIG. 18 VERTICAL VIBRATIONS OF DRILL HEAD OF RADIAL DRILLING MACHINE WHEN DRILLING  $7/8$ -IN-DIAM HOLES IN MILD STEEL AT VARIOUS FEED RATES

the peak-to-peak fluctuations were almost as large as the average torque. During break-through the feed rose substantially, and thus the 0.020-in. displacement corresponding to the deflection of the machine was regained as the thrust load acting on it was released.

The periodic fluctuations in drill displacement, torque, and thrust during drill break-through are shown with an extended time scale in Fig. 17(b). The frequency of the main component of vibration was 12.3 cps, which was near the natural frequency of the machine in its first mode of vibration. Also present in the torque and thrust records is a component at 6.5 cps, corresponding to the frequency of spindle rotation. The phase relationships between torque, thrust, and drill displacement are illustrated in the large-scale diagram in Fig. 17(c). At break-through the forces acting on the drill point lead the drill displacement by 90 to 120 deg; the forces acting on the drill point are opposite in sense to the dynamometer reactions shown in Fig. 17(b). As shown in Appendix 5, this would be in accord with the forces produced by a chip thickness-variation effect, and would suggest that the self-regenerative mechanism of chatter may play an important part in the vibrations occurring at break-through.

The increase in average feed rate and the vibration set up during break-through impose severe loads on the drill. This is demonstrated by the large fluctuations in torque shown in Fig. 17(a), where it can be seen that the maximum torque during break-through exceeded that prior to break-through by 40 per cent. Since this maximum torque occurs while the cutting edges adjacent to the chisel edge are emerging from the work, the remainder of the cutting edges and outer corners must be subjected to high specific loads. Even if the drill does not break or the cutting edges chip badly at break-through, the cumulative effect of successive break-through cycles will shorten the life of the drill.

**Vibrational Forces.** Chatter vibrations commonly occur on radial drilling machines, which, as pointed out in an earlier paper,<sup>2</sup> have comparatively flexible structures possessing little damping in the lower modes of vibration. The nature of the vibrations is demonstrated by the vibration records in Fig. 18, which were taken vertically on the drill head of a radial drilling machine during drilling operations. Chatter vibrations occur at frequencies closely related to the natural frequency of the machine in one of its modes of vibration. In the tests referred to previously the frequency of vibration was slightly higher than the natural frequency of the machine in its first mode of vibration.

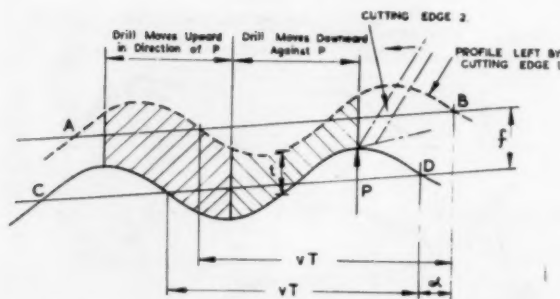


FIG. 19 MECHANISM OF SELF-REGENERATIVE CHATTER VIBRATION IN DRILLING

The frequency of vibration and the manner in which the amplitude builds up at the commencement of the records shown in Fig. 18 suggest that the vibrations may be self-inductive in origin. It can be shown that vibrational energy may be fed into the system comprising the machine, drill, and work when certain phase relationships exist between the vertical vibratory motion of the drill and the profile of the surface to be cut. Consider for example the thrust forces acting on the drill cutting edge shown diagrammatically in Fig. 19. It will be assumed that during the previous half revolution of the drill the machine has been set in vibration at its natural frequency  $\nu$  by a small shock force. As a result the surface  $AB$  produced by cutting edge 1 is sinusoidal in profile with a wave length  $\nu T$ . Depending on the relationship between the speed of rotation of the drill and the frequency of vibration, the vibration trace  $CD$  of cutting edge 2 will be displaced in phase from the profile of the surface by an amount  $\alpha$ . Thus the chip thickness  $t$  and the thrust force  $P$  acting on the cutting edge will vary periodically at the natural frequency of the system as indicated by the shaded area in the diagram. If the phase displacement of the successive cut surfaces is as shown in the diagram, the thrust force  $P$  will be least when the drill is moving downward and greatest when it is moving upward. Hence the work done on the drill during its upward motion exceeds the work done by the drill during its downward motion, and, unless the net gain of energy is dissipated by the damping forces of the system, the amplitude of vibration will gradually increase.

An analysis of self-regenerative vibration is given in Appendix 5 to help clarify some of the significant features of this type of vibration, and to contribute to previous discussions by Hahn, Tlustý, Tobias and Fishwick, and others. The main results of the analysis in terms of dimensionless quantities  $\delta$ ,  $\rho$ , and  $n$  are shown on the stability charts in Fig. 20. The quantity  $\delta$  represents the logarithmic decrement of a system comprising the machine, tool, and work;  $\rho$  denotes the ratio of the increase in drilling thrust to the stiffness of the system as the chip thickness increases; and  $n$  is a measure of the phase relationship between the undulating profiles of successively cut surfaces. By definition  $n$  increases as the spindle speed is decreased. The quantity  $\delta/\rho$  is determined by certain characteristics of the machine and work material; large values of  $\delta/\rho$  correspond to high damping, high natural frequency, or low increase in drilling thrust with increasing chip thickness.

The shaded areas on the stability charts indicate the regions of instability or chatter. Below a certain value of  $\delta/\rho$ , alternate regions of stability and instability are met as the spindle speed is reduced, until at low spindle speeds the curves of borderline stability overlap and form a continuous region of instability. Above a certain value of  $\delta/\rho$ , there are no unstable regions and

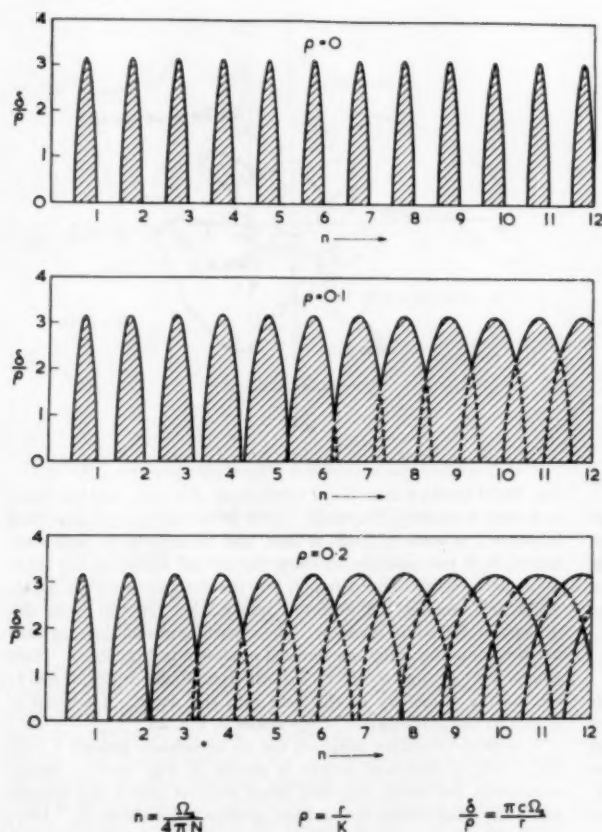
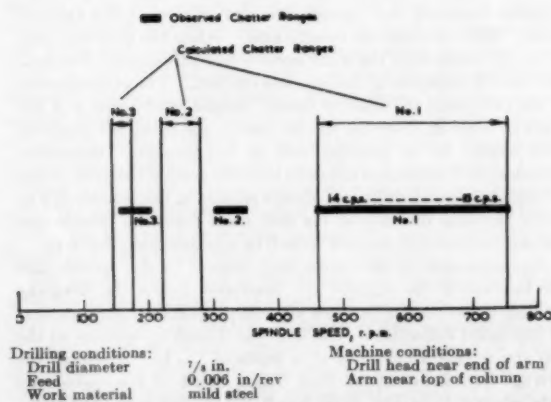


FIG. 20 VIBRATION STABILITY CHARTS

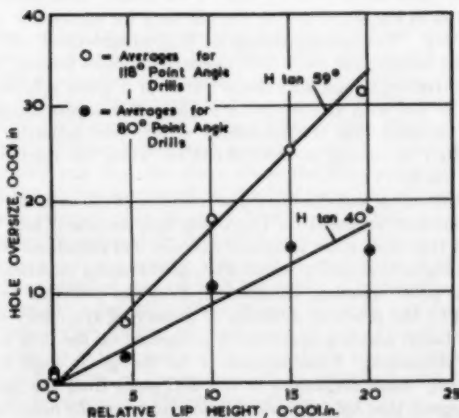
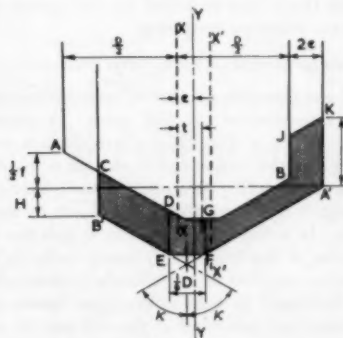


the system is stable irrespective of  $n$ . It is shown in Appendix 5 that the requirements for this unconditional stability are defined approximately by the formula  $\delta/\rho > \pi$ . Thus  $\delta/\rho$  should be as large as possible if the system is to be very stable for all values of  $n$ . This implies that one or more of the following conditions should be satisfied: (a) High damping in the system, (b) relatively high stiffness of the system, and (c) relatively low increase

in drilling thrust with increasing chip thickness.

In our present state of knowledge the analysis in Appendix 5 can only be expected to provide an indication of the general behavior of a machine tool susceptible to self-regenerative chatter. Self-induced vibrations of different origin are known to exist in machining operations, and the pattern of behavior may then be quite different from the one described. When interpreting the stability charts it should be kept in mind that the quantities  $\delta$  and  $\rho$  do not necessarily remain constant as the cutting speed is changed; if for example the ratio  $\delta/\rho$  increases sufficiently as the spindle speed is reduced the higher order chatter ranges will not be encountered. Nevertheless, certain characteristics associated with individual chatter bands, notably the variation of chatter frequency with speed and the location of the band in relation to the mean chatter frequency, help to identify self-regenerative chatter in practical cases.

Fig. 21 gives the results of some preliminary drilling tests on a radial drilling machine to investigate the theory of self-regenerative chatter. The observed ranges of spindle speed in which chatter occurred are shown together with the first three ranges obtained from the stability chart. The values of  $n$ ,  $\delta$ , and  $\rho$  were derived from vibration records obtained in the first observed range of chatter. It



b) Effect of relative lip height on size of  $1/8$ -in-nominal-diam holes drilled in steel (results are averages of tests at feed rates of 0.005, 0.008, and 0.012 in/rev)

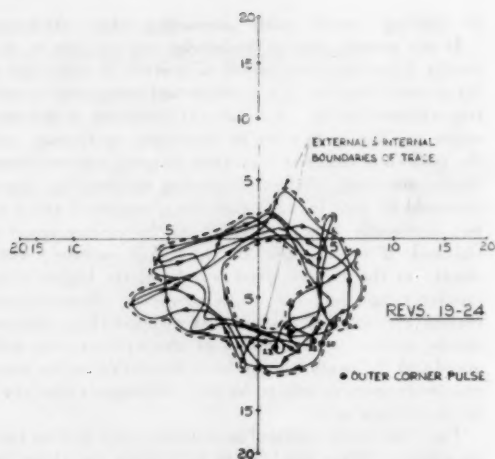


Fig. 23(a) Derivation of boundary diagrams from deflection records

will be seen that the location and width of chatter ranges are reasonably consistent with the theory. Despite some discrepancies in detail, the evidence of the tests carried out so far lends support to the self-regenerative theory, and suggests that further investigation along lines indicated by the theory may help to solve vibration problems in drilling.

#### RESULTS OF INVESTIGATIONS INTO DRILLING ACCURACY

**Hole Size and Roundness.** Hole accuracy is markedly dependent on the symmetry of the drill point. A common error in symmetry is shown in Fig. 22(a) where the lips are inclined at equal angles  $\kappa$  to the drill axis, but one lip is in advance of the other by the distance  $H$ . As a result of the relative lip height  $H$ , the chisel edge is displaced from the drill axis by an amount  $t = \frac{1}{2} H \tan \kappa$ . It is shown in Appendix 6 that the hole oversize due to an error of this type is very nearly equal to  $2t$ , or  $H \tan \kappa$ . Typical results obtained in experiments to determine the effects of relative lip height on hole accuracy are shown in Fig. 22(b). Hole diameters were measured at the top, middle, and bottom of the holes, but as the variation in hole diameter beyond a depth of  $\frac{1}{16}$  in. did not exceed 0.002 in. attention was confined to measurements taken at the middle of the holes. Also shown on the graph in Fig. 22(b) are the lines  $H \tan \kappa$  for values of  $\kappa = 40$  and  $59$  deg. The calculated lines are in good agreement with the observed results; the mean hole oversize increases linearly with the relative lip height, and the oversize for a given relative lip height is less with smaller point angles. Roundness measurements revealed that the roundness errors were generally less than 0.001 in., rising to 0.002–0.003 in. when the relative lip height was 0.015 in.

Point thinning, and chamfering or rounding of the outer corners, are sometimes proposed for improving hole accuracy, but tests showed that they often increased oversize and roundness errors. The loss of hole accuracy which often accompanies modifications such as point thinning, chamfering, etc., can probably be explained by the practical difficulty of preserving symmetry when an additional grinding operation is performed on the drill point.

**Hole Alignment.** Consideration of the changes in slope which accompany small deflections of the drill point from the spindle axis suggests that hole alignment is dependent on the behavior of the drill at the onset of drilling. Continuous records of point displacement for a  $\frac{3}{8}$ -in.-diam drill were obtained using capacitive gages, and a contactor on the machine spindle which injected a pulse to mark the position of the outer corners along the trace.

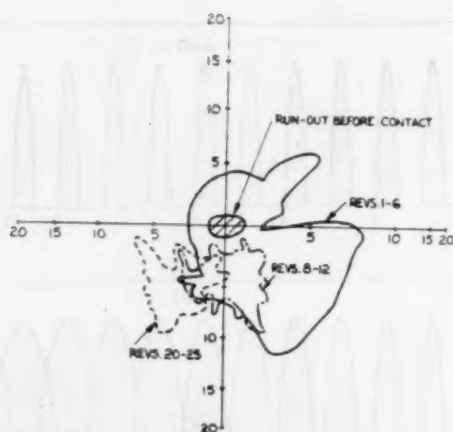


Fig. 23(b) Relative lip height  $< 0.001$  in. without center hole

Fig. 23(a) shows a trace for 6 revolutions of a drill, and the inner and outer boundary diagrams. Over 20 revolutions are involved in phase 1 of each  $\frac{3}{8}$ -in.-diam hole, and because of the space required it is not possible to show the actual traces of the drill-point path in the present paper, but the diagrams in Figs. 23(b), (c), (d), (e), convey the essential information derived from the drill-point deflection records. The closed figures on the diagrams are the boundary diagrams derived as shown in Fig. 23(a). They extend over several revolutions at different stages during phase 1; i.e., during the entry of the drill into the work. Attention is drawn to the nonlinearity of the scales in Fig. 23.

A typical boundary diagram for an accurately ground  $\frac{3}{8}$ -in.-diam drill of standard length is shown in Fig. 23(b). Before contacting the work, the drill point rotated about the spindle axis with a maximum run-out not greater than 0.0025 in. During the first few revolutions following contact the drill point was deflected away from the spindle axis by amounts up to about 0.012 in. As the drill continued to penetrate the work, the deflections decreased and became centered around a point approximately 0.005 in. from the spindle axis. When the drill had completed 20 revolutions the outer corners had just entered the work and the full diameter of the hole was reached. The general center of the drill-point movements finally became established at a distance of 0.006 in. from the spindle axis in the front left quadrant with respect to the principal axes of the machine. Successive records of drill deflection revealed that the general behavior of the accurately ground drills was always similar to that shown in Fig. 23(b), the final distance of the drill point from the spindle axis varying in a random manner from 0 to approximately 0.006 in.

Measurements to determine with respect to the spindle axis the location of the shallow hole produced during the foregoing drilling operation were in close agreement with the measurements of drill-point deflection. The hole was 0.0055 in. oversize at the top and 0.0025 in. oversize at a depth of  $\frac{1}{16}$  in. Although the average oversize over the first  $\frac{1}{16}$ -in. depth of the  $\frac{3}{8}$ -in.-diam hole referred to in Fig. 23(b) was 0.004 in., the boundary curve for revolutions 20 to 25 shows that the drill point was able to move in an orbit of about 0.010-in. diam. At the beginning of the hole the drill point is located only by the narrow land surfaces at the outer corners. Thus along a direction perpendicular to the diameter across the lands, the drill point is free to move substantially further than the limits defined by the clearance between hole and drill diameters, at least until the drill has penetrated far enough for the land helix to provide additional guidance for the drill.

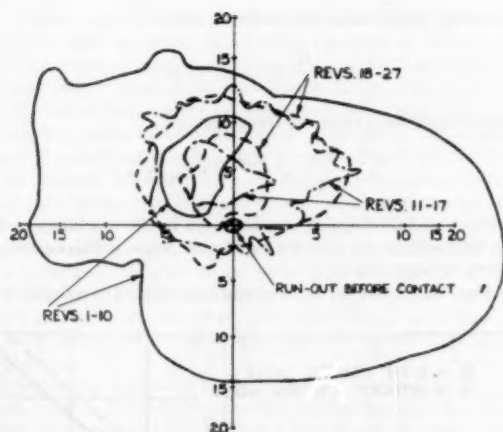


Fig. 23(c) Relative lip height: 0.005 in. without center hole

NOTE: Axes of diagrams graduated in units of 0.001 in.  
 Drill diameter  $\frac{1}{8}$  in.  
 Body length of drill  $\frac{5\frac{11}{16}}{16}$  in.  
 Work material steel  
 Spindle speed 300 rpm  
 Feed 0.006 in./rev

FIG. 23 DIAGRAMS SHOWING BOUNDARIES OF RADIAL DEFLECTIONS OF DRILL POINT AT COMMENCEMENT OF DRILLING

A typical diagram for a drill having a 0.005-in. relative lip height is shown in Fig. 23(c). During the first few revolutions after contact, the drill point was deflected in a wide orbit ranging more than 0.020 in. from the spindle axis. After 10 revolutions, however, the general motion of the drill point became established as a rough circle about 0.010-in. average diameter, with the center about 0.005 in. from the spindle axis. This type of motion continued without any substantial change to the end of the test, when the outer corners had penetrated the work to a depth of  $\frac{1}{16}$  in. The final position of the center of the general circle of motion of the drill was approximately 0.005 in. from the spindle axis toward the rear of the machine. The average diameters of the inner and outer boundary diagrams were approximately 0.007 in. and 0.014 in., respectively, so that the drill point was generally moving in a path about 0.010-in. diam. Measurements showed that the actual hole was displaced from the spindle axis by 0.007 in. toward the rear of the machine, and that the average hole oversize was 0.011 in. over the first  $\frac{1}{16}$ -in. depth of hole. Taking into account possible sources of error, there is fair agreement between the measurements of drill deflection and hole location. The average hole oversize is seen to be almost equal to the diameter of the average circle of motion of the drill.

The general indications of the diagram in Fig. 23(c) are that, after the initial skidding of the chisel edge, the axis of rotation of a drill with substantial relative lip height rapidly establishes itself at a new center of rotation displaced from the general axis of the drill point. The magnitude of the displacement is approximately equal to the eccentricity of the center of the chisel edge arising from relative lip height. Thus the drill point rotates about an axis which is displaced from the spindle axis by an amount equal to the eccentricity of the chisel edge with a run-out equal to twice the eccentricity of the chisel edge. Clearly, therefore, in addition to the effects on hole size and drill life which already have been discussed, relative lip height also can seriously affect hole straightness and alignment.

The effect of a center hole on the deflection of the accurately ground drill and a drill having a 0.005-in. relative lip height is shown in Figs. 23(d) and (e). The center hole which was ac-

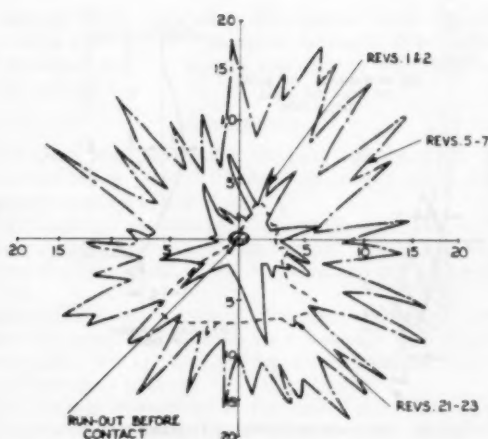


Fig. 23(d) Relative lip height &lt; 0.001 in. with center hole

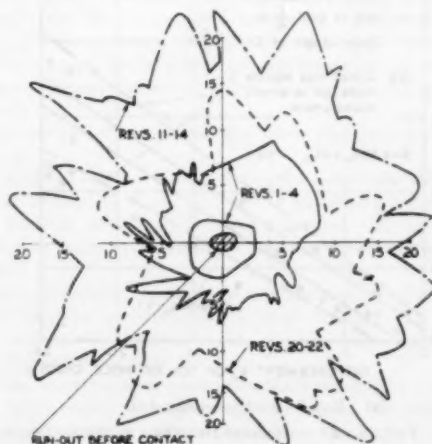


Fig. 23(e) Relative lip height: 0.005 in. with center hole

curately drilled from the machine spindle, was large enough in diameter to just contain the chisel edge and slightly deeper than the penetration over phase 1. Comparison of the diagram in Fig. 23(d) for the accurately ground drill with the diagram in Fig. 23(b) for the same drill without a center hole, shows that the drill-point displacements were generally much greater with a center hole and that the character of the motion was different. The trace of the movement of the drill point formed a series of triangles centered about a point close to the spindle axis. The maximum excursion of the drill point amounted to approximately 0.020 in. about the spindle axis after 6 revolutions of the drill from the instant of contact with the work. The behavior of the drill after the outer corners had entered the work was similar to that found when drilling without a center hole, except that the final position of the general center of motion was always within 0.002 or 0.003 in. of the spindle axis as compared with 0.006-0.007 in. for the tests without a center hole.

The diagram in Fig. 23(e) for the drill with 0.005-in. relative lip height is similar in character to that for the accurately ground drill with a center hole. The important effect of the center hole was to constrain the center of motion of the drill point to within 0.002 in. or 0.003 in. of the spindle axis as compared with 0.005

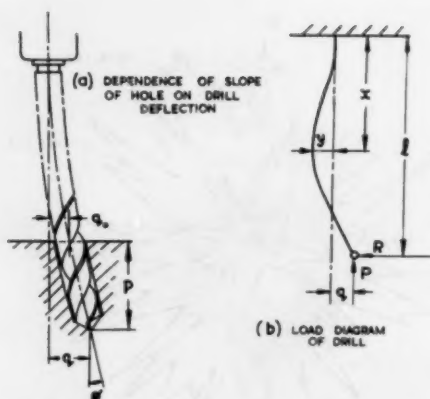
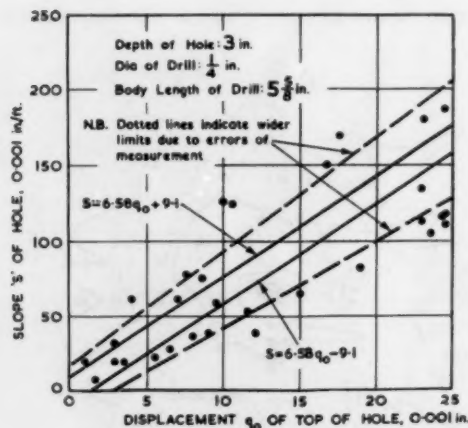
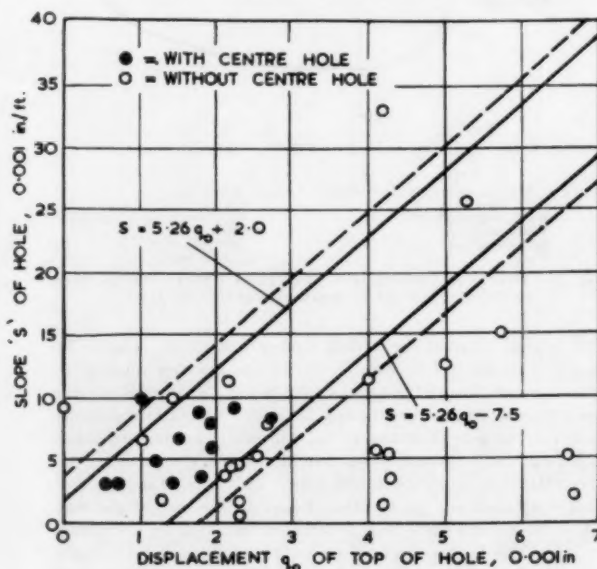


FIG. 24 ANALYSIS OF SLOPE OF DRILLED HOLES



(a) Results for 1/8-in.-diam drill



(b) Results for 5/16-in.-diam drill

FIG. 25 RELATIONSHIP BETWEEN SLOPE OF DRILLED HOLE AND DISPLACEMENT OF TOP OF HOLE FROM SPINDLE AXIS

in. without a center hole. The average hole oversize over the first 1/16-in. depth was 0.013 in.; i.e., 0.002 in. greater than the oversize for the same drill without a center hole. However, the hole diameter just beyond a depth of 1/16 in. was the same, approximately 0.010 in. larger, for holes drilled both with and without a center hole.

The general conclusion to be drawn from the results is that the center hole should improve hole alignment by reducing the displacement at the top of the hole. A center hole will not, however, reduce hole oversize due to relative lip-height errors and it may make matters worse.

The final deflection of the drill point in phase 1, as discussed in the foregoing, has an important effect on the slope of the drilled hole which is illustrated in Fig. 24(a). Because of the initial deflection, the axis of the drill point has become inclined to the spindle axis and, with increasing depth, the deflection and slope have become progressively larger, so that the path of the drill tends to wander further and further from the true axis. It is shown in Appendix 7 that, except under conditions where the drilling thrust approaches the buckling load for the drill, the deflection  $q$  is related to the initial deflection  $q_0$ , the length of the drill  $l$ , and the depth of the hole  $p$ , by the exponential equation

$$q = q_0 e^{3p/2l}$$

The average slope  $s$  of a hole of depth  $p$  is

$$s = \frac{12}{p} (q - q_0) \text{ in./ft}$$

or substituting for  $q$  from the foregoing

$$s = \frac{12q_0}{p} (e^{3p/2l} - 1) \text{ in./ft}$$

The effect on hole slope of certain errors in the machine can be taken into account by introducing further terms in this equation, as shown in Appendix 7.

In Figs. 25(a) and (b) the slopes of holes drilled to a depth of 3

in. in mild steel with 1/8-in. and 5/16-in.-diam drills are shown plotted against the displacements of the tops of the holes from the spindle axis. Some of the test pieces for the tests with the 5/16-in.-diam drill were accurately center drilled from the machine spindle to provide a center hole of diameter just greater than the chisel-edge length; in the remainder of the tests, however, no such guidance for the drill point was provided. The full lines on the graphs are the calculated limits based on equations similar to those above for slope ( $s$ ), but modified to take account of spindle misalignment and clearance (see Appendix 7). The dotted lines indicate the amount by which the limits are effectively widened due to possible errors in measurement of the slope of the holes.

It will be seen that the results in Fig. 25(a) for the 1/8-in.-diam drills are grouped around the lines calculated from the equations, although there are some deviations from theory. There is some evidence in the graph that the drill has two modes of deflection, one resulting in slopes rather higher and one in slopes rather lower than those predicted by the theory. It is believed that the two modes may be caused by additional distortions arising from the torsional load on the drill, but a more detailed analysis together with further experimental observations would be required to clarify this more complex behavior of the drill.

The results in Fig. 25(b) show that the initial displacements and

hole slopes were much smaller with the more rigid  $\frac{5}{16}$ -in.-diam drill, and that the center hole limited the slope to within 0.010 in./ft as compared with a maximum slope of 0.033 in./ft without a center hole. Most of the results were in the neighborhood of the calculated range, although there were some large deviations among the results of tests without a center hole. A consideration of the changes in the hole slope corresponding to known errors in the machine alignment suggests that these deviations may be due to the presence of small indeterminate errors in the machine and test setup. The wide calculated limits of hole slope on the graph (+0.002 in./ft to -0.0075 in./ft), for example, correspond to a misalignment error of no more than 0.002 in. over 3-in. movement of the quill and a clearance of only  $\pm 0.0005$  in. in the quill slide. Clearly, therefore, quite small errors in the machine or setup may have a considerable influence on the slope of the drilled holes.

**Effect of Jig Bushes on Hole Alignment.** Jig bushes are commonly used to facilitate hole location and to improve hole alignment. To determine the effect of a jig bush on the alignment of comparatively deep holes, some tests were carried out in a simple drilling jig which could be fitted with either a short or long standard jig bush to suit  $\frac{1}{4}$ -in.-diam drills; the bush was rigidly mounted at a distance of 0.010 in. clear of the work. Groups of 24 holes were drilled in steel test pieces clamped in the jig, which was used under the various conditions specified in Table 1.

TABLE 1 RESULTS OF TESTS TO DETERMINE EFFECT OF JIG BUSH ON HOLE ALIGNMENT

Test Conditions	Range of hole slope with respect to spindle axis in groups of 24 holes (0.001 in./ft.)
Without jig bush; jig fastened to machine table.	8 - 170
$\frac{5}{16}$ in. long jig bush accurately aligned with spindle axis; jig fastened to machine table	4 - 28
$\frac{5}{16}$ in. long jig bush; jig free on machine table.	3 - 152
$\frac{3}{4}$ in. long jig bush; jig free on machine table.	4 - 65

Dia. of Drill :  $\frac{1}{4}$  in.  
 Body Length of Drill :  $5\frac{5}{8}$  in.  
 Depth of Hole : 3 in.

The results in Table 1 show that the short jig bush considerably reduced the slope of the drilled hole when the jig was fastened down similarly to a fixture and the bush was accurately aligned with the spindle axis. When, however, the jig was free on the machine table so that the jig and work were positioned by entering the drill into the bush, the range of hole slope was almost as great as that obtained without a jig bush. Under the same conditions, the long jig bush gave smaller values of slope, although the hole alignment was still worse than that obtained with the accurately aligned short jig bush.

The better hole alignment with the accurately aligned short jig bush is a direct result of the reduction of the initial drill deflection by the jig bush. The results demonstrate, however, that even with a jig bush large misalignments may still occur if the

normal type of loose jig is used. The extent of the misalignment will clearly depend on such factors as the length of the jig bush, the rigidity of the drill, and the resistance to sliding of the jig on the machine table.

#### CONCLUSIONS

**Drill Life.** Medium-duration life tests under carefully controlled conditions provide a valid indication of the practical effects of variations in drill shape.

Point angle has a marked effect on drill life, the optimum point angle varying from material to material. Typical optimum point angles were 60-80 deg for cast iron; and 130 deg for steel En 30B.

There is an optimum value of relief angle, although the differences from material to material are less marked than those for point angle. The optimum relief angle for steel and cast iron lies in the range 9 to 15 deg.

Drill life may be improved by a method of point thinning providing greater clearance near the corners of the chisel edge [method C, Fig. 12(b)].

Drill life is substantially reduced by large relative lip height.

**Drilling Forces.** Reducing the point angle of the drill generally lowers the thrust and raises the torque. Exceptions arise with small drills and when drilling titanium Alloy Ti 150A.

Within practical limits, relief angle has little effect on the drilling forces. Some reduction in thrust may be achieved by use of clearance.

An increase in helix angle generally lowers the torque and thrust in drilling.

The thrust of thick-web drills can be reduced by suitable point thinning; method C, Fig. 12(b), gave a significant reduction in thrust without weakening the cutting edges. No significant reduction in thrust is obtained by thinning the points of thin-web drills.

Under unfavorable conditions of machine rigidity, drill breakthrough may be accompanied by large increases in drilling torque and specific loading at the cutting edges. This may hasten drill failure or cause breakage.

The chatter vibrations which sometimes occur during drilling appear to be mainly self-regenerative in origin. An analysis of this type of vibration leads to conclusions which are in general accord with test results and practical experience. According to the analysis increases in machine damping and machine rigidity help to prevent unstable machining conditions.

**Drilling Accuracy.** Hole size is markedly dependent on the symmetry of the drill point. Asymmetry resulting from relative lip height causes the axis of rotation of the drill point to move to the center of the displaced chisel edge; the resulting hole oversize is given by  $H \tan \kappa$ , where  $H$  is the relative lip height and  $\kappa$  is half the point angle. Point thinning, outer-corner chamfering, and so on, may tend to impair hole accuracy by disturbing the symmetry of the drill point.

Hole alignment is dependent on drill deflection at the commencement of drilling and certain types of errors in the machine. Methods of drill-point location such as the use of an accurately located center hole, a jig bush or a fixture bush reduce hole misalignment by effectively preventing the initial deflection of the drill.

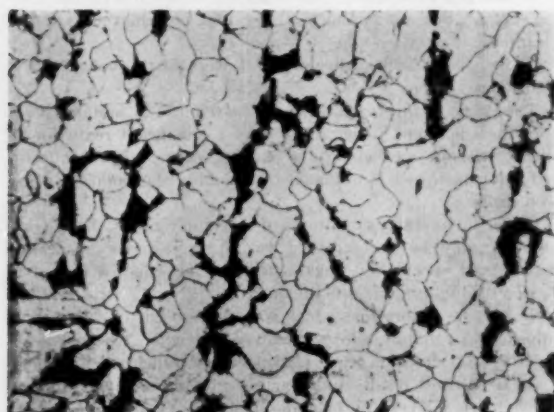
The common method of locating a loose jig by entering the drill into the jig bush is not effective in preventing large misalignments of drilled holes. The extent of misalignment will depend on the length of the jig bush, the rigidity of the drill, and the resistance to sliding of the jig on the machine table.

#### ACKNOWLEDGMENTS

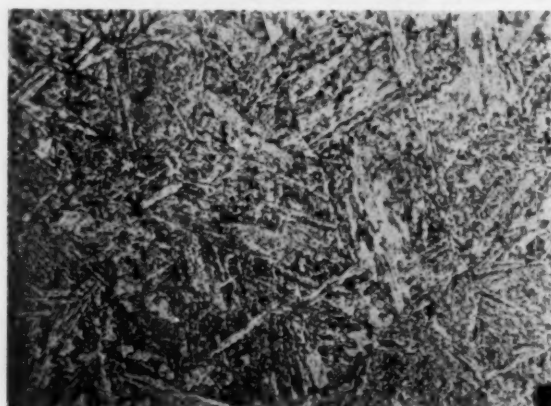
The author is indebted to the Production Engineering Re-

TABLE 2 CHEMICAL COMPOSITION AND PHYSICAL PROPERTIES OF STEELS USED IN DRILLING INVESTIGATIONS

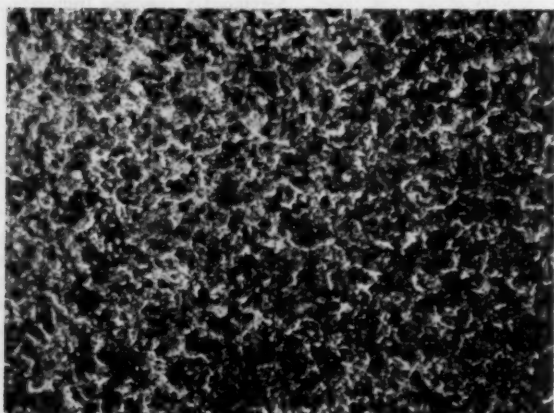
Material	Chemical Composition, %								Physical Properties					Heat Treatment
	Carbon	Silicon	Mang.	Nickel	Chrom.	Molyb.	Sulphur	Phos.	% Elong. on 2 in. Gauge Length	U.T.S. tons/sq.in.	Brinell No.	Drilling at 760 R.P.M. 0.006 in. feed/rev.		
												Torque lb.ft.	Thrust lb.	
Analysis En 32A Specification	0.11	0.29	0.60	-	-	-	0.021	0.022	45.3	25.4	131 to 162	9.18	714	Annealed
	0.15 max.	0.05 0.35	0.41 0.70	-	-	-	0.050 max.	0.050 max.						
Analysis En 10 Specification	0.58	0.24	0.60	0.80	-	-	0.019	0.013	21.9	50.8	230 to 298	9.97	955	Hardened and Tempered
	0.50 0.60	0.05 0.35	0.50 0.80	0.50 0.80			0.06 max.	0.06 max.						
Analysis En 30B Specification	0.33	0.28	0.55	4.45	1.41	0.26	0.012	0.007	15.4	64.1	308 to 325	13.29	1,041	Subcritical Annealed
	0.26 0.34	0.10 0.35	0.40 0.60	3.90 4.30	1.10 1.40	0.20 0.40	0.05 max.	0.05 max.						
Analysis En 12 Specification	0.30	0.10	1.50	0.60	-	-	0.05	0.05						
	0.45	0.35	max.	1.00			max.	max.						
Analysis En 1A Specification	0.07	0.10	0.80	-	-	-	0.20	0.07						
	0.15	max.	1.20				0.30	max.						



(a) Carbon case-hardening steel En 32A  
Condition: annealed



(c) 4 1/4 per cent nickel-chromium-molybdenum steel En 30B  
Condition: subcritical annealed



(b) "55" carbon 3/4 per cent nickel steel En 10  
Condition: oil-quenched 830 C, tempered 550 C

FIG. 26 TYPICAL PHOTOMICROGRAPHS OF STEELS USED IN DRILLING INVESTIGATIONS  
(Etched with 2 per cent nital. Magnification  $\times 250$ .)

search Association for permission to use the research results given in the paper, and to numerous members of PERA staff for their co-operation in this research.

## Appendix 1

### MATERIAL DRILLED

*Steels.* The steels used were as follows:

- 1 Carbon case-hardening steel En 32A.
- 2 "55" carbon 3/4 per cent nickel steel En 10 heat-treated to 55 tons per sq in.
- 3 4 1/4 per cent nickel-chromium-molybdenum steel En 30B.
- 4 35/45 ton 1 per cent nickel steel En 12 (axle steel).
- 5 Free-cutting carbon steel En 1A.

The chemical composition, physical properties, and heat-treatments of the four steels are tabulated in Table 2. Photomicro-

graphs of typical structures of the steels En 32A, En 10, and En 30B are shown in Fig. 26.

Steels En 32A and En 30B were supplied in rolled bars 4 in. square  $\times$  6 ft long, and steel En 10 was supplied in forged bars  $4\frac{1}{2}$  in. square  $\times$  6 ft long. Workpieces 9 in. long were cut from each bar and  $\frac{1}{4}$  in. was shaped off two opposite faces. These faces were filed smooth and Brinell hardness readings taken. Steel En 12 was supplied in the form of round bars.

Variations in test material from one billet to another and even within the same billet constitute a major difficulty in drilling investigations. As the tests were conducted with standard steels manufactured to commercial limits, wide variations in material hardness were to be expected, particularly in steel En 10. Fig. 27 shows the hardness gradient at cross sections taken at  $\frac{7}{16}$  in. and 3 in. from the end of an En 10 steel test billet. Photomicrographs revealed that there was a marked increase in the amount of ferrite towards the center, while the outside of the billet exhibited a fine structure of coalesced carbide. To avoid the influence of changes in structure within the billet, the tests in En 10 steel were confined to the center section of the billet and not less than 1 in. from the edges. Even this precaution did not prove completely satisfactory, as in many tests the drills failed suddenly due to a heavy build-up on the lands, while another drill tested in another billet would wear an equal amount without failure.

**Cast Iron.** Pearlitic gray cast iron (cylinder material) to BS

1425/14 was used for the tests with cast iron. The chemical composition and physical properties of the test blocks are shown in Table 3.

**Titanium.** The chemical composition of titanium alloy Ti 150A is given in Table 4. Test specimens measuring  $\frac{3}{4}$  in. long were cut from the 2-in.-diam bars, and hardness tests were made with a 30-kg load on a Vickers hardness testing machine. Readings taken at  $\frac{1}{8}$ -in. intervals across the diameter of each specimen are tabulated in Table 5.

## Appendix 2

### VARIATIONS IN SHAPE AND OTHER PROPERTIES OF NOMINALLY SIMILAR DRILLS

All drills used in the tests were examined to insure that shape and physical properties were within specified limits. Sample analyses and photomicrographs also were taken.

A large number of drills supplied for ordinary use in factories was examined to establish the approximate range of some of the main variables in normal industrial practice. Typical examples of the range of properties observed at that time are shown in Table 6.

Limits based on the preliminary observations were subsequently established for the test drills. An indication of these limits is given in the following abridged version of a drill specification:

TABLE 3 COMPOSITION AND ULTIMATE TENSILE STRENGTH OF CAST IRON USED IN DRILLING INVESTIGATIONS

Sample or Spec.	Chemical Composition, %								Physical Properties	
	Total Carbon	Combined Carbon	Silicon	Sulphur	Phosphorus	Manganese	Nickel	Chromium	Gauge Dia.	Ultimate Tensile Strength Tons/sq.in.
Analysis										
Sample No. 1	3.01	0.63	2.19	0.095	0.253	0.82	0.14	0.23	0.564	16.0
Sample No. 2	2.69	0.61	2.15	0.098	0.203	0.87	0.14	0.22	0.564	14.0
Specification										
B.S. 1452/14	-	-	-	-	-	-	-	-	0.564	15.0 (min.)

TABLE 4 CHEMICAL COMPOSITION OF TITANIUM ALLOY Ti 150A USED IN DRILLING INVESTIGATIONS

Material or Spec.	Chemical Composition, %				
	Carbon	Iron	Nitrogen	Chromium	Titanium
Analysis	0.050	1.48	0.10	2.75	Remainder
Manufacturer's Spec.	0.047	-	0.10	2.58	Remainder

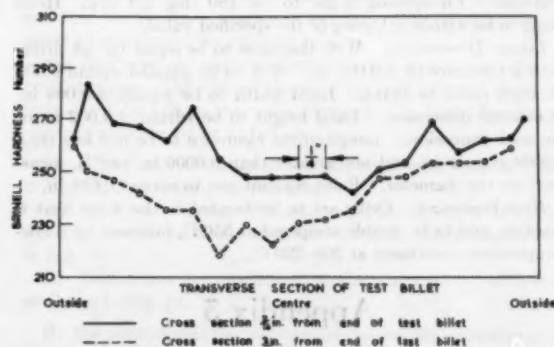


FIG. 27 HARDNESS VARIATIONS WITHIN A BILLET OF EN 10 STEEL

TABLE 5 HARDNESS READINGS TAKEN ON THE FACE OF TITANIUM TEST SPECIMENS AT  $\frac{1}{8}$ -IN. INTERVALS ACROSS THE DIAMETER

Specimen No.	Hardness Reading (D.P.N. 30 Kg. Load)															
	393	404	391	391	383	389	385	364	396	402	393	391	377	389	381	387
4																
59	385	368	375	362	366	357	355	344	353	351	366	357	360	370	357	385
98	362	366	379	379	373	377	368	360	371	375	375	381	375	370	373	391

TABLE 6 RANGE OF VARIATION OF DRILL SHAPE AND HARDNESS OBSERVED IN NOMINALLY SIMILAR 1/2-IN.-DIAM DRILLS

Element	Max.	Min.	Average	Range
Drill Point Dia. (in.)	0.6254	0.6236	0.6246	0.0018
Web Thickness at Point (in.)	0.122	0.070	0.0977	0.052
Web Thickness near Shank (in.)	0.160	0.113	0.1353	0.047
Land Height (in.)	0.040	0.012	0.0237	0.028
Land Width (in.)	0.080	0.020	0.048	0.060
Longitudinal Relief (in. per in.)	0.0026	0.0008	0.0015	0.0018
Relative Lip Height near Chisel Edge (in.)	0.008	0.0005	0.0036	0.0075
Relative Lip Height (in.) near Outer Corner	0.011	0.0000	0.0034	0.011
Point Angle (Degrees)	127	115	119.6	12
Relief Angle (Degrees) near Chisel Edge	35.5	16	23.65	19.5
Relief Angle (Degrees) near Outer Corner	25	5	14.10	20
Chisel Edge Angle (Degrees)	145	122	131.9	23
Helix Angle (Degrees)	31	28	29.5	3
Lip Spacing Angle (Degrees)	184	180	181.5	4
Hardness (D.P.N. No.) over Length of 1/4 in. from Point	1,016	256	832	760

*Abridged PERA Test Drill Specification.* Drills to conform to British Standard No. 328: 1950 with the following exceptions:

*Material.* Drills to be manufactured from 18-4-1 high-speed steel obtained from the same cast and, if possible, from the same bar. Carbon content to be between 0.70 and 0.75 per cent.

*Hardness.* Hardness readings taken on drill lands to be not less than 800 DPN and not greater than 910 DPN. Hardness readings taken at the center of a cross section of the drill to have a difference of less than 90 DPN from the hardness at the drill lands. Differences in hardness between the two lands of one drill to be less than 70 DPN.

*Angles.* Lip-spacing angle to be 180 deg  $\pm$  1 deg. Helix angle to be within  $\pm 1/2$  deg of the specified value.

*Linear Dimensions.* Web thickness to be equal for all drills, with a tolerance of  $\pm 0.004$  in. Web to be parallel within 0.006 in. from point to shank. Land width to be within  $\pm 0.004$  in. of nominal dimension. Land height to be within  $\pm 0.002$  in. of nominal dimension. Longitudinal clearance to be not less than 0.0004 in. per in. and not greater than 0.0006 in. per in. measured on the diameter. Point run-out not to exceed 0.001 in.

*Heat-Treatment.* Drills are to be treated in the same heat if possible, and to be double tempered at 550 C, followed by a low-temperature treatment at 200-230 C.

## Appendix 3

### TWIST-DRILL NOMENCLATURE

Various drill elements, angles, and dimensions mentioned in the following nomenclature are illustrated in Fig. 5.

#### Elements

*Axis.* The longitudinal center line.

*Body.* The part of the drill extending from the chisel edge to the shank end of the flutes.

*Shank.* The part of the drill by which it is held and driven.

*Tang.* The tongued portion on the end of the drill shank.

*Flutes.* The grooves in the body of the drill which provide lips and chip space.

*Web.* The central part of the drill situated between the roots of the flutes and extending from the point end towards the shank; the point end of the web forms the chisel edge.

*Lands.* The cylindrically ground surfaces on the leading edges of the drill flutes. The width of the land is measured at right angles to the flute helix.

*Body clearance.* The part of the body surface reduced in diameter to provide diametral clearance.

*Heel.* The edge formed by the intersection of the flute surface and the body clearance.

*Point.* The sharpened end of the drill, consisting of all that part of the drill which is shaped to produce lips, faces, flanks, and chisel edge.

*Face.* The part of the flute surface adjacent to the lip on which the chip impinges as it is cut from the work.

*Flank.* The surface or surfaces on a drill point which extend behind the lip to the following flute.

*Relief flank.* That part of flank immediately adjacent to lip.

*Clearance flank.* That part of the flank extending behind the relief flank.

*Lip (cutting edge).* The edge formed by the intersection of the flank and face.

*Outer corner.* The corner formed by the intersection of the lip and the leading edge of the land.

*Chisel edge.* The edge formed by the intersection of the flanks.

*Chisel-edge corner.* The corner formed by the intersection of a lip and the chisel edge.

*Diametral flute shape.* The contour or profile of the flute in a specified plane at right angles to the axis of the drill.

*Helical flute shape.* The contour or profile of the flute in a plane at right angles to the flute helix at the lands.

#### Measurements

*Diameter.* The measurement over the lands at any specified distance from the shank end of the body.

*Over-all length.* The length over the extreme ends of the point and the shank.

*Flute length.* The axial length from the extreme end of the point to the termination of the flutes at the shank end of the body.

*Lead of helix.* The distance measured parallel to the drill axis between corresponding points on the leading edge of a flute in one complete turn of the flute.

*Back taper (longitudinal clearance).* The reduction in diameter per inch length of drill from the point towards the shank.

*Land height.* The height of the land surface above the body surface behind the land, where it merges with the land surface.

*Web thickness.* The minimum dimension of the web measured at the point end of the drill.

*Web taper.* The increase in the web thickness per inch length from the point of the drill to the shank.

*Lip length.* The minimum distance between the outer corner and the chisel-edge corner of the lip.

*Relative lip height.* The axial displacement of the lips measured at a given radius and determined by the axial distance of the lips from a reference plane perpendicular to the drill axis.

*Relief-flank width.* The dimension (or angle) which defines the extent of the relief flank from the lip.

*Point run-out.* The radial run-out, with respect to the axis of the shank, of the circle containing the lands at the point end of the drill.

*Percentage flute area.* The sum of the areas of the flutes measured in a specified plane perpendicular to the drill axis expressed as a percentage of the area of a circle equal in diameter to the diameter of the drill in the specified plane.

### Angles

**Helix angle.** The acute angle between the leading edge of a land and the drill axis.

**Rake.** The angle between the face and a plane parallel to the drill axis and the line joining the corresponding outer and chisel-edge corners, measured in a plane perpendicular to this line.

**Point angle.** The sum of the acute angles between the drill axis and the lines joining each outer corner to the corresponding corners of the chisel edge (the two angles should be equal).

**Inclined relief angle.** The angle between the relief flank and a surface generated by the corresponding lip as the drill rotates about its axis, measured around the surface of a cone whose included angle is supplementary to the drill-point angle; i.e., around the surface of a cone coaxial with the center of the drill having an included angle of  $180^\circ$  minus drill-point angle and with its apex pointing toward the shank.

**Nominal relief angle.** The nominal relief angle is the angle between the relief flank and a plane perpendicular to the drill axis, measured in a plane parallel to the drill axis and perpendicular to a radius. The angle is usually measured from the lip.

**Clearance angle.** The clearance angle is the angle between the clearance flank and a plane perpendicular to the drill axis, measured in a plane parallel to the drill axis and perpendicular to a radius.

**Chisel-edge angle.** The obtuse angle included by the chisel edge and a line from either outer corner to the corresponding end of the chisel edge; the angle is measured in a plane perpendicular to the drill axis.

**Lip-spacing angle.** The angle between the lips at any specified radius measured in a diametral plane.

## Appendix 4

### CONICAL GRINDING AND THE GEOMETRY OF THE DRILL POINT

A common method of grinding the flank surfaces of the point of a twist drill is shown diagrammatically in Fig. 28. The drill is

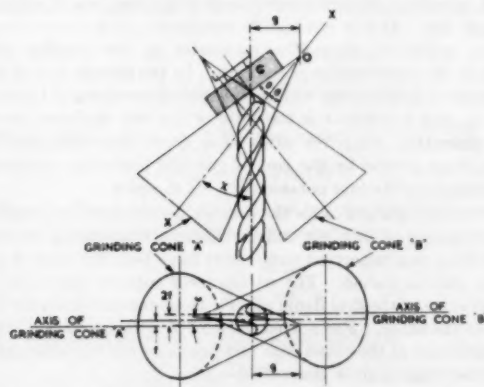


FIG. 28 PRINCIPLE OF CONICAL GRINDING OF DRILL FLANKS

rotated about the axis  $XX$ , which is fixed in space, and the flank is ground by the plane face of the grinding wheel  $G$ ; the axis  $XX$  and the plane of the grinding-wheel face intersect in the point  $O$ . The motion of the wheel face in relation to the drill point may be deduced by considering the drill point as fixed and the wheel face as rotating about the axis  $XX$ , the virtual motion of the wheel face being equal and opposite to the actual motion of the drill. A plane rotating about a fixed axis envelops a cone, so that the

grinding-wheel face envelops part of a conical surface in its motion relative to the drill point, and the flank surface produced on the drill point is part of the surface of this cone. The vertex of the cone is the point  $O$  and the cone semiangle is the angle  $\theta$  between the axis  $XX$  and the wheel face. The cone may be termed the grinding cone and this method of drill-point grinding is therefore usually referred to as conical grinding. In the first part of this Appendix a mathematical analysis is given which relates the grinding cone and the position and inclination of the drill within the grinding cone to certain features of drill-point shape.

In many drill-grinding machines the grinding motion is more complex than that shown in Fig. 28. Nevertheless, in most cases the motion is equivalent to a conical motion at any instant of time, and the flank surface which is produced may be regarded as a blending of portions of the surfaces belonging to a large number of different grinding cones. The motion of the plane face of a grinding wheel relative to the drill point is reducible at any instant to a motion of the conical type together with a sliding motion along the line of contact between the drill point and wheel face. If this sliding motion is omitted, flank grinding consists of a series of purely conical motions, the axis of rotation gradually changing its position and the cone its form as grinding proceeds. This reduction to equivalent conical motions enables the results of the analysis in the first part of this Appendix to be applied to a wide class of drill-grinding machines; even where grinding takes place against the wheel periphery the results are frequently applicable since in many cases the curvature of the wheel has little influence on the form of the flank surface produced.

In the second part of this Appendix relationships are derived between various angles of special significance due to their effect on drill life and other criteria of drill performance. Expressions also are deduced which determine the flute shape required to give straight cutting edges when a drill is ground to a specified point angle.

### DRILL-POINT SHAPE AND THE GRINDING CONE

Formulas will now be derived which relate the point shape ground on the drill to the grinding cone used and the position and inclination of the drill within the grinding cone. Throughout the analysis it will be assumed that the cutting edges are straight, and that the lip-spacing angle is  $180^\circ$ . The cutting edge lies along a generator of the grinding cone.

Fig. 29 shows end and side views of a drill ground with straight cutting edges. The web thickness of the drill is  $2t$  and the radius from the drill axis to the outer corner is  $R$ . Right-handed co-ordinate axes are set up as follows:

- The  $z$ -axis along the axis of the drill, with sense as shown in Fig. 29; i.e., toward the drill shank.
- The  $y$ -axis along the common perpendicular which intersects the extensions of the two cutting edges, with sense as shown in Fig. 29.
- The  $x$ -axis perpendicular to the  $y$  and  $z$ -axes, with sense as shown in Fig. 29.

By the definition of the co-ordinate system, the extension of the lower cutting edge shown in the end view, Fig. 29, passes through the point  $(0, -t, 0)$ , which is independent of the point shape for a given web thickness  $2t$ . The tangent plane to the drill flank at the cutting edge contains this (fixed) point, so that this plane is completely specified relative to the co-ordinate axes providing that the direction of its normal is known. Two parameters are required to determine the direction of the normal; they may be chosen as follows:

- $\kappa$  (half the point angle)—the angle between a cutting edge and the  $z$ -axis.

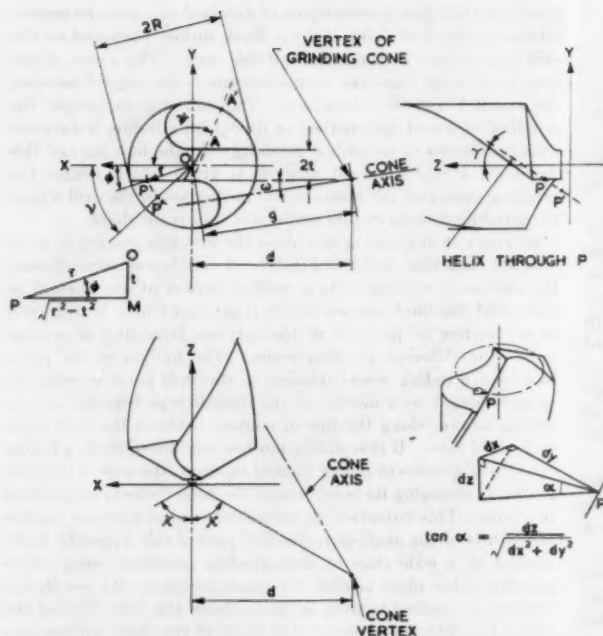


FIG. 29 VIEWS OF DRILL POINT SHOWING CO-ORDINATE AXES AND VARIOUS QUANTITIES REQUIRED IN GEOMETRICAL ANALYSIS

(b)  $\psi$ —the angle between the  $x$ -axis and the line of intersection  $AA'$  of the tangent plane with the  $x$ - $y$ -plane (sense as in Fig. 29). When the effect of the curvature of the flank surface in the vicinity of the chisel edge may be neglected,  $\psi$  will coincide with the chisel-edge angle.

In order to specify completely the grinding cone in relation to the drill point (having determined a tangent plane to the cone by means of the parameters  $\kappa$ ,  $\psi$ ) two further quantities are required; the following may be chosen:

- (c)  $\theta$ —the semiangle of the grinding cone.
- (d)  $-d$ —the  $x$ -co-ordinate of the vertex of the grinding cone.

The direction cosines ( $l$ ,  $m$ ,  $n$ ) of the grinding-cone axis will now be expressed in terms of the parameters  $\kappa$ ,  $\psi$ , and  $\theta$ .

By the choice of co-ordinate axes the co-ordinates of the vertex of the grinding cone are

$$(-d, -t, -d \cot \kappa) \dots \dots \dots [1]$$

The direction cosines of the cutting edge are

$$(\sin \kappa, 0, \cos \kappa) \dots \dots \dots [2]$$

The direction cosines of the line of intersection of the tangent plane at the cutting edge with the  $x$ - $y$ -plane are

$$(\cos \psi, \sin \psi, 0) \dots \dots \dots [3]$$

The direction ratios of the normal to the tangent plane at the cutting edge are, from [2] and [3]

$$(-\sin \psi \cos \kappa : \cos \psi \cos \kappa : \sin \psi \sin \kappa) \dots \dots \dots [4]$$

Since the cutting edge, the normal to the tangent plane at the cutting edge, and the cone axis all lie in the same plane, the direction ratios of the cone axis may be expressed by the use of [2] and [4] in the form

$$(-\sin \psi \cos \kappa + k \sin \kappa : \cos \psi \cos \kappa : \sin \psi \sin \kappa + k \cos \kappa) \dots \dots [5]$$

where  $k$  is a constant which is at yet undetermined.

The condition that the cone axis makes an angle  $\theta$  with the cutting edge is from [5] and [2]

$$\frac{k}{(\sin^2 \psi + \cos^2 \psi \cos^2 \kappa + k^2)^{1/2}} = \cos \theta$$

whence

$$\frac{k}{(\sin^2 \psi + \cos^2 \psi \cos^2 \kappa)^{1/2}} = \cot \theta \dots \dots [6]$$

and

$$(\sin^2 \psi + \cos^2 \psi \cos^2 \kappa + k^2)^{1/2} = (\sin^2 \psi + \cos^2 \psi \cos^2 \kappa)^{1/2} \operatorname{cosec} \theta \dots \dots [7]$$

From [5], [6], and [7] the direction cosines  $l$ ,  $m$ , and  $n$  of the cone axis are given by

$$\left. \begin{aligned} l &= \frac{-\sin \psi \cos \kappa \sin \theta}{(\sin^2 \psi + \cos^2 \psi \cos^2 \kappa)^{1/2} + \sin \kappa \cos \theta} \\ m &= \frac{\cos \psi \cos \kappa \sin \theta}{(\sin^2 \psi + \cos^2 \psi \cos^2 \kappa)^{1/2}} \\ n &= \frac{\sin \psi \sin \kappa \sin \theta}{(\sin^2 \psi + \cos^2 \psi \cos^2 \kappa)^{1/2} + \cos \kappa \cos \theta} \end{aligned} \right\} \dots [8]$$

Formulas [8] determine the direction of the axis of the grinding cone in terms of  $\psi$ ,  $\kappa$ , and  $\theta$ ; [1] determines the position of the cone vertex in terms of  $d$  and  $\kappa$  (for a specified web thickness  $2t$ ); and the cone semiangle equals  $\theta$ ; hence the grinding cone is completely determined in relation to the drill point by the four parameters  $\psi$ ,  $\kappa$ ,  $\theta$ , and  $d$  (for a specified web thickness  $2t$ ).

The parameters  $\psi$  and  $\kappa$  govern features of drill-point shape which have been found by experiment to have an important effect on drill life. As  $\psi$  is not readily measurable, it is more convenient to specify an alternative parameter  $\alpha_0$ , the nominal relief angle at the outer corner of the drill. In the second part of this Appendix a relationship will be deduced determining  $\psi$  in terms of  $\kappa$ ,  $\alpha_0$ , and  $\tau$ , where  $\tau$  is the ratio of the web thickness to the drill diameter. Thus for drills of a given web thickness the flank shape ground by the conical grinding process is completely determined by the four parameters  $\kappa$ ,  $\alpha_0$ ,  $\theta$ , and  $d$ .

The values of  $\kappa$  and  $\alpha_0$  for the drill are usually fixed by practical considerations of drill life and the forces set up during drilling; after these two important parameters have been specified,  $\theta$  and  $d$  may still be varied. The parameter  $\theta$  controls the variation in curvature of the drill flank, moving from one end of the cutting edge to the other. For a fixed value of  $\theta$ , a variation in  $d$  alters the curvature at the chisel edge and hence, as will be shown later, the chisel-edge angle is also varied.

Considering possible approximations in cases where the grinding motion is not purely conical, it is clear that the general form of the drill flanks ground on machines whose motions are reducible to an instantaneous conical motion depends on four parameters of the type just discussed for pure conical grinding.  $\kappa$  and  $\alpha_0$  have the same meaning irrespective of the detailed motion of the machine; depending on the machine, however, the parameter  $\theta$  may be replaced by an average cone semi-angle, and the parameter  $d$  by some measure of the average curvature at the chisel edge. It should be mentioned that on most drill-grinding machines the range of possible variations in point shape is not very large, and

frequently the design of the machine prevents the four parameters from being varied independently.

The Formulas [1] and [8] suffice to determine the alignment of the drill relative to the grinding cone, but it is nevertheless convenient to introduce a new set of parameters which enables the alignment of the drill relative to the grinding cone to be more readily visualized; formulas will now be derived which determine the alignment of cone and drill in terms of the new set of parameters. The parameters are the following:

- $\theta$  = semiangle of grinding cone
- $\chi$  = angle between drill axis and cone axis
- $f$  = distance between cone axis and drill axis
- $g$  = projected distance between cone vertex and drill axis on to a plane parallel to cone axis and drill axis

These parameters are shown in Fig. 28.

Now

$$\cos \chi = \frac{\sin \psi \sin \kappa \sin \theta}{(\sin^2 \psi + \cos^2 \psi \cos^2 \kappa)^{1/2}} + \cos \kappa \cos \theta \dots [9]$$

For  $\chi$  is the angle which the cone axis makes with the drill axis, the  $z$ -axis of the system of co-ordinates shown in Fig. 29; thus  $n$  in the Formulas [8] represents the same quantity as  $\cos \chi$ .

Continuing to refer to the co-ordinate system shown in Fig. 29,  $f$  is the perpendicular distance between the  $z$ -axis and a line passing through the cone vertex ( $-d, -t, -d \cot \kappa$ ) and having direction cosines ( $l, m, n$ ) where  $l, m, n$  are given by [8].

Hence

$$f = \frac{lt - md}{(l^2 + m^2)^{1/2}} \dots [10]$$

The direction ratios of a line parallel to a plane which is parallel to both the drill axis and the cone axis is of the form

$$(kl:km:1+kn)$$

where  $k$  is a constant as yet undetermined. If this line is perpendicular to the  $z$ -axis,  $k = -1/n$ , so that its direction ratios are

$$\left(-\frac{l}{n} : -\frac{m}{n} : 0\right) \dots [11]$$

By [1] the co-ordinates of the cone vertex are

$$(-d, -t, -d \cot \kappa)$$

Hence by projection of the line joining the origin of co-ordinates to the cone vertex on the direction given by [11]

$$g = \frac{ld + mt}{(l^2 + m^2)^{1/2}} \dots [12]$$

Eliminating  $d$  between Equations [10] and [12]

$$lf + mg = (l^2 + m^2)^{1/2} \dots [13]$$

Thus Equation [9] determines the angle between the cone axis and the drill axis when the cone angle and the point and relief angles of the drill are fixed, and Equation [13] gives the relationship which  $f$  and  $g$  must satisfy for the cutting edge to lie on the appropriate generator of the grinding cone. As  $g$  increases, the curvature of the relief surface at the chisel edge will decrease and hence the chisel-edge angle will also decrease, although it will of course always remain greater than  $\psi$ .

Since to be straight the cutting edge must lie along a generator of the grinding cone, it will generally be inclined to a plane parallel to the cone and drill axes (see Fig. 28). To complete the dis-

cussion of the alignment of the drill relative to the grinding cone an angle  $\omega$  will be determined which specifies this inclination:  $\omega$  is the angle between the projection of the cutting edge on the  $x$ - $y$ -plane and a plane parallel to both cone and drill axes (see Figs. 28 and 29).

Now the direction cosines of a line perpendicular to the cone axis and the drill axis are

$$\left(\frac{-m}{(l^2 + m^2)^{1/2}}, \frac{l}{(l^2 + m^2)^{1/2}}, 0\right) \dots [14]$$

The angle  $\omega$  is equal to the angle between [14] and the  $y$ -axis. Thus

$$\cos \omega = \frac{l}{(l^2 + m^2)^{1/2}}$$

whence

$$\tan \omega = -\frac{m}{l} \dots [15]$$

#### THE GEOMETRY OF THE DRILL POINT

*Relationship Between  $\psi$  and the Nominal Relief Angle.* In terms of the quantities  $r$  and  $\phi$  which are shown in Fig. 29, the  $x$  and  $y$ -co-ordinates of an arbitrary point  $P$  on the cutting edge of the drill are

$$x = r \cos \phi$$

$$y = -r \sin \phi$$

The direction ratios of the normal to the tangent plane at the cutting edge have been found previously; they are

$$(-\sin \psi \cos \kappa : \cos \psi \cos \kappa : \sin \psi \sin \kappa) \dots [4]$$

Hence

$$-\sin \psi \cos \kappa dx + \cos \psi \cos \kappa dy + \sin \psi \sin \kappa dz = 0. [16]$$

Where  $(dx, dy, dz)$  is a displacement in the tangent plane at the cutting edge.

In the measurement of nominal relief angle  $r$  is kept constant, corresponding to a displacement of the form

$$\left. \begin{aligned} dx &= -r \sin \phi d\phi \\ dy &= -r \cos \phi d\phi \end{aligned} \right\} \dots [17]$$

Now

$$\tan \alpha = \frac{dz}{(dx^2 + dy^2)^{1/2}} \text{ (see Fig. 29)}$$

where  $\alpha$  is the nominal relief angle at the point  $(r, \phi)$  on the cutting edge,  $(dx, dy, dz)$  is a displacement in the tangent plane at the cutting edge, and  $dx$  and  $dy$  are of the form of Equations [17].

Hence from Equations [16] and [17]

$$\tan \alpha = \frac{-r \cos \phi \cos \psi \cos \kappa + r \sin \phi \sin \psi \cos \kappa}{r \sin \psi \sin \kappa}$$

i.e.

$$\tan \alpha = (\sin \phi - \cos \phi \cot \psi) \cot \kappa \dots [18]$$

Denoting  $r/R$  by  $\rho$  and  $t/R$  by  $\tau$

$$\sin \phi = \frac{t}{r} = \frac{\tau}{\rho} \dots [19]$$

and

$$\cos \phi = \frac{(\rho^2 - \tau^2)^{1/2}}{\rho} \dots [20]$$

so that

$$\tan \alpha = \frac{\cot \kappa}{\rho} [\tau - (\rho^2 - \tau^2)^{1/2} \cot \psi] \dots [21]$$

And, by transposition

$$\cot \psi = -\frac{1}{(\rho^2 - \tau^2)^{1/2}} [\rho \tan \kappa \tan \alpha - \tau] \dots [22]$$

Equations [21] and [22] enable either one of  $\alpha, \psi$  to be determined if the other quantity is given.

At the outer corner of the drill  $\rho = 1$ ; substituting this value in Equation [22]

$$\cot \psi = -\frac{1}{(1 - \tau^2)^{1/2}} [\tan \kappa \tan \alpha_0 - \tau] \dots [23]$$

where  $\alpha_0$  is the nominal relief angle at the outer corner of the drill.

*Variation of Nominal Relief Angle Along Cutting Edge.* Substituting for  $\cot \psi$  from Equation [23] into [21]

$$\tan \alpha = \frac{\tau}{\rho} \left[ 1 - \left( \frac{\rho^2 - \tau^2}{1 - \tau^2} \right)^{1/2} \right] \cot \kappa + \frac{1}{\rho} \left( \frac{\rho^2 - \tau^2}{1 - \tau^2} \right)^{1/2} \tan \alpha_0 \dots [24]$$

From Equation [24] the relief angle at any point  $P$  along the cutting edge may be determined given  $\alpha_0, \kappa$ , and  $\tau$ .

*Relationship of Nominal Relief Angle to Angle Between Machined and Flank Surfaces.* In considering the cutting action at the drill lip it may be useful to consider measures of relief other than the nominal relief angle. A particularly simple one from a theoretical viewpoint, although it is not readily measurable in practice, is the angle between the machined and the flank surfaces measured in a plane perpendicular to the cutting edge. A relationship between this angle  $\alpha_n$  and the nominal relief angle  $\alpha$  will now be derived. The feed rate will be assumed to be sufficiently small for its influence on the machined surface to be neglected.

The direction ratios of the normal to the tangent plane of the flank surface at the cutting edge are

$$(-\sin \psi \cos \kappa; \cos \psi \cos \kappa; \sin \psi \sin \kappa) \dots [4]$$

The tangent plane to the machined surface at a given point  $P$  of the cutting edge is determined by any two distinct tangents through the given point; the cutting edge will be taken together with the tangent to the circular path described by the point when cutting. The direction cosines of the cutting edge are

$$(\sin \kappa, 0, \cos \kappa) \dots [2]$$

and, by inspection of Fig. 29, the direction cosines of the tangent to the circular path at  $P$  are

$$(\sin \phi, \cos \phi, 0)$$

Or, from Equations [19] and [20]

$$\left( \frac{\tau}{\rho}, \frac{(\rho^2 - \tau^2)^{1/2}}{\rho}, 0 \right) \dots [25]$$

From Equations [2] and [25], the direction ratios of the normal to the machined surface are

$$\left( -\frac{(\rho^2 - \tau^2)^{1/2}}{\rho} \cos \kappa; \frac{\tau}{\rho} \cos \kappa; \frac{(\rho^2 - \tau^2)^{1/2}}{\rho} \sin \kappa \right) \dots [26]$$

From Equations [4] and [26], the angle between the machined and flank surfaces is given by

$$\cos \alpha_n = \frac{(\rho^2 - \tau^2)^{1/2} \sin \psi + \tau \cos^2 \kappa \cos \psi}{[(\sin^2 \psi + \cos^2 \kappa \cos^2 \psi)(\rho^2 - \tau^2 \sin^2 \kappa)]^{1/2}}$$

whence

$$\tan \alpha_n = \frac{\tau \cos \kappa - (\rho^2 - \tau^2)^{1/2} \cos \kappa \cot \psi}{(\rho^2 - \tau^2)^{1/2} + \tau \cos^2 \kappa \cot \psi} \dots [27]$$

From Equations [22] and [23],  $\alpha_n$  may be expressed directly in terms of  $\alpha$  or  $\alpha_0$  by the formulas

$$\tan \alpha_n = \frac{\rho(\rho^2 - \tau^2)^{1/2} \sin \kappa \tan \alpha}{\rho^2 - \tau^2 \sin^2 \kappa - \rho \tau \sin \kappa \cos \kappa \tan \alpha} \dots [28]$$

$$\tan \alpha_n = \frac{\tau \{ (1 - \tau^2)^{1/2} - (\rho^2 - \tau^2)^{1/2} \} \cos \kappa + (\rho^2 - \tau^2)^{1/2} \sin \kappa \tan \alpha_0}{\{ (1 - \tau^2)^{1/2} (\rho^2 - \tau^2)^{1/2} + \tau^2 \cos^2 \kappa - \tau \sin \kappa \cos \kappa \tan \alpha_0 \}} \dots [29]$$

*Relationship Between Rake  $\gamma_n$ , as Defined in Appendix 3, and Drill Helix Angle.* In terms of the quantities  $r$  and  $\phi$  which are shown in Fig. 29, the  $x$  and  $y$ -co-ordinates of an arbitrary point  $P$  on the cutting edge of the drill are

$$x = r \cos \phi \\ y = -r \sin \phi$$

Let  $\gamma$  be the helix angle of the flute helix which passes through  $P$ ; then the equations of this helix may be written in the following parametric form

$$\left. \begin{aligned} x &= r \cos \nu \\ y &= -r \sin \nu \\ z &= -r(\nu - \phi) \cot \gamma + (r^2 - \nu^2)^{1/2} \cot \kappa \end{aligned} \right\} \dots [30]$$

where  $\nu$  corresponds to a general point  $P'$  along the helix through  $P$  ( $\nu = \phi$  at the point  $P$  on the helix).

By differentiation of Equations [30] with respect to  $\nu$ , the direction ratios of the tangent to the helix at  $P$  are

$$(\sin \phi; \cos \phi; \cot \gamma) \dots [31]$$

The direction cosines of the cutting edge are

$$(\sin \kappa, 0, \cos \kappa) \dots [2]$$

Hence, since the directions [31] and [2] are both parallel to the rake face at  $P$ , the direction ratios of the normal to the rake face at  $P$  are given by

$$(\cos \phi \cos \kappa; \cot \gamma \sin \kappa; -\sin \phi \cos \kappa) \dots [32]$$

From the definition of rake given in Appendix 3,  $\gamma_n$  is the angle between Equation [32] and the  $y$ -axis (which is normal to both the cutting edge and the drill axis).

Hence

$$\cos \gamma_n = \frac{\cot \gamma \sin \kappa - \sin \phi \cos \kappa}{[\cos^2 \phi \cos^2 \kappa + (\cot \gamma \sin \kappa - \sin \phi \cos \kappa)^2 + \cos^2 \phi \sin^2 \kappa]^{1/2}}$$

whence

$$\cot \gamma_n = \sec \phi \cot \gamma \sin \kappa - \tan \phi \cos \kappa$$

Using Equations [19] and [20],  $\phi$  can be expressed in terms of  $\rho$  and  $\tau$ , where

$$\rho = \frac{r}{R} \text{ and } \tau = \frac{f}{R}$$

Hence

$$\cot \gamma_n = \frac{1}{(\rho^2 - \tau^2)^{1/2}} (\rho \cot \gamma \sin \kappa - \gamma \cos \kappa) \dots [33]$$

$\gamma$  is easily determined when  $\gamma_0$ , the drill helix angle, and  $\rho = r/R$  are given.  $\gamma_0$  is the angle of the helix passing through  $P$  when  $P$  coincides with the outer corner of the drill; the pitch of the helix is equal to

$$2\pi R \cot \gamma_0$$

But the pitch of the helix is equal to the pitch of the drill flutes and is therefore equal to the pitch of the helix passing through a general point  $P$  on the cutting edge; thus

$$2\pi R \cot \gamma_0 = 2\pi r \cot \gamma$$

whence

$$\tan \gamma = \rho \tan \gamma_0 \dots [34]$$

**Relationship Between Normal Rake  $\gamma_n$  and Drill Helix Angle.** Corresponding to  $\alpha_n$ , the relief angle between the drill flank and the machined surface of the work, an analogous rake angle  $\gamma_n$  also may be defined at a given point on the cutting edge.  $\gamma_n$  is the angle between the drill face and the plane which contains the cutting edge and which is perpendicular to the machined surface at the given point on the cutting edge; this angle is often referred to as "normal" rake.

An expression for  $\gamma_n$  in terms of the quantities  $\rho$  and  $\tau$  and the helix angle may be derived immediately from the Expression [28] for the analogous angle  $\alpha_n$ , for the nominal relief angle  $\alpha$  in Equation [28] is by definition the complementary angle of a helix which is tangential to the flank at the cutting edge. Thus by writing  $\cot \gamma_n$  for  $\tan \alpha_n$  and  $\cot \gamma$  for  $\tan \alpha$ , in Equation [28] the following equation is obtained for  $\gamma_n$

$$\tan \gamma_n = \frac{(\rho^2 - \tau^2 \sin^2 \kappa)}{\rho(\rho^2 - \tau^2)^{1/2} \sin \kappa} \tan \gamma - \frac{\tau}{(\rho^2 - \tau^2)^{1/2}} \cos \kappa \dots [35]$$

From Equation [34],  $\gamma_n$  may be expressed in terms of the helix angle  $\gamma_0$  as follows

$$\tan \gamma_n = \frac{(\rho^2 - \tau^2 \sin^2 \kappa)}{(\rho^2 - \tau^2)^{1/2} \sin \kappa} \tan \gamma_0 - \frac{\tau}{(\rho^2 - \tau^2)^{1/2}} \cos \kappa \dots [36]$$

**Shape of Flute Cross Section Required to Produce a Straight Cutting Edge.** Taking a section of the flutes (produced if necessary) in the  $x$ - $y$  plane gives the flute section shown in Fig. 30. One half of each flute section is commonly determined so that

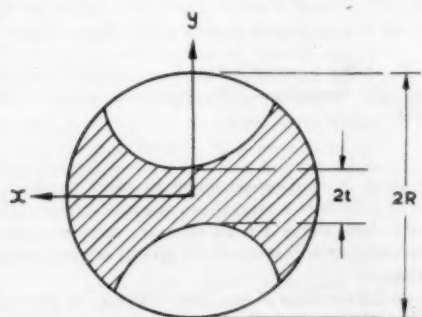


FIG. 30 DIAGRAMMATIC SECTION THROUGH DRILL SHOWING FLUTE CONTOUR

a straight edge is ground on the drill for a specified point angle; the form of the other half is not critical and is chosen to give extra strength while still leaving sufficient space for chip disposal. The form of that half of the flute associated with a straight cutting edge will now be determined.

Referring to Fig. 29

$$r = t \operatorname{cosec} \phi \dots [37]$$

Hence, making this substitution in Equations [30], and utilizing [34]

$$\left. \begin{aligned} x &= t \operatorname{cosec} \phi \cos \nu \\ y &= -t \operatorname{cosec} \phi \sin \nu \\ z &= -R \cot \gamma_0 (\nu - \phi) + t \cot \phi \cot \kappa \end{aligned} \right\} \dots [38]$$

Equations [38] are a set of parametric equations for the relevant half of the flute surface, which is traced out by varying  $\nu$  and  $\phi$  in a suitable manner. The intersection of Equations [38] with the  $x$ - $y$  plane is obtained by putting  $z = 0$ . Then

$$0 = -R \cot \gamma_0 (\nu - \phi) + t \cot \phi \cot \kappa$$

i.e.

$$\nu = \phi + \frac{t}{R} \tan \gamma_0 \cot \phi \cot \kappa$$

or

$$\nu = \phi + \tau \tan \gamma_0 \cot \phi \cot \kappa \dots [39]$$

where  $\tau$  again denotes the ratio of the web thickness to the drill diameter.

Also Equation [37] may be rewritten in the form

$$\rho = \tau \operatorname{cosec} \phi \dots [40]$$

where  $\rho = r/R$ .

Equations [39] and [40] are a pair of parametric equations which determine the form of the flute cross section; each value of the parameter  $\phi$  determines the values of  $\rho$  and  $\nu$ , which are, in effect, the polar co-ordinates of a point on the flute cross section.

**Chisel-Edge Angle.** The line  $OQ$  of Fig. 31(a) represents half of the drill chisel edge as seen when looking down on to the drill point; in Fig. 31(b) this portion of the chisel edge has been enlarged and a circular arc  $OS$  has been drawn to touch  $OQ$  at  $O$ . This circular arc corresponds to part of the circle of curvature at  $O$  of the section of the grinding cone by the plane at right angles to the drill axis which touches the drill at its tip (the grinding cone considered corresponds to the left-hand drill flank shown in Fig. 31a). Assuming that the curve of section of the cone may be adequately approximated by the circle of curvature (of radius  $a$ ), the angle  $E-S-T = \psi$ , where  $S-T$  is the tangent to the circle at the point  $S$  (see Fig. 31b).

By projecting  $SC$  and  $CO$  on to a line at right angles to  $SE$ , the following relationship is obtained

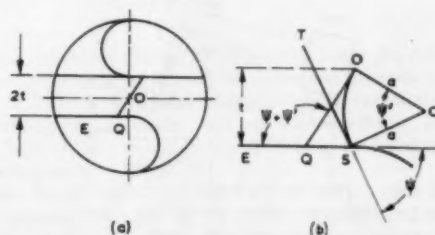


FIG. 31 GEOMETRICAL RELATIONSHIPS AT CHISEL EDGE

$$a \cos \psi - a \cos (\psi + \psi') = t$$

whence

$$\cos (\psi + \psi') = \cos \psi - \frac{t}{a}$$

i.e.

$$\cos \lambda = \cos \psi - \frac{t}{a} \dots \dots \dots [41]$$

where  $\lambda = (\psi + \psi')$  equals the chisel-edge angle.

From Equations [41] and [23] the chisel-edge angle may be determined for drills of a specified web thickness, provided that the point angle and the nominal relief angle at the outer corner of the drill are given, together with the curvature of the grinding cone at the drill tip.

## Appendix 5

### A THEORETICAL ANALYSIS OF SELF-REGENERATIVE CHATTER

**Introduction.** In many metal-cutting operations metal is removed by a series of adjacent cuts, so that if one cut is unduly heavy the next is correspondingly reduced and the force acting on the tool fluctuates accordingly. Under certain conditions these fluctuations in the cutting force supply energy to the vibrating cutter. If the stiffness and damping of the system comprising the machine, the cutting tool, the workpiece, and so on, are insufficient to dissipate this energy at a faster rate than it is produced, a chatter vibration, triggered off by some slight chance disturbance of the steady cutting conditions and built up by the successive increments of energy which are then supplied by each new cut, may be generated. In the following mathematical analysis of this mechanism of self-regenerative chatter specific reference will be made to the drilling operation; however, the results of the analysis may be applied to other metal-cutting operations in which metal is removed by successive cuts.

**Derivation of Equation Governing Chatter Mechanism.** Vibration tests carried out on radial drilling machines have shown that the chatter vibrations which occur during the drilling operation commonly correspond to what may be termed a cantilever mode of vibration of the drilling machine, from the analogy with the motion of a cranked cantilever vibrating in its fundamental mode (see Fig. 32). A similar cantilever mode is obtained by excitation tests, but the motion in this case does not coincide exactly with the motion which takes place during drilling since the constraining effect of the workpiece material is absent. In the following analysis, the mode of vibration considered will be that corresponding to the vibrations which take place during drilling; this mode of vibration involves a system comprising the machine, cutting tool, workpiece, and so on. Only the vertical motion  $x$  of the drill is indicated in Fig. 32, although in fact there may be components of motion in directions along the ma-

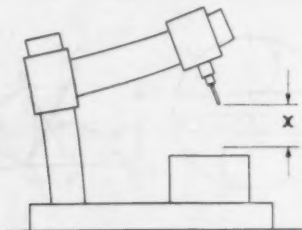


FIG. 32 CANTILEVER MODE OF VIBRATION OF RADIAL DRILLING MACHINE

chine arm and perpendicular to the plane of the arm and spindle axes. In the present analysis these additional motions will not be considered.

When the machine is vibrating in the cantilever mode its equation of motion at the time  $t$  may be written in the form

$$m\ddot{x} + c\dot{x} + kx = \text{increase in thrust force on drill point} \dots [42]$$

where  $x$  is the axial displacement of the drill from its steady cutting condition, and  $m$ ,  $k$ , and  $c$  are, respectively, an equivalent mass, spring stiffness, and damping constant characteristic of the system in the cantilever mode of vibration. It now remains to express the right-hand side of Equation [42] in an appropriate mathematical form.

The increase in the metal-removal rate at time  $t$  over the metal-removal rate under steady cutting conditions is proportional to the increase in chip thickness:  $-(x - x_l)$ , where  $x_l$  is the corresponding displacement in the previous cut,  $l$  being the time interval between consecutive cuts. In the case of drilling with the drill lips spaced 180 deg apart,  $l$  is the time corresponding to  $1/2$  revolution of the drill. Making the assumption that the increase in the thrust force acting on the drill point is proportional to this increase in the metal-removal rate, the increase in thrust force  $= -r(x - x_l)$ , where  $r$  is independent of  $x$  and  $t$  but may depend on the cutting conditions.

Thus Equations [38] may be rewritten in the form

$$m\ddot{x} + c\dot{x} + kx = -r(x - x_l) \dots \dots \dots [43]$$

Equation [43] is the equation governing the chatter mechanism under consideration.

The method of derivation which has just been given may be modified in detail to cover other types of metal-cutting operation, and an equation ultimately obtained which is formally equivalent to [43]. Thus the conclusions to be drawn from Equation [43] are applicable to a variety of metal-cutting operations.

**Solution of Equation Governing Chatter Mechanism.** The complete solution of Equation [43] presents difficulties, but certain special solutions are sufficient to indicate whether or not self-regenerative chatter vibrations will build up under given cutting conditions.

Consider the (complex) function of  $t$  given by

$$z = Ae^{st} \dots \dots \dots [44]$$

where  $A$  and  $s$  are complex constants. It follows that

$$z_l = Ae^{s(t-l)}$$

The function [44] satisfies

$$m\ddot{z} + c\dot{z} + kz = -r(z - z_l) \dots \dots \dots [45]$$

providing that

$$ms^2 + cs + k = -r(1 - e^{-sl}) \dots \dots \dots [46]$$

$as$  is readily shown by substituting Equation [44] into [45] and cancelling  $Ae^{st}$  throughout. Equation [46] may be rewritten in the form

$$ms^2 + cs + K - re^{-sl} = 0 \dots \dots \dots [47]$$

where  $K = k + r$ . Corresponding to every complex root of Equation [47] there is a special solution of Equation [45] given by Equation [44], where  $A$  is an arbitrary complex number; by taking the real part of this solution a special solution of Equation [43] is obtained.

These special solutions of Equation [43] may be given a physical interpretation in the following way: Suppose that during the interval of time from  $t = -l$  to  $t = 0$  the cutting tool is constrained to vibrate in a manner corresponding to the real part of

$Ae^{st}$ , where  $s$  satisfies Equation [47]. From the previous discussion,  $Ae^{st}$  will satisfy Equation [45] for  $t \geq 0$ , and so the motion will continue to be determined by the real part of  $Ae^{st}$  when  $t \geq 0$ . Thus the special solutions given by Equation [44] are the motions arising subsequent to the constrained motion just described, which may conveniently be termed a triggering vibration. A triggering vibration may be of arbitrarily small amplitude, since the constant  $A$  may be small in absolute magnitude; consequently, such a triggering vibration may be produced by a very slight disturbance of the steady cutting conditions. Triggering vibrations of a more general character may be considered by resolution into component motions of the form  $Ae^{st}$ , where values of  $s$  are taken which correspond to the roots of Equation [47]. As before, the form of the motion remains unaltered when  $t \geq 0$ .

The motion subsequent to a triggering vibration will decrease in amplitude provided that the real part of  $s$  in  $z = Ae^{st}$  is negative for all the component motions; but if any real part is positive, the amplitude of the motion will increase indefinitely. This leads to the following condition for the dynamical stability of the system: The system is stable only if all the roots of Equation [47] have negative real parts. If this condition is not satisfied, the system will be dynamically unstable and chatter vibrations will be liable to occur.

**Zones of Instability.** The stability of the system, as determined by the roots of Equation [47], depends on the ratios

$$m:c:K:r$$

and on the value of  $l$ ; that is, on four independent parameters. In the subsequent analysis it will be found convenient to utilize the four alternative parameters:  $\Omega_a$ ,  $\delta$ ,  $\rho$ , and  $n$ , defined as follows

$$\Omega_a = \sqrt{\left(\frac{K}{m}\right)}; \quad \delta = \frac{\pi c}{\sqrt{(mK)}}; \quad \rho = \frac{r}{K}; \quad n = \frac{l}{2\pi} \sqrt{\left(\frac{K}{m}\right)}$$

$\Omega_a$  is the augmented undamped circular natural frequency of the system;  $\delta$  is the logarithmic decrement expressed in terms of the augmented spring stiffness  $K$  of the system ( $K = k + r$ );  $\rho$  measures the rate of increase of the reaction force on the cutting tool (with increasing chip thickness) as a fraction of the augmented spring stiffness of the system;  $n$  is the number of vibrations at the augmented undamped natural frequency which will take place in time  $l$ .

The dimensionless quantities  $\delta$ ,  $\rho$ , and  $n$  may be considered as measuring, respectively, the damping of the system, the rate of increase of the reaction force due to the work material, and the time interval between consecutive cuts. A knowledge of these three quantities is sufficient to determine whether or not the system is unstable. The result which is finally obtained is that the system is unstable for a given value of  $\rho$  when the point  $(n, \delta/\rho)$  lies within certain regions of the  $(n, \delta/\rho)$ -plane. These regions are termed the zones of instability for this particular value of  $\rho$ ; Fig. 20 shows some of the instability zones for  $\rho = 0$ ,  $\rho = 0.1$ , and  $\rho = 0.2$  (as calculated from Formulas [55] and [56]).

To determine the instability zones, first substitute  $s = u + iv$  in Equation [47]. The following equations are obtained for  $u$  and  $v$ , the real and imaginary parts of  $s$

$$mu^2 - mv^2 + cu + K - re^{-u} \cos vl = 0 \dots [48]$$

$$2muv + cv + re^{-u} \sin vl = 0 \dots [49]$$

Equations [48] and [49] may be rewritten in dimensionless terms after introducing the quantities  $\delta$ ,  $\rho$ ,  $n$ , and the additional dimensionless quantities  $\beta$  and  $V$  which are defined by

$$\beta = 2\pi u \sqrt{\left(\frac{m}{K}\right)}; \quad V = v \sqrt{\left(\frac{m}{K}\right)}$$

$\beta$  measures the logarithmic increment of the chatter; the amplitude of the chatter vibration is multiplied by  $e^\beta$  after a time corresponding to one cycle of an oscillation at the augmented undamped natural frequency.  $V$  is the ratio of the chatter frequency to the augmented undamped natural frequency. After substitution of these five quantities in Equations [48] and [49] and after simplification, the following equations are obtained

$$\beta^2 + 2\delta\beta + 4\pi^2 - 4\pi^2 V^2 - 4\pi^2 \rho e^{-\beta n} \cos 2\pi n V = 0 \dots [50]$$

$$\beta V + \delta V + \pi \rho e^{-\beta n} \sin 2\pi n V = 0 \dots [51]$$

The boundaries of the instability zones are now obtained from Equations [50] and [51] by making the substitution  $\beta = 0$ , which is the condition that the system lie on the borderline between dynamical stability and dynamical instability; Equations [50] and [51] then reduce to

$$1 - V^2 - \rho \cos \theta = 0 \dots [52]$$

$$\delta V + \pi \rho \sin \theta = 0 \dots [53]$$

where  $\theta$  has been written for  $2\pi n V$ . By definition of  $\theta$

$$n = \frac{\theta}{2\pi V}$$

From Equation [52]

$$V = \sqrt{(1 - \rho \cos \theta)} \dots [54]$$

the positive square root being taken since  $V$  is a positive quantity. Hence

$$n = \frac{\theta}{2\pi \sqrt{(1 - \rho \cos \theta)}} \dots [55]$$

By substitution of Equation [54] in [53]

$$\frac{\delta}{\rho} = - \frac{\pi \sin \theta}{\sqrt{(1 - \rho \cos \theta)}} \dots [56]$$

As the parameter  $\theta$  varies, the point  $(n, \delta/\rho)$  given by Equations [55] and [56] traces out the boundaries of the instability zones. For each position of the point on the boundary, Equation [54] gives the ratio of the chatter frequency to the augmented undamped natural frequency.

The form of Equation [56] shows that for a positively damped system with  $\rho > 0$ , the curve defined by Equations [55] and [56] has physical significance only when

$$(2p - 1)\pi < \theta < 2p\pi \dots [57]$$

where  $p$  is a positive integer, for only when Equation [57] is satisfied is  $\delta/\rho > 0$ . By substituting  $\theta = (2p - 1)\pi$ ,  $\theta = 2p\pi$  in Equation [55], Condition [57] may be expressed in terms of  $n$

$$\frac{p - 1/2}{\sqrt{(1 + \rho)}} < n < \frac{p}{\sqrt{(1 - \rho)}} \dots [58]$$

Thus the boundary curves lie within the limits given by [58]. It may be verified by formal mathematical analysis that the points  $(n, \delta/\rho)$  which lie below the boundary curves are the points of instability for the system; this will become evident, however, in the light of the physical interpretations to be developed later in this Appendix.

**Chatter Bands.** If  $n$  is increased while  $\delta$  and  $\rho$  remain substantially constant, the point  $(n, \delta/\rho)$  moves first into and then out of the successive instability zones (it is assumed that  $\delta/\rho$  is not too large). This may readily be seen by reference to Fig. 20,

or directly by consideration of Equations [55] and [56]. Thus the system is unstable for certain ranges of  $n$  determined by the instability zones and the magnitude of  $\delta/\rho$ ; these ranges may be termed the chatter bands for the given  $\delta$  and  $\rho$ .

In the case of the drilling operation,  $n$  can be increased by increasing the time interval  $l$ ; i.e., by drilling at a lower spindle speed. Hence, according to the present theory, drilling chatter should be observed within definite bands of speeds and should be absent outside these bands (assuming that  $\delta$ ,  $\rho$ , and  $\Omega_0$  remain fairly constant as the spindle speed is reduced). Some experimental evidence in support of the existence of chatter bands has been given in the body of the paper. From experimental data obtained for the principal chatter band it was possible to determine the basic parameters occurring in the theoretical analysis.

*Experimental Determination of Basic Parameters of System.* The method is based on the relationship connecting the chatter frequency under borderline-stability conditions with the parameter  $\theta$ . From Equation [54]

$$V^2 = 1 - \rho \cos \theta$$

whence

$$\left(\frac{v}{2\pi}\right)^2 = \left(\frac{\Omega_0}{2\pi}\right)^2 (1 - \rho \cos \theta) \dots \dots \dots [59]$$

The form of Equation [59] indicates that a linear relationship exists between the square of the chatter frequency and  $\cos \theta$ . The intercept of this line on  $\cos \theta = 0$  equals the square of the augmented undamped natural frequency, and the slope of the line divided by this intercept equals  $-\rho$ .

In the course of the drilling tests described in the body of the paper, the chatter frequencies were noted which corresponded to a range of evenly spaced spindle speeds covering the whole of the principal chatter band. These observations enabled the linear relationship between

$$\left(\frac{v}{2\pi}\right)^2$$

and  $\cos \theta$  to be determined empirically; hence, from the intercept and slope of the line, experimental values for the parameters  $\Omega_0$  and  $\rho$  could be found. The observed chatter frequencies gave immediately the values of

$$\left(\frac{v}{2\pi}\right)^2$$

required in this procedure, and the corresponding values of  $\cos \theta$  were obtained from the chatter frequency and the spindle speed by making use of the formula

$$\frac{\theta}{2\pi} = \frac{\text{chatter frequency}}{2 \times \text{spindle speed}} \dots \dots \dots [60]$$

The formula is easily deduced from the definition of  $\theta$ :  $\theta = 2\pi nV$ , so that

$$\frac{\theta}{2\pi} = \frac{lv}{2\pi}$$

$l$  equals the time for  $1/2$  revolution of the drill

$$l = \frac{1}{2 \times \text{spindle speed}}$$

hence

$$\frac{\theta}{2\pi} = \frac{\text{chatter frequency}}{2 \times \text{spindle speed}}$$

The borderline-stability conditions required for the application of this method were found to hold at all the spindle speeds for which tests were carried out, due to the increase in the damping of the system for increasing amplitudes of vibration. In this connection, it should be noted that Formula [54], on which the method is based, does not contain the damping  $\delta$ .

Having found the parameters  $\Omega_0$  and  $\rho$  as just described, the value of  $\delta/\rho$  for the principal chatter band was determined by taking the greatest and least values of  $\cos \theta$  which were observed and substituting these, with the corresponding values of  $\sin \theta$ , in Equation [56]. In this way two values of  $\delta/\rho$  were obtained which were averaged to give the final result. Multiplication by the value of  $\rho$  already found then gave the value of  $\delta$  for the principal chatter band.

The quantity  $n$  is related to the spindle speed by the formula

$$n = \frac{\Omega_0}{2\pi} / 2 \times \text{spindle speed} \dots \dots \dots [61]$$

which follows from the definition of  $n$  and the fact that

$$l = \frac{1}{2 \times \text{spindle speed}}$$

Thus, for any spindle speed which lies inside the principal chatter band, all four parameters  $n$ ,  $\Omega_0$ ,  $\rho$ , and  $\delta$  could be determined. If it is assumed that the parameters  $\rho$  and  $\delta$  are unaltered as  $n$  is varied, the values of  $n$  marking the ends of the remaining chatter bands may be found by solving Equation [56] for  $\theta$  and then substituting in Equation [55]. The corresponding bands of spindle speeds may be obtained from Equation [61] by making the additional assumption that  $\Omega_0$  is also constant for all the chatter bands; it was in this way that the calculated bands of spindle speeds shown in Fig. 26 were obtained.

The experimental results in Fig. 21 for the principal chatter band were in good agreement with the present theory of self-regenerative chatter; the values of  $\theta$  given by Equation [60] were evenly distributed about the value  $\theta = (3\pi/2)$  and they satisfied Condition [57],  $\pi < \theta < 2\pi$  in this case. Agreement was less good for the other chatter bands, possibly indicating that the parameters  $\Omega_0$ ,  $\rho$ , and  $\delta$  may vary from chatter band to chatter band.

*Characteristic Features of Instability Zones.* Certain general characteristics of the instability zones may be deduced readily from Equations [54], [55], [56], and [58]. First, as is apparent on reference to Fig. 20, the successive zones of instability defined by Condition [58] eventually overlap (for  $\rho > 0$ ;  $\rho = 0$  is merely a limiting case). To show this, suppose that the  $q$ th instability zone overlaps its successor, then from Equation [58] the interval

$$\frac{q-1/2}{\sqrt{1+\rho}} < n < \frac{q}{\sqrt{1-\rho}}$$

overlaps the interval

$$\frac{q+1/2}{\sqrt{1+\rho}} < n < \frac{q+1}{\sqrt{1-\rho}}$$

whence

$$\frac{q+1/2}{\sqrt{1+\rho}} < \frac{q}{\sqrt{1-\rho}}$$

from which is obtained

$$q > \frac{1}{2 \left[ \sqrt{\left( \frac{1+\rho}{1-\rho} \right)} - 1 \right]} \dots \dots \dots [62]$$

Equation [62] is the required condition for overlapping.

The ratio of the chatter frequency under borderline-stability conditions to the augmented undamped natural frequency depends only on the corresponding values of  $\delta$  and  $\rho$ . This may be seen by substituting the value  $(1 - V^2)/\rho$ , obtained for  $\cos \theta$  from Equation [54], into

$$\frac{\delta^2}{\rho^2} = \frac{\pi^2(1 - \cos^2 \theta)}{1 - \rho \cos \theta}$$

obtained from Equation [56]. The following expression, quadratic in  $V^2$ , is obtained after simplification

$$V^4 - 2 \left(1 - \frac{\delta^2}{2\pi^2}\right) V^2 + (1 - \rho^2) = 0 \dots \dots [63]$$

Hence

$$V^2 = \left(1 - \frac{\delta^2}{2\pi^2}\right) \pm \sqrt{\left[\left(1 - \frac{\delta^2}{2\pi^2}\right)^2 - (1 - \rho^2)\right]} \dots [64]$$

Equation [64] gives two values for  $V$ , the ratio of the chatter frequency under borderline-stability conditions to the augmented undamped natural frequency. Referring to Fig. 20, Equation [64] determines  $V$  at the points of intersection of the borderline-stability curves with a line drawn parallel to the axis of  $n$  so as to correspond to the given value of  $\delta/\rho$ . When the quantity under the root sign in Equation [64] is positive, the line intersects the boundary of each zone of instability in two distinct points; from Equation [54] it may be seen that the value of  $V$  at the left-hand point corresponds to taking the positive sign in Equation [64], the negative sign giving the value at the right-hand point.

When the quantity under the root sign in Equation [64] is negative, no real roots of Equation [63] exist, and a line drawn parallel to the axis of  $n$  for a corresponding value of  $\delta/\rho$  lies wholly within the region of stability. Thus the system is stable irrespective of  $n$ , and chatter bands corresponding to particular ranges of the time interval  $l$  do not occur; under these circumstances the system may be said to be unrestrictedly stable. The condition for unrestricted stability is then

$$\left(1 - \frac{\delta^2}{2\pi^2}\right)^2 - (1 - \rho^2) < 0$$

i.e.

$$\frac{\delta^2}{\rho^2} > \frac{2\pi^2}{\rho^2} [1 - \sqrt{(1 - \rho^2)}] \dots \dots \dots [65]$$

When  $\rho$  is fairly small Expression [65] may be approximated adequately by the relationship

$$\frac{\delta}{\rho} > \pi \dots \dots \dots [66]$$

Expression [66] is less than 1 per cent in error when  $\rho$  does not exceed 0.2. By transforming Inequality [66] the physical significance of the condition for unrestricted stability may be made immediately apparent. For

$$\begin{aligned} \frac{\delta}{\rho} &= \frac{\pi c}{\sqrt{mK}} \bigg/ \frac{r}{K} \\ &= \pi \frac{c}{r} \sqrt{\left(\frac{K}{m}\right)} \\ &= \pi \frac{c}{r} \Omega_n \end{aligned}$$

Substitution in Inequality [66] gives the following equivalent relationship

$$\frac{c}{r} \Omega_n > 1 \dots \dots \dots [67]$$

From [67] it can be seen that the augmented undamped natural frequency of the system  $(\Omega_n)/(2\pi)$ , the effective damping  $c$ , and the cutting force parameter  $r$  may be regarded as equally important in determining the stability of the system. A given percentage increase in the dimensionless quantity  $(c/r)\Omega_n$  on the left-hand side of Inequality [67] may be secured by the same percentage change in any one of  $\Omega_n$ ,  $c$ , or  $r$ , provided that the percentage involved is not too large. Economic and other considerations obviously will have to be taken into account before deciding whether a high stability is best secured by a high natural frequency, or by a high effective damping, or by an appropriate adjustment in the cutting conditions, or by a suitable combination of all three.

**Physical Significance of Parameter  $\theta$ .** The formal analysis which has just been given may be supplemented to advantage by a more intuitive explanation. Consider the physical significance of the parameter  $\theta$ . As has been pointed out immediately following Equation [60],  $\theta/(2\pi) = lv/(2\pi)$ , that is,  $\theta/(2\pi)$  equals the number of chatter cycles occurring in the time interval  $l$  under borderline-stability conditions. Since the characteristic features of the zones of instability may be deduced from Equations [54], [55], [56], and [57], all of which are expressed in terms of  $\theta$ , it may be inferred that an explanation of these characteristics is obtainable in terms of the physical equivalent of  $\theta$ : the number of chatter cycles occurring in the time interval  $l$ .

The existence of bands of chatter is easily explicable in these terms. Consider first the left-hand ends of the chatter bands which correspond to given values of  $\delta$  and  $\rho$ ; these end points are determined by the intersections with the borderline-stability curves of a line drawn parallel to the axis of  $n$  so as to correspond to the given value of  $\delta/\rho$ . From Equation [56], the following quadratic equation in  $\cos \theta$  is obtained

$$\cos^2 \theta - \frac{\delta^2}{\pi^2 \rho} \cos \theta - \left(1 - \frac{\delta^2}{\pi^2 \rho^2}\right) = 0$$

The smaller root of this equation determines the values of  $\theta$  which correspond to the left-hand points of intersection. For the  $p$ th chatter band the point is given by

$$\theta = -\alpha + 2p\pi$$

where  $0 < \alpha < \pi$  from Equation [57]. The number of cycles of chatter which occur in the time interval  $l$  is given by

$$\frac{\theta}{2\pi} = \frac{-\alpha}{2\pi} + p$$

where  $p$  is a positive integer. Hence each successive chatter band corresponds to an increase in the time interval  $l$  such that one further cycle of chatter can be accommodated in this interval; the chatter frequency remains constant, as is shown by Equation [54], assuming that the augmented undamped natural frequency remains constant. For each chatter band the same fraction of a cycle,  $\alpha/(2\pi)$ , remains uncompleted, constituting a constant phase lag between consecutive cuts. From a diagram (Fig. 19) it may be seen that the effect of such a phase lag on the variation of the metal-removal rate is to supply energy to the system (see the account given in the body of the text). The rate of supply of energy and the rate of its absorption are the same for all the chatter bands irrespective of the change in the number of completed chatter cycles in the interval  $l$ . The dy-

namical instability of the system for a point lying in the interior of a chatter band is due to the phase lag  $\alpha$  being such that energy is supplied faster than it can be dissipated by the damping of the system.

*Phase Relationships in Self-Regenerative Chatter.* The effects of the phase lag between consecutive cuts may be studied in greater detail by making use of the expressions

$$z = a \sin vt \dots \dots \dots [68]$$

$$x_1 = a \sin (vt + \alpha) \dots \dots \dots [69]$$

Equation [68] represents a chatter vibration of frequency  $v/(2\pi)$  and Equation [69] represents the corresponding drill displacement occurring during the preceding cut. It is assumed that the chatter takes place under borderline-stability conditions so that the amplitude  $a$  remains constant; as is clear from the form of Equations [68] and [69], the phase lag between consecutive cuts equals  $\alpha$  radians.

From Equations [68] and [69], the increase in the metal-removal rate is proportional to

$$a \sin (vt + \alpha) - a \sin vt$$

which equals

$$a (\cos \alpha - 1) \sin vt + a \sin \alpha \sin \left( vt + \frac{\pi}{2} \right)$$

Assuming that the thrust-force increment acting on the drill point is proportional to the increase in the metal-removal rate, it is seen from this last expression that the thrust-force increment can be divided into two components: (i) a force in phase with the displacement [68], of amplitude proportional to  $a (\cos \alpha - 1)$ ; (ii) a force  $\pi/2$  ahead of the displacement [68], of amplitude proportional to  $a \sin \alpha$ . The force (i) does no net work over a complete chatter cycle; the force (ii) does work on the system provided that  $\sin \alpha$  is positive; i.e., provided that  $0 < \alpha < \pi$ .

The expression

$$a \sin (vt + \alpha) - a \sin vt$$

which is proportional to the increase in the thrust force, also may be written in the equivalent form

$$2a \sin \frac{\alpha}{2} \sin \left[ vt + \left( \frac{\pi}{2} + \frac{\alpha}{2} \right) \right]$$

From this last expression it is apparent that the increment of the thrust force is ahead of the displacement [68] by a phase angle of

$$\left( \frac{\pi}{2} + \frac{\alpha}{2} \right) \text{ radians}$$

*Chatter at Drill Break-Through.* Examination of the experimental results in Fig. 17(b) for the chatter at drill break-through indicates that the phase relationship which was observed between the thrust and the drill displacement is compatible with a phasing of

$$\left( \frac{\pi}{2} + \frac{\alpha}{2} \right)$$

From the experimental results, the chatter frequency was equal to 12.3 cps at a spindle speed of 400 rpm so that in each half revolution of the drill there were

$$\frac{12.3 \times 60}{400 \times 2} \text{ cycles of chatter} \\ = 0.922 \text{ cycle of chatter}$$

Hence the phase lag between consecutive cuts was

$$360 \times (1 - 0.922) \text{ deg} = 28 \text{ deg}$$

From this, the thrust force should have been ahead in phase by

$$\left( 90 + \frac{28}{2} \right) = 104 \text{ deg}$$

according to the principles just developed; the experimental results showed that in fact the thrust force was ahead by a phase angle which varied from 90 to 120 deg.

It appears, then, that the self-regenerative chatter mechanism which has formed the subject of this Appendix may play a significant part in the production of chatter at drill break-through. The reduction in the constraining effect of the material at break-through will facilitate the mechanism; also, the release of the strain energy stored in the system during cutting may be expected to produce an oscillatory motion of the drill point which will serve as an effective triggering vibration.

## Appendix 6

### ANALYSIS OF EFFECT OF RELATIVE LIP HEIGHT ON HOLE SIZE

It is shown in the body of the paper that hole accuracy is markedly dependent on the symmetry of the drill point. A common error in symmetry is shown in Fig. 22(a), where the lips are inclined at equal angles  $\kappa$  to the drill axis but one lip is in advance of the other by the distance  $H$ . As a result of the relative lip height  $H$ , the chisel edge is displaced from the drill axis by an amount  $t = \frac{1}{2} H \tan \kappa$ . The behavior of the drill at the beginning of the drilling operation and at a depth where the drill point is fully engaged in the hole will now be considered.

Assuming that there are no serious errors in the machine, the drill rotates about its general axis  $XX$  until the chisel edge makes contact with the surface of the work. The records of drill-point deflection in Fig. 23(c) show that after some initial skidding of the chisel edge, the drill will tend to rotate about a new axis passing through the center of the chisel edge; i.e., passing through the point at distance  $t$  from the original axis  $XX$ . It will now be supposed that the drill continues its passage into the work and that the axis of rotation is finally established at a distance  $e$ , not necessarily equal to  $t$ , from the original axis; this is the situation depicted in Fig. 22(a). During a half revolution of the drill at a feed of  $f$  per revolution the outer corners move from  $A$  to  $A'$  and  $B$  to  $B'$ , respectively, as the drill rotates about the axis  $YY$ . The chip section along the cutting edges is shown shaded in the diagram. Along the shorter lip (to the left of  $YY$ ) the chip thickness measured in the direction of feed is  $\frac{1}{2}f + H - 2e \cot \kappa$ , and along the greater part of the longer lip (to the right of  $YY$ ) it is  $\frac{1}{2}f - H + 2e \cot \kappa$ . At the outer corner of the longer lip, however, the chip thickness becomes equal to the feed  $f$ , since only this lip is engaged in the cut near the periphery of the hole. At the chisel edge, which is shown drawn for a web thickness-to-diameter ratio of  $\frac{1}{8}$  and a chisel-edge angle of 135 deg, the chip thickness is mainly equal to  $\frac{1}{2}f$ .

Because of the inclination  $\kappa$  of the lips to the drill axis, each lip will have a radial-force component which is directed towards the drill axis and is roughly proportional in magnitude to the cross-sectional area of the chip. For equilibrium the two radial forces must be equal; to a good approximation this condition will be satisfied when the chip sections along each lip are equal in area. Strictly, the force required to deflect the drill also should be included with the radial-force components, but simple tests show that the standard-length drill is a comparatively flexible structure. For example, a radial load of only about 10 lb is required at the end of a standard-length  $\frac{5}{8}$ -in-diam drill to deflect the

drill by 0.010 in. On the other hand, the very large difference in chip section at the two lips caused by small displacements of the axis of rotation of the drill suggests that the unbalanced radial forces originating from the cutting action will be large by comparison with the resistance to bending of the drill. To determine  $\epsilon$ , therefore, the chip area  $B'CDE$  in Fig. 22(a) may be equated to the area  $A'FGBJK$ ; the area  $EDGF$  at the chisel edge is omitted from the equation on the assumption that there is no significant unbalanced radial-force component at the chisel edge. Thus after simplifying and collecting terms for the chip area, we obtain

$$\frac{5}{6} HD - \frac{5}{3} De \cot \kappa - \frac{H^2}{2} \tan \kappa - \frac{Hf}{2} \tan \kappa - \epsilon f + 2\epsilon^2 \cot \kappa = 0$$

Provided  $\kappa$  does not approach 90 deg, all terms except the first two are of the second order of magnitude and can be neglected. Hence, solving for  $\epsilon$

$$\epsilon = \frac{H}{2} \tan \kappa \dots \dots \dots [70]$$

i.e.

$$\epsilon = t$$

Thus for all practical purposes  $\epsilon$  is equal to the displacement of the chisel edge from the drill axis due to the relative lip height  $H$ . It would appear, therefore, that the axis of rotation initiated during the early stages of the drilling operation remains practically unchanged by the necessary conditions for equilibrium when the point of the drill is fully engaged in the hole.

From Fig. 22(a) the amount the hole is oversize due to the relative lip height  $H$  is equal to  $2\epsilon$ . Substituting for  $\epsilon$  from the foregoing equation

$$\text{Hole oversize} = H \tan \kappa \dots \dots \dots [71]$$

The lines calculated from this equation were found to be in good agreement with the typical test results presented in Fig. 22(b).

## Appendix 7

### APPROXIMATE ANALYSIS OF PATH OF DRILL POINT DURING DRILLING

This analysis concerns the effect of deflections of the drill at the commencement of drilling on the alignment and slope of the drilled hole with respect to the spindle axis. In Fig. 24(a) a drill which has received an initial deflection  $q_0$  is shown after penetrating  $p$  inches into the work. Because of the initial deflection, the axis of the drill point will be inclined to the spindle axis, and as the drill penetrates into the work the deflection  $q$  and slope  $\phi$  at the drill point will become progressively larger, so that the drill point will tend to follow a path deviating further and further from the spindle axis. In the analysis, equations are deduced for the path of the drill point through the work, and hence for the deviation  $q$  at any depth  $p$  for a given initial deflection  $q_0$ .

In the approximate analysis the following assumptions are made:

- 1 The drill deflects in the same manner as an equivalent column or beam of uniform section.
- 2 The clearance between the drill and hole is sufficient to permit the drill to bend without constraint.
- 3 The drill is fixed at the shank end.
- 4 Only the drill point participates in the cutting action.

The truth of the first assumption has been investigated by more exact calculations and simple deflection tests, the results of which are given later in this Appendix. The second assumption is probably satisfied in the majority of cases since the hole is nearly always larger than the diameter of the drill, and the curvature of the deflected drill axis is in the same sense as the curvature of the hole axis. In deep holes, however, it would be necessary to consider possible interference between the deflected drill and the curved hole; this factor has not been included in the present analysis. The third assumption that the drill is fixed at the shank end will be substantially true for well-fitting taper shanks or chucks. The fourth assumption implies that the lands do not make a significant contribution to the cutting action of the drill.

*Relationship Between Drill Deflection and Slope of Drill Point.* For the purposes of an approximate analysis the drill may be regarded at any instant during the drilling operation as a column of length  $l$ , fixed at the upper end and hinged at the lower end, with a deflection  $q$  imposed at the lower end, as shown in Fig. 24(b). Because of the deflection  $q$  and thrust load  $p$  there will be a transverse reaction  $R$  at the drill point. Thus the differential equation for the deflected shape of the drill is

$$EI \frac{d^2y}{dx^2} = -P(y + q) + R(l - x) \dots \dots \dots [72]$$

where

$E$  = modulus of elasticity of drill material

$I$  = second moment of area of equivalent uniform column

Putting  $P/(EI) = k^2$ , and rearranging terms

$$\frac{d^2y}{dx^2} + k^2y = k^2 \left[ -q + \frac{R}{P} (l - x) \right]$$

The solution of this differential equation is

$$y = A \cos kx + B \sin kx - q + \frac{R}{P} (l - x) \dots \dots [73]$$

The constants  $A$  and  $B$  are determined from the end conditions  $y = 0$  at  $x = 0$ ,  $y = -q$  at  $x = l$ . Hence

$$A = q - \frac{Rl}{P}$$

$$B = -\left(q - \frac{Rl}{P}\right) \cot kl$$

Substituting for  $A$  and  $B$  in Equation [73]

$$y = \left(q - \frac{Rl}{P}\right) \cos kx - \left(q - \frac{Rl}{P}\right) \cot kl \sin kx - q + \frac{R}{P} (l - x) \dots \dots [74]$$

The slope equation of the deflection curve is obtained by differentiating Equation [74]. Carrying out the differentiation

$$\frac{dy}{dx} = -k \left(q - \frac{Rl}{P}\right) \sin kx - k \left(q - \frac{Rl}{P}\right) \cot kl \cos kx - \frac{R}{P} \dots \dots [75]$$

To determine  $R$  in terms of known quantities, use is made of the condition  $dy/dx = 0$  when  $x = 0$ . Hence

$$R = \frac{P q k \cot kl}{kl \cot kl - 1}$$

Substituting for  $R$  in Equation [75] the following expression for  $dy/dx$  is obtained

$$\frac{dy}{dz} = kq \left( \frac{kl \cot kl}{kl \cot kl - 1} - 1 \right) (\sin kz + \cot kl \cos kz) - \frac{kq \cot kl}{kl \cot kl - 1} \dots [76]$$

In the discussion of the path followed by the drill point the slope at the drill point, denoted by  $\phi$  in Fig. 24(a), is required. Putting  $z = l$  in Equation [76] and simplifying, the following equation is obtained for  $\phi$

$$\phi = kq \left( \frac{1 - \cos kl}{kl \cos kl - \sin kl} \right) \dots [77]$$

where

$$k = \sqrt{\left( \frac{P}{EI} \right)}$$

In Equation [77]  $\phi$  becomes infinitely large as the denominator of the expression in brackets approaches zero; this corresponds to the application of the buckling load  $P_c$ . Thus putting  $kl \cos kl - \sin kl = 0$  the following transcendental equation is obtained in  $k$

$$kl = \tan kl \dots [78]$$

The smallest root satisfying Equation [78] is

$$kl = 4.493$$

Hence, substituting

$$\sqrt{\left( \frac{P_c}{EI} \right)}$$

for  $k$ , the following formula is found for  $P_c$

$$P_c = \frac{20.16 EI}{l^2} \dots [79]$$

If, as is usually the case, the drilling thrust is well below the buckling load for the drill, the expression for  $\phi$  may be replaced by an approximate simpler expression. Temporarily writing  $z = kl$  in Equation [77] and expanding the sine and cosine terms

$$\phi = \frac{q}{l} \left[ -\frac{3}{2} \left( 1 - \frac{1}{12} z^2 + \frac{1}{360} z^4 \dots \right) \left( 1 - \frac{1}{10} z^2 + \frac{1}{280} z^4 \dots \right)^{-1} \right]$$

Simplifying this expression

$$\phi = -\frac{q}{l} \left( \frac{3}{2} + \frac{1}{40} z^2 + \frac{11}{8400} z^4 \dots \right) \dots [80]$$

By using Equation [79] the quantity  $z$  can be expressed in terms of the ratio  $P/P_c$ . Thus

$$z = kl = 4.493 \sqrt{(P/P_c)}$$

For a ratio of  $P/P_c$  of  $1/4$  the value of  $z$  is roughly 2, and on inserting  $z = 2$  in Equation [80] it is found that the terms involving  $z$  are small compared with the constant term of the series. Therefore, for values of  $P$  well below the critical value Equation [80] reduces to

$$\phi = \frac{3q}{2l} \dots [81]$$

or

$$\frac{\phi l}{q} = 1.5 \dots [82]$$

The negative sign can be omitted since  $q$  has been taken negative for deflections to the right in Fig. 24(b). It will be seen that Equation [82] is simply the relationship between the maximum deflection and slope of a uniform cantilever subjected to a transverse end load. Thus for values of  $P$  which are small compared with the buckling load the deflection is substantially the same as if there were no thrust load acting on the drill.

The Relationship [81] between slope, deflection, and length only strictly applies to a uniform-section cantilever, whereas the body of a drill varies from a helical fluted section to a plain circular section near the taper shank. However, simple deflection tests show that Relationship [81] may be used without great error provided the length  $l$  is taken as the fluted length of the drill. The results of deflection tests in which a radial load was applied at the point end of  $1/8$ -in. and  $1/4$ -in.-diam drills rigidly supported in a taper socket at the shank end are shown in Table 7. The direction of radial loading was turned through 20 deg between measurements to determine the deflection characteristics of the drills in different longitudinal planes. It will be seen that in spite of the presence of the helical flutes the deflection and slope of the drills varied very little as the radial direction of loading was altered. The average value of  $\phi l/q$  (based on the fluted

TABLE 7 RESULTS OF DEFLECTION TESTS ON  $1/8$ -IN. AND  $1/4$ -IN.-DIAM DRILLS

Angle turned through by drill relative to Radial Direction of Load Degrees	5/8 in. dia. drill. Body length = 5.11/16 in. Fluted length = 5 in. Radial load at end of drill = 6 lb.			1/4 in. dia. drill. Body length = 3.17/32 in. Fluted length = 2.7/8 in. Radial load at end of drill = 0.66 lb.		
	Deflection $q$ at end of drill. in.	Slope $\phi$ at end of drill. rad.	$\frac{\phi}{q}$	Deflection $q$ at end of drill in.	Slope $\phi$ at end of drill rad.	$\frac{\phi}{q}$
0	0.0073	0.00203	1.39	0.0036	0.00199	1.59
20	0.0069	0.00195	1.41	0.0038	0.00204	1.55
40	0.0068	0.00189	1.39	0.0036	0.00201	1.61
60	0.0065	0.00185	1.43	0.0033	0.00189	1.65
80	0.0064	0.00183	1.43	0.0034	0.00188	1.59
100	0.0066	0.00186	1.41	0.0032	0.00186	1.67
120	0.0070	0.00192	1.37	0.0032	0.00180	1.62
140	0.0073	0.00201	1.38	0.0032	0.00186	1.67
160	0.0074	0.00204	1.38	0.0033	0.00185	1.61
180	0.0072	0.00199	1.38	0.0035	0.00195	1.60

length of the drill) for each size of drill is seen to be within 10 per cent of the value 1.5 given by Equation [82].

**Slope of Drilled Hole.** By the initial assumption that the cutting action is confined to the lips and chisel edge of the drill, it follows that the drill point will cut in the direction inclined at the angle  $\phi$  to the spindle axis. Thus the drill point will move along a path whose tangent  $dq/dp$  at any instant is equal to  $\phi$ , the slope at the drill point. Therefore, from Equation [81] we can write

$$\frac{dq}{dp} = \frac{3q}{2l} \dots \dots \dots [83]$$

The solution of this equation is

$$q = Ae^{3p/2l} \dots \dots \dots [84]$$

where  $A$  is an arbitrary constant. At  $p = 0$ ,  $q = q_0$  (the initial deflection of the drill point) and therefore Equation [84] can be written

$$q = q_0 e^{3p/2l} \dots \dots \dots [85]$$

This is the equation of the path of the drill point through the work and therefore of the axis of the drilled hole.

A convenient measure of the slope of a hole is the slope  $s$  of the line joining the two points on the hole axis at the top and bottom of the hole. From inspection of Fig. 24(a)  $s$  is given by

$$s = \frac{q - q_0}{p} \dots \dots \dots [86]$$

Substituting for  $q$  from Equation [85], the slope equation becomes

$$s \text{ (in./in.)} = \frac{q_0}{p} (e^{3p/2l} - 1) \dots \dots \dots [87]$$

Where  $p$ ,  $q_0$ , and  $l$  are in inches.

**Effect of Machine Errors on Slope of Drilled Hole.** The slope of the axis of the drilled hole with respect to the spindle axis will be affected by misalignments of the drilling machine and clearances in the spindle bearings and slides. If the axis of the quill is not parallel to the spindle axis, the spindle nose will be displaced transversely as the spindle and quill are fed downwards. The displacement will be proportional to the vertical movement of the spindle, so that in a hole of depth  $p$  the top of the drill will have been displaced transversely by the amount  $fp$ , where  $f$  is the tangent of the angle between the quill and spindle axes. Also in addition to the movement  $fp$  there may be a further movement  $c$  due to necessary clearance in the spindle bearings or quill slide. The top of the drill will therefore be subject to a maximum transverse movement  $\delta$ , where  $\delta = fp + c$ .

If the drill deflection  $q$  falls in the same direction as the movement  $\delta$ , the effect of  $\delta$  will be to reduce the slope  $\phi$  of the drill point. Therefore, instead of  $q$ , the quantity  $q - \delta$  will appear on the right-hand side of Equation [83]. Thus

$$\frac{dq}{dp} = \frac{3(q - \delta)}{2l}$$

or

$$\frac{dq}{dp} = \frac{3(q - fp - c)}{2l} \dots \dots \dots [88]$$

Solving this modified differential equation for  $q$  and using the condition  $q = q_0$  at  $p = 0$

$$q = q_0 e^{3p/2l} - f \left[ \frac{2l}{3} (e^{3p/2l} - 1) - p \right] - c(e^{3p/2l} - 1) \dots [89]$$

Unless the drilling conditions are such that the initial drill deflection is biased in one direction,  $q$  may have any orientation with respect to the misalignment error  $fp$ . If, instead of being in the same direction,  $fp$  and  $q$  are in opposite directions, the second term on the right-hand side of Equation [89] will have a positive sign. With regard to the clearance error  $c$ , it is probable that the clearance will always be taken up in the direction of  $q$  when comparatively stiff drills are used, but this may not be true in the case of small slender drills, where the drill-deflection forces are extremely small. Thus, whether or not the third term on the right-hand side of Equation [89] should be assigned positive/negative or only negative will usually depend on the drilling setup. It would appear, therefore, that in practice  $q$  will vary between the limits given by the following equations

$$q = q_0 e^{3p/2l} \pm f \left[ \frac{2l}{3} (e^{3p/2l} - 1) - p \right] - c(e^{3p/2l} - 1) \dots \dots [90]$$

for comparatively stiff drills

$$q = q_0 e^{3p/2l} \pm \left\{ f \left[ \frac{2l}{3} (e^{3p/2l} - 1) - p \right] + c(e^{3p/2l} - 1) \right\} \dots \dots [91]$$

for slender drills.

To determine the general slope  $s$  of the holes,  $q$  from Equation [90] or [91] is again substituted in Equation [86]. Hence

$$s = \frac{q_0}{p} (e^{3p/2l} - 1) \pm \left\{ f \left[ \frac{2l}{3p} (e^{3p/2l} - 1) - 1 \right] + \frac{c}{p} (e^{3p/2l} - 1) \right\} \dots \dots [92]$$

for slender drills

$$s = \frac{q_0}{p} (e^{3p/2l} - 1) \pm f \left[ \frac{2l}{3p} (e^{3p/2l} - 1) - 1 \right] - \frac{c}{p} (e^{3p/2l} - 1) \dots \dots [93]$$

for comparatively stiff drills.

It will be noticed that these equations are simply Equation [87] with additional terms depending on the machine-misalignment error  $f$  and the clearance  $c$ .

**Calculation of Theoretical Limits of Hole Slope in Fig. 25.** Formulas [92] and [93] have been used to calculate the theoretical limit lines in Fig. 25 for the slope of holes drilled with  $1/8$ -in. and  $3/8$ -in.-diam drills. By way of example, the basis of calculation for the results of the tests with the  $1/8$ -in.-diam drill will be given. The following quantities will be used in the calculation of the limit lines:

Body length of drill	5 $\frac{1}{4}$ in.
Fluted length of drill	4 $\frac{1}{4}$ in.
Minimum second moment of area of drill section	49.6 $\times 10^{-8}$ in. <sup>4</sup>
Modulus of elasticity of drill material	30 $\times 10^6$ psi
Drilling thrust in medium carbon steel at feed rate of 0.004 in./rev.	200 lb
Depth of hole	3 in.
Misalignment of spindle and quill axes of drilling machine	0.0007 in./in.
Clearance in quill slide	$\pm 0.0005$ in.

To assess whether the critical load for the drill is high enough

compared with the drilling thrust to permit the equations based on the approximate Expression [81] to be used, a lower limit for the critical load will be calculated on the assumption that the drill will not buckle before a uniform column of the same length having a second moment of area equal to the minimum second moment of area of the drill. On inserting the appropriate values in Equation [79] the lower limit for the critical load is found to be 950 lb. As the ratio of drilling thrust to the lower limit is only 0.21, Equation [92] or [93] can be used to calculate the limit lines for the relationship between the displacement  $q_0$  at the top of the hole and the slope  $s$  of the hole. Substituting the given values of fluted length, hole depth, misalignment error, and clearance in Equation [92] for a slender drill, the following equations to the limit lines for the  $1/8$ -in.-diam drill are obtained

$$s(0.001 \text{ in./ft}) = 6.58 q_0 \pm 9.1 \quad (q_0 \text{ in units of } 0.001 \text{ in.})$$

By similar substitution of the appropriate values in Equation [93] for a more rigid drill, the equations for the  $5/8$ -in.-diam drill were found to be

$$s(0.001 \text{ in./ft}) = 5.26 q_0 + \frac{2.0}{7.5} \quad (q_0 \text{ in units of } 0.001 \text{ in.})$$

## Discussion

R. G. KENNEDY.\* It is always refreshing to have new light shed on the many factors affecting drill performance. Both drill

\* The Cleveland Twist Drill Company, Cleveland, Ohio.

users and manufacturers will benefit from the author's work in this field.

The author is to be complimented on his drill dynamometer data, recordings of which are shown in his Figs. 8 and 17. His tests show that increase of torque is a more sensitive indicator of drill failure than is an increase in thrust. In general we have found this to be true. The wide fluctuations in torque, observed when the drill is breaking through the bottom of the test billet, as depicted in Fig. 17(a), clearly reveal the stresses placed on a drill in through-hole drilling. These records emphasize the destructive vibrations commonly occurring during break-through, and furnish an explanation of the reason drill life is so much shorter when drilling through holes rather than blind holes.

We were much interested in the author's ingenious method of depicting point displacement at the onset of drilling as shown in his Fig. 23.

The relation between hole displacement and slope, as shown in Fig. 25, comprises new information of value to drill users.

The author has demonstrated remarkably well the effect of difference in lip height or "relative lip-height error" on the size of holes drilled and their alignment. The fact that a poorly pointed drill, having lips of different height, produces larger sized holes than a correctly pointed drill is revealed in Fig. 22(b). This subject has been explored in a limited manner in our own laboratory. A chart (Fig. 33) of our data is hereby offered in the hope that it will supplement the author's data of Fig. 22(b). In our work we did not explore lip-height errors larger than 0.010 in. However, we did collect data from tests in both soft steel and hard cast iron

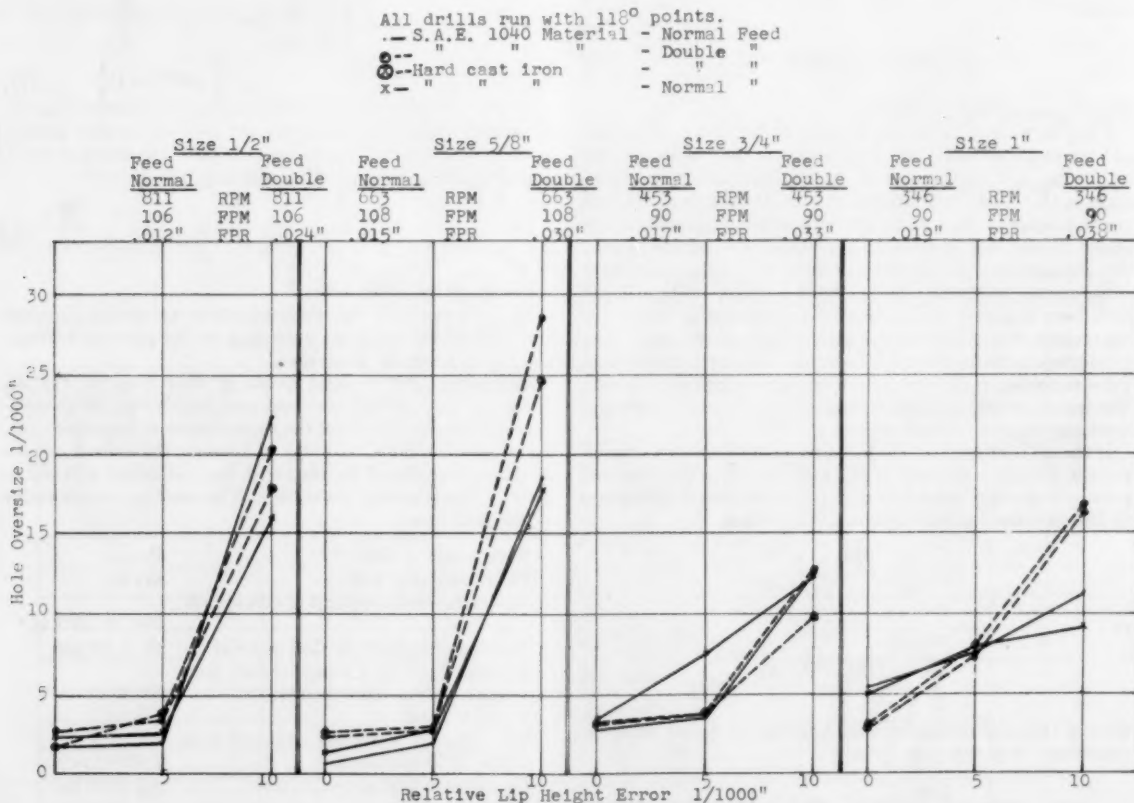


FIG. 33 EFFECT OF DIFFERENCE IN LIP HEIGHT ON HOLE OVERSIZE

run with four different sizes of drills. Our tests showed that a relative lip-height error of 0.010 in. results in a greater amount of oversize of holes when drilling with smaller sized drills than when drilling with larger sizes, at least in the drill sizes we used, which were  $1/2$  in.,  $5/8$  in.,  $3/4$  in., and 1 in.

The author is to be congratulated for the quantitative evaluation he has made of many important factors affecting drill performance. The writer also offers the hope that he will submit the results of future work in this field for publication in our country.

R. S. HAHN.<sup>7</sup> This discussion deals with the section on vibrational forces which is based upon an analysis of regenerative chatter in drilling. In this analysis the author derives the equation

$$m\ddot{x} + c\dot{x} + kx = -r(x - x_l)$$

where the argument of  $x_l$  is retarded by the time interval  $l$ . This equation is essentially identical to that derived by the writer.<sup>8</sup>

The author's method of analysis is preferable to that of the writer's since it gives information regarding the frequencies of chatter which the author uses to compute the undamped augmented natural frequency  $\Omega_a$  and the "work constant"  $r$ . However, this procedure should be used with care since the experimental measurement of frequency requires a finite amplitude; i.e., the self-excited vibration has grown and reached a limit cycle where its amplitude is usually halted because of nonlinearities which the original differential equation does not contemplate.

The author's condition for unconditional stability Equation [65] is identical to the writer's.<sup>8</sup> The regions of conditional stability shown in Fig. 20 are also in agreement.<sup>8</sup> The example computed by the writer (Fig. 7)<sup>8</sup> corresponds exactly to the situation represented in Fig. 20 for  $\rho = 0.1$ ,  $\delta/\rho = 2.5$ .

In addition to the conditions for "unconditional stability" and "conditional stability" Equation [62] of the paper gives the condition for "unconditional instability" (for zero damping).

In connection with Fig. 20 for the case where  $\rho = 0$  it is not clear what meaning the ordinate  $\delta/\rho$  has since the denominator is zero.

The abscissa of Fig. 20 may be interpreted in general as the number of cycles of vibration between consecutively adjacent cutting edges. For example, in single-point turning, it would be the number of cycles for one work revolution. With a two-fluted drill, it is the number of cycles occurring in a half revolution. For a tool with  $j$  cutting edges

$$n = \frac{f}{jN} \text{ (cycles per tooth interval)}$$

The author's analysis is well done and as he points out, applies to many types of operations, such as turning, boring, drilling, counterboring, and even dressing internal-grinding wheels.

C. J. OXFORD, JR.<sup>9</sup> The author is to be commended for this fine paper describing the Production Engineering Research Association experimental program to obtain basic data on drilling. The work covers many important factors influencing drill performance, and the paper is a valuable addition to the literature on drilling. The writer regrets that the author did not describe some of the work in greater detail, but realizes that several papers would be required to do this adequately.

As is always the case with good work of this type, more new

<sup>7</sup> Consulting Engineer, The Heald Machine Company, Worcester, Mass. Mem. ASME.

<sup>8</sup> "On the Theory of Regenerative Chatter in Precision-Grinding Operations," by R. S. Hahn, Trans. ASME, vol. 76, 1954, pp. 593-597.

<sup>9</sup> Research Engineer, National Twist Drill & Tool Company, Rochester, Mich. Mem. ASME.

questions are raised than old questions answered. The writer hopes that the PERA will continue its work on drilling to follow up the many leads uncovered in the present program.

The writer is pleased to see the author has recognized that wide variations in drill performance are normal and has used statistical techniques in evaluating the results of life tests. This procedure is especially necessary if small performance variations are sought, and here it may be necessary to use a very large number of drills in the tests. This point is often overlooked by drill users who attempt to conduct tests under production conditions.

The writer has found that drill-life test data tend to be normally distributed about the average, but that the standard deviation range is relatively wide, of the order of  $\pm 30$  to 40 per cent. By careful selection of drills and workpiece materials it is possible to reduce these ranges somewhat. This was done by Wolfe, Kinman, and Lennard<sup>10</sup> in their evaluation of cutting fluids by drilling test. Such selected drills gave reasonably satisfactory results in evaluating cutting fluids. However, this procedure is certainly not proper in the testing of drills where one wishes to take into account the normal variations encountered in production-drilling operations.

The author's use of a portal-frame drilling machine to minimize machine deflection and vibration is to be commended. Because of this, the tests more nearly reflect performance of the twist drills rather than the twist drills in combination with a particular drilling machine. It is unfortunate that the portal-frame construction is not more widely used. One manufacturer of drilling machines in this country attempted to introduce a machine of portal-frame construction, but was compelled to drop it because his customers would not accept the loss of versatility and accessibility which is inherent to this type of design.

In describing his dynamometers the author gives data as to the full-load torsional and vertical deflections, but neglects to indicate the capacities of the unit. It would be of interest to know the vertical and torsional spring constants.

The writer would like to inquire whether the author has observed any effect of the dynamometer upon drill life. Certainly, when the workpiece is mounted upon the dynamometer it is not as rigidly mounted as if it were clamped directly to the machine table. In tests of  $1/2$ -in. end mills with the workpiece mounted upon a dynamometer having a spring constant of about 250,000 lb per in. the writer has observed a reduction of life of about 40 per cent as compared to the case where the workpiece was mounted rigidly on the machine table. Of course, in drilling, the tool forces are more nearly balanced than in the case of end mills, and this effect may be less.

The author's device for measuring relief angle at any radius on the drill point by optical sectioning is very good. This apparatus simplifies this type of measurement and probably possesses greater accuracy than the usual indirect method.

The variation in design of nominally similar  $5/8$ -in. drills supplied by various British manufacturers is of interest. Actually, it appears that some of the manufacturers furnished a heavy-duty drill while others furnished a drill of substantially standard design. In this country the standard drill designs used by most manufacturers are quite similar, but most manufacturers also carry a line of heavy-duty drills. The heavy-duty drills are usually made with heavy webs to provide greater torsional stiffness when drilling tough materials. The heavy-duty designs of different manufacturers differ considerably.

The drills used by the author in his test program are somewhat unusual in that they have straight parallel webs. The straight-

<sup>10</sup> "A Preliminary Investigation of the Effectiveness of Various Chlorinated Hydrocarbon Compounds as Cutting Oil Additives," by K. J. B. Wolfe, M. D. Kinman, and G. Lennard, *Journal of the Institute of Petroleum*, vol. 40, September, 1954, pp. 253-256.

web construction has the obvious advantage of not requiring thinning during resharpener, but there may be a considerable loss of stiffness which could affect drill life in varying degrees, depending upon the drill and flute length. The writer feels that the difficulties encountered in web thinning are more than offset by the increased life obtained with drills having tapered webs. However, the accurate thinning of heavy drill webs is a real problem in some shops. The author does not touch upon the effect of drill length upon drill life. In the writer's laboratory it is always observed that shortening a  $\frac{3}{16}$ -in. taper-shank drill about  $\frac{1}{2}$  in. from its original length will increase the average drill life by 10 to 15 per cent when drilling a chrome-nickel-alloy steel having a hardness of about 220 Bhn. In the case of some of the very tough alloys the increase in life with drill shortening can be even more dramatic. The accompanying Fig. 34 shows the case of drilling S-816 cobalt-base high-temperature alloy. This particu-

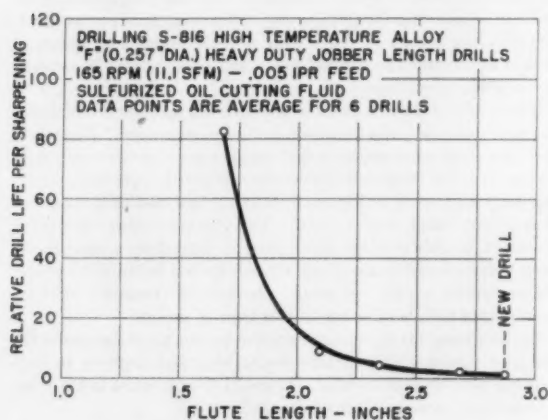


FIG. 34 INFLUENCE OF DRILL LENGTH UPON DRILL LIFE WHEN DRILLING S-816 HIGH-TEMPERATURE ALLOY

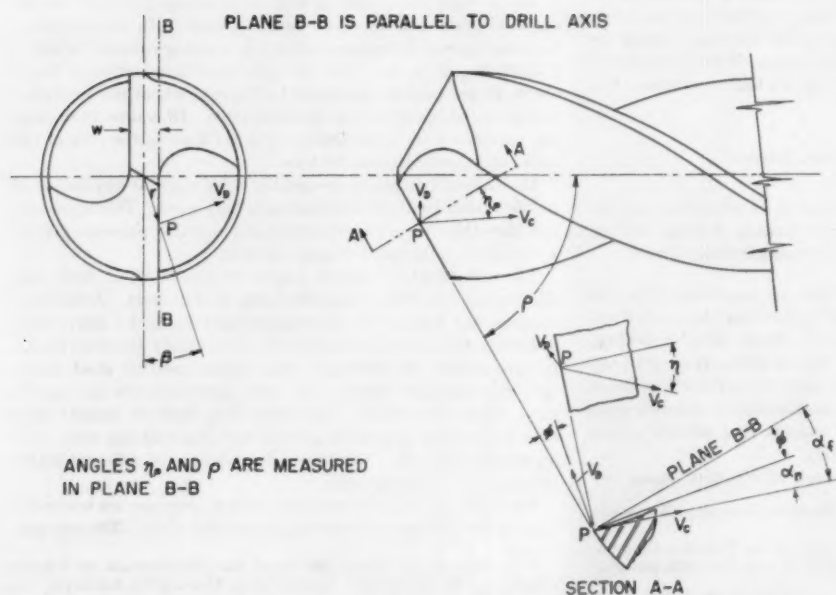


FIG. 35 ELEMENTS OF DRILL POINT SHOWING FACE RAKE ANGLE AND NORMAL RAKE ANGLE

lar alloy has extreme work-hardening tendencies. In the figure it will be noted that a new letter "F" (0.257) drill, with a  $\frac{27}{8}$ -in. flute length, has a relative life of one corresponding to the drilling of two holes through  $\frac{1}{2}$ -in. bars. As the drill was shortened during successive regrinds the life increased gradually at first, and then when the flute length was finally shortened to  $1\frac{11}{16}$  in. the drill life increased more than 80 times. With normal work materials the increase in life is not as great but it is always observed.

It is further noted that the drills were made of a tungsten high-speed steel, apparently in accordance with usual British and European practice. In this country, all or nearly all manufacturers are now making their standard drills of molybdenum high-speed steel. While the lower cost and the strategic value of the molybdenum high-speed steels in the United States is certainly a factor, the main reason for the change from tungsten to molybdenum high-speed steels has been improved drill performance.

The author's analysis of the nominal relief angle as produced by conical-point grinding is a valuable addition to the literature. He shows that misalignment of the drill point with the sharpening cone generator will modify the theoretical relief angle. It should be noted that deliberate misalignment sometimes can be used to modify drill relief angles for particular applications.

The writer must take issue with the author's definition of drill rake angle. The author uses the plane containing the cutting edge which is parallel to the drill axis as the zero rake plane. The rake angle is then measured in a plane perpendicular to the drill cutting edge. This angle is the same as the face rake angle defined by the writer in an analysis of twist-drill geometry presented several years ago.<sup>11</sup> The face rake angle is not an angle of fundamental importance in metal cutting. Its only merit is that it is an angle which is readily measured and visualized on the twist drill. The normal rake angle, which is measured with reference to the finished surface produced by the drill point is a basic angle. The author has correctly defined the normal rake angle in his Appendix 4. The normal rake angle always has a lower value than the face rake angle and on a twist drill is usually

quite negative at small radii. Another important rake angle is the effective rake angle which is a measure of the angle through which the chip is deflected in cutting. This angle is partly a function of the properties of the work material. The accompanying Fig. 35 shows the relationship between face rake angle and normal rake angle; Fig. 36 shows the variation of face rake angle, normal rake angle, and effective rake angle for various radii on a  $\frac{3}{16}$ -in. drill.

It has not yet been established completely which rake angle is of major importance in determining drill performance. Stabler<sup>12</sup> claims that metal-cut-

<sup>11</sup> "On the Drilling of Metals, I—Basic Mechanics of the Process," by C. J. Oxford, Jr., Trans. ASME, vol. 77, 1955, p. 103.

<sup>12</sup> "The Basic Nomenclature of Cutting Tools," by G. V. Stabler, Institution of Production Engineers Journal, vol. 34, May, 1955, pp. 264-279.

ting forces are principally determined by the normal rake angle, but Shaw<sup>12</sup> has shown that both the normal rake angle and the inclination angle (which influences the effective rake angle) are important in oblique cutting.

In Fig. 36 it can be seen that all of these rake angles tend to approach each other at larger radii and here they are principally functions of the drill helix angle. The values of all of these rake angles are reasonably close together for the outer half of the drill lips. This portion of the drill removes 75 per cent of the metal and hence dissipates most of the cutting energy. The problem is further complicated by the continuity of the chips across the drill lips which affects the direction of chip flow.

The writer is in full agreement with the author in his view that short-duration accelerated-life tests are of little value because the wear mechanism may change completely in accelerated tests. This factor has been overlooked often by tool users who attempt to conduct tests by accelerating the rate of metal removal by four or five times over the contemplated shop practice.

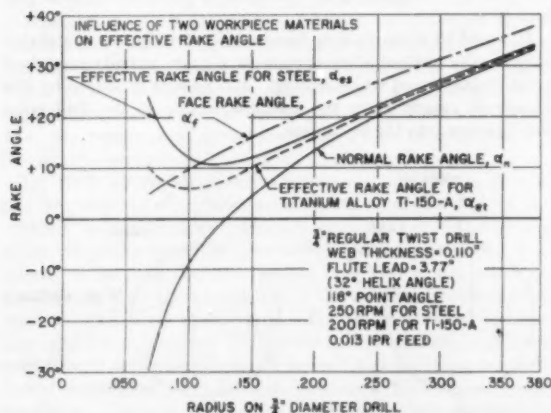


FIG. 36 COMPARISON OF FACE RAKE ANGLE, NORMAL RAKE ANGLE, AND EFFECTIVE RAKE ANGLE AT VARIOUS RADII ON A  $\frac{1}{8}$ -IN. TWIST DRILL

The author is correct in stating that many factors must be considered in determining the end of drill life. As yet no single criterion which will apply in all cases has been discovered. The writer has found that in drilling high-strength steels and other materials where considerable flank wear is encountered, the thrust force appears to be a good indicator of dulling. However, on ordinary materials, the wear pattern seems to depend considerably upon the combination of speed and feed used to give a particular penetration rate.

In the writer's laboratory it has also been found that the titanium alloys have unique drilling characteristics. In determining torque and thrust versus feed characteristics, enough drill wear may occur during a test to make the results obtained dependent upon the order in which the tests are run. With these materials it is essential that the first point be rechecked at the end of a test to be sure that no appreciable change in the drill has taken place.

The author states that none of the web-thinning methods he investigated appeared to be worth using on thin-web drills. This is probably true for routine drilling operations but the writer feels that web thinning of such drills is justified for drilling deep holes

<sup>12</sup> "Metal Cutting Principles," by M. C. Shaw and N. H. Cook, Massachusetts Institute of Technology, Cambridge, Mass., third edition, 1954.

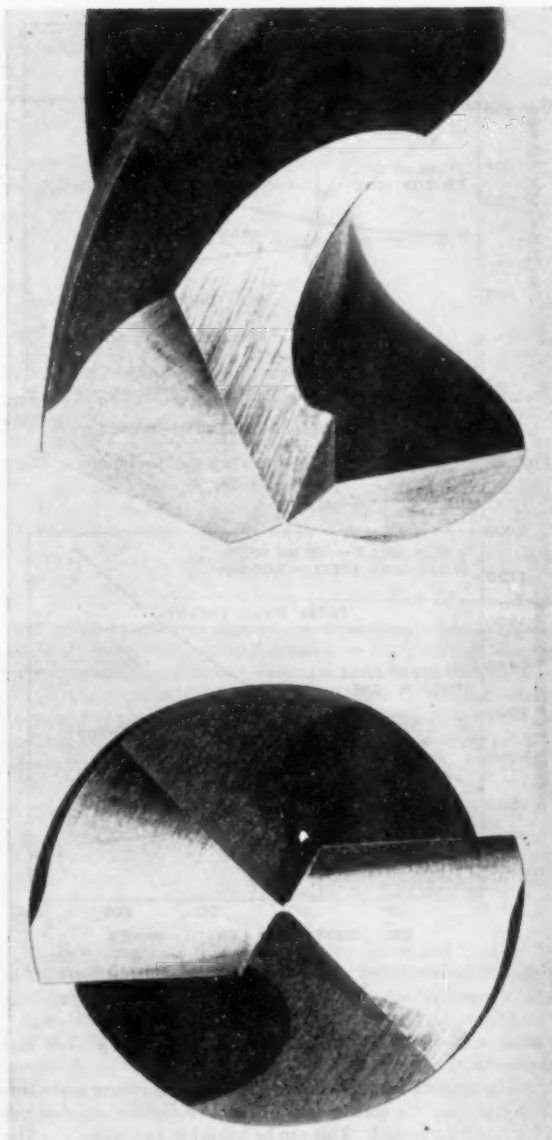


FIG. 37 SPLIT (CRANKSHAFT) DRILL POINT  
(Note new cutting edges created by splitting operation.)

in tough materials and where the drills are used in portable drilling equipment. For this purpose a style of thinning which is related to the author's method B is most effective. This is called a split (crankshaft) point and it is usually ground approximately as shown in Fig. 37. Here, the effective length of the chisel edge is reduced to nearly zero because the thinning cuts form additional cutting edges which extend to the center of the drill. With this style of thinning the torque is reduced very little but the thrust can be reduced to very nearly the theoretical minimum. Figs. 38(a) and 38(b) show how the drill torque and thrust are partitioned between the lips and the web for various lengths of drill chisel edge. These plots are based upon a recent analysis of the

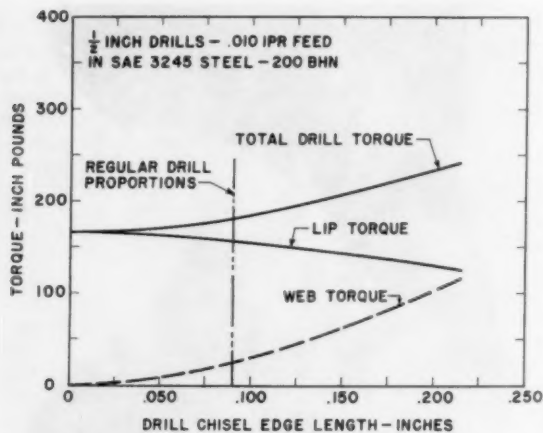


FIG. 38(a) INFLUENCE OF DRILL CHISEL-EDGE LENGTH UPON DRILL TORQUE

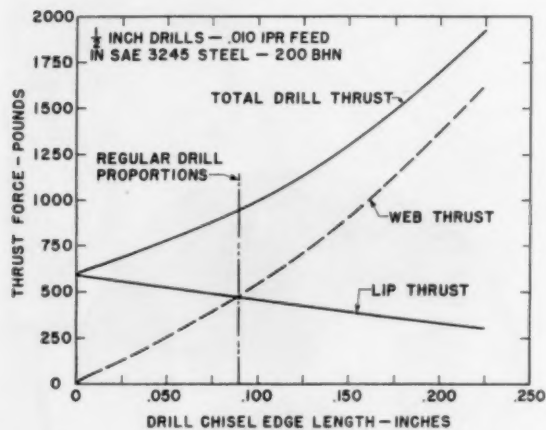


FIG. 38(b) INFLUENCE OF DRILL CHISEL-EDGE LENGTH UPON DRILL THRUST FORCE

torque and thrust in drilling presented by M. C. Shaw and the writer.<sup>14</sup>

As the author mentions, the split point sometimes gives difficulty in that the intersection of the two cutting edges is not adequately supported. This can be helped in two ways: (1) The included angle of the drill point can be increased and this is usually done when drilling tough materials. (2) The new cutting edges can be ground so that they are swung more toward the main lips of the drill and this reduces the relief angle behind the new cutting edges and gives more support to the edges. This has been found particularly effective in the drilling of high-strength steels.

The author claims that his method C reduced drill thrust by 25 to 40 per cent when drilling cast iron and steel. The writer attempted to check this, but was unable to discover a thrust reduction of more than 10 to 15 per cent when drilling two types of steel. The fact that there is any reduction in thrust with this thinning method is probably due to the fact that it permits easier

escape of the chips and extrusion products formed by the drill chisel edge.

The experiments which determined the difference between the actual and theoretical paths of the drill are particularly enlightening. These clearly show that machine deflection can far exceed the nominal feed per revolution and can cause a large and damaging increase in feed during the break-through. This situation is unfortunately very little appreciated by drill users and by some drilling-machine manufacturers. It further points out that a twist drill can take a surprising amount of abuse and still give a good account of itself.

In connection with the investigation of chatter, was any evidence of high-frequency vibration involving the tool itself rather than the complete system encountered? There is some indication that this does happen when drilling certain materials.

The tests relating hole size to relative lip height and point eccentricity clearly point out the need for accurate drill sharpening and thinning. As the work material becomes harder, accurate sharpening and thinning are essential to satisfactory drill performance.

It would be interesting to have a brief description or a sketch showing the method of using capacitive gages to make records of point displacement while drilling. The records produced by this apparatus clearly show the unstable nature of the drill point during entry into the workpiece.

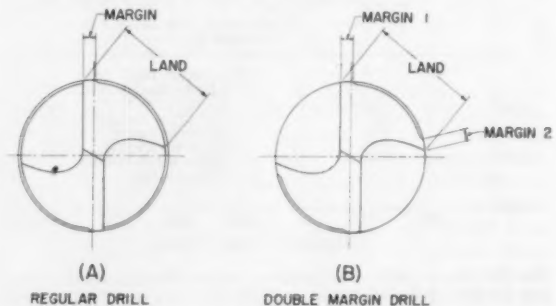


FIG. 39 COMPARISON OF A REGULAR DRILL AND A DOUBLE-MARGIN DRILL SHOWING EXTRA MARGIN ON DOUBLE-MARGIN DRILL WHICH IMPROVES GUIDING OF THE DRILL

The tests on the use of jig bushings are very interesting. They clearly show that the common radial-drill-press practice of allowing the drill bushing to pull the drill head into approximate alignment with the desired hole location can give very poor holes. It should be noted that alignment with short bushings can be improved considerably through the use of double-margin drills. Double-margin construction is shown in the accompanying Fig. 39. Here an additional margin is provided at the trailing edge of each drill land with the result that initial guiding is greatly improved.

The writer again wishes to compliment the author and his staff at the PERA on a well-designed comprehensive investigation of drilling. It is to be hoped that the experimental work and the analysis of data will be continued and reported in future papers.

#### AUTHOR'S CLOSURE

The author is very appreciative of the interest shown in the paper and the valuable comments made by contributors to the discussion.

Mr. Kennedy's charts of hole oversize against relative lip height are of considerable interest and exhibit characteristics which were not revealed by the author's experiments. A puzzling

<sup>14</sup> "On the Drilling of Metals, 2—The Torque and Thrust in Drilling," by M. C. Shaw and C. J. Oxford, Jr., Trans. ASME, vol. 79, 1957, pp. 139-148.

feature of the graphs shown in Fig. 33 is that in two cases the hole oversize for a relative lip height of 0.005 in. is considerably less than that which might be expected from considerations of equilibrium at the drill point. There are many factors other than relative lip height which could affect hole oversize and one might expect therefore to find values which were greater than those given by Equation [71] in Appendix 6 rather than smaller. The results in Fig. 33 suggest that it would be worth while to carry out more extensive investigations into the effects of the various factors on hole size.

Dr. Hahn's comment on the apparent obscurity of  $\delta/\rho$  in Fig. 20 when  $\rho = 0$  was accepted, but in this instance the author had sacrificed explicitness of statement for the sake of brevity. It was intended to represent the limiting case when  $\rho$  is approaching zero and is very small. The analysis of self-regenerative vibration given in the paper was based on essentially the same equation as that first discussed by Dr. Hahn some years ago in his paper on chatter in precision grinding operations. In that paper he derived the condition for unrestricted stability expressed by Formula [65]. Certain additional results are presented in the author's analysis, notably the instability zones and the equation relating the chatter frequency to the parameters of the system. The instability zones provide a general view of the phenomenon of regenerative chatter, while the frequency equation enables the basic parameters of an actual vibrating system to be determined by simple observation of a range of chatter frequencies.

Dr. Hahn's remarks on effects due to nonlinearities in the system are very relevant, since such effects were observed in the author's tests and indeed commonly serve to limit the amplitude of the vibrations occurring in an unstable vibrating system. It is interesting to note that the method described in the paper for determining the basic parameters of the system is applicable in most practical cases of this type. The parameters  $\Omega_a$ ,  $\delta$ , and  $\rho$  may still be determined by observing the chatter frequencies even though nonlinear effects are present and the frequencies observed correspond to vibrations having a finite nonconstant amplitude. The type of vibration which can be dealt with may be described as essentially sinusoidal in character in the sense that it may be represented with good accuracy over any complete period by a sine wave, although the amplitude of the sine wave used to represent it varies from period to period. The chatter vibrations occurring in the chatter bands shown in Fig. 21 fell into this category, as do many chatter vibrations—at least in their initial stages. Vibrations having a markedly nonsinusoidal character commonly supervene only when the amplitude of the chatter vibration exceeds the feed, so that impact takes place between tool and work.

Equation [43] is applicable in the case of a nonlinear system undergoing vibrations which are essentially sinusoidal in character providing that the coefficients in the equation are suitably interpreted. The quantities  $m$ ,  $c$ ,  $k$ , and  $r$  are no longer to be treated as constants, but as functions of  $a$ , the amplitude of the chatter vibration. For clarity Equation [43] may be revised to make explicit this dependence on amplitude, thus

$$m(a)\ddot{x} + c(a)\dot{x} + k(a)x = -r(a)[x - x_1] \dots [43a]$$

An "essentially sinusoidal" solution of Equation [43a] is obtained by substituting

$$x = a \sin vt \dots [68a]$$

where  $a$  is a function of  $t$  such that  $\dot{a}$  is a quantity small enough to be neglected over the period  $2\pi/v$  of the chatter vibration. After substitution of Equation [68a] in Equation [43a] and some slight simplification

$$\begin{aligned} & \left[ -m(a)v^2 + \frac{\dot{a}}{a}c(a) + k(a) + r(a) - r(a)\cos vt \right] \sin vt \\ & + \left[ 2\frac{\dot{a}}{a}m(a)v + c(a)v + r(a)\sin vt \right] \cos vt = 0 \end{aligned}$$

The coefficients of  $\sin vt$  and  $\cos vt$  must both be equal to zero for this equation to be satisfied, hence

$$-m(a)v^2 + \frac{\dot{a}}{a}c(a) + K(a) - r(a)\cos vt = 0$$

$$2\frac{\dot{a}}{a}m(a)v + c(a)v + r(a)\sin vt = 0$$

where  $K(a)$  has been written for  $[k(a) + r(a)]$ .

New parameters  $\Omega_a(a)$ ,  $\delta(a)$ ,  $\rho(a)$ , and  $\Delta(a)$  are now introduced, where

$$\Omega_a(a) = \frac{K(a)}{m(a)}, \quad \delta(a) = \frac{\pi c(a)}{\sqrt{[m(a)K(a)]}}$$

$$\rho(a) = \frac{r(a)}{K(a)}, \quad \text{and} \quad \Delta(a) = \frac{2\pi}{\Omega_a(a)} \frac{\dot{a}}{a}$$

The parameters  $\Omega_a(a)$ ,  $\delta(a)$ , and  $\rho(a)$  are obvious generalizations of the parameters  $\Omega$ ,  $\delta$ , and  $\rho$  which appear in the paper, and it is readily shown that if  $a$  and  $a + h$  are the amplitudes for corresponding points in consecutive chatter cycles then  $h/a = \Delta(a)$  approximately; i.e.,  $\Delta(a)$  approximates to the logarithmic increment of the chatter. Rewriting the pair of equations in terms of the new parameters, the following relationships are obtained, after some simplification

$$\left(\frac{v}{2\pi}\right)^2 = \left(\frac{\Omega_a}{2\pi}\right)^2 \left(1 + \frac{1}{2\pi^2} \Delta\delta - \rho \cos \theta\right)$$

$$\frac{v}{\Omega_a} (\Delta + \delta) = -\pi\rho \sin \theta$$

In these equations  $\theta$  has been written for  $vt$ , and for ease of writing the dependence of the quantities  $\Omega_a$ ,  $\delta$ ,  $\rho$ , and  $\Delta$  on the amplitude  $a$  has not been indicated explicitly as hitherto.

From the first equation it may be seen that in practical cases  $v = \Omega_a$  to a first approximation; hence, by substitution in the second equation,  $\Delta + \delta = -\pi\rho \sin \theta$  approximately; it follows that the inequality  $(\Delta + \delta) < \pi\rho$  holds approximately. From this inequality it follows that the inequality

$$\frac{1}{2\pi^2} \Delta\delta < \frac{1}{8} \rho^2$$

is also approximately true. Finally, then, since  $(\rho^2/8)$  is normally a small second-order quantity in practical cases, the term  $(1/2\pi^2)\Delta\delta$  may commonly be neglected, so that the two equations may be simplified to give

$$\left(\frac{v}{2\pi}\right)^2 = \left(\frac{\Omega_a}{2\pi}\right)^2 (1 - \rho \cos \theta) \dots [59a]$$

$$\frac{\Delta + \delta}{\rho} = -\sqrt{\frac{\pi \sin \theta}{(1 - \rho \cos \theta)}} \dots [56a]$$

The close formal similarity between these equations and the corresponding Equations [59] and [56] of the paper is at once apparent. In particular, Equations [59a] and [59] are identical

in form and do not include the damping parameter  $\delta$ . It follows that the method described in the paper for determining the basic parameters of a vibrating system is unaffected by nonlinearity in the system, providing the amplitude  $a$  of the chatter vibration is small enough for the parameters  $\Omega_a(a)$  and  $\rho(a)$  not to differ substantially from the parameters  $\Omega_a$  and  $\rho$ , which appear in the paper. This is the situation which was indicated in the author's tests. The amplitude of the chatter vibration assumed a fairly small limiting value and no appreciable dependence of  $\Omega_a$  or  $\rho$  on this limiting amplitude was detected.

With a slight extension, the method for determining the basic parameters of the vibrating system may still be applied even when the dependence of  $\Omega_a(a)$  and  $\rho(a)$  on the amplitude of the chatter vibration is appreciable. The square of the chatter frequency is plotted against  $\cos \theta$  as before, only in this case, since  $\Omega_a(a)$  and  $\rho(a)$  are no longer constants, Equation [59a] shows that a curve is obtained which deviates from the straight line of Equation [59]. However, the ends of the curve will lie on the straight line since at the ends the amplitude  $a$  of the chatter vibration is small. Thus, if a suitable regression curve is fitted to data obtained in a case such as this, the desired straight line corresponding to Equation [59] of the paper is obtained by joining the ends of the curve. Having obtained this straight line, the rest of the method described in the paper is unaffected by the nonlinearity of the system.

The scatter of drill life reported by Mr. Oxford agrees very well with that observed during drilling tests in steel and cast iron carried out at PERA. These showed that the average coefficient of variation of drill life in steel was about 35 per cent, of which only a comparatively small amount could be attributed to the variability of test drills. The distribution of drill-life values in cast iron was markedly asymmetrical and it would be misleading therefore to quote a coefficient of variation, but in general the scatter of drill life in this material was about twice that occurring in steel.

The capacity of the large drilling dynamometer shown in Fig. 3(a) can be varied by changing the steel diaphragms in the load-measuring elements; thrust loads up to 2 tons and torques up to 100 lb-ft may be measured readily. The spring constants of the dynamometer when fitted with the diaphragms used in the majority of the tests were 300,000 lb/in. for thrust and 19 lb-ft/min of arc for torque. The maximum capacity of the small drilling dynamometer shown in Fig. 3(b) is 20-lb thrust and 0.09 lb-ft torque, and the respective spring constants are 10,000 lb/in. and 0.03 lb-ft/min of arc.

The author has not carried out comparative drill-life tests with and without a dynamometer, but feels that the stiffness of the dynamometer is high enough compared with the stiffnesses of the drill and machine to insure that the dynamometer effect will be relatively small. For example, the vertical deflection of the dynamometer table was roughly only  $1/4$  the vertical deflection of the drill caused by the elastic twisting of shafts in the drill-feed mechanism, and the torsional deflection of the dynamometer was less than 1 per cent of that of a standard  $1/8$ -in.-diam drill. It is appreciated that reference only to stiffness in a dynamic system could be misleading, but it is thought that the figures given indicate the general order of the dynamometer characteristics as compared with those of the drilling setup.

The author is not convinced that the conventional tapered web can always be justified in terms of drill life. It is argued that the tapered web increases the torsional and flexural rigidity of the drill and thereby improves drill life, but the extent of this improvement will depend on how sensitive drill life is to changes in rigidity of the drill. Tests by the author in cast iron and medium-carbon steels with standard length  $1/8$ -in.-diam drills did not reveal a significant improvement in drill life as the fluted length of the drill was reduced from 4 to 3 in., and it would appear therefore

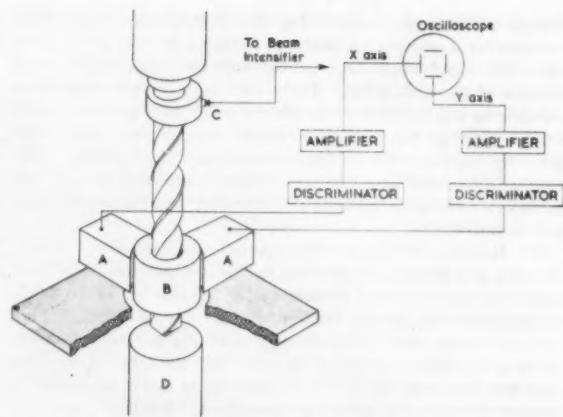


FIG. 40 DIAGRAM OF EQUIPMENT USED FOR MEASURING DRILL POINT DISPLACEMENTS

that under these conditions an increase of approximately 25 per cent in the torsional rigidity of the drill was of little consequence. If, therefore, standard length drills were made with a parallel web for say, two thirds of the fluted length it does not appear likely that drill life in normal engineering materials would be impaired seriously, and the elimination of the possibility of incorrect or poorly executed point thinning might well result in substantially improved drill life in practice. When tough, work-hardening materials are drilled, however, the drill performance seems to be much more sensitive to changes in rigidity and the tapered web may then become essential. Mr. Oxford's results showing the effect on drill life of the length of the drill when drilling S-816 high-temperature alloy (Fig. 34) point very clearly to the marked effect of drill rigidity during drilling operations on this type of work material.

The greater sensitivity of drill life to changes in drill rigidity when drilling certain materials may well be due to the occurrence of high-frequency torsional vibrations involving only the drill. It has been shown by Arnold<sup>15</sup> that self-induced vibrations of the tool may occur if the material being machined has a negative cutting force/cutting speed characteristic. This type of vibration is quite different in origin from the self-regenerative vibration discussed in the paper and further equipment would have been required to detect it. However, the author has often noted audible signs of drill vibrations during the drilling of certain materials, and the squeal that is frequently heard when a drill is near failure certainly points to torsional vibration. It is hoped that it will shortly be possible to investigate the problem of drill vibration in greater detail.

The author agrees that the rake specified in Appendix 3 is not a fundamental metal-cutting angle, but is of the opinion that the advantages of ready measurement and visualization mentioned by Mr. Oxford are of major importance in a practical workshop nomenclature. Even if our knowledge of metal cutting was sufficiently advanced to enable a fundamental rake to be defined clearly, it is doubtful whether the definition of such an angle could be applied readily in the workshop. Workshop personnel are principally concerned with the facility with which a tool can be specified, ground, and measured as a separate entity, and the definitions given in Appendix 3 have been prepared with these essential workshop requirements in mind. The author feels that

<sup>15</sup> "The Mechanism of Tool Vibration in the Cutting of Steel," by R. N. Arnold, Proceedings of The Institution of Mechanical Engineers, vol. 154, 1946, pp. 261-276.

the onus is on the research worker to translate metal-cutting fundamentals into terms which are familiar to workshop personnel, and which are best suited to the practical requirements of workshop specification and tool servicing.

As pointed out by Mr. Oxford the split or crankshaft point has considerable advantages for the drilling of deep holes in tough materials. In this type of drilling operation the structural properties of the drill mainly set the limits of drill performance. The thick web which is necessary for maximum rigidity must be thinned at the point with the primary object of reducing the drilling thrust, and the split point described by Mr. Oxford fulfills this purpose very well. Provided the thinning is done accurately, the type of point produced also should facilitate the starting of the drill.

The reduction in thrust achieved with the method C type of point thinning is almost certainly due in part to the fact that it permits the material removed at the chisel edge to escape readily into the flutes; this also may account for the improved drill life shown in Fig. 12(a). The author notes that Mr. Oxford obtained a rather smaller reduction in thrust than that quoted in the paper. The behavior of the twist drill is governed by a very large number of factors and even small changes in these factors can have a

pronounced effect on drilling forces and drill life. Without a detailed comparison of the conditions of the author's tests and those of Mr. Oxford's, it is not possible to determine the causes of the observed difference in the results.

A diagram of the equipment used to record the point displacements of the drill is shown in Fig. 40 of this closure. Two insulated condenser plates A were positioned close to a concentric sleeve B, located on the lands of the drill. The changes in capacitance across the sleeve and the two plates as the drill deflected were converted to voltage changes, amplified and presented on the X and Y-plates of an oscilloscope fitted with a high-speed cine-recording camera. A contactor C was arranged to trigger a pulse on the trace once per revolution of the drill and thus to mark the position of the outer corners along the trace. By photographing the movements of the spot on the face of the cathode-ray tube as the drill entered the workpiece D, a continuous polar record could be obtained of the transverse deflections of the drill point.

The double margin drill described by Mr. Oxford would appear to have considerable advantages where greater accuracy of the hole is required, and the author hopes to be able to include drills of this type in future tests.



# Seal Leakage in the Rotary Regenerator and Its Effect on Rotary-Regenerator Design for Gas Turbines<sup>1</sup>

By D. B. HARPER,<sup>2</sup> MONTREAL, QUEBEC, CANADA

An analysis of rotary-regenerator seal leakage is presented which predicts the leakage quantity and the variations of pressure gradient under the sealing shoe. The verifying results obtained from tests of a simulated sealing arrangement also are given. The optimum efficiency conditions of the gas-turbine cycle including leakage and pressure loss are studied; and a sample regenerator design for a specific gas-turbine plant is carried as far as the presentation of design-point curves for sizing the rotary regenerator. A method of reducing leakage is presented and the results of experimental verification are shown. Conclusions are drawn regarding the best general configuration of the rotary regenerator with respect to the leakage problem.

## NOMENCLATURE

The following nomenclature is used in the paper:

- $A$  = leakage-area constant =  $\alpha\gamma\delta L_s \left[ \frac{2g}{RT_c n} \right]^{1/2}$   
 $A'$  = matrix area/unit volume  
 $B$  = leakage displacement-area constant =  $\frac{\vartheta}{RT_c L}$   
 $c$  = specific heat of matrix material  
 $C_p$  = specific heat of gas, constant pressure  
 $D_R$  = rotor diameter  
 $G'$  = mass velocity (matrix frontal area)  
 $h$  = coefficient of heat transfer  
 $k$  = ratio of specific heats  
 $L$  = length of seal shoe in direction of leakage  
 $L_s$  = length of seal shoe perpendicular to leakage path  
 $L_R$  = length of matrix flow path  
 $m'$  = matrix mass/unit volume  
 $n$  = number, number of passages under seal  
 $p$  = pressure  
 $r$  = pressure ratio  
 $S$  = matrix velocity at seal shoe  
 $\vartheta$  = rotor, matrix, free volume under seal shoe  
 $W, W_T$  = flow rate, total leakage  
 $W_L$  = flow rate, clearance leakage  
 $W_D$  = flow rate, displacement leakage  
 $\frac{\Delta W}{W}$  = leakage/compressor-flow ratio  
 $\alpha$  = flow coefficient

- $\gamma$  = carry-over factor for labyrinth  
 $\delta$  = seal-shoe clearance  
 $\rho$  = density  
 $\xi$  = matrix-voids fraction  
 $\theta$  = time period  
 $\eta$  = efficiency, cycle  
 $\eta_{RI}$  = regenerator effectiveness, internal  
 $\eta_{RE}$  = regenerator effectiveness, external  
 $\Lambda$  = reduced length =  $\frac{A'hL_R}{G'C_p}$   
 $\Lambda_0 = \Lambda_c \left[ \frac{1}{1 + \frac{\Lambda_s}{\Lambda_R} \frac{(wC_p)_c}{(wC_p)_H}} \right]$   
 $\pi$  = reduced time period =  $\frac{A'h\theta}{m'c}$   
 $\frac{BS}{A}$  = dimensionless leakage parameter

## INTRODUCTION

The efficiency of a simple gas-turbine plant can be increased by using a regenerative cycle in which a heat exchanger is used to transfer heat from the hot turbine-exhaust gas to the cooler compressor-discharge air. A brief study of the flow-friction and heat-transfer relationships indicates that small heat-exchanger volume can be attained with passages of small hydraulic diameter (neglecting fouling problems for the present). As passage size is reduced the number of passages required increases, while the passage length must decrease if the pressure losses are to be maintained constant. The conventional shell-and-tube heat exchanger cannot exploit this characteristic very far as a large number of small tubes introduce construction difficulties and short tube lengths prevent the use of counterflow.

The crossflow plate-fin heat exchanger, Fig. 1(a), can utilize small passages without such difficulty. This type of heat exchanger has been analyzed for the conditions of a gas-turbine cycle having a cold stream at 60 psia and 400 F, a hot stream at 15 psia and 1140 F, and a flow rate of 45 lb/sec. The heat exchanger is assumed to have a constant temperature effectiveness  $\eta_R$  of 0.80 and a constant pressure loss

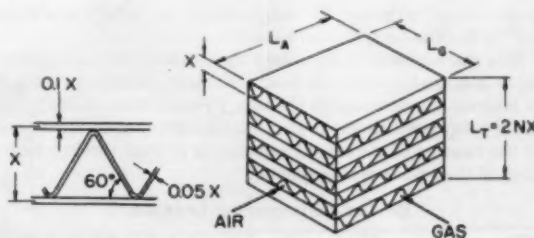


Fig. 1(a) PLATE-FIN SURFACE

<sup>1</sup>The material in this paper is derived from a research project carried out by the author at the Massachusetts Institute of Technology under the direction of Prof. W. M. Rohsenow.

<sup>2</sup>Project Engineer, Aluminum Company of Canada, Ltd.

Contributed by the Heat Transfer Division and presented at the Diamond Jubilee Annual Meeting, Chicago, Ill., November 13-18, 1955, of THE AMERICAN SOCIETY OF MECHANICAL ENGINEERS.

NOTE: Statements and opinions advanced in papers are to be understood as individual expressions of their authors and not those of the Society. Manuscript received at ASME Headquarters, April 5, 1955. Paper No. 55-A-109.

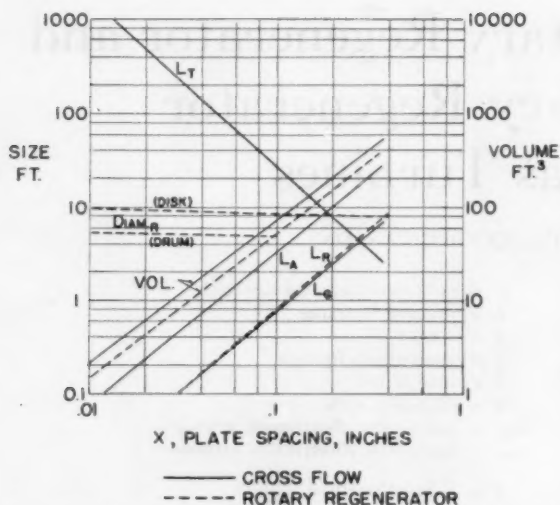


FIG. 1(b) EFFECT OF HYDRAULIC DIAMETER ON HEAT-EXCHANGER SIZE

$$\Sigma \frac{\Delta P}{P} = 0.04$$

The solution for minimum exchanger volume as a function of plate spacing  $X$  is shown in Fig. 1(b).

Fig. 1(b) shows the decrease in exchanger volume, the decrease in passage length ( $L_A$  and  $L_O$ ), and a rapid increase in the height of the plate pile  $L_T$  as plate spacing  $X$  is reduced. For 25 plates per inch ( $X = 0.04$  in.) the exchanger dimensions are 0.16 ft  $\times$  0.7 ft  $\times$  130 ft. Thus, while the plate-fin heat exchanger can be of small volume its dimensions become unwieldy. The total length  $L_T$  would have to be divided into a number of interconnected units.

The rotary-regenerator type of heat exchanger, similar to the Ljungström air preheater, has a rotor disk or drum to carry energy-storage material having adequate transfer surface (the matrix). The rotor is continuously rotated and any element of matrix is intermittently in the hot and cold streams. During rotation, heat is transferred to the matrix while in the exhaust-gas stream, and heat is transferred from the matrix while in the cooler compressed-air stream.

A rotary regenerator has been analyzed under the same assumptions as the preceding crossflow exchanger, using the same plate-fin type of surface, and solving for minimum exchanger volume as a function of plate spacing  $X$ . The results of this calculation are shown by dotted lines in Fig. 1(b). Here the volume can be seen as essentially the same as for the crossflow type, but exchanger dimensions as given by length  $L_R$  and diameter  $D_R$  remain reasonable even for the smallest plate spacings. Thus a rotary regenerator can be made small in volume and still be built in a single unit up to quite large flow capacities.

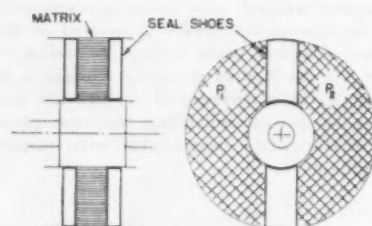
This characteristic of the rotary regenerator leads to considering it as a gas-turbine-cycle heat exchanger. However, there is an inherent disadvantage in the rotary regenerator; namely, the loss of compressed air due to the positive displacement occasioned by the rotation of the matrix and due to leakage through clearances of the sealing arrangements.

#### ROTARY-REGENERATOR LEAKAGE

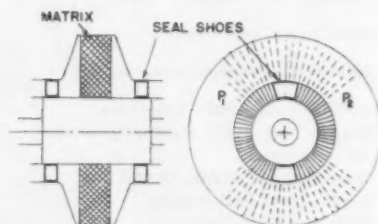
The prevention of leakage flow between hot and cold streams in the rotary regenerator is a factor which will determine the

success of this form of heat exchanger for gas-turbine cycle use. The sealing arrangements must adequately prevent leakage flow, and at the same time not introduce high frictional resistance to rotation. Neglecting small aerodynamic effects—Hrynyszak (6)\* proposes the use of stator and rotor (matrix) blades to rotate the regenerator by aerodynamic forces alone—the power required to rotate the rotor is entirely absorbed in friction. Since this power input is charged directly against the heat exchanger it must be kept small.

The sealing arrangements will be of two general types; continuous cylindrical seals similar to a shaft seal, and main seals which divide the high and low-pressure sides. The continuous cylindrical seals can be handled by careful mechanical design. The main seals present a more difficult problem because of the effect of the displacement or carry-over loss, the pressure forces under the seal faces which must be balanced, and allowances to be made for thermal distortion of the rotor.



(a) CONTINUOUS PASSAGE ROTOR



(b) COMPARTMENT ROTOR

Fig. 2

The two possible classes of main seal arrangements are illustrated diagrammatically in Fig. 2. Fig. 2(a) shows the case where the seal bears directly upon the regenerator matrix. This type demands the use of a matrix of continuous passages, the walls of which prevent the direct flow of air from the high to the low-pressure side. Fig. 2(b) shows the case where the seal bears against a system of rotor compartments. This type of rotor must be used where packed screens or other porous matrix types are to be used. This configuration has the advantage that the seal length, being independent of matrix dimensions, may be short, but with it there will be rotating ducting or "dead" compartments which will increase the displacement loss under the seal. In either sealing arrangements a number of compartments or passages will be under the seal shoe at any instant.

A cross section through either arrangement is illustrated schematically in Fig. 3(a) where the important relationships are reproduced. Here the clearance  $\delta$  through which leakage will take

\* Numbers in parentheses refer to the Bibliography at the end of the paper.

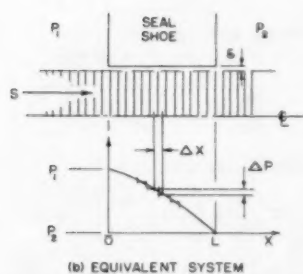
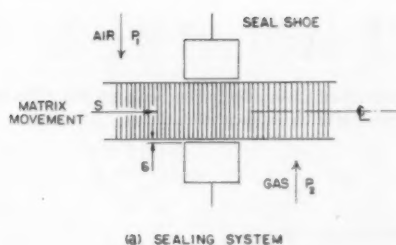


FIG. 3

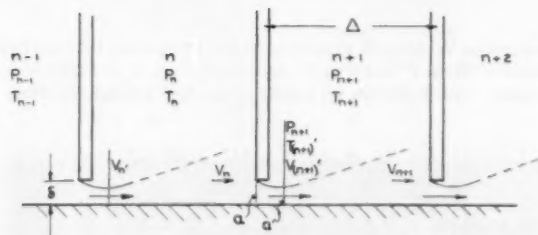
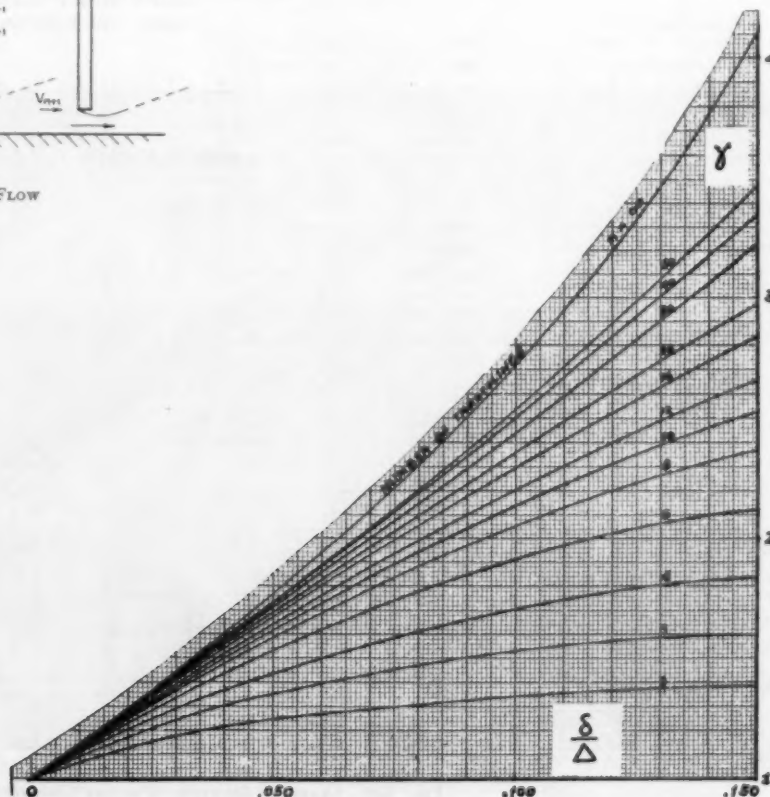


FIG. 4(a) LABYRINTH FLOW

FIG. 4(b) CARRY-OVER FACTOR  $\gamma$ 

place is shown. Movement of the matrix with velocity  $S$  will cause a positive displacement of air from one side to the other.

#### ROTARY-REGENERATOR SEAL-SHOE ANALYSIS

Fig. 3(b) may be taken as being equivalent, with respect to leakage, to Fig. 3(a) if the following assumptions are made:

- (a) Low air and gas velocities approaching the matrix.
- (b) Neglecting flow resistance from within a passage; i.e., the air pressure within the passage is equal to that at the seal face.
- (c) That a mean temperature can be used for the air trapped within a passage.

The analysis of the leakage occurring in Fig. 3(b) has been made with the following additional assumptions:

- (d) Low velocity of matrix movement compared with the air velocities under the sealing restrictions.
- (e) That the flow under the seal shoe past a passage end is similar to flow through an orifice.
- (f) A sufficiently large number of passages,  $n$ , under the seal shoe for  $(\Delta P/P)$  between adjacent passages to be small.
- (g) That the temperature during expansion (or compression) of the air trapped in a compartment is constant (isothermal expansion).

The flow rate through a given restriction Fig. 4(a) is thus a function of the pressure and the pressure difference, similar to flow through an orifice where the critical pressure ratio has not been reached

$$W_{Ls} = \alpha \gamma \delta L_s \left[ -\frac{2g}{RT_x} P_x \Delta P_x \right]^{1/2} \dots \dots \dots [1]$$

where  $\gamma$  is Egli's (4) velocity carry-over factor, Fig. 4(b), for labyrinth-type flow.

Assuming a sufficiently large number of passages under the seal at one time the mean pressure gradient, Fig. 3(b), may be taken as a continuous function of  $X$ . Hence

$$\Delta P = \frac{dp}{dx} \Delta x; \quad \Delta x = \frac{L}{n}; \quad \Delta P = \frac{L}{n} \frac{dp}{dx} \dots \dots \dots [2]$$

and Equation [1] may be written

$$W_{Ls} = A \left( -Lp \frac{dp}{dx} \right)^{1/2} \dots \dots \dots [3]$$

The local displacement flow rate due to rotor movement can be written as

$$\begin{aligned} W_{Ds} &= \varphi_x \text{ (free volume flow rate)} \\ &= Bp_x S \dots \dots \dots [4] \end{aligned}$$

The total flow rate due to leakage through clearances plus displacement due to rotation may be written

$$W_{Ts} = W_{Ls} + W_{Ds} \dots \dots \dots [5]$$

However, this is a function of  $p$  only, and  $p$  is a function of  $x$  in the steady state; thus from continuity we may write

$$\frac{dW_T}{dx} = 0; \quad \therefore \frac{dW_L}{dx} = -\frac{dW_D}{dx}$$

which leads to

$$\left( \frac{dp}{dx} \right)^2 + p \left( \frac{d^2p}{dx^2} \right) = 2BS/AL^{1/2} \left( -\frac{dp}{dx} \right)^{1/2} p^{1/2} \dots [6]$$

This differential equation, describing leakage under the seal shoe, may be solved with the substitutions

$$\frac{dp}{dx} = -y, \quad \text{and} \quad \frac{y}{p} = Z \dots \dots \dots [7]$$

to give after integration

$$Z = \left[ \frac{1}{pc} - \frac{BS}{AL^{1/2}} \right]^2 \dots \dots \dots [8]$$

where  $c$  is a constant of integration.

Substitution for  $Z$  in Equation [8] gives

$$\frac{dp}{dx} = -p \left[ \frac{1}{pc} - \frac{BS}{AL^{1/2}} \right]^2 \dots \dots \dots [9]$$

Writing Equation [5], using [3] and [4]

$$W_T = A \left[ -Lp \frac{dp}{dx} \right]^{1/2} + BS p$$

and introducing Equation [9] evaluates the constant  $c$  as

$$c = \frac{AL^{1/2}}{W_T} \dots \dots \dots [10]$$

Separating variables in Equation [9] and integrating between the limits of  $P_1$  to  $P$  and 0 to  $X$ , and using  $P/P_2 = r$ ,  $P_1/P_2 = r_T$  together with Equation [4] results in the final leakage equation

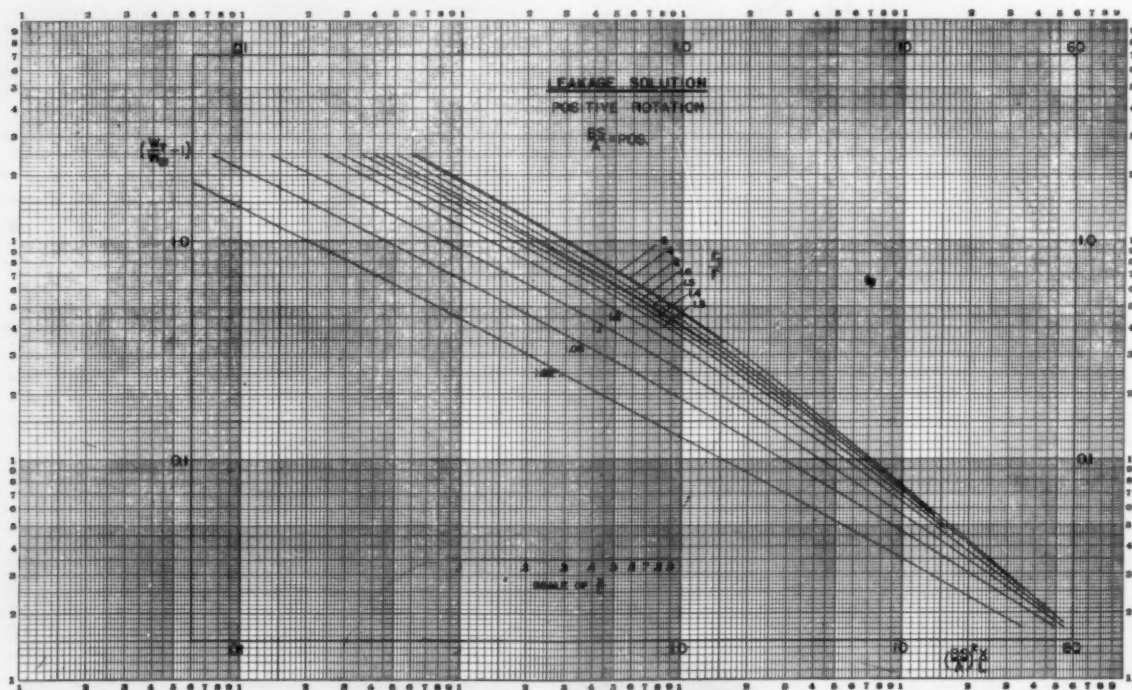


FIG. 5(a) LEAKAGE SOLUTION—POSITIVE ROTATION

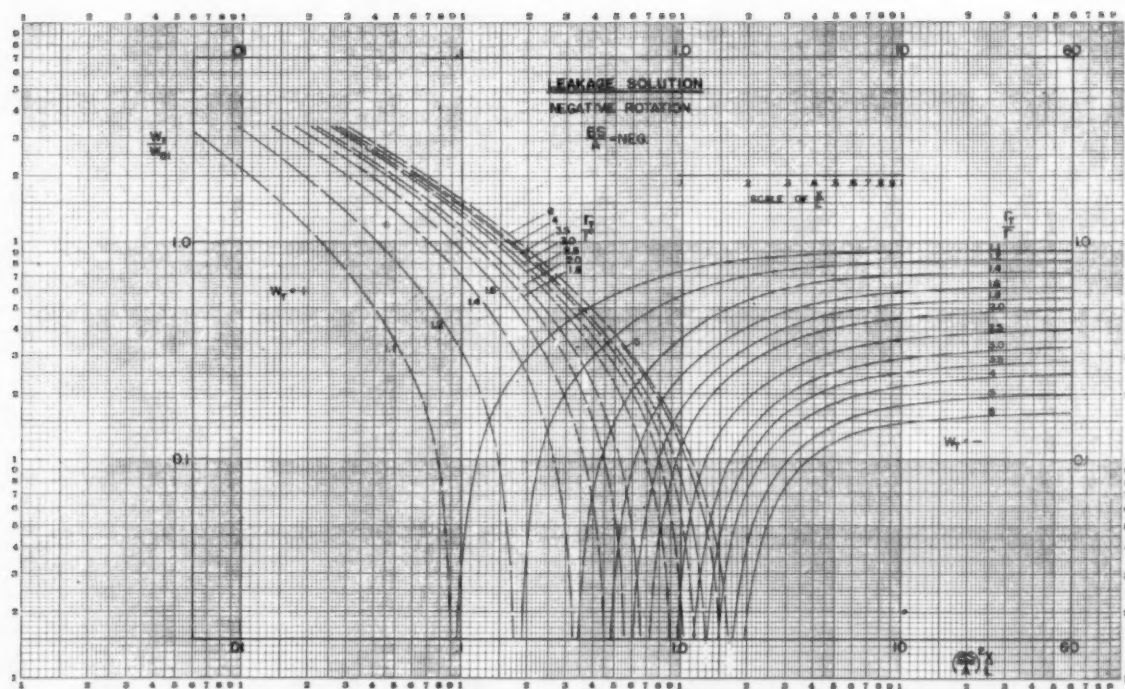


FIG. 5(b) LEAKAGE SOLUTION—NEGATIVE ROTATION

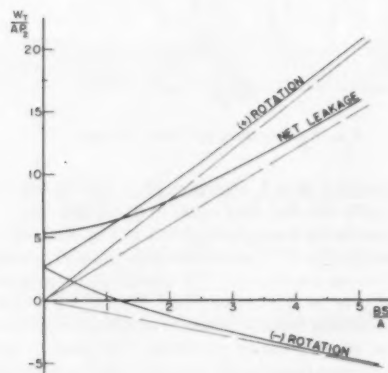


FIG. 6(a) SEAL LEAKAGE

$$\frac{1}{1 - \frac{W_T}{W_D1}} - \frac{1}{1 - \frac{W_D1}{W_T} \frac{r}{r_T}} - \ln \frac{1 - \frac{W_D1}{W_T} \frac{r}{r_T}}{1 - \frac{W_T}{W_D1}} = \left( \frac{BS}{A} \right)^2 \frac{X}{L} \dots \dots \dots [11]$$

where  $W_T$  is unknown and  $r/r_T$  is an unknown function of  $X/L$ .

Systematic solution of Equation [11] by trial and error is tedious so the solution curves of Fig. 5 have been prepared. Fig. 5(a) is for positive rotation (i.e., rotor moving from high to low-pressure sides) while Fig. 5(b) is for negative rotation (i.e., rotation from low to high-pressure sides). The results are given in terms of the leakage parameter  $BS/A$ . For visualization of the results,  $BS/A$  may be considered primarily as proportional to

rotational speed times voids volume, divided by leakage-flow-clearance area. The abscissa is entered with the known value of  $(BS/A)^2$  with  $X/L$  taken as unity. With  $X/L$  equal to unity  $r = P_1/P_2 = 1$ , thus read up to  $r_T/r = r_T$ . Now the corresponding value of  $W_T/W_{D1}$  is read off.  $W_{D1}$  is known and equal to  $BSP_1$ , thus  $W_T$  is known. Since  $W_T/W_{D1}$  is a constant, the pressure gradient may be obtained by reading along this constant horizontal line corresponding values of  $r_T/r$  and  $(BS/A)^2 X/L$  giving values of  $r$  versus  $X/L$ . A scale of  $X/L$  is shown for convenience. In Fig. 5(b) for negative rotation ( $S = \text{neg}$ ),  $W_T/W_{D1}$  goes to zero at a certain value of  $BS/A$  and then reappear with opposite sign as  $W_T$  becomes negative; that is, above a certain value of  $BS/A$  the rotor is pumping from the low to the high-pressure sides.

For direct and more accurate numerical solution, Equation [11] is best written in the form

$$\frac{1}{1 - \left( \frac{BS}{A} \right) \left( \frac{AP_2}{W_T} \right) r_T} - \frac{1}{1 - \left( \frac{BS}{A} \right) \left( \frac{AP_2}{W_T} \right) r} - \ln \frac{1 - \left( \frac{BS}{A} \right) \left( \frac{AP_2}{W_T} \right) r}{1 - \left( \frac{BS}{A} \right) \left( \frac{AP_2}{W_T} \right) r_T} = \left( \frac{BS}{A} \right)^2 \frac{X}{L} \dots \dots \dots [12]$$

The results of such a solution are shown in Fig. 6 for  $r = 4$ . Fig. 6(a) shows the total leakage for positive and negative rotation and the net rotary-regenerator leakage which results from addition of leakages from both seal sets. It can be noted by comparison with the asymptotes that while increased rotational speed increases total leakage it decreases that part of the leakage due to the clearances. Fig. 6(b) shows the corresponding pressure gradients occurring under the seal shoes.

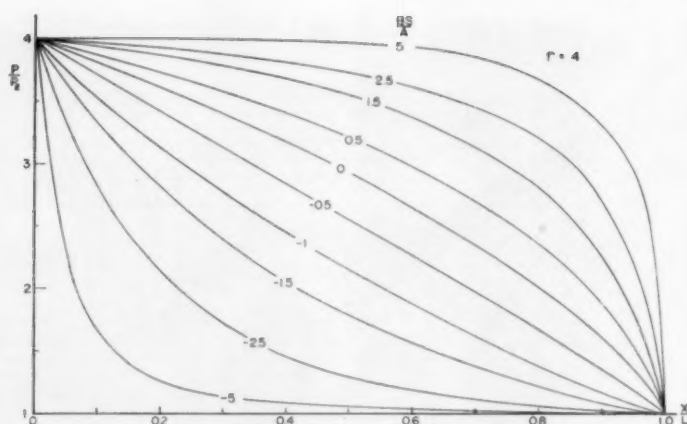


FIG. 6(b) PRESSURE GRADIENTS UNDER SEAL SHOE

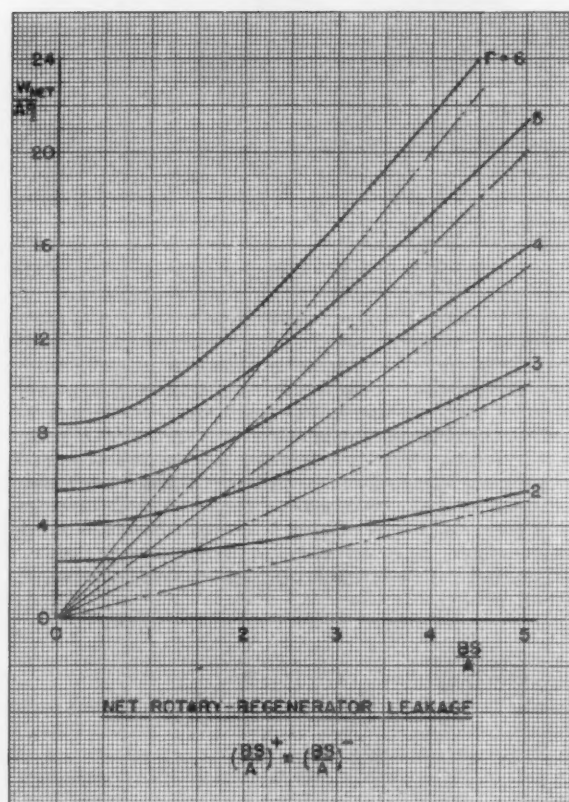


FIG. 7 NET ROTARY-REGENERATOR LEAKAGE

Fig. 7 shows the net rotary-regenerator leakage for a range of pressure ratios.

#### EXPERIMENTAL INVESTIGATION

Experimental apparatus was built to test the validity of the preceding relationships. The apparatus is shown diagrammatically in Fig. 8. The ranges of the variables were pressure ratio 4 to

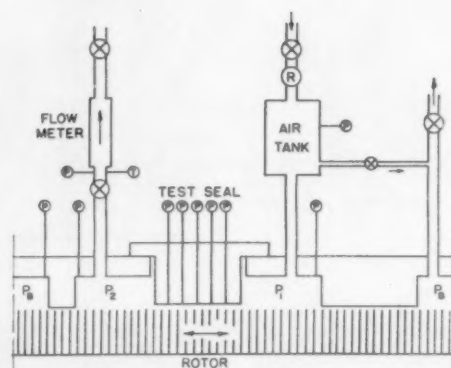


FIG. 8 DIAGRAM OF TEST APPARATUS

1, rotational speed 10 to 1, clearance 10 to 1, with the number of partitions under the seal shoe equal to 8, 12, and 16.

Typical results for leakage are shown in Fig. 9(a) and for pressure gradient by Fig. 9(b), where the experimental points and the theoretical curves are shown. The agreement for pressure gradient became poor as  $BS/A$  increased beyond unity due to the effect of extraneous leakage passages within the apparatus being subjected to steep pressure gradients. In general the experimental results were found to substantiate the theoretical analysis.

#### EFFECT OF ROTARY-REGENERATOR PERFORMANCE ON GAS-TURBINE-CYCLE PERFORMANCE

To evaluate the effect of a rotary-regenerator in a gas-turbine cycle it is necessary to consider not only the regenerator effectiveness but also the pressure and leakage losses occurring due to its use.

The internal regenerator effectiveness  $\eta_{RI}$ , given by regenerator heat-transfer theory, may be approximated (2) by

$$\eta_{RI} = \left[ \frac{1}{\frac{1}{2} \left( 1 + \frac{(wC_p)_g}{(wC_p)_H} \right) \Lambda_0 + 1} \right] \left[ 1 - \frac{1}{9} \left( \frac{\pi}{\Lambda} \right)^2 \right] \quad [13]$$

The regenerator actual external effectiveness  $\eta_{RE}$  is lower than  $\eta_{RI}$  because of the leakage flow mixing of air and gas. This correction is given (5) as

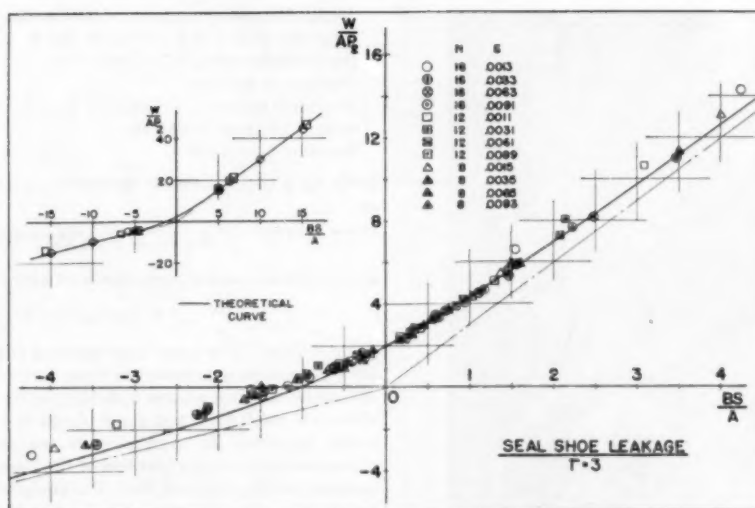


FIG. 9(a) SEAL-SHOE LEAKAGE

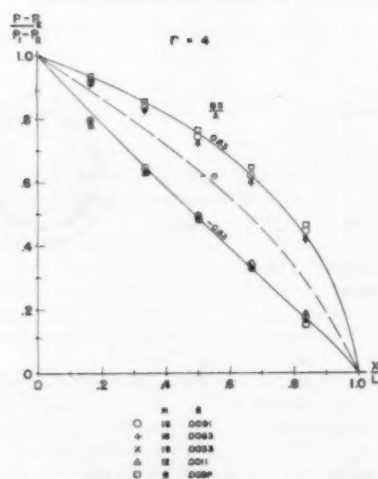


FIG. 9(b) SEAL-SHOE PRESSURE GRADIENTS

$$\eta_{RI} - \eta_{RE} = \frac{\eta_{RI} \left( \frac{\Delta W}{W} \right) (1 - \eta_{RI})}{2 - \left( \frac{\Delta W}{W} \right) (1 + \eta_{RI})} \dots [14]$$

Considering the gas-turbine cycle of Fig. 10 a cycle analysis has been carried out on the basis of 1 lb of air compressed per sec and including the effect of leakage and pressure loss due to the introduction of the regenerator into the cycle. An expression was obtained for cycle efficiency and differentiated with respect to compression ratio  $r_c$  and set equal to zero to obtain the compression ratio for maximum efficiency. The compression ratio for maximum efficiency is given as

$$r_c^{\frac{K-1}{K}} = \frac{\eta_r \frac{T_3}{T_1} (1 + \psi)}{\phi - (\phi + \eta) \frac{T_3}{T_1}} \left[ 1 \pm \sqrt{\frac{\frac{T_3}{T_1} - 1}{\eta_r \frac{T_3}{T_1}} \frac{\phi}{1 + \psi} \left( \frac{\eta_r \frac{T_3}{T_1}}{\frac{T_3}{T_1} - 1} \psi + 1 + \xi \eta_r \left[ \left( \frac{T_3}{T_1} - 1 \right) \phi - \eta_r \frac{T_3}{T_1} \right] \right)} \right] \dots [15]$$

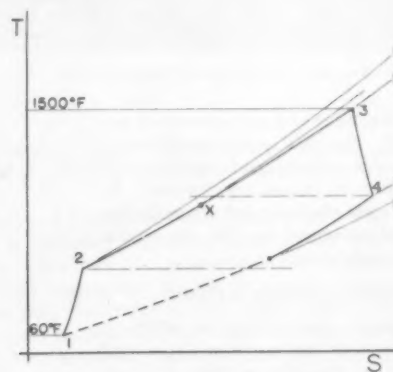


FIG. 10 T-S DIAGRAM OF CBTX CYCLE

where

$$\phi = \frac{1 - \eta_{RE}}{\xi - (1 + \phi)\eta_{RE}}$$

$$\xi = 1 - \frac{\Delta W}{W}$$

$$\psi = \frac{K-1}{K} \sum \frac{\Delta P}{P}$$

Equation [15] has been solved for a cycle operating between 60 and 1500 F with compressor and turbine efficiencies of 0.85 and 0.88, respectively. A range of regenerator effectiveness, pressure loss, and leakage loss have been used. These results were used to obtain a family of curves describing plant performance. One such curve, for  $\Sigma(\Delta P/P) = 0.10$  is reproduced as Fig. 11.

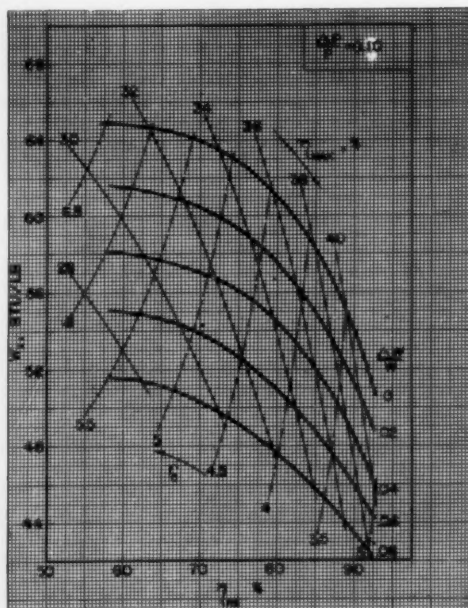


FIG. 11 CBTX CYCLE DESIGN POINTS

The curve is entered with a given value of  $\eta_{RE}$  and  $\Delta W/W$ . The maximum cycle efficiency, the compression ratio for maximum efficiency, and the net work output may be read off. The loss in cycle efficiency and the reduction of work output caused by the regenerator leakage is clearly shown.

#### ROTARY-REGENERATOR DESIGN

A preliminary analysis of the effect of matrix dimensions was made by Harper and Rohsenow (5). This showed that, for optimum plant performance there exists a best rotational speed, matrix flow length, and frontal area. In addition, for a fixed  $(\Delta P/P)_{air} + (\Delta P/P)_{gas}$  there is an optimum ratio of the hot to cold frontal areas. Therefore, for a fixed gas-turbine plant performance there must exist an optimum set of regenerator dimensions. The analysis here was made for a gas-turbine cycle of 4000 hp output with maximum cycle efficiency of 34 per cent. Fig. 11, together with the corresponding curves for other pressure losses, was used to determine the cycle design points along 34 per cent efficiency lines.

The matrix type chosen has the geometry found by Coppage (3) to have the most favorable heat transfer-friction power characteristics. This matrix consists of layers of wire screen arranged perpendicularly to the flow direction. The mesh chosen ( $20 \times 20$ ) will not give as compact a unit as closer meshes, but it probably is about the closest mesh practical for an open-cycle plant where combustion products must be passed.

Matrix data are as follows:

Mesh,  $20 \times 20$  wires per in.  $\times 0.01$  in. diam 18/8 stainless steel  
specific heat,  $c = 0.12$  Btu/lb deg F  
Heat-transfer area,  $A' = 784$  ft<sup>2</sup>/ft<sup>3</sup>  
Mass  $m' = 82.5$  pcf  
Hydraulic radius,  $r_h = 1.0625 \times 10^{-3}$  ft  
Screen thickness = 0.02 in.  
Porosity,  $\xi = 0.832$

From fig. 6 of reference (3) the heat-transfer correlation is given as

$$N_{St}N_{Pr} = 1.50(N_{Re}')^{-0.59} \quad [16]$$

and the friction-factor curve has been approximated by

$$f = 36(N_{Re}')^{-0.715} \quad [17]$$

**Rotor Type.** The rotor type assumed is shown in Fig. 12(a). Here the matrix is mounted in drum form and a section of inlet and outlet ducting rotates with the matrix. This arrangement allows for small main seal shoes placed at the ends of the drum which simplifies the equalizing of seal-shoe thrust and the allowance for thermal expansion of the rotor. It does, however, increase the displacement loss. For analysis the voids volume of matrix plus rotor is assumed to be five times the total matrix volume. The drum diameter-to-length ratio is assumed to be 1.50 to allow space within the drum for internal ducting.

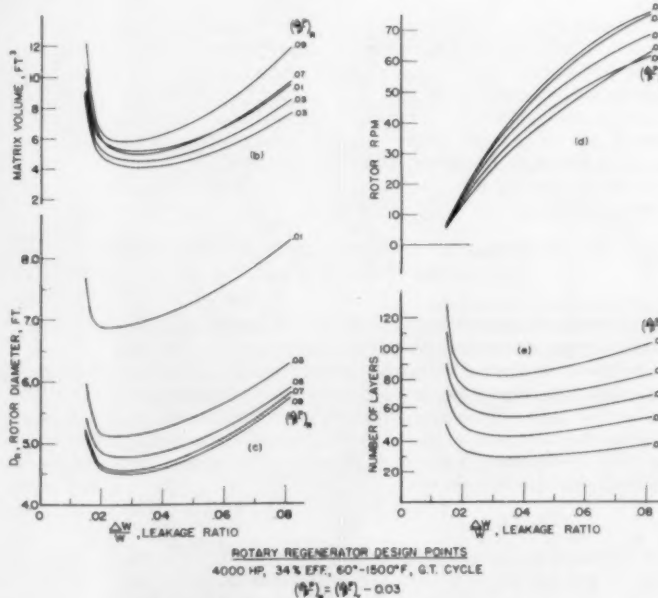
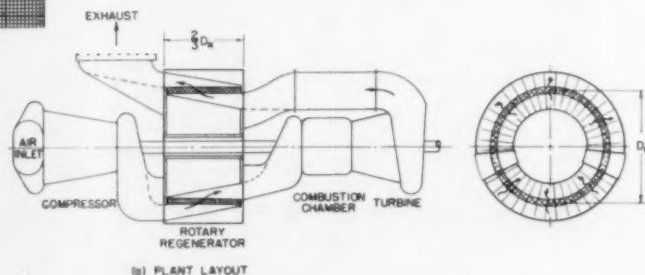


FIG. 12 ROTARY-REGENERATOR DESIGN POINTS

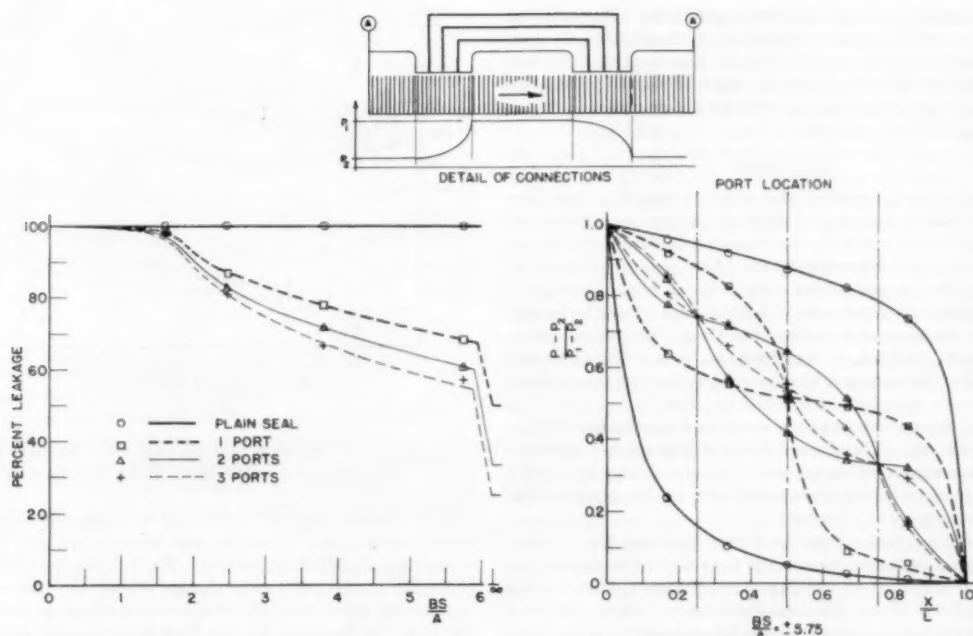


FIG. 13 TEST OF PORTED SEAL SHOES

Five rotor partitions are assumed to be under the seal shoe at one time. Each seal shoe is assumed to cover 20 deg of angle; that is, the useful matrix volume is 320/360 of the total matrix volume.

Equation [13], with the assumption of equal heat-capacity rates, has been used to determine theoretical regenerator effectiveness; the  $(\pi/\Lambda)$  term being related to leakage. Equation [14] corrects the effectiveness for leakage. The air-to-gas-side ratios at each point were chosen to give a regenerator of minimum volume.

The results of this analysis are shown by Fig. 12 plotted against  $\Delta W/W$  as a parameter. All points on these design curves define a regenerator which will give the gas-turbine plant analyzed the desired output and efficiency.

Fig. 12(b) gives the matrix volume for various pressure drops through the regenerator. A constant  $\Delta P/P = 0.03$  for cycle ducting has been assumed. A minimum matrix volume is seen to occur at  $\Delta W/W = 0.035$  and  $\Delta P/P_R = 0.03$ .

Fig. 12(c) shows the regenerator diameter which is perhaps a more significant measure than matrix volume. This minimum occurs at  $\Delta W/W = 0.03$  and  $\Delta P/P_R = 0.09$ , however, there is no significant difference in diameter between the minimum for  $\Delta P/P_R = 0.03$  and 0.09.

Fig. 12(d) gives rotor rpm which has a value of about 30 at minimum diameter.

Fig. 12(e) shows the number of screen layers required in the matrix, and is a measure of the matrix length in the flow direction (the radial direction).

With the rotor type here analyzed, the main seal-shoe length is short compared to the rotor voids volume; hence, even for clearances of 0.003 in. under the seals the leakage parameter  $BS/A$  is large. This indicates that the displacement leakage constitutes almost the entire regenerator leakage.

In conclusion, this design study of a 4000-hp gas-turbine plant incorporating a rotary regenerator shows that this type of heat exchanger can attain the required effectiveness within a small

space. Careful design of plant layout and ducting should enable this type of plant to be incorporated in a locomotive, or in small ships.

**Reduction of Leakage in Rotary Regenerator.** The amount of leakage in the rotary regenerator when applied to a gas-turbine cycle has been shown to be intimately connected with the design of the cycle components; that is, an increase of leakage at the optimum design point decreases the work output of the cycle per pound of air compressed at a greater rate than the leakage increase. Thus all the components of the cycle must accommodate an increased flow rate. To attain a given cycle efficiency, the regenerator leakage also requires an increase in regenerator effectiveness, and hence its size.

**Cross-Connected Seal Shoes.** Rotary regenerators with small clearance areas (small seal shoes) and large rotating volumes will establish large values of the leakage parameter  $BS/A$ . Large  $BS/A$  cause large differing pressure gradients under the seal-shoe pairs. The pressure gradient where the rotor rotates into the high-pressure region is low, and where it rotates out of the high-pressure region it is high. Thus, if a pipe or series of pipes were connected between ported seal shoes, the pressure gradient would be equalized between shoes at each port. It can readily be shown that as  $BS/A \rightarrow \infty$  the pressure gradients become stepped at each port, and that for this case the leakage is given by

$$\frac{W_{NET}}{BSP_2} = \frac{r-1}{N_P+1} \quad [18]$$

where  $N_P$  is the number of ports. This will give adequate results for  $BS/A > 10$  providing the cross-connecting pipes are sized to give negligible pressure drop.

Fig. 13 shows the results of an experimental test of a ported seal shoe set in the range  $0 \leq BS/A \leq 6$ . The per cent leakage curve shows that no effect is obtained below a value of  $BS/A = 1$  and then, with increased  $BS/A$  the leakage is approaching the asymptotic value given by Equation [18].

The measured pressure gradients graphically illustrate the equalization of the pressure between shoes at each port.

From Equation [18], or from Fig. 13 it is clear that the successive reduction of leakage becomes less with each added connection. Thus more than three or four cross connections between seals would not be warranted.

### CONCLUSION

In the preceding sections the rotary regenerator has been analyzed in detail with respect to its application in a gas-turbine cycle. This has shown that, even though a definite small leakage cycle. This has shown that, even though a definite small leakage between high and low-pressure sides must exist it will not detract from the size advantages of this type of heat exchanger.

An analysis and experimental investigation of seal leakage in the rotary regenerator have been described. The theoretical results are quite adequate for seal-design purposes. The method of reducing the displacement loss by cross-connecting ported seal shoes is shown and gives considerable promise.

A rotary regenerator has been sized for a specific gas-turbine-plant requirement. The effect of choice of pressure drop and leakage rate are shown by design-point curves. A suggested plant layout is presented to enable visualization of the space requirements of the rotary regenerator.

A general conclusion may be drawn that the best over-all rotary-regenerator arrangement will have a rotor containing the matrix and a system of rotating compartmented ducts leading out to small seal shoes. The seal shoes can be pressure balanced by a diaphragm or piston which can be pressurized by a port in the seal shoe itself. The location of this port along the pressure gradient will depend on the seal area and piston area. This loading force should be just sufficient to keep the seal in close contact with the rotor compartments, but not to cause excess friction. If the seals act on opposite faces of a drum-type rotor, thermal expansion of the rotor will not result in great difficulties. As such a rotor will contain large rotating volumes, a system of seal porting and cross connection should be used to minimize leakage. This general arrangement with the matrix mounted in a number of separate compartments would facilitate provision for separate removal and replacement of matrix elements.

### BIBLIOGRAPHY

- 1 "Analysis of Rotary Regenerator for Gas Turbine Applications and Investigation of Regenerator Seal Leakage," by D. B. Harper, Technical Report No. 5, M.I.T., August, 1954.
- 2 "The Periodic-Flow Regenerator—A Summary of Design Theory," by J. E. Coppage and A. L. London, Trans. ASME, vol. 75, 1953, pp. 779-787.
- 3 "Heat Transfer and Flow Friction Characteristics of Porous Media," by J. E. Coppage, Department of Mechanical Engineering, Stanford University, Stanford, Calif., Technical Report No. 16, 1952.
- 4 "Leakage Through Labyrinth Seal," by A. Egli, Trans. ASME, vol. 57, 1935, pp. 115-122.
- 5 "Effect of Rotary Regenerator Performance on Gas-Turbine-Plant Performance," by D. B. Harper and W. M. Rohsenow, Trans. ASME, vol. 75, 1953, pp. 759-765.
- 6 "The Turbo-Regenerator as Applied to Gas Turbines," by W. Hrynissak, The Institution of Mechanical Engineers, General Discussions on Heat Transfer, Section 5, 1951.
- 7 "Gas Turbine Plant Heat Exchangers," by W. M. Kays, A. L. London, and D. W. Johnson, The American Society of Mechanical Engineers, 1951.

### Discussion

W. W. CHAO.<sup>4</sup> This paper is an excellent contribution to the subject of seal leakage in rotary regenerators. In order to limit the discussion to a reasonable length, the writer would like to

<sup>4</sup>Section Supervisor, Combustor and Heat Exchanger Section, Gas Turbine Department, Scientific Laboratory, Ford Motor Company, Dearborn, Mich. Assoc. Mem. ASME.

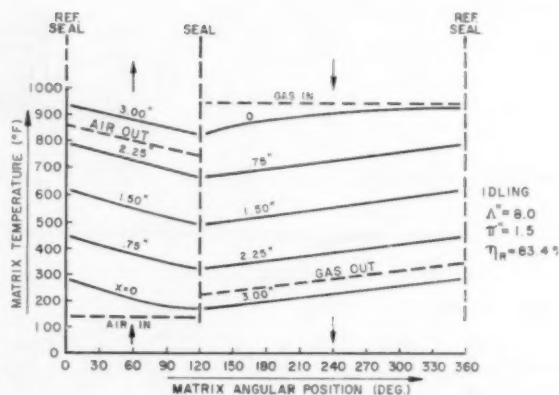


Fig. 14

comment on the subject of leakage only and also make reference to the author's earlier work<sup>5</sup> from which the present paper is abstracted.

In the actual design and operation of rotary regenerators, the running clearance  $\delta$  under the seal shoes is probably the most difficult parameter to determine. The temperature of the rotor undergoes continuous cyclic change during the operation and large temperature gradient exists across the rotor as illustrated in Fig. 14 of this discussion for the Ford experimental regenerator.<sup>6</sup> This would cause the rotor to deflect and the clearances to assume values different from those when cold. Hence the leakage parameter ( $BS/A$ ) is such an uncertain quantity that accurate calculation of seal-leakage loss and pressure distribution becomes very difficult to realize in practice.

It is rather unfortunate that the author neglected to discuss the values of flow coefficient  $\alpha$  and the labyrinth carry-over factor  $\gamma$  in his presentation of leakage experiments, since the accuracy of these values would assume first-order importance in estimating the leakage parameter ( $BS/A$ ) if the clearance is assumed to be accurately known and maintained. It should be noted that the values of carry-over factor  $\gamma$ , shown in Fig. 4(b), were based on clearances ranging from 0.015 to 0.040 in. and did not check with the test results performed with clearances ranging from 0.006 to 0.010 in. (see author's reference 4). Such discrepancy is expected to be even greater for smaller clearances at higher values of clearance to pitch ratio such as encountered in flame-trap matrix rotor seals. In such cases the use of Fig. 4(b) would result in considerable error in leakage calculations.

It would be very useful, therefore, to determine the carry-over factor from experimental results obtained for Fig. 9(a) of the paper by using the recent data on flow coefficient for staggered-type labyrinths.<sup>7</sup> In order to cover the range of clearance-to-pitch ratios of practical interest to flame-trap-type matrix-regenerator design, labyrinth spacings closer than a 3-deg interval would have to be used in the author's test rig.

The definitions of  $A$  as leakage-area constant and  $B$  as leakage displacement-area constant are rather misleading inasmuch as these parameters are dimensional and do not have the dimension of area. Furthermore, since these parameters, defined as they were by Equations [3] and [4], are based on the actual seal length,

<sup>5</sup>See author's reference (1).

<sup>6</sup>"Research and Development of an Experimental Rotary Regenerator for Automotive Gas Turbines," by W. W. Chao, Proceedings of the American Power Conference, 17th Annual Meeting, March, 1955.

<sup>7</sup>"Leakage of Air Through Labyrinth Glands of Staggered Type," by W. J. Kearton and T. H. Keh, Proceedings of The Institution of Mechanical Engineers, vol. 166, 1952, pp. 180-188.

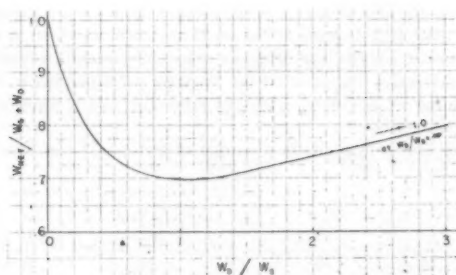


FIG. 15

the values of net leakage ( $W_{NET}/(AP_1)$ ), as shown in Figs. 6 and 7, should really be divided by a factor of 2.

It is interesting to note that the results presented by the author in Fig. 7 can be reduced to a single curve, as shown in Fig. 15, herewith, in terms of the static leakage  $W_s$  and displacement leakage  $W_d$  which are more familiar to practical designers. These leakage values can be computed readily from the following equations

$$W_s = \alpha \gamma \delta L_s \sqrt{\frac{g}{RT_m n} (p_1^2 - p_2^2)} \dots \dots \dots [19]$$

$$W_d = \frac{VN}{60} \frac{1}{RT_m} (p_1 - p_2) \dots \dots \dots [20]$$

where

$V$  = void space of entire rotor, cu ft

$N$  = rotor speed, rpm

$L_s$  = total main seal length, ft

The net leakage value under the main seals  $W_{NET}$  can now be obtained from Fig. 15, once the values for  $W_s$  and  $W_d$  are known. It should be noted that in order to evaluate the total regenerator air loss, leakages through seals other than the main seals should be accounted for and added to the value of  $W_{NET}$ . It can be shown that the ratio, ( $W_d/W_s$ ), is a function of the author's leakage parameter ( $BS/A$ ) and the air-side to gas-side pressure ratio  $r_T$

$$\frac{W_d}{W_s} = \left( \frac{BS}{A} \right) \left[ \frac{r_T - 1}{2(r_T + 1)} \right]^{1/2} \dots \dots \dots [21]$$

The foregoing appears to suggest the use of ( $W_d/W_s$ ) instead of ( $BS/A$ ) as the principal leakage parameter.

Finally, Equations [18] and [7.1]<sup>6</sup> should be corrected to give

$$\frac{W_{NET}}{BSP_1} = \frac{r_T - 1}{N_P + 1} \dots \dots \dots [22]$$

W. E. HAMMOND.<sup>8</sup> It is a well-known fact that the only serious problem in the rotary-type regenerator for gas-turbine application is that of leakage. The author is certainly to be commended for his excellent paper dealing with this subject.

The writer's company feels that, because of the many advantages of the rotary design and the marked improvement in thermal performance of a gas-turbine plant so equipped, a practical solution to the problem of leakage control will be developed.

The company has been engaged for approximately 30 years in the design and manufacture of the rotary-type air preheater. Naturally, we have been very interested in the application of this heater to the gas-turbine cycle since economically it offers much

<sup>8</sup> Chief Engineer, The Air Preheater Corporation, Wellsville, N. Y. Mem. ASME.

more attractive possibilities than the recuperative type, particularly where high effectiveness heat exchangers are required. We have come over much the same ground as has the author and are in general agreement with his results. In addition to this, we have carried on considerable research as to the cause of fires in dense matrices and believe we can avoid them. In fact, the result of this effort has resulted in the manufacture of a rotary regenerative air heater of 40 psi for the General Electric Company. This unit will be on test in the near future and a description of it is to be presented to the Society, as well as the results of tests.

STUART MISENER.<sup>9</sup> The author is to be complimented on completing a fine piece of work. His analysis presents a good picture of the leakage process between a seal shoe and a moving matrix and it is supported by good experimental verification. The problems connected with such a seal are many and the author's method of computing leakage and pressure distribution under the seal will be most helpful.

His analysis deals entirely with the case where a seal is in contact with a finely divided matrix and the movement of this matrix influences the pressure distribution experienced by the seal. He mentions briefly the possibility of designing a regenerator with another type of seal and illustrates this in Fig. 2(b). It may be helpful to consider some of the design problems encountered in connection with this other type of seal and some of the ideas that have been used to overcome these problems.

The type of regenerator in question is one in which the rotor is divided into a number of segments separated by radial dividers. In such a machine the sealing usually takes place between the dividers and a seal shoe. In our particular case, the flow path was annular and was divided into 24 segments, each segment being separated from the others by a radial wall. The ends of the rotor constituted a rotating seal which in turn mated with the stationary seal over a portion of the annulus. This stationary seal thus has two circumferential portions and two radial portions as can be seen in the exploded view, Fig. 16 of this discussion.

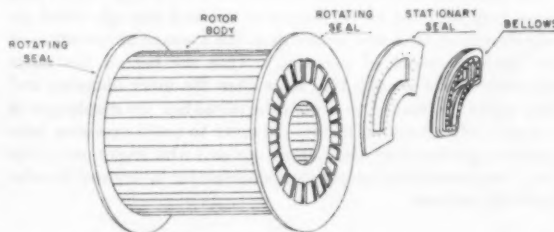


FIG. 16 SCHEMATIC EXPLODED VIEW OF SEAL ARRANGEMENT

The leakage through the circumferential portion of these seals is reasonably predictable and in our particular case, with about 60 psi inside and about 15 psi pressure outside the seal, the flow was laminar and subsonic. As a matter of interest, the leakage path was approximately  $2\frac{3}{4}$  in. long and the clearance was in the neighborhood of 0.002 in.

It is the radial portions of this seal, however, that might be of greatest interest. These, of course, are sealed against the radial dividing walls of the rotor and as the rotor moves, these dividing walls sweep across the face of the stationary seal. On one side of this dividing wall the pressure is approximately 60 psi and on the other side approximately 15 psi. The result, of course, is that the force, tending to lift the stationary seal away from the rotor, varies with the position of the divider on the face of the stationary

<sup>9</sup> Carrier Corporation, Syracuse, N. Y.

seal. This means that the seal has to be loaded to counteract the largest pressure encountered or provided with some means of automatically balancing this variable load.

In order to do this we installed a series of three bellows with accompanying mechanical linkages on the back side of the radial portion of the seal. Each of these bellows was connected through a passage in the seal to a different point on the sealing surface. The net result was that as the radial dividing wall of the rotor swept across the radial portion of the stationary seal, it exposed these holes in sequence to the high-pressure air region. As each hole was exposed, the bellows connected to it was activated thus applying an increased force to the rear of the seal. In this way we provided a three-step balancing force for the continuously varying lifting force on the face of the seal. As will be realized, space on the back of the seal is limited and we were unable to work in three bellows of the desired size. Thus we had to settle for smaller bellows and a linkage supplied the necessary mechanical advantage. This linkage engaged a fulcrum on the end of the regenerator casing.

Our work is far from complete. However, results thus far indicate that this arrangement provides the desirable balancing forces and keeps the seal from lifting off the rotor, at the same time greatly reducing the loading from what it would otherwise be.

Another design problem that arose in the course of our work has to do with thermal deformations in the stationary and rotating seals of the regenerator. It will be noted from Fig. 16 that the passages containing the hot gases are completely surrounded by the metal of the seals which is in turn surrounded by areas containing cooler air. Thus there is a continuous flow of heat outward from the gas passages and unless special precautions are taken serious distortions could result. To understand this more clearly, consider for a moment an annular ring of metal similar to a washer. If the outer diameter of this ring is cold and the inner diameter is hot, the ring cannot stay flat but must take on a conical or perhaps a twisted shape and, of course, such deformation of the seal must be avoided at all costs.

In order to prevent any such distortion we first provided passages very near the circumference of the seal through which air was circulated that was hotter than the average temperature of the inner diameter of the seal. Thus we heated the outer diameter of our annular ring more than the inner diameter and this, naturally, tended to stretch the metal like the diaphragm of a drum and hence keep it flat. In order to avoid excessive temperature gradients we also backed our seal with high-purity copper. As a result the temperature distribution in our seal is satisfactorily uniform.

P. T. VICKERS.<sup>10</sup> The author is to be congratulated not only for a splendid piece of research work but also for the fine manner in which he has presented it. This is an excellent example of one of the many basic research projects which are being carried out by our universities and which are applicable to current or soon-to-be current problems in industry. Too often, engineers in industry are so involved in the details of day-to-day problems that they fail to study the basic concepts of their ultimate goal.

In this instance, Professor Roshenow and the author were farsighted enough to see that if the rotary regenerator was to be practicable in the gas-turbine application, the seal leakage had to be minimized. Before one can hope to minimize the leakage, it is first necessary to determine the parameters affecting leakage. Then, if possible, study experimentally the relative effect of these parameters, thereby indicating what the designer should strive for in design of a seal for a rotary regenerator.

<sup>10</sup> Research Engineer, General Motors Research Laboratories, Detroit, Mich. Assoc. Mem. ASME.

This is the first time any work has been done toward the study of the basic seal problem. The usual approach has been to work out a seal for a given type of rotary-regenerator matrix with which an organization happens to be working at a particular time. Here, however, is a paper written about sealing rotary regenerators in its basic elements.

Could the author clarify a couple of questions? In Equation [11]

$$\frac{1}{1 - \frac{W_{D1}}{W_T}} - \frac{1}{1 - \frac{W_{D1}}{W_T} \frac{r}{r_i}} - \ln \frac{1 - \frac{W_{D1}}{W_T} \frac{r}{r_i}}{1 - \frac{W_{D1}}{W_T}} = \left( \frac{BS}{A} \right)^2 \frac{x}{L}$$

$W_{D1}$  is described as the displacement leakage and is often called "carry-over" leakage. Numerically, this is equal to the product of the density of the air entrained in the matrix and the rate at which the void volume is passing through the seal from the high-pressure side to the low-pressure side. In the case of the seal where the matrix rotates from the low-pressure side to the high-pressure side, the displacement carry-over is minus (or negative). Thus Equation [11] would then be written

$$\frac{1}{1 + \frac{W_{D1}}{W_T}} - \frac{1}{1 + \frac{W_{D1}}{W_T} \frac{r}{r_i}} - \ln \frac{1 + \frac{W_{D1}}{W_T} \frac{r}{r_i}}{1 + \frac{W_{D1}}{W_T}} = \left( \frac{BS}{A} \right)^2 \frac{x}{L}$$

where  $W_{D1}$  is defined as the "carry-over" leakage. Could the author tell us if this conclusion is valid?

In using these equations for design, one must be able to evaluate all of the terms in the dimensionless parameter  $(BS/A)$ .  $B$  is a function of geometry and fluid properties,  $S$  is a function of speed and geometry. However,  $A$  which is equal to

$$\alpha \gamma \delta L_s \left( \frac{2g}{RTn} \right)^{1/2}$$

is not only a function of geometry and fluid properties but also a function of labyrinth-flow coefficient and velocity carry-over factor. The author cites Egli's work on carry-over factor, which is completely defined and in a usable form. The flow coefficient for labyrinth seals is not so well known. Could the author direct us to a reliable source of information on this subject?

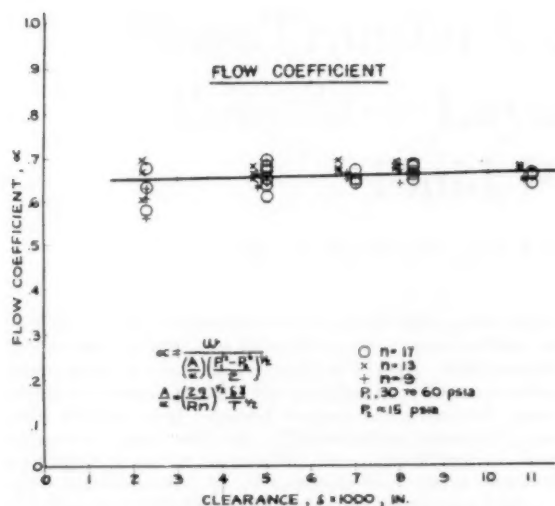
Incidentally, this leakage theory has been tried on some test results with a practical regenerator. It can be affirmed that the theory does work in practice.

#### AUTHOR'S CLOSURE

The discussors of this paper are to be commended for greatly adding to its scope and general interest. The following comments have been limited to particular items for reasons of space:

In W. W. Chao's discussion the carry-over factor  $\gamma$  is considered. As mentioned, the curves of Fig. 4(b) were used to determine  $\gamma$  in a range not verified by reference (4). However, preliminary experimental tests were carried out that are not reported here or in reference (1). In these tests  $\gamma$  was taken from Fig. 4(b) for a range of  $\delta/\Delta$  and  $n$ , and the flow coefficient  $\alpha$  calculated from the experimental results. These results are shown by Fig. 17. If we now assume  $\alpha$  constant we could use these same results as an experimental determination of  $\gamma$  for the specified conditions. The spread of the points increases at the smaller clearances due primarily to increasing error in clearance measurement.

With regard to Figs. 6 and 7, if the length of the seal  $L$ , occurring in the parameter  $A$  is taken as the total length of both seal shoe sets then in fact the net leakage  $(W_{NET}/AP_2)$  should be divided

FIG. 17 FLOW COEFFICIENT; SPACING,  $\Delta = 0.2$  INCHES

by a factor of 2. However, all other figures and equations except Equation [18] are based on considering each seal set inde-

pendently. That is,  $W_{NET}$  of Figs. 6 and 7 equals  $W_T$  (positive seal) plus  $W_T$  (negative seal) where  $L_s$  is intended to be the length of the clearance on a single seal set.

Fig. 15 is a useful curve for designers and is certainly easy to use. However, use of the factor  $W_s$  of Equation [19] does not give a true picture of the fundamental form of the leakage. This is because  $W_s$  is only a correct figure for seal clearance leakage in the case of the stationary rotor (considering, of course, the rotor type used in the analysis). The actual clearance leakage in fact becomes less as rotational speed increases due to changing pressure gradients. Theoretically, at infinite rotor speed there is zero clearance leakage and of course infinite displacement leakage.

Mr. Misener's discussion gives a very interesting coverage of the more practical problems encountered in designing an actual rotary regenerator.

P. T. Vicker's discussion brings out the question of the minus (—) signs in Equation [11] when it is used for study of the negative rotation seal. The signs are best left as shown and a negative value of rotational velocity  $S$  and hence  $W_D$ , introduced, which is the conclusion this discussor reached. In the solution of this equation the value of  $W_T$  changes from positive to negative as  $(BS/A)$  increases. Thus if the sign is arbitrarily changed in the written equation confusion may result although essentially the suggestion is correct.

The flow coefficient and the carry-over factor have been reviewed earlier in this discussion.

THE  
JOURNAL  
OF  
THE  
ROYAL  
ANTHROPOLOGICAL  
INSTITUTE  
OF GREAT  
BRITAIN  
AND IRELAND  
VOLUME  
LXXV  
PART I  
1945

CONTENTS  
PAGES  
The Journal of the Royal Anthropological Institute of Great Britain and Ireland, Volume LXXV, Part I, 1945  
1-100

THE  
JOURNAL  
OF  
THE  
ROYAL  
ANTHROPOLOGICAL  
INSTITUTE  
OF GREAT  
BRITAIN  
AND IRELAND  
VOLUME  
LXXV  
PART II  
1945

CONTENTS  
PAGES  
The Journal of the Royal Anthropological Institute of Great Britain and Ireland, Volume LXXV, Part II, 1945  
101-200

THE  
JOURNAL  
OF  
THE  
ROYAL  
ANTHROPOLOGICAL  
INSTITUTE  
OF GREAT  
BRITAIN  
AND IRELAND  
VOLUME  
LXXV  
PART III  
1945

CONTENTS  
PAGES  
The Journal of the Royal Anthropological Institute of Great Britain and Ireland, Volume LXXV, Part III, 1945  
201-300

THE  
JOURNAL  
OF  
THE  
ROYAL  
ANTHROPOLOGICAL  
INSTITUTE  
OF GREAT  
BRITAIN  
AND IRELAND  
VOLUME  
LXXV  
PART IV  
1945

CONTENTS  
PAGES  
The Journal of the Royal Anthropological Institute of Great Britain and Ireland, Volume LXXV, Part IV, 1945  
301-400

THE  
JOURNAL  
OF  
THE  
ROYAL  
ANTHROPOLOGICAL  
INSTITUTE  
OF GREAT  
BRITAIN  
AND IRELAND  
VOLUME  
LXXV  
PART V  
1945

CONTENTS  
PAGES  
The Journal of the Royal Anthropological Institute of Great Britain and Ireland, Volume LXXV, Part V, 1945  
401-500

# Mass-Transfer Cooling in a Laminar Boundary Layer With Constant Fluid Properties<sup>1</sup>

By J. P. HARTNETT<sup>2</sup> AND E. R. G. ECKERT,<sup>3</sup> MINNEAPOLIS, MINN.

Mass transfer or transpiration cooling offers great possibilities for maintaining tolerable surface temperatures on high-speed aircraft or on turbine blades. The present study is concerned with the prediction of heat transfer, skin friction, and required coolant flows for such transpiration-cooled surfaces. The solutions presented were collected in so far as possible from the literature, and were supplemented by new calculations where required for the case of the flat plate and plane stagnation flows.

## NOMENCLATURE

The following nomenclature is used in the paper:

- $C_{f,x}$  = local skin-friction coefficient
- $c_p$  = specific heat at constant pressure
- $f$  = dimensionless stream function, defined in Equations [8]
- $g_c$  = conversion factor
- $h_{fg}$  = latent heat of evaporation
- $h_{sg}$  = latent heat of sublimation
- $h_x$  = local heat-transfer coefficient, defined in Equation [26]
- $k$  = thermal conductivity of fluid
- $\dot{m}_1$  = mass-flow rate of coolant
- $p$  = static pressure
- $r$  = recovery factor, defined in Equation [25]
- $T$  = temperature
- $u$  = velocity parallel to surface
- $v$  = velocity normal to surface
- $w$  = mass fraction; ratio of partial density to total density
- $x$  = distance along surface
- $y$  = distance normal to surface
- $D$  = coefficient of diffusion
- $\alpha$  = thermal diffusivity
- $\nu$  = kinematic viscosity
- $\mu$  = absolute viscosity
- $\rho$  = density
- $\eta$  = dimensionless distance from wall, defined in Equations [8]
- $\theta$  = dimensionless temperature profile, defined in Equations [8]
- $\Phi$  = dimensionless mass fraction profile defined in Equations [8]
- $Nu_x$  = local Nusselt number  $h_x x/k$

- $Re_x$  = local Reynolds number  $u_\infty x/\nu$
- $Pr$  = Prandtl number  $c_p \mu/k = \nu/\alpha$
- $Sc$  = Schmidt number  $\nu/D$

## Subscripts

- $e$  = cooling gas entering porous wall
- $\infty$  = free stream
- $w$  = wall
- $t$  = total
- $r$  = recovery
- 1 = diffusing gas
- 2 = main flow gas (air)

## INTRODUCTION

The maintenance of tolerable surface temperatures on high-speed aircraft or on turbine blades presents a very challenging problem. One method which appears to have great promise is the use of transpiration or mass-transfer cooling. Such a cooling process can be realized, for example, by the use of porous surfaces through which a coolant is forced. The coolant may be a gas such as air, helium, or hydrogen, or it may be a liquid such as liquid oxygen. Mass-transfer cooling could also be obtained by fabricating the surface of the aircraft of a material which will evaporate under the influence of the hot boundary layer and in this way apply effective cooling by its heat of vaporization.

This study is concerned with the prediction of the heat transfer, skin friction, and required coolant flows for such transpiration-cooled surfaces. A logical preliminary approach is the examination of the laminar boundary-layer equations of momentum, diffusion, and energy for the case where the properties of the gas diffusing through the wall are identical with the properties of the free-stream fluid. Such a constant-properties analysis could be applied immediately to two-component systems when the properties of the two components are not too different. More important, however, this preliminary analysis may indicate basic behavior patterns of the boundary-layer solutions under conditions of simultaneous mass and heat transfer. Accordingly, these solutions were collected in so far as available in the literature, were supplemented by new calculations where required, and are presented herein for the case of the flat plate and the plane stagnation flow.

In addition to solutions for fluid injection from the wall, solutions of the energy equations also are presented for the case of boundary-layer suction over a range of suction values for both the flat plate and the plane stagnation flow. Such solutions are of value since the use of suction for boundary-layer control is quite common. Moreover, these suction results may be applied to the mass-transfer case where icing of the surface occurs.

The recovery factor is evaluated for the flat plate and is found to be sensitive to both fluid injection and to suction. With this recovery-factor information the heat-transfer results can be applied to high velocities where viscous dissipation is important.

<sup>1</sup> Publication of the Heat Transfer Laboratory, University of Minnesota.

<sup>2</sup> Assistant Professor of Mechanical Engineering, University of Minnesota. Assoc. Mem. ASME.

<sup>3</sup> Professor of Mechanical Engineering, University of Minnesota. Mem. ASME.

Contributed by the Heat Transfer Division and presented at the Diamond Jubilee Annual Meeting, Chicago, Ill., November 13-18, 1955, of THE AMERICAN SOCIETY OF MECHANICAL ENGINEERS.

NOTE: Statements and opinions advanced in papers are to be understood as individual expressions of their authors and not those of the Society. Manuscript received at ASME Headquarters, August 15, 1955. Paper No. 55-A-108.

## ANALYSIS

For the case of two-dimensional steady laminar flow with negligible dissipation of an incompressible fluid with constant properties, the boundary-layer equations of continuity, momentum, diffusion, and energy may be written as follows:

## Continuity

$$\frac{\partial u}{\partial x} + \frac{\partial v}{\partial y} = 0 \quad [1]$$

## Momentum

$$\rho u \frac{\partial u}{\partial x} + \rho v \frac{\partial u}{\partial y} = \mu \frac{\partial^2 u}{\partial y^2} - \frac{dp}{dx} \quad [2]$$

## Diffusion

$$u \frac{\partial w_1}{\partial x} + v \frac{\partial w_1}{\partial y} = D \frac{\partial^2 w_1}{\partial y^2} \quad [3]$$

## Energy

$$u \frac{\partial T}{\partial x} + v \frac{\partial T}{\partial y} = \alpha \frac{\partial^2 T}{\partial y^2} \quad [4]$$

## Boundary Conditions:

## Momentum

$$\left. \begin{aligned} u &= 0 & \text{at} & y = 0 \\ v &= v_w(x) & \text{at} & y = 0 \\ u &= u_\infty & \text{as} & y \rightarrow \infty \end{aligned} \right\} \quad [5]$$

## Diffusion

$$\left. \begin{aligned} w_1 &= w_{1w} & \text{at} & y = 0 \\ w_1 &= w_{1\infty} & \text{as} & y \rightarrow \infty \\ v_{\text{air}} &= 0 & \text{at} & y = 0 \end{aligned} \right\} \quad [6]$$

(i.e., no net flow of boundary-layer air into the porous wall surface.)

## Energy

$$\left. \begin{aligned} T &= T_w & \text{at} & y = 0 \\ T &= T_\infty & \text{as} & y \rightarrow \infty \end{aligned} \right\} \quad [7]$$

It may be noted that eight boundary conditions are listed, whereas a study of the differential equations indicates that only seven conditions are required. It will be demonstrated that this system actually contains only seven independent parameters; however, for clarity of presentation it was found to be more desirable to introduce the boundary conditions as shown.

A few words regarding the last boundary condition in Equations [6], i.e.,  $v_{\text{air}} = 0$ , may be helpful. For evaporation or sublimation from a solid surface this condition is self-evident. It is, however, believed that it also describes best the actual conditions occurring on a porous wall through which a cooling gas is ejected. In general, the mass fraction of the coolant gas will be less than unity at the wall surface, while somewhere within the wall surface practically pure coolant gas will exist with a mass fraction of unity. This means that a mass-fraction (or concentration) gradient of the diffusing cooling gas occurs within the wall and correspondingly a mass-fraction gradient of the air exists. As a consequence of this gradient a diffusive flow of air into the wall must occur. However, this diffusive flow of air into the wall is just balanced by the convective flow of coolant gas toward the wall surface when the net flow of air in the wall and through the surface is zero, Equations [6].

The foregoing equations may be transformed to a more usable form by introducing the stream function

$$\Psi, \left( u = \frac{\partial \Psi}{\partial y}, v = -\frac{\partial \Psi}{\partial x} \right)$$

as well as the following substitutions

$$\left. \begin{aligned} f &= \frac{\Psi}{\sqrt{\mu x u_\infty}} \\ \eta &= \frac{y}{x} \sqrt{\frac{u_\infty x}{\nu}} \\ \Phi &= \frac{w_{1w} - w_1}{w_{1w} - w_{1\infty}} \\ \vartheta &= \frac{T - T_w}{T_\infty - T_w} \end{aligned} \right\} \quad [8]$$

In addition, the free-stream velocity  $u_\infty$ , just outside the boundary layer, is assumed to vary according to the law

$$u_\infty = Ax^m \quad [9]$$

Such a velocity is, for instance, found in two-dimensional flow over an infinite wedge of angle  $\beta\pi$  where

$$\beta = \frac{2m}{m+1} \quad [10]$$

The foregoing substitutions, with the assumption that  $f$ ,  $\Phi$ , and  $\vartheta$  are functions of  $\eta$  only (also the temperature  $T_w$  and mass-fraction  $w_{1w}$  are constant along the surface, i.e., independent of  $x$ ) yield the following ordinary differential equations for the constant-property momentum, diffusion, and energy equations:

## Momentum

$$\frac{d^3 f}{d\eta^3} + \frac{m+1}{2} f \frac{d^2 f}{d\eta^2} - m \left[ \left( \frac{df}{d\eta} \right)^2 - 1 \right] = 0 \quad [11]$$

## Diffusion

$$\frac{d^2 \Phi}{d\eta^2} + \frac{m+1}{2} \text{Sc} f \frac{d\Phi}{d\eta} = 0 \quad [12]$$

## Energy

$$\frac{d^2 \vartheta}{d\eta^2} + \frac{m+1}{2} \text{Pr} f \frac{d\vartheta}{d\eta} = 0 \quad [13]$$

## Boundary conditions

$$\left. \begin{aligned} \frac{df}{d\eta} &= 0 & \text{at} & \eta = 0 \\ \frac{df}{d\eta} &= 1 & \text{as} & \eta \rightarrow \infty \\ f_w &= -\frac{2}{m+1} \frac{v_w}{u_\infty} \sqrt{\text{Re}_x} & \text{at} & \eta = 0 \end{aligned} \right\} \quad [14]$$

$$\left. \begin{aligned} \Phi &= 0 & \text{at} & \eta = 0 \\ \Phi &= 1 & \text{as} & \eta \rightarrow \infty \end{aligned} \right\} \quad [15]$$

$$\left. \begin{aligned} \vartheta &= 0 & \text{at} & \eta = 0 \\ \vartheta &= 1 & \text{as} & \eta \rightarrow \infty \end{aligned} \right\} \quad [16]$$

It follows from the boundary conditions that the normal ve-

locity at the wall must either be zero or it must vary as  $\sqrt{u_\infty/x}$  to comply with the assumption that  $f$  is a function only of  $\eta$ .

For a constant-property fluid as considered here, the momentum equation may be solved for a range of values of  $f_w$  independently of the diffusion and energy equations. Such solutions may then be utilized to obtain the solutions of the energy and diffusion equation by direct integration.

Inspection of the differential equations and the boundary conditions shows immediately that solutions of the diffusion equation for  $\Phi$  are also solutions of the energy equation in  $\vartheta$  when the Schmidt number in the diffusion equation is equal to the Prandtl number in the energy equation. There is one major difference, however, in that the boundary conditions for the diffusion equation are not yet completely satisfied, since the boundary condition  $v_{air} = 0$  at  $y = 0$  has not yet been fulfilled. This may be done as follows: The velocity of the air is composed of a diffusive velocity

$$\left( -\frac{D}{w_2} \frac{\partial w_2}{\partial y} \right)$$

and a convective velocity  $v$

$$v_{air} = -\frac{D}{w_2} \frac{\partial w_2}{\partial y} + v \dots \dots \dots [17]$$

As explained previously, this velocity vanishes within the wall and this condition applies up to the wall surface.

Therefore, for  $y = 0$

$$v_{air} = 0 = -\left( \frac{D}{w_2} \frac{\partial w_2}{\partial y} \right)_w + v_w \dots \dots \dots [18]$$

$$v_w = \left( \frac{D}{w_2} \frac{\partial w_2}{\partial y} \right)_w \dots \dots \dots [18a]$$

The resulting convective velocity at the wall surface  $v_w$  is the velocity associated with the momentum equation and therefore Equation [18a] gives a relationship between the mass fraction at the wall and the blowing value at the wall  $f_w$ . The following relationships may be used to modify Equation [18a]

$$\left. \begin{aligned} w_1 + w_2 &= 1 \\ \frac{\partial w_1}{\partial y} &= -\frac{\partial w_2}{\partial y} \end{aligned} \right\} \dots \dots \dots [19]$$

There results

$$v_w = -\frac{D}{1-w_{1w}} \left( \frac{\partial w_1}{\partial y} \right)_w \dots \dots \dots [20]$$

By rearranging, after introducing the variable  $\eta$  and the Schmidt number  $\nu/D$ , the final relationship is obtained

$$\frac{1-w_{1w}}{w_{1w}-w_{1\infty}} = -\frac{\left( \frac{d\Phi}{d\eta} \right)_w}{Sc \left( \frac{m+1}{2} f_w \right)} \dots \dots \dots [21]$$

Thus we find that a definite relationship exists between the blowing value  $f_w$  and the values  $w_{1w}$  and  $w_{1\infty}$  of the mass fraction of the diffusing gas at the wall surface and in the free stream; consequently, we are not free to choose arbitrarily all three values  $f_w$ ,  $w_{1w}$ , and  $w_{1\infty}$ . This then is the relationship which demonstrates that the boundary conditions shown in Equations [5], [6], and [7] contain only seven independent conditions. For example, if the mass fraction of the diffusing gas is zero in the free stream ( $w_{1\infty} =$

0), as is generally the case in transpiration cooling, we are free to prescribe either the blowing rate  $f_w$  or the mass fraction at the wall.

The total mass flow of the diffusing medium away from the wall is composed not only of the quantity being carried away by the convective velocity  $v_w$  but also of the quantity being removed by diffusion. The total mass flow may be obtained from the following expression

$$\begin{aligned} \dot{m}_1 &= \rho_{1w} v_{1w} = \rho_{1w} \left( -\frac{D}{w_1} \frac{\partial w_1}{\partial y} \right)_w + \rho_{1w} v_w \\ &= \rho_{1w} \left( -\frac{D}{w_1(1-w_1)} \frac{\partial w_1}{\partial y} \right)_w \dots \dots \dots [22] \end{aligned}$$

This mass-flow rate also must be equal to the product of the convective velocity and the total density and by noting Equation [20] and the definition of the mass fraction, it is seen that Equation [22] reduces to the following

$$\dot{m}_1 = \rho_{1w} v_{1w} = \rho v_w \dots \dots \dots [23]$$

## RESULTS

**Flat Plate.** For flow with constant velocity  $u_\infty$  the value  $m$  is zero according to Equation [9]. The two-dimensional steady-state solutions of the boundary-layer momentum equation for a constant-property fluid have been reported by references (1, 2, 5, 13)<sup>4</sup> and recently in more detail by Emmons and Leigh (9).

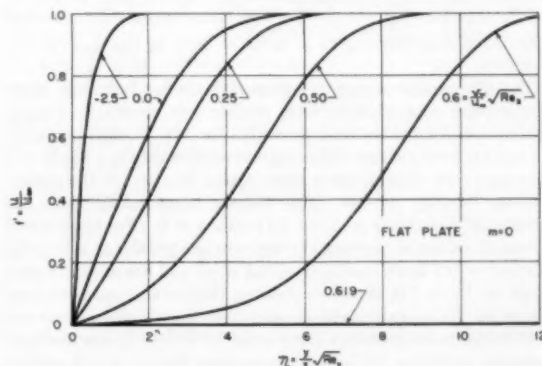


FIG. 1 DIMENSIONLESS VELOCITY PROFILES  $u/u_\infty$  FOR LAMINAR FLOW OVER FLAT PLATE FOR A RANGE OF VALUES OF THE INJECTION PARAMETER  $\left( \frac{v_w}{u_\infty} \right) \sqrt{Re_x}$

They are shown in Figs. 1 and 2. In Fig. 1, the velocity profile is shown for a range of values of the mass-transfer parameter  $(v_w/u_\infty) \sqrt{Re_x}$ . Positive values of this parameter indicate "blowing" or fluid injection while negative values indicate "suction" or mass transfer toward the wall which would occur, for example, in the case of icing. Two important conclusions may be drawn from these profiles. The first conclusion is that blowing destabilizes the boundary-layer flow along a flat plate as evidenced by the S-shaped velocity profiles. As reported by Emmons and Leigh (9), at a relatively small value of  $(v_w/u_\infty) \sqrt{Re_x}$  (i.e., 0.619) boundary-layer equations yield a solution in which  $\partial u/\partial y = 0$  at  $y = 0$  and  $u = 0$  for any finite  $y$ . The velocity boundary is completely lifted off the plate—it is "blown away." This indicates obviously that the boundary-layer equation does not describe properly the actual conditions in laminar flow as the blowing velocity approaches the value  $0.619 u_\infty / \sqrt{Re_x}$ .

<sup>4</sup> Numbers in parentheses refer to the Bibliography at the end of the paper.

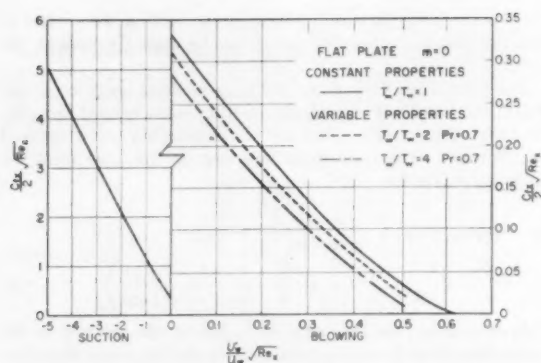


FIG. 2 DIMENSIONLESS LOCAL SKIN-FRICTION VALUES  $\frac{C_{f,x}}{2} \sqrt{Re_x}$  FOR LAMINAR FLOW OVER FLAT PLATE AS A FUNCTION OF INJECTION

$$\text{PARAMETER } \frac{v_w}{u_\infty} \sqrt{Re_x}$$

The dimensionless skin-friction parameter  $(C_{f,x}/2) \sqrt{Re_x}$  which is given by the slope of the dimensionless velocity profile at the wall is shown in Fig. 2. In the case of suction, this coefficient increases from the well-known Blasius value of 0.332 to a value greater than 5 for a suction parameter of  $(v_w/u_\infty) \sqrt{Re_x} = -5.0$ . For blowing, the skin-friction value continually decreases with increasing blowing to a value of zero at  $(v_w/u_\infty) \sqrt{Re_x} = 0.619$ .

The dimensionless constant-property laminar boundary-layer temperature and mass-fraction profiles are shown in Fig. 3. The temperature profiles are presented for two Prandtl numbers, 0.7 and 1.0, over a range of blowing and suction values. For  $Pr = 1$  they are in the dimensionless presentation identical to the dimensionless velocity profiles. This follows immediately from the differential Equations [11] and [13] with  $m = 0$ . For suction and for small values of blowing the temperature profiles at a Prandtl number = 0.7 have a smaller initial slope and are always below those for  $Pr = 1.0$ , therefore yielding thicker thermal-boundary layers for the lower Prandtl number. At high blowing rates the wall-temperature gradients are greater for  $Pr = 0.7$ , but the temperature profile for  $Pr = 0.7$  crosses over the  $Pr = 1.0$  profiles again yielding thicker thermal-boundary layers for the lower Prandtl numbers.

The dimensionless mass-fraction profiles are also represented in Fig. 3. They are identical with the dimensionless temperature profiles except that now the profiles apply to Schmidt numbers of 0.7 and 1.0. However, as pointed out in the analysis, there is a relationship between the mass fraction at the wall and the blowing rate as given by Equation [21]. As a result, if the free-stream mass fraction is assumed to be zero each mass-fraction profile pertains to a particular value of the mass fraction of the diffusing gas at the wall  $w_{1,w}$ . These values are shown on the curves in parentheses. (For example, the mass-fraction curve corresponding to a blowing value of 0.25 for a Schmidt number of 0.7 is valid for a  $w_{1,w} = 0.513$ , if  $w_{1,\infty} = 0$ .) No value of  $w_{1,w}$  is shown for the suction profile at the assumed value  $w_{1,\infty} = 0$ , since this obviously has no meaning physically. If however, the value of  $w_{1,\infty}$  is specified as some finite value, the value of  $w_{1,w}$  for which the profile is valid may be calculated from Equation [21].

The dimensionless heat-transfer coefficient  $Nu_x/\sqrt{Re_x}$  as well as the value of the slope of the mass-fraction profiles at the wall are shown in Fig. 4 for Prandtl (or Schmidt) numbers of 0.7 and 1.0. For the solid wall the value of  $Nu_x/\sqrt{Re_x}$  is 0.332 for  $Pr = 1.0$  and 0.293 for  $Pr = 0.7$ . These values increase with increasing

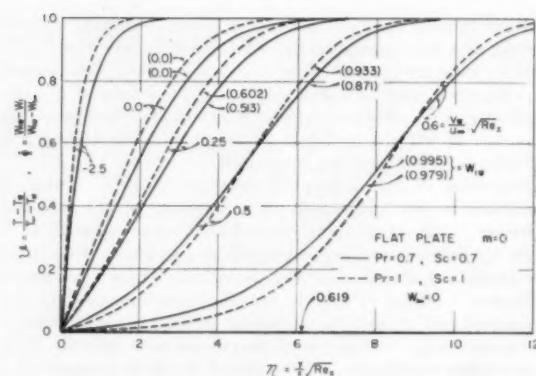


FIG. 3 DIMENSIONLESS TEMPERATURE PROFILES AND MASS-FRACTION PROFILES FOR LAMINAR FLOW OVER FLAT PLATE FOR A RANGE OF VALUES OF INJECTION PARAMETER  $\frac{v_w}{u_\infty} \sqrt{Re_x}$  FOR PRANDTL NUMBERS OF 1.0 AND 0.7

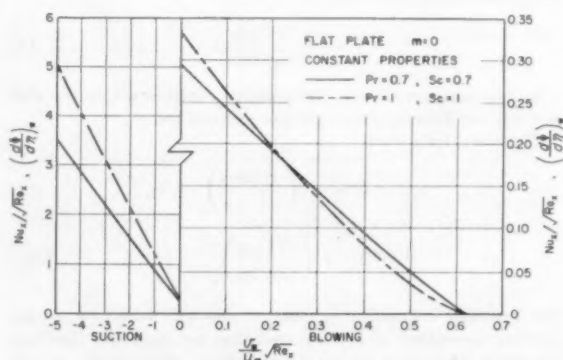


FIG. 4 DIMENSIONLESS LOCAL HEAT-TRANSFER COEFFICIENTS  $Nu_x/\sqrt{Re_x}$  AND LOCAL MASS-TRANSFER COEFFICIENTS  $(\frac{d\Phi}{d\eta})_w$  FOR LAMINAR FLOW OVER FLAT PLATE AS A FUNCTION OF INJECTION PARAMETER  $\frac{v_w}{u_\infty} \sqrt{Re_x}$

suction (i.e., with increasing mass transfer toward the wall surface from the free stream), with the influence of Prandtl number being greatest at the highest value. In the case of blowing the  $Nu_x/\sqrt{Re_x}$  curves for the two Prandtl numbers cross at a value of  $(v_w/u_\infty) \sqrt{Re_x}$  equal to 0.25 and at this value the dimensionless heat-transfer coefficients are equal. At smaller mass transfer rates  $[(v_w/u_\infty) \sqrt{Re_x}]$  less than 0.25 the higher Prandtl number demonstrates the higher coefficient while at higher blowing rates (greater than 0.25), the lower Prandtl number of 0.7 shows the higher coefficient. Both curves coincide at the limiting blowing value of 0.619 resulting in a zero value for the heat transfer and for the diffusive mass transfer at this condition.

The preceding discussion on the dimensionless heat-transfer coefficient also applies to the mass transfer, where the Prandtl number is now replaced by the Schmidt number and the  $Nu_x/\sqrt{Re_x}$  parameter by

$$\left(\frac{d\Phi}{d\eta}\right)_w$$

The mass-fraction profiles for a free stream free of the diffusing

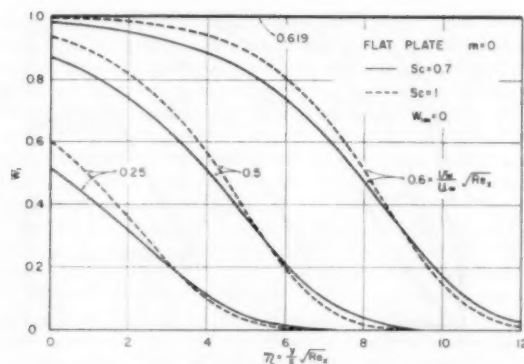


FIG. 5 MASS-FRACTION PROFILES FOR LAMINAR FLOW OVER FLAT PLATE FOR SEVERAL DIFFERENT INJECTION RATES  $w_{1\infty} = 0$

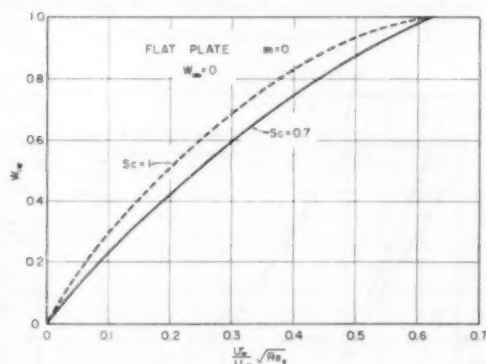


FIG. 6 MASS-FRACTION VALUES AT WALL SURFACE FOR LAMINAR FLOW OVER FLAT PLATE AS A FUNCTION OF INJECTION PARAMETER  $\frac{U_\infty}{U_w} \sqrt{Re_x}$ , FOR  $w_{1\infty} = 0$

gas ( $w_{1\infty} = 0$ ) are shown in Fig. 5 over a range of blowing values for Schmidt numbers of 0.7 and 1.0. The effect of increasing the blowing rate for a constant Schmidt number is to increase the wall mass fraction for a given mass transfer or blowing rate. The Schmidt number of 0.7, in general, demonstrates a thicker boundary layer than the unity Schmidt number, although the higher Schmidt number has the higher value of the mass fraction at the wall. The limiting case where the diffusion boundary layer lifts off the wall and where the mass fraction  $w_{1\infty}$  becomes unity is seen at the blowing value of 0.619.

Fig. 6 emphasizes the interrelationship between the mass fraction at the wall and the blowing parameter for the usual case where the main flow is free of the diffusing coolant gas. It is apparent from this figure that at a given Schmidt number setting the blowing rate also fixes the value of the mass fraction at the wall.

The effects of a variation of properties with temperature have been studied in reference (2) for a Prandtl number 0.7. For these calculations it was assumed that the properties vary proportionally to a power of the absolute temperature and the following exponents were chosen: 0.7 for viscosity, 0.85 for heat conductivity, 0.19 for specific heat, and  $-1$  for density. These results also are shown in Figs. 7 and 2 with the physical properties evaluated at the wall temperature. In general, the effect of increasing  $T_w/T_\infty$  is to decrease the skin friction and the heat transfer, with the skin friction exhibiting greater changes particularly at low

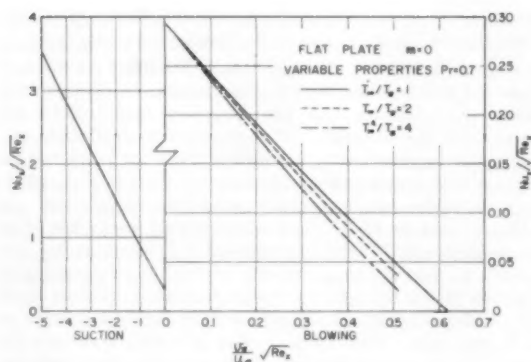


FIG. 7 DIMENSIONLESS LOCAL HEAT-TRANSFER COEFFICIENTS  $Nu_x/\sqrt{Re_x}$  FOR LAMINAR FLOW OVER FLAT PLATE AS A FUNCTION OF INJECTION PARAMETER  $\frac{U_\infty}{U_w} \sqrt{Re_x}$  FOR CASE OF VARIABLE PROPERTIES (References 1, 2.)

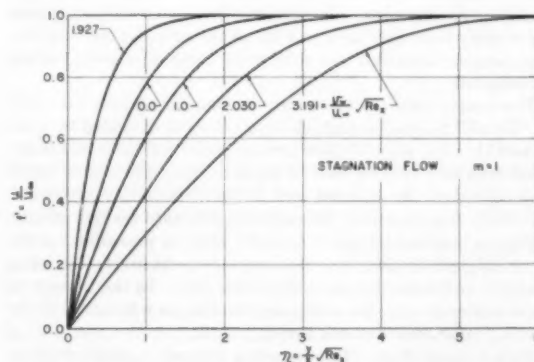


FIG. 8 DIMENSIONLESS VELOCITY PROFILES  $u/u_\infty$  FOR LAMINAR PLANE STAGNATION FLOW FOR A RANGE OF VALUES OF INJECTION PARAMETER  $\frac{U_\infty}{U_w} \sqrt{Re_x}$

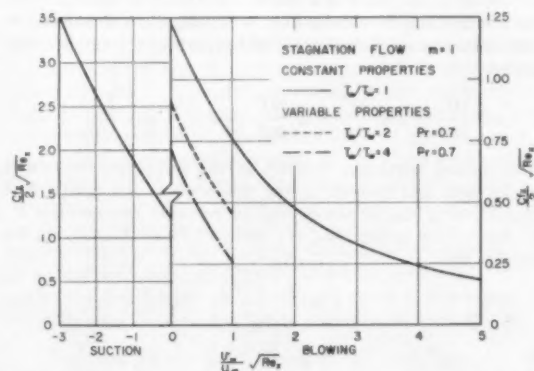


FIG. 9 DIMENSIONLESS LOCAL SKIN-FRICTION VALUES  $\frac{C_f}{2} \sqrt{Re_x}$  FOR LAMINAR PLANE STAGNATION FLOW AS A FUNCTION OF INJECTION PARAMETER  $\frac{U_\infty}{U_w} \sqrt{Re_x}$

blowing rates. Both the heat-transfer and skin-friction results indicate that the limiting value of the blowing parameter  $(v_w/u_\infty) \cdot \sqrt{\text{Re}_x}$  will be reached at a value lower than 0.619 for the case where the wall is cooler than the free stream. No calculations which would yield the same information for mass transfer are available in the literature. Dimensionless concentration and temperature profiles are again identical when the properties do not vary with concentration and where the product  $\rho D$  exhibits the same temperature dependency as the heat conductivity.

**Plane Stagnation Flow.** For two-dimensional steady flow of an incompressible fluid in the neighborhood of a stagnation line, the velocity  $u_\infty$  increases proportionally to  $x$  and the exponent  $m$  in Equation (9) has the value 1. Results for such a boundary-layer flow are shown in Figs. 8 to 13 and cover the same information as for the flat plate. These results include previously reported solutions [13] and [5] as well as some new solutions which were obtained to cover the range of interest more completely.

The major difference between the stagnation and flat-plate cases lies in the solution of the momentum equation with the resulting stagnation-flow velocity profiles and skin-friction values shown in Figs. 8 and 9. For the plane stagnation flow the velocity profiles are quite stable over a large range of blowing values. This is indicated by the fact that they do not exhibit the S-shapes found for the flat plate. In addition, there is no indication that the velocity boundary layer will lift off the wall and the skin friction remains finite over the substantial range of blowing values investigated.

The temperature and mass-transfer boundary layers, however, do "lift off" the wall at high blowing values as indicated by Figs. 10 and 11. The slope of these profiles at the wall approaches the value zero at a blowing rate of approximately 2.0 and at larger blowing values the thermal and diffusion boundary layers are effectively displaced from the wall surface toward the free stream.

Figures similar to Figs. 5, 6, and 7 may be presented for the plane stagnation case, and demonstrate qualitatively the same behavior as for the flat plate, Equation (15). In the interest of space economy, only the wall mass fraction as a function of the blowing parameter is shown here in Fig. 12.

**High-Velocity Flow.** The foregoing analysis is satisfactory at low speeds since compressibility and viscous dissipation effects have been neglected. At high velocities these become important and it is desirable to have available some analyses accounting for such effects.

Inspection of the boundary-layer energy equation reveals that for constant properties it is linear in  $T$  and that, therefore, a complete solution may be obtained by combining a complete solution of the homogeneous Equation (4) with a particular solution of the equation

$$\rho c u \frac{\partial T}{\partial x} + \rho c v \frac{\partial T}{\partial y} = k \frac{\partial^2 T}{\partial y^2} + u \frac{\partial P}{\partial x} + \mu \left( \frac{\partial u}{\partial y} \right)^2 \quad [24]$$

The desired particular solution of the complete equation is that for zero heat transfer at the wall surface and results in a specification of the adiabatic wall or recovery temperature  $T_r$ . The results may be reported as a recovery factor  $r$  defined in the following way

$$r = \frac{T_r - T_\infty}{\frac{u_\infty^2}{2g_c c_p}} \quad [25]$$

In all cases where a free-stream pressure gradient exists there also exists a gradient of the free-stream static temperature  $T_\infty$ . In such cases the recovery temperature will vary along the surface if the thermal conductivity of the body approaches zero. Combining such a solution with the incompressible solution (homogeneous

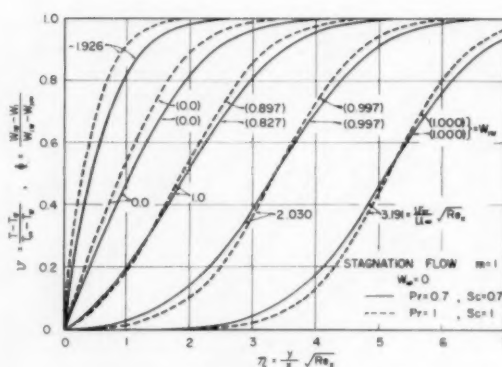


FIG. 10 DIMENSIONLESS TEMPERATURE PROFILES AND MASS-FRACTION PROFILES FOR LAMINAR PLANE STAGNATION FLOW FOR A RANGE OF VALUES OF INJECTION PARAMETER  $\frac{v_w}{u_\infty} \sqrt{\text{Re}_x}$  FOR PRANDTL NUMBERS OF 1.0 AND 0.7

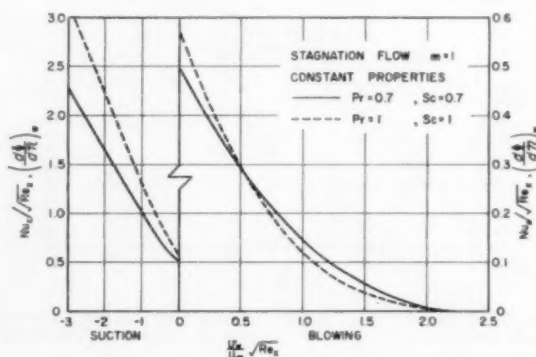


FIG. 11 DIMENSIONLESS LOCAL HEAT-TRANSFER COEFFICIENT  $Nu_x / \sqrt{\text{Re}_x}$  AND LOCAL MASS-TRANSFER COEFFICIENTS  $\left( \frac{dW}{dy} \right)_w$  FOR LAMINAR PLANE STAGNATION FLOW AS A FUNCTION OF INJECTION PARAMETER  $\frac{v_w}{u_\infty} \sqrt{\text{Re}_x}$

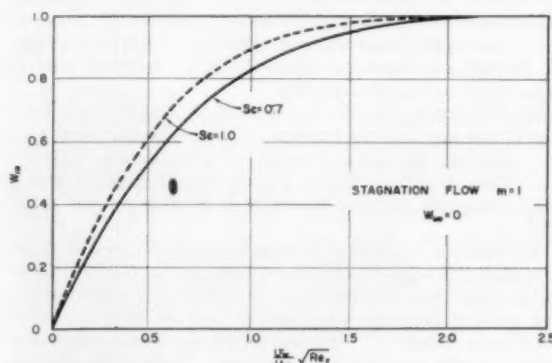


FIG. 12 MASS-FRACTION VALUES AT WALL SURFACE FOR LAMINAR PLANE STAGNATION FLOW AS A FUNCTION OF INJECTION PARAMETER  $\frac{v_w}{u_\infty} \sqrt{\text{Re}_x}$ , FOR  $w_{1\infty} = 0$

equation) yields a wall temperature which varies along the surface, that is, such a combination will satisfy only a particular wall-temperature variation, for instance not the condition of constant wall temperature. A different recovery temperature will be obtained if the thermal conductivity of the body approaches infinity, for in this case the recovery temperature will be constant. Therefore considerable care must be taken in the specification of the recovery factor for flows with free-stream pressure gradient (7).

On the flat plate with constant velocity  $u_\infty$  the stream temperature is constant as long as the flow is laminar and the recovery temperature of the plate does not vary along the surface. In this case there is no ambiguity with respect to the recovery temperature, and its specification immediately yields the complete solution of the constant-property energy equation including dissipation. The heat-transfer coefficient  $h_x$  is obtained from the solution neglecting dissipation (from the complete solution of the homogeneous equation); however, the heat transfer is obtained from the expression

$$\left. \begin{aligned} q_x &= h_x(T_w - T_r) \\ &= \frac{k}{x} \sqrt{\text{Re}_x} \left( \frac{d\theta}{d\eta} \right)_w (T_w - T_r) \end{aligned} \right\} \dots \dots [26]$$

The information on heat-transfer coefficients presented in the foregoing paragraphs can be used in connection with Equation [26].

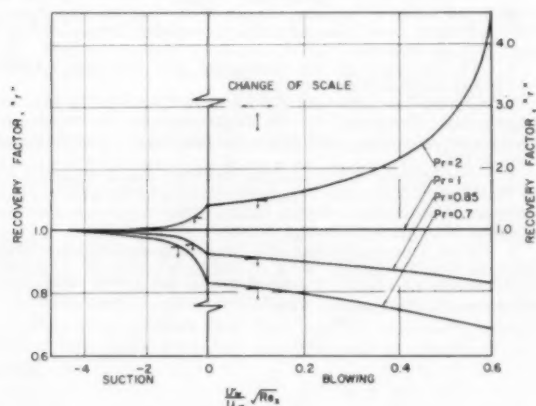


FIG. 13 RECOVERY FACTORS FOR LAMINAR FLOW OVER A FLAT PLATE AS A FUNCTION OF INJECTION PARAMETER  $\frac{v_w}{u_\infty} \sqrt{\text{Re}_x}$  FOR SEVERAL VALUES OF THE PRANDTL NUMBER

The recovery temperature is conveniently reported in terms of the recovery factor  $r$ , as defined, where  $r$  is the solution of the complete equation for  $\partial T / \partial y = 0$  at  $y = 0$  and may be found in Fig. 13. The results for  $\text{Pr} = 0.7$  have been reported previously in reference (8).

For the case of blowing the recovery temperature is here defined as that particular temperature of the porous wall and of the gases leaving that wall such that there is no convective heat transfer

$$\left( k \frac{\partial T}{\partial y} = 0 \right)$$

at the wall.

Much of the flexibility of the results obtained for a constant-property fluid disappears when those properties are considered to

be variable. If the actual property variations are prescribed for a particular fluid the results must then be restricted to that fluid. Such is the case with the results of Brown and Donoughe (2) which are discussed briefly in this paper and which apply only to air.

#### APPLICATION OF RESULTS

**Mass-Transfer Cooling With a Gas.** In the considered application the surface temperature is the parameter of major importance. This temperature may be obtained by writing a heat balance for the cooling gas on its path through the porous wall. This balance reads

$$\dot{m}_1 c_p (T_w - T_r) = h_x (T_w - T_\infty) + q_r - q_s \dots \dots [27]$$

where

$q_r$  = net radiative heat transfer to porous wall surface  
 $q_s$  = net conduction heat flow away from control area along porous wall surface

If the conduction and radiation terms are neglected this may be rearranged to read as follows

$$\frac{T_w - T_r}{T_\infty - T_w} = \frac{h_x}{\rho v_w c_p} = \frac{\frac{\text{Nu}_x}{\sqrt{\text{Re}_x}}}{\text{Pr} \left( \frac{v_w}{u_\infty} \sqrt{\text{Re}_x} \right)} \dots \dots [27a]$$

The free-stream conditions, the mass flow rate  $\dot{m}_1$ , and the gas-inlet temperature  $T_r$  will generally be known. For constant-property flow the knowledge of the mass flow rate  $\dot{m}_1$  and the free-stream conditions fix the blowing velocity  $v_w$  by Equation [23] and consequently  $(v_w / u_\infty) \sqrt{\text{Re}_x}$ . Then from Fig. 4 or 11, the necessary values may be obtained for substitution into Equation [27a] for the determination of the wall temperature  $T_w$ . In addition, Equation [21] or Fig. 6 allows the determination of the mass fraction of the diffusing gas at the wall surface.

High-velocity flow with viscous dissipation may easily be treated for the flat plate. The free-stream temperature then is replaced by the recovery temperature, which may readily be obtained from the recovery-factor values shown in Fig. 13.

**Mass Transfer or Film Cooling With a Liquid.** If the cooling is obtained by the evaporation of a thin film of liquid distributed uniformly along the surface which is to be cooled, the constant-property analysis may again be used as a first approximation. However, in this case there is an interrelationship between the surface temperature and the concentration at the wall if the wall surface remains wet; namely, the partial pressure of the diffusing vapor at the surface must equal the vapor pressure of the liquid at the temperature  $T_w$ . Thus, when the wall temperature  $T_w$  is fixed, this fixes the partial pressure of the vapor at the surface, which means that the wall concentration or mass fraction is uniquely determined. Equation [21] must still be valid and yields the dimensionless convective velocity  $f_w$ . Thus, when free-stream conditions are known, fixing the wall temperature uniquely fixes the mass-fraction profile and the diffusion rate.

The wall temperature may be determined in this case from the following heat balance, neglecting radiation and conduction

$$\dot{m}_1 c_p (T_w - T_r) + \dot{m}_1 h_{fg} = h_x (T_w - T_\infty) \dots \dots [28]$$

$$\frac{T_w - T_r + \frac{h_{fg}}{c_p}}{T_\infty - T_w} = \frac{\frac{\text{Nu}_x}{\sqrt{\text{Re}_x}}}{\text{Pr} \frac{v_w}{u_\infty} \sqrt{\text{Re}_x}} \dots \dots [28a]$$

For liquid-film cooling the assumption of a value of the wall temperature fixes the partial pressure at the wall and this, in effect, determines the mass fraction at the wall surface. With this information and knowing the free-stream conditions the blowing value  $(v_w/u_\infty) \sqrt{Re_\infty}$  may be determined from Equation [21] or from Figs. 6 or 12. With this information the value of  $Nu_w/\sqrt{Re_\infty}$  may be obtained from Fig. 4 or 11. All of the required values may then be substituted into Equation [28a] and it may be determined if this equation is satisfied. If it is not satisfied a new wall temperature is assumed and the procedure again followed until agreement is found. Thus, for fixed free-stream conditions and a fixed entrance temperature of the coolant gas  $T_s$ , the evaporative flow adjusts itself to a unique value fulfilling both the energy and mass balance. This is the amount of liquid that one should introduce if full advantage of the film-cooling process is to be utilized. If less liquid is introduced the liquid will boil within the porous wall. This usually results in an unstable condition in which part of the wall will be wet while other sections will be completely dry. If more liquid than the calculated equilibrium amount is introduced, it will flow downstream along the surface or be blown away and therefore very little additional cooling will be obtained, resulting in a waste of cooling liquid. High-velocity flow over a flat plate may be treated by replacing the free-stream temperature  $T_\infty$  by recovery temperature  $T_r$  in Equations [28] and [28a]. The extension of the foregoing analysis to sublimation cooling is accomplished readily.

#### ACKNOWLEDGMENTS

This investigation was carried out with financial support of the Mechanics Division, Office of Scientific Research, Air Research and Development Command under Contract No. AF-18(600)-1226.

The authors are indebted to Mr. R. L. Sampson, who performed the major portion of the calculations reported herein, and in addition, made many helpful suggestions during the course of the investigation.

The authors acknowledge the assistance of Dr. Fulton Koehler of the Institute of Technology, Mathematics Department of the University of Minnesota, in obtaining solutions to the plane stagnation flow case.

#### BIBLIOGRAPHY

- 1 "Exact Solution of the Laminar Boundary Layer Equations for a Porous Flat-Plate With Variable Fluid Properties and a Pressure Gradient in the Main Stream," by W. B. Brown, Proceedings of the First U. S. National Congress of Applied Mechanics, June, 1951.
- 2 "Tables of Exact Laminar-Boundary-Layer Solutions When the Wall Is Porous and Fluid Properties Are Variable," by W. B. Brown and P. L. Donoughe, NACA TN No. 2479, September, 1951.
- 3 "Solutions of Laminar-Boundary-Layer Equations Which Result in Specific-Weight-Flow Profiles Locally Exceeding Free-Stream Values," by W. B. Brown and J. N. B. Livingood, NACA TN 2800, September, 1952.
- 4 "Exact Solutions of Laminar-Boundary-Layer Equations With Constant Property Values for Porous Wall With Variable Temperature," by P. L. Donoughe and J. N. B. Livingood, NACA TN 3161, September, 1954.
- 5 "Heat Transfer and Temperature Profiles in Laminar Boundary Layers on a Sweat Cooled Wall," by E. R. G. Eckert, Technical Report No. 5646, Air Materiel Command, November, 1947.
- 6 "Method for Calculation of Heat Transfer in Laminar Region of Air Flow Around Cylinders of Arbitrary Cross-Section," by E. R. G. Eckert and J. N. B. Livingood, NACA TN 2733, June, 1952.
- 7 "Convective Heat Transfer at High Velocities," by E. R. G. Eckert, Heat-Transfer Symposium, Engineering Research Institute, University of Michigan, University of Michigan Press, 1953.
- 8 "Transpiration and Film Cooling," by E. R. G. Eckert, *ibid.*
- 9 "Tabulation of the Blasius Function With Blowing and Suction," by H. W. Emmons and D. C. Leigh, Fluid Motion Sub-Committee, Aeronautical Research Council, Report No. FM1915, June, 1953.
- 10 "Exact Calculation of Laminar Boundary Layer in Longitudinal Flow Over a Flat-Plate With Homogeneous Suction," by R. Iglish, NACA TN 1205, April, 1949.
- 11 "Effect of Large Temperature Changes (Including Viscous Heat) Upon Laminar Boundary Layers With Variable Free Stream Velocity," by S. Levy, *Journal of the Aeronautical Sciences*, vol. 21, July, 1954, pp. 459-474.
- 12 "Die Grenzschicht mit Absaugung und Ausblasen," by H. Schlichting, *Luftfahrtforschung* 19, 1942.
- 13 "Exakte Lösungen für die laminare Grenzschicht mit Absaugung und Ausblasen," by H. Schlichting and K. Bussmann, *Schriften der Deutschen Akademie der Luftfahrtforschung*, series B, vol. 7, no. 2, 1943.
- 14 "The Solution of the Laminar-Boundary-Layer Equation for the Flat-Plate Velocity and Temperature Fields for Variable Physical Properties and for the Diffusion Field at High Concentration," by H. Schuh, NACA TN 1275, May, 1950.
- 15 "Mass Transfer Cooling in a Laminar Boundary Layer With Constant Fluid Properties," by J. P. Hartnett and E. R. G. Eckert, Heat Transfer Laboratory Technical Report No. 4, 1955, University of Minnesota, Minneapolis, Minn.

# The New Zealand Thermal Area and Its Development for Power Production

By C. J. BANWELL,<sup>1</sup> LOWER HUTT, NEW ZEALAND

The main thermal area in the North Island of New Zealand is described, and a short account given of its geological history and of its relation to the Pacific seismic and volcanic belt. The prospecting and development drilling program, commenced at Wairakei in 1950, is presented. Temperature information from the drill holes has been used to prepare several temperature sections through the development area. Wairakei drill holes have nearly all tapped a mixture of steam and water, with a mean enthalpy for all producing holes of 450 Btu/lb. In the month of November, 1954, 16 producing holes were discharging a total mass of 1.38 million lb/hr, the steam fraction of which, at 70 psi wellhead pressure, represents a generated power output of 20,000 kw. The total estimated natural heat output of the Wairakei area is equivalent to approximately 100,000 kw of generated power.

## EARLY DEVELOPMENT

THE first practical application of heat from the New Zealand thermal area appears to have been made by the Maoris, who were found by the first European arrivals using natural steam vents and hot pools for cooking and washing. A few still do this, but the newcomers soon began pumping hot water from springs for swimming baths and for various forms of curative treatment. In the past few decades, many successful bores, mostly only a few hundred feet deep, have been drilled in Rotorua and a few other parts of the thermal area, and the steam and hot water they deliver have been used for space and water heating, as well as for timber drying, hothouses, and some other rather small-scale industrial purposes. Most of the bores have been privately drilled and owned, and no large-scale district heating schemes have been put into operation, though there is little doubt that they would be both practical and economic.

## POWER PRODUCTION

The intensive geothermal prospecting and development program that was instituted by the New Zealand Government in 1950 in the Wairakei area was stimulated to a very great extent by the electric-power shortages that had become increasingly serious over the preceding few years. Electric power has become of major importance in New Zealand, both for domestic and industrial use, and, as is the case in many other countries, consumption is increasing very nearly according to an exponential law, the annual increase being of the order of 7 to 10 per cent. Practically all the electrical energy used at the present time is generated from water power and, because of shortages of labor and materials, new construction has not kept pace with the

growing demand. Shortages of this kind can be overcome to some extent by importing other types of generating plant from abroad, and by projects, such as geothermal development, which do not compete too seriously with the existing hydro projects for men and materials.

The hydroelectric power potential of the North Island is relatively limited, and the total capacity developable in 1 megawatt or larger schemes has been estimated to be about 1250 mw. Of this, nearly 72 per cent should be in use by the end of 1961, if the program outlined in the paper can be carried out. The potential of the South Island is much greater both absolutely, and still more in relation to population. The South Island is slightly larger in area than the North but at the 1951 census had only 34 per cent of the population. In 1953 the South Island had only 27.5 per cent of the total developed power and so was still at a disadvantage in this respect, but the current development program in the two islands should give it nearly 43 per cent by the end of 1959 and, unless there is a marked change in current population trends in the interval, the South Island power position should be relatively satisfactory.

To supplement the North Island hydro development program, the following additional schemes have been proposed:

- 1 A steam-generating station of 120,000 kw capacity, located in the Waikato coal field between Hamilton and Auckland. Some of this coal can be worked by opencast methods, and many of the shipping and other difficulties associated with the use of coal from the West Coast of the South Island would be avoided.

- 2 A gas-turbine station of 60,000 kw capacity. This would use imported oil fuel, and would be located at Wellington, which represents an important load center.

- 3 A geothermal steam station at Wairakei, with a final output of 80,000 kw. This will be combined with a heavy-water production plant, and will, in all, take considerably more than the estimated natural heat flow from the area.

## NORTH ISLAND DEVELOPMENT PROGRAM

Table 1 is based on information contained in a report presented to the New Zealand House of Representatives in 1955 (First Report of the Combined Committee on the North Island Electric Power Supply, Government Printer, D-4B).

This program leaves two further hydro schemes, Aratiatia and Kaituna, with a total capacity of about 160 mw, and a unit cost of 0.58 cent per kwhr, for development, and, including these, accounts for all but about 200 mw of hydro power available from the larger schemes. At the estimated rate of increase of demand, deficiencies rising to between 14 and 25 per cent of the demand in 1957-1958 are forecast. In 1961-1962 there may be a surplus of about 7 per cent or a deficiency of about 6 per cent, depending on rainfall, and after this, deficiencies increasing to between 12 and 22 per cent in 1964-1965, the last year considered.

Several further ways of supplementing the North Island supply, either in the course of, or after the end of, the foregoing program, have been considered. These include wind and tidal power, transmission from the South Island by a cable across Cook Strait, further geothermal development, and the use of atomic energy.

<sup>1</sup> Chief Physicist, Research, Dominion Physical Laboratory.

Contributed by the Heat Transfer Division and presented at a joint session of the Heat Transfer and Power Divisions at the Diamond Jubilee Annual Meeting, Chicago, Ill., November 13-18, 1955, of THE AMERICAN SOCIETY OF MECHANICAL ENGINEERS.

NOTE: Statements and opinions advanced in papers are to be understood as individual expressions of their authors and not those of the Society. Manuscript received at ASME Headquarters, June 27, 1955. Paper No. 55-A-58.

TABLE 1 POWER PROJECTS PLANNED FOR NORTH ISLAND

Type of plant	Location	Scheduled completion date	Capacity, megawatts	Cost of power, cents/kwhr
Existing fuel.....	Wellington } Auckland }	...	49	Over 0.88
Existing hydro.....	...	...	595	0.27
Hydro.....	Whakamaru	Middle 1957	100	0.27
Steam (geothermal).....	Wairakei	Middle 1958	40	0.47
Gas turbine <sup>a</sup> .....	Wellington	End 1958	60	0.88
Hydro.....	Atiamuri	End 1959	50	...
Steam (geothermal).....	Wairakei	Middle 1960	40	0.47
Steam (coal).....	Waikato	End 1960	120	0.88
Hydro.....	Ohakuri	End 1961	100	...
Hydro.....	Waipapa	End 1961	50	...
Less fuel stations closed down			1960	49
				955
			Total	1004

<sup>a</sup> This program is by no means final. In a press release dated July 30, 1955, it was announced that the gas-turbine proposal had been abandoned, and that the capacity of the projected Waikato coal-steam plant would be increased to 180,000 kw.

Of these, the first two do not appear to be economic at the present time, while the cable proposal depends both on technical problems of cable manufacture, laying, and maintenance, all rather difficult to assess at present, and on the rate of South Island power development. The estimated total natural heat flow from the thermal area is equivalent to between 250 and 300 mw of generated power, and, subject to the Wairakei project proving satisfactory, there seems to be no reason why most of this capacity should not be developed. In addition, there appears to be enough stored heat in the Wairakei area to permit the rate of draw-off to be increased to several times the natural heat flow without shortening the useful life unduly, and it is to be expected that similar conditions will be found in many of the other hot areas. Thus it seems possible that, by overdrawing the natural heat flow, the thermal area might be able to provide about 1000 mw for a period of 10 to 15 years, and if generating plants using atomic energy become generally available within this period, large-scale geothermal development should easily meet the expected power deficiencies. At the present stage of exploration, it is not possible to decide whether a permanent increase over the natural heat flow is possible with properly sited holes.

#### DIRECT INDUSTRIAL USE OF HEAT FROM THERMAL AREA

The main thermal areas are located toward the center of the North Island, but with a few exceptions, none is conveniently close to any industrial center that could use large quantities of process heat. Hence the costs of transporting raw and processed materials to and from the heat supply, or the cost of long pipe lines have to be considered. The quantities of heat available are such that, provided a large enough demand could be built up, pipe lines of considerable length would become economic, but such an undertaking would involve a large capital investment and much planning, so that, at present, the alternative of generating electric power and feeding it into the existing networks has many attractions.

Currently, there are two enterprises in hand in which it is intended or hoped to make fairly large-scale direct use of the heat. One is the Wairakei combined power and heavy-water plant, where some of the available heat will be used for concentrating heavy water. In this case the raw material, ordinary water, is available on site, and the concentrated product has a high enough value to make transport costs negligible. The other is the almost completed Tasman pulp and paper mill at Kawerau, which is close to the Te Teko thermal area in the Bay of Plenty. Bores to test the steam supply are now being drilled, and if it is found satisfactory, it will be used to take over part of the load of the plant's fuel-fired boilers.

#### COST OF HEAT AND STEAM AT WELLHEAD

From drilling experience at Wairakei, it is possible to make a

rough estimate of the cost of a bore with a given output, and if we take the useful life of the bore to be, say, 10 years, which seems to be a conservative estimate, some idea of costs can be obtained. Taking as an example borehole No. 20 with a diameter of 8 in. and a depth of 2000 ft, approximately, the cost, including interest at 5 per cent over a 10-year amortization period, would amount to about \$128,000. This bore delivers a mass output of 563,000 lb/hr with an enthalpy of 481 Btu/lb and a wellhead pressure of 150 psi, so that the heat delivery relative to 212 F will be  $1.0 \times 10^6$  Btu for 1 cent and the steam delivery at 75 psi 780 lb for 1 cent. No maintenance costs have been included here, as bores in this area do not appear to require any major maintenance such as cleaning out, and wear and corrosion of wellhead fittings are not serious. Costs of unsuccessful holes should be included, but with a better knowledge of the area, the proportion of these should be relatively small.

#### WASTE HEAT FROM GENERATING PLANT

Before borehole steam can be used for power generation, it must be separated from a large quantity of water, and it seems probable that this water will be discarded at a temperature of 212 F or higher.

Taking into account the heat used by the heavy-water plant, the steam consumption will be approximately 30 lb/kwhr, and the mass of water discarded (for an initial enthalpy of the discharge of 450 Btu/lb) 78 lb/kwhr, so that plant generating 80 mw will provide  $6.24 \times 10^6$  lb/hr (27.8 cu sec) of water at 212 F. This represents  $1.12 \times 10^6$  Btu/hr relative to 32 F, which is sufficient to provide space heating for a population of the order of 200,000. The Auckland urban area, with a total population of 350,000, is approximately 175 miles by road from Wairakei, and calculation shows that it would be possible to pipe the required amount of water this distance without excessive losses. The cost of the heat at the delivery end would be from one third to one quarter of that from oil or electricity, though the cost of the local reticulation system and of heating plants in individual dwellings would have to be considered.

It has been suggested that it might be advantageous to return some or all of the separated water to the producing area by pumping it into bores placed at the perimeter, to prevent or delay cooling off by incoming ground water. Such a procedure might be effective if enough were known about ground-water movements to enable the necessary extra holes to be sited properly. In this case, the amount of water available for other uses might be greatly reduced.

#### GEOGRAPHICAL-STRUCTURAL RELATIONSHIPS

The main thermal area of the North Island of New Zealand lies near the southern and western end of the great seismic and volcanic belt that extends around almost the whole perimeter of the Pacific basin, to the antarctic region to the south of

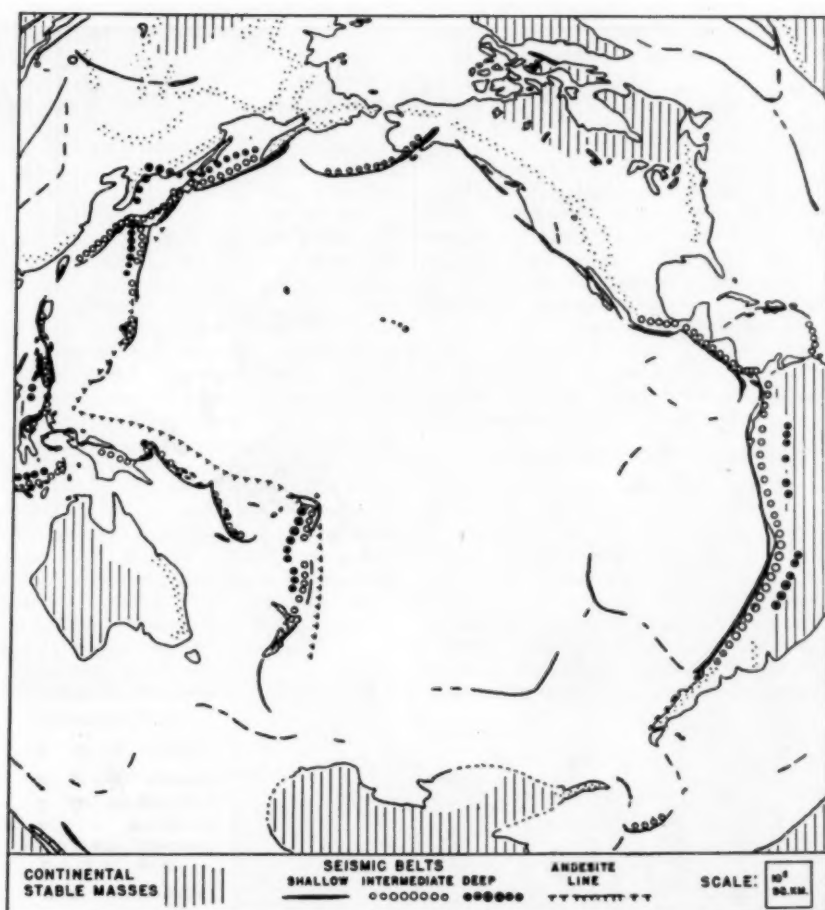


FIG. 1 SEISMIC AND VOLCANIC BELT OF PACIFIC AREA  
(Fig. 33, p. 90 of "Seismicity of the Earth"—Gutenberg and Richter.)

South America. Fig. 1<sup>2</sup> shows the manner in which most of the earthquake epicenters are concentrated in this belt. In particular, all the intermediate and deep-focus shocks are confined to the fringes or to groups within the fringes of the basin, and volcanic activity also follows this grouping in general. Almost without exception, the shallow-focus shocks are nearest the basin, and the intermediate and deep shocks at increasing distances behind them.

A profile through the northern Japanese region<sup>4</sup> shows that the earthquake centers lie close to a plane surface which dips away from the Pacific at an angle of about 30 deg. The present-day active volcanoes in Japan lie above the zone of earthquakes of intermediate depth (about 125 miles), and a line of extinct volcanoes is located behind them. In the case of New Zealand, the fewness of deep-focus (i.e., up to 435 miles deep) shocks does not permit such a satisfactory profile to be made, but the general similarity of the relationship between volcanic activity and earthquake depth is apparent from Fig. 2.<sup>5</sup> The almost

extinct volcano of Mt. Egmont and the extinct volcanic region about Auckland lie on a line roughly parallel with and behind the present active area, as in Japan, though the volcanoes to the south, all extinct, at Banks Peninsula near Christchurch, and the Auckland and Campbell Islands (the latter about 400 miles to the south of the South Island) do not seem to belong to the general pattern.

The zone of activity in the New Zealand area lies in the apex of the acute angle formed by the two main structural axes apparent in the North Island<sup>6</sup> and extends in a general NNE direction from the active volcanoes of Ruapehu and Ngauruhoe south of Lake Taupo to White Island in the Bay of Plenty, a distance of some 150 miles. White Island, although it does not appear to have erupted in the true volcanic sense in historic times, has a crater which is the scene of intense and high-temperature fumarole activity, and can probably be regarded as an active volcano. An intense, though short-lived volcanic eruption took place from Mt. Tarewera in 1886, but in the remainder of the area, thermal activity takes the form of localized areas of hot springs, fumaroles, and the like.

<sup>2</sup> Reference (3), fig. 33, p. 90.

<sup>3</sup> Numbers in parentheses refer to the Bibliography at the end of the paper.

<sup>4</sup> Reference (3), fig. 6, p. 29.

<sup>5</sup> Ibid., fig. 14, p. 46.

<sup>6</sup> Reference (1), p. 53

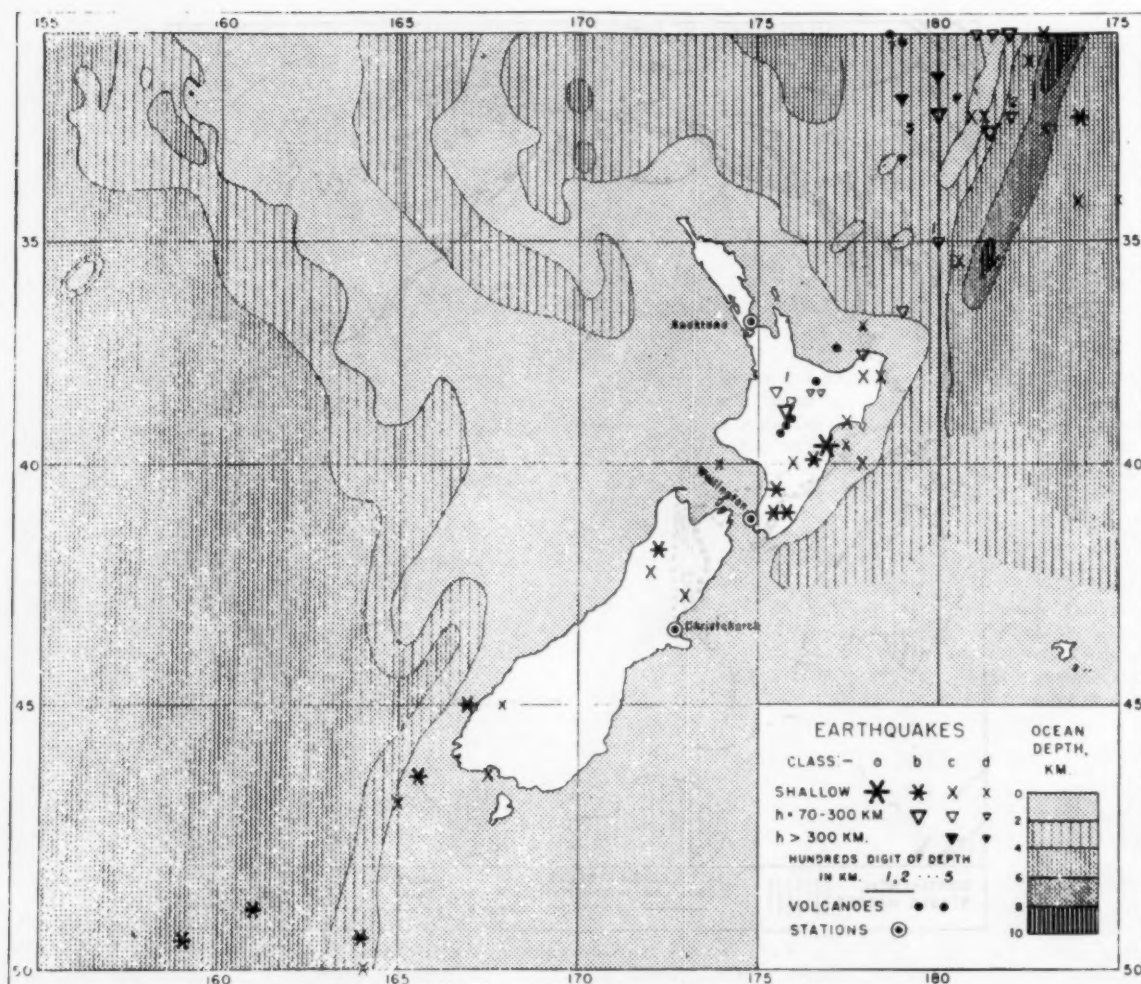


FIG. 2 LOCATIONS OF VOLCANOES AND EARTHQUAKE EPICENTERS IN NEW ZEALAND AREA  
(Fig. 14, p. 46 of "Seismicity of the Earth"—Gutenberg and Richter.)

#### RECENT GEOLOGICAL HISTORY OF THERMAL AREA

In geologically recent times sudden explosive eruptions have occurred that have scattered pumice and basalt ash over most of the North Island. The deposits vary in thickness from a few inches to several feet, and follow the present contours of the land surface. One of the most recent of these explosions produced the so-called Taupo shower, which covered an area of some 8800 square miles with an ash deposit varying in thickness from more than 2 ft over upward of 1000 sq miles to 6 to 15 in. on the East Coast, some 90 miles away. The total volume is estimated by Cotton to be 4 to 5 cu miles. It is evident that there were intervals between these showers long enough for well-established forests to develop, since buried trees are common, and the charred condition of many of them indicates temperatures of the order of 250 C for the deposited ash. Some of this carbonized material has been used by Fergusson and Rafter (5) to date the showers by the carbon-14 isotope method, and ages of  $1700 \pm 150$  years for wood found in coarse Taupo pumice a

few miles north of Taupo,  $1850 \pm 50$  years for wood from a site west of Lake Taupo, and  $3150 \pm 200$  years for wood from fossil soil in a quarry a few miles southeast of Taupo, have been determined. Carbonized material from a depth of 200 ft in the Taupo area was found to have an age of approximately 5000 years (G. J. Fergusson, private communication). These results seem to indicate a cycle of about 1700 years for the eruptions, but it is by no means certain that all the showers are from a single source, since the vents or explosion craters from which the showers came are seldom identifiable, and it is not evident that the eruptions of different sources should be correlated in this way.

#### STRUCTURE OF THERMAL AREA

From seismic evidence Bullen (4) concludes that the upper part of the N.Z. crustal structure consists of some 30,000 ft of greywacke overlying 15,000 ft of granitic material. Greywacke is a close-grained, hard, impermeable rock of sedimentary origin, with an age of the order of 200 to 500 million years, and it is

on this greywacke, possibly overlain with some thickness of other sedimentary beds, that the volcanic rocks lie (1). The results of a gravity survey of the area, carried out in 1950 by the New Zealand Geophysical Survey, indicate that the greywacke dips steeply along the eastern boundary of a trough or "graben," to a depth of about 7000 ft below the present surface, and rises again more slowly to the west. The gravity survey also indicates a ridge rising some 2000 to 3000 ft from the floor of the graben, and all the major activity, including that of the important Wairakei area, lies above this ridge, which may thus be associated with important fractures in the basement rocks.

The process of formation of the graben appears to have been more or less continuous up to the present time, and earthquakes associated with fault movements have been recorded in the Taupo district in 1896 and 1922 (1). As the graben formed it became partly filled with volcanic material. During its most recent history (and probably over much of its earlier history also) the land surface has been partly covered by fairly extensive lakes. The form and location of these lakes, as well as the course of rivers and streams draining the area, must have undergone sudden and sometimes extensive changes as the topography was altered by new ash and pumice showers, fault movements, and so on. The loose ash deposits also would erode rapidly, leading to further filling up of hollows and lake beds, alterations of drainage, and the like, and much of the material in the present surface of the graben evidently has been built up in this way. Relatively impermeable mudstones from old lake beds, highly permeable water-sorted gravels and sands, deposits from recent eruptions, and material altered to varying degrees by the action of hot water and steam all occur in great profusion. It is not surprising to find that geological correlation over even a limited

area is often unsatisfactory, although petrological examination of cores from holes in the Wairakei area has shown the presence of continuous formations of some size.

### PRESENT DISTRIBUTION OF THERMAL ACTIVITY

The locations of the principal active thermal areas over the central part of the previously mentioned graben are shown in Fig. 3 by the hatched circles. The total natural-heat discharge from hot springs, geysers, fumaroles, etc., as estimated by J. Healy in 1949-1950 for each, is shown by the attached figures (millions of Btu per hour). The heat discharge is relative to 0°C, and since the mean enthalpy is about 342 Btu/lb, reference to the average local ground-water temperature (approx 53°F) will reduce these figures by 6 to 7 per cent. Several of the areas are well-known tourist attractions, but some are little known and still difficult of access. The faults shown in Fig. 3 nearly all follow the main structural trend of the region, though there is no very obvious connection between the surface traces of these faults and the thermal activity.

## HEAT SUPPLY OF HOT SPRINGS AND GEYSERS

The question of the origin and mode of transfer to the surface of the heat that maintains thermal activity has been discussed at some length in two forthcoming publications (Geothermal Steam for Power, issued by D.S.I.R., N.Z., and Physics of the N.Z. Thermal Area, D.S.I.R., N.Z.). The conclusion from this discussion is that the heat flow is most probably supplied by high-temperature (of the order of 1000 C) steam entering the area from below, and becoming mixed with ground water on its way to the surface. A possibility that seems less likely, on present evidence, is that deeply circulating water of surface origin be-

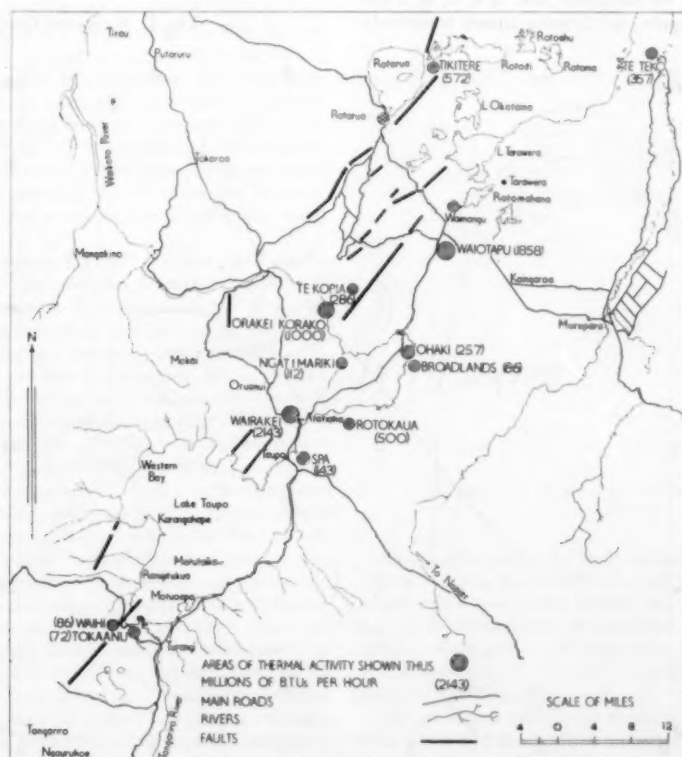


FIG. 3 MAP OF MAIN NEW ZEALAND THERMAL AREA

comes heated by contact with hot rock, and rises again to the surface either because of its smaller density or as a result of the general ground-water movement.

#### TEMPERATURE SECTIONS

Since the Wairakei prospecting and development program was commenced in 1950, frequent temperature-depth observations have been made in all holes during drilling and for some time after completion until the hole was opened. From the resulting large mass of data, a selection has been made of what appear to be the values best representing true ground temperature, and from these temperatures, a series of horizontal temperature sections has been prepared, at intervals of 50 m (164 ft) from 50 m below datum to 350 m above datum. Datum is approximately sea level, and the depth of the uppermost section ranges from a few feet to about 400 ft below ground level.

Fig. 4 is a map of the area, showing locations of drill holes, and so on, and Figs. 5, 6, and 7 are horizontal temperature sections at 350 m (1148 ft) and 200 m (656 ft above datum) and 50 m (164 ft) below datum, respectively. The isotherms are drawn for 10-deg C intervals, with 50, 100, 150, 200, and 250 deg indicated by heavier lines. The location of the surface trace of one of the principal faults in the area is shown on each section by the dashed line. The uppermost section, Fig. 5, shows two centers of high temperature, at A, near borehole No. 20, and B, between boreholes Nos. 6 and 3. B appears to be the northern extremity of a separate hot zone that probably extends south and east to include the areas of surface activity about Karapiti fumarole, just south of boreholes Nos. 12 and 13. The continuity of this zone is inferred from the existence of surface activity over most of its length, as there is no direct information from drill holes. None of the boreholes Nos. 5, 6, 3, or 7 has maintained useful heat outputs, No. 3 being almost completely

unproductive, and No. 5 productive for only a short time. The form of the isotherms about A show little relationship to surface features, except that the spread to the E and SE of A may be related to the expected direction of general water movement toward the Waikato River.

In Fig. 6, the hot area A has moved farther eastward, and B has shifted south and tended to become merged with A. The form

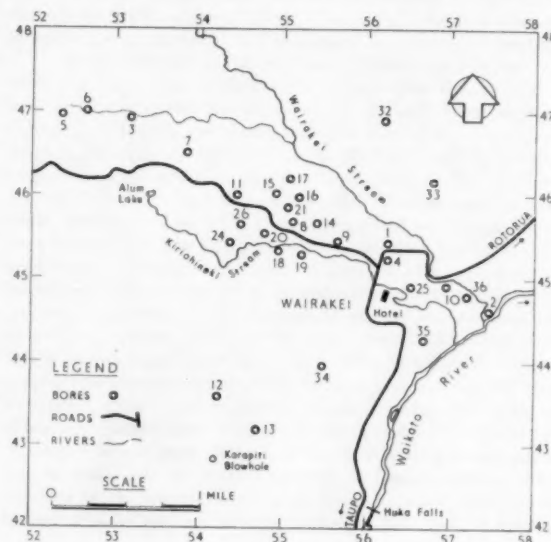


FIG. 4 WAIRAKEI THERMAL AREA

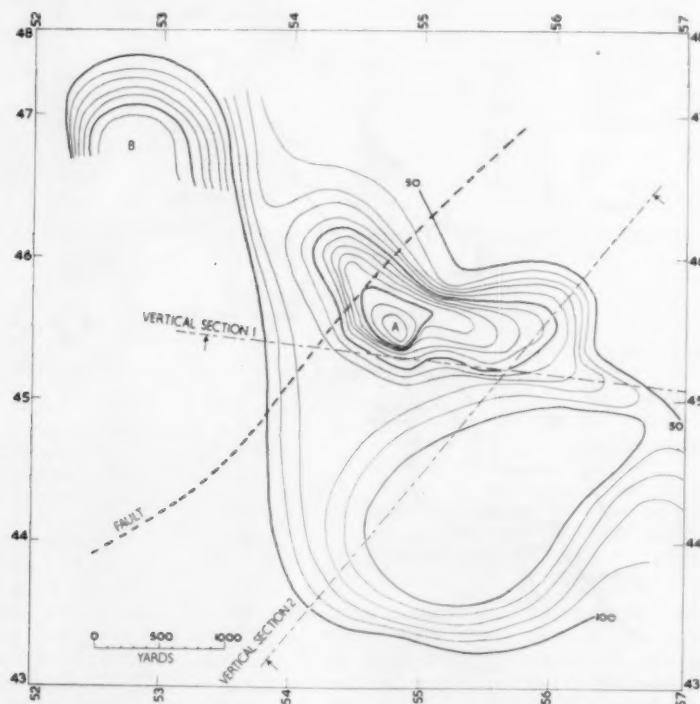


FIG. 5 HORIZONTAL TEMPERATURE SECTION (1), 1148 FT ABOVE DATUM

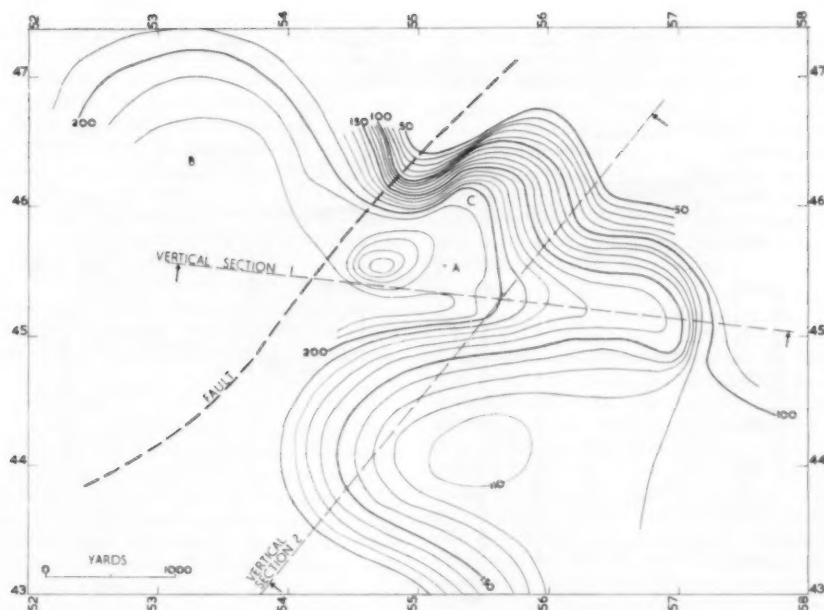


FIG. 6 HORIZONTAL TEMPERATURE SECTION (2), 656 FT ABOVE DATUM

of the isotherms to the north of A now shows a marked relationship to the fault trace, while the extension C of the hot area lies beneath the region of most intense natural activity in the Wairakei Valley. The spreading of the isotherms to the east is much more evident, and suggests the presence of a well-defined drainage channel toward the river in this direction. However, there is no strong thermal activity near the river here though hot springs are known to occur in parts of the river bed, and may be fed by this flow. The fault is believed to dip in a SE direction, and the form of the isotherms near C strongly suggests an inward movement of cool water, possibly derived from the Wairakei stream, along the fault as well as an outflow of hot water nearly at the same level.

The deepest horizontal section 3, Fig. 7, covers a much smaller area because only a few of the boreholes have been drilled deep enough to provide the necessary temperature data. However, it shows a very interesting feature in the hot area A, which has moved still farther east, and has become separated from area B. The form and extent of B are now only roughly defined because of lack of data. Although A has moved to the east, the isotherms on this side have not moved correspondingly, and consequently have become much more crowded. The situation is made clearer by the vertical section 1, Fig. 8, through boreholes Nos. 24 and 4/1 (vertical scale 5 × horizontal scale). In this particular plane, it has been possible to take the isotherms to much greater depths by using temperature information from boreholes Nos. 18 and 19, which lie close to the plane. It is evident from this section that a separate high-temperature zone exists, approximately under borehole No. 4/1, and separated from the hot area further westward by a deep minimum which is probably associated with the fault. The spreading of the upper part of the isotherms to the right at D once more indicates outward movement of hot water in that direction, and the crowding of the isotherms below a corresponding inward movement. There is also some evidence, from the spreading of the isotherms, of an upward and westward movement, which most probably represents part of the hot water supply to the Wairakei Valley.

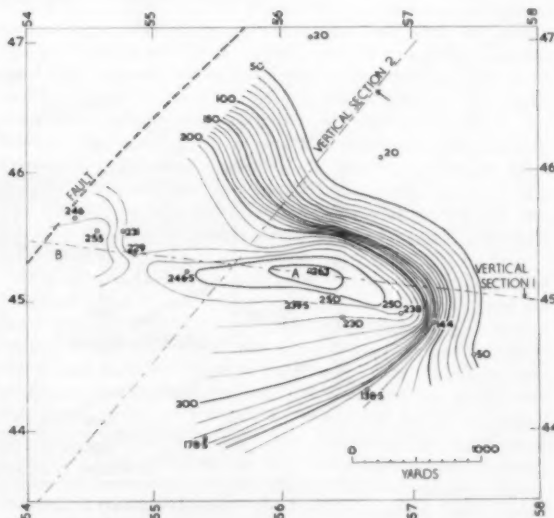


FIG. 7 HORIZONTAL TEMPERATURE SECTION (3), 164 FT BELOW DATUM

The vertical section 2, Fig. 9, intersects only a small part of the hot zone A near its western side, but indicates an outward movement with a component toward the Wairakei Valley, supporting the inferences from the previous section. This section also shows a steep rise in the isotherms toward the left (SW) edge, in the direction of Karapiti fumarole, indicating another heat source in this direction.

The geological sections for the area, which coincide very nearly with 1 and 2 of the vertical temperature sections, show a bed of ignimbrite lying under the whole area with its upper surface at depths ranging from 100 to 200 ft above datum below Karapiti

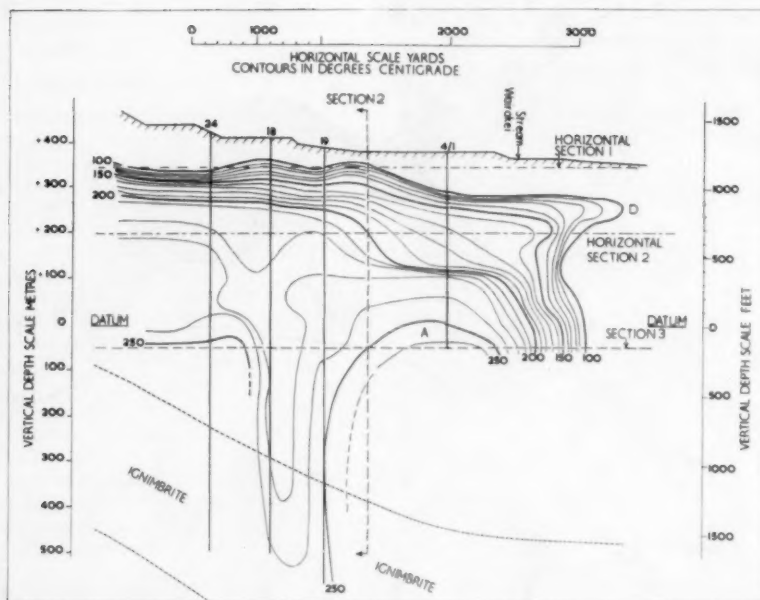


FIG. 8 VERTICAL TEMPERATURE SECTION (1) THROUGH BOREHOLES NOS. 24 AND 4/2  
(Location of ignimbrite boundaries from "Geological Section" by J. Healy.)

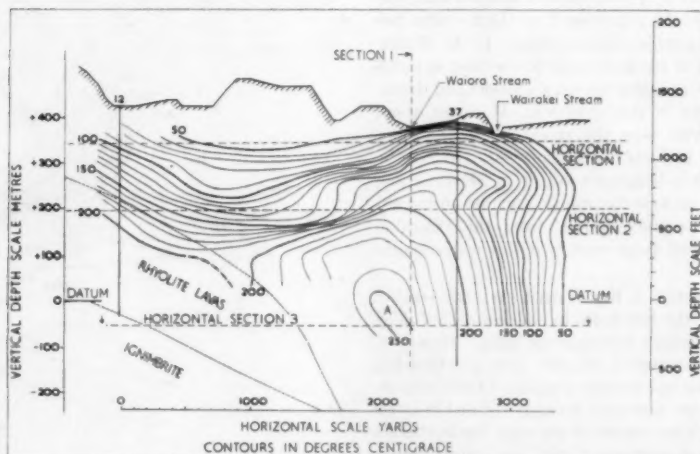


FIG. 9 VERTICAL TEMPERATURE SECTION (2) THROUGH BOREHOLES NOS. 12 AND 37  
(Location of rhyolite and ignimbrite boundaries from "Geological Section" by J. Healy.)

fumarole and boreholes Nos. 5, 6, and 3 to about 1200 ft below datum below borehole No. 4/1, where the hot zone is located. It appears quite possible that this zone is due to the escape of hot fluid through a fissure or joint in the ignimbrite in this neighborhood, and if this is the case, there is an excellent opportunity both to obtain a steam supply with a minimum of contamination by local ground water, and to determine whether the hot fluid from below is mainly steam or hot water. The indications of another heat source toward Karapiti fumarole, taken in combination with the corresponding geological section, also suggests some interesting possibilities. Here, rhyolite lavas up to a thickness of 800 ft lie above the ignimbrite in a broad dome formation that could form a steam reservoir, or a region in which

the steam from a considerable area below could be tapped. Neither of the boreholes drilled in this neighborhood (Nos. 12 and 13) has reached the bottom of the rhyolites, so that the precise location and physical properties (i.e., permeability, existence of fissures or joints, etc.) of the ignimbrite are still unknown.

The upper surface of the ignimbrite also appears to rise into a broad dome with its top beneath boreholes Nos. 5, 6, 3, and 7 (area B of Fig. 5). The discharge from these holes has generally been much richer in gas than that from bores further east, and this, combined with the relative absence of water in the natural activity here and to the south, has led to the suggestion that this area is fed principally by steam escaping through fissures

in the ignimbrite from a trap structure below. The large flows of hot chloride water, relatively free from gas, found in the Wairakei Valley, and the very similar hot chloride water tapped by the holes to the east of No. 11 may then be derived from water that has become separated from the steam in the dome formation, and is escaping through fissures down the flanks. On this interpretation, holes to the east will tap only hot water, at temperatures of perhaps up to 300 C, while deep holes sited over the dome structure to the west, and penetrating the ignimbrite, would tap a supply of steam that might be comparatively free from water. None of the boreholes Nos. 5, 6, 3, or 7 has been drilled far enough to reach the supposed depth of the top of the ignimbrite, nor is the thickness of the latter accurately known, so that more work of an exploratory character is still necessary before the potentialities of this area can be assessed properly.

#### RESULTS OF DRILLING

The original exploratory drilling program at Wairakei, commenced in 1950, called for the drilling of a series of bores, at 1200-ft intervals along a line (D line) about 3½ miles long, running in a general NNW direction from the left bank of the Waikato River, Fig. 4. This line passes between the two principal regions of natural activity in the vicinity, the Wairakei and Waiora Valleys, and is roughly parallel with them. It was originally intended to drill the bores to depths of 500 to 700 ft only, but those at either end of the line, Nos. 5 and 2A, were taken to approximately 1000 ft, and several of the others were deepened later. This program was completed before the end of 1951 by which time the heat and mass outputs from all the more promising holes had been measured, and something was known of the form of their pressure-output characteristics and general behavior. The conclusions from operations up to this stage were as follows:

- 1 The best-producing section of D line, for shallow drilling, lay between and included the locations of boreholes Nos. 4 and 11.

- 2 The output from nearly all the better-producing bores consisted of a mixture of steam and water with an enthalpy corresponding closely to that of hot water at the temperature measured at the bottom of the hole. Two bores in the producing region, Nos. 4 and 8A, had given flows of dry steam in considerable quantity, but in both cases deepening the holes resulted in a discharge differing little in composition from the remainder.

- 3 The output from the bores in the best-producing section did not fall off markedly with time. Changes that did occur (e.g., in borehole No. 1, completed in May, 1950) tended to be in the direction of a fall in the total mass discharge, but little or no change in total heat discharge.

- 4 The more active bores would discharge stably over a considerable range of wellhead pressures, from a few tens of pounds per square inch to 300 or more, for the most active. Generally, the enthalpy of the discharge remained nearly constant over the full pressure range, with a tendency to fall by a few per cent toward the high-pressure end. In some cases, the enthalpy showed a small maximum toward the low-pressure end. A few holes showed a steep rise in enthalpy as the discharge was throttled or the flow became partly blocked. This characteristic appears to have been a feature of newly opened bores, and borehole No. 4/2, which showed the effect strongly at first, had developed a falling characteristic within a year, and at the same time showed a marked increase in total output, enthalpy, and operating pressure range.

- 5 The gas content of the total discharge ranged from about 0.04 to 0.14 per cent by weight for bores in the producing section,

and from 10 to 100 times as much for bores to the west. The gas consists usually of 80 to 90 per cent carbon dioxide, a few per cent of hydrogen sulphide, and smaller quantities of hydrogen, hydrocarbons, nitrogen, and other gases. Substances dissolved in the water include chloride (1000 to over 2000 ppm) as the largest constituent, up to a few hundred parts per million of silica (metasilicic acid) and smaller quantities of other compounds. The discharges are generally slightly alkaline, with a pH up to about 8, measured at ordinary temperature. The general chemical composition is similar to that of the hot-spring discharges in the Wairakei Valley.

#### FURTHER EXPLORATION

From the information gained from the D-line bores, further prospecting bores were sited to the north and south of the most productive section of D-line, and by March 31, 1952, a total of 16 bores had been drilled, mostly in this area. The results from these boreholes generally confirmed the conclusions of the previous exploration and in April, 1953, the first of the larger and deeper boreholes, No. 20, was completed. This hole was drilled to a depth of 2003 ft, and with an 8½-in.-OD inner casing to 1400 ft. It delivered an output of 563,000 lb per hr with an enthalpy of 481 Btu/lb, at a wellhead pressure of 150 psi, compared with the previous highest value of 146,000 lb/hr, and 456 Btu/lb at 79 psi from borehole No. 15 (drilled 836 ft, cased 6 in.) completed 8 months previously.

Two further 8-in. boreholes, No. 19, drilled to 3189 ft, and completed July 1, 1953, and No. 18, drilled to 3144 ft and completed September 8, 1953, were located in the same area, but neither has produced a very large output. No. 19 was drilled through hard and impermeable material over a considerable part of its depth, especially toward the bottom, and appears to have gone some distance into the ignimbrite. It became blocked a few minutes after opening, and after a second attempt was made to start it a month later, with similar results, an inward bulge was found to have developed in the casing about 100 ft from the top. This bulge was finally removed by milling, but the performance of this hole has remained unsatisfactory, and it is closed at the present time.

Borehole No. 18, when opened on November 4, 1953, discharged large quantities of rock debris, totaling some 500 cu yd, and became partially blocked several times during this process. Severe erosion of the 8-in. upper discharge section (above the control valve) and parts of the wellhead occurred, and a fault had developed in the inner casing a few feet from the top of the well. The upper section of the well was excavated and the damaged section cut out and replaced. The damage had taken place at a socketed joint, which appeared to have failed initially through weakening by erosion. Further damage and rupture were caused by stresses during discharge and quenching of the hole. After the repair, the bore was reopened and discharged only a little more rock, but the output obviously was relatively low, and has not increased appreciably up to the present time.

Of the other deep 8-in. bores so far drilled, No. 26 produced a large output very similar to that from No. 20. No. 25, drilled to 2236 ft between Nos. 20 and 26, became blocked several times after opening, and has thrown out some 800 cu yd of debris. At the present time the discharge appears relatively small, and the bore is probably partially blocked. The latest 8-in. hole, No. 24, drilled to 1885 ft and completed at the end of March, 1955, was opened at the beginning of April, and appears to have a satisfactory output, although no measurements had been made up to the time of writing.

In general, the results obtained from these larger and deeper boreholes have been rather disappointing. Of six so far drilled,

two have large outputs, and one, No. 24, appears to be similar. However, the performance even of Nos. 20 and 26 is not especially striking in comparison with the outputs obtained from some of the shallower 6-in. bores in other parts of the area. Borehole No. 4/1, after deepening to 1494 ft in May, 1954, gave an output of 286,000 lb/hr, with an enthalpy of 476 Btu/lb; No. 4/2 drilled to 1500 ft, 232,000 lb/hr and 504 Btu/lb; and No. 21 drilled to 1002 ft, 205,000 lb/hr and 450 Btu/lb. If the output obtainable from a bore is determined by casing cross section, which is probably true of the more active ones, the performance of the 6-in. bores is little inferior to the 8 in.

The results from borehole No. 21 are particularly interesting as the enthalpy of the discharge is considerably higher than would have been expected from its position in relation to the isotherms of Figs. 8 and 9. However, it should be remarked that it was found impossible to take normal temperature runs either in this bore or in the nearby Nos. 14 and 15 because of unstable conditions, and a tendency for the hole to fill with steam, so that higher ground temperatures may exist here. Alternatively, in view of the discharge of almost dry steam given by borehole No. 14 (drilled to 605 ft),<sup>7</sup> there may be a considerable proportion of steam in the underground flow here, or a steam-bearing stratum which these bores intersect, without outstandingly high ground temperatures.

The reasons for the foregoing results are made fairly clear by Figs. 8 and 9. All the 8-in. bores with the possible exception of No. 24 have entered a relatively cool region which is quite probably due to the entry of surface water along a fault zone. The temperature information from the shallower holes previously drilled in the neighborhood gave little indication of the presence of this cool region, and its existence did not become evident until the deeper boreholes were drilled. Boreholes Nos. 4, 4/1, and 4/2 are located above what appears to be an important heat source for the area as a whole, and Nos. 14, 15, and 21 have tapped some of the flow from this source on its way to the surface. As already remarked, it is still difficult to decide whether the heat source is mainly steam or mainly hot water. The high proportion of steam from borehole No. 14 could be interpreted as being part of a primary steam flow that has escaped mixing with local ground water. However, the flows of dry steam obtained previously all appear to have been quite localized, and we may be dealing only with secondary steam that has become separated from the hot water by some favorable distribution of permeable and impermeable formations near the surface.

#### DEVELOPMENT FOR POWER PRODUCTION

The final decisions regarding type and location of generating plant, choice of steam-producing area, depth of holes, and other details will be governed by many engineering and economic considerations which it is not proposed to discuss here. Rather, an attempt will be made to give some idea of the possible alternatives that now appear to exist, and of some of the factors that may influence the eventual selection.

At the outset it is evident that it would be very desirable to obtain a supply of steam free from water. None of the areas so far explored holds out any promise of this at any of the depths reached. If a permeable dome structure exists under the ignimbrite in the vicinity of boreholes Nos. 3 and 6, or to the south of here, it could contain supplies of steam separated from water by gravity. The evidence for such a supply is indirect, and the possibility would have to be tested by drilling, probably to depths of at least two to three thousand feet. Dry or drier

steam might be obtained in the hot area under the No. 4 group by drilling closer to or into the ignimbrite at about 2500 ft, but this possibility also would require testing.

Then, too, it would be advantageous to have the steam-producing area as close as possible to the Waikato River, which represents the only adequate supply of condenser cooling water in the district. The bores of the No. 4 group are about 1300 yd from the nearest part of the river, and some 250 ft above it, and a large steam source in this neighborhood would be very attractive. The relative costs of piping steam or pumping cooling water would be factors in deciding whether to locate the powerhouse near the river or near the producing area, but in either case the shorter distance must weigh in favor of this area. A factor against it is the need for drilling deeper bores, and in this respect shallow development (with bores to, say, 1000 or 1500 ft) in the area outlined by the 200°C contour of Fig. 7, as far west as Nos. 15 and 24, would have advantages.

Finally, the probable useful life of the producing area is of importance. If the rate of heat withdrawal by bores is limited to that of the natural heat discharge—a rate that presumably could be maintained indefinitely if all this heat could be diverted to the bores—the total available generated power output from the whole Wairakei area would be about 100,000 kw. Just how much the available heat flow can be permanently increased by properly placed bores is not at all clear, but it has been calculated (independently by Mr. J. Healy and the author) that the amount of heat stored in hot water under the area so far investigated, could maintain the present natural rate for a period of 100 to 120 years without any further supply from below. There is little doubt that heat could be withdrawn at a much higher rate by drilling a large enough number of shallow bores, at the cost of probable exhaustion in a correspondingly short time, and also at some risk of early invasion of the area by cold ground water or other disturbances of the original equilibrium. The desirability of heavily overdrawing an area in this way will be influenced by the urgency of the need for power and similar considerations, as well as by the possible effect on the area.

#### OUTPUT AND PRESENT STATE OF BORES

Table 2 (taken from the D.S.I.R. Bulletin "Physics of the N.Z. Thermal Area") gives the locations, depths, casing dimensions, and other details of the bores drilled from the beginning of the project in 1950, up to the end of March, 1955. The two bores in the Te Teko thermal area (Fig. 3) are part of a project for supplying process heat to a large pulp and paper mill approaching completion a short distance away at Kawerau.

Table 3 taken from the same publication gives the wellhead pressures at which the holes are normally allowed to discharge, and the mass flows and enthalpies at these pressures.

Normally, bores are left to discharge continuously, but occasional shutdowns occur for maintenance and other reasons so that the totals given should be taken as the maximum rather than the average rate. The average rate of discharge for the month of November, 1954, was 1.38 million lb per hr with an enthalpy of 450 Btu/lb. Assuming the mean effective wellhead pressure for the whole group to be 70 psi, the steam fraction will be 19.2 per cent and the steam discharge 359,000 lb/hr. From calculations given in the Ministry of Works Progress Report to March 31, 1953, the steam consumption of a typical steam-generating plant operating at an exhaust pressure of 28 in. of mercury from a steam pressure of 70 psi will be 18.2 lb/hr per kw, so that the foregoing steam output represents almost 20,000 kw of generated power. It is evident that efficiency might be increased by grouping the holes according to their optimum working pressure and using them to supply steam to a specially de-

<sup>7</sup> On March 13, 1955, after further drilling operations, the mean output of bore hole No. 14 at 70 psi wellhead pressure, had increased to 53,600 lb/hr and the enthalpy had fallen to 576 Btu/lb.

TABLE 2 LOCATIONS AND DIMENSIONS OF BORES, WAIRAKEI AND TE TEKOK (FPS UNITS)

Borehole no. Wairakei	A				B	C	D	E	Date completed
	(E)	(N)	(E)	(N)					
1	356	232	445	407	1250	600	470	4	2. 5.50
2	357	509	444	588	1105	205	60	4	16. 5.50
2A	357	502	444	588	1109	1005	195	4	30. 8.50
3	353	150	446	922	1490	1006	768	4	29. 8.50
4	356	204	445	256	1245	1140	878	4	8.12.50
4/1	356	226	445	246	1242	1494	954	6	31. 5.54
4/2	356	209	445	221	1250	1500	498	6	31.12.52
5	352	316	446	973	1550	1020	1010	2.5	30. 9.50
6	352	682	446	988	1525	600	543	4	28.10.50
7	353	812	446	520	1520	1220	866	3	30. 6.52
8	355	108	445	658	1302	525	115	6	30.11.50
8A	355	131	445	718	1320	645	591	4	31.10.51
9	355	630	445	440	1270	574	400	4	19. 6.51
10	356	951	444	915	1170	1130	981	4	17. 7.51
11	354	449	446	007	1490	895	728	4	1. 6.51
12	354	231	443	554	1395	1515	853	4	3. 5.51
13	354	697	443	159	1340	1411	736	4	30. 4.52
14	355	419	445	672	1285*	605	508	6	25. 7.52
15	354	873	446	007	1370*	836	501	6	19. 8.52
16	355	204	445	966	1350*	1001	686	6	20. 4.53
16/1	355	206	445	964	1350*	1001	686	4	15. 4.53
17	355	084	446	212	1470*	995	773	6	2. 5.53
18	354	897	445	359	1300	3144	1477	8	28. 9.53
19	355	282	445	255	1295	3189	2200	8	1. 7.53
20	354	769	445	536	1330*	2003	1400	8	22. 4.53
21	355	010	445	861	1420	1002	854	6	30. 4.53
23	356	511	444	878	1240	1351	489	4	6. 7.53
24	354	432	445	426	1390	1885	1133	8	31. 3.55
25	354	599	445	535	1365	2236	1359	8	31.12.54
26	354	451	445	640	1410	1816	1486	8	22. 1.54
32	356	258	466	993	1320	1813	321	6	8. 8.53
33	356	741	446	160	1260	1589	236	6	15. 9.53
34	355	361	443	998	1325	2013	999	4	4. 3.54
35	356	714	444	303	1155	1990	238	6	31. 7.54
36	357	241	444	840	1145	2005	1040	4	30. 9.54
Te Teko									
1						900	695	4	31. 7.54
2						242	100	4	31. 5.54

\* Measured from ground surface. In most other bores reference datum is the casing flange which may be up to 10 ft below ground surface.

NOTE: Dates given in last column are those of completion to depths tabulated. A few bores have been tested at shallower depths and deepened later.

TABLE 3 WELLHEAD PRESSURES

Borehole no.	WHP		Date	Mass		Heat		Enthalpy	
	Kg/cm <sup>2</sup> gage	Psig		Kg/sec (10 <sup>3</sup> lb/hr)	Kg/sec (10 <sup>3</sup> lb/hr)	Kg. cal/sec × 10 <sup>3</sup>	(10 <sup>3</sup> Btu/hr)	Cal/gm	(Btu/lb)
1				1.26*	10.0	0.469*	6.7	372	671
2A			7/54	7.57	60.0	0.705	10.0	93.2	168
4	4.15	(60.5)	8/54	7.2	57.0	1.957	28.0	272	490
4/1	6.9	(84.0)	8/54	36	286.0	9.51	135.5	264	476
4/2	6.33	(90.0)	7-8/53	29.3	232.0	8.18	116.5	279	504
6	2.67	(38.0)	9/50	2.27*	18.0	0.643*	9.2	283	510
7			4/53	1.64*	13.0	0.455*	6.5	278	503
8A	5.2	(73.0)	5/54	3.3	26.0	1.089	15.5	330	595
9	7.03	(100.0)	3/54	7.89	62.5	2.38	34.0	302	545
10	2.6	(37.0)	6/54	3	24.0	0.600	8.6	200	360
11	4.92	(70.0)	4/54	11.6	92.0	2.67	38.0	230	415
12	4.92	(70.0)		12.3	97.5	2.34	33.4	190	343
13	4.5	(64.0)		17.6	140.0	3.25	46.4	185	334
14 <sup>b</sup>	2.32	(33.0)	4/54	0.74	5.9	0.48	6.8	651	1172
15	5.55	(79.0)	6/54	18.4	146.0	4.66	66.5	253	456
16	4.85	(69.0)		16.6	132.0	3.98	56.7	240	432
16/1	0.915	(13.0)	8/54	7.7	61.0	2.0	28.5	260	469
17	4.57	(65.0)	8/54	14.75	117.0	3.34	47.6	226	407
20	10.35	(150.0)	5/54	71	563.0	19.0	271.0	267	481
21	5.91	(84.5)		25.3	205.0	6.33	90.5	250	450
26	14.1	(200.0)		72.5	575.0	18.9	270.0	261	470
Totals:				362.8	2880	91.3	1300	250	450
								(Weighted mean)	

\* Omitted from total.

<sup>b</sup> Just prior to closing for deepening.

NOTE: The date column gives the month and year when the bore was operating at the discharge and pressure given.

signed generating plant, and that also, a considerable further quantity of power could be obtained from the hot water. The desirability of such alternatives, or of using the hot water or some of the exhaust steam for process heat will depend upon many economic factors which space does not permit to discuss here.

#### INTERACTION BETWEEN BOREHOLES

In order to decide upon the maximum possible or desirable

rate of withdrawal from a given area by bores it is important to know how much neighboring bores affect one another's performance. Since no noticeable mutual interference was found between the bores at 1200 ft spacing along D-line, two further boreholes were drilled close to No. 4, forming a triangle with sides approximately 24 yd (4-4/1), 30 yd (4/1-4/2), and 31 yd at the surface. Later, another pair of boreholes, Nos. 16 and 16/1, 10 ft apart at the surface, were drilled for interaction tests.

A series of measurements of the output characteristic of borehole No. 4/1, with No. 4/2 successively closed and open, was carried out in January, 1955. The holes were now of nearly equal depths (1494 and 1500 ft, respectively), and the mass output of No. 4/1 was found to be about 10 per cent lower with No. 4/2 open. The steam output was about 14 per cent lower at 80 psi wellhead pressure, and almost unchanged at the maximum pressure of 200 psi.

Boreholes Nos. 16 and 16/1 were both drilled to 1001 ft, and much larger effects were found, though the rather complex behavior under some operating conditions hindered measurements considerably. Satisfactory output characteristics of the smaller (4 in.) borehole No. 16/1, with No. 16 open and closed were obtained. These showed a fall in the mass output to less than one third at the lowest operating pressure (40 psi) and a reduction of the maximum pressure at which the bore would discharge from more than 150 psi to about 100 psi. The enthalpy was almost independent of operating pressure under both conditions, but was about 24 per cent higher with No. 16 open. Satisfactory output measurements on the 6-in. borehole, No. 16, were possible with No. 16/1 open, but with No. 16/1 closed pressure oscillations of large amplitude made output measurements very difficult. However, opening No. 16/1 appears to have reduced the mass output by about 20 per cent and increased the enthalpy slightly.

#### INFORMATION FROM DRILL CORES

The first sixteen prospecting bores drilled in the Wairakei area up to March 31, 1952, were cored over the full length, to obtain information about the geology and physical structure of the country. In a number of formations core recovery was poor, and these had to be identified and described as well as possible from cuttings. In general, the structure found was not greatly different from what would have been expected from the previous geological knowledge of the area, though some new knowledge has been added. The detailed information obtained has been of much value in locating impermeable bands, setting casing, and the conduct of drilling operations generally.

The main contribution to the geological knowledge of the area has been the discovery of hydrothermally altered ignimbrite at depth of approximately 2200 ft in the deeper bores. Experience has shown that the hydrothermal alteration of the ignimbrite decreases with depth indicating that the geothermal steam supply is to be found above the ignimbrite rather than in it.

In the more recent prospecting and development bores, core has been taken only occasionally, for control of drilling operations, or when the geological information appeared to be of particular importance.

#### CORROSIVE PROPERTIES OF STEAM

In order to investigate the corrosive and other chemical characteristics of the bore discharges, borehole No. 9 was taken over in 1953 by D.S.I.R., and used by the Chemical Engineering Section, Dominion Laboratory, and other branches of the Department as a source of steam for various tests. In addition to the chemical work, the performance of various designs of steam-water separators, flow-measuring methods, pressure drop along pipe lines, sampling methods, and the like, have been studied, and the results have been described in a number of Departmental Reports. The amount of information is too great even to summarize here, and only a few notes on the corrosion aspect will be given.

As a result of a very thorough investigation of the rates of corrosion, in both a stressed and an unstressed condition, of a large variety of metals and alloys in wet steam, dry steam, and

a wet steam/air mixture, the following general conclusions have been reached.

- 1 No unusual corrosion troubles are likely to be encountered in equipment handling dry-steam condensate with a composition similar to that used in the tests at borehole No. 9.

- 2 Corrosion rates of most of the metals tested in the wet steam-air mixture are far higher than those in wet steam or dry steam alone. Thus stand-by corrosion in plant handling the steam is likely to be important unless suitable precautions are taken.

- 3 Serious stress-corrosion cracking of a martensitic stainless steel occurred in both dry and wet steam. This is a type of material often used for steam-turbine blading, so that its lack of resistance is of some importance.

- 4 Austenitic stainless steels show a very high resistance to general corrosion, but all except the molybdenum-bearing variety are susceptible to pitting. The nonaustenitic stainless steels show a generally lower resistance to corrosion, and are also susceptible to pitting.

- 5 Copper-base alloys (except brass) have high enough corrosion rates to make their use undesirable in most applications.

- 6 The rate of corrosion of mild steel is low enough to make its use satisfactory for thick-walled piping and similar applications, provided stand-by corrosion can be kept to a minimum.

The foregoing is intended only as a very brief and incomplete summary of the results obtained, and for further information, reference should be made to the original reports. The general conclusion from these tests, and from some others with metal specimens buried in the soil at several points, is that the Wairakei area presents no unusually severe corrosion problems, though it does present a few special ones.

#### DRILLING METHODS

Rotary drills have been used exclusively for all prospecting and development work at Wairakei. Many of the shallower bores were drilled with Sullivan 37 rigs, and later a Failing rig was used for bores to about 1500 ft. The deeper development bores have been drilled with a larger portable rotary rig capable of drilling to 4000 ft nominal depth. For straightforward drilling, fishtail bits are commonly used in the softer formations, and rolling-cutter rock bits in the harder silicified material. Rates of drilling can vary from 40 ft or more per shift down to a foot or two per day. Rate of wear of bits is very high in the harder materials, but rock hard enough to justify the use of diamond-tipped bits has not yet been encountered. For coring and reaming, core barrels tipped with a weldable tungsten-carbide compound or special roller core cutters are used. In the year ending March 31, 1954, seven major bores, totaling 14,970 ft were drilled in the Wairakei area, and in the year ending March 31, 1955, five bores (including deepening of 4/1) were drilled at Wairakei, and one at Te Teko, totaling 10,072 ft.

The drill rods pass through a gland (or, in later operations with the larger rig, a hydraulically operated blowout preventer), so that pressure can be held if the hole heats up suddenly, and a recovery tube above the main valve allows core barrels or bits to be withdrawn from the bore while it is under pressure. Temperature is controlled and cuttings carried out of the bore by circulating a water/bentonite mixture. The bentonite also serves to seal minor permeable sections of the bore against loss of fluid. Larger leaks and fissures, which cannot be sealed in this way, often occur, and are then dealt with, if possible, by grouting and redrilling. As a rule, no attempt is made to use a high-density drilling mixture, and the fluid temperature is controlled carefully in order to keep the hydrostatic pressure of the fluid in the bore as close as possible to the pressure in the country

outside. The coarser cuttings are separated from the return fluid on a vibrating screen, and some of the finer material in a settling labyrinth. The fluid is then returned to a large holding tank, and its temperature adjusted by diverting part of it through a splash cooling tower.

All bores are now drilled from a concrete pit over which the rig stands. Casing consists of an outermost surface casing to a depth of about 50 ft, an anchor casing to a depth of from 200 to 500 ft, and an inner casing which extends to a depth ranging from a few feet to up to 1500 ft or more short of the bottom of the hole. All casings are grouted in place immediately after running. Some holes with very short uncased lengths have been completed for experimental purposes, but most of these have been deepened later. The length left uncased is based on estimates of the permeability of the country in which the bore is drilled, the object being to leave a large enough area of uncovered wall to allow the entry of the steam-water mixture without the production of too much debris. There is seldom any difficulty in keeping a bore under complete control until drilling has been completed to the planned depth. In a few bores it has been necessary to suspend drilling because of loss of circulation. Normally, after completion and removal of the rig, the bore is allowed to heat up for several days or weeks before opening. During the heating period frequent temperature runs are made over the full clear length of the bore.

Most bores have discharged considerable quantities of broken rock when opened, and soundings taken later almost invariably have shown the bore to be obstructed a short distance below the bottom of the inner casing. Since the enthalpy of the discharge obtained usually corresponds to that of water at the bottom bore temperature or hotter, it seems likely that the cavity left by the initial discharge becomes more or less filled with larger fragments, which form a permeable mass through which fluid can rise from the deeper parts of the bore. In some cases, where the discharge has almost certainly come from a permeable zone higher up the bore, the lower part has probably become blocked completely.

Borehole No. 20 has not discharged any appreciable quantity of solid material since it was opened, most probably because it has intersected fissures large enough to maintain the full discharge without any breakup of the formation. No. 26, 400 yd to the west of No. 20, also has discharged very little rock, but No. 25, located about halfway between, and drilled slightly deeper, does not seem to have intersected fissures of any importance, and as already noted, has so far proved incapable of clearing itself of debris. The actual form and distribution of the fissures is still far from clear. Fissures of useful size may be rather localized, and so far they appear to have played an important role in only a few bores.

#### CHANGES OF BORE OUTPUT WITH TIME

In general, boreholes in the production area between Nos. 4 and 11 have shown only moderate changes in output characteristics since they were first opened. A bore with one of the longest histories of unaltered depth and regular careful measurement is No. 9. In the first 10 months of its life, the mass output fell about 18 per cent and the enthalpy rose about 7 per cent. In the following 21 months (up to March, 1954) the mass output fell by a further 15 per cent and the enthalpy increased by 13 per cent. Changes of a similar kind were found in No. 8A, the mass output falling about 30 per cent, and the enthalpy increasing about 20 per cent in the course of a year. In this case, there was also a marked change in the shape of the output characteris-

tic, to a form with a steeper fall in output with pressure at the lower pressures, and a lower maximum operating pressure. In contrast with this, neither the mass output, enthalpy, nor form of output characteristic of No. 11 has changed measurably in an interval of about 2½ years.

The very large increase in output and enthalpy, and improvement in form of the output characteristic of borehole No. 4/2 already has been mentioned. It seems likely that the flow of hot fluid into the bottom of the bore has gradually increased the permeability in the neighborhood, or that the change in the underground pressure distribution eventually has resulted in the bore drawing its supply from a nearby fissure that was not intersected during drilling.

#### GENERAL CHANGES IN AREA

Regular observations of the heat discharge from the natural activity in the Wairakei and Waiora Valleys have been maintained since 1950, and ground temperatures (measured by buried thermocouples) down to a depth of 50 to 90 ft have been recorded and reobserved several times at points within and outside the development area. Also, weirs have been installed at points in the Wairakei stream above and below the principal active region, and a flume in the small hot stream from the Waiora Valley. Flow and temperature of the Wairakei stream are recorded continuously at both weirs, and similar measurements are taken daily at the Waiora flume.

A buried chain of thermocouples near borehole No. 11 showed a fall of nearly 30 deg C at 60 ft depth in a period of 2 years up to November, 1953, and a further fall of about 3 deg C in the next 8 months. Falls of 20 and 8 deg C at 50 ft depth near No. 9 have been found over the same intervals, but changes of only a few degrees C down to 90 ft near No. 10. A thermocouple chain between boreholes Nos. 12 and 13, approximately 1½ miles south of the development area showed a rise of about 6 deg C between 1951 and 1953, followed by a fall of 27 deg C in the next 8 months, at depths between 30 and 60 ft, and total changes of about 7 deg C at 80 ft. Except for this last chain, the form of the temperature/depth curve has shown little change with time.

In the period of 4 years between the end of 1950 and the end of 1954, there has been a marked fall in the heat discharge from certain hot springs in the Wairakei Valley, and a fall in the ground temperatures recorded by the thermocouples in the development area. Most of the springs affected are located on the northern slopes of the Wairakei Valley, and the flow from several has ceased completely. The heat discharge from one of the springs still flowing has fallen to about one third of its initial value, most of the change taking place before the end of 1953. The period of a small geyser in this valley has increased markedly and become irregular in the same time interval, and the Great Wairakei Geyser appears not to have played since the middle of 1954.

#### BIBLIOGRAPHY

- 1 "The Geology of the Rotorua-Taupo Subdivision," by L. I. Grange, New Zealand Geological Survey, Bulletin No. 37 (New Series), 1937, pp. 1-132.
- 2 "Volcanoes as Landscape Forms," by C. A. Cotton, Whitcombe & Tombs, Ltd., London, England, 1944, pp. 1-416.
- 3 "Seismicity of the Earth," by B. Gutenberg and C. F. Richter, Princeton University Press, Princeton, N. J., 1949.
- 4 "The Crystal Structure of the New Zealand Region as Inferred From Studies of Earthquake Waves," by K. E. Bullen, Sixth Pacific Science Congress, vol. 50, 1940, pp. 103-110.
- 5 "New Zealand C<sup>14</sup> Age Measurements," by C. J. Fergusson and T. A. Rafter, *New Zealand Journal of Science and Technology*, section B, vol. 35, no. 1, July, 1953, pp. 127-128.

## Discussion

O. P. BERGELIN.<sup>8</sup> Having had the good fortune to take part in this interesting project during the first half of 1952, the writer would like to mention the exceptionally good work done by the Ministry of Works in developing drilling methods and in overcoming the many problems which arose in handling the output of the wells. The time factor was important and therefore the research, exploration, and drilling all had to be carried out at one time. The progress that has been made and the good record of safety that has been maintained are a tribute to all who have worked on the project.

H. B. NOTTAGE.<sup>9</sup> In reading this fascinating story of New Zealand's great natural source of power, keen interest naturally arises in the harnessing of this potential for useful output. It is believed that many of us are sincerely interested in hearing further remarks on the varied aspects of the industrial development program itself. What are some of the major plans and

<sup>8</sup> Professor, Department of Chemical Engineering, University of Delaware, Newark, Del. Mem. ASME.

<sup>9</sup> Project Manager, Propulsion Research Corporation, Santa Monica, Calif. Mem. ASME.

problems involved in establishing an industrial region; such as plant sites, raw materials, harnessing the geothermal power, availability of by-products or low-potential thermal energy, and in designing, installing, and operating the actual equipment involved?

### AUTHOR'S CLOSURE

The author wishes to express his appreciation of the opportunity given to present this and the companion paper<sup>10</sup> on steam sampling at the Diamond Jubilee Meeting of the ASME, and of the assistance rendered by Dr. Bergelin in preparing the papers for publication. Dr. Bergelin's own visit to New Zealand came at a most opportune time, and his work there in 1951 and 1952 contributed greatly to the establishment of a sound foundation for steam measurements and other research.

In the period between the writing of this paper and the present time, the rate of drilling at Wairakei has been considerably accelerated, and the results obtained have fully confirmed the promise of earlier exploration. There is every reason to expect that in the course of the next twelve months, enough progress will have been made, and enough new information obtained, to justify further publication along the lines of the present paper.

<sup>10</sup> Published in this issue, pp. 269-278.

# Flow Sampling and Discharge Measurement in Geothermal Bores

By C. J. BANWELL,<sup>1</sup> LOWER HUTT, NEW ZEALAND

The development of a sampler for measuring the heat and mass discharges of steam bores is described, and the results obtained in a number of test runs are compared with those given by full-scale separating and metering equipment. The sampler also has been used to investigate the flow distribution across a free steam-water jet, and the results are shown in graphical form and some of their implications discussed.

## INTRODUCTION

IN THE course of the development of the natural heat resources of the Wairakei thermal area in the North Island of New Zealand, borehole outputs ranging from 10 million Btu per hr and 20,000 lb per hr for the smaller and earlier boreholes, to 200 million Btu per hr and 500,000 lb per hr for the larger and more recent, have been obtained. Wellhead pressures range from about 50 psig up to 300 psig at these outputs, and the average discharge consists of about 25 per cent steam and 75 per cent water, measured at atmospheric pressure. It is important to measure and sample these flows as accurately and expeditiously as possible, and the problem presents considerable difficulties.

With the smaller boreholes, measurements of heat and mass output can be made satisfactorily by means of a steam calorimeter. However, the size of the calorimeter (which must be mobile) and other operating difficulties become troublesome above about 25 million Btu and 100,000 lb per hr, and measurements on the larger bores have been made with a separating and metering plant that deals with the whole flow. For the smaller bores, a mobile unit has been built, but for the larger a special installation is required at each bore. These installations are relatively large and costly and take several weeks to set up, so that despite the reliability of the method there would be considerable use for an auxiliary measuring system that could be installed quickly and used often. Since sampling methods were becoming of importance for chemical analysis, measurement of gas content, checking of separator performance, etc., it was decided to try to develop a sampling system that would both enable bore outputs to be measured, and give some preliminary information about the behavior and distribution of the steam-water mixtures in the pipe lines.

Bores are normally allowed to discharge to atmosphere during the testing period, so that many difficulties can be avoided by sampling the mixed jet at the point of discharge. However, critical flow conditions may occur at the discharge point, the flow is often very irregular and turbulent, and may carry rock particles and abrasive material. Thus there was some doubt whether a collecting device could be made that would stand up to these conditions for long enough to be useful, and the position of which in the jet could be controlled satisfactorily.

<sup>1</sup> Chief Physicist, Research, Dominion Physical Laboratory.

Contributed by the Heat Transfer Division and presented at a joint session of the Heat Transfer and Power Divisions at the Diamond Jubilee Annual Meeting, Chicago, Ill., November 13-18, 1955, of THE AMERICAN SOCIETY OF MECHANICAL ENGINEERS.

NOTE: Statements and opinions advanced in papers are to be understood as individual expressions of their authors and not those of the Society. Manuscript received at ASME Headquarters, June 27, 1955. Paper No. 55-A-97.

## FIRST DESIGN

Some preliminary calculations showed that, at the flow rates usually found, a nozzle with an area of 0.25 to 0.5 sq in. would collect steam and water at a rate that could be handled by a calorimeter of convenient size and, at the same time, would be large enough to keep heat losses from connecting lines conveniently small. A water calorimeter was chosen as the measuring instrument because it has several advantages. It measures both steam and mass flow; it has the useful characteristic of integrating the flows (which may be quite variable) over the period of measurement; it offers a minimum of back pressure; it is simple to build and operate. The choice of back pressure at the nozzle to give correct sampling presents some interesting problems, which will be discussed later, but at this point in the design it was assumed that the collecting nozzle should present as little obstruction to the flow as possible. Since the fluid in the jet would be escaping freely to atmosphere, the attempt was made to simulate this condition inside the nozzle by expanding to a larger diameter (1.5 in.) fairly rapidly and keeping back pressure low. To allow tests at different back pressures, a throttling valve and pressure gauge were included in the line at the calorimeter.

The calorimeter used for all the work described herein consisted of a 55-gal drum, uninsulated except at the bottom. Temperature was measured by a pair of copper-constantan thermocouples immersed to two different depths, and water level by an air-purge system and external manometer. In the first series of tests, flow from the sampler was controlled by means of the throttling valve or by traversing the collecting nozzle into and out of the jet. Later, a pair of coupled quick-change valves were fitted, to enable the sample flow to be switched quickly between calorimeter and waste without interruption. The final arrangement is shown in Fig. 1.

The mechanical specification for the collecting nozzle and mount aimed at producing a piece of equipment that could be fitted to flanged or unflanged pipe endings of any diameter between 4 and 12 in. could be handled and fitted conveniently by one man, and would allow the nozzle to be traversed across the pipe mouth along any diameter. The supporting structure was designed for a thrust of 200 lb on the nozzle and parts exposed to the jet. Surfaces facing upstream were made of heavy material and faired to reduce thrust and damage by rock particles, and the nozzle, which was thin-edged to reduce uncertainty in the effective collecting area, was hardened and made easily replaceable. The construction is shown in Fig. 2. The nozzle and supporting frame are pivoted on two removable pins, and traversed by a worm and quadrant. In use, the nozzle is placed much closer to the pipe end than shown in Fig. 2. The adjustable V-shaped yokes can be clamped to the pipe first in the required position, and the nozzle assembly then attached with the nozzle swung out of the jet, so that it is not essential to close off or divert the discharge to install the sampler. However, diversion is usually desirable because of the uncomfortably high noise level at the jet, and because objects touching the jet are liable to be sucked in and thrown to a considerable distance.

## SAMPLING SCHEDULE

Provision for traversing the nozzle across the mouth of the



FIG. 1 CALORIMETER INSTALLATION AT BOREHOLE NO. 26

pipe is necessary because the distributions of both composition and velocity across the emerging jet are likely to be nonuniform. In a long horizontal section of pipe and at the velocities normally occurring, the liquid component of the discharge tends to travel along the lower part, and irregularities in the pipe wall, due to valves and branches, or changes in direction at bends, also lead to changes in distribution. If the flow is symmetrical about the center of the pipe, measurements at a series of points across any diameter will give all the information required and, if the distribution of flow is uniform across some diameter, a traverse along this diameter will again give satisfactory sampling, though the results will have to be weighted differently to find the total flow. More irregular distributions obviously will demand sampling at more points but in such cases it usually would be advisable to try to improve uniformity by adding flow-spreading orifices upstream or altering the layout of the piping.

The heat content, mass flow, and so on, of a sample taken with the nozzle in a particular position will have a "weight" or significance with respect to the whole discharge that will depend on the distance between the nozzle and pipe axes. Assuming axial symmetry of the flow, a sample taken with the axes coincident represents only the discharge through a central area equal to that of the nozzle, while at positions away from the axis, the sample taken with a circular nozzle represents, very nearly, the flow through an annulus with outer and inner radii equal to the distance between the axes plus and minus the radius of the nozzle. In averaging the results from a series of point-by-point observations, in order to find the total flow, each result should be multiplied by a weighting factor proportional to the area of this annulus.

Similarly, if there is reason for assuming some other form of flow distribution, other weighting procedures could be worked out, but in calculating all the results given here, axial symmetry has been assumed; the only precaution taken has been to insure that the diameter traversed always lay in the direction in which greatest separation of steam and water would be expected from

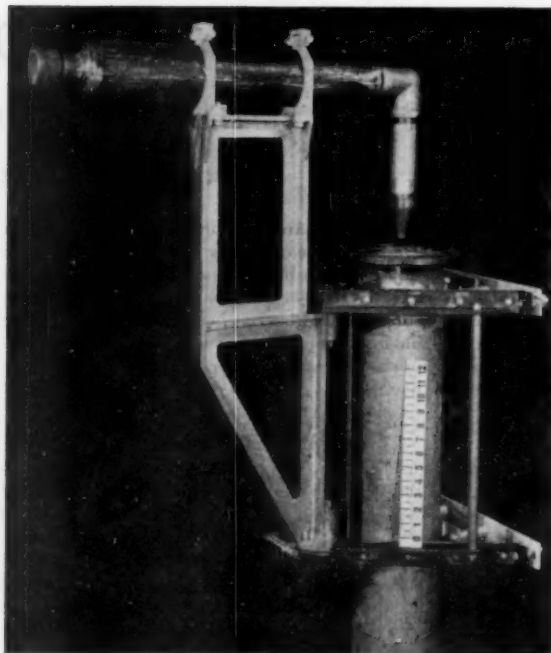


FIG. 2 MK I SAMPLER

upstream conditions. Experience has shown that the composition and rate of flow change only slowly over the central parts of the pipe, but change rapidly and drastically toward the wall, so that it is necessary to take more samples in the outer parts of the flow.

#### TIMED TRAVERSES

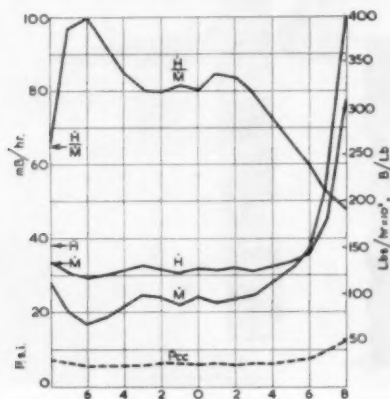
Where the purpose of using the sampler is primarily to measure the total output, the foregoing sampling procedure can be simplified and expedited greatly by making a single traverse across the jet with a time schedule such that the time spent at each point is proportional to the weight assigned to the sample at that point. The mass of water and quantity of heat collected in the calorimeter during the traverse will then give the required weighted total. Every point in the jet is sampled in this way, only one set of calculations is required, and the time for the traverse is of the same order (5 to 10 min) as that for each single-point observation. An equally thorough point-by-point set would take almost 10 hr and, apart from the time involved, could result in prohibitively heavy wear on the sampler in bores discharging much abrasive material.

#### TESTS OF FIRST MODEL

This sampler was first set up at borehole No. 12, which was discharging horizontally through a 6-in-ID pipe, and was throttled to a wellhead pressure of 60 psi by a gate valve, approximately  $7/8$  closed, 70 in. upstream of the open end. The chord of traverse was arranged to be parallel to the valve spindle, since it was expected that the asymmetry in the flow due to the form of the gage opening would be greatest in this direction. A preliminary traverse across the jet with the valve in the calorimeter line closed showed a rise in pressure toward the side opposite the valve opening. Observations of heat output and mass flow were made at 16 uniformly spaced positions across the jet, three runs, each lasting one minute, being taken at each position. The calorimeter tem-

perature rise in each run was 10 to 15 deg C and 25 to 30 lb of water was collected.

The results from borehole No. 12 are plotted in Fig. 3. The right-hand side of the diagram corresponds to the side of the pipe mouth opposite the throttling-valve opening, and the separation of steam and water (presumably due to the presence of this eccentric opening) is quite apparent. From the enthalpy curve, there is evidently much water at the pipe wall at both sides, but opposite the valve opening the flow at the wall is almost entirely water. Despite this, the high mass flow results in the heat flow also being a maximum along this side. Values for the total heat and mass discharge from the bore, calculated from the weighted means just discussed, are shown by the horizontal arrows.



STEAM SAMPLER, HOLE 12, RUN 1, AUGUST 12, 1953.  
Pw. 60 psi. A.O.S. THROTTLED BY VALVE

FIG. 3 FLOW DISTRIBUTION ACROSS PIPE MOUTH

The next measurements were made at borehole No. 4/2, which was discharging through 160 ft of horizontal 60-in. pipe. A vertical direction of traverse was used, because it was expected that much of the water would be traveling along the lower part of the pipe. The pressure distribution found in a traverse with the calorimeter valve closed showed a sharp peak of approximately 77 psig near the lower edge of the pipe mouth, which supports this supposition, but as only timed traverses were made on this occasion, it could not be checked further. Altogether, four timed traverses each lasting 3 min in alternate directions were run and the results are given in Table 1.

TABLE 1 RESULTS OF TRAVERSES

Run No.	Date	Borehole	Million Btu/hr Samp.	Million Btu/hr Sep.	Thousands lb/hr Samp.	Thousands lb/hr Sep.	Btu/lb Samp.	Btu/lb Sep.	Pw, psi
1	Aug. 12, 1953	12	36	37	139	110	261	336	60
2	Aug. 21, 1953	4/2	112		284		395		
3	Aug. 21, 1953	4/2	107		290		371		
4	Aug. 21, 1953	4/2	106		285		372		
5	Aug. 21, 1953	4/2	106		284		375		
	Means	4/2	108	109	285.6	228	378	478	120
6	Aug. 24, 1953	20	240	207	649	440	370	470	290

The final run with this sampler was made at borehole No. 20. This borehole was the first of the larger and deeper development boreholes to be completed and its output, judged by wellhead pressure and observation of the discharge, appeared much greater than that from any of the previous boreholes. The discharge was vertical, through a section of 8-in. pipe, and the flow was throttled at the base of this section by a 5 1/2-in. venturi valve fully open. The wellhead pressure was 290 psi. Much difficulty was found in forcing the sampling nozzle into the jet from this

borehole, and marked deflection and vibration of the nozzle mount were noted; a closed-in pressure of 85 psi was read with the nozzle in the edge of the jet, and a 5-min timed traverse was started. About 1 1/2 min after starting, the light-alloy casting supporting the nozzle fractured and the nozzle was thrown out of the jet. Calorimeter water level and temperature were noted at this point, and a calculation of output made, based on the time spent in the jet. The results given in Table 1 agree reasonably well with the separator results obtained later, indicating that the flow distribution across the jet must have been fairly uniform. The vertical discharge and the presence of the venturi orifice would both be expected to help maintain uniformity.

#### RESULTS WITH Mk I SAMPLER

Results are given in Table 1. The columns headed "Sep." give values obtained by the Ministry of Works Measurements Group, using the full-scale separating and measuring plant.

The agreement between the separator and sampler results for boreholes Nos. 12 and 4/1 is good for the heat outputs, but the sampler invariably gives a considerably larger mass output, and consequently a lower enthalpy. For borehole No. 12, the difference could be attributed in part to water accumulated in the connecting hose between runs, but this trouble would not occur in the timed runs at borehole No. 4/2, because these runs begin and end with the nozzle out of the jet, and the hose was drained between runs. Also, the results from the four runs agree well among themselves. The reasons for the difference have not yet been cleared up completely but a contributory factor appears to be the carry-over of water with the separated steam that comes from the U-bend separator in the full-scale plant. This water has a negligible effect on the measured steam flow, but recent checks by chemical methods show that the quantity may be appreciable, and this water would not appear in the final total flow measurement by the separator plant. The high mass and heat flows and low enthalpy for borehole No. 20 are probably due to the sampler run being confined to the outer part of the jet.

#### DESIGN OF SECOND SAMPLER—Mk II

The experience with the Mk I sampler showed that much heavier construction would be needed to deal with the larger bores, and a new model was developed to withstand shock loads of 500 psi of projected area of all parts exposed to the jet. To reduce jet velocity, a special discharge section, expanding from 8 to 12 in. ID with a 7-deg included angle, having a total length of 5 ft, was constructed. The sampler was mounted on the 12-in. flange by a ring clamp which allowed it to be rotated into any position about the pipe axis. The general appearance of the

nozzle and traversing mount is shown in Fig. 4, which shows the installation at borehole No. 26. The final assembly with electric drive and control unit is shown in Fig. 5.

The nozzle traverse with the Mk II sampler is linear and at a rate of 0.2 in. per revolution of the driving worm. The electric drive will rotate the worm one complete revolution each time a button on the control unit is pressed, and the position of the nozzle is shown by the dial indicator on this unit. Automatic stops at 33 turns either side of center are provided, and these

positions are normally used as the starting points for timed traverses.

The Mk II sampler was first set up at borehole No. 26. This borehole had been completed in January, 1954, to a depth similar to No. 20, and when opened had shown a similar performance, except that an appreciable quantity of rock fragments had been thrown out. It had been closed down for several weeks prior to the installation of the sampler. The wellhead fittings on this occasion consisted of the main well-control valve, an auxiliary throttling valve, both 8 in., an 8-in. spool piece, 5 ft 2 in. long, and the special expanding discharge section. This supported the sampler directly above the well and about 6 ft above the drilling platform. No by-pass was fitted so the well had to be opened with the sampler in position and the sampler was exposed to the discharge as long as the well was running, though the collecting nozzle could be left outside the jet.

The borehole was opened on May 13, and was found to be still throwing out an appreciable quantity of hard-rock fragments. The nozzle was kept out of the jet for the opening period, but considerable damage occurred to the sheet-metal coverings over the slide, and to the cast-aluminum shroud at the base of the nozzle. The condition of the nozzle carriage and shrouds after a period of about 10 hr in the jet is shown in Figs. 6 and 7. The battered appearance of the sheet-metal cover in the lower left of Fig. 6 is due to rock particles, but the grooving shown in



FIG. 4 Mk II SAMPLER INSTALLATION AT HOLE NO. 26

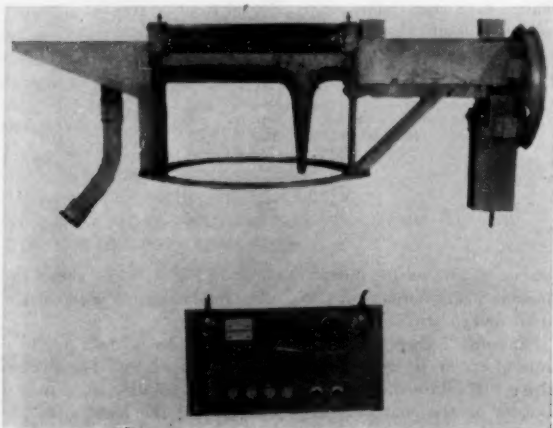


FIG. 5 Mk II SAMPLER WITH ELECTRIC DRIVE AND CONTROL UNIT

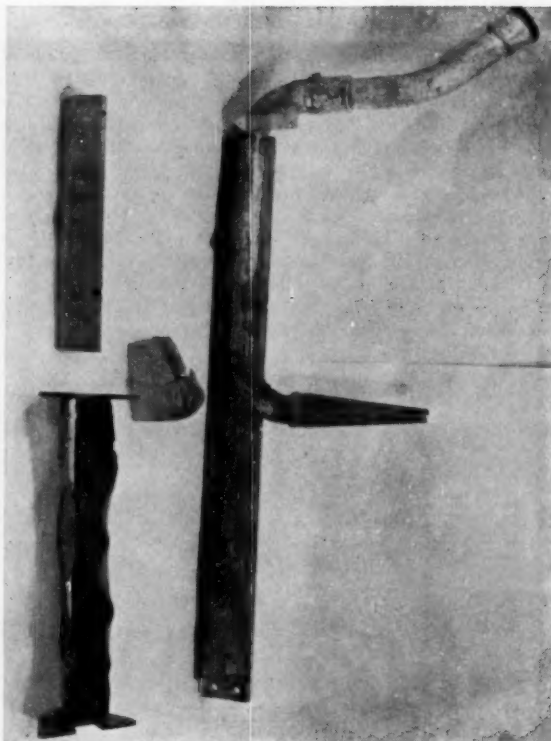


FIG. 6 NOZZLE MOUNT AND SHEATHING AFTER EXPOSURE TO DISCHARGE AT BOREHOLE NO. 26

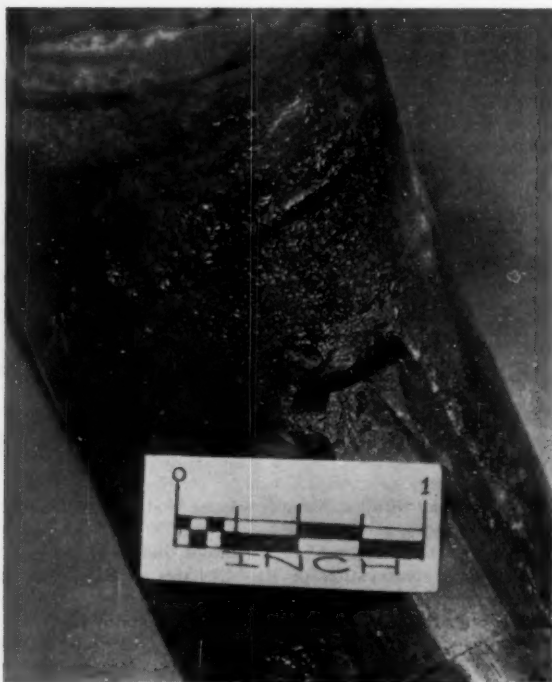


FIG. 7 DETAIL OF EROSION AT BASE OF NOZZLE

TABLE 2 RESULTS OF BOREHOLE NO. 26 TESTS

Run No.	Date 1954	Output		Btu/lb	M	A	P <sub>w</sub> , psi	P <sub>cc</sub> , psi
		mB/hr	10 lb/hr					
7	May 14	397.3	691.8	548.7	1	0.5	140-95	
8	May 26	356.8	808.0	441.52	Gate	0.25	165-140	
9(a)	May 27	See Fig. 9			Gate	0.25	167-145	50
9(b)	May 27	See Fig. 9			Gate	0.5	165	33
10	May 28	301.7	725.7	415.8	Gate	0.5	178	
11	Aug. 16	280.4	626.4	447.8	0.4	0.25	200	
12	Aug. 17	207.3	433.2	478.8	0.2	0.25	300	
13	Aug. 18	245.5	533.3	460	0.3	0.25	250	
13/1 <sup>a</sup>	Aug. 18	241.8	553.2	437.1	0.3	0.25	250	
13/2 <sup>a</sup>	Aug. 18	243.2	526.5	461.7	0.3	0.25	250	
13/3 <sup>a</sup>	Aug. 18	248	561	442	0.3	0.25	250	
13/4 <sup>a</sup>	Aug. 18	249.2	547	455.6	0.3	0.25	250	
13/5 <sup>a</sup>	Aug. 18	247.3	531.8	465.06	0.3	0.25	250	
13/6 <sup>a</sup>	Aug. 18	248	537.6	461.5	0.3	0.25	250	

<sup>a</sup> Timed traverse taken immediately before point-by-point run No. 13.<sup>b</sup> Timed traverse taken immediately after point-by-point run No. 13.<sup>c</sup> Mass determined by chloride method.

the aluminum shroud (center) and in the steel nozzle carriage (Fig. 7) is typical of the erosion occurring even in relatively clean mixed flows, usually at points of direct impact or change of direction of the fluid.

The well was left closed overnight and reopened the next morning when a set of point-by-point runs (No. 7) was taken with the throttling valve fully open. Results are given in Table 2. Because of the high rate of wear on the sampler, it was not possible to allow enough time for the well condition to stabilize, and the wellhead pressure was falling throughout the period of measurement, most rapidly at the beginning.

After this run, an 8-in. by-pass with a throttling valve was fitted at the wellhead, so that the well could be left to stabilize overnight by discharging through the by-pass at the desired pressure, and the flow diverted past the sampler only during the measurement period. Also, the portable thermocouple potentiometer was replaced by a multipoint recording potentiometer, which avoided the need for a balancing operation made extremely tedious by galvanometer instability resulting from the high noise level near the bore. Runs with the new arrangement were started on May 26 and Nos. 8, 9(a), 9(b), and 10 were taken by May 28 when the sampler was removed for repairs and improvements.

The sheet-metal shrouds, some of which had disappeared during the period of operation, were replaced by much heavier material and other improvements made to keep steam and water out of the slides and driving mechanism. The electric drive was fitted, and tests resumed at borehole No. 26 on August 9, 1954. The calorimeter was now installed in the operating hut, which protected it from falling water, and enabled one operator to run a series of tests without leaving the hut. An orifice assembly was installed at the lower mounting flange of the expanding section immediately above the valve and throttling of both vertical and by-pass discharge was done by means of orifices of suitable size. This avoided wear on the valves, which were now required only for shutoff purposes, and gave a much more symmetrical flow into the expanding section. Except for minor changes these arrangements have been used in all the later observations and have proved essentially satisfactory.

**Results From Borehole No. 26.** Results of point-by-point sets are given in the graphs of Figs. 8 to 12, and the weighted averages of the sets in Table 2.

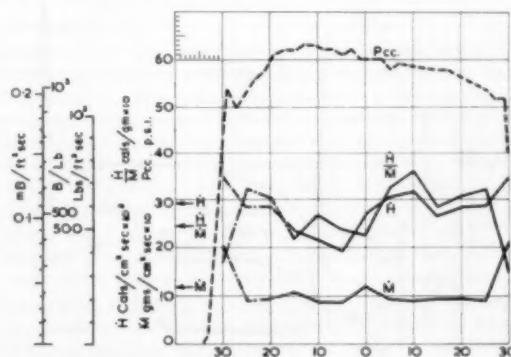
#### DISCUSSION OF RESULTS

The various graphs showing measured flows as a function of nozzle position were plotted initially in terms of cgs units, and scales showing the corresponding fps values have been added at the left-hand edge. The pipe axis corresponds to  $N = 0$ , and the nozzle axis is in line with the inner wall of the mount of the expanding section at  $N = 30$  on either side. The rate of flow to the sampler is greatly reduced at  $N = 31$ , and this has been taken as the effective position of the edge of the jet for reducing the measured flows to total discharge. Because of the weighting procedure

used, little or no error is introduced by the inclusion of the low values at the jet edge in the calculations.

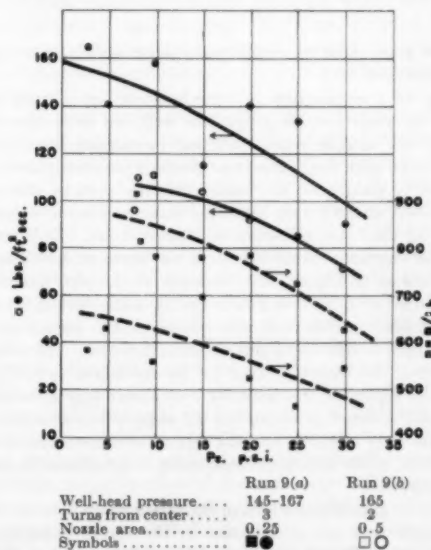
Fig. 8, for Run 8, where the flow is only slightly throttled, shows fairly uniform shut-in pressures and flows across most of the jet, except for a fall in enthalpy near the wall to a value indicating the flow is mostly water. Fig. 10, Run 10, shows the same effect, but there is also a marked asymmetry, the enthalpy curve showing that much of the water is traveling up the side of the pipe opposite the

valve opening. Both heat and mass flows become very large near the walls, and this increase is accompanied by very much higher shut-in nozzle pressure, an effect which is even more noticeable in Figs. 11 and 12. These pressures, especially the higher ones, always took a considerable time to reach a final value, and the pressure gage showed wide and rapid fluctuations, so that



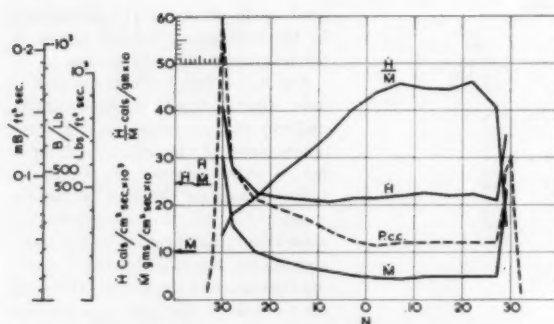
STEAM SAMPLER, HOLE 26, RUN 8, MAY 26, 1954.  
WELLHEAD PRESS 145-140 psi, A.O. 25 sq. in., THROTTLED BY VALVE

FIG. 8 FLOW DISTRIBUTION ACROSS PIPE MOUTH



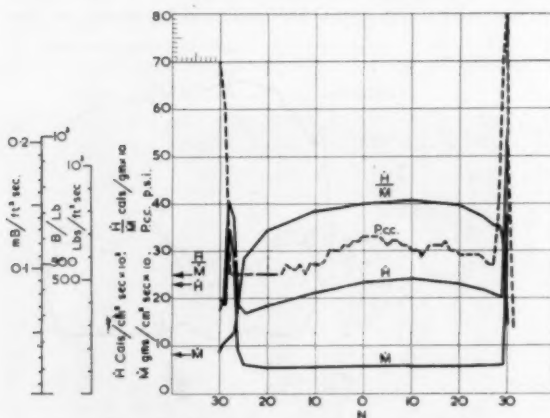
Well-head pressure.... Run 9(a) Run 9(b)  
Turns from center.... 145-167 165  
Nozzle area.... 3 2  
Nozzle area.... 0.25 0.5  
Symbols..... ■● □○

FIG. 9 RATE OF SAMPLING AT DIFFERENT BACK PRESSURES



STEAM SAMPLER, HOLE 26, RUN 10, MAY 28, 1954.  
WELLHEAD PRESS. 178 p.s.i., A=0.5 sq. in., THROTTLED BY VALVE.

FIG. 10 FLOW DISTRIBUTION ACROSS PIPE MOUTH



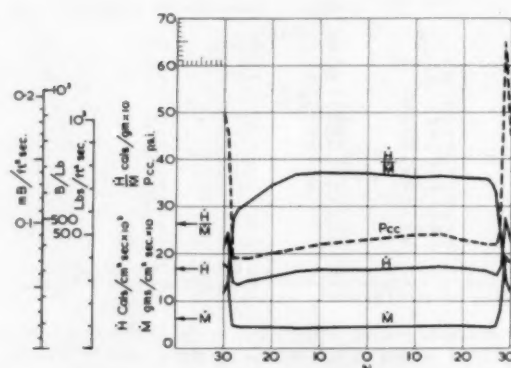
STEAM SAMPLER, HOLE 26, RUN 11, AUGUST 16, 1954.  
Pw. 200 p.s.i., M=0.4, A=0.25 sq. in.

FIG. 11 FLOW DISTRIBUTION ACROSS PIPE MOUTH

the values given must be considered as estimates of the final mean pointer position.

In Fig. 13 a comparison is made between the outputs measured for borehole No. 26 at various wellhead pressures in the course of the sample runs described previously, and the results obtained with the Ministry of Works separating plant. The agreement is good over the higher-pressure part of the range, but the trend of the curves indicates that the sampler values are too high at the lower pressures and larger flows. This may be due to the sampling nozzle collecting too much under these conditions because of higher static pressure at the pipe mouth, but the well was far from being in a steady state during the early sampler measurements, and the scatter of the points scarcely justifies much weight being put on the difference. The comparison between the output curves for borehole No. 4/1 (Fig. 16) made with separator and sampler also shows higher values for the sampler at lower pressure, but the sampler observations were made soon after opening, and the separator measurements some months later, so the difference could easily be attributed to changes in bore behavior.

In order to gain a better idea of the relationship between nozzle back pressure and rate of collection by the nozzle, Runs 9(a) and 9(b) at borehole No. 26 and Runs 14 and 15 at borehole No. 4/2 were made. In Figs. 9 and 14 the lines are the estimated best



STEAM SAMPLER, HOLE 26, RUN 12, AUGUST 17, 1954.  
WELLHEAD PRESS. 305 p.s.i., M=0.2, A=0.25 sq. in.

FIG. 12 FLOW DISTRIBUTION ACROSS PIPE MOUTH

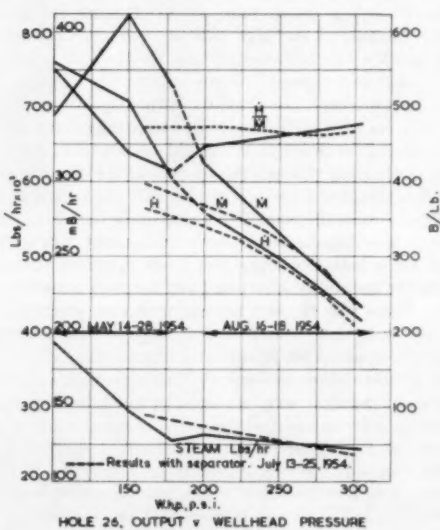


FIG. 13 BOREHOLE NO. 26—COMPARISON WITH SEPARATOR MEASUREMENTS

curves through experimental points. Because of the relatively small output from borehole No. 4/2, the maximum closed-in pressure obtainable was considerably smaller than at borehole No. 26, so that the same pressure range could not be covered as in Runs 9(a) and 9(b), but the discharge was relatively steady as the smaller scatter in the plotted points shows. All these runs show the tendency to collect relatively more water as the back pressure is increased, and show that the smaller nozzle collects more water than the large nozzle at a given back pressure. From elementary single-phase flow theory, one would expect to obtain the correct sampling rate by throttling to a back pressure equal to the closed-in pressure minus the dynamic head corresponding to the velocity of flow of the sample in the line at the pressure gage. Calculation shows the dynamic head to be about 0.5 psi and the theoretical back pressure therefore from Fig. 14 is about 11.0 to 11.7 psig. However, the best agreement with separator results, both for mass flow and enthalpy, is obtained by operation close to zero back pressure on the flat parts of the curves of Fig. 14. On the other hand, the curves in Fig. 9 show a much smaller droop with increasing back pressure and, if the sampling rate at, say, 30 psi

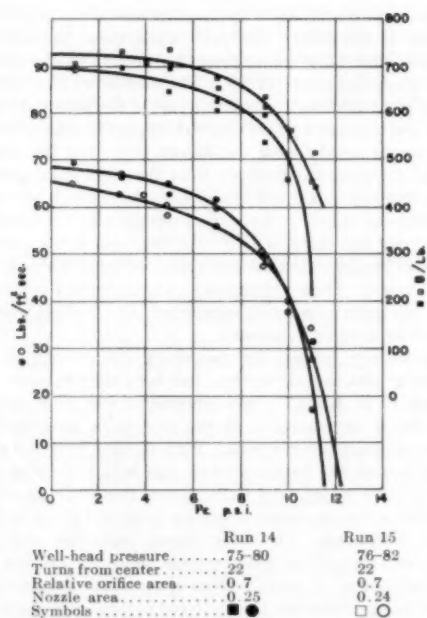


FIG. 14 RATE OF SAMPLING AT DIFFERENT BACK PRESSURES—HOLE 4/2, NOV. 10, 1954

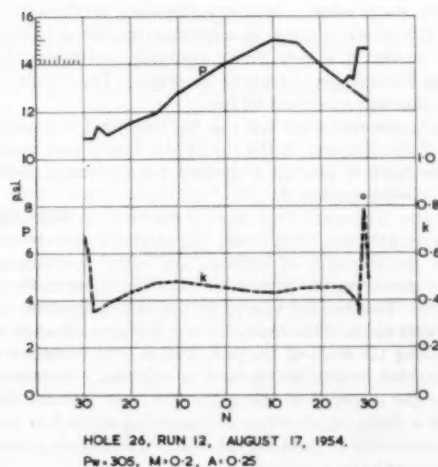


FIG. 15 VELOCITIES AND PRESSURES AT SAMPLING POINT

back pressure in Run 9(b) could be assumed to represent the correct rate, much of the discrepancy between the lower-pressure sampler and separator mass flows of Fig. 13 would disappear, but the disagreement in the enthalpies would be made worse. It is clear that much more experimental work, over a wide range of flow rates and mixture compositions, is needed to provide adequate experimental data, and meanwhile these few results are presented as some indication of the nature of the problem.

The high closed-in pressures associated with the very wet parts of the flow near the pipe wall are difficult to explain unless one assumes a very high momentum for the water. Since these high

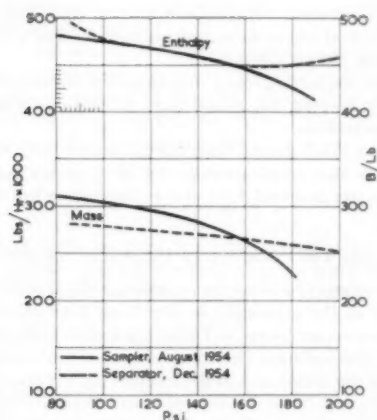


FIG. 16 BOREHOLE No. 4/1 OUTPUT CURVES

pressures have been found only when the flow has been throttled through a relatively small opening, with an upstream pressure that would produce critical-flow conditions at some point in dry steam and could produce a velocity approaching that of sound in the wet mixture, it is suggested that the high pressures are due to the impact at the nozzle of water that has retained a considerable part of this velocity. The high velocity is most likely to be retained where the water is most concentrated, near the edge of the pipe mouth, whereas the water is more likely to be broken up into small particles and transfer its momentum to the surrounding steam in the drier parts of the flow. If one assumes some arbitrary static pressure at a given point in the plane traversed by the sampling nozzle at the pipe mouth, it is possible, from the measured sampling rate, to calculate a value for the steam velocity and for the water velocity then needed to bring the total pressure up to the observed shut-in pressure (see Appendix). By trial it is also possible to find a static pressure that will make water and steam velocities equal at each point, except in the region of high closed-in pressures and high water flow near the edges, where the method fails. Here, one is forced to assume either an increasing static pressure toward the edge of the jet, which seems inherently improbable, or a higher water velocity, which seems possible.

Fig. 15 gives the static pressures ( $P$ ) at the pipe mouth from Run 12 calculated on the assumption of equal steam and water velocities over the central part, and of constant static pressure at the edge equal to the last calculable value. Velocities ( $k$ ) are shown as a fraction of the velocity of sound in saturated water vapor at 130 C (1392 fps). Extrapolation of the pressure curve to the pipe wall as shown by the dashed line would result in only a small increase in  $k$  (to point shown by circle), at the position of highest pressure ( $N = 29$ ). Similar calculations for Runs 14 and 15 at borehole No. 4/2 give static pressures of 6.5 psi and 8.0 psi, and values of  $k$  of 0.48 and 0.44, respectively. The contributions of water momentum to total closed-in pressure are 2.46 psi and 2.02 psi, and if we ignore these in calculating the proper sampling back pressure, we have values of 9.04 and 10.24 psi, respectively. Reference to Fig. 14 shows that operation at these pressures would give a large disagreement between the results from the different-sized nozzles, also comparison with separate measurements shows that the measured flows would be too small and too low in enthalpy.

The conclusions from the foregoing discussion appear to be as follows:

1 Good agreement between sampler and separator measurements is obtained where the sampler is used for flow rates not exceeding about 150 psf per sec.

2 In a jet discharging freely to atmosphere, correct sampling is obtained by keeping the nozzle back pressure as close to atmospheric as possible.

3 At flows much greater than 150 psf per sec there may be no back pressure that simultaneously will give correct sampling of steam and water in mixed flows of the composition found in these bores.

#### FLOW AND PRESSURE AT THROTTLING ORIFICE

The water flows ( $F$ ) in psf per sec through the throttling orifice at the base of the expanding section have been calculated for several runs and are given in Table 3, together with orifice area ratios ( $M$ ) and wellhead pressures ( $P_w$ ) measured immediately upstream of the orifice and steam fraction ( $x$ ) at pressure  $P_w$ .

TABLE 3 WATER FLOWS THROUGH THROTTLING ORIFICE

Run no.	$F$	$M$	$P_w$	$x$	Hole no.
7	401	1.0	100	0.27	26
11	1122	0.4	200	0.10	26
13	1300	0.3	250	0.09	26
12	1550	0.2	305	0.10	26
14	397	0.7	75-80	0.20	4/2
15	392	0.7	75-80	0.21	4/2

Comparison of these results with those obtained with mixed flows of steam and water by Benjamin and Miller<sup>2</sup> and shown in graphical form in their Figs. 8 and 14, indicate that reasonable agreement will be obtained if we assume a pressure differential of about 60 psi across the orifice for Run 12 down to 10 to 15 psi for Runs 13 and 14. The experimental ranges do not overlap, and some extrapolation is necessary for the comparison, which is thus rather rough, but it appears there must still be considerable pressure immediately downstream of the orifice, and a correspondingly large pressure drop along the expanding section. Benjamin and Miller conclude from their experimental results that no critical pressure will exist in a sharp-edged orifice passing saturated water even when downstream conditions are such that flashing can occur. The calculated value for  $k$  in the orifice for the conditions of Run 12 is 0.2, assuming the mixture to have the composition corresponding to the upstream pressure, and 0.29 immediately downstream of the orifice, assuming equilibrium composition corresponding to a 60-psi pressure drop. A water particle escaping from the upstream pressure region to atmospheric pressure without energy loss would have a velocity corresponding to  $k = 0.15$ , so that the high velocities shown in Fig. 15 of this paper must have occurred somewhere downstream of the orifice, possibly close to the end of the expanding section. It is intended to measure the pressure distribution along the expanding section in some further experiments, and thus perhaps throw some further light on the flow conditions there.

#### SAMPLING AND DENSITY MEASUREMENTS IN PIPE LINES

A number of members of the Dominion Physical Laboratory staff have been engaged in experimental work with mixed flows of known composition at borehole No. 9, Wairakei. A separating and metering plant has been set up at this bore, so that controlled steam velocities of up to about 150 fps, pressures up to 100 psi, and water flows up to about 0.2 cfs in 4 or 6-in. pipe lines, are available.

M. L. Horlor has tested a 1/4-in. pitot assembly which can be traversed across a diameter of a 6-in. pipe at this bore. At a pressure of 120 psia, and a wet-steam velocity of 89.3 fps, he has

found the average wetness of the mixture near the pipe wall about twice that at the center, and that nearly three quarters of the total water flow takes place along the bottom of the pipe at a velocity of approximately 11 fps. The total water flow calculated from the pitot velocity in the lower part of the pipe and from the velocity and average wetness of the steam in the remainder of the section agrees closely with the known flow, but the velocities calculated by standard methods from the differential pitot pressures in this region are not of the correct order; if the density used in the calculation is the mean value for the wet mixture the result is only one third of that expected, and if the mixture is assumed to be dry steam the calculated velocity is about double the true value. These experiments were intended primarily to test the equipment and gain experience, and further work with an improved sampler is planned.

A satisfactory method for measuring the density in mixed flows, using beta-ray absorption, has been developed by R. E. Belin and F. B. Knox. Their equipment will allow the mean density across any diameter of the pipe to be measured to an accuracy of about  $\pm 5$  per cent. With it, they have studied the flow distribution in a horizontal 4-in. pipe with increasing quantities of injected water, and have shown that substantially dispersed flow occurs at steam velocities down to 130 fps and water flows of 0.026 cfs. At lower steam velocities and higher water flows, most of the water travels along the bottom of the pipe. Only one set of combinations of water flow, steam velocity, and pipe-line pressure has been covered in these experiments, and much more work is still necessary to give a complete picture.

Belin and Knox also have used the beta-absorption method to study the effectiveness of an orifice for making mixed flows more homogeneous. Their observations show that an orifice that increases the steam velocity from an initial value of 90 fps (in a 6-in. pipe) to 225 fps will disperse an accompanying flow of 12 lb per sec of water so that it is very nearly uniformly distributed through the steam 2 to 3 ft downstream of the orifice. The velocity of the water in this region is about 90 fps.

The beta-absorption method also has been used to measure the density of the discharge in the throat of a critical-flow nozzle and from this work a promising method for measuring bore discharges is being developed.

The water discharged from most of the bores at Wairakei contains about 2000 ppm of chloride, and attempts have been made to check the efficiency of cyclones and other water-separating plants by measuring the quantity of chloride present in the nearly dry steam. This had led to a further sampling problem, since it appears that much of the residual water becomes attached to and travels along the walls of the pipe, and is thus missed or incorrectly sampled by any simple form of collector. Proposed solutions are the dispersal of the water film back into the flow by means of a sharp-edged orifice and sampling of the flow immediately downstream or trapping the film in a collecting groove, but these have yet to be developed.

#### ACKNOWLEDGMENTS

The author wishes to express his appreciation of the willing assistance given by the Geothermal Project Engineer, Wairakei, and members of his staff in making bores available for test, installing special wellhead arrangements, supplying information, and in doing other work, without which it would not have been possible to produce this and its companion paper in their present form. Nearly all the observational work in connection with sampler measurements up to August, 1954, was done by the author, but the observations at borehole No. 4/1 in August, 1954, were done in conjunction with members of the Ministry of Works Measurement Group, and the operation of the sampler has since been taken over completely by this Group.

<sup>2</sup> "Flow of Saturated Water Through Throttling Orifices," by M. W. Benjamin and J. G. Miller, Trans. ASME, vol. 63, 1941, pp. 419-429.

The author also wishes to acknowledge the assistance given by the Design Office, Dominion Physical Laboratory, in dealing with the many detailed problems involved in instrument development. The author wishes to express his thanks to Prof. O. P. Bergelin for arranging presentation of the papers and for his comments and assistance in preparing them for publication.

## Appendix

### NOMENCLATURE

The following nomenclature is used in the Appendix:

- $A$  = area of collecting nozzle, sq in.  
 $D$  = radial distance of nozzle axis from pipe axis, in.  
 $\dot{H}$  = heat flow, Btu/sq ft/sec or kg-cal/sq cm/sec  
 $L$  = latent heat of steam at atmospheric pressure (538.7 cal/gm)  
 $\dot{M}$  = mass flow, psf per sec or gm/sq cm/sec  
 $M$  = throttling orifice area as fraction of pipe area  
 $M_1$  = mass of water in calorimeter at beginning of run, grams  
 $M_2$  = mass of water in calorimeter at end of run, grams  
 $N$  = number of turns of traversing screw from center position  
 $P$  = static pressure at sampling point, dynes/cm<sup>2</sup>  
 $P_s$  = mean dynamic pressure due to water flow, dynes/cm<sup>2</sup>  
 $P_a$  = pressure at calorimeter, psi, or dynes/cm<sup>2</sup>  
 $P_{cc}$  = closed-in pressure at calorimeter, psi, or dynes/cm<sup>2</sup>  
 $P_v$  = dynamic pressure due to steam flow, dynes/cm<sup>2</sup>  
 $P_w$  = wellhead pressure, psi  
 $r$  = radius of nozzle opening, in.  
 $t_1$  = temperature of water in calorimeter at beginning of run, deg C  
 $t_2$  = temperature of water in calorimeter at end of run, deg C  
 $V$  = specific volume of water vapor, cc/gm  
 $v_w$  = velocity of water, cm/sec  
 $W_N$  = weighting factor at  $N$ th turn from center  
 $x$  = steam fraction, by weight  
 $\rho$  = density of water, gm/cc

NOTE: Absolute cgs units have been used in the equations and numerical results converted to fps units for plotting of graphs and discussion.

### DERIVATION OF FORMULAS

The formulas used for reducing observed calorimeter temperatures and water levels are derived in a straightforward manner, and the values of the constants involved are peculiar to the calorimeter used, so they need not be given here. The weighting factor (ratio of nozzle area to area of annulus represented by the sample) is given by

$$W_N = 4D/r \text{ when } D \text{ is greater than } r. \quad [1]$$

and

$$W_N = (D/r + 1)^2 \text{ when } D \text{ is less than } r. \quad [2]$$

The rate of traverse of the Mk II sampler is 0.2 in. per turn, so that Equation [2] applies only to one or two turns near the center with the nozzle sizes used. For greater values of  $N$ ,  $W$  is given by

$$W_N = 2.005N \text{ for a 0.5-sq-in. nozzle}$$

and

$$W_N = 2.836N \text{ for a 0.25-sq-in. nozzle}$$

The time schedule for timed traverses has been calculated by treating each weighting factor as a time interval and finally scal-

ing each interval so that the total traverse time is some convenient value, either 5 or 10 min.

**Nozzle Pressure.** The following equations show the way in which the static pressure and steam and water velocities shown in Fig. 15 have been found. It has been assumed that all pressures are directly additive, and that the steam and water can be considered separately. The observed closed-in pressure in the nozzle is then

$$P_{cc} = P + P_s + P_a. \quad [3]$$

where  $P$  is static pressure in mixture at sampling point,  $P_s$  is dynamic pressure due to steam flow, and  $P_a$  is mean dynamic pressure due to water flow. Then, by conventional flow theory

$$P_s = \frac{1}{2} (\dot{M}x)^2 V. \quad [4]$$

where  $\dot{M}$  is the total mass flow,  $x$  is the steam fraction, and  $V$  the specific volume of steam at pressure  $P$ . Note that  $x$  is calculated from the enthalpy of the observed flow, and it will not be the same as the average composition of the mixture at the sampling point except when steam and water velocities are equal.

Assuming that the water fraction travels at a velocity  $v_w$  and enters the nozzle only during a fraction  $y$  of the total time, the peak pressure  $P'$  while water is entering will be

$$P' = \frac{1}{2} \rho v_w^2. \quad [5]$$

where  $\rho$  is the density, and the mean pressure averaged over a sufficient period will be

$$P_a = yP' = \frac{1}{2} \rho v_w^2 y. \quad [6]$$

and since evidently  $y = \dot{M}(1-x)/\rho v_w$ , we have, substituting this expression for  $y$  in Equation [6]

$$P_a = \frac{1}{2} \dot{M}(1-x)v_w. \quad [7]$$

Substituting expressions for  $P_s$  and  $P_a$  from Equations [4] and [7] in [3] and rearranging gives

$$v_w = \left[ P_{cc} - \left( P + \frac{1}{2} (\dot{M}x)^2 V \right) \right] / \left( \frac{1}{2} \dot{M}(1-x) \right). \quad [8]$$

while the steam velocity is

$$v_s = \dot{M}xV. \quad [9]$$

Taking the mass flow  $\dot{M}$  and enthalpy to be those observed at some defined calorimeter back pressure (in all these calculations the results obtained at or as close as possible to zero-gage pressure have been used) and taking some trial value for  $P$ , the steam and water velocities can be found from Equations [8] and [9]. If some definite relationship between these two velocities is now assumed, it is possible to find, by trial, for most parts of the flow, values for  $P$  which satisfy this condition.

As already noted, the condition of equality of velocities has been assumed in calculating the values for  $k$  and  $P$  plotted in Fig. 15. However, even without this assumption, the range of values possible for  $P$  is rather limited because of large variations in calculated water velocity resulting from a relatively small change in  $P$ . As an upper limit, it seems extremely unlikely that the water velocity can exceed the velocity of sound in water vapor under the flow conditions considered here, while, in view of the high water

velocities, that appear necessary to assume at the edges of the jet, it seems improbable that the water velocity is much less than that of the steam in the central parts. In some preliminary calculations, in which  $P$  was assumed to be uniform across the jet and equal to 10.8 psi, water velocities of over 0.9 the velocity of sound were necessary at some points. Thus it seems likely that the static pressures calculated must be within a few psi of the actual values, except possibly near the edges, where the calculated values are probably too high. In this connection it is worth remarking that there was evidence of a considerable quantity of air being collected by the nozzle at positions near the edge of the jet, which suggests pressures less than atmospheric in this region. Visual examination of the escaping jet also suggests strong entrainment of air and stray steam into the lower parts.

## Discussion

O. P. BERGELIN.<sup>3</sup> The difficulties in obtaining representative samples from a multiphase stream are known to anyone who has worked in this field. In the present case these difficulties appear to have been increased by the choice of equipment. Sonic velocities in steam-water mixtures are relatively low and probably are exceeded just beyond the vena contracta of the back-pressure orifice. Without any guiding wall there will be over-expansion and, even with a single phase, a complex flow pattern with shock waves might be expected in the expanding nozzle section. The addition of a heavy phase, which partially vaporizes as the pressure is released, and which rapidly assumes a nonuniform distribution across the stream, makes theoretical analysis even more difficult. Therefore it would not seem feasible to attempt to predict the correct sample-nozzle back pressure which may vary in an erratic manner across the stream and change in a different manner for each flow rate.

Some of the difficulties might be eliminated or minimized if the sampling nozzle were moved upstream out of the zone of critical flow at the pipe exit. Following the well-head control valve a relatively large orifice might be used to disperse the wall layer of water into the main stream. The sampling nozzle would traverse this jet at the vena contracta. Following the sampler a straight section of pipe ending in a flow-control orifice or nozzle would complete the assembly. The usual troubles in sampling would remain but the sampling conditions would be under far better control because shock waves would be eliminated and the stream would be at a higher pressure and a lower velocity. The nozzle assembly would doubtless be too much for one man to handle, but it still could be classed as portable.

Another modification to obtain a better sample would be to measure the pressure drop across the sampling nozzle. Experience has shown that, in order to get a representative sample, the pressure just inside the tip of the sampling nozzle should be at

or slightly below the static pressure of the stream. If shock waves are eliminated and acceleration effects are negligible, the static pressure across the stream should be essentially constant. Then by measuring the pressure difference between a tap on the pipe wall opposite the sampler, and another tap located just inside the sampling nozzle, and adjusting this pressure by means of a valve in the sampling line, the most satisfactory nozzle differential pressure for sampling could be maintained. This method would somewhat complicate the design of the sampling nozzle but the improved control should make it worth while.

The author and his associates have made great progress in measuring and handling large flows of two-phase mixtures. It seems probable that they will soon develop a successful metering method along the lines of their current efforts.

## AUTHOR'S CLOSURE

Although the author is inclined to agree with Dr. Bergelin's contention that sampling at a point of higher pressure and lower velocity would avoid some of the theoretical and practical difficulties that could result from the possible presence of shock waves, it should be remarked that the original purpose was to build as simple a device as possible. A design to permit traversing the collecting nozzle across a section of the pipeline under pressure would have added too many mechanical difficulties in the early stages of development, but now that the sampler appears to be well established as an empirically, if not a theoretically, satisfactory device, it is hoped to build a new model that will incorporate some of the improvements that Dr. Bergelin suggests. The fact that it has been found necessary to add the rather massive expanding section for the free discharge measurement means that a pipeline model would have little disadvantage on a weight basis, and could possibly be lighter.

In the course of a series of runs with the sampler at Bore No. 20, in August, 1955, pressures at the tapings on the expanding section were measured. The bore on this occasion was throttled with an  $M = 0.5$  orifice plate at the bottom of the expanding section, wellhead pressure was 142 psi, and the measured mean mass flow 100 lb/ft<sup>2</sup> sec. Pressure at the lowest tapping, 6 in. above the orifice plate, was 17 psi, and at successive tapings at 6-in. intervals downstream pressures were 10, 6, less than 5, and less than zero psi, respectively, all the remaining tapings to the discharge end showing pressures below atmospheric. This does not suggest much constraint of the jet within the expanding section, and leaves some doubt as to whether critical flow conditions would occur except in a region near the vena contracta. In particular, it does not seem evident that the free end of the expanding section, at the plane of traverse of the nozzle, will have an associated shock wave, or that the high closed-in nozzle pressures observed near the edge are due to such a shock wave. The author is still disposed to believe that these pressures are the result of a large momentum acquired by the water in passing through a shock-wave system in the region of the orifice or vena contracta.

<sup>3</sup> Professor, Department of Chemical Engineering, University of Delaware, Newark, Del. Mem. ASME.

# Temperature and Velocity Distribution and Transfer of Heat in a Liquid Metal

By H. E. BROWN,<sup>1</sup> B. H. AMSTEAD,<sup>2</sup> AND B. E. SHORT,<sup>3</sup> AUSTIN, TEXAS

The results of an experimental investigation of the velocity and temperature distributions, together with the corresponding eddy diffusivity and heat-transfer results in a cooled stream of turbulently flowing mercury are presented. The temperature and velocity traverses of the mercury stream were made in a 1.61-in-ID nickel pipe over a range of Reynolds moduli of from approximately 250,000 to 800,000, with constant heat flux, and with the Prandtl modulus maintained substantially constant at 0.02. The relative radial position in a circular pipe at which the bulk mean temperature corresponds to the local temperature was found to be substantially constant and independent of the Reynolds modulus for the range of Reynolds moduli employed. A similar velocity relationship was found to exist. The ratio  $\alpha$  of the eddy diffusivity for heat transfer to the eddy diffusivity for momentum transfer at the mean radius was between 0.7 for the lower Reynolds number and 0.9 for the higher Reynolds number. It was found that, in the absence of an interfacial resistance effect, the Martinelli-Lyon equation represents the heat-transfer data reasonably well, especially if allowance is made for the variation of the eddy-diffusivity ratio  $\alpha$  with the Reynolds number.

## NOMENCLATURE

The following nomenclature is used in the paper:

- $A$  = local heat-transfer surface, sq ft
- $A_0$  = heat-transfer surface at wall, sq ft
- $a$  = thermal diffusivity, sq ft per sec
- $B$  = experimental constant
- $C$  = experimental constant
- $C_1$  = experimental constant
- $C_2$  = experimental constant
- $c_p$  = specific heat at constant pressure, Btu per lb F
- $f$  = friction factor
- $M$  = experimental constant
- $N$  = experimental constant
- $q$  = heat-transfer rate, Btu per sec
- $q_0$  = heat-transfer rate for stream as a whole, Btu per sec
- $r$  = radius at any point in stream, ft
- $r_0$  = inside radius of pipe, ft
- $T^*$  = friction temperature =  $q_0/u^*c_p\gamma A_0$ , deg F
- $t$  = temperature in stream at any point, deg F
- $t_{a1}$  = mean temperature of stream at downstream station, deg F

- $t_{a2}$  = mean temperature of stream at upstream station, deg F
- $t_b$  = temperature base for plotting temperature profile for integration purposes, deg F
- $t_w$  = wall temperature at any axial station, deg F
- $u$  = velocity at any point in stream, fps
- $u_m$  = mean stream velocity, fps
- $u^*$  = friction velocity,  $\sqrt{(\tau_0/\rho)}$ , fps
- $y$  = radial distance from wall, ft
- $\Delta y$  = constant increment of wall distance, ft
- $y^+$  = friction-distance parameter,  $\frac{\sqrt{(\tau_0/\rho)y}}{\nu}$
- $\Delta y^+$  = constant increment of friction-distance parameter
- $\alpha$  = ratio,  $\epsilon_h/\epsilon_m$
- $\epsilon_h$  = eddy diffusivity for heat transfer, sq ft per sec
- $\epsilon_m$  = eddy diffusivity for momentum transfer, sq ft per sec
- $\gamma$  = specific weight of fluid, pcf
- $\nu$  = kinematic viscosity, sq ft per sec
- $\rho$  = density of fluid,  $\gamma/g$
- $\tau$  = shearing stress at any point in stream, psf
- $\tau_0$  = shearing stress at wall, psf

## INTRODUCTION

Many investigators (1 to 4) have reported values of the heat-transfer coefficient for mercury in forced convection that were considerably smaller than predicted by the Martinelli-Lyon analogy (5, 6). In general, the values of the heat-transfer coefficient reported in the literature have been based on the difference in temperature between the bulk mean temperature of the mercury and the wall temperature of the confining tube. These values of the heat-transfer coefficient could have been affected by an interfacial resistance at the tube wall, as has often been claimed. The values of the heat-transfer coefficient reported by Isakoff and Drew (7) were based on a "fluid-wall" temperature that was obtained by extrapolating the experimentally determined temperature profiles of the mercury stream back to the wall. These data are in reasonable agreement with the Martinelli-Lyon analogy but show a rate of change of the Nusselt modulus with respect to the Peclet modulus that is greater than the rate of change predicted by the Martinelli-Lyon analogy.

The discrepancies between the theoretical heat-transfer results and the usual experimental results could be caused by a variation of the ratio  $\alpha$  of the eddy diffusivity for heat transfer to the eddy diffusivity for momentum transfer, as well as by an interfacial resistance. Therefore it was thought that additional data as obtained by the probing method would be of value.

## DESCRIPTION OF APPARATUS

The arrangement of the apparatus is shown in Fig. 1. It consists of a closed loop of nickel pipe with a centrifugal pump for mercury circulation. The mercury is discharged directly into a heating section and returned through a cooling section. The heating section consists of 1 1/4-in. standard nickel pipe jacketed with a 2 1/4-in. brass tube which is approximately 20 ft long. Steam is used for heating the mercury which flows downward in the heater. The cooling section consists of a 25-ft length of 1 1/2-

<sup>1</sup> Associate Professor of Mechanical Engineering, University of Texas.

<sup>2</sup> Associate Professor of Mechanical Engineering, University of Texas. Assoc. Mem. ASME.

<sup>3</sup> Professor of Mechanical Engineering, University of Texas. Fellow ASME.

Contributed by the Heat Transfer Division and presented at the Diamond Jubilee Annual Meeting, Chicago, Ill., November 13-18, 1955, of THE AMERICAN SOCIETY OF MECHANICAL ENGINEERS.

NOTE: Statements and opinions advanced in papers are to be understood as individual expressions of their authors and not those of the Society. Manuscripts received at ASME Headquarters, August 15, 1955. (A combined condensation of ASME Papers Nos. 55-A-106 and 55-A-107.)

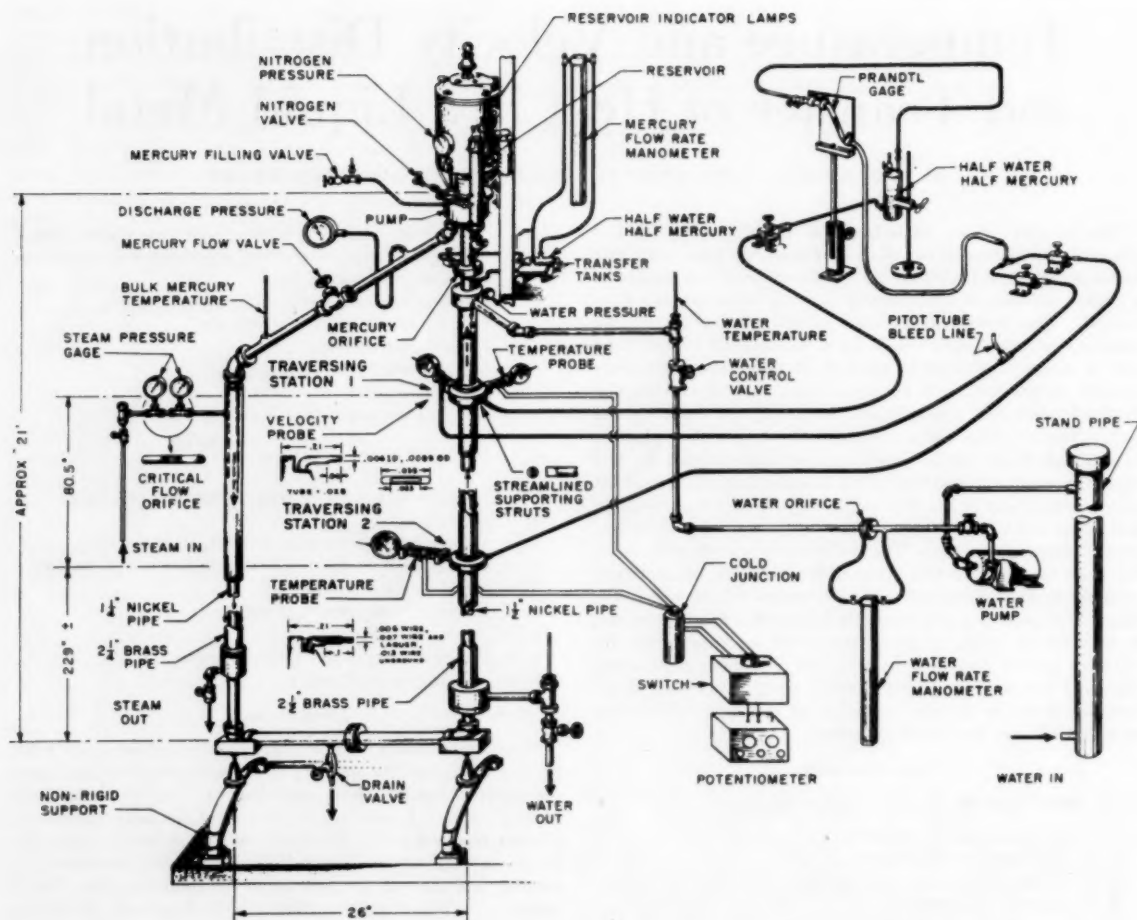


FIG. 1 SCHEMATIC DIAGRAM OF TEST EQUIPMENT

in. standard nickel pipe (1.6-in. ID) jacketed with a 20-ft section of  $2\frac{1}{2}$ -in. brass tube. Water is used for cooling of the mercury as it flows upward through the inner pipe. Calibrated orifices, one in the steam line and one in the water line, are used to set the desired rates of flow of each of these substances. An orifice in the mercury line ahead of the pump suction permits the mercury rate to be determined.

Two probing stations for temperature and pressure measurements are located in the cooling section, one (Station 2) 90 diameters downstream from the beginning of the cooling section, and the other (Station 1) 140 diameters downstream from the beginning of the cooling section. A temperature profile and the static pressure were obtained at each station, and a velocity profile also was obtained at Station 1. A Prandtl type gage, having a least count of 0.001 ft, was used to measure the velocity pressure and the static pressure drop between the two probing stations.

The velocity-pressure probe consisted of a small flattened and ground hypodermic tube fastened to a thin drilled strut (Figs. 1 and 2). The measuring head was formed by pressing, axially, a short length of 0.028-in. tubing into the strut and bending the tubing to point upstream. The tip of the probe was flattened and ground until the over-all thickness of the tip was 0.0089 in. The inside dimensions of the finished probe tip were  $0.006 \times 0.023$  in.,

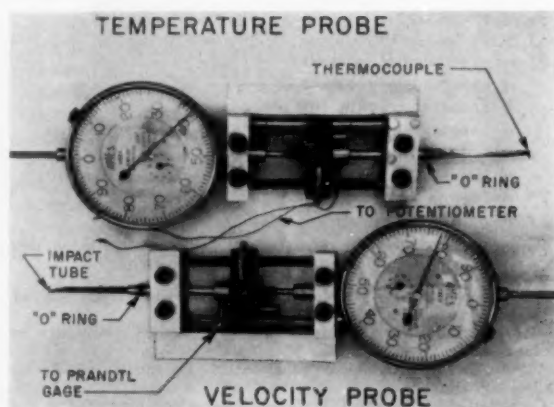


FIG. 2 PROBING DEVICES AND HOLDERS

the longer dimension being perpendicular to the pipe radius. This permitted velocity measurements to within a point 0.0045 in. from the pipe wall.

The two temperature probes were similar in appearance to the total-pressure probe. In forming the thermocouple for a temperature probe, 0.013-in. cotton-covered iron and constantan wires were spot-welded and slipped into a thin drilled strut. Approximately 0.18 in. of the wires was bent at an angle of 90 deg to point upstream when in use. The cotton covering was removed from the portion of the wires exposed to the mercury, and Sauereisen No. 1 Insulate cement was used to hold the wires firmly in the drilled strut. The surfaces of the thermocouple were ground to frontal dimensions of  $0.006 \times 0.026$  in., the long dimension being perpendicular to the radius of the pipe. All of the wires exposed to the mercury were lacquered except about  $\frac{3}{4}$  of the junction. An ice bath was used for the reference-junction temperature for the temperature probes, and a portable potentiometer with a minimum scale graduation of 0.01 mv was used for the temperature measurements.

The holders for the velocity and temperature probes consisted of a small metal frame which was fitted with a lead screw and a guide rod. A knurled nut on the lead screw caused the probe to move axially through the strut and transversely in the mercury stream. A dial indicator, with a minimum scale graduation of 0.001 in., was attached to the probe holder and permitted accurate measurement of the probe position along a radial line in the mercury stream.

Prior to charging the system with mercury, the test section was polished with fine-grain abrasive paper and then it was wiped with a cloth swab. Following the polishing and wiping, the system was washed with ammonia, then water, and then acetone, and this was followed with forced-air-circulation drying. The system was then evacuated to a pressure of 0.25 psia. The mercury was syphoned into the system after being filtered through a cloth to remove possible foreign matter floating on the surface. During operation, the system was pressurized with nitrogen at 15 psig at the pump reservoir at the top of the system.

#### PROCEDURE

The velocity probe (pitot tube) was calibrated over a Reynolds number (based on the frontal diameter of pitot tube) from 50 to 200, in a small calibrated water tunnel, and over a range of 400 to 1000 in a wind tunnel using a standard ASHVE pitot tube. The calibration coefficient for the pitot tube was constant over the range of Reynolds numbers encountered in the mercury experiments. The mercury orifice was calibrated, in place, by a 10-point velocity traverse over the pipe cross section. The temperature probes were calibrated in a heavily insulated ceramic vessel fitted with a steam coil and a stirrer using a certified mercurial thermometer for comparison. The thermocouples were attached to the bulb of the thermometer during calibration.

Values of the thermal conductivity of mercury were obtained from the "Liquid Metals Handbook" (8). All other properties of the mercury were obtained from "The Handbook of Chemistry and Physics" (9).

The apparatus was operated over a range of Reynolds numbers in the cooling section of about 250,000 to 800,000. The water rate in the cooling jacket was adjusted to give the same thermal capacity as the flowing mercury so that the axial temperature gradient of the water would be equal to the axial temperature gradient of the mercury. The mercury was heated sufficiently for the center-line temperature to be as close to 140 F at the upstream probing station as was practicable.

After temperature stabilization had been obtained, the downstream temperature probe and the velocity probe were retracted to avoid disturbance of the mercury stream, and a radial-temperature traverse was made at the upstream station. Temperature data were obtained at the center and at ten radial positions, corresponding to centers of equal area increments, and at three radial positions

near the far wall of the mercury stream. The temperature was obtained to within 0.0045 in. of the wall. Calculations indicated that the position nearest the pipe wall at which data were obtained was always in the turbulent core. Following completion of the traverse at the upstream (No. 2) station the probe was retracted and the procedure repeated for the temperature traverse at the downstream (No. 1) station. The two temperature traverses were followed by a velocity traverse at the downstream station at the same radial positions as were used for the temperature traverse, both temperature probes being retracted during this procedure. Several measurements of the static-pressure drop between the two stations were made during the velocity traverse. Upon completion of the temperature and velocity traverses and the static-pressure drop measurements, the flow of steam, water, and mercury was stopped as quickly as possible, and the deflections of the Prandtl type manometer were observed to obtain "zero" readings for static-pressure drop and for velocity pressure. These zero readings were obtained as quickly as possible so that they would be recorded at the same bulk temperature of the mercury as with flow.

#### TEMPERATURE-DATA REDUCTION

The change in the temperature of the mercury from the center of the pipe to the pipe wall was only of the order of 20 F, and the change in temperature from the upstream probing station to the downstream probing station was about 20 F; hence constant physical properties of the mercury could be assumed.

With the mercury properties being substantially independent of radius, the bulk mean temperature at a particular probing station may be defined by

$$t_a = \frac{2 \int_0^r ur(t - t_b)dr}{u_a r_0^2} + t_b \dots \dots \dots [1]$$

The mean velocity was obtained by an arithmetic mean of the velocities from the ten-point velocity traverse. The integral was evaluated graphically.

Temperature data were obtained sufficiently close to the wall to show a linear variation of temperature with distances from the wall for the three or four data points nearest the wall. The mer-

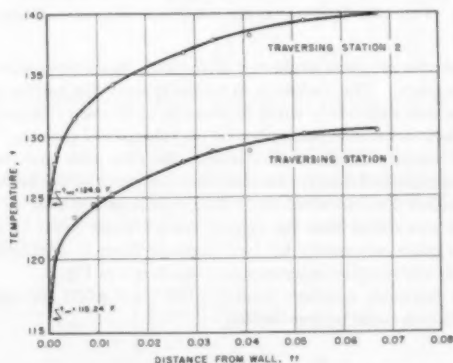


FIG. 3 TEMPERATURE PROFILES AT  $N_R = 660 \times 10^3$

cury fluid-wall temperature at a particular probing station was obtained by plotting temperature versus distance from the wall and extrapolating to the wall. Fig. 3 shows a typical plot of this type.

#### VELOCITY DISTRIBUTION

Velocity-distribution data were obtained with isothermal conditions as well as during the regular runs with heat transfer. For

the so-called isothermal runs, cooling water was circulated through the jacket of the test section for temperature stabilization, but no heat was added to the mercury in the heater. By plotting the ratio of the local velocity to the friction velocity against the logarithm of the friction-distance parameter, as shown in Fig. 4, it was found possible to represent both the isothermal and non-isothermal data reasonably well by the same line. However, the data were found to lie below the line commonly associated with smooth pipe-velocity distribution. For the runs with heat trans-

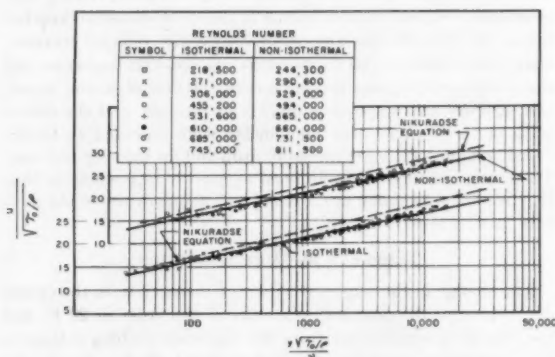


FIG. 4 VELOCITY DISTRIBUTIONS FOR ISOTHERMAL AND NONISOTHERMAL CONDITIONS

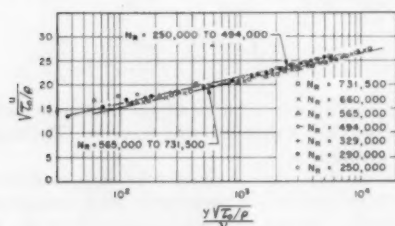


FIG. 5 VELOCITY DISTRIBUTIONS FOR NONISOTHERMAL CONDITIONS

fer, the viscosity was evaluated at the bulk mean temperature of the mercury. The variation in viscosity over the radius of the stream was sufficiently small to make it unnecessary to evaluate the friction-distance parameter by an integration process.

The velocity-distribution data from the runs with heat transfer also were plotted singly, and attention was given to the individual runs rather than to all of the velocity data as a whole. In this case it was found that the velocity distribution could be represented more accurately by two separate lines in a generalized velocity-distribution representation, as shown in Fig. 5.

For Reynolds numbers from 250,000 to 494,000 the velocity distribution could be represented by

$$\frac{u}{u^*} = 4.76 + 2.44 \ln y^* \quad [2]$$

and for Reynolds numbers from 565,000 to 731,000 the velocity distribution could be represented by

$$\frac{u}{u^*} = 3.96 + 2.44 \ln y^* \quad [3]$$

These two velocity distributions were used, together with pressure-drop data, to evaluate the eddy diffusivities for momentum

transfer. The velocity distribution, as related to the friction factor  $f$ , may be shown by an equation of the form

$$\frac{u/u_s - 1}{\sqrt{f}} = C_1 \log(y/r_0) + C_2 \quad [4]$$

By trial and error with the experimental data, the constants  $C_1$  and  $C_2$  in Equation [4] were determined so that Equation [4] becomes

$$\frac{u/u_s - 1}{\sqrt{f}} = 2.25 \log(y/r_0) + 1.37 \quad [5]$$

For the ratio of the center line (or maximum velocity)  $u_c$  to the average velocity  $u_s$ , Equation [5] becomes

$$u_c/u_s = 1.37 \sqrt{f} + 1 \quad [6]$$

since  $y = r_0$  at this point. Friction factors were determined from measurements of pressure drop and of average velocity, and indicated a relative pipe roughness of 0.00015 on the Moody (10) chart.

#### TEMPERATURE DISTRIBUTIONS

The relative temperature distributions are shown in Fig. 6 for a range of Reynolds numbers from 250,000 to 731,000. The Martinelli predictions are also shown for Reynolds numbers of  $10^4$  and  $10^5$ . The temperature gradients measured were somewhat larger than indicated by the Martinelli predictions, especially in the vicinity of the wall. Martinelli derived an equation for the transverse temperature gradient in a fluid flowing turbulently in a smooth pipe as

$$\frac{\partial t}{\partial y} = \frac{(2.5/\alpha)T^*}{y + \frac{5}{\alpha N_{Pr} N_R^*} (1 - y/r_0)} \quad [7]$$

The equation contains two terms involving radial position; namely  $(1 - y/r_0)$  and  $\alpha$ , if  $\alpha$  is assumed to vary with radial position. For a fixed value of the Prandtl number and for a fixed value of the friction Reynolds number, the Martinelli equation can be approximated by

$$\frac{\partial t}{\partial y} = \frac{BT^*}{y + \Phi(y)} \quad [8]$$

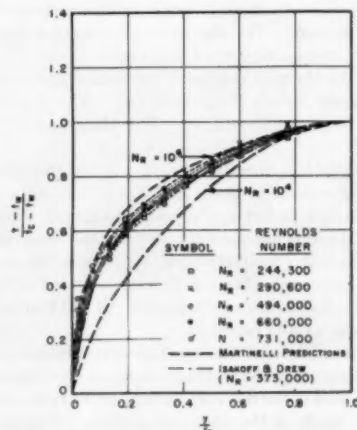


FIG. 6 TEMPERATURE DISTRIBUTION AT UPSTREAM STATION

which is empirical in nature. The symbols  $\Phi(y)$  represent some function of  $y$  which is to be determined from the experimental data. In testing this equation, the simplest function was tried first, namely

$$\Phi(y) = \text{a constant distance} \dots \dots \dots [9]$$

It was found that the data could be represented by the resulting temperature-distribution equation within the limits of experimental error. In general, the constant distance varied with the Reynolds number, decreasing as the Reynolds number increased. An integrated form of Equation [8] which utilizes Equation [9] is

$$\frac{t - t_w}{T^*} = C + B \ln(y^+ + \Delta y^+) \dots \dots \dots [10]$$

Equation [10] is a dimensionless temperature-distribution equation that is applicable to the turbulent core only. Fig. 7 shows a plot of the dimensionless temperature as a function of the friction-distance parameter, according to the form of Equation [10]. The reason for fitting such an equation to the data was to have a convenient means of evaluating the temperature gradients.

The relative distance from the pipe wall at which the average velocity corresponds to the local velocity and the relative distance from the pipe wall at which the bulk mean temperature corresponds to the local temperature is shown in Fig. 8, together with the results of other investigators. In the present study the average velocity corresponded to the local velocity found at  $(y/r_0) = 0.251$ . The calculations of Jakob (11), based on the data of Nikuradse, indicated an average value of  $(y/r_0) = 0.239$  for this point, for a range of Reynolds numbers as was employed in the current investigation.

For the present study, the value of the bulk mean temperature corresponded to the local temperature at the relative distance from the wall of  $(y/r_0) = 0.301$ . The calculations of Jakob (12) on

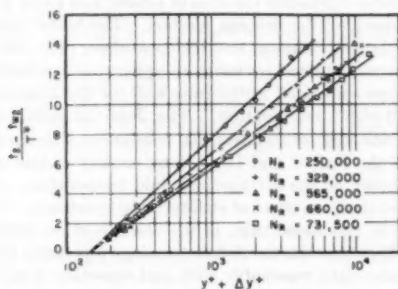


FIG. 7 DIMENSIONLESS TEMPERATURE AT UPSTREAM STATION WITH ABSCISSA DISPLACEMENT

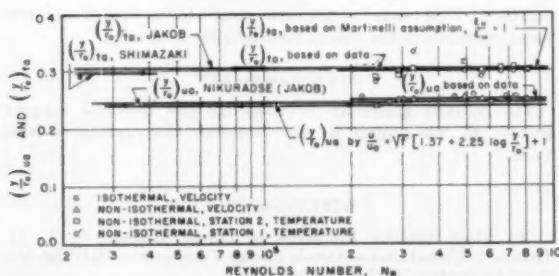


FIG. 8 VALUES OF  $(y/r_0)$  AT WHICH AVERAGE VELOCITY AND TEMPERATURE OCCUR

the location of the point at which the average temperature can be found were based on the predictions of Martinelli, and represent the average position with the Prandtl number varying between 0.01 and 10. The Martinelli predictions indicate a small Prandtl number effect but only a very small Reynolds number effect. The Shimazaki (13) data were obtained with a heated stream of air and indicate a value of  $(y/r_0)$ , at which the bulk mean temperature corresponds to the local temperature, that is, slightly smaller than the average value for the current mercury data.

#### EDDY-DIFFUSIVITY RESULTS

Heat is transferred in a turbulent stream by both thermal (molecular) diffusivity and by the eddy diffusivity (for heat) of turbulent flow. It is customary to assume the two diffusivities directly additive. Following Martinelli's analysis (5), consider a general core of fluid having a surface area  $A$ ; the local heat-transfer rate  $q$ , in terms of thermal and eddy diffusivities, is

$$q = A \gamma c_p (a + \epsilon_h) \frac{\partial t}{\partial y} \dots \dots \dots [11]$$

The problem of determining the eddy diffusivity for heat  $\epsilon_h$  therefore involves the determination of the local heat-transfer rate as a function of the radial position in the fluid stream and the determination of the temperature gradient as a function of the radial position considered. Considering a stream of fluid having a constant axial temperature gradient and substantially constant properties, in accordance with the experimental conditions, a heat balance on an element of fluid shows the local heat-transfer rate may be expressed by

$$q = \left( \frac{q_0}{r_0^2} \right) \int_0^r \left( \frac{u}{u_a} \right) 2r dr \dots \dots \dots [12]$$

The local velocity can be expressed in dimensionless form by

$$\frac{u}{u_a} = M + N \ln y^+ \dots \dots \dots [13]$$

By combining Equations [12] and [13], and by integrating the resulting expression, there is obtained

$$q = \frac{q_0 u_a}{u_a} \left[ \left( M - \frac{N}{2} + N \ln y^+ \right) \left( 1 - \frac{y}{r_0} \right)^2 - N \left( 1 - \frac{y}{r_0} - \ln \frac{r_0}{y} \right) \right] \dots \dots \dots [14]$$

The heat-transfer rate for the stream as a whole may be found from

$$q_0 = \pi r_0^2 u_a \gamma c_p (t_{a2} - t_{a1}) \dots \dots \dots [15]$$

As shown previously, the local transverse temperature gradient can be represented by Equation [8]. The substitution of Equations [8] and [14] into Equation [11], together with rearrangement, yields

$$\epsilon_h = \frac{(u^*)^2 (y + \Delta y)}{u_a B} \left[ \left( M - \frac{N}{2} + N \ln y^+ \right) \times \left( 1 - \frac{y}{r_0} \right) - N + \frac{N \ln \frac{r_0}{y}}{1 - \frac{y}{r_0}} \right] - a \dots \dots \dots [16]$$

Equation [16] was employed to calculate values of  $\epsilon_h$ , the eddy diffusivity for heat transfer.

The following analysis will illustrate the method employed for the determination of values  $\epsilon_m$ , the eddy diffusivity for momentum

transfer. The shear stress at any radial position may be expressed by

$$\tau = \rho(\nu + \epsilon_m) \frac{\partial u}{\partial y} \quad [17]$$

The local shear stress varies linearly with the radial position and is given by

$$\tau = \tau_0 \left(1 - \frac{y}{r_0}\right) \quad [18]$$

The velocity gradient was evaluated by differentiating the velocity distribution Equations [2] and [3], which have the general form of Equation [13]. The combination of Equations [17], [18], and the differentiated form of Equation [13], results in

$$\epsilon_m = \frac{u^* \left(1 - \frac{y}{r_0}\right) y}{N} - \nu \quad [19]$$

Having determined the values of the two diffusivities  $\epsilon_a$  and  $\epsilon_m$ ,

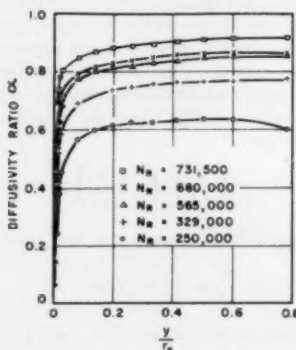


FIG. 9 VARIATION OF  $\alpha$  WITH DISTANCE FROM THE WALL-UPSTREAM STATION

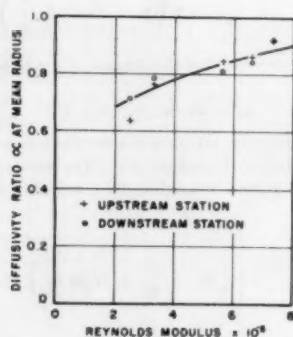


FIG. 10 VARIATION OF  $\alpha$  AT MEAN RADIUS WITH THE REYNOLDS MODULUS

values  $\alpha$ , the ratio of the eddy diffusivity for heat transfer to the eddy diffusivity for momentum transfer, were then computed. Fig. 9 shows the variation of  $\alpha$  with the relative distance from the tube wall for a range of Reynolds numbers. The diffusivity ratio was found to be reasonably constant over the radius except in the

vicinity of the wall. The diffusivity ratio was also found to vary with the Reynolds number, tending to increase in magnitude with an increase in the value of the Reynolds number.

In Fig. 10 the values of  $\alpha$  at the mean pipe radius have been plotted against the Reynolds number, with data being shown for both probing stations.

#### HEAT-TRANSFER RESULTS

Values of the Nusselt modulus were plotted against values of the Peclet modulus, together with the results of other investigators, as shown in Fig. 11. The values of the Nusselt modulus were found to be somewhat lower than the values predicted by the Martinelli-Lyon analogy equation at the lower flow rates and were found to be in reasonable agreement at the higher flow rates.

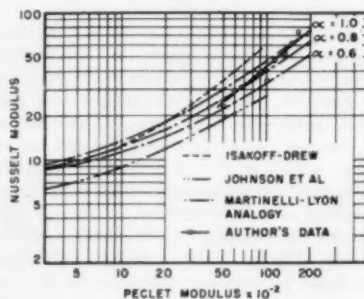


FIG. 11 HEAT-TRANSFER RESULTS WITH MERCURY

The Martinelli-Lyon analogy equation has been shown for values of  $\alpha = 0.8$  and  $\alpha = 0.6$  in addition to the value of  $\alpha = 1.0$ . The topmost curve represents the data of Isakoff and Drew which also were obtained by the probing method. The lower curve represents the data of Johnson and his co-workers (4). The data of Johnson were obtained by using an apparatus in which thermocouples were embedded in the tube wall for the measurement of the "solid-wall" temperature. The Johnson data can show, therefore, the effect of an interfacial resistance. The current data, as well as the Isakoff and Drew data, employ a fluid-wall temperature based on the extrapolated fluid temperature, and therefore cannot show the effect of an interfacial resistance.

It may be concluded that, in the absence of an interfacial-resistance effect, the Martinelli-Lyon analogy represents the current heat-transfer data reasonably well, and especially if allowance is made for the variation of  $\alpha$  with the Reynolds number. Further, in both cases where the probing method has been used, it is seen that the values of the Nusselt modulus are appreciably greater than those obtained by measurements of the solid-wall temperature. This tends to lend some weight to the idea of an interfacial resistance in the case of heat transfer to mercury.

#### ACKNOWLEDGMENT

The authors gratefully acknowledge the financial support granted to this project by the Research Corporation of New York.

#### BIBLIOGRAPHY

- 1 "Heat Transfer Properties of Liquid Metals," by L. M. Trefethen, United States Atomic Energy Commission, Oakridge National Laboratory NP 1788, July, 1950.
- 2 "Heat Transfer Properties of Mercury," by D. English, Atomic Energy Research Establishment, Report Number EIR 547, 1950.
- 3 "Heat Transfer to Mercury," by E. R. Gilliland, R. J. Musser,

and W. R. Page, General Discussion on Heat Transfer, London Conference, London, England, September, 1951.

4 "Heat Transfer to Mercury in Turbulent Pipe Flow," by H. A. Johnson, W. J. Clabaugh, and J. P. Hartnett, *Trans. ASME*, vol. 76, 1954, pp. 505-511.

5 "Heat Transfer to Molten Metals," by R. C. Martinelli, *Trans. ASME*, vol. 69, 1947, pp. 947-959.

6 "Liquid-Metal Heat Transfer Coefficients," by R. N. Lyon, *Trans. AICHE*, vol. 47, 1951, pp. 75-79.

7 "Heat and Momentum Transfer in Turbulent Flow of Mercury," by S. E. Isakoff and T. B. Drew, General Discussion on Heat Transfer, London Conference, London, England, September, 1951.

8 "Liquid Metals Handbook," by R. N. Lyon, Atomic Energy Commission and Bureau of Ships, Navy Department, June, 1952.

9 "Handbook of Chemistry and Physics," by C. D. Hodgman, Chemical Rubber Publishing Company, thirty-third edition, 1951.

10 "Friction Factors for Pipe Flow," by L. F. Moody, *Trans. ASME*, vol. 66, 1944, pp. 671-684.

11 "Velocity Distribution of Fluids in Turbulent Flow," by H. T. Bates, *Trans. AICHE*, vol. 36, 1940, pp. 269-284; discussion by M. Jakob.

12 Discussion of Martinelli paper, reference (5), by M. Jakob.

13 "Temperature Distribution in Heated Fluids in Turbulent Pipe Flow," by T. T. Shimazaki, MS thesis in Mechanical Engineering, University of California, 1949.

## Discussion

C. A. SLEICHER, JR.<sup>5</sup> It is instructive to compare the reported values of the diffusivity ratio  $\alpha$  to those predicted by Jenkins.<sup>6</sup> Although Jenkins' values are somewhat lower than most experimental ones, his analysis correctly predicts that  $\alpha$  will approach unity as turbulence increases. This trend is observed here for liquid metals, in which  $\alpha$  is less than 1, and for air,<sup>7</sup> in which  $\alpha$  is greater than 1. The trend is observed not only by comparing  $\alpha$  at the same radius for different Reynolds numbers, but also by comparing  $\alpha$  at different radii for a given Reynolds number. Jenkins' analysis also predicts that  $\alpha$  will decrease with decreasing

<sup>5</sup> Shell Development Company, Emeryville, Calif.

<sup>6</sup> "Variation of Eddy Conductivity With Prandtl Modulus and Its Use in Prediction of Turbulent Heat Transfer Coefficients," by R. Jenkins, Heat Transfer and Fluid Mechanics Institute Preprints, 147-158, Stanford University Press, Stanford, Calif., 1951.

<sup>7</sup> "Temperature Gradients in Turbulent Gas Streams," by W. H. Corcoran, F. Page, Jr., W. G. Schlenger, and B. H. Sage, *Industrial and Engineering Chemistry*, vol. 44, 1952, pp. 410-430.

Prandtl number. Were it not for these trends, the authors could not have determined the wall temperature as they did; that is, if near the wall the temperature is to be linear with distance from the wall, it must be true that  $\alpha N_{Pr} (\epsilon_m/\nu) \ll 1$ . Their closest temperatures were made at 0.0045 in. from the wall, which for  $N_{Re} = 660,000$  corresponds to about  $y^+ = 80$  and  $\epsilon_m/\nu = 31$ . Thus, if  $\alpha = 1$ ,  $\alpha N_{Pr} (\epsilon_m/\nu) = 0.64$ , whereas, according to Jenkins,  $\alpha = 0.16$  or  $\alpha N_{Pr} (\epsilon_m/\nu) = 0.10$ .

Recently a more rigorous analysis for the variation of  $\alpha$  with Prandtl number and degree of turbulence has been developed by Baron and Barkelew. The results are slightly higher than those of Jenkins, but they do give a more rigorous theoretical foundation for showing that  $\alpha$  is considerably less than unity for liquid-metal flows. The experimental work of the authors is substantial confirmation of these analyses.

It is the low values of  $\alpha$  that account for most of the literature data being lower than the Lyon-Martinelli prediction. In fact, many of the experimental liquid-metal Nusselt numbers in the literature are higher than those for smooth pipes in the absence of entrance effects. For example, the Nusselt numbers of the present paper are slightly high, particularly at the highest Reynolds numbers, because the pipe was not quite smooth. It can be shown that other data have been obtained under conditions in which thermal-entrance effects cause Nusselt numbers to be higher than the asymptotic value.

### AUTHORS' CLOSURE

The authors appreciate the comments of Dr. C. A. Sleicher, Jr. It is thought that the extrapolation procedure for securing fluid-wall temperatures does not introduce a serious error in the case of liquid metals. The order of magnitude of the temperature extrapolation was 1 F, whereas the difference between the fluid wall temperature and the center-line temperature was of the order of magnitude of 20 F.

As pointed out by Dr. Sleicher, the values of the diffusivity ratio  $\alpha$  as predicted by Jenkins are somewhat lower than determined by experiment in the present study. In view of the simplifying assumptions necessary to the development of such a prediction, it would not be expected that the magnitude of  $\alpha$  would be predicted with the degree of accuracy of the trend of  $\alpha$  with the level of turbulence.

The first of these is the fact that the  
the second is the fact that the  
the third is the fact that the

the fourth is the fact that the  
the fifth is the fact that the  
the sixth is the fact that the

the seventh is the fact that the  
the eighth is the fact that the  
the ninth is the fact that the

the tenth is the fact that the  
the eleventh is the fact that the  
the twelfth is the fact that the

the thirteenth is the fact that the  
the fourteenth is the fact that the  
the fifteenth is the fact that the

the sixteenth is the fact that the  
the seventeenth is the fact that the  
the eighteenth is the fact that the

the nineteenth is the fact that the  
the twentieth is the fact that the  
the twenty-first is the fact that the

the twenty-second is the fact that the  
the twenty-third is the fact that the  
the twenty-fourth is the fact that the

the twenty-fifth is the fact that the  
the twenty-sixth is the fact that the  
the twenty-seventh is the fact that the

the twenty-eighth is the fact that the  
the twenty-ninth is the fact that the  
the thirtieth is the fact that the

### Conclusion

The above facts show that the  
the following facts show that the  
the following facts show that the

the following facts show that the  
the following facts show that the  
the following facts show that the

the following facts show that the  
the following facts show that the  
the following facts show that the

the following facts show that the  
the following facts show that the  
the following facts show that the

the following facts show that the  
the following facts show that the  
the following facts show that the

# Mean-Temperature Difference in One, Two, and Three-Pass Crossflow Heat Exchangers

By R. A. STEVENS,<sup>1</sup> J. FERNANDEZ,<sup>1</sup> AND J. R. WOOLF,<sup>2</sup> FORT WORTH, TEXAS

A review is presented of the mean-temperature-difference equations for all previously solved cases of crossflow exchangers. A numerical integration procedure was used to obtain data for the single-pass case with both fluids unmixed. All of the previously unsolved cases of two and three-pass crossflow exchangers were also solved by numerical integration, using a cyclical reiteration process for the countercurrent cases. Design data in the form of correction factors are presented for all cases not previously solved.

## NOMENCLATURE

The following nomenclature is used in the paper:

$A$  = heat-transfer area  
 $C_p$  = specific heat

$$E = \text{effectiveness, } E_A = \frac{\Delta t_A}{t_1 - T_1}, E_B = \frac{\Delta t_B}{t_1 - T_1}$$

$e$  = natural base of logarithms  
 $K = 1 - e^{-NTU} = 1 - e^{-Z \Delta NTU}$

$M$  = mass flow rate

$n$  = number of channels in numerical integration; number of passes

$$NTU = \text{number of transfer units, } NTU = \frac{UA}{MC_p} = \frac{\Delta t}{\Delta t_m}$$

$Q$  = heat-transfer rate

$T$  = temperature of fluid  $B$

$t$  = temperature of fluid  $A$

$U$  = over-all heat-transfer coefficient

$Z$  = thermal capacity ratio,  $Z_A = (MC_p)_A / (MC_p)_B$ ,  $Z_B = (MC_p)_B / (MC_p)_A$

$\Delta t$  = temperature difference

$$\delta = \text{crossflow factor, } \delta = \frac{E}{NTU} = \frac{\Delta t_m}{t_1 - T_1}$$

## Subscripts

$A$  = fluid  $A$

$a$  = fluid  $A$  per pass of a multipass exchanger

$B$  = fluid  $B$

$b$  = fluid  $B$  per pass of a multipass exchanger

CF = true counterflow

$m$  = mean

PF = true parallel flow

1 = inlet; 2 = exit

<sup>1</sup> Propulsion Engineer, Convair—Division of General Dynamics Corporation. Assoc. Mem. ASME.

<sup>2</sup> Propulsion Group Engineer, Convair—Division of General Dynamics Corporation. Mem. ASME.

Contributed by the Heat Transfer Division and presented at the Diamond Jubilee Annual Meeting, Chicago, Ill., November 13-18, 1955, of THE AMERICAN SOCIETY OF MECHANICAL ENGINEERS.

NOTE: Statements and opinions advanced in papers are to be understood as individual expressions of their authors and not those of the Society. Manuscript received at ASME Headquarters, August 8, 1955. (Condensed from Paper Nos. 55-A-89 and 55-A-90.)

## INTRODUCTION

The crossflow exchanger is one which is used extensively, particularly in the aircraft industry. Nearly all of the exchangers using the so-called compact heat-exchanger surfaces are of this type. Solutions of the mean-temperature difference are available for only part of the possible cases. Bowman, Mueller, and Nagle (1)<sup>3</sup> have presented the most complete survey to date. The present paper covers solutions of the mean-temperature difference for one, two, and three passes with countercurrent and co-current flow. The following assumptions apply to all cases:

- 1  $U$  is constant throughout.
- 2 The heat-transfer area of each pass is the same.
- 3 No change of phase.
- 4 Constant specific heat.
- 5 Steady flow.

All of the theory following is based on effectiveness  $E$ , thermal-capacity ratio  $Z$ , and number of transfer units  $NTU$ . The authors prefer these relations for design. For those more familiar with other relations, the following summary of relations is given

$$E_A = \frac{t_1 - t_2}{t_1 - T_1}$$

$$E_B = \frac{T_2 - T_1}{t_1 - T_1} = Z_A E_A$$

$$NTU_A = \frac{UA}{(MC_p)_A} = \frac{\Delta t_A}{\Delta t_m}$$

$$NTU_B = \frac{UA}{(MC_p)_B} = \frac{\Delta t_B}{\Delta t_m} = \frac{(MC_p)_A \Delta t_A}{(MC_p)_B \Delta t_m} = Z_A NTU_A$$

$$(MC_p)_A \Delta t_A = -(MC_p)_B \Delta t_B$$

$$\delta = \frac{\Delta t_m}{t_1 - T_1} = \frac{\Delta t_A}{NTU_A(t_1 - T_1)} = \frac{E_A}{NTU_A}$$

Since the true counterflow exchanger gives maximum mean-temperature difference (all other variables being constant), it is used as a standard of comparison for countercurrent exchangers. The effectiveness relation for true counterflow is

$$E_A = \frac{1 - e^{-NTU_A(1-Z_A)}}{1 - Z_A e^{-NTU_A(1-Z_A)}} \dots \dots \dots [1]$$

For  $Z_A = 1$ , the equation reduces to

$$E_A = \frac{NTU}{1 + NTU_A} \dots \dots \dots [1a]$$

The true parallel-flow exchanger can be used as a standard of comparison of multipass co-current crossflow exchangers. The effectiveness equation for parallel flow is

<sup>3</sup> Numbers in parentheses refer to the Bibliography at the end of the paper.

$$E_A = \frac{1 - e^{-NTU_A(1+Z_A)}}{1 + Z_A} \quad [2]$$

## ANALYSIS

**Single-Pass Crossflow Exchangers.** Since either fluid can be mixed or unmixed, there are three possible flow combinations for the single-pass crossflow exchanger. These are shown in Fig. 1. Smith (2) has derived equations for two cases and presented design data for the third.

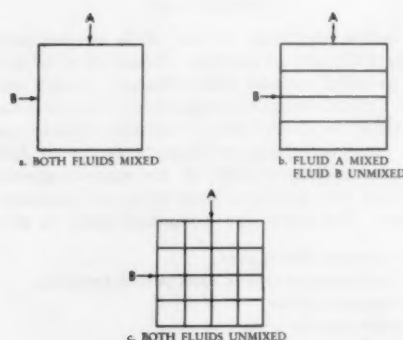


FIG. 1 VARIATIONS OF SINGLE-PASS CROSSFLOW EXCHANGERS

1 Both Fluids Mixed—Case a, Fig. 1. The equation for this case is

$$E_A = \frac{1}{\frac{1}{1 - e^{-NTU_A}} + \frac{Z_A}{K} - \frac{1}{NTU_A}} \quad [3]$$

2 Fluid A Mixed, Fluid B Unmixed—Case b, Fig. 1. The relation for effectiveness is

$$E_A = 1 - e^{-Z_A K} \quad [4]$$

3 Both Fluids Unmixed—Case c, Fig. 1. Nusselt (3, 4) presented equations for the mean-temperature difference in a cross-flow exchanger having both fluids unmixed. Brimley, Eggleston, and Muenzer (5) recently calculated the solutions from the following equation of Mason (6)

$$E_A = \frac{1}{Z_A NTU_A} \sum_{n=0}^{\infty} \left\{ \left[ 1 - e^{-NTU_A} \sum_{m=0}^n \frac{(NTU_A)^m}{m!} \right] \left[ 1 - e^{-Z_A NTU_A} \sum_{m=0}^n \frac{(Z_A NTU_A)^m}{m!} \right] \right\} \quad [5]$$

Their report gives values of  $\delta$  as a function of effectiveness on both sides (four significant figures). The authors have used a numerical integration method for obtaining the same data. Referring to the element in Fig. 2, the heat-balance and transfer equations are

$$dQ = \frac{(MC_p)_A}{n} (t_{i-1,j} - t_{i,j}) = \frac{(MC_p)_B}{n} (T_{i,j} - T_{i,j-1}) \dots [6]$$

and

$$dQ = \frac{UA}{n^2} \left( \frac{t_{i-1,j} + t_{i,j}}{2} - \frac{T_{i,j-1} + T_{i,j}}{2} \right) \dots [7]$$

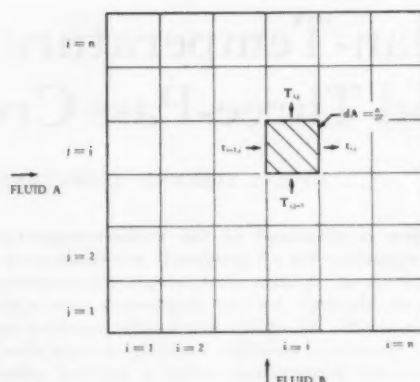


FIG. 2 MATRIX FOR SINGLE-PASS UNMIXED CROSSFLOW EXCHANGER

To make the numerical integration more accurate, the arithmetic-mean temperatures were used in Equation [7] for heat-transfer temperature difference. The exit temperatures are

$$t_2 = \frac{1}{n} \sum_{j=1}^n t_{n,j}; \quad T_2 = \frac{1}{n} \sum_{i=1}^n T_{i,n}$$

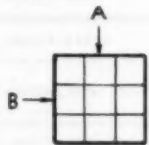
The equations were set up on an electronic digital computer, the IBM 701 Data Processing Machine, and values of effectiveness computed for  $Z_A = 0$  to 1 and  $NTU_A = 0$  to 7. The results are given in Table 1. The number of channels  $n$  was taken as 20. A check was made with the data of reference (5) and it was found that they agreed to the fourth significant figure. Our purpose in recalculating the data was to obtain the effectiveness as a function of arbitrary values of  $NTU$  and  $Z$ .

The effect of the number of channels on the calculated values of effectiveness is shown in Table 2. This table also includes similar data for all cases in this paper which were solved by numerical integration.

**Two-Pass Countercrossflow Exchangers.** Fig. 3 shows schematically the possible flow variations for two-pass countercrossflow exchangers. Since six of these are repetitions obtained by reversing the notation for the fluids, there are ten possible cases. Table 3 summarizes the solutions for these ten cases. Equations are given for the cases for which analytical solutions can be obtained.

The equation for the first three cases in Table 3 presents the over-all effectiveness ( $E_A$ ) as a function of single-pass effectiveness ( $E_s$ ) and thermal-capacity ratio. Since this equation relates two identical exchangers in series, the single-pass effectiveness should be determined using the single-pass  $NTU$ . For a two-pass exchanger, the single-pass  $NTU$  is one half the total  $NTU$ .

The last five cases in Table 3 were not susceptible to analytical solution. They were solved by a cyclical reiteration process of numerical integration, following the method proposed by Korst (7). Consider Fig. 4. The temperature of the mixed fluid between passes  $t_i$  is assumed. With this assumed temperature of fluid A entering pass II, and the known temperature  $T_1$  of fluid B, the numerical integration methods of Equations [6] and [7] can be applied to obtain the average temperature  $t_2$  and the temperature distribution of fluid B leaving pass II. With the calculated temperature distribution  $T_i$  and the known temperature  $t_1$  of fluid A, the same procedure is applied to pass I and the averaged temperatures  $t_i$  and  $T_2$  are obtained. One cyclical integration has now been completed. The calculated  $t_i$  is compared

TABLE 1  $\epsilon_A$  FOR SINGLE-PASS CROSSFLOW, BOTH FLUIDS UNMIXED


$z_A$	0	0.1	0.2	0.3	0.4	0.5	0.6	0.7	0.8	0.9	1.0
NTUA											
0	0	0	0	0	0	0	0	0	0	0	0
0.25	0.2212	0.2188	0.2164	0.2141	0.2117	0.2095	0.2072	0.2050	0.2028	0.2007	0.1985
0.5	0.3935	0.3860	0.3787	0.3716	0.3646	0.3578	0.3512	0.3448	0.3385	0.3323	0.3263
0.85	—	0.5574	0.5427	0.5285	0.5147	0.5014	0.4885	0.4760	0.4640	0.4523	0.4410
1.0	0.6321	0.6141	0.5966	0.5797	0.5633	0.5475	0.5323	0.5175	0.5033	0.4896	0.4763
1.25	—	0.6916	0.6702	0.6496	0.6296	0.6103	0.5917	0.5737	0.5563	0.5396	0.5234
1.5	0.7769	0.7522	0.7281	0.7046	0.6819	0.6598	0.6385	0.6179	0.5980	0.5788	0.5603
1.75	—	0.8000	0.7741	0.7487	0.7239	0.6998	0.6763	0.6536	0.6316	0.6104	0.5899
2.0	0.8647	0.8378	0.8109	0.7843	0.7582	0.7325	0.7075	0.6831	0.6594	0.6365	0.6143
2.5	0.9179	0.8920	0.8652	0.8379	0.8104	0.7830	0.7559	0.7291	0.7030	0.6774	0.6526
3.0	0.9502	0.9270	0.9018	0.8753	0.8479	0.8199	0.7917	0.7635	0.7357	0.7082	0.6814
3.5	0.9698	0.9501	0.9273	0.9024	0.8758	0.8480	0.8194	0.7904	0.7613	0.7325	0.7041
4.0	0.9817	0.9654	0.9454	0.9225	0.8971	0.8699	0.8414	0.8120	0.7821	0.7522	0.7226
5.0	0.9933	0.9830	0.9683	0.9495	0.9273	0.9019	0.8742	0.8447	0.8140	0.7826	0.7511
6.0	0.9975	0.9914	0.9809	0.9661	0.9470	0.9239	0.8975	0.8685	0.8375	0.8052	0.7723
7.0	0.9991	0.9955	0.9883	0.9767	0.9605	0.9397	0.9149	0.8866	0.8557	0.8229	0.7889

TABLE 2 EFFECT OF NUMBER OF CHANNELS ON NUMERICAL RESULTS  
Effectiveness at NTU = 7.0, Z = 1.0

Case	n = 10	12	15	20	25
One Pass Fig. 1-c	0.7896		0.7891	0.7889*	0.7888
Counter-Current Flow					
Two Passes Fig. 3, II-b	0.8117		0.8114*	0.8113	
" II-c	0.8206		0.8204*	0.8203	
" III-c	0.8509		0.8508*	0.8507	
" IV-b	0.8169		0.8166*	0.8166	
" IV-c	0.8355		0.8353*	0.8352	
Three Passes Fig. 3, II-b	0.8296	0.8295*	0.8294		
" II-c	0.8406	0.8405*	0.8405		
" III-c	0.8633	0.8633*	0.8632		
" IV-b	0.8351	0.8350*	0.8349		
" IV-c	0.8513	0.8512*	0.8512		
Co-Current Flow					
Two Passes Fig. 3, II-b	0.3626		0.3626*	0.3627	
" II-c	0.4163		0.4166*	0.4167	
" III-c	0.4700		0.4705*	0.4705	
" IV-b	0.3894		0.3896*	0.3897	
" IV-c	0.4432		0.4435*	0.4436	
Three Passes Fig. 3, II-b	0.5469	0.5469*	0.5470		
" II-c	0.5088	0.5088*	0.5087		
" III-c	0.4992	0.4992*	0.4992		
" IV-b	0.5255	0.5255*	0.5255		
" IV-c	0.5018	0.5017*	0.5017		

\* Indicates number of channels used in results

with the assumed  $t_4$ . If these agree within an arbitrary difference, the effectiveness is taken from the values of  $t_2$  and  $T_3$ . If not, the cycle is reiterated with the last calculated values of  $t_4$  until the comparison checks. This procedure was set up on the IBM 701 machine with 15 channels per pass, and nondimensional temperatures were used, i.e.

$$\tau = \frac{t - T_1}{t_1 - T_1}; \quad \tau' = \frac{T - T_1}{t_1 - T_1}$$

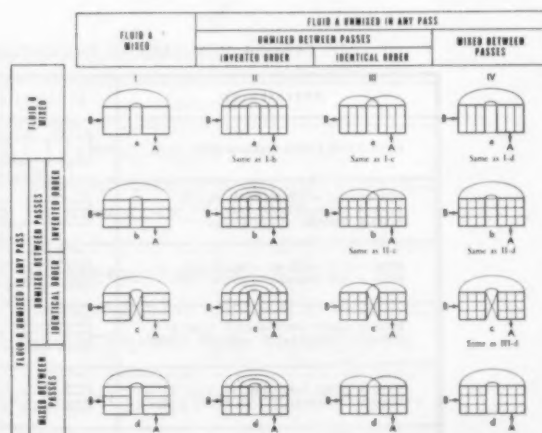


FIG. 3 VARIATIONS OF TWO-PASS CROSSFLOW EXCHANGERS

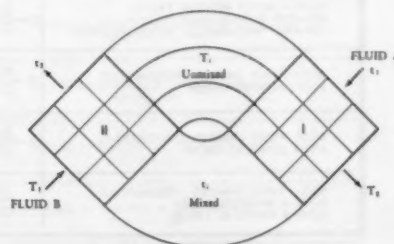


FIG. 4 MATRIX FOR CYCLICAL ITERATION ANALYSIS

TABLE 3 SUMMARY OF TWO-PASS COUNTERCROSSFLOW EXCHANGERS

DESCRIPTION	SCHEMATIC	SOLUTION
BOTH FLUIDS MIXED THROUGHOUT		$E_A = \frac{2E_s - E_s^2(1+Z_A)}{1 - E_s^2 Z_A}$ COMPUTE $E_s$ FROM EQUATION (3), USING $1/2$ OF THE TOTAL NTU
BOTH FLUIDS MIXED BETWEEN PASSES; FLUID A MIXED IN EACH PASS; FLUID B UNMIXED IN EACH PASS		$E_A = \frac{2E_s - E_s^2(1+Z_A)}{1 - E_s^2 Z_A}$ COMPUTE $E_s$ FROM EQUATION (4), USING $1/2$ OF THE TOTAL NTU
BOTH FLUIDS MIXED BETWEEN PASSES; BOTH FLUIDS UNMIXED IN EACH PASS		$E_A = \frac{2E_s - E_s^2(1+Z_A)}{1 - E_s^2 Z_A}$ OBTAIN $E_s$ FROM TABLE 1, USING $1/2$ OF THE TOTAL NTU
FLUID A MIXED THROUGHOUT; FLUID B UNMIXED THROUGHOUT, INVERTED ORDER		$E_A = 1 - \frac{1}{\frac{K}{2} + (1 - \frac{K}{2})e^{2KZ_B}}$
FLUID A MIXED THROUGHOUT; FLUID B UNMIXED THROUGHOUT, IDENTICAL ORDER		$E_A = 1 - \frac{1}{e^{2KZ_B} - K^2 Z_B e^{KZ_B}}$
FLUID A MIXED BETWEEN PASSES, UNMIXED IN EACH PASS; FLUID B UNMIXED THROUGHOUT, INVERTED ORDER		SOLVED BY NUMERICAL INTEGRATION (SEE FIG. 5)
FLUID A MIXED BETWEEN PASSES, UNMIXED IN EACH PASS; FLUID B UNMIXED THROUGHOUT, IDENTICAL ORDER		SOLVED BY NUMERICAL INTEGRATION (SEE FIG. 6)
BOTH FLUIDS UNMIXED THROUGHOUT; BOTH INVERTED ORDER		SOLVED BY NUMERICAL INTEGRATION (SEE FIG. 7)
BOTH FLUIDS UNMIXED THROUGHOUT; BOTH IDENTICAL ORDER		SOLVED BY NUMERICAL INTEGRATION (SEE FIG. 8)
BOTH FLUIDS UNMIXED THROUGHOUT; FLUID A INVERTED ORDER FLUID B IDENTICAL ORDER		SOLVED BY NUMERICAL INTEGRATION (SEE FIG. 9)

TABLE 4 SUMMARY OF THREE-PASS COUNTERCROSSFLOW EXCHANGERS

DESCRIPTION	SCHEMATIC	SOLUTION
BOTH FLUIDS MIXED THROUGHOUT		$E_A = \frac{3E_s - 3E_s^2(1+Z_A) + E_s^3(1+Z_A+Z_A^2)}{1 - E_s^3 Z_A(3 - E_s - E_s^2 Z_A)}$ COMPUTE $E_s$ FROM EQUATION (3), USING $1/3$ OF THE TOTAL NTU
BOTH FLUIDS MIXED BETWEEN PASSES; FLUID A MIXED IN EACH PASS; FLUID B UNMIXED IN EACH PASS		$E_A = \frac{3E_s - 3E_s^2(1+Z_A) + E_s^3(1+Z_A+Z_A^2)}{1 - E_s^3 Z_A(3 - E_s - E_s^2 Z_A)}$ COMPUTE $E_s$ FROM EQUATION (4), USING $1/3$ OF THE TOTAL NTU
BOTH FLUIDS MIXED BETWEEN PASSES; BOTH FLUIDS UNMIXED IN EACH PASS		$E_A = \frac{3E_s - 3E_s^2(1+Z_A) + E_s^3(1+Z_A+Z_A^2)}{1 - E_s^3 Z_A(3 - E_s - E_s^2 Z_A)}$ OBTAIN $E_s$ FROM TABLE 1, USING $1/3$ OF THE TOTAL NTU
FLUID A MIXED THROUGHOUT; FLUID B UNMIXED THROUGHOUT, INVERTED ORDER		$E_A = 1 - \frac{1}{(1 - \frac{K}{2})e^{3KZ_B} + (K(1 - \frac{K}{4}) - K^2 Z_B(1 - \frac{K}{2}))e^{KZ_B}}$
FLUID A MIXED THROUGHOUT; FLUID B UNMIXED THROUGHOUT, IDENTICAL ORDER		$E_A = 1 - \frac{1}{(e^{KZ_B} - 2K^2 Z_B)e^{2KZ_B} - (1 - K - \frac{K}{2} Z_B)K^2 Z_B e^{KZ_B}}$
FLUID A MIXED BETWEEN PASSES, UNMIXED IN EACH PASS; FLUID B UNMIXED THROUGHOUT, INVERTED ORDER		SOLVED BY NUMERICAL INTEGRATION (SEE FIG. 10)
FLUID A MIXED BETWEEN PASSES, UNMIXED IN EACH PASS; FLUID B UNMIXED THROUGHOUT, IDENTICAL ORDER		SOLVED BY NUMERICAL INTEGRATION (SEE FIG. 11)
BOTH FLUIDS UNMIXED THROUGHOUT; BOTH INVERTED ORDER		SOLVED BY NUMERICAL INTEGRATION (SEE FIG. 12)
BOTH FLUIDS UNMIXED THROUGHOUT; BOTH IDENTICAL ORDER		SOLVED BY NUMERICAL INTEGRATION (SEE FIG. 13)
BOTH FLUIDS UNMIXED THROUGHOUT; FLUID A INVERTED ORDER FLUID B IDENTICAL ORDER		SOLVED BY NUMERICAL INTEGRATION (SEE FIG. 14)

TABLE 5 SUMMARY OF TWO-PASS COCROSSFLOW EXCHANGERS

DESCRIPTION	SCHEMATIC	SOLUTION
BOTH FLUIDS MIXED THROUGHOUT		$E_A = 2E_s - E_s^2(1+Z_A)$ COMPUTE $E_s$ FROM EQUATION (3), USING $1/2$ OF THE TOTAL NTU
BOTH FLUIDS MIXED BETWEEN PASSES; FLUID A MIXED IN EACH PASS; FLUID B UNMIXED IN EACH PASS		$E_A = 2E_s - E_s^2(1+Z_A)$ COMPUTE $E_s$ FROM EQUATION (4), USING $1/2$ OF THE TOTAL NTU
BOTH FLUIDS MIXED BETWEEN PASSES; BOTH FLUIDS UNMIXED IN EACH PASS		$E_A = 2E_s - E_s^2(1+Z_A)$ OBTAIN $E_s$ FROM TABLE 1, USING $1/2$ OF THE TOTAL NTU
FLUID A MIXED THROUGHOUT; FLUID B UNMIXED THROUGHOUT, INVERTED ORDER		$E_A = (1 - \frac{K}{2})(1 - e^{-2KZ_B})$
FLUID A MIXED THROUGHOUT; FLUID B UNMIXED THROUGHOUT, IDENTICAL ORDER		$E_A = 1 - e^{-KZ_B}(e^{-KZ_B} + K^2Z_B)$
FLUID A MIXED BETWEEN PASSES, UNMIXED IN EACH PASS; FLUID B UNMIXED THROUGHOUT, INVERTED ORDER		SOLVED BY NUMERICAL INTEGRATION (SEE FIG. 15)
FLUID A MIXED BETWEEN PASSES, UNMIXED IN EACH PASS; FLUID B UNMIXED THROUGHOUT, IDENTICAL ORDER		SOLVED BY NUMERICAL INTEGRATION (SEE FIG. 16)
BOTH FLUIDS UNMIXED THROUGHOUT; BOTH INVERTED ORDER		SOLVED BY NUMERICAL INTEGRATION (SEE FIG. 17)
BOTH FLUIDS UNMIXED THROUGHOUT; BOTH IDENTICAL ORDER		SOLVED BY NUMERICAL INTEGRATION (SEE FIG. 18)
BOTH FLUIDS UNMIXED THROUGHOUT; FLUID A INVERTED ORDER FLUID B IDENTICAL ORDER		SOLVED BY NUMERICAL INTEGRATION (SEE FIG. 19)

TABLE 6 SUMMARY OF THREE-PASS COCROSSFLOW EXCHANGERS

DESCRIPTION	SCHEMATIC	SOLUTION
BOTH FLUIDS MIXED THROUGHOUT		$E_A = 3E_s - 3E_s^2(1+Z_A) + E_s^3(1+Z_A)^2$ COMPUTE $E_s$ FROM EQUATION (3), USING $1/3$ OF THE TOTAL NTU
BOTH FLUIDS MIXED BETWEEN PASSES; FLUID A MIXED IN EACH PASS; FLUID B UNMIXED IN EACH PASS		$E_A = 3E_s - 3E_s^2(1+Z_A) + E_s^3(1+Z_A)^2$ COMPUTE $E_s$ FROM EQUATION (4), USING $1/3$ OF THE TOTAL NTU
BOTH FLUIDS MIXED BETWEEN PASSES; BOTH FLUIDS UNMIXED IN EACH PASS		$E_A = 3E_s - 3E_s^2(1+Z_A) + E_s^3(1+Z_A)^2$ OBTAIN $E_s$ FROM TABLE 1, USING $1/3$ OF THE TOTAL NTU
FLUID A MIXED THROUGHOUT; FLUID B UNMIXED THROUGHOUT, INVERTED ORDER		$E_A = 1 - (1 - \frac{K}{2})^2 e^{-3KZ_B} - [\frac{K}{2} + (1 - \frac{K}{2})(\frac{K}{2} + K^2Z_B)] e^{-KZ_B}$
FLUID A MIXED THROUGHOUT; FLUID B UNMIXED THROUGHOUT, IDENTICAL ORDER		$E_A = 1 - e^{-3KZ_B} - 2K^2Z_B e^{-2KZ_B} - K^2Z_B(1 - K + \frac{K^2}{2}Z_B) e^{-KZ_B}$
FLUID A MIXED BETWEEN PASSES, UNMIXED IN EACH PASS; FLUID B UNMIXED THROUGHOUT, INVERTED ORDER		SOLVED BY NUMERICAL INTEGRATION (SEE FIG. 20)
FLUID A MIXED BETWEEN PASSES, UNMIXED IN EACH PASS; FLUID B UNMIXED THROUGHOUT, IDENTICAL ORDER		SOLVED BY NUMERICAL INTEGRATION (SEE FIG. 21)
BOTH FLUIDS UNMIXED THROUGHOUT; BOTH INVERTED ORDER		SOLVED BY NUMERICAL INTEGRATION (SEE FIG. 22)
BOTH FLUIDS UNMIXED THROUGHOUT; BOTH IDENTICAL ORDER		SOLVED BY NUMERICAL INTEGRATION (SEE FIG. 23)
BOTH FLUIDS UNMIXED THROUGHOUT; FLUID A INVERTED ORDER FLUID B IDENTICAL ORDER		SOLVED BY NUMERICAL INTEGRATION (SEE FIG. 24)

The arbitrary accuracy check was

$$\frac{|\tau_{i, \text{assumed}} - \tau_{i, \text{calculated}}|}{\tau_{i, \text{assumed}}} < 5 \times 10^{-6}$$

Korst showed that the reiteration would converge. To reduce the machine calculation time,  $t_i$  was assumed to be that which would obtain if both fluids were mixed between passes.

For the cases where both fluids are unmixed between passes, the procedure is the same except that a temperature distribution must be assumed rather than a single mixed temperature. A linear distribution was assumed such that the average temperature was the same as for an exchanger with both fluids mixed between passes.

**Three-Pass Countercrossflow Exchangers.** Fig. 3 also represents the flow variations for this type of exchanger, if it is assumed that each fluid follows a consistent flow pattern; i.e., if fluid A is unmixed inverted order between passes I and II, it will be unmixed inverted order between passes II and III also. The ten three-pass countercrossflow cases are presented in Table 4.

**Two-Pass Cocrossflow Exchangers.** Although the cocrossflow arrangement is inherently inferior to the countercrossflow arrangement, installation problems may dictate its use.

Fig. 3 represents the possible flow arrangements for two-pass cocrossflow exchangers if the direction of flow of one of the fluids is reversed. The ten cases are summarized in Table 5. The last five cases were solved by the same type of numerical integration procedure used for the countercrossflow cases, except that no reiteration was necessary.

**Three-Pass Cocrossflow Exchangers.** The solutions for these ten cases are summarized in Table 6.

#### GENERAL

Kays, London, and Johnson (8) give the following equation for any countercrossflow multipass exchanger with both fluids mixed between passes

$$E_A = \frac{\left( \frac{1 - E_c Z_A}{1 - E_c} \right)^n - 1}{\left( \frac{1 - E_c Z_A}{1 - E_c} \right)^n - Z_A} \dots \dots \dots [8]$$

where  $n$  is the number of passes. The authors did not derive this equation in its general form. However, our equations for two and three passes did check Equation [8].

#### RESULTS AND CONCLUSIONS

In the basic work, effectiveness was calculated to four significant figures for all cases. Values of NTU were from 0.25 to 7.0 and thermal-capacity ratio was taken from 0 to 1.0 in increments of 0.1, except for the more impractical cases where the increment was 0.5. These data were arranged in tables which may be found in references (9 to 11). Derivations of all equations derived by the authors may be found in references (9) and (10).

Owing to space limitations, only data for those cases that were solved by numerical integration are given here. These data are presented in the form of correction factors in Figs. 5 through 24. The correction factor is the effectiveness of the exchanger divided by the effectiveness of a true counter or parallel-flow exchanger having the same NTU and thermal-capacity ratio.

For all of the "unsymmetrical" cases (where the flow patterns of the two fluids are different), the value of  $E_A$  for given values of NTU and  $Z_A$  is slightly different from  $E_B$  for the same values of NTU and  $Z_B$ . For the cocurrent cases this difference was appreciable, so that in the correction-factor graphs it was necessary to plot different curves for intermediate values of  $Z_A$  and  $Z_B$ .

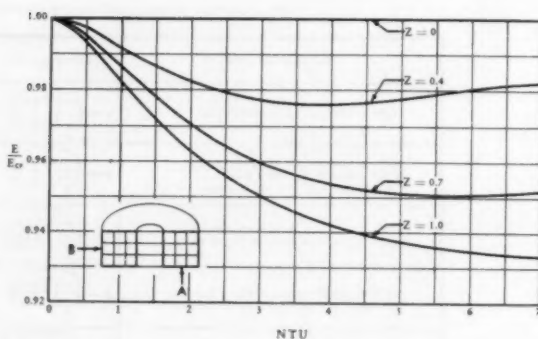


FIG. 5 CORRECTION FACTOR FOR TWO-PASS COUNTERCROSSFLOW; FLUID A MIXED BETWEEN PASSES, UNMIXED IN EACH PASS; FLUID B UNMIXED THROUGHOUT, INVERTED ORDER

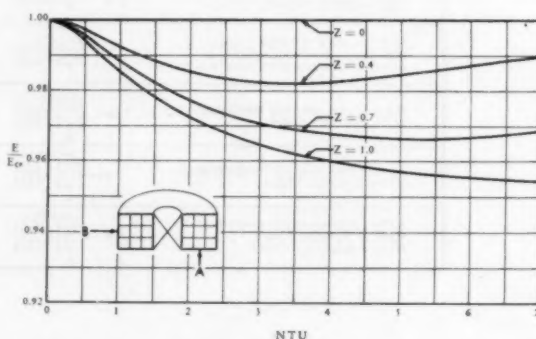


FIG. 6 CORRECTION FACTOR FOR TWO-PASS COUNTERCROSSFLOW; FLUID A MIXED BETWEEN PASSES, UNMIXED IN EACH PASS; FLUID B UNMIXED THROUGHOUT, IDENTICAL ORDER

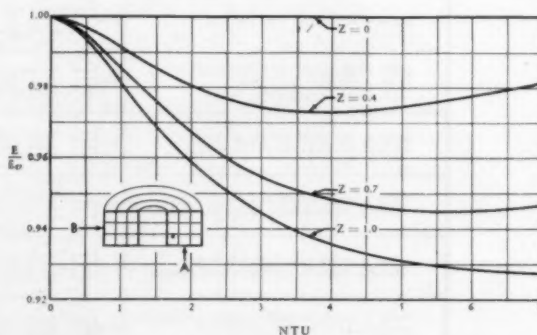


FIG. 7 CORRECTION FACTOR FOR TWO-PASS COUNTERCROSSFLOW; BOTH FLUIDS UNMIXED THROUGHOUT; BOTH INVERTED ORDER

For the countercurrent flow arrangements the differences were very small, and separate curves were impractical. It should be noted, however, that in those countercurrent cases where the fluids have different flow patterns within the passes,  $E_A$  and  $E_B$  can differ by larger amounts.

Examination of the correction-factor curves for the cocrossflow exchangers reveals that nearly all of the two-pass graphs have areas where the effectiveness is lower than that of a true parallel-flow exchanger with the same NTU and thermal-capacity ratio, and considerably lower than the corresponding single-pass

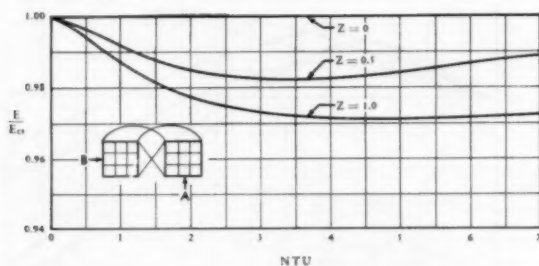


FIG. 8 CORRECTION FACTOR FOR TWO-PASS COUNTERCROSSFLOW; BOTH FLUIDS UNMIXED THROUGHOUT; BOTH IDENTICAL ORDER

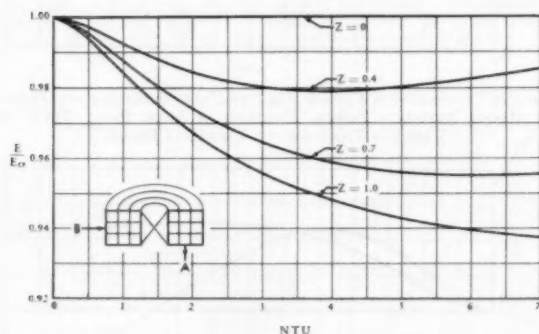


FIG. 9 CORRECTION FACTOR FOR TWO-PASS COUNTERCROSSFLOW; BOTH FLUIDS UNMIXED THROUGHOUT; FLUID A INVERTED ORDER, FLUID B IDENTICAL ORDER

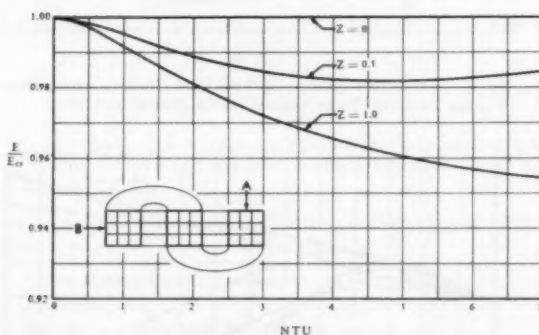


FIG. 10 CORRECTION FACTOR FOR THREE-PASS COUNTERCROSSFLOW; FLUID A MIXED BETWEEN PASSES, UNMIXED IN EACH PASS; FLUID B UNMIXED THROUGHOUT, INVERTED ORDER

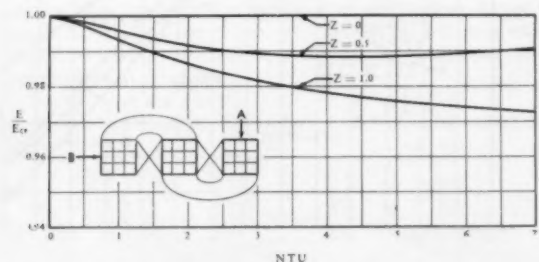


FIG. 11 CORRECTION FACTOR FOR THREE-PASS COUNTERCROSSFLOW; FLUID A MIXED BETWEEN PASSES, UNMIXED IN EACH PASS; FLUID B UNMIXED THROUGHOUT, IDENTICAL ORDER

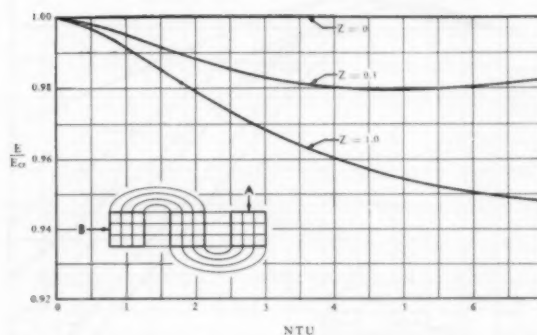


FIG. 12 CORRECTION FACTOR FOR THREE-PASS COUNTERCROSSFLOW; BOTH FLUIDS UNMIXED THROUGHOUT; BOTH INVERTED ORDER

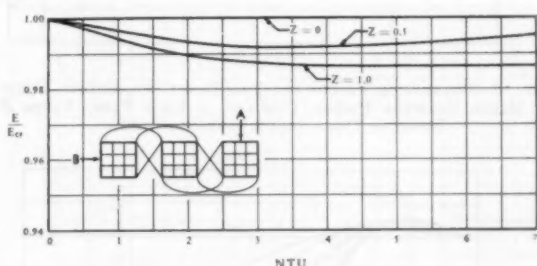


FIG. 13 CORRECTION FACTOR FOR THREE-PASS COUNTERCROSSFLOW; BOTH FLUIDS UNMIXED THROUGHOUT; BOTH IDENTICAL ORDER

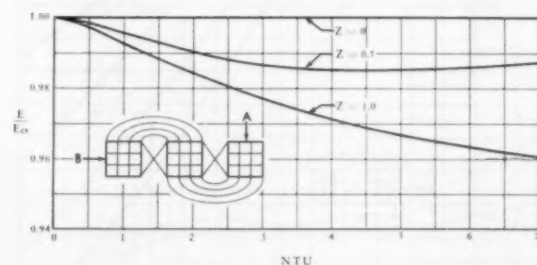


FIG. 14 CORRECTION FACTOR FOR THREE-PASS COUNTERCROSSFLOW; BOTH FLUIDS UNMIXED THROUGHOUT; FLUID A INVERTED ORDER, FLUID B IDENTICAL ORDER

crossflow exchanger. These results are due to the fact that in cocurrent flow it is possible in certain parts of the exchanger for the "cold" fluid to reach a higher temperature than the "hot" fluid, resulting in reversed heat flow and decreased effectiveness for both fluids. This does not occur at low values of NTU, because for low NTU, which means low effectiveness, the temperature change of each fluid is low and there is little chance for reversed heat flow. The effect is present in the three-pass cases, but it is less pronounced because of the lower NTU per pass for a given total NTU.

In using the correction-factor curves, it is necessary to use consistent notation. That is, if the known quantities are  $NTU_A$  and  $Z_A$ , the correction factor is  $E_A/E_{CF}$  (for the countercurrent cases) or  $E_A/E_{PF}$  (for the cocurrent cases). If the known quantities are  $NTU_B$  and  $Z_B$ , the correction factor is  $E_B/E_{CF}$  or  $E_B/E_{PF}$ .

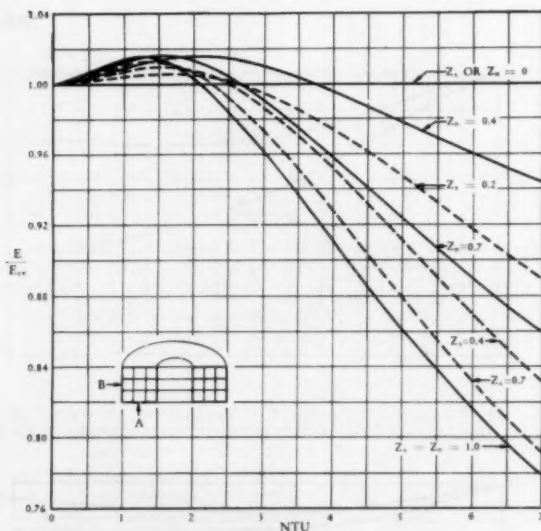


FIG. 15 CORRECTION FACTOR FOR TWO-PASS COCROSSFLOW; FLUID A MIXED BETWEEN PASSES, UNMIXED IN EACH PASS; FLUID B UNMIXED THROUGHOUT, INVERTED ORDER

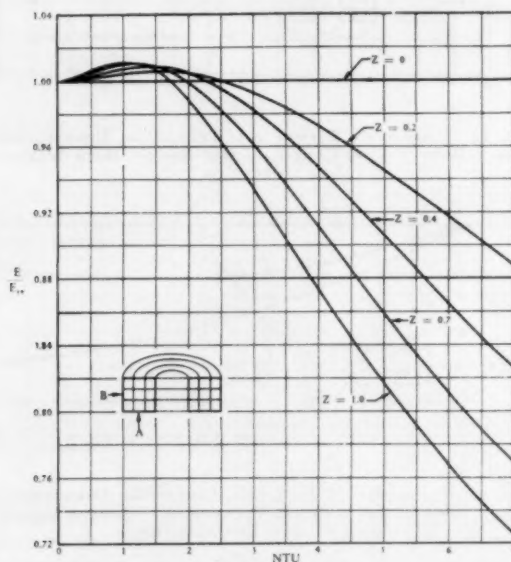


FIG. 17 CORRECTION FACTOR FOR TWO-PASS COCROSSFLOW; BOTH FLUIDS UNMIXED THROUGHOUT; BOTH INVERTED ORDER

From the data on three-pass countercrossflow exchangers, it appears that for four or more countercrossflow passes the effectiveness relation for true counterflow may be used with very little error. For four or more cocrossflow passes, the true parallel-flow equation should give accurate results.

To obtain maximum mean-temperature difference, the preferred order of flow arrangement within the passes for all cases is as follows:

- Both fluids unmixed.
- One fluid unmixed, one mixed.
- Both fluids mixed.

For all two and three-pass countercrossflow cases and for all

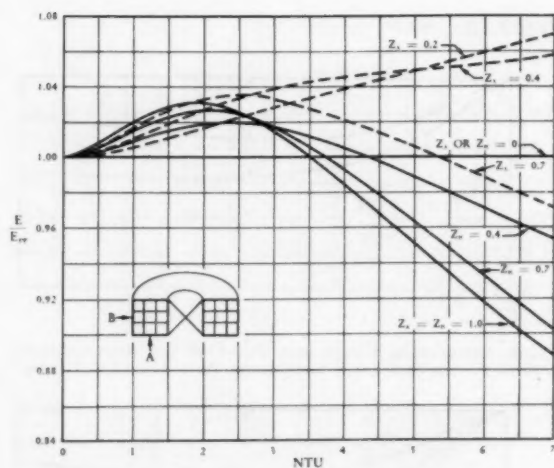


FIG. 16 CORRECTION FACTOR FOR TWO-PASS COCROSSFLOW; FLUID A MIXED BETWEEN PASSES, UNMIXED IN EACH PASS; FLUID B UNMIXED THROUGHOUT, IDENTICAL ORDER

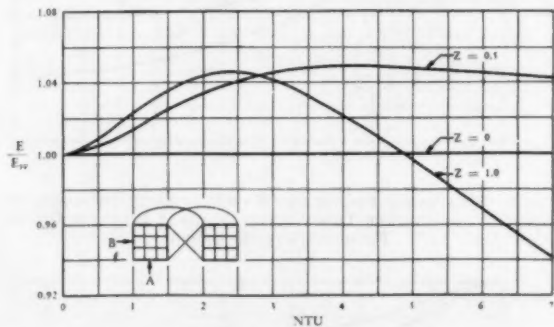


FIG. 18 CORRECTION FACTOR FOR TWO-PASS COCROSSFLOW; BOTH FLUIDS UNMIXED THROUGHOUT; BOTH IDENTICAL ORDER

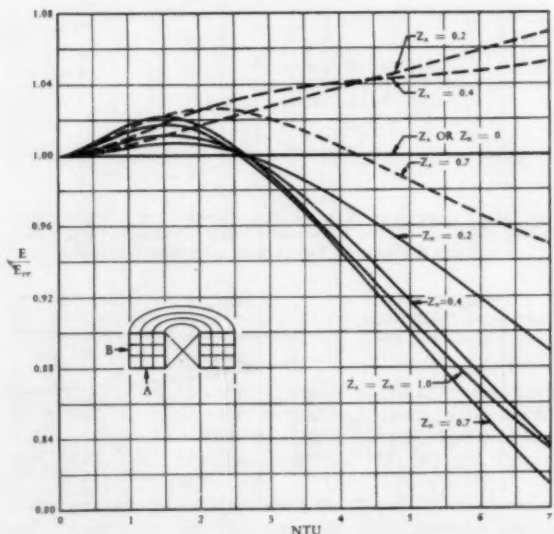


FIG. 19 CORRECTION FACTOR FOR TWO-PASS COCROSSFLOW; BOTH FLUIDS UNMIXED THROUGHOUT; FLUID A INVERTED ORDER, FLUID B IDENTICAL ORDER

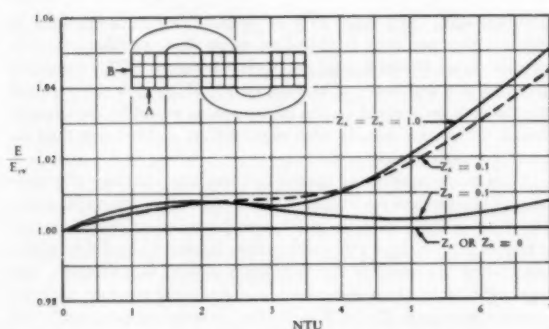


FIG. 20 CORRECTION FACTOR FOR THREE-PASS COCROSSFLOW; FLUID A MIXED BETWEEN PASSES, UNMIXED IN EACH PASS; FLUID B UNMIXED THROUGHOUT, INVERTED ORDER

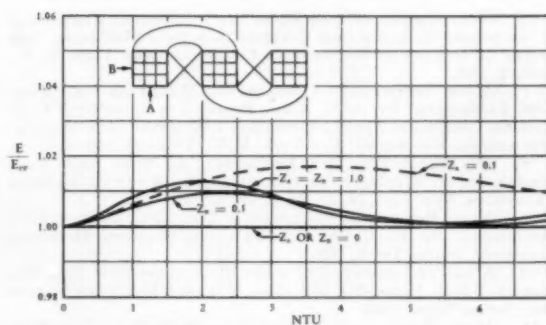


FIG. 21 CORRECTION FACTOR FOR THREE-PASS COCROSSFLOW; FLUID A MIXED BETWEEN PASSES, UNMIXED IN EACH PASS; FLUID B UNMIXED THROUGHOUT, IDENTICAL ORDER

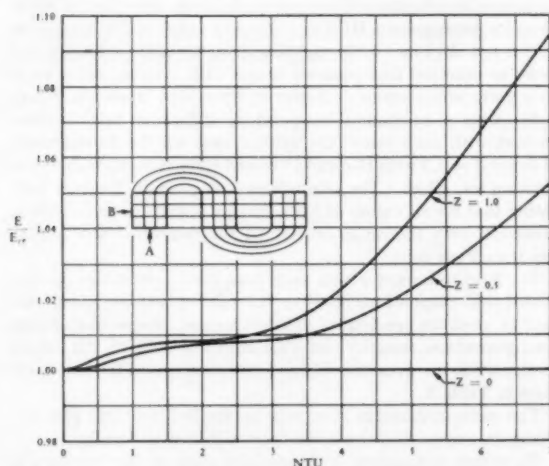


FIG. 22 CORRECTION FACTOR FOR THREE-PASS COCROSSFLOW; BOTH FLUIDS UNMIXED THROUGHOUT; BOTH INVERTED ORDER

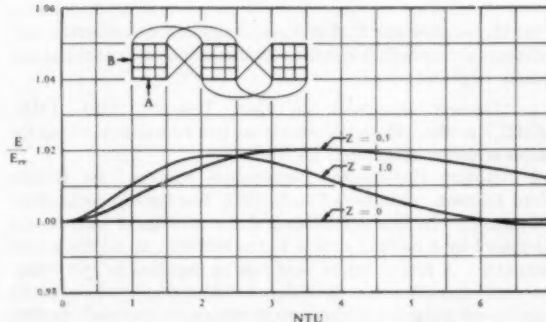


FIG. 23 CORRECTION FACTOR FOR THREE-PASS COCROSSFLOW; BOTH FLUIDS UNMIXED THROUGHOUT, BOTH IDENTICAL ORDER

two-pass cocrossflow cases the following is the preferred order of flow arrangement between the passes:

- (a) Unmixed, identical order.
- (b) Mixed.
- (c) Unmixed, inverted order.

For three-pass cocrossflow, the foregoing order is reversed.

Because of the possibility of reverse heat flow, cocrossflow exchangers in which the effectiveness of a single pass is equal to or greater than the maximum parallel-flow effectiveness should be avoided. Table 7 shows the maximum NTU per pass which should be used in cocrossflow exchangers in which both fluids are unmixed in the passes.

TABLE 7 MAXIMUM DESIGN NTU PER PASS, COCROSSFLOW EXCHANGERS

Z	NTU	Z	NTU
0.1	2.73	0.6	1.42
0.2	2.18	0.7	1.33
0.3	1.89	0.8	1.24
0.4	1.69	0.9	1.18
0.5	1.55	1.0	1.12

#### BIBLIOGRAPHY

- 1 "Mean Temperature Difference in Design," by R. A. Bowman,

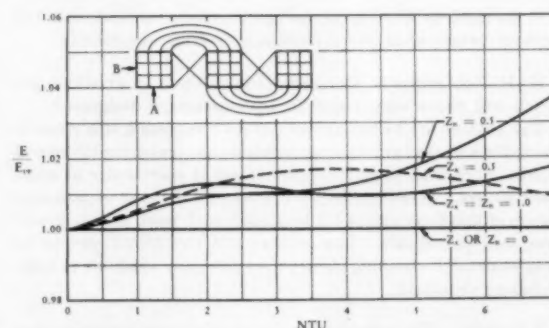


FIG. 24 CORRECTION FACTOR FOR THREE-PASS COCROSSFLOW; BOTH FLUIDS UNMIXED THROUGHOUT; FLUID A INVERTED ORDER, FLUID B IDENTICAL ORDER

A. C. Mueller, and W. M. Nagle, Trans. ASME, vol. 62, 1940, pp. 283-294.

2 "Mean Temperature Difference in Cross-Flow," by D. M. Smith, *Engineering*, vol. 138, November 2, 1934, pp. 479-481; vol. 138, November 30, 1934, pp. 606-607.

3 "Der Wärmeübergang im Kreuzstrom," by W. Nusselt, *Zeitschrift des Vereines deutscher Ingenieure*, vol. 55, 1911, pp. 2021-2024.

4 "Eine Neue Formel für den Wärmedurchgang im Kreuzstrom," by W. Nusselt, *Technische Mechanik und Thermodynamik*, vol. 1, 1930, pp. 417-422.

5 "Nusselt Cross Flow Factors," by D. E. Brimley, G. E. Eggleston, and H. E. Muenzer, Douglas Aircraft Company Report SM-14933, Santa Monica, Calif., November 1, 1953.

6 "Heat Transfer in Cross Flow," by J. L. Mason, Proceedings of the Second U. S. National Congress of Applied Mechanics, THE AMERICAN SOCIETY OF MECHANICAL ENGINEERS, New York, N. Y., 1955, p. 801.

7 "Mean Temperature Difference in Multi-Pass Cross-Flow Heat Exchangers," by H. H. Korst, Proceedings of the First U. S. National Congress of Applied Mechanics, THE AMERICAN SOCIETY OF MECHANICAL ENGINEERS, New York, N. Y., 1952, pp. 949-955.

8 "Gas Turbine Plant Heat Exchangers," by W. M. Kays, A. L. London, and D. W. Johnson, THE AMERICAN SOCIETY OF MECHANICAL ENGINEERS, New York, N. Y., April, 1951.

9 "Mean Temperature Difference in Counter-Cross-Flow Heat Exchangers," by R. A. Stevens, MS thesis, Southern Methodist University, Dallas, Texas, 1956.

10 "Mean Temperature Difference in Co-Cross-Flow Heat Exchangers," by J. Fernandez, MS thesis, Southern Methodist University, Dallas, Texas, 1956.

11 "Mean Temperature Difference in Multi-Pass Cross-Flow Heat Exchangers," by R. A. Stevens, J. Fernandez, and J. R. Woolf, Convaire Report FZA-095, 1955.

## Discussion

G. M. DUSINBERRE.<sup>4</sup> For those interested in numerical calculations as applied to crossflow exchangers, two additional references might be noted:

1 "General Discussion on Heat Transfer, 1951, IME-ASME," p. 304. Here the relaxation and iteration methods for simple crossflow exchangers are outlined.

2 "Rotary Regenerator Performance Factors," by Robert Ward Johnson. (Master's Thesis, 1954, The Pennsylvania State University.) In this unpublished thesis a range of factors was calculated by a method similar to the authors', on a punch-card computer. A rotary regenerator can be regarded as two cross-flow exchangers in series. But, since machine time came out of the department budget, a preliminary investigation was made to estimate the minimum number of subdivisions for three-figure accuracy. For most cases a five-by-five or six-by-six subdivision of each side was quite adequate.

If the need for four significant figures can be justified, then the authors' twenty-channel subdivision is probably desirable.

G. E. EGGLESTON.<sup>5</sup> The authors have done an excellent job which will prove very useful to heat-exchanger designers.<sup>6</sup>

The authors are to be commended for completing this more or less tedious work of grinding out numbers and preparing tables and charts. Such work in print is possibly not as spectacular as some other papers. There has been a tendency in the past to pass over papers of this type and to fail to publish such work in universally circulated periodicals. The authors and the ASME are to be congratulated for making these papers generally available to heat-exchanger designers.

F. LANDIS.<sup>7</sup> The authors are to be congratulated for presenting these solutions for multipass crossflow heat exchangers. Their work effectively completes the efforts which have previously produced many attempts but only few partial solutions.

It may, however, be worth while to put the results into proper perspective as far as the designer is concerned. The analysis is based on the assumptions of constant over-all heat-transfer coefficients, constant specific heats, and no change of phase in either fluid. These conditions are practically never met and over-all heat-transfer coefficients are rarely known with an accuracy of

$\pm 10$  per cent. Any analysis that permits design predictions to within a few per cent is therefore more than satisfactory. In practice either the exchange area (and therefore NTU) would be increased to a maximum of about 4 or 5 NTU to give the required effectiveness or a slight loss in effectiveness would be acceptable. Design difficulties usually also require that at least one fluid be mixed between passes.

It can be demonstrated thermodynamically that the effectiveness must decrease for constant NTU whenever irreversibilities take place. These may be due to mixing between passes, or due to higher local temperature differences between the fluids which occur when the order of the flow arrangement is inverted. The irreversibility and loss of effectiveness also must increase with the capacity rate ratio  $Z$ ; at  $Z = 0$  (the "condenser problem") the flow arrangement can have no effect, and it will show its maximum effect when  $Z = 1.0$ . When the worst arrangement for identical counterflow, two-pass exchangers (Arrangement IV-d, Fig. 3), is compared with the best (Arr. III-c) at  $Z = 1.0$ , the maximum difference is only about 3.0 per cent, Table 8, herewith. Corrections for Arrangement III-d and all other values of  $Z$  must be less.

It is not obvious whether mixing between passes with identical order or unmixed flow between passes with inverted order leads to a lower effectiveness. However, since flow inversion brings fluids with a maximum temperature difference into thermal contact with each other, the critical case will be Arrangement II-b, for  $Z = 1.0$  with II-c and IV-b and other capacity-rate ratios showing less effect. The comparison also given in Table 8, indicating that for all values of NTU mixing is slightly preferable to inversion, over the range considered the correction amounts to less than 2 per cent.

For fluids unmixed within each pass it may therefore be concluded that calculations based on full mixing between passes will lead to accurate predictions of effectiveness irrespective of flow arrangements or capacity ratios for values of NTU  $\leq 7.0$ . Such a calculation involves only Table 1 and solutions to the first three cases in Table 3.

The same arguments also can be applied to three-pass exchangers, except that the corrections will be even smaller.

To permit comparison with previous work in the literature it also should be noted that in all derived relations of the authors  $Z_A < Z_B$ .

TABLE 8 COMPARISON OF EFFECTIVENESS FOR  $Z = 1.0$

NTU	$\frac{E_{Arr. III-c}}{E_{Arr. IV-d}}$	$\frac{E_{Arr. II-b}}{E_{Arr. IV-d}}$
	$E_{Arr. IV-d}$	$E_{Arr. IV-d}$
0.5	1.001	0.9997
1.0	1.003	0.9972
2.0	1.010	0.9907
3.0	1.016	0.9861
4.0	1.021	0.9836
5.0	1.025	0.9823
6.0	1.028	0.9819
7.0	1.030	0.9818

## AUTHORS' CLOSURE

The authors would like to thank Professor Dusinberre, Mr. Eggleston, and Professor Landis for their kind remarks and pertinent comments.

Regarding the need for four-digit accuracy, it was considered desirable to determine the relative influence of different flow arrangements on exchanger effectiveness. In view of the small differences between similar flow arrangements, as pointed out by Professor Landis, it was anticipated that four-digit accuracy would be necessary to give a true picture.

Test problems were run to determine the minimum number of subdivisions necessary for four-digit accuracy, as shown in Table 2, using NTU = 7.0 and  $Z = 1.0$ . For the single-pass unmixed arrangement (Fig. 1(c) and Table 1) it was found that a  $15 \times 15$  matrix was required for three-figure accuracy and  $20 \times 20$  for four

<sup>4</sup> Professor of Mechanical Engineering, The Pennsylvania State University, University Park, Pa. Fellow ASME.

<sup>5</sup> Design Engineer, Air Conditioning Division, Douglas Aircraft Company, Inc., Santa Monica, Calif. Assoc. Mem. ASME.

<sup>6</sup> See reference (1) of the Bibliography.

<sup>7</sup> Assistant Professor of Mechanical Engineering, New York University, New York, N. Y. Assoc. Mem. ASME.

figures. A five-by-five subdivision for this case resulted in an error of three units in the third decimal place.

The authors agree with Professor Landis' remarks on the limitations imposed on the analysis by the assumptions. It is hoped that future work will establish the relative magnitudes of the approximations involved.

Professor Landis' main point is well taken, namely, that the fairly simple relations for Arrangement IV-d, Fig. 3, may be used with excellent accuracy to predict the performance of any two-pass countercrossflow exchanger in which both fluids are unmixed within the passes. However, the authors must take issue with two of Professor Landis' statements.

First, Arrangement IV-d is described as the "worst" of the two-pass countercrossflow arrangements. This is not the case. Of the ten different arrangements shown in Fig. 3, Arrangement IV-d ranks not as the worst, but as the third best. Table 9 shows all of the arrangements compared with Arrangement III-c in increasing order of efficiency.

It should perhaps be pointed out that the flow arrangement within the passes has a much greater influence on effectiveness than the arrangement between passes.

TABLE 9 COMPARISON OF EFFECTIVENESS FOR  $Z = 1.0$ 

NTU	$\frac{E_{III-c}}{E_{I-a}}$	$\frac{E_{III-c}}{E_{I-b}}$	$\frac{E_{III-c}}{E_{I-d}}$
1.0	1.008	1.007	1.006
4.0	1.093	1.073	1.060
7.0	1.181	1.128	1.111
NTU	$\frac{E_{III-c}}{E_{I-c}}$	$\frac{E_{III-c}}{E_{IV-d}}$	$\frac{E_{III-c}}{E_{II-d}}$
1.0	1.004	1.006	1.004
4.0	1.049	1.038	1.031
7.0	1.096	1.049	1.042
NTU	$\frac{E_{III-c}}{E_{II-c}}$	$\frac{E_{III-c}}{E_{IV-d}}$	$\frac{E_{III-c}}{E_{III-d}}$
1.0	1.003	1.003	1.001
4.0	1.025	1.021	1.012
7.0	1.037	1.030	1.019

Second, the statement that in all derived relations  $Z_A$  must be less than or equal to  $Z_B$  is incorrect. Since  $Z_A$  is the reciprocal of  $Z_B$ , the statement implies that  $Z_A \leq 1$  and  $Z_B \geq 1$ . There are no restrictions of this type either in the mathematical derivations or in the physical system. This can easily be verified by substitution in any of the derived equations, making use of the summary of relations in the Introduction.



# Convection Phenomena in Fluids Heated From Below

By SIMON OSTRACH,<sup>1</sup> CLEVELAND, OHIO

A review of nearly a century's research on the effects of heating a fluid from below in a body force field reveals many unusual aspects of the resulting flow which had previously been of meteorological interest only. For horizontal fluid layers, the flow was found to depend on a single parameter (the Rayleigh number). Below certain critical values of the Rayleigh number the configuration is in stable equilibrium; for Rayleigh numbers exceeding the critical either columnar or cellular flows occur with increased heat-transfer rates. It is pointed out herein that configurations with heating from below also are encountered in present-day problems in various fields. A recent experiment and an analysis of fluids heated from below in a vertical enclosure (which more closely simulates current configurations) are discussed and there appears to be a correlation between the previous research for meteorological purposes and new problems of current interest in fluid mechanics and heat transfer.

## INTRODUCTION

UNTIL the past few years free or natural convection, that is, convective motion due entirely to buoyancy forces, had been of little interest except to the meteorologist or astrophysicist. The lack of interest in other applications was possibly due to two causes: (a) The complexities of the phenomenon resulting from the inseparable interaction of its dynamics and thermodynamics, and (b) in most problems of interest, the prime factors governing natural convection, namely, the body force, fluid volumetric expansion coefficient, and temperature difference were small.

However, with the advent of jet propulsion and nuclear power the three prime factors governing natural convection can all very greatly exceed their previously considered bounds. Hence in many practical present-day problems in the fields of aeronautics, atomic power, electronics, and chemical engineering, natural convection effects can be important. Accordingly, more interest has recently been shown in this phenomenon and a number of research papers have already been published; for example (1)<sup>2</sup> to (13). Many of these recent studies were concerned with internal flows, that is, flows which are bounded by fixed surfaces, and several new and interesting aspects of the natural-convection phenomenon were encountered. However, in the afore-mentioned papers one of the most unusual aspects of natural convection, namely, the instability of the flow with heating from below, was not considered except for a mention in (13) of its possible importance in present-day problems.

It is clear that two layers of fluid of different densities with

the heavier above the lighter are in a state of unstable equilibrium. Any disturbance of this configuration will establish a transient motion in which the heavier fluid moves to the bottom. The limit of this motion is a rest state with the heavier fluid below. An analogous situation appears to be that in which a fluid of initially uniform density is heated from below. However, it was found that the fluid remains stationary until a certain critical temperature gradient (depending on the fluid and configuration) is reached. The equilibrium then becomes unstable for infinitely small disturbances and the fluid starts to move. The heat from below is, moreover, a source of energy which serves to maintain a motion once started, since the descending heavier fluid is heated and becomes lighter. In this case the final state is not one of a stable equilibrium but is an essentially steady motion.

Most of the existing studies of heating from below were made for horizontal fluid layers with particular regard to meteorological applications. It was found both theoretically and experimentally that the flow was generally of an unusual columnar or cellular type depending on a critical parameter (the Rayleigh number). A detailed and complete review of this work up to 1939 with application to meteorology is given in (14).

There are now, in various fields, actual configurations wherein the fluid layers are not horizontal but the fluid is still heated from below. For example, a discussion of such a configuration in an atomic power unit is presented in (15), and such a configuration is also found in conjunction with the cooling of turbine blades by natural convection. To the best of the author's knowledge, the important turbine-blade cooling problem was only recently classified as one of an "unstable-type" natural convection flow (16). In (16) and (17) there is the first account of a theoretical analysis of heating from below in a vertical channel or, more generally, in one whose axis is parallel rather than normal to the body force direction. It was found therein that the basic characteristics of the flow and heat transfer were similar to those for horizontal fluid layers. In addition, the velocity and temperature distributions were determined in detail so that they could be compared to an identical configuration wherein, however, the fluid was not heated from below. The effects of heating from below were shown in this manner to be marked.

In the present paper the various theoretical and experimental studies dealing with the development of the flow patterns and stability criteria are discussed as are also those investigations in which a steady flow is superposed on the natural-convection flow with heating from below. Finally, the analogy of this unstable type of natural-convection flow with flows between two parallel surfaces in relative motion and with flows over wavy walls is indicated.

It is hoped that the present paper will aid in the understanding of numerous new fluid mechanics and heat-transfer problems which are of growing significance and will also perhaps serve as a basis for future research on a scientific phenomenon which has been of interest for almost a century.

## EARLY EXPERIMENTS

It is well known that a fluid motion is set up if in the presence of a body force field there exists a density variation transverse to

<sup>1</sup> Aeronautical Research Scientist, NACA, Lewis Flight Propulsion Laboratory.

<sup>2</sup> Numbers in parentheses refer to the Bibliography at the end of the paper.

Contributed by the Heat Transfer Division and presented at the Diamond Jubilee Annual Meeting, Chicago, Ill., November 13-18, 1955, of THE AMERICAN SOCIETY OF MECHANICAL ENGINEERS.

NOTE: Statements and opinions advanced in papers are to be understood as individual expressions of their authors and not those of the Society. Manuscript received at ASME Headquarters, August 8, 1955. Paper No. 55-A-88.

the force direction. In 1882, however, Thomson (18) was the first to describe a "tessellated structure" which he observed casually in a tub of warm soapy water cooling in the yard of an inn. The configuration in which this cellular convective pattern occurred was one wherein there was a density gradient parallel but opposite to the direction of the body force. The first laboratory-controlled experiments of this apparently new phenomenon were made by Bénard and are reported in (19) among others. Bénard worked with very thin liquid layers (on the order of several millimeters) lying on a metallic plate which was heated and maintained at a uniform temperature. The upper surface of the liquid layer was free and was at a lower temperature than at the plate surface since it was in contact with the ambient air. The detailed development of the flow is described in many sources and basically occurs in two phases as follows:

When the vertical temperature difference is sufficiently large, a random motion of the fluid results. Shortly, thereafter, the first phase of relatively short duration (increasing with fluid viscosity from a few seconds to several minutes) appears in which the fluid forms cells of semiregular shape. In this phase the cellular cross sections are nearly regular polygons of, in general, four to seven sides. During the second phase the cells become equal and regular and align themselves. The limit of the second phase is thus a permanent regime of cells with vertical boundaries and hexagonal cross sections (see Fig. 1) in which the liquid rises in the core of the cell, moves outward at the top, descends at the outer periphery, i.e., in the vertical boundary between adjacent

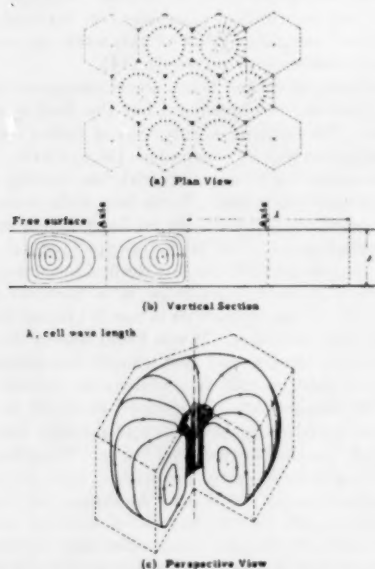


FIG. 1 SCHEMATIC SKETCH OF BÉNARD CELL STRUCTURE  
(Reproduced from reference 14.)

cells, and moves inward at the bottom. These cells are often called Bénard cells. Fig. 2 is a reproduction of a photograph of the cellular pattern in a layer of spermaceti taken during Bénard experiments.

#### EARLY THEORIES

In the mathematical formulation of so complicated a physical phenomenon simplifying assumptions must be made. All theoretical analyses of natural convection to date are based on the assumption that density variations are negligible except in so far

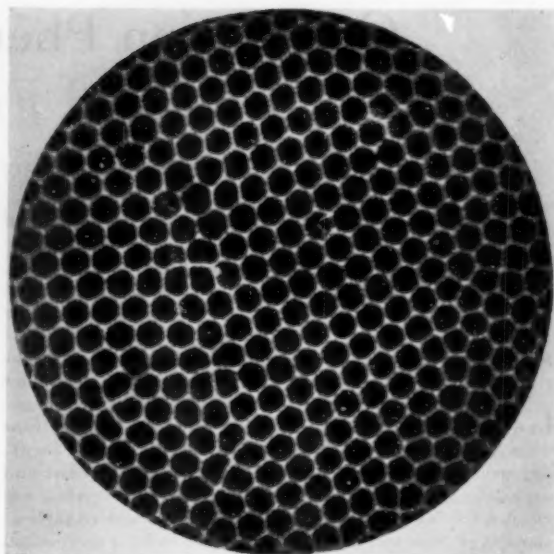


FIG. 2 VIEW OF BÉNARD CELLS IN LAYER OF SPERMACE TI  
(Reproduced from reference 14.)

as they modify the action of the body force. Justification of this assumption can be found in many papers. In addition, for the problem at hand, several different configurations can be specified. The top and bottom surfaces (see Fig. 1) of the fluid are taken to be plane and parallel and these surfaces may further be rigid or free and conducting or insulated. If rigid, the no-slip condition of viscous fluids must be imposed and if free, tangential (horizontal) velocities are permitted at the horizontal surfaces. The vertical boundary or cell wall can either be a rigid boundary or a surface of symmetry between two adjacent cells. In all the studies of horizontal layers the vertical cell boundaries are taken to be insulated and it is further assumed that the fluid temperature decreases linearly upward.

Lord Rayleigh (20) was the first to investigate the problem theoretically. Jeffreys (21) and (22) and Low (23) later extended and verified Rayleigh's analysis. Each analysis is made in two parts, (a) the investigation of the geometry of the convection, and (b) the determination of a criterion for the onset of free convection in a fluid layer of limited depth. It was assumed that the equations for neutral stability are obtained by neglecting time-dependent and second-order velocity terms and hence the analysis deals with only the first phase of the flow development. In this way, assuming further that the cells were rectangular in cross section, the form of small disturbances which are neither amplified nor damped was determined as was also the relation of the fundamental parameters as a function of cell size for this to occur.

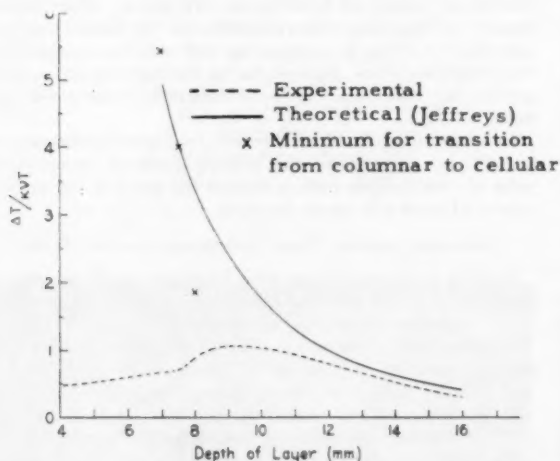
The limitations of the analyses because of the many assumptions will be discussed subsequently, but the analyses did yield the surprising and fundamental result that a top-heavy fluid layer was statically stable under the joint influence of viscosity and conduction until the vertical temperature gradient became sufficiently large. In particular, it was found that the sole parameter determining stability was the product of the Prandtl and Grashof numbers. This product, called the Rayleigh number, is independent of the cell shape and is given by  $\beta g h^3 \Delta T / \nu$  where  $\beta$  is the fluid volumetric expansion coefficient ( $1/T$  for gases),  $g$  is the gravitational (or body) force,  $h$  is the layer depth,  $\Delta T$

is the temperature difference between the bounding surfaces,  $\kappa$  is the thermal diffusivity, and  $\nu$  is the kinematic viscosity coefficient. For two rigid conducting parallel surfaces above and below, for example, the critical Rayleigh number is approximately 1700.

#### REFINEMENTS OF EARLY RESEARCH

Although there was qualitative agreement between Bénard's early experiments and the theoretical analyses just described, several not fully justified assumptions were made to simplify the mathematics. More careful experiments accordingly were made [see references (24) and (25) for details of apparatus and procedure] which not only verified the qualitative picture again but also substantiated quantitatively the predicted critical Rayleigh number. In addition, Schmidt and Milverton (24) showed that there was a sudden increase in heat transfer when the motion started.

Chandra's experiments (25) in which the depth of fluid layer was varied, however, shed a completely new light on the problem. Comparison of Chandra's results with those analytically determined by Jeffreys is shown in Fig. 3. Note that  $\Delta T/\kappa\nu T$  is



( $\Delta T$ , critical temperature difference;  $\kappa$ , thermal diffusivity;  $\nu$ , kinematic viscosity;  $T$ , mean temperature.)

FIG. 3 COMPARISON OF CHANDRA'S EXPERIMENTAL AND JEFFREY'S THEORETICAL CRITICAL TEMPERATURE DIFFERENCES  
(Reproduced from reference 25.)

plotted against the layer depth; where  $\Delta T$  denotes the critical temperature difference between the two plates,  $\kappa$  denotes the thermal diffusivity,  $\nu$  denotes the kinematic viscosity, and  $T$  denotes the mean temperature; from the definition of the Rayleigh number it is clear that the critical temperature difference varies inversely as the cube of the layer depth (from Jeffreys's criterion then  $\Delta T/\kappa\nu T = 1709/gh^3$ ).

The experimental results show reasonable agreement with the theoretical in layers of depth exceeding 10 mm, and, in fact, it was again verified for such layers that no motion occurred until the critical was exceeded. However, for more shallow layers Chandra observed initial motions whose character differed from that for the deeper layers. For example, in layers 6 mm or less in depth, the flow pattern bore no resemblance to the previously described polygonal prismatic cells. Instead, after a brief inter-

val vertical columns of rising air appeared and this ascending motion seemed to continue indefinitely. The centers of convection drifted about so that after a time it was difficult to recognize any definite pattern. This type of motion was described as being "columnar" in contradistinction to the cellular and will be referred to as such hereafter. It was not possible to obtain cellular convection in the shallow layers no matter how large the temperature difference was made by heating the lower plate.

With fluid layers between 7 and 10 mm, columnar convection first appears for relatively small temperature differences. For larger temperature differences the motion essentially becomes cellular. The minimum temperature differences for the transition from columnar to cellular patterns are indicated by crosses in Fig. 3. There is excellent agreement between these observations and Jeffreys's theory, particularly for layers of 7 and 7.5 mm.

Detailed descriptions and photographs of the development of the flows are presented in (25). Thus Chandra confirmed the theories for relatively deep layers and showed that for relatively shallow layers a distinct new type of instability is encountered which was not predicted by the earlier research. Chandra also showed that the columnar-type flow passes into the cellular type for layers of medium depth. In any event, these experiments show that significant natural-convection flows can be obtained in thin fluid layers. In addition, observations of the cellular flow with air showed that the motion was the reverse of that found by Bénard for liquids; that is, the fluid descended in the central core and rose in the outer peripheries. It can thus be concluded that the flow direction in the cells depends on the particular configuration. The theories give no indication of the flow direction.

At this point it is perhaps appropriate to digress from the chronological sequence of events in order to appraise the research discussed in the foregoing. In this regard the work of Sutton (26) is noteworthy. Sutton was concerned with resolving the differences between the theory and Chandra's experiments for shallow layers. From the definition of the critical Rayleigh number, the theory implies that the critical temperature (or density) difference required for sustained convection increases indefinitely as the layer depth approaches zero. However, Chandra's experiments showed a more complicated state of affairs for shallow layers for which there was no theoretical treatment. Sutton, therefore, critically examined the three fundamental assumptions made in the theories, viz., that (a) density variations are negligible except for their influence on the buoyancy, (b) the initial motion is slow, and (c) a linear temperature profile extends throughout the entire fluid layer at the start of the motion. Sutton accepts the first two as reasonable, but on the basis of Chandra's and other experiments, argues that the validity of the third assumption is doubtful. Sutton suggests that a small boundary layer with a large temperature gradient forms as the heating of the lower surface begins. As the heating continues the boundary layer becomes unstable and yields the columnar flow described by Chandra. Further heating then leads to the establishment of the condition postulated in the theories and hence cellular flow and agreement for large temperature differences.

Sutton does point out that the theoretical formulation would correspond to an experimental one in which the heat is added so slowly as to preclude the possibility of the formation of a boundary layer. He dismisses the possibility that the experimental procedures were such and re-examines the problem according to his postulate that the columnar motion occurs because of an instability of a shallow boundary layer whose depth is unrelated to the distance between the upper and lower boundaries. On this basis Sutton derives a criterion for the columnar flow which in-

volves only the ratio of the absolute temperatures of the upper and lower rigid boundaries and agrees with Chandra's observations. Another expression is derived and experimentally verified for the critical temperature difference at which transition takes place from the columnar to the cellular flow. Finally, it is shown, in agreement with Chandra, that the cellular type will occur for fluid layers exceeding a certain depth, but that for more shallow layers the columnar type is generated initially, passing to the cellular for increased temperature differences.

All the research described up to this point was aimed at determining the criterion for the onset of a flow and the form of this flow. Schmidt and Saunders (27) undertook an investigation to see if there was any change in the motion of air or water between two parallel and horizontal plates for temperature differences in excess of those for the start of a flow. It was found that the length of the horizontal side of a cell was twice the layer depth when the flow was cellular. As the Rayleigh number was increased beyond the critical, the temperature gradients at the plane midway between the boundary surfaces decreased to negligible values indicating that all the heat was being convected. Experiments on several layer depths show that on further heating the layer becomes completely turbulent at Rayleigh numbers of approximately 45,000. The turbulence developed suddenly in the tests with water, but in air the transition was much more gradual, the first signs of turbulence appearing at a Rayleigh number of about 5000. The increase in the rate of heat transfer at the change from equilibrium to cellular motion was found to be greater than that at the change from cellular to turbulent flow.

In 1940 Pellew and Southwell (28) reformulated the theoretical analyses. In a rigorous mathematical manner they showed that any motion with a temporal periodicity will decay or subside so that the basic equations used in the early theories were reconfirmed. They further point out that for vertical boundaries which are thermal insulators the two horizontal boundaries must be conductors for maintained motion.

The most novel aspects of the Pellew and Southwell analysis is, however, that the shape of the cell is left indefinite in terms of a cell wave length. In the previous analyses the cell was assumed to be rectangular in cross section. Pellew and Southwell thus reduced the problem to, (a) relating the Rayleigh number to the wave length, and (b) evaluating the wave length for a specified cell shape for the purpose of determining the "preferred" cell shape. However, it was found that the wave length was essentially dependent on the ratio of the depth of the fluid layer to a characteristic length which defines the cell size. Therefore, for a fluid layer of indefinite horizontal extent, any symmetrical cell pattern can be formed in which the cells can be of any shape. Consequently, all wave lengths are possible for such configurations and the cell pattern which forms will be the one associated with the smallest possible Rayleigh number. The apparent preference for a hexagonal pattern must then possibly be explained on the basis of a nonlinear theory.

Contours of the vertical velocity component computed from an exact solution of the linearized equations for a hexagonal cell was shown to have all the basic qualities of the flow as observed experimentally. Finally, it was demonstrated that cells bounded by two rigid vertical boundaries could not be analyzed in the same manner as for layers of indefinite horizontal extent.

Although the linear theory yields a definitive stability criterion and provides a qualitative picture of the detail and form of a convective cell, it deals only with the first phase of the motion. That is, it demonstrates that the fluid remains at rest until the critical Rayleigh number is reached. The fluid then becomes unstable to small disturbances and a semiregular cellular pattern forms. Above the critical Rayleigh number an increasing range of wave lengths will be amplified. One of these wave

lengths establishes itself by being selectively amplified until nonlinear effects intervene in a stabilizing manner and prevent further growth. The steady motion so attained then corresponds to the second or final phase of the flow development. It, therefore, becomes clear that the actual heat transfer and fluid flux can only be determined from a nonlinear theory.

Pillow (29) accordingly formulates the nonlinear problem for the two-dimensional flow between two horizontal plates. For Rayleigh-number magnitudes of the order sufficient for steady flows, the basic equations are in a form analogous to the classical boundary-layer equations and hence can be studied by a singular perturbation technique; that is, the effects of viscosity and heat conduction need be considered only near the cell boundaries. Solutions for the cell interior (i.e., away from the boundaries) indicate that both the vorticity and temperature are constant there. Recall that Schmidt and Saunders' experiments also indicated that the temperature gradients vanish in the center of the cell.

A satisfactory solution for the flow near the boundaries has not as yet been found. Pillow, therefore, assumes two-dimensional flow and employs an approximate method to show that the heat transfer will be proportional to the five-fourths power of the temperature difference between the two plates. This proportionality also was found experimentally, but the Nusselt numbers calculated by Pillow do not agree too well with the experimental. The discrepancies are perhaps due to the approximate method and the fact that the actual flow is three rather than two-dimensional.

In recent years Chandrasekhar (see, for example, references 30 and 31) has investigated the problem from an astrophysical point of view but his work is beyond the scope of the present paper and hence will not be discussed.

#### UNSTABLE LAYERS WITH SUPERPOSED STEADY FLOW

In order to explain various cloud formations in the presence of winds many of the previous experiments also were run with a steady superposed motion in the horizontal direction (25, 32, 35). The superposed motion was established either by moving one of the boundaries in its plane or by forced methods such as fans and pumps. Since it is conceivable that similar configurations will be encountered in present-day applications in fields other than meteorology a summary of that research will be presented.

The results are divided into two categories; viz., the effects of a steady flow on (a) cellular convection patterns, and (b) on columnar flows. For a configuration in which cellular flows could occur, the steady flow did not alter the stability condition; that is, if the temperature difference was lower than the critical no flow pattern (other than the steady) was discernible. When the critical temperature difference was exceeded polygonal cells were, of course, obtained with no superposed flow. However, when the steady flow rate is maintained below a certain low limiting value, say,  $u_1$ , the original polygonal pattern is distorted as shown in Fig. 4. When the steady flow exceeds  $u_1$  but is below another limit, say,  $u_2$ , the fluid aligns itself into a series of vortexes or rolls with axes transverse to the steady-flow direction (see Fig. 5). For steady velocities greater than  $u_2$  the flow pattern is a series of longitudinal rolls; that is, vortexes with axes parallel to the flow direction, Fig. 6.

For a fluid layer of a given depth,  $u_1$  and  $u_2$  both increase with the temperature difference between the top and bottom boundaries. It is not possible to state the values of  $u_1$  and  $u_2$  for given configurations.

When a columnar flow was subjected to a steady flow the fluid appeared to be filled with irregular short spindlelike structures, Fig. 7. As the steady-flow velocity is increased the lengths of the spindlelike structures increase and the structures appear to

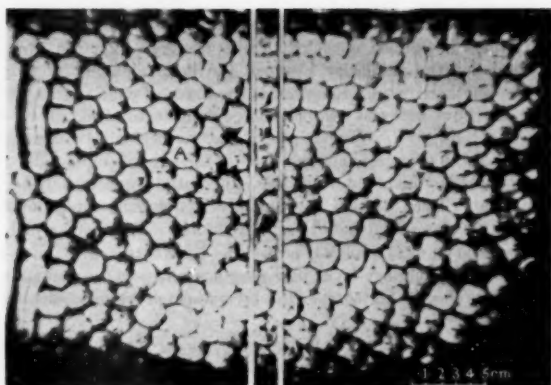


FIG. 4 TYPICAL VIEW OF DISTORTED CELLS WITH LOW-VELOCITY SUPERPOSED STEADY FLOW (Reproduced from reference 25.)

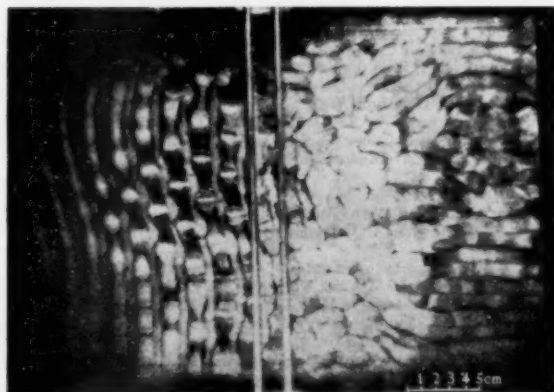
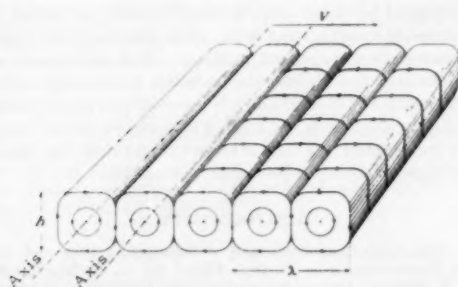


FIG. 5 TYPICAL SCHEMATIC SKETCH AND VIEW OF TRANSVERSE ROLLS WITH SUPERPOSED STEADY FLOW OF INTERMEDIATE VELOCITY ( $A$ , fluid-layer depth;  $\lambda$ , cell wave length;  $V$ , superposed velocity. Reproduced from references 25 and 14.)

be more regular, but long continuous rolls or transverse rolls were never encountered.

To the author's knowledge no more details (such as relative heat-transfer rates and the like) are available for the superposed flows described, and no theoretical treatment has been attempted.

#### FLOWS IN VERTICAL ENCLOSURES

In order to analyze the effects of heating from below in the configuration more representative of present-day problems, con-

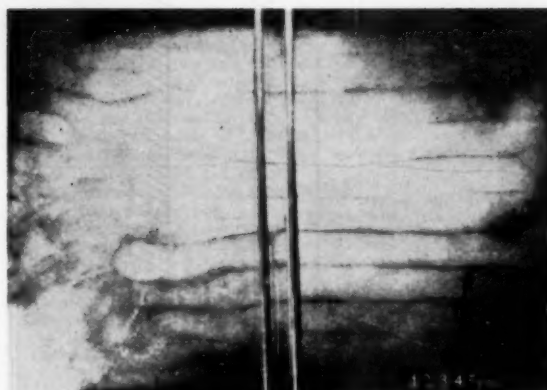
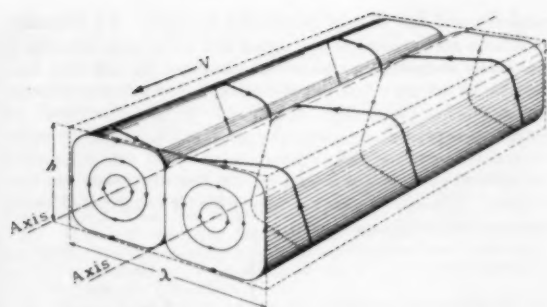


FIG. 6 TYPICAL SCHEMATIC SKETCH AND VIEW OF LONGITUDINAL ROLLS WITH LARGE VELOCITY SUPERPOSED STEADY FLOW ( $A$ , fluid-layer depth;  $\lambda$ , cell wave length;  $V$ , superposed velocity. Reproduced from references 25 and 14.)

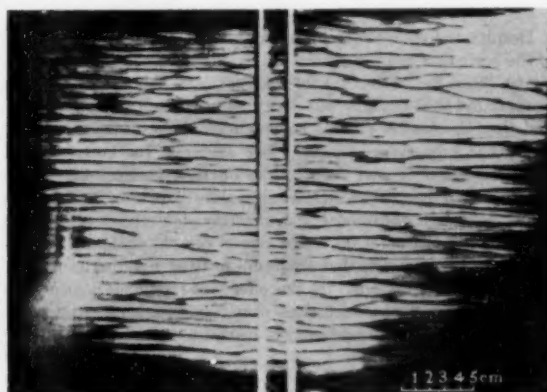


FIG. 7 TYPICAL VIEW OF SPINDLELIKE STRUCTURE OBTAINED BY SUPERPOSING STEADY FLOW ON COLUMNAR-TYPE FLOW (Reproduced from reference 25.)

sideration was given in (16) and (17) to the fully developed flow of a viscous fluid subject to the gravitational force between two plane vertical parallel surfaces open at both ends, Fig. 8. (More generally, the surfaces could be taken to be oriented parallel to any generating body force.) The vertical temperature gradient is specified to be uniform and negative so that the fluid is, in effect, heated from below. This configuration differs from those for horizontal fluid layers in that the depth of the layer is not

restricted and the vertical boundaries are rigid. No boundary conditions are specified at the upper and lower ends although a completely enclosed channel can be simulated by requiring that there be no net mass flow in the channel. The primary assumption of this analysis is then that the flow is fully developed; no restriction is placed on the velocity magnitudes. Detailed velocity and temperature distributions are obtained not only when the vertical surfaces are insulators but also when they are conductors. The solutions are also applicable for a superposed forced flow parallel to the channel axis.

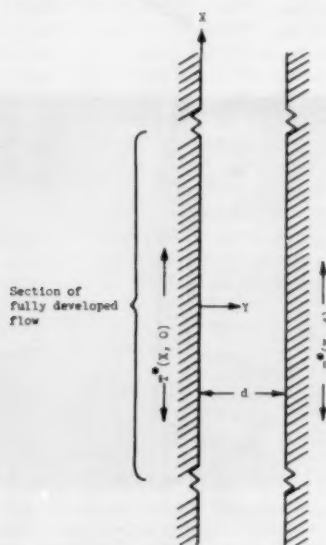


Fig. 8 SCHEMATIC SKETCH OF VERTICAL CHANNEL CONFIGURATION

Despite the differences between the two configurations some of the basic flow characteristics in the vertical enclosures are similar to those for horizontal fluid layers. In this regard, it was again found that the flow was dependent on the Rayleigh number and that there exist critical Rayleigh numbers on either side of which the flow type changes. For example, for both vertical walls insulated it was found that no flow ensues unless the Rayleigh number takes on certain values; for conducting side walls, flows are obtained for every Rayleigh number, but the flow changes character on either side of certain critical Rayleigh numbers. It is shown that frictional heating may be important in these critical regions. If the effects of frictional heating are considered, two distinct solutions were found for each set of parametric equations as had previously been discovered by the author (4, 13).

Comparison of the results of (16) and (17) with an identical configuration (13) wherein, however, the fluid was not heated from below, indicated that the flow and heat transfer can be increased appreciably by heating from below.

In (15) there is an account of an experiment in which a surprisingly large amount of heat transfer was obtained by natural convection in tall narrow vertical enclosures when the fluid was heated from below. The unusual heat-transfer rates were explained by the observation of "convection loops" or cells in the fluid. Thus some experimental evidence of cellular flows in vertical enclosures exists.

#### ANALOGIES

The research on fluid layers heated from below takes on addi-

tional significance because of the analogy between those problems and others in applied mechanics. For example, Low (36) first pointed out the similarity between the flow bounded by two conducting horizontal rigid surfaces the lower of which is heated and the flow between two coaxial cylinders rotating at different speeds (37). Comparison of the mathematical developments for the two problems reveals that the two sets of boundary conditions are identical, but the differential equations differ somewhat. Even though the analogy is not exact, a general qualitative correspondence exists between the two problems which is discussed in (22) and (23) as well as elsewhere. Certain aspects of the boundary-layer flow over a slightly wavy wall (38) and of the flow in horizontal fluid layers heated from below also appear to be similar.

The problem of the flow in vertical enclosures neglecting frictional heating is directly analogous to the whirling instability of a rotating shaft. The critical Rayleigh numbers correspond to the critical or whirling speeds of the shaft.

#### CONCLUSION

Despite the differences between the configurations studied for meteorological purposes and the simplified one simulating those encountered in various other fields, there appears to be a correlation between the two types of problems. New problems in which there is heating from below can be better understood and more properly evaluated if cognizance is taken of this correspondence. For example, the flow in the cooling passages of turbine blades is usually one in which the fluid is heated from below, but the problem has apparently never been analyzed as such.

#### BIBLIOGRAPHY

- 1 "The Analytical Prediction of Superposed Free and Forced Viscous Convection in a Vertical Pipe," by R. C. Martinelli and L. M. K. Boelter, University of California Press (Berkeley and Los Angeles), 1942.
- 2 "Free Convection Through Enclosed Gas Layers," by M. Jakob, Trans. ASME, vol. 68, 1946, pp. 189-195.
- 3 "Analysis of Turbulent Free Convection Boundary Layer on Flat Plate," by E. R. G. Eckert, NACA Report 1015, 1951.
- 4 "Laminar Natural-Convection Flow and Heat Transfer of Fluids With and Without Heat Sources in Channels With Constant Wall Temperatures," by S. Ostrach, NACA TN 2863, 1952.
- 5 "Theoretical Considerations on Free Convection in Tubes," by M. J. Lighthill, Aeronautical Research Council 15, 074 F.M. 1758, 1952.
- 6 "Experiments on Mixed Free- and Forced-Convection Heat Transfer Connected With Turbulent Flow Through a Short Tube," by E. R. G. Eckert, A. J. DiGiulio, and A. N. Curren, NACA TN 2974, 1953.
- 7 "New Aspects of Natural-Convection Heat Transfer," by S. Ostrach, Trans. ASME, vol. 75, 1953, pp. 1287-1290.
- 8 "Free Convection in Heat Generating Fluid (Laminar Flow)," by J. Woodrow, Atomic Energy Research Establishment, England, A.E.R.E. E/R 1267, 1953.
- 9 "Laminar Free Convection Between Heat Producing Vertical Plates in a Liquid," by D. V. Wordsworth, Atomic Energy Research Establishment, England, A.E.R.E. E/R 1270, 1953.
- 10 "Natural-Convection Heat Transfer at Reduced Pressures," by J. R. Kyte, A. J. Madden, and E. L. Piret, *Chemical Engineering Progress*, vol. 49, 1953, pp. 653-662.
- 11 "Nonisothermal Flow and Heat Transfer Inside Vertical Tubes," by R. L. Pigford, Presented at Heat Transfer Symposium, Annual Meeting American Institute of Chemical Engineering, preprint no. 15, 1953.
- 12 "Heat Transfer by Free Convection in an Open Thermosyphon Tube," by B. W. Martin and H. Cohen, *British Journal of Applied Physics*, vol. 5, no. 3, 1954, pp. 91-96.
- 13 "Combined Natural- and Forced-Convection Laminar Flows and Heat Transfer of Fluids With and Without Heat Sources in Channels With Linearly Varying Wall Temperatures," by S. Ostrach, NACA TN 3141, 1954.
- 14 "Tourbillons Thermoconvectifs dans L'Air, Application à la Météorologie," by D. Avsec, Publications Scientifiques et Techniques du Ministère de L'Air, no. 155, 1939.

- 15 "Free Convection in Narrow Vertical Sodium Annuli," by D. P. Timo, Knolls Atomic Power Laboratory, General Electric Co., KAPL-1082, 1954.
- 16 "Unstable Convection in Vertical Channels With Heating From Below, Including Effects of Heat Sources and Frictional Heating," by S. Ostrach, NACA TN 3458, 1955.
- 17 "On the Flow, Heat Transfer, and Stability of Viscous Fluids Subject to Body Forces and Heated From Below in Vertical Channels," by S. Ostrach, 50 Jahre Grenzschichtforschung, Eine Festschrift in Originalbeiträgen, Verlag Friedrich Vieweg und Sohn, Braunschweig, Germany, 1955.
- 18 "On a Changing Tessellated Structure in Certain Liquids," by J. Thomson, Proceedings Glasgow Philosophical Society, vol. 13, 1882, p. 469.
- 19 "Tourbillions cellulaires dan une nappe liquide," by H. Bénard, *Revue générale des Sciences pures et appliquées*, vol. 11, 1900, pp. 1261-1271, and 1309-1328.
- 20 "On Convection Currents in a Horizontal Layer of Fluid, When the Higher Temperature Is on the Under Side," by Lord Rayleigh, *Philosophical Magazine and Journal of Science*, vol. 32, no. 192, 1916, pp. 529-546.
- 21 "The Stability of a Layer of Fluid Heated Below," by H. Jeffreys, *Philosophical Magazine*, vol. 2, 1926, pp. 833-844.
- 22 "Some Cases of Instability in Fluid Motion," by H. Jeffreys, Proceedings of the Royal Society of London, England, vol. 118, 1928, pp. 195-208.
- 23 "On the Criterion for Stability of a Layer of Viscous Fluid Heated From Below," by A. R. Low, Proceedings of the Royal Society of London, England series A, vol. 125, 1929, pp. 180-195.
- 24 "On the Instability of a Fluid When Heated From Below," by R. J. Schmidt and S. W. Milverton, Proceedings of the Royal Society of London, England, series A, vol. 152, 1935, pp. 586-594.
- 25 "Instability of Fluids Heated From Below," by K. Chandra, Proceedings of the Royal Society of London, England, series A, vol. 164, 1938, pp. 231-242.
- 26 "On the Stability of a Fluid Heated From Below," by O. G. Sutton, Proceedings of the Royal Society of London, England, series A, vol. 204, 1950-1951, pp. 297-309.
- 27 "On the Motion of a Fluid Heated From Below," by R. J. Schmidt and O. A. Saunders, Proceedings of the Royal Society of London, England, series A, vol. 165, 1938, pp. 216-228.
- 28 "On Maintained Convective Motion in a Fluid Heated From Below," by A. Pellew and R. V. Southwell, Proceedings of the Royal Society of London, England, series A, vol. 176, 1940, pp. 213-243.
- 29 "The Free Convection Cell in Two Dimensions," by A. F. Pillow, Aeronautical Research Laboratories, Report A 79, Melbourne, Australia, 1952.
- 30 "The Instability of a Layer of Fluid Heated Below and Subject to Coriolis Forces," by S. Chandrasekhar, Proceedings of the Royal Society of London, England, series A, vol. 217, 1953, p. 306.
- 31 "The Instability of a Layer of Fluid Heated Below and Subject to the Simultaneous Action of a Magnetic Field and Rotation," by S. Chandrasekhar, Proceedings of the Royal Society, series A, vol. 225, 1954, pp. 173-184.
- 32 "Some Experiments on Periodic Columnar Formation of Vortices Caused by Convection," by T. Terada, Report of the Aeronautical Research Institute, Tokyo Imperial University, vol. 3, no. 31, 1928, p. 3.
- 33 "Forms of Stratified Clouds," by S. Mal, *Beiträge zur Physik der freien Atmosphäre*, Leipzig, Germany, vol. 17, no. 1, 1930.
- 34 "The Forms of Stratified Clouds," by A. C. Phillips and Sir G. T. Walker, *Quarterly Journal of the Royal Meteorological Society*, vol. 58, no. 243, 1932, pp. 23-30.
- 35 "Shear Patterns in an Unstable Layer of Air," by A. Graham, Philosophical Transactions of the Royal Society of London, England, series A, vol. 232, 1933, pp. 285-296.
- 36 "Instability of Viscous Fluid Motion," by A. R. Low, *Nature*, vol. 115, 1925, pp. 299-300.
- 37 "Stability of a Viscous Fluid Between Two Rotating Cylinders," by G. I. Taylor, Philosophical Transactions of the Royal Society, series A, vol. 223, 1923, pp. 289-343.
- 28 "Influence of a Slight Wall Undulation on the Distribution of the Laminar Boundary Layer," by H. Görtler, Kaiser Wilhelm Institute for Aerodynamical Research, Göttingen, Germany, October, 1949, TPA3/T1B Translation, No. GDC 10/5556T, Issued by the Ministry of Supply.



# Experimental Superheater for Steam at 2000 Psi and 1250 F—Report After 14,281 Hours of Operation

By J. H. HOKE<sup>1</sup> AND F. EBERLE,<sup>2</sup> ALLIANCE, OHIO

In order to investigate the reactions of superheater alloys to operating conditions producing steam at 1250 F, a test element constructed of 2-in.-OD alloy tubes was installed in an operating boiler at the Twin Branch Plant. Operating conditions and experience after 5000 and 12,000 hr as well as metallurgical examination of specimens removed from the element after nearly 7000 hr of operation were described in previous papers. The present paper describes the results of the metallurgical examinations after 14,281 hr of operation, when the experiment was discontinued and the test element removed for complete examination and evaluation.

## INTRODUCTION

POWER-PLANT cycle efficiency is improved by increasing operating temperatures and pressures. The present limitation to this trend appears to be due to the properties of the currently used materials of construction and the understandable reluctance of plant officials to use newly developed alloys without prior information as to their serviceability under actual operating conditions.

In order to obtain a practical and long-time demonstration of the suitability of certain new alloys, developed during and after World War II, for higher steam temperatures, a superheater test element was constructed and installed in an operating boiler at the Twin Branch Plant, receiving steam at 2000 psi, 950 F, and discharging 1250 F steam at the outlet. Field operation began in March, 1950, and an account of the experience gained during the first two years of operation was presented in a previous paper.<sup>3</sup> A second paper<sup>4</sup> has been presented dealing with the succeeding two years of operation which included preliminary information obtained from the metallurgical examination of a number of samples removed from the element after nearly 7000 hr of operation. The test element was finally removed from service in May, 1954, because changes in operating schedule reduced the rate of accumulation of service time and prevented the effective continuation of the test.

<sup>1</sup> Research Metallurgist, The Babcock & Wilcox Company Research Center.

<sup>2</sup> Chief Metallurgical Engineer, The Babcock & Wilcox Company Research Center.

<sup>3</sup> "Experimental Superheater for Steam at 2000 Psi and 1250 F—Progress Report of Field Operation," by F. G. Ely and F. Eberle, Trans. ASME, vol. 74, 1952, pp. 803-812.

<sup>4</sup> "Experimental Superheater for Steam at 2000 Psi and 1250 F—Progress Report After 12,000 Hours of Operation," by F. Eberle, F. G. Ely, and J. A. Dillon, Trans. ASME, vol. 76, 1954, pp. 665-677.

Contributed by the Research Committee on High-Temperature Steam Generation and presented at a joint session with the Power Division, Diamond Jubilee Annual Meeting, Chicago, Ill., November 13-18, 1955, of THE AMERICAN SOCIETY OF MECHANICAL ENGINEERS.

NOTE: Statements and opinions advanced in papers are to be understood as individual expressions of their authors and not those of the Society. Manuscript received at ASME Headquarters, August 19, 1955. Paper No. 55-A-102.

The element at that time had accumulated 14,281 hr of operating service of which 50 per cent had been with steam-outlet temperatures in excess of 1200 F, 31.5 per cent in the temperature range of 1100 to 1200 F, and the remainder of the time at temperatures below 1100 F. During the same period (due to customary banked periods at night and week-end outages) the element also had been subjected to 828 temperature cycles of which 332 included temperatures below saturation when the steam was shut off.

Upon removal, the element was returned to the laboratory for a complete metallurgical investigation of the various tube materials and weldments. This investigation has included complete metallographic examinations of the tube materials and weldments, particularly with respect to the extent of external and internal oxidation and microstructural changes, and mechanical testing of tube materials and weldments such as room and elevated temperature (1350 F), tensile and impact tests, hardness determinations, flaring tests, and side-bend tests of weldments. Records had been made periodically during the test period of any changes in external dimensions of the tubes. Stress-rupture testing of the tube materials and weldments has been initiated, but owing to the long-range nature of these tests, conclusive results are not yet available. This study of the stress-rupture properties will be reported later. Steam-oxidation tests on conventional superheater materials, conducted with cylindrical specimens shrink-fitted on the core rods of the test element at locations of increasing steam temperatures, likewise will be reported at a later date.

## REVIEW OF OPERATIONAL AND EXPERIMENTAL DETAILS

As fully described in the first progress report, the test element was constructed of 2-in.-OD alloy tubes in the form of four hair-pin loops connected in series and arranged for semiportable insertion through the rear wall of boiler No. 42 at the Twin Branch Plant of American Gas and Electric Service Corporation and its affiliate the Indiana and Michigan Electric Company. Its location in the boiler setting is shown in Fig. 1. At this location, it was swept by the gas stream approaching the main superheater, at temperatures in the range of 2000 F, and was exposed to the action of a Type IK soot blower operated on normal schedule. Steam from the main superheater outlet was supplied to the inlet of the test element, and passed through the four consecutive loops to the final outlet for disposal.

Fig. 2 illustrates graphically the relation of the tube-metal temperature to outlet steam temperature for the various sections of the test elements as determined from thermocouple data. The average increase in steam temperature in the probe is shown in Fig. 3, based on an inlet temperature of 950 and an exit temperature of 1250 F.

The first progress report also contained a brief commentary on methods of test operation which were maintained during most of the service life. The types of alloy materials used in the original construction, as well as changes in the arrangement of the test element resulting from alterations and repairs, from the removal

of specimens, and from the introduction of new materials, are described fully in the second progress report.

Fig. 4 illustrates the arrangement of the superheater test element for the fourth or final period of operation, and Table 1 gives pertinent information and operational data for the various tube materials. Table 2 contains information on the weldments that were examined after termination of the field test.

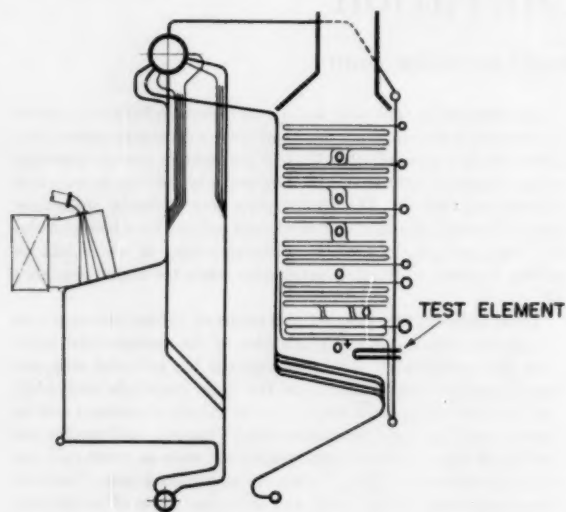


FIG. 1 LOCATION OF SUPERHEATER TEST ELEMENT IN BOILER SETTING

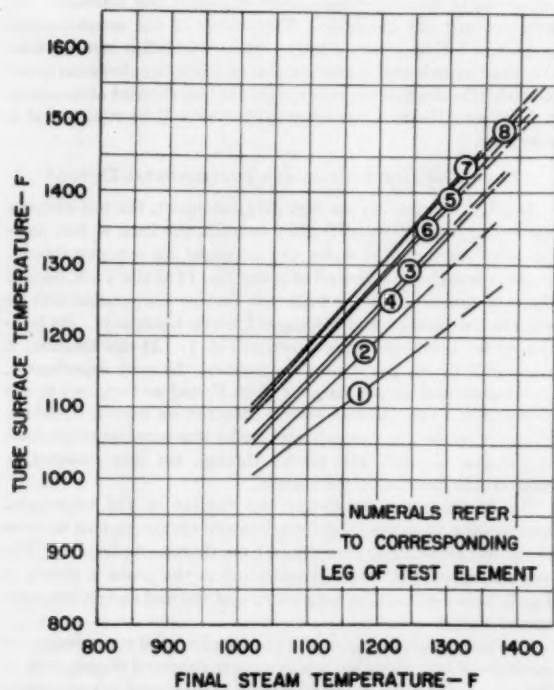


FIG. 2 SUMMARY OF METAL TEMPERATURE VERSUS FINAL STEAM TEMPERATURE FOR VARIOUS TUBE SECTIONS IN TEST ELEMENT

#### EXAMINATION OF MATERIALS AT END OF SERVICE

At the end of service, the test element was removed to the laboratory for dissection and evaluation. The various tube sections appeared to be in good condition and showed no general indication of deterioration. The soot-blower side of most of the tubes was covered with a smooth, thin, and tightly adherent red oxide, and the fireside with an ash-and-scale mixture which was of

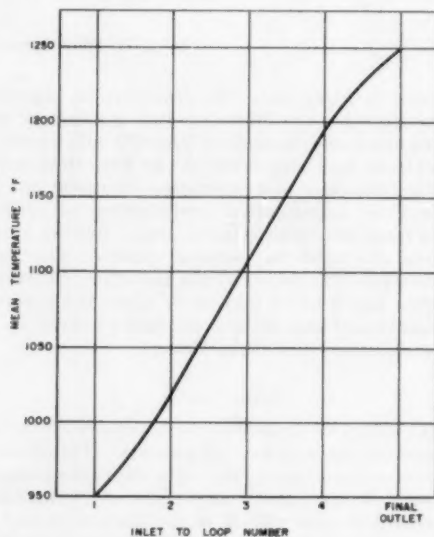


FIG. 3 AVERAGE INCREASE OF STEAM TEMPERATURE IN PROBE BASED ON 950 F INLET AND 1250 F OUTLET STEAM TEMPERATURE

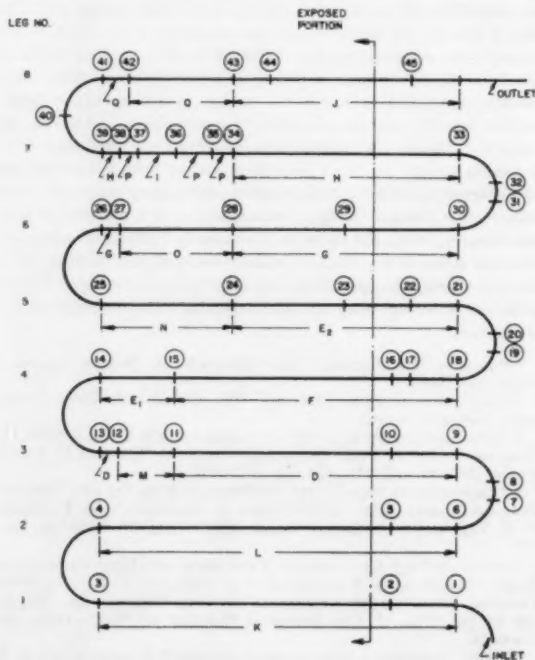


FIG. 4 FINAL ARRANGEMENT OF TEST ELEMENT SHOWING LOCATION OF MATERIALS AND WELDS

TABLE 1 TUBE DATA AND OPERATIONAL INFORMATION FOR VARIOUS SECTIONS OF TEST ELEMENT

Leg no.	Material	Base composition	Section	Service, hrs	Tube dimensions—		Average <sup>1</sup> metal temperature, °F	Stress at 2000 psig— ASME	Allowable working stress— ASME
					OD	Min. wall thickness			
1	AISI 304	18Cr8Ni	K	13133	2.00	0.512	1161	1907	5475 <sup>2</sup>
2	304	18Cr8Ni	L	13133	2.00	0.512	1236	1907	3250
3	304	18Cr8Ni	D, M	14281	2.00	0.512	1279	1907	3250
4	347	18Cr8NiCb	E <sub>1</sub>	14281	2.00	0.398	1270	3025	4275
5 <sup>3</sup>	321	18Cr8NiTi	F	14281	2.00	0.521	1270	1863	3190
6 <sup>3</sup>	321	18Cr8NiTi	N	7323	2.00	0.520	1314	1863	3197
7 <sup>4</sup>	347	18Cr8NiCb	E <sub>2</sub>	14281	2.00	0.398	1314	3025	4275
8	316	16Cr13Ni3Mo	G	14281	2.00	0.504	1309	1970	3300
9	304	18Cr8Ni	O	7323	2.00	0.492	1309	2063	3393
10	318	16Cr13Ni3MoCb	H	14281	2.00	0.509	1340	1932	3270
11	Timken	16Cr25Ni6Mo	I	14281	2.00	0.273	1340	5330	6490
12	15-15N	15Cr15NiWMoCb	P	7323	2.00	0.281	1340	5040	6205
13	Armco	17-14CuMo	J	14281	2.00	0.268	1341	5460	6650
14	15-15N	15Cr15NiWMoCb	Q	7323	2.00	0.284	1341	5040	6205

<sup>1</sup> Corresponding to an outlet steam temperature of 1250 F.<sup>2</sup> Old piece, improperly heat-treated, moved from Leg 5 at end of third period.<sup>3</sup> Replacement tube.<sup>4</sup> Moved from Leg 4 at end of third period.<sup>5</sup> Interpolated for average metal temperature shown.<sup>6</sup> Taken as equal to that for Type 316.<sup>7</sup> Sixty per cent of the rupture strength in 100,000 hr at 1350 F.<sup>8</sup> Value reported for 15-15N has been revised from that reported in footnote 4 due to more complete results.

TABLE 2 SUMMARY INFORMATION FOR WELDS INVESTIGATED

Weld no.	Leg no.	Service time hr	Materials joined		Electrode <sup>a</sup>
			A	B	
14	4	14281	347	304	19-9Cb
15	4	7323	321	347	19-9Cb
23	5	11339	347	347	19-9Cb
24	5	7323	321	347	19-9Cb
25	5	7323	316	321	18-12Mo
29	6	11339	316	316	18-12Mo
34	7	7323	15-15N	318	17-14CuMo
35	7	7323	15-15N	15-15N	17-14CuMo
37	7	7323	15-15N	16-25-6	17-14CuMo
38	7	7323	318	15-15N	17-14CuMo
39	7	14281	316	318	18-12Mo
40	Bend 7-8	7323	316	316	18-12Mo
42	8	7323	15-15N	15-15N	17-14CuMo
44	8	11339	17-14CuMo	17-14CuMo	17-14CuMo

<sup>a</sup> The first number refers to the chromium content and the second to the nickel content.

a reddish brown color and contained an underlying dark scale. However, the soot-blower side of Sections O (Type 304—Leg 6), N (Type 321—Leg 5), Q (15-15N—Leg 8), and I (Timken 16-25-6—Leg 7) was covered with a dark scale which was not as smooth and polished as the red surface of the other sections. There was no observed indication of soot-blowing damage such as blistering, exfoliation, or craze cracking of scale or metal underneath. Ring sections of the various alloys were descaled in the laboratory and re-examined. In general, appearances were quite similar, the soot-blower sides being fairly smooth and the firesides showing some roughening. This roughening effect was not centered on the fireside, but was present as two distinct areas on each side of the fireside center with a relatively smooth region between.

Periodically, during service and after termination of the field test, tube-diameter measurements were made on the various sections to check for the possible occurrence of circumferential creep or tube wastage. As mentioned in the second progress report,<sup>4</sup> a slight progressive enlargement of tube diameter was noted in the Type 321 material at the hotter end of Leg 5. This deformation was subsequently found to have resulted from the inadvertent lack of a solution heat-treatment of the tube prior to its installation. Consequently, a replacement Type 321 tube was inserted and the unaffected portion of the old tube was relocated in Leg 4. However, this old material continued to show creep at the new location to the extent of 0.85 per cent increase in diameter at the end of service. The section of Type 304 located in Leg 6 showed a 1.0 per cent increase in diameter at the hotter end, but little change at the cooler end indicating that this material was being used near its temperature-stress limit. On the other hand, the 15-15N alloy had an external metal loss of approximately 0.010 in. on the horizontal diameter. Types 316, 318, and Armco 17-14CuMo showed a slight decrease particularly

on the horizontal diameter which is perpendicular to the direction of gas flow.

## HIGH-TEMPERATURE CORROSION BEHAVIOR

Two methods are available for the determination of the corrosion behavior of commercial tubing in service. One consists of measuring the change in tube dimensions after scale removal. This method is somewhat questionable for determining external corrosion because the change in outside diameter caused by corrosion may be offset by tube enlargement from creep. The change in internal diameter is also not practical for measuring internal corrosion because the original values are not known with sufficient accuracy. As previously mentioned, the 15-15N alloy had a diameter decrease of 0.010 in. and Types 316, 318, and Armco 17-14CuMo had smaller and variable losses which were likewise greater on the diameter perpendicular to the gas flow.

The second method employs the scale thickness formed in service as a measure of the corrosion behavior. Such measurements are of little use for evaluating external corrosion of tubes removed from service due to the mixtures of oxide and ash deposits formed as well as soot-blower action which produces a very variable layer. However, it may be used with certain reservations for measuring internal corrosion, that is, the resistance of the metal to steam attack. Such a method is useful for comparing various materials and may serve as an approximation for determining corrosion rates providing exfoliation has not occurred.

TABLE 3 STEAM-CORROSION RATES CALCULATED FROM AVERAGE MAXIMUM SCALE THICKNESS

Alloy	Location	Average <sup>a</sup> metal temperature internal surface, °F	Corrosion rate, —mils per year—	
			At 6950 hrs	At end of service
304	Leg 3	1258 F	1.5	.9
321	Leg 4	1255	1.5	.5
321	Leg 5	1292	...	2.2
347	Leg 5	1292	.4	.5
316	Leg 6	1288	6.0	2.8
304	Leg 6	1288	...	.95
318	Leg 7	1326	.5	.85
16-25-6	Leg 7	1326	.5	.85
15-15N	Leg 8	1352	...	3.2
17-14CuMo	Leg 8	1352	.65	2.5

<sup>a</sup> Corresponding to 1250 F outlet steam temperature.

In comparing the corrosion rates of the various alloys of the test element, the differences in temperature at which the individual sections had been operating must be taken into consideration. Such data are included in Table 3 along with average values of steam-corrosion rates. The corrosive effect of high-pressure superheated steam is a matter of considerable interest inasmuch as some investigators have shown by laboratory tests that corrosion rates in steam are higher than in air.

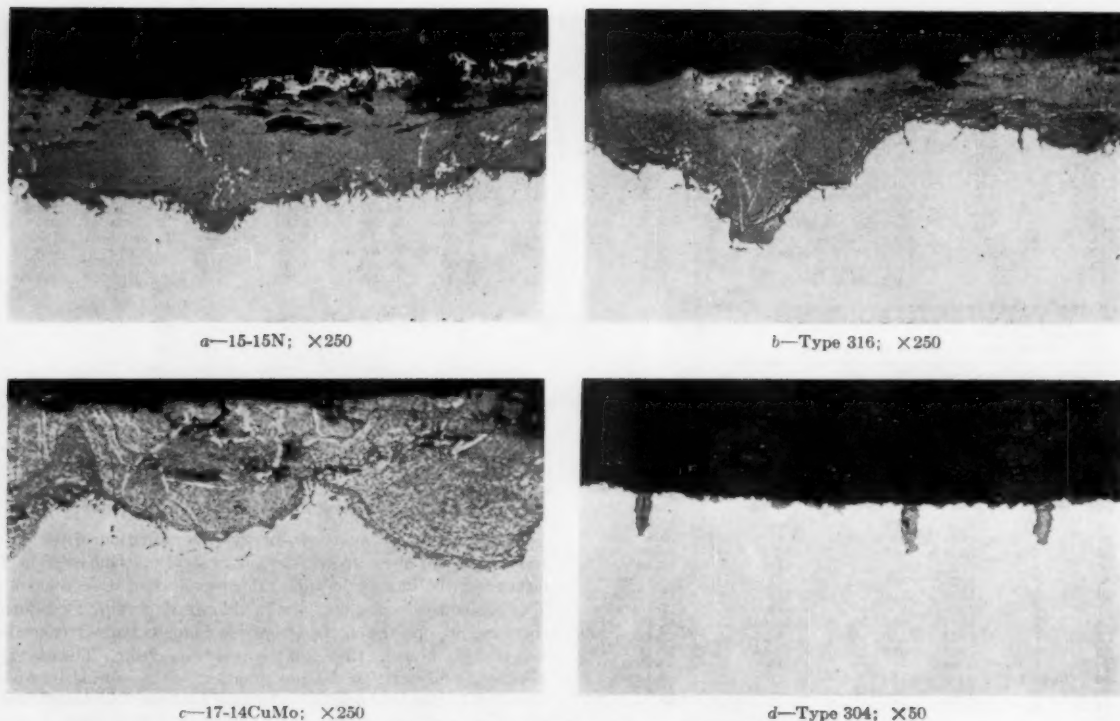


FIG. 5 TYPICAL STEAM-SIDE SCALE LAYERS. UNETCHED

A close inspection of the corrosion rates of the various alloys indicates that Types 304, 321, and 316 displayed decreasing corrosion rates with time, that the corrosion rates of Types 318, 347, and Timken 16-25-6 did not change appreciably, and that Armeo 17-14CuMo showed an increasing corrosion rate. Whether these differences in corrosion rates are of significance is not known, but the data indicate that for the service conditions encountered, alloys 316, Armeo 17-14CuMo, and 15-15N showed least resistance to attack by steam. These alloys were coated with fairly thick, well-defined layers such as illustrated by the cross-sectional views in Fig. 5. It is felt that the various degrees of surface oxidation observed are within the range acceptable for high-temperature superheater design. There was no indication of an intergranular steam attack in any of the alloys even though the oxide layers were irregular and varied from angular penetrations to smooth sinusoidal contours. Except for the Armeo 17-14CuMo material, flaring tests produced no cracks or tears on either the internal or external surfaces.

The observed propagation of internal seams, die marks, etc., in some of the tubes may be cause for some concern. These defects originate during the fabrication of seamless tubing and may be regarded as stress raisers although there is no record of a service failure in practical experience which has been caused or aggravated by such seams. Fig. 5(d) illustrates the appearance of the cross section of Type 304 tubing after 14,281 hr of service containing such oxide-filled penetrations. Again, owing to the comparative nature of such observations, accurate growth data are not available, but such defects were found to penetrate more rapidly than general oxidation.

#### MECHANICAL PROPERTIES

Of particular interest in this investigation was the possible

effect of prolonged service at elevated temperatures on the mechanical properties of the materials of construction. It is important to know whether significant deterioration of the stress-rupture properties, as well as the short-time room-temperature and elevated-temperature mechanical properties of tube materials and weldments, has occurred. The change in the stress-rupture properties has been made the subject of a special study because of the long test durations involved and will be reported separately at a later date. The results of the short-time tests that were employed are presented as well as results available for the materials prior to service and after 6950 hr for comparative purposes.

**Tensile Properties at Room Temperature and 1350 F.** Tensile tests were conducted at room temperature and at 1350 F on specimens made from the tube materials as well as on pertinent weldments of the test element. The effect of time, temperature, and stress on the tensile properties at room temperature and 1350 F on the tube materials is shown in Tables 4 and 5, and is graphically illustrated in Figs. 6, 7, 8, and 9. There was a slight tendency for the room-temperature strength values to increase after service, particularly for the more complex alloys, while the ductility values decreased more markedly. However, these results, when compared with those obtained after 6950 hr, show that such trends are decreasing and in fact occasionally are reversed. Long-time service appears to have little deleterious effect upon the elevated-temperature tensile properties, various trends being observed though none resulted in a serious loss of values. Room-temperature tensile-test values presented in the second progress report<sup>4</sup> for Type 347 material after 6950 hr have since been found to be in error and have been deleted.

As a part of the program for the evaluation of weldments after service, room-temperature and elevated-temperature (1350 F)

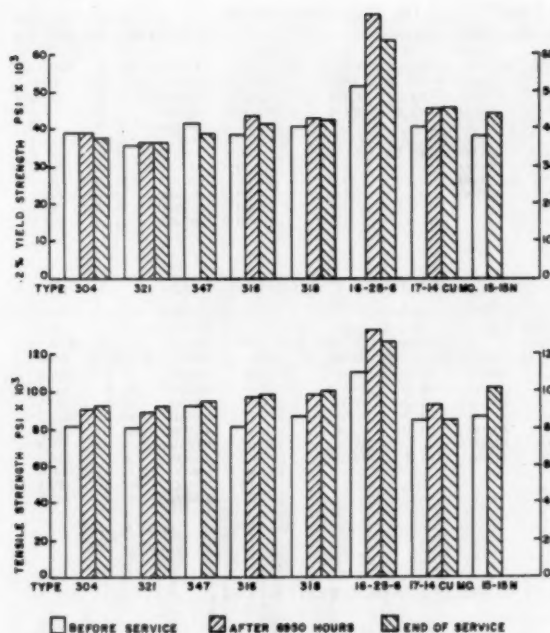


FIG. 6 ROOM-TEMPERATURE YIELD AND TENSILE STRENGTHS OF TUBE MATERIALS BEFORE AND AFTER SERVICE

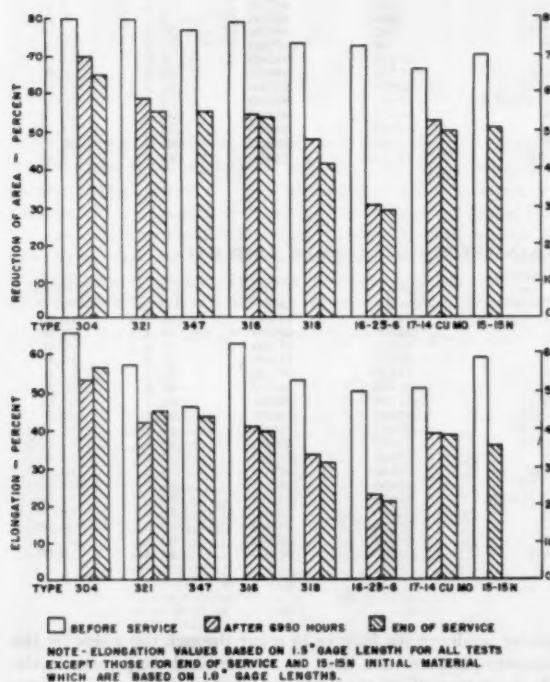


FIG. 7 ROOM-TEMPERATURE DUCTILITY VALUES FOR TUBE MATERIALS BEFORE AND AFTER SERVICE

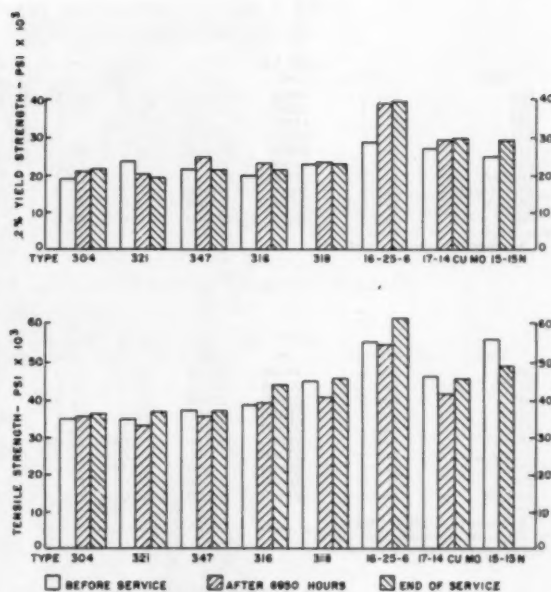


FIG. 8 YIELD AND TENSILE STRENGTHS OF TUBE MATERIALS AT 1350 F BEFORE AND AFTER SERVICE

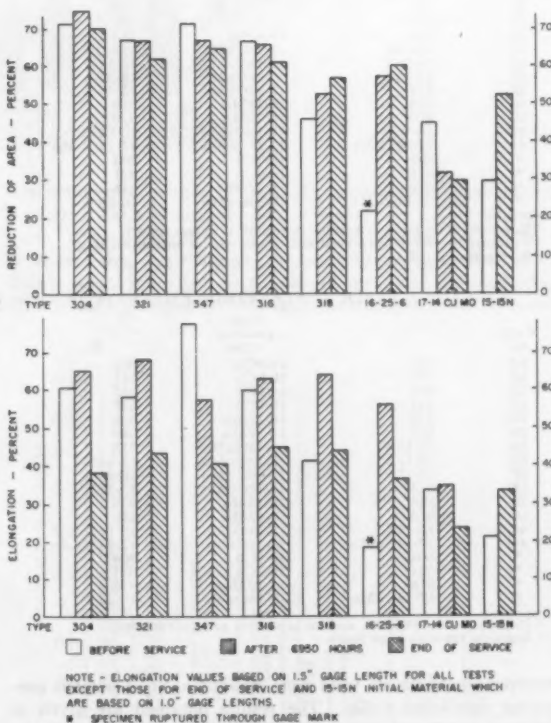


FIG. 9 DUCTILITY VALUES FOR TUBE MATERIALS AT 1350 F BEFORE AND AFTER SERVICE

TABLE 4 ROOM-TEMPERATURE TENSILE PROPERTIES OF TUBE MATERIALS

Alloy	Location	Before service				After 6950 hr service				At end of service <sup>a</sup>			
		0.2% YS, psi	UTS, psi	% Elong. in 1.5 in.	% Red. of area	0.2% YS, psi	UTS, psi	% Elong. in 1.5 in.	% Red. of area	0.2% YS, psi	UTS, psi	% Elong. in 1.0 in.	% Red. of area
304	Leg 3	39000	82000	66.0	80.0	39200	90900	53.3	69.2	37900	92500	56.5	64.9
321	Leg 4	35900	80100	37.3	79.2	36300	80000	42.0	38.4	36500	92200	45.5	55.1
347	Leg 5	41800	91800	46.0	76.8	...	...	...	...	38350	94150	43.5	55.2
321	Leg 5	34750	80600	64.5	76.0	...	...	...	...	33350	84150	50.0	65.3
316	Leg 6	38900	80600	63.3	79.1	43200	96700	40.7	54.2	41750	98750	39.5	53.8
318	Leg 7	41000	86300	52.6	73.7	43100	99600	33.3	48.0	42350	100450	31.5	41.2
16-25-6	Leg 7	51300	109100	50.0	72.5	70600	132000	22.7	30.7	63700	126400	21.0	28.9
17-14CuMo	Leg 8	40900	84900	50.7	66.3	45800	92500	39.3	52.5	45950	95400	38.5	49.3
15-15N	Leg 8	38200	87300	59.0	70.1	...	...	...	...	44500	102350	36.0	50.6
304	Leg 6	39000	82000	66.0	80.0	...	...	...	...	39050	95400	46.5	52.0

<sup>a</sup> Average of duplicate tests.

TABLE 5 ELEVATED-TEMPERATURE (1350 F) TENSILE PROPERTIES OF TUBE MATERIALS

Alloy	Location	Before service				After 6950 hr service				At end of service <sup>a</sup>			
		0.2% YS, psi	UTS, psi	% Elong. in 1.5 in.	% Red. of area	0.2% YS, psi	UTS, psi	% Elong. in 1.5 in.	% Red. of area	0.2% YS, psi	UTS, psi	% Elong. in 1.0 in.	% Red. of area
304	Leg 3	19600	35500	60.0	71.5	21200	35900	64.7	75.2	21850	38100	38.0	69.9
321	Leg 4	23900	34900	58.0	67.1	20100	33100	68.0	66.9	19750	36750	43.0	61.8
347	Leg 5	21800	37600	78.0	72.9	25200	35700	57.3	67.0	21450	38750	40.5	64.5
316	Leg 6	19400	38300	60.0	67.1	23000	38700	62.7	66.0	21450	43950	45.0	61.2
318	Leg 7	22800	45100	40.7	45.8	23600	40200	64.0	52.4	25500	45500	44.0	56.8
16-25-6	Leg 7	28600	55100	18.0 <sup>b</sup>	22.0 <sup>b</sup>	38900	54500	56.0	57.6	39700	61750	30.0	60.8
17-14CuMo	Leg 8	27400	46000	33.3	45.4	29300	41400	34.7	32.0	29650	45500	23.5	30.1
321	Leg 5	22900	36100	55.5 <sup>c</sup>	54.0	...	...	...	...	19300	35950	39.5	53.3
304	Leg 6	19600	35500	60.0	71.5	...	...	...	...	17300	36450	43.5	60.1
15-15N	Leg 8	24800	56000	21.0 <sup>c</sup>	26.2	...	...	...	...	29550	48350	33.5	52.8

<sup>a</sup> Average of duplicate tests.<sup>b</sup> Ruptured through gage mark.<sup>c</sup> Per cent elongation in 1.0 in.

TABLE 6 ROOM-TEMPERATURE TRANSVERSE-WELD TENSILE TEST DATA

Weld no.	A	Com- position weld	B	Location of failure	0.2% YS, psi	UTS, psi	% Red. of area	% Elong. in 1.0 in.
14	347	19-9Cb	304	304	47300	92600	76.0	33.0
15	321	19-9Cb	347	321	45000	95600	41.7	26.0
23	347	19-9Cb	347	Weld	51700	97300	23.9	23.0
24	321	19-9Cb	347	321	47500	90400	63.9	29.0
25	316	18-12Mo	321	Weld	47000	86400	16.6	14.0
29	316	18-12Mo	316	Weld	48700	68700	9.2	5.0
34	15-15N	17-14CuMo	318	Weld	52400	86700	3.7	5.0
35	15-15N	17-14CuMo	15-15N	Weld	52700	97000	3.7	8.0
37	15-15N	17-14CuMo	16-25-6	15-15N	55000	99400	22.7	14.0
38	318	17-14CuMo	15-15N	318	52700	103200	23.1	14.0
39	316	18-12Mo	318	Weld	48800	96700	9.0	13.0
40	316	18-12Mo	316	Weld	47700	98800	20.2	28.0
42	15-15N	17-14CuMo	15-15N	15-15N	50800	95500	21.8	11.0
44	17-14CuMo	17-14CuMo	17-14CuMo	17-14CuMo	47600	84400	15.2	10.0
*	304	19-9Cb	304	304	45000	93600	68.6	40.0 <sup>b</sup>
*	321	19-9Cb	321	321	39700	91200	58.2	31.3 <sup>b</sup>
*	318	18-12Mo	318	318	47100	99600	48.6	27.3 <sup>b</sup>
*	17-14CuMo	17-14CuMo	16-25-6	Weld <sup>a</sup>	41700	74400	32.8	9.3 <sup>b</sup>

<sup>a</sup> Reported after 6950 hr service in second progress report.<sup>b</sup> Fracture in 17-14CuMo weld metal induced by entrapped slag.<sup>c</sup> Elongation in 1.5 in.

TABLE 7 ELEVATED-TEMPERATURE (1350 F) TRANSVERSE-WELD TENSILE TEST DATA

Weld no.	A	Com- position weld	B	Location of failure	0.2% YS, psi	UTS, psi	% Red. of area	% Elong. in 1.0 in.
14	347	19-9Cb	304	304	29100	41600	51.3	16.0
15	321	19-9Cb	347	321	25500	40000	29.4	22.0
23	347	19-9Cb	347	347	29500	41100	55.4	19.0
24	321	19-9Cb	347	321	27000	41400	27.5	19.0
25	316	18-12Mo	321	321	24600	40200	32.5	12.0
29	316	18-12Mo	316	316	28100	44700	47.6	20.0
34	15-15N	17-14CuMo	318	318	31700	48700	52.7	20.0
35	15-15N	17-14CuMo	15-15N	15-15N	33900	48000	52.4	22.0
37	15-15N	17-14CuMo	16-25-6	15-15N	37000	51800	49.1	15.0
38	318	17-14CuMo	15-15N	15-15N	31000	49400	30.7	11.0
39	316	18-12Mo	318	318	31300	49200	17.7	14.0
40	316	18-12Mo	316	Weld	25700	47200	15.6	16.0
42	15-15N	17-14CuMo	15-15N	15-15N	33400	48200	51.9	22.0
44	17-14CuMo	17-14CuMo	17-14CuMo	17-14CuMo	31600	44100	20.6	11.0
*	304	19-9Cb	304	304	25200	38900	70.2	18.7 <sup>a</sup>
*	321	19-9Cb	321	321	21700	34600	60.0	29.3 <sup>a</sup>
*	318	18-12Mo	318	318	25600	42000	60.4	37.3
*	17-14CuMo	17-14CuMo	16-25-6	Weld	26200	36400	40.4	8.0 <sup>a</sup>

<sup>a</sup> Reported after 6950 hr. service in second progress report.<sup>b</sup> Rupture through gage mark.

transverse-weld tensile tests were conducted on specimens containing significant welds. The results obtained are given in Tables 6 and 7, and Figs. 10 and 11 show the broken specimens, thus illustrating the relative location of failures with respect to weld metals and base materials as well as qualitatively illustrating the relative ductility of the various components. There was a

greater tendency for failures to occur through the welds for the room-temperature tests than for the elevated-temperature tests. These results indicate that there is a greater change in properties for weld metals than for tube materials after long-time elevated-temperature service.

*Charpy Impact Tests at Room Temperature and 1350 F.* An

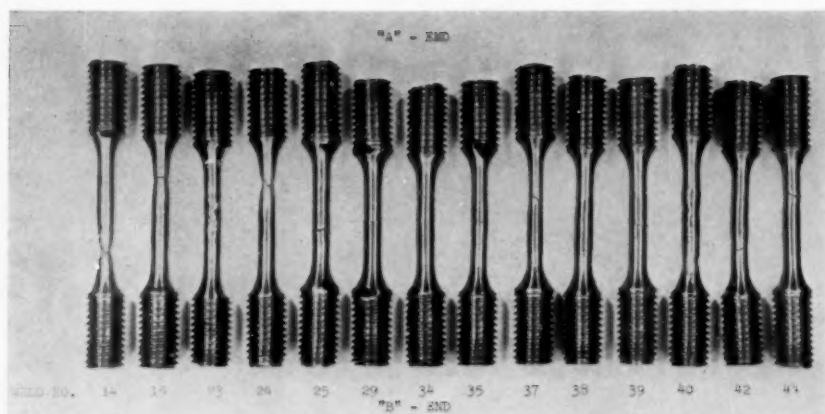


FIG. 10 APPEARANCE OF ROOM-TEMPERATURE WELD TENSILE TEST SPECIMENS AFTER RUPTURE

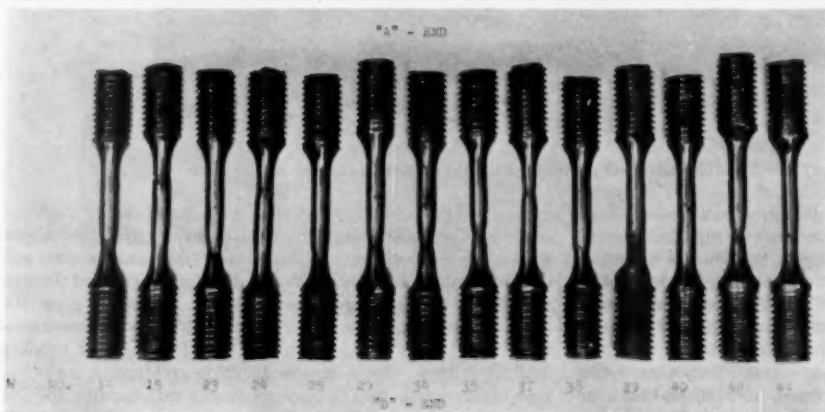


FIG. 11 APPEARANCE OF ELEVATED TEMPERATURE (1350 F) WELD TENSILE TEST SPECIMENS AFTER RUPTURE

important type of deterioration that frequently occurs at elevated temperatures is embrittlement resulting from certain structural phase changes. Such changes, causing a decrease in shock resistance, are particularly evident for alloys, such as Types 321, 318, 347, Armeo 17-14CuMo, and Timken 16-25-6, known to form sigma phase or other brittle constituents as well as for many types of weld deposits. The test results for the tube materials are presented in Table 8 and the room-temperature results are

TABLE 8 CHARPY IMPACT PROPERTIES OF TUBE MATERIALS

Alloy	Service	Location	Ft-Lb room temperature		Ft-Lb 1350 F	
			Full size	Half- width	Full size	Half- width
304	Before service	...	94	56	...	...
304	After 6950 hr	Leg 3	...	25	...	...
304	After 14281 hr	Leg 3	47	...	49	...
304	After 7323 hr	Leg 6	28.5	...	42	...
321	Before service	...	92	52	...	...
321	After 6950 hr	Leg 5	25	15	...	...
321	After 14281 hr	Leg 4	25	...	34	...
321	Before service	...	79	...	51	...
321	After 7323 hr	Leg 5	42	...	48	...
347	Before service	...	...	42	...	...
347	After 6950 hr	Leg 4	...	19	...	...
347	After 14281 hr	Leg 5	...	18	...	21
316	Before service	...	88.5	49	...	...
316	After 6950 hr	Leg 6	...	18	...	...
316	After 14281 hr	Leg 6	28	...	48.5	...
318	Before service	...	85.5	43.5	...	...
318	After 6950 hr	Leg 7	...	9.0	...	...
318	After 14281 hr	Leg 7	14.5	...	25	...
16-25-6	Before service	...	...	35	...	...
16-25-6	After 6950 hr	Leg 7	...	6	...	...
16-25-6	After 14281 hr	Leg 7	...	4	...	8
17-14CuMo	Before service	...	...	25	...	...
17-14CuMo	After 6950 hr	Leg 8	...	13	...	...
17-14CuMo	After 14281 hr	Leg 8	...	11	...	11
15-15N	Before service	...	...	31.5	...	20.0
15-15N	After 7323 hr	Leg 8	...	10.5	...	12.5

compared graphically in Fig. 12. It appears, from these results, that there was a considerable loss of impact strength for all materials. However, most of this loss occurred during the first 6950 hr of exposure, and there was relatively little change thereafter. This is encouraging because the results previously obtained after 6950 hr indicated possible serious embrittlement if the observed

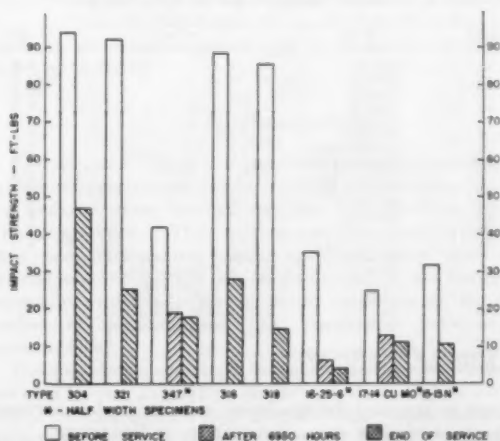


FIG. 12 ROOM-TEMPERATURE CHARPY IMPACT VALUES FOR TUBE MATERIALS BEFORE AND AFTER SERVICE

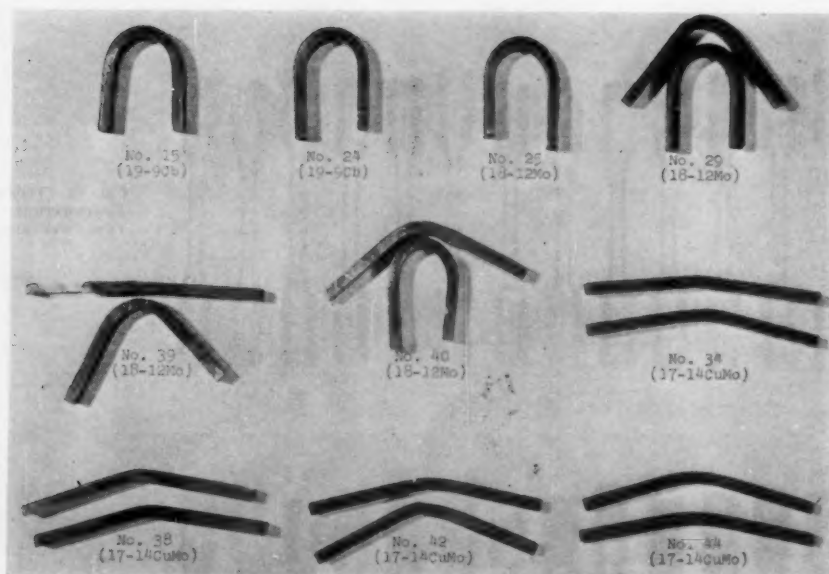


FIG. 13 TYPICAL EXAMPLES OF WELD SIDE-BEND TEST SPECIMENS

rates of decrease were continued. However, in all cases, there appears to be adequate shock resistance left for superheater service with the possible exception of Timken 16-25-6. In addition, it is further encouraging to note that all materials had as good as or better impact resistance at 1350 F than at room temperature.

The Charpy impact tests on the weldments are actually tests of the weld metal rather than of the complete weldment, since the keyhole notch was located in the weld metal. Only three types of welds were present—those made with 19-9Cb, 18-12Mo, or 17-14CuMo electrodes. The results are given in Table 9 and indicate marked embrittlement, particularly for the 17-14CuMo weld metal. However, an improved 17-14CuMo electrode is now reported to be commercially available. Again, it was noted in all cases that tests conducted at 1350 F gave somewhat higher results than those at room temperature. One should be cautioned when comparing the impact values to note that half-width

more important consideration than impact resistance, duplicate side-bend tests were conducted on samples cut from the various weldments. These samples were  $\frac{1}{8} \times \frac{1}{4}$  in. cross section and were bent using a tup of  $\frac{3}{8}$  in. diam. Bending was carried through to 180 deg, unless failure occurred earlier. Table 10 gives the data obtained from these tests. The 19-9Cb welds had considerable ductility, and all specimens withstood 180 deg of bending without failure. Tests on the 18-12Mo weldments, however, gave rather erratic results, some specimens withstanding 180 deg of bend while others failed. Duplicate specimens did not necessarily give duplicate results. These fractures were very coarse. Results from the 17-14CuMo weldments were uniform in that all specimens fractured with relatively little deformation. Fig. 13 shows the appearance of typical specimens after testing.

TABLE 9 CHARPY IMPACT DATA FOR WELD METALS

Weld no.	Weld metal	Ft-Lb <sup>a</sup>	
		room temperature	1350 F
14	19-9Cb	3.8	8.3
15	19-9Cb	6.2	10.8
23	19-9Cb	6.0	10.0
24	19-9Cb	7.4	9.0
25	18-12Mo	5.3	8.1
29	18-12Mo	5.6	6.5
34	17-14CuMo	1.4	3.3
35	17-14CuMo	1.1	2.8
37	17-14CuMo	1.5	2.6
38	17-14CuMo	1.1	2.6
39	18-12Mo	3.3	4.1
40	18-12Mo	5.0	7.4
42	17-14CuMo	0.9	2.4
44	17-14CuMo	0.7	2.5
*	19-9Cb	21.0 (full size)	
*	19-9Cb	8.0 (half-width)	
*	19-9Cb	10.3 (full size)	
*	19-9Cb	4.8 (half-width)	
*	18-12Mo	2.0 (half-width)	
*	17-14CuMo	1.0 (half-width)	

\* Reported after 6950 hr service.

<sup>a</sup> Half-width specimens.

as well as standard-size specimens were used when necessary, owing to restrictions of material quantity or dimensions.

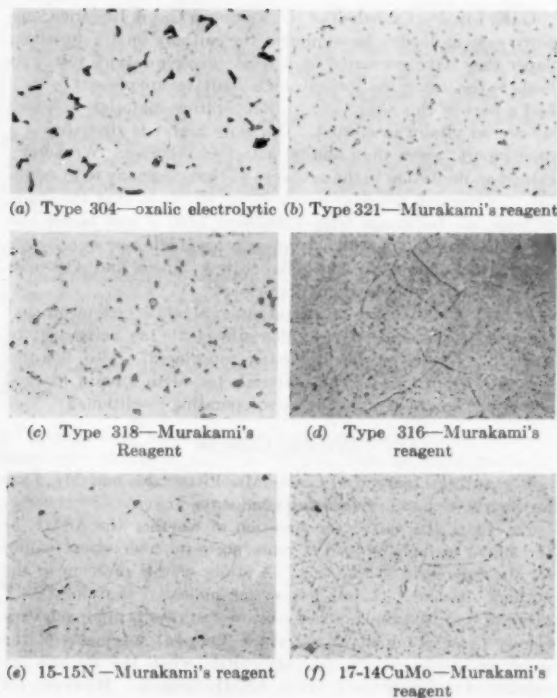
**Side-Bend Tests.** To evaluate further the effects of elevated temperature upon the ductility of these materials, which may be a

TABLE 10 SIDE-BEND TEST RESULTS

Weld no.	Weld metal	Bend angle	
		#1	#2
14	19-9Cb	180	180
15	19-9Cb	180	180
23	19-9Cb	180	180
24	19-9Cb	180	180
25	18-12Mo	180	180
29	18-12Mo	80	180
34	17-14CuMo	8	24
35	17-14CuMo	47	43
37	17-14CuMo	27	28
38	17-14CuMo	23	26
39	18-12Mo	108	0
40	18-12Mo	180	62
42	17-14CuMo	43	26
44	17-14CuMo	37	24

#### MICROSTRUCTURAL OBSERVATIONS

The changes in mechanical properties are due to changes in the internal structure of the various materials at elevated temperatures over long periods of time. Such changes were anticipated, and the important consideration was the extent of such changes and their effect upon the mechanical properties. Sigma phase became quite prevalent in the stabilized alloys 318, 321, and 347, but the microstructures showed rather insignificant changes since being observed after 6950 hr of service. This sigma is distributed as discontinuous particles in a grain-boundary pattern. In addition, Type 318 had a considerable amount of a fine matrix pre-

FIG. 14 TYPICAL TUBE METAL MICROSTRUCTURES.  $\times 500$ 

cipitate. The unstabilized alloys 304 and 316 showed grain-boundary carbide precipitation, while Type 316 also displayed a fine matrix precipitate. Sigma was also observed rather extensively in the 304 material. It was present quite uniformly in the section exposed in Leg 6 for 7323 hr; but, for the section exposed in Leg 3 for 14,281 hr, the sigma distribution was most pronounced in the metal taken from the fireside of the tube and here also increased in amount from the inside to the outside. Such an occurrence was not reported after 6950 hr of service in Leg 3.

The more complex alloys, 15-15N, Armco 17-14CuMo, and Timken 16-25-6, showed extensive general and grain-boundary carbide precipitation, and the 17-14CuMo had a few scattered sigma particles as well. Typical microstructures are shown in Fig. 14.

Notable amounts of sigma were observed in the various weld deposits. Such occurrences were rather discontinuous for the 19-9Cb materials, but the 18-12Mo welds frequently had very large grain sizes, with a rather continuous sigma precipitation along the boundaries. The structure within these grains was quite varied, apparently depending upon local composition variations, usually containing a fairly random matrix precipitate or sigma particles. The 17-14CuMo weld metal frequently contained discontinuous sigma particles in a general grain-boundary pattern, as well as a fine uniform Widmanstätten pattern. Typical weld-metal microstructures are shown in Fig. 15. There was no evidence of stress oxidation at the tube-weld metal interfaces. Frequently, the transition zone had an enlarged grain size and less grain-boundary precipitate such as illustrated in Fig. 15(d) for the 321/19-9Cb boundary of weld No. 15.

#### CONCLUSIONS

The results obtained from the final examination of the various alloys exposed in the Twin Branch probe indicate that no serious

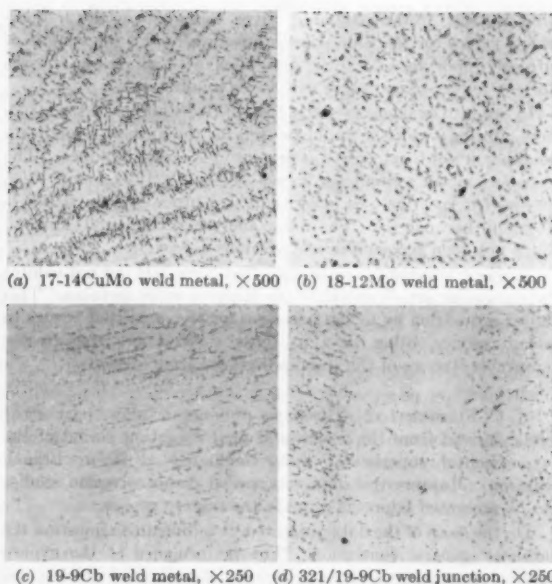


FIG. 15 TYPICAL WELD MICROSTRUCTURES. MURAKAMI'S REAGENT

deterioration of the essential properties has occurred in this pulverized-coal-fired unit. The property most notably affected was impact strength but, with the possible exception of Timken 16-25-6 there appears to be adequate shock resistance remaining for superheater service, particularly at elevated temperatures. Changes in properties were most rapid during the first 6950 hr of service followed by a lower rate of change thereafter. The various weld deposits, particularly Armco 17-14CuMo, had quite low-impact resistance after service. The desirability for an electrode which will deposit weld metal of a greater retained impact toughness is evident.

The oxidation resistance of all alloys appears to be adequate for the service for which they were employed. The investigation also revealed that the nonstabilized alloys 304 and 316 suffered no intergranular attack.

The performance of the experimental superheater and the behavior of the alloys of which it was constructed indicate that materials are available for use in superheaters for high-pressure steam up to 1250 F.

## Discussion

C. L. CLARK,<sup>6</sup> Those concerned with the application of metals in high-temperature service are indebted to the authors for making available these results from their extended-time tests on tubular specimens. Their findings are of particular value since they were obtained on tubular specimens under more commercial conditions than can be duplicated in the laboratory, especially with respect to the steam conditions on the inner surface of the tubes, and the combustion gases on the outer surface.

The fiber stresses existing in the tube wall, Table 1 of the paper, are seen to vary as much as 50 per cent, depending on the particular formula used for their determination. Have the authors undertaken any work to determine which of these two formulas,

<sup>6</sup> Metallurgical Engineer, Special Steel Developments, Steel and Tube Division, The Timken Roller Bearing Company, Canton, Ohio.

that is, the ASME or Lamé, gives the more accurate fiber-stress values for the tube sizes in question? This question is of utmost importance to those concerned with allowable stresses for the higher-temperature and stress conditions.

In order to evaluate properly the relative stability of the structures during service it would be well for the authors to indicate whether or not free ferrite was present in the original tubes. The reported nickel content for Types 347 and 321, 11.1 and 10.36 per cent, respectively, is lower than that often used for seamless tubes of this analysis. The actual analyses of Types 304 and 316 have not been reported in the previous papers.

It was gratifying for us to note that Type 304 did not exhibit intergranular attack on either the inner or outer surfaces. This raises a question as to the necessity for the stabilized grades in steam service, other than in those cases where the greater allowable stresses of the stabilized grades are a factor.

R. C. FITZGERALD.<sup>6</sup> This paper presents the major part of the data derived from the fourth and final operating period of the experimental superheater tests conducted at Twin Branch Station. Rupture-test data and special steam-corrosion studies to be presented later will amplify the present report.

On the basis of the data presented, it is difficult to question the authors' general conclusion, "The performance of the experimental superheater and the behavior of the alloys of which it was constructed indicate that materials are available for use in superheaters for high-pressure steam up to 1250 F." It should be remembered, however, that the 14,000-hr duration of this test was in the order of 1/10 to 1/20 the expected service life of present installations. It would have been desirable (had it been possible in the operating schedule of the test boiler) to continue the testing if only better to establish a realistic life expectancy for materials in this temperature range.

It appears from the data that life expectancy will be a function of corrosion rate and probably the corrosion rate in steam. It appears also that in the test environment of this boiler, at least, external corrosion is not important. The steam-side corrosion rates are not excessive on a mile per year basis. However, as reported by the authors the determination of these rates by scale thickness or diameter measurements is fraught with peril. Evaluation of the cylindrical steam-corrosion specimens probably will provide more accurate corrosion rates than those determined on the walls of the tube samples themselves. Oxide penetration at internal surface defects certainly warrants serious consideration. If accelerated corrosion may be expected at such points, the additional expense of elimination of such defects might well be justified. It is believed that a program of quantitative evaluation of internal seams from a corrosion standpoint and means of their detection and elimination would be valuable at this time.

It seems much easier to interpret the results of the bend test in terms of practical ductility than the notched-bar impact results. In terms of actual energy absorbed all the impact test values are low. However, the bend-test results demonstrate that adequate ductility remains in the 19-9 Cb deposit but not in the other welds.

The authors of this paper and the co-operating companies deserve the sincere thanks of all industry for this valuable contribution to the knowledge of the behavior of materials at high temperatures.

<sup>6</sup> Senior Engineer, Power Production Stations, Baltimore Gas & Electric Company, Baltimore, Md. Mem. ASME.

G. E. LIEN.<sup>7</sup> On behalf of the American Gas & Electric Company system I wish to commend the authors on the excellent paper they have presented on a most effective service test. As hosts to the test at the Twin Branch Plant, we are pleased to have had a part in this study of high-temperature materials in which we are so vitally interested. Our only regret is that this is a final report rather than one on a test in progress. We hereby extend an invitation to the authors and their company to re-establish this research program in one of our plants so that the study of materials for steam temperatures at 1250 F and higher can keep ahead of the new higher-temperature, higher-economy commercial installations in which Babcock & Wilcox and American Gas & Electric are playing a major part.

Does lack of evidence of intergranular steam attack mean that the need for stabilized weld deposits is not as necessary for steam-line service as was previously considered? Also, has this test shown any one of the materials tested to have a marked advantage over the others at these operating conditions?

#### AUTHORS' CLOSURE

The authors thank Dr. Clark, Mr. Fitzgerald, and Mr. Lien for their useful and stimulating comments.

Dr. Clark has raised the question of whether the ASME or the Lamé formula gives the more accurate fiber stress values for the tube sizes in question. A study of this problem in the authors' Research Center has so far indicated that for  $OD/T$  ratios of 8 to 10, tubular stress-rupture test results approach very closely those obtained on bar stock (coupon) specimens of the same materials—ferritic and austenitic—when the stresses are calculated by either the Lamé or ASME formula. However, for heavy wall tubular specimens with  $OD/T$  ratios of 4 and 5, the results obtained on the tubular specimens are close to those of the coupon specimens when the stress is calculated by Lamé, but are significantly lower when the stress is calculated by the ASME formula.

With respect to the second question raised by Dr. Clark, i.e. as to whether free ferrite was present in the original tubes, no free ferrite has been metallographically observed. The chemistries of the various alloys employed have been reported in the first paper presented at the 1951 Annual Meeting of the Society and published in the July, 1952, issue of the ASME TRANSACTIONS, but the authors agree with Dr. Clark that it would be desirable to have them repeated in this final presentation. They are as follows:

	Alloy	C	Mn	Si	Cr	Ni	Mo	Other Elements
	Type 304	0.066	1.61	0.35	18.86	10.18	...	...
	Type 347	0.064	1.55	0.39	17.68	12.42	...	0.80Cb
	Type 321	0.050	1.78	0.60	18.07	12.22	...	0.48Ti
	Type 316	0.077	1.66	0.45	16.32	13.42	2.36	...
	Type 318	0.07	1.62	0.51	17.17	14.96	2.03	0.72Cb
	16-25-6	0.075	1.64	0.45	16.18	26.42	6.40	0.167N
	17-14CuMo	0.11	0.99	0.45	15.50	13.48	2.18	3.15Cu, 0.45Cb, 0.30Ti
	15-15N	0.10	1.25	0.60	15.5	14.5	1.5	1.5W, 0.9CbTa

The authors admit that the nickel content in the Type 304 alloy is on the low side, especially when considering that the chromium is relatively high. This may account for the occurrence of sigma in this tubing after long-time service. In this connection, the authors wish to point out again that the tubing used in the test element was randomly picked from the mill stock pile, principally from the viewpoint of finding suitable wall thicknesses to meet the design requirements. The nickel contents quoted by Dr. Clark for the Type 321 and 347 tubing are in error.

The authors are of the opinion that the service behavior of these alloys is more significantly influenced by the mechanical

<sup>7</sup> Senior Engineer, Piping and Metallurgy Section, Mechanical Engineering Division, American Gas & Electric Service Corporation, New York, N. Y. Mem. ASME.

and thermal history of the materials than by variations in chemistry within specification limits.

The absence of intergranular corrosion in the nonstabilized grades Types 304 and 316 at the termination of the test is evidence that these nonstabilized grades are suitable for steam service. These alloys had been purposely employed in order to demonstrate this.

The authors agree with Mr. Fitzgerald that it would have been desirable to extend the test beyond 15,000 hours, but this was not practicable. However, the test duration was long enough to obtain a realistic indication of the response of the chosen materials to actual service conditions.

The authors wish to caution that the good external corrosion behavior of the alloys in the test boiler should not be taken as an indication that these materials would be similarly resistant to the corrosion products of other types of coal. Resistance to steam attack at the given temperatures, however, appears to be satisfactory.

The authors agree with Mr. Fitzgerald that the potential hazard presented by surface seams in tubing should not be underestimated. However, since no deterioration or harm resulted from the presence of "conventional" surface seams in these tubes in over 15,000 hours of actual service under the aggravating con-

ditions of sootblowing, such unavoidable seams should not be looked upon with alarm.

Mr. Lien and the American Gas & Electric Company deserve special thanks for their generous support of this long drawn-out experiment. Mr. Lien's question as to whether the observed absence of intergranular steam attack indicates that stabilized weld deposits are not necessary for steam-line service must be answered in the affirmative. The authors have conducted another superheater field test with nonstabilized Type 304 and have there likewise found no evidence of intergranular attack by high-temperature steam.

The second question raised by Mr. Lien, as to whether any one of the materials tested has a marked advantage over the others at the given operating conditions, does not permit a simple answer. The stabilized Grades 321 and 347 are generally looked upon as interchangeable as far as high-temperature service is concerned. No broad field experience is available on the nonstabilized Grades 304 and 316, but they may possibly prove to be preferable to the stabilized grades, especially at metal temperatures of 1300 F and higher. Strengthwise, the superalloys are definitely superior to the standard grades. The potential service performance of all these alloys is significantly influenced by the manufacturing and fabrication conditions imposed upon them prior to service.



# High-Temperature Corrosion of Alloys Exposed in the Superheater of an Oil-Fired Boiler

By D. W. McDOWELL, JR.,<sup>1</sup> R. J. RAUDEBAUGH,<sup>2</sup> AND W. E. SOMERS<sup>3</sup>

A series of heat-resistant alloy test racks containing some 30-odd test specimens was installed in the gas inlet of the second bank of the superheater in a Public Service Electric and Gas Company boiler. This boiler had been burning bunker C fuel oil for the three-year period before the test and used bunker C during the entire test period. Gas temperatures varied from 1560 F at full load to 1100 F at minimum load. The loading on the boiler during the investigation was considered typical of steam-boiler operation. Scale taken from the build-up on the test specimens analyzed as high as 36 per cent vanadium pentoxide and 32 per cent sulphuric anhydride. An analysis of the ash constituents present in the oil-fired boiler during the tests also showed high vanadium, sulphur, sodium, and calcium contents. All corrosion rates were measured by metallographic examination and were expressed as inches penetration for the duration of the test and extrapolated to inches per year (IPY). Corrosion results were obtained on both cast and wrought alloys as well as some alloys with various coatings. An extensive metallographic investigation was conducted on all alloys exposed to determine the type of attack each material underwent during the exposure period. Some alloys had a corrosion rate as much as ten times greater than others.

## INTRODUCTION

A PROGRAM which assists in the determination of which heat-resistant alloys perform most satisfactorily in various high-temperature corrosive environments has been conducted for the past several years by the Stainless Steel and Heat Resistant Alloys Section of the Development and Research Division, International Nickel Company, Inc. This information has been accumulated by the installation of heat-resistant test racks containing a wide variety of test specimens in actual industrial environments where information is desired and needed. By testing materials in the actual service environment, much more realistic information is obtained than by conducting similar tests in the laboratory. After a suitable exposure time, the

racks are removed from the high-temperature environment and each test specimen is sectioned and examined under the microscope to determine the type and extent of attack. For comparative purposes, these results are extrapolated to inches penetration of attack per year (IPY) for each alloy. Results of such tests materially aid in the selection of materials which are most suitable for a given industrial high-temperature environment.

In co-operation with the Public Service Electric and Gas Company, Newark, N. J., a high-temperature alloy investigation was instigated by exposing a series of test racks in the superheater of an oil-fired boiler using bunker C fuel oil. The presence of large percentages of sulphur, vanadium, sodium, calcium, etc., in this bunker C oil led to the belief that such an environment would show high deterioration rates for all alloys that were exposed.

This assumption proved to be true. Nevertheless, it is of importance, from the economics point of view, to have a basis for judgment as to how much longer certain alloys would last than others. In other words, the investigation would ascertain whether the exploitation of certain of the studied alloys, in preference to the others, would be justified on the basis of economic considerations and their length of service.

## PROCEDURE

The boiler selected for the installation of the three racks is a Babcock & Wilcox Company radiant-type boiler, designed for a full-load steam output of 550,000 lb per hr at 1350 psi, and 950 F at the superheater outlet with either pulverized coal or oil firing. This boiler, No. 52, Marion Generating Station, Jersey City, N. J., went into service in 1941, and had been fired with bunker C oil since April, 1952.

All three test racks were supported from a hook clamped to one of the first-row tubes of the second bank of the high-temperature superheater about 3 ft from boiler side wall in such a manner that they hung clear of the superheater tubes in the cavity on the furnace side of the bank. Because of this method of support, the specimens may be said to have been at the gas temperature.

Bare thermocouples were used to measure the gas temperature adjacent to the racks in the cavity in which they were suspended. It was determined that this temperature reached 1560 F at full boiler load, was 1220 F at half load, and ranged from 1050 F to 1100 F at the minimum loads at which the boiler was operated during the tests. The boiler was operated in the normal manner during the tests; that is, it was run at a full load or close to full load during the day for five days a week, and at half load and lower during the early morning hours and during week ends. Table 1 indicates the boiler load during the test period for each test rack.

Samples were taken of deposits on the racks. A typical analysis of these deposits is shown in Table 2, as is a partial analysis of the ash in the bunker C oil fired during these tests.

Heat-resistant alloy test rack No. 50 with eight test specimens was installed on April 15, 1954. This rack, shown in Fig. 1, supported 1-in.  $\times$  1/4-in.  $\times$  4-in. test specimens by means of 1/4-

<sup>1</sup> Metallurgist, Stainless Steel and Heat Resistant Alloy Section, Development and Research Division, The International Nickel Company, Inc., New York, N. Y.

<sup>2</sup> In charge of Iron Alloy Section, Bayonne Research Laboratories, Development and Research Division, The International Nickel Company, Inc., Bayonne, N. J.

<sup>3</sup> Engineer, Electric Engineering Department, Public Service Electric and Gas Company, Newark, N. J. Assoc. Mem. ASME.

Contributed by the Research Committee on High-Temperature Steam Generation and presented at a joint session of the Research Committee on High-Temperature Steam Generation and Power Division, at the Diamond Jubilee Annual Meeting, Chicago, Ill., November 13-18, 1955, of THE AMERICAN SOCIETY OF MECHANICAL ENGINEERS.

NOTE: Statements and opinions advanced in papers are to be understood as individual expressions of their authors and not those of the Society. Manuscript received at ASME Headquarters, October 5, 1955. Paper No. 55-A-203.

TABLE 1 TEMPERATURE VERSUS LOADING ON BOILER NO. 52 MARION GENERATING STATION, PUBLIC SERVICE ELECTRIC AND GAS COMPANY, JERSEY CITY, N. J., DURING PERIOD OF TEST

Temperature, F.	Steam loading, lb per hr		
	70000-100000 1050-1100	100000-250000 1100-1220	250000-550000 1220-1560
Exposure time, hr:			
1 Test rack No. 50; total exposure, 648 hr	174	40	434
2 Test rack No. 54; total exposure, 504 hr	176	53	275
3 Test Rack No. 65; total exposure, 707 hr	105	326	276
Rack no.	Installation date	Removal date	Exposure, boiler service, hrs
50	April 15, 1954	May 17, 1954	648
54	May 22, 1954	June 14, 1954	504
65	August 28, 1954	September 27, 1954	707

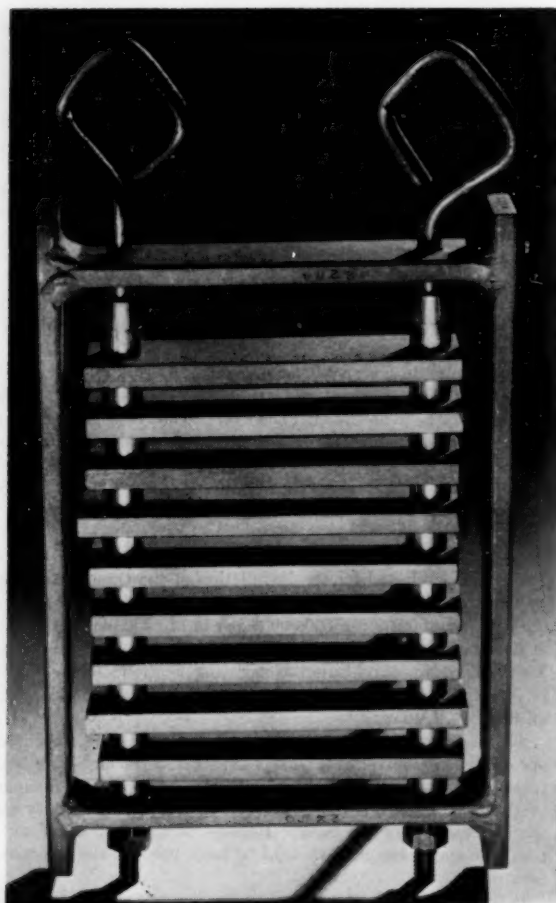


FIG. 1 TEST RACK NO. 50 BEFORE 648 HR EXPOSURE IN THE SUPERHEATER SECTION OF OIL-FIRED BOILER AT PUBLIC SERVICE ELECTRIC AND GAS COMPANY, MARION GENERATING STATION, JERSEY CITY, N. J.

in. rods. The specimens were separated from one another by means of alloy spool spacers.

Rack No. 50 was removed on May 17, 1954, after having been exposed to the flue gases for 648 boiler service hrs. Fig. 2 shows this rack after this exposure. Exposure data for the three racks tested are given in Table 1 and the condition of racks 54 and 65 after exposure are shown in Figs. 3 and 4.

#### RESULTS AND DISCUSSION

Wrought alloys, cast alloys, and cast alloys with various coat-

TABLE 2 ANALYSES OF SCALE AND ASH CONSTITUENTS DURING TESTS

Typical analysis of deposits (scale) taken from test specimens	Typical partial analysis of ash constituents in oil-fired boiler during tests	
	Per cent	
Silica	7.8	
Aluminum oxide	2.0	Sulphur, per cent
Ferric oxide	5.2	Ash, ppm
Vanadium pentoxide	36.37	Sodium, ppm
Sulphuric anhydride	32.89	Magnesium, ppm
Nickel oxide	2.16	Calcium, ppm
Sodium oxide	5.12	Vanadium, ppm
Magnesium oxide	2.35	
Phosphate anhydride	0.50	

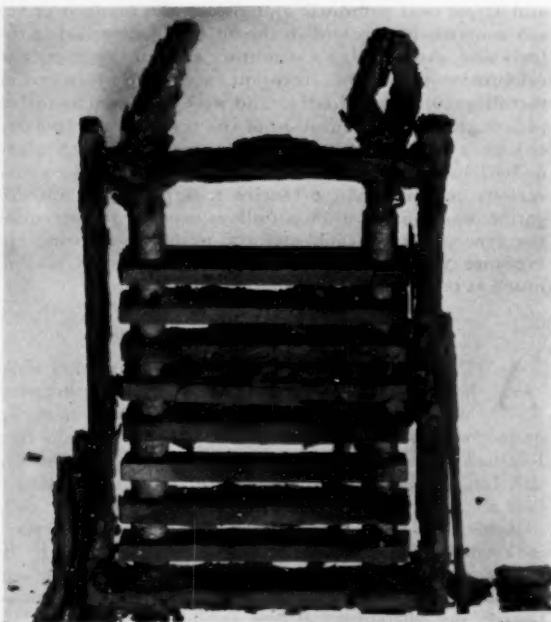


FIG. 2 TEST RACK NO. 50 AFTER 648 HR EXPOSURE IN SUPERHEATER SECTION OF OIL-FIRED BOILER AT MARION GENERATING STATION, PUBLIC SERVICE ELECTRIC AND GAS COMPANY

ings were tested. Before installation into the test rack all specimens were carefully gaged for thickness with micrometers. After exposure, prepared sections were measured under a micrometer microscope in order to record the thickness of unaffected metal remaining and structural discontinuities in the scale.

The maximum deterioration rates of all of the test specimens are expressed in inches penetration at the surface for the duration of exposure and by linear extrapolation for a year's interval. This extrapolated value makes it possible to compare the corrosion rates. These results are given in Table 3. The data from

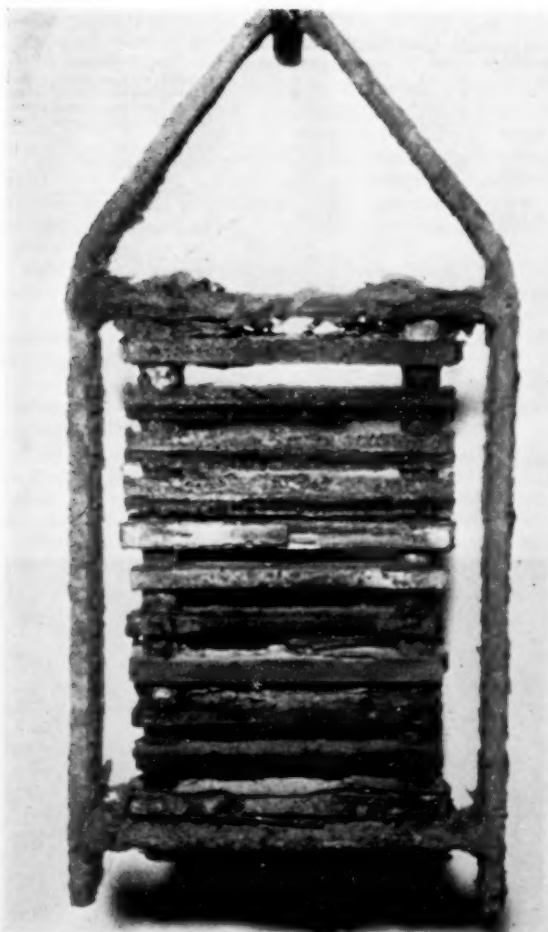


FIG. 3 TEST RACK NO. 54 AFTER 504 HR EXPOSURE IN SUPER-HEATER SECTION OF OIL-FIRED BOILER AT MARION GENERATING STATION, PUBLIC SERVICE ELECTRIC AND GAS COMPANY

this table are arranged in order of the severity of the parent-metal attack with the material suffering the least attack at the top and the severity of corrosion getting progressively greater down the list. It is interesting to note that the four coated samples had rather a fast corrosion attack on the coating; however, the duration of the test was not long enough to allow complete penetration of the coating. What would happen to the parent metal when and if the coatings were penetrated by the attack of the corrosive atmosphere is not known. The reason for putting these coated specimens at the top of the list is merely to show that there was no base-metal attack in this case. It should be pointed out that it was not considered practical to extrapolate the corrosion rates to inches penetration per year for coated specimens. These coated specimens will be discussed in greater detail later.

The test rack was positioned vertically, the samples being in a horizontal position, one above the other. As can be seen from the data given in Table 3 a number of the specimens were thinned more along one edge than the other, with maximum attack occurring along the leading edge relative to gas flow. In those cases where a consistent difference in the degree of attack was observed along opposite edges, two penetration rates are given.

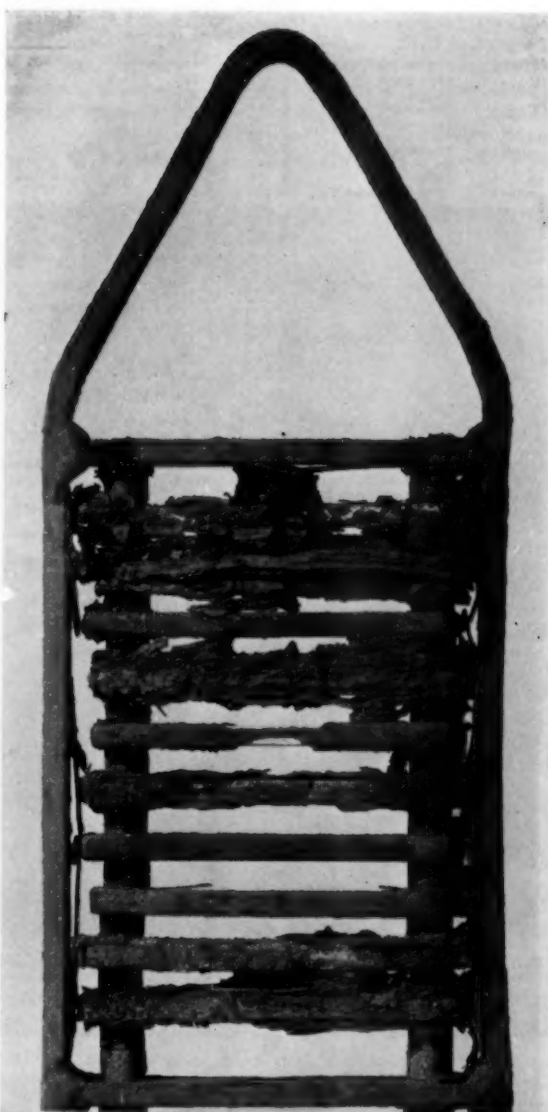


FIG. 4 TEST RACK NO. 65 AFTER 707 HR EXPOSURE IN SUPER-HEATER SECTION OF OIL-FIRED BOILER AT MARION GENERATING STATION, PUBLIC SERVICE ELECTRIC AND GAS COMPANY

#### TEST RACK No. 50

Results of microscopic examination of the various specimens and of the Type 330 rack material and the Type 310 rods used to hold the specimens in the rack are summarized in the following.

*Type 406.* Best base material for resisting corrosive attack; evidently the 3 to 4 per cent Al included in its composition is helpful in this respect. The surface of the material was characterized by broad shallow depressions with no evidence of intergranular attack. As can be seen from Fig. 5, the grain structure is extremely coarse and is characterized by a heavy intergranular carbide network. That these are carbides is evident in Fig. 6, since Murakami's etch has stained them dark.

*Type 446.* The 28 per cent Cr specimen had a surface that

TABLE 3 SUMMARY OF TEST RACKS NOS. 50, 54, AND 65

Material	Composition	Thickness, in.		Metal loss inches penetration <sup>a</sup>			Remarks
		Before exposure	After exposure	per 504 hr	per 648 hr	per 707 hr per year	
HK	25Cr-20Ni	0.262	0.240		0.011 <sup>b</sup>	...	Coated; no base-metal attack
HE	28Cr-10Ni	0.265	0.238		0.0135 <sup>b</sup>	...	Coated; no base-metal attack
HT	15Cr-35Ni	0.269	0.240		0.0145 <sup>b</sup>	...	Coated; no base-metal attack
HF	21Cr-9Ni	0.237	0.227		0.015 <sup>b</sup>	...	Coated; no base-metal attack
406	12Cr-3Al	0.254	0.238			0.108	
Inconel	78Ni-15Cr-7Fe	0.257	0.244	0.007		0.113	Sulphidized to about 0.004 in.
HE	28Cr-10Ni	0.247	0.227		0.014	0.010	Some sulphidation
446	28Cr	0.254	0.226			0.189	
Incoloy	37Ni-20Cr-rest Fe	0.253	0.228	0.013		0.217	Shallow carburization
309	25Cr-12Ni	0.247	0.219-0.212	0.014-0.018		0.244-0.305	
302	18Cr-8Ni	0.253	0.194		0.030	0.406	
HF	21Cr-9Ni	0.250	0.182			0.422	Some sulphidation
430	18Cr	0.248	0.213-0.195	0.018-0.027		0.305-0.426	
502	5Cr	0.255	0.228-0.192	0.014-0.032		0.244-0.557	Some sulphidation
...	5Cr-Mo <sup>c</sup>	0.219	0.173-0.158	0.023-0.030		0.4-0.522	Some sulphidation
...	5Cr-Mo-Si <sup>c</sup>	0.220	0.169-0.153	0.025-0.033		0.435-0.575	Some sulphidation
410	12Cr	0.262	0.181		0.041	0.555	
...	5Cr-Si <sup>c</sup>	0.226	0.173-0.163	0.027-0.032		0.557-0.575	Some sulphidation
HW	12Cr-60Ni	0.268	0.231-0.134			0.230-0.601	Some sulphidation
321	18Cr-10Ni-0.50Ti	0.250	0.148		0.051	0.69	
C steel	Plain carbon	0.253	0.173	0.04		0.095	Excessively coarse surface grains, little if any carbides
T-22	2.25Cr + Mo	0.211	0.103-0.090		0.067	0.054-0.0605	Some sulphidation
431	18Cr-2Ni	0.254	0.120			0.906	
431		0.255	0.198-0.108			0.353-0.930	Very severe attack
431		0.254	0.211-0.132	0.022-0.061		0.374-1.06	

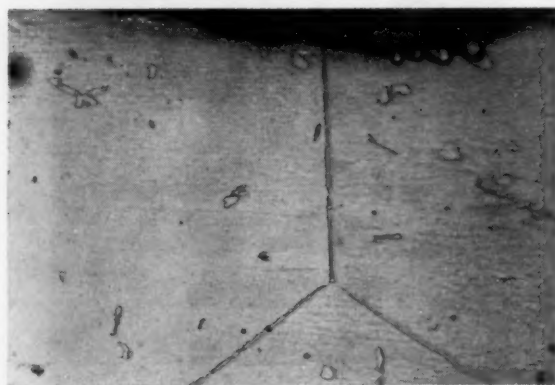
<sup>a</sup> Where differences exist between leading and trailing edges, two values are given.<sup>b</sup> These values represent the attack on the coating.<sup>c</sup> Curved samples cut from boiler-tube stock.

FIG. 5 PORTION OF ONE EDGE OF CROSS SECTION OF TYPE 406 SPECIMEN

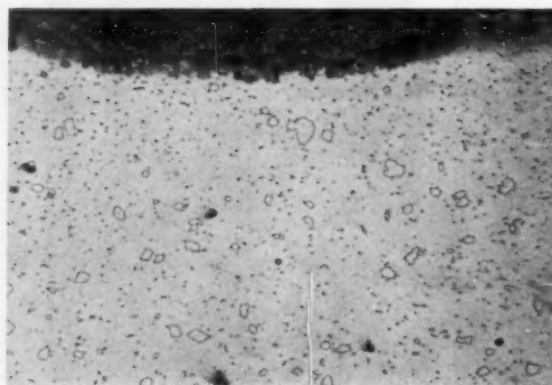
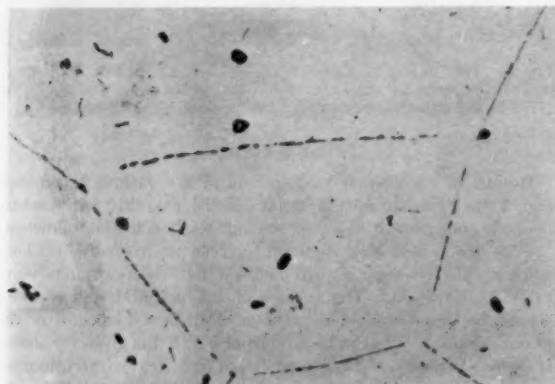
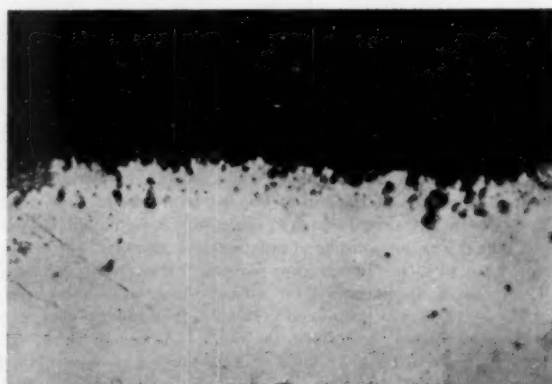
(Heavy grain boundary carbide and coarse grain condition existed throughout the cross section. Glyceregia etch;  $\times 250$ .)

FIG. 7 PORTION OF ONE EDGE OF CROSS SECTION OF TYPE 446 SPECIMEN

(Structure at mid-section similar to that shown in this view. Glyceregia etch;  $\times 250$ .)FIG. 6 TYPE 406 SHOWING CARBIDE NETWORK (Murakami's etch;  $\times 250$ .)FIG. 8 TYPE 446 SHOWING A FEW SMALL GLOBULAR SULPHIDES AT EXPOSED SURFACE (Glyceregia etch;  $\times 500$ .)

was more evenly attacked than that of test specimen Type 406. Here again, there is no evidence of intergranular attack. As can be seen in Fig. 7, the structure is characterized by fine and coarse carbides distributed throughout the matrix. The attack at the surface also included some sulphidation. This attack is shown in Fig. 8.

**Type 302.** The exposed surface of the 18-8 alloy was free from intergranular attack; however, precipitated carbides were present throughout the cross section of this specimen in uniform amounts. There did not seem to be a gradation of this precipitated phase from surface to mid-thickness.

**Type 410.** This 12-Cr alloy was much more heavily corroded than any of the previous types. However, there was still no evidence of intergranular attack. Its structure was characterized by carbides distributed throughout the matrix and with some carburization at the surfaces.

**Type 321.** This stabilized Type 18-8 showed evidence of sulphidation and somewhat spotty carburization. Carbides were present through the grains and at the grain boundaries.

**Type 431.** This alloy was included in each of the test racks. In this test rack it was the most heavily corroded of the 400 series. There is considerable carburization and subsurface structural alteration (compare Figs. 9 and 10). Severe intergranular attack can be noted which caused whole clusters and grains to be corroded away, Fig. 9.

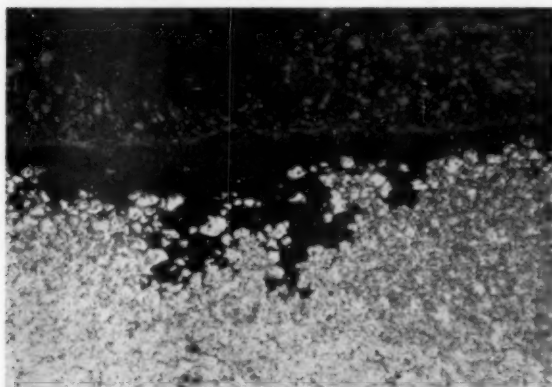


FIG. 9 PORTION OF ONE EDGE OF CROSS SECTION OF TYPE 431 SPECIMEN  
(Carburization and intergranular corrosion revealed. Glyceregia etch;  $\times 250$ .)

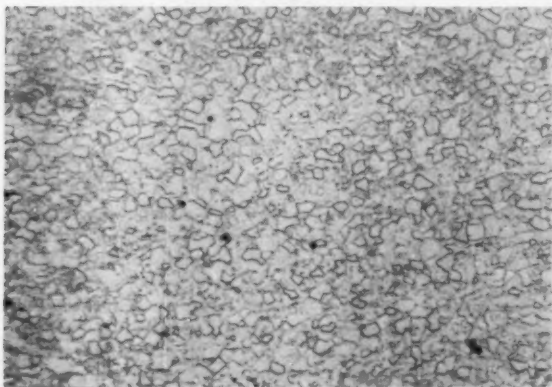


FIG. 10 MID-THICKNESS OF TYPE 431 SPECIMEN  
(Carbide in a two-phase structure of martensite and ferrite. Glyceregia etch;  $\times 250$ .)

The test rack material, Type 330 (15 Cr-35 Ni) and Type 310 rod material (25 Cr-20 Ni) were both sulphidized and slightly carburized. Of these materials, Type 330 was apparently attacked the severest. Fig. 11 is typical of the sulphidation found at the surface of the Type 310 rods. Note the tendency for sulphides to oxidize preferentially. Aside from this sulphide attack Type 310 seemed to perform about like Type 309 soon to be discussed.

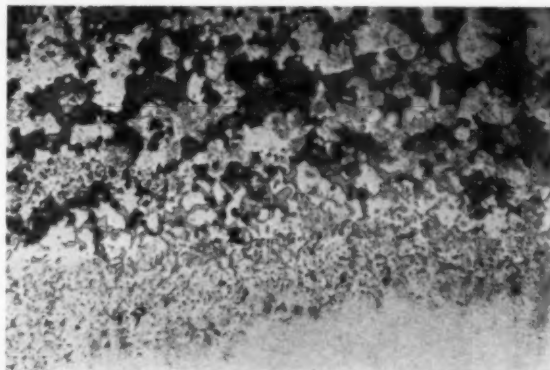


FIG. 11 SULPHIDATION AT SURFACE OF RODS USED TO HOLD SPECIMENS  
(Material is 25 Cr-20 Ni. Etched lightly in glyceregia;  $\times 250$ .)

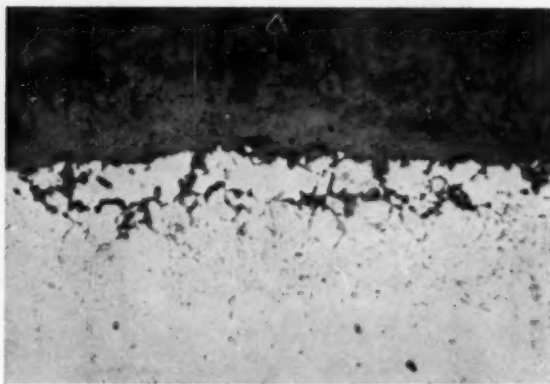


FIG. 12 SULPHIDATION AND OXIDE PENETRATION ON INCONEL  
(Etched lightly in glyceregia;  $\times 250$ .)

#### TEST RACK NO. 54

Results of the microscopic examination of the specimens included in test rack No. 54 and exposed for 504 hr on the same hook in the superheater section of the oil-fired boiler with bunker C oil at the Marion Generating Station are given in the following.

**Inconel.** Inconel showed the lowest rate of penetration with a very uniform attack over the entire specimen. This attack was typified by oxide penetration into a rather heavily sulphidized zone, about 0.004 in. in depth as shown in Fig. 12.

**Incoloy.** The surface of the Incoloy specimen was pitted and, as can be seen from Fig. 13, carburized. This carburization was both intergranular and intragranular in nature. When subjected to Murakami's reagent, this carbide phase was uniformly darkened.

**Type 309.** By comparison with the other alloys exposed, Type 309 is apparently quite good in this service. It is true, however, that the specimen had thinned more along one edge than

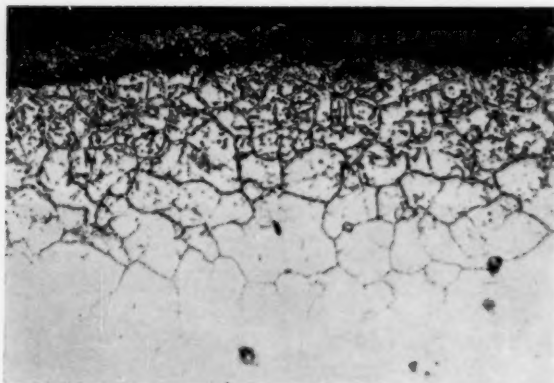


FIG. 13 INCOLOY SHOWING INTERGRANULAR AND SOME INTRA-GRANULAR CARBURIZATION (Glyceric acid etch;  $\times 100$ )

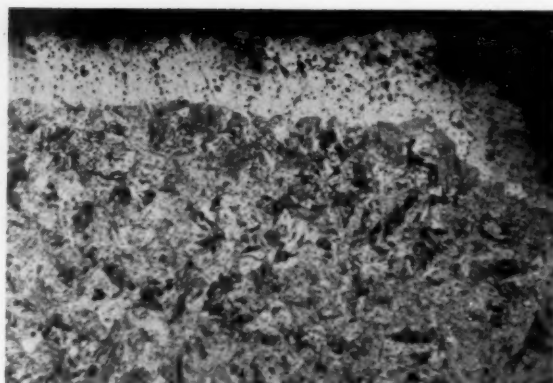


FIG. 15 GLOBULAR SULPHIDES IN SHALLOW DECARBURIZED ZONE OF 5 PER CENT CHROMIUM STEEL (Picral HCl etch;  $\times 250$ )

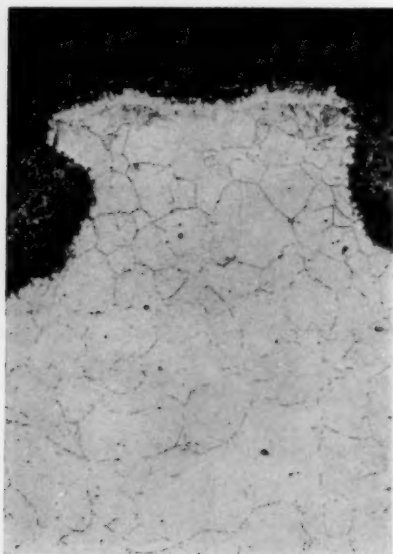


FIG. 14 PITTED AND CARBURIZED CONDITION ALONG MORE SEVERELY CORRODED EDGE OF TYPE 309 SPECIMEN (Glyceric acid etch;  $\times 250$ )

the other. A representative cross-sectional view extending back from the surface along the more severely corroded edge is shown in Fig. 14. (Note the pitting attack.)

**Type 430.** A characteristic microstructure of the Type 430 specimen showed carbides in a ferritic matrix. Corrosion attack was uniform along a given edge but was greater at the leading edge than at the trailing edge.

**5-Cr and 5-Cr Modified Specimens.** The four lower alloy steels (5-Cr grades) corroded at a fairly similar rate along their respective leading edges where the attack was most severe. The Type 502 specimen (straight 5-Cr) was a flat specimen whereas the three 5-Cr modified specimens (modified with Mo or Si or both) were cut from a boiler tube. Each of these was curved and represented  $1/4$  of the circumference of a standard  $2\frac{1}{2}$ -in.-OD superheater tube. It is interesting to note that the greatest spread in rates between opposite edges of these specimens was noted on the plain 5-Cr sample (the flat specimen). The other

three specimens, being curved, the differences in penetration along their opposite edges may have been considerably influenced by specimen contour. A portion of the cross section just beneath an exposed surface of the 5-Cr specimen is shown in Fig. 15. Small globular sulphide particles may be seen in a shallow decarburized zone. In the 5-Cr modified specimens, the results indicate that additions of silicon do not seem to be as beneficial as additions of molybdenum.

**Carbon Steel.** Microstructure of the C-steel specimen after test resembled that of ingot iron. There were excessively coarse ferrite grains with little or no visible carbide phase.

**Type 431.** This type was the most heavily corroded of the specimens exposed in this test rack. Its microscopic appearance was identical to that already given for the specimen exposed in test rack No. 50 and shown in Figs. 9 and 10.

#### TEST RACK NO. 65

Results of the microscopic examination of the specimens included in test rack No. 65 and exposed for 707 hr on the same hook in the superheater section of the boiler fired with bunker C oil at the Marion Generating Station are given in the following.

**Coated Specimens of HK, HE, HT, and HF.** In the case of these coated specimens, the original thickness given in Table 3 includes the coating. These original coating thicknesses per surface for the four specimens were found to be as follows

HK	—0.017 in.
HE	—0.020 in.
HT	—0.020 in.
HF	—0.022 in.

This coating which was applied by the Duraloy Corporation, Scottdale, Pa., was composed of a mixture of oxides of Al, Fe, Cr, Ni, with traces of Cu, Mo, Si, and Mn, and fired at a temperature above 1800 F.

Microscopic examination of these specimens revealed that in all cases the base metal was still completely covered by coating material. Coatings were cracked, chipped, and thinned to various degrees, but penetration did not go beyond the inner banded surface. The "alloy" inner surface was hard, tenacious, and seemingly quite resistant to attack. Much of the cracking and chipping which is shown in Figs. 16 to 19 (coatings prior to exposure) may have occurred in cutting, polishing, and mounting of the specimens. Figs. 20 to 23 show the coated specimens after exposure.

Although none of the coatings was penetrated during the time

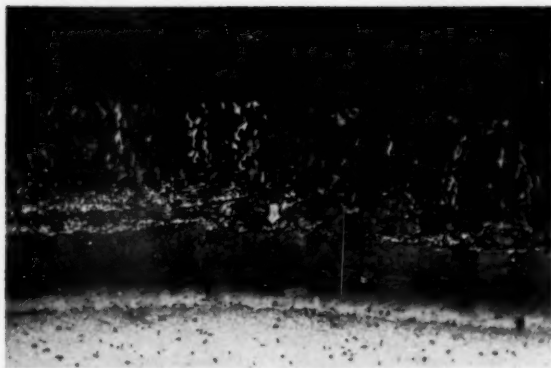


FIG. 16 TYPE HE PRIOR TO EXPOSURE  
(Glyceria etch for 15 sec;  $\times 150$ .)

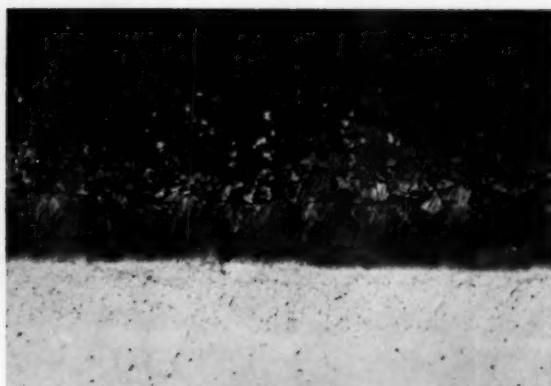


FIG. 17 TYPE HF PRIOR TO EXPOSURE  
(Glyceria etch for 15 sec;  $\times 150$ .)

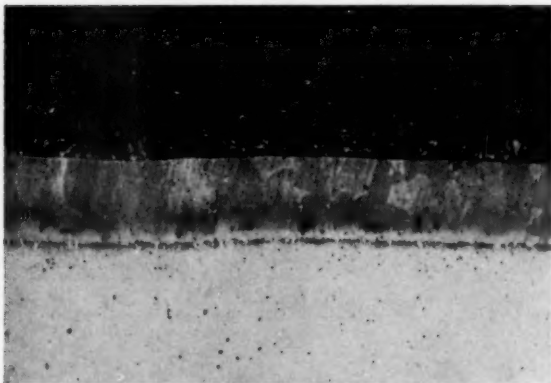


FIG. 18 TYPE HK PRIOR TO EXPOSURE  
(Glyceria etch for 15 sec;  $\times 150$ .)

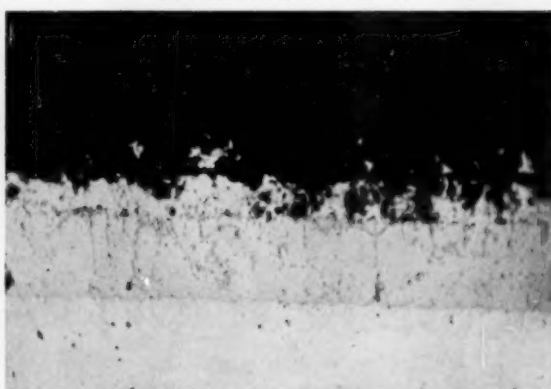


FIG. 19 TYPE HT PRIOR TO EXPOSURE  
(Glyceria etch for 15 sec;  $\times 150$ .)

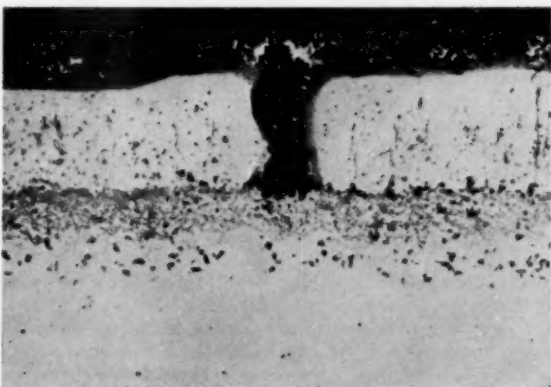


FIG. 20 COATED TYPE HE AFTER EXPOSURE SHOWING AREA OF DEEPEST PENETRATION FOUND ON ENTIRE SPECIMEN  
(Glyceria etch for 20 sec;  $\times 150$ .)

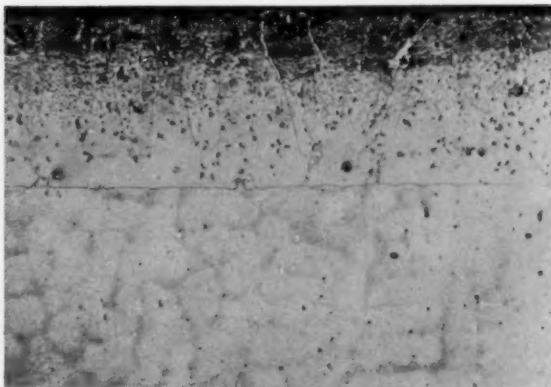


FIG. 21 COATED TYPE HF AFTER EXPOSURE  
(Glyceria etch;  $\times 150$ .)

of exposure (707 hr), it is a matter of conjecture what might have occurred upon longer time exposure to this environment.

Results of analyses made of the coating materials taken from four unexposed samples are shown in Table 4.

The reason for the variation in the compositions of the coatings is that an attempt has evidently been made to match up the

coefficient of expansion of the coating with that of the base material.

**Type HE.** Of the uncoated cast materials, HE exhibited the lowest corrosion rate. Microscopic examination revealed the typical duplex structure of an HE alloy, with evidence of some surface carburization. This test specimen also shows some evidence of sulphidation.

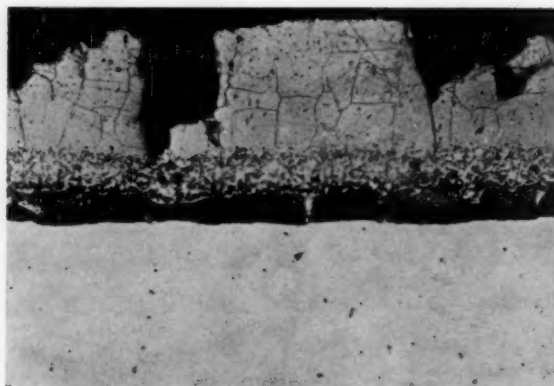


FIG. 22 COATED TYPE HK AFTER EXPOSURE  
(Glyceric etch;  $\times 150$ .)

**Type HF.** This specimen was quite similar to the uncoated HE specimen, just described, giving the typical duplex structure with the addition of some carbides and also showing some surface carburization and sulphidation.

TABLE 4 COMPOSITION OF COATING ON CAST ALLOYS\*

	Per cent—			
	HK	HE	HT	HF
Al.....	53.1	49.2	50.4	50.5
Fe.....	16.2	8.2	11.6	9.7
Cr.....	2.9	4.4	1.4	2.8
Ni.....	5.3	2.4	9.0	1.2
Cu.....	Trace	Trace	Trace	Trace
Mo.....	Trace	Trace	Trace	Trace
Si.....	Trace	Trace	Trace	Trace
Mg.....	Trace	Trace	Trace	Trace
Thickness of coating (per surface), in.....	0.017	0.020	0.020	0.022

\* Coatings applied by Duraloy Corporation, Scottsdale, Pa.

**Type HW.** As shown in Fig. 24, this specimen showed some sulphidation with rather severe general attack. The carbides were more massive than exhibited by the HF specimen.

**T-22 ( $2\frac{1}{4}\%$  Cr + 1 Mo).** Considerable sulphidation was evidenced also in this wrought, low-alloy Cr-Mo steel. It exhibited a relatively carbide-free ferritic structure of well-rounded grains. The attack was not uniform over the surface with some areas being more severely attacked than others. In general, the attack was about the same as that found in the carbon-steel specimen.

**Type 431.** This specimen was again the control specimen in that it was the common alloy tested in each of the three racks. Here again, the microstructure observed was similar to that shown in Figs. 9 and 10.

#### CONCLUSIONS

1 (a) The reproducibility of test results for the three racks is indicated by the figures below for Type 431 specimens which were included on all three test racks. This alloy was included on each of the three racks because it was thought that its attack might be rather severe.

Rack No. 50—0.906 IPY (extrapolated from 648 hr)

Rack No. 54—0.374 to 1.06 IPY (extrapolated from 504 hr)

Rack No. 65—0.353 to 0.930 IPY (extrapolated from 707 hr)

(b) A further comparison between racks may be made with reference to the 2.25 per cent Cr + 1 per cent Mo specimen of test rack No. 65 and the 5 per cent Cr + Mo specimen of test rack No. 54.

2.25 Cr + 1 Mo—0.670 to 0.750 IPY (extrapolated from 707 hr)



FIG. 23 COATED TYPE HT AFTER EXPOSURE  
(Glyceric etch for 30 sec;  $\times 150$ .)

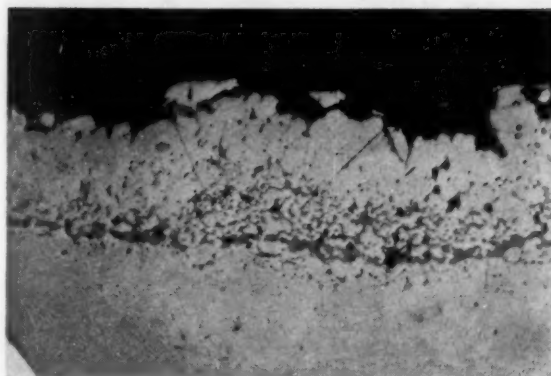


FIG. 24 EDGE OF CROSS SECTION OF TYPE HW SPECIMEN SHOWING SOME SULPHIDATION  
(Etched lightly in glyceric;  $\times 100$ .)

5.0 Cr + 0.5 Mo—0.400 to 0.522 IPY (extrapolated from 504 hr—curved specimen)

(c) The reproducibility of test results on a given rack is shown in the close grouping of the 5-Cr and 5-Cr modified test specimens. The maximum corrosion rates along the leading edge of these four materials were similar.

2 Of the specimens without coatings, Type 406 alloy gave the lowest corrosion rate. Inconel, although exhibiting the second lowest corrosion rate, gave evidence of sulphidation. It is believed that the rate of sulphidation would be greatly increased if the location of the test rack had been in a hotter part of the superheater section of the boiler.

3 Coatings as applied to the cast materials were rather severely attacked; however, they did protect the base metal from attack. It is a matter of conjecture as to what might have occurred upon a longer time exposure to this environment. However, after 707 hr, these coatings had still not been penetrated.

4 Alloys which exhibit a corrosion rate of as high as 0.4 IPY (this means the dividing line is between Type 309 and 302) would certainly be considered unsatisfactory for such applications as hangers, spacers, tube supports, and so on, in the superheater section of a boiler which is using bunker C fuel. However, as anticipated, none of the alloys shows a rate of oxidation low enough to make them outstanding in this service. The differences in oxidation rates were found to be profound and could well serve

as a basis for intelligent considerations in relation to the type of alloy to be used.

#### ACKNOWLEDGMENTS

The authors would like to thank Mr. Walter Ames, Superintendent of Marion Generating Station, Public Service Electric and Gas Company, Jersey City, N. J., Mr. Frank Pierson, Boiler Room Engineer, and Mr. Stanley Grysko, Assistant Boiler Room Engineer at Marion Generating Station, for their permission and co-operation in conducting these tests.

We also would like to thank Mr. F. B. Foley, and Dr. V. N. Krivobok of International Nickel Company, Inc., New York, N. Y., and Mr. Lee W. Lemon of Public Service Electric and Gas Company, for their review and criticism of the manuscript.

## Discussion

E. M. ANGER.<sup>4</sup> This discussion relates to one of the most active and devastating reactions, namely, the attack by  $V_2O_5$  and vanadates on metal and alloys used for equipment for the generation of steam.

The authors are to be congratulated for work done on this subject and reported in detail.

We have found the same result as described in the paper with bare metals and alloys and have supplied "Duralized" equipment for some years, which is resistant to the attack of fly ash from vanadium-type oils for other processes than the generation of steam.

We Duralized a Type 310 welded assembly approximately 2 years ago for color-pigment production which was fired with bunker C oil with an operational temperature up to 1750 F. The coating was applied to all sections in contact with the impinging flame.

The operating life of the Duralized equipment was several times greater than the former bare-metal assemblies. A new requirement has now presented a problem, as the increase in the operating time has caused the pigment-carrying Type 310 tubes to fail from the inside from reaction of sulphur gases by sulphidation. In this case new equipment will be designed using Duralized centrifugal tubing cast from an alloy which will be more resistant to these gases and thus increase the operational life of the equipment.

The authors state: "It is interesting to note that the four coated samples had rather a fast corrosion attack on the coating; however, the duration of the test was not long enough to allow complete penetration of the coating. What would happen when and if the coatings were penetrated by the corrosive atmosphere is not known."

This question, perhaps, can be answered as follows:

The Duralized samples or other process equipment are furnished with the Duralize reaction approximately 35 per cent completed, and when the coated alloy is heated for several months, the former surface coating changes and continuous penetration sets in and all former measurements of coating thickness are lost. The assumption exists that the coating has disappeared or is disappearing.

This is really not so, as the reaction is penetrating deeper and deeper into the alloy base.

The analysis of the coating given in Table 4 of the paper is as the samples were furnished as stated in the paper and can only be construed this way.

The chemical analysis of the coating when under operation runs very much lower in total aluminum and higher in oxides of iron, nickel, chromium, silicon compounds, etc.

<sup>4</sup> The Duraloy Company, Scottdale, Pa.

A typical analysis of the Duralized surface coating after several months of service, using 28 per cent chromium-alloy base metal, is as follows:

Percent			
Al.....	30	Cu.....	Trace
Fe.....	22	Mo.....	Trace
Cr.....	11	Si.....	Trace

Compounds present are alpha, alumina,  $Al_2O_3$ ,  $Fe_2O_3$ ,  $Cr_2O_3$ , NiO,  $Al_2Cr$ , and possibly some  $Fe_2Al_3$ .

The thicknesses of the coating given in Table 2 of the paper are assumed to be taken as a reading of thicknesses of the coating above the base-metal surface and are given for the alloys as follows:

HK—25 Cr 20 Ni 0.017 in. HE—28 Cr 10 Ni 0.020 in.  
HT—15 Cr 35 Ni 0.020 in. HF—18 Cr 8 Ni 0.022 in.

The amount of penetration of the Duralize into these alloys should be added to these measurements, as we have found the base-metal line has changed and a new deeper line is formed. We believe the coating protective thickness may be twice the coating thickness measurements as shown in the foregoing.

E. L. SIMONS.<sup>4</sup> These comments will be confined to the data of Table 2 and to the photomicrograph, Fig. 11 of the paper.

(a) *Analytical Data of Table 2.* The weight ratios of V/Na and V/Mg in the deposit are very much larger than they are in the oil ash; and the Mg/Na ratio is significantly larger in the deposit.

(b) There is a surprisingly large percentage of  $SO_2$  in the deposit. Even if all of the Al, Fe, Ni, Na, and Mg were present as sulphates, the per cent  $SO_2$  would be only about 26. Although not reported in the analysis, calcium is also likely to be found in the deposit as calcium sulphate. This would account, at least in part, for both the additional  $SO_2$  and the missing 5 per cent in the total analysis reported for the deposit.

*Photomicrograph of Fig. 11.* The sulphidation and oxidation of the Type 310 rods of the specimen holder shown in Fig. 11 of the paper is strikingly similar to the type of attack which has been observed at the General Electric Research Laboratory when specimens of Type 310 alloy, coated with a thin layer of sodium sulphate, have been exposed to cycling, reducing, and oxidizing conditions at temperatures above 750 C (1380 F).

It does not resemble the catastrophic attack of this same alloy which we have observed with thin layers of vanadium pentoxide. Such attack is catastrophic only in oxidizing atmospheres above 850 C (1560 F).

That the attack noted in Fig. 11 is primarily through sulphide penetration even though the deposit is more than 36 per cent  $V_2O_5$  suggests two features of the boiler operation: (1) The maximum temperature of 850 C (1560 F) was not maintained for sustained periods in an oxidizing atmosphere. (2) The metal-deposit interface was subject to alternating reducing and oxidizing conditions. As our experiments have indicated, lower valent sulphur can be produced by transient reducing conditions either in the atmosphere or as contaminants in the deposit or at the metal surface. The sulphide inclusions which result from the penetration of the alloy by a metal-metal sulphide eutectic are more susceptible to oxidation than is the alloy itself.

NOTE: The sodium-sulphate work referred to in the foregoing comments is described in a paper entitled, "Sodium Sulfate in

<sup>4</sup> Research Laboratory, General Electric Company, Schenectady, N. Y.

Gas Turbine," presented at the meeting of The National Association of Corrosion Engineers in Chicago in March, 1955, and published in *Corrosion*, vol. 11, 1955, 505t.

#### AUTHORS' CLOSURE

The authors wish to thank Messrs. E. M. Anger and E. L. Simons for their respective discussions of the paper. Concerning Mr. Anger's comments on the Duralized specimens, it is indeed true that the coating-metal interface advances during exposure at elevated temperatures. It should be pointed out, however, that the over-all thickness of the coated material may decrease simultaneously. This is illustrated in the case of a Duralized HE specimen which was exposed on a test rack for 326 days at about 1550 F to less severely corrosive hot combustion gases in a furnace burning gas in conjunction with fuel oil,

the latter having relatively little  $V_2O_5$ , 30 ppm, and less than 0.75 per cent sulphur. The over-all coated sample thickness decreased 0.032 in., that is, from 0.267 in. to 0.235 in. during the 326-day exposure, whereas the thickness of the altered coating plus the broadened diffusion zone was about the same as the thickness of the coating originally present on the sample prior to exposure, respectively, 0.0195 and 0.020 in.

With reference to the comments on the sulphidation and oxidation of the Type 310 rods, Mr. Simons' suspicion that conditions at the metal surface were alternately reducing and oxidizing rather than predominantly oxidizing for long periods of time is a very justifiable one. Furthermore, his observation concerning the preferential oxidation of the sulphide constituent in the metal matrix is further illustrated in Fig. 12 which typifies the nature of the attack observed on Inconel.

# Use of Nonlinear Valve Characteristics in the Control of a Simple Blending Process

By J. L. SHEARER,<sup>1</sup> CAMBRIDGE, MASS.

A simple, continuous, energy-blending process is analyzed to attain an understanding of its dynamic performance when the flow rate of either the hot or cold fluid is time variant. A linearized analysis based on small changes of all variables is employed to estimate the static and dynamic performance of the process when simple controllers are used to regulate temperature of the out-flowing mixture. Possible advantages are indicated for the use of nonlinear flow versus stroke characteristics of the flow-control valve together with its connecting lines. Graphical analyses show the performance of various control schemes when the system variables undergo large changes and indicate how valve characteristics may be chosen for the blending process under control.

## NOMENCLATURE

The following nomenclature is used in the paper:

- $C_h$  = specific heat of mixture in tank, Btu/lb-deg F
- $D$  = denotes derivative with respect to time,  $d/dt$ , 1/sec
- $h_1$  = enthalpy of cold fluid, Btu/lb
- $h_2$  = enthalpy of hot fluid, Btu/lb
- $i$  = subscript to denote initial steady value
- $K_t$  = loop gain, dimensionless
- $k_1$  = process constant,  $(\partial T/\partial W_1)_{ss}$ , deg F-sec/lb
- $k_2$  = process constant,  $(\partial T/\partial W_2)_{ss}$ , deg F-sec/lb
- $k_3$  = process constant,  $(\partial T/\partial h_1)_{ss}$ , deg F-lb/Btu
- $k_4$  = process constant,  $(\partial T/\partial h_2)_{ss}$ , deg F-lb/Btu
- $k_c$  = controller gain, in/deg F
- $k_v$  = valve gain (installed with connecting lines), lb/sec-in.
- $ss$  = subscript to denote steady state
- $T$  = temperature of mixture in tank, deg F abs
- $T^*$  = desired temperature, deg F abs
- $t$  = time, sec
- $V$  = volume of tank, cu ft
- $W_1$  = weight rate of flow of cold fluid, lb/sec
- $W_2$  = weight rate of flow of hot fluid, lb/sec
- $W_3$  = weight rate of flow of mixture from tank, lb/sec
- $\gamma$  = weight density of mixture in tank, lb/cu ft
- $\Delta$  = denotes a small change of the following variable
- $\zeta$  = damping ratio of system
- $\lambda$  = exponential coefficient, 1/in.
- $\tau$  = time constant of process, sec
- $\tau_c$  = time constant of controller, sec
- $\tau_1$  = time constant of system, sec

## INTRODUCTION

The process to be considered takes place in a well-stirred,

<sup>1</sup> Assistant Professor of Mechanical Engineering, Massachusetts Institute of Technology, Cambridge, Mass. Mem. ASME.

Contributed by the Instruments and Regulators Division and presented at the Diamond Jubilee Annual Meeting, Chicago, Ill., November 13-18, 1955, of THE AMERICAN SOCIETY OF MECHANICAL ENGINEERS.

NOTE: Statements and opinions advanced in papers are to be understood as individual expressions of their authors and not those of the Society. Manuscript received at ASME Headquarters, August 5, 1955. Paper No. 55-A-70.

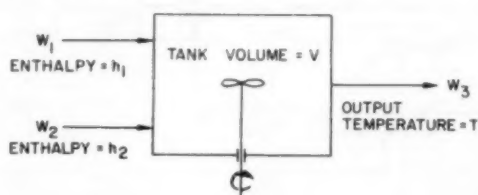


FIG. 1 SCHEMATIC DIAGRAM OF SIMPLE BLENDING PROCESS

liquid-filled, fixed-volume tank that is used to blend a hot flow of a given fluid with a cold flow of the same substance. The temperature of the resulting mixture flowing from the tank is the output of the process. The process is shown schematically in Fig. 1. The cold-flow rate, cold-flow enthalpy, hot-flow rate, and hot-flow enthalpy all may be varied by external means, and they all are possible inputs to the system. The tank is well insulated to prevent heat transfer through its walls. The mass of the walls is small compared to the mass of the liquid in the tank, with the result that negligible heat is required to vary the temperature of the walls. Since the density and specific heat of the liquid in the tank are taken to be constant and perfect mixing is assumed to take place, the temperature is uniform through the mixture and equal to the instantaneous temperature of the flow leaving the tank.

## PROCESS ANALYSIS

Application of the unsteady-flow energy equation to the space enclosed by the tank gives

$$W_1 h_1 + W_2 h_2 = W_3 C_h T + C_h \gamma V \frac{dT}{dt} \quad [1]$$

and the continuity equation yields

$$W_1 + W_2 = W_3 \quad [2]$$

Therefore

$$W_1 h_1 + W_2 h_2 = (W_1 + W_2) C_h T + C_h \gamma V \frac{dT}{dt} \quad [3]$$

Although this is a single-capacity system, as demonstrated by the fact that it has a single reservoir of energy storage and is described by a first-order differential equation when all variables undergo small changes, it becomes a nonlinear system whenever any or all of  $W_1$ ,  $h_1$ ,  $W_2$ ,  $h_2$ , and  $T$  undergo large changes. Fig. 2, a block diagram of the process, shows one scheme of simulation for study on an analog computer when large changes occur.

For reasons of relative simplicity and ease of comprehension, the performance of the system is considered first when all variables undergo only small changes from a set of initial equilibrium conditions. For small changes, then

$$W_{1i} \Delta h_1 + h_{1i} \Delta W_1 + W_{2i} \Delta h_2 + h_{2i} \Delta W_2 = (W_{1i} + W_{2i}) C_h \Delta T + C_h \gamma V (\Delta W_1 + \Delta W_2) + C_h \gamma V \frac{d\Delta T}{dt} \quad [4]$$

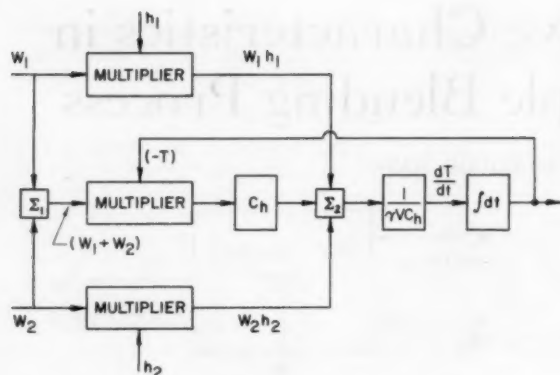


FIG. 2 ANALOG BLOCK DIAGRAM OF BLENDING PROCESS

Collecting terms yields

$$C_A(W_{1s} + W_{2s} + \gamma V D)\Delta T = (h_{1s} - C_A T_s)\Delta W_1 + (h_{2s} - C_A T_s)\Delta W_2 + W_{1s}\Delta h_1 + W_{2s}\Delta h_2 \quad [5]$$

where  $D$  denotes  $d/dt$ . Solution for  $\Delta T$  gives

$$\Delta T = \frac{k_1 \Delta W_1 + k_2 \Delta W_2 + k_3 \Delta h_1 + k_4 \Delta h_2}{\tau D + 1} \quad [6]$$

where

$$k_1 = \frac{h_{1s} - C_A T_s}{C_A(W_{1s} + W_{2s})}$$

$$k_2 = \frac{h_{2s} - C_A T_s}{C_A(W_{1s} + W_{2s})}$$

$$k_3 = \frac{W_{1s}}{C_A(W_{1s} + W_{2s})}$$

$$k_4 = \frac{W_{2s}}{C_A(W_{1s} + W_{2s})}$$

and

$$\tau = \frac{\gamma V}{W_{1s} + W_{2s}}$$

The tank temperature change  $\Delta T$  is seen to lag changes in  $W_1$ ,  $W_2$ ,  $h_1$ , and  $h_2$  with a time constant  $\tau$  which varies inversely with the initial equilibrium flow rate through the tank; hence the process responds much more quickly to input changes when the initial rate of flow through the tank is high. It is also interesting to note that the time constant varies directly with the weight of liquid in the tank but is independent of the specific heat of the liquid mixture. The steady-state response to changes in  $W_1$  and  $W_2$  is given by  $k_1$  and  $k_2$ , respectively, which show that the respective gains vary directly with the initial equilibrium enthalpy changes of the respective flows as they traverse the tank and vary inversely with the specific heat of the mixture and the initial equilibrium rate of flow through the tank. The steady-state response to changes in  $h_1$  and  $h_2$  are given by  $k_3$  and  $k_4$ , respectively, which show that each gain is dependent on the ratio of its respective initial equilibrium rate of flow to the total initial rate of flow through the tank and varies inversely with the specific heat of the mixture.

#### REGULATION FOR SMALL DISTURBANCES

A problem of practical significance is that of holding the mixture temperature  $T$  as nearly constant as possible while the rate or

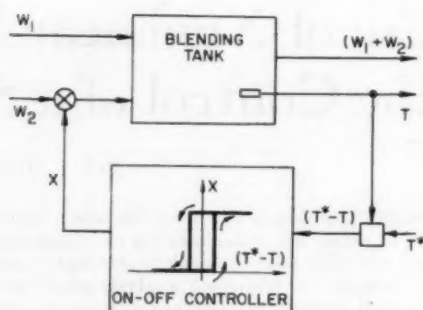


FIG. 3 SCHEMATIC DIAGRAM SHOWING USE OF AN ON-OFF CONTROLLER FOR SIMPLE BLENDING PROCESS

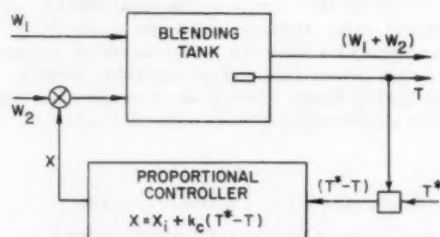


FIG. 4 SCHEMATIC DIAGRAM OF REGULATION OF THE BLENDING PROCESS WITH A PROPORTIONAL CONTROLLER

enthalpy of one of the input flows varies arbitrarily with time. If a cyclic variation of  $T$  with time within prescribed limits were permissible under steady-state conditions, a simple on-off controller with dead zone would be satisfactory to vary the other flow by rapidly opening and closing a simple control valve, as shown in Fig. 3. If a steady cyclic variation of  $T$  is not permissible, then some means of continuous control is appropriate. In many cases, a proportional controller having very fast response compared to the process is available to stroke a linear control valve, as shown in Fig. 4. The following equation may be used to express the controller action on the flow  $W_2$

$$W_2 = W_{2s} + k_c k_p (T^* - T) \quad [7]$$

where

$$k_c = \text{controller gain} = \frac{\text{valve motion}}{\text{temperature change}}$$

$$k_p = \text{valve gain} = \frac{\text{small change of flow rate}}{\text{small valve motion}}$$

$$T^* = \text{desired value of } T$$

The flow rate  $W_{2s}$  can be set with a bias adjustment in the controller to give the desired value of  $T$  for  $W_{1s}$ ,  $h_{1s}$ , and  $h_{2s}$ . For small changes

$$\Delta W_2 = k_c k_p (\Delta T^* - \Delta T) \quad [8]$$

Combining the process and controller Equations [6] and [8] gives

$$\Delta T = \frac{K_1 \Delta T^* + k_1 \Delta W_1 + k_3 \Delta h_1 + k_4 \Delta h_2}{(1 + K_1)(\tau D + 1)} \quad [9]$$

where

$$\tau_1 = \frac{\tau}{1 + K_1}$$

$$K_1 = k_2 k_c k_p$$

The process under control is still represented by a first-order differential equation. If a large value of  $K_1$  is used ( $K_1 \gg 1$ ), then  $(\Delta T / \Delta T^*)_{ss} \approx 1$ , and the steady-state response of  $T$  to changes in  $W_1$ ,  $h_1$ , and  $h_2$  will be small. Using a large value of  $K_1$  also makes the closed-loop response time  $\tau_1$  correspondingly small and creates no stability problem as long as other system lags remain negligible. However, it is not sufficient for other system lags to be small compared to the uncontrolled process lag; in order to be negligible, they also must be small compared to the lag time  $\tau_1$ . Situations almost inevitably will arise when sufficiently large values of  $K_1$  will be used to make necessary the inclusion of otherwise negligible lags in the control system. The controller itself often has a dynamic response characteristic which may be approximated by a single lag.

For the purposes of illustration, an assumption is made that a controller lag exists which cannot be neglected. Then the controller characteristic may be written

$$W_2 = W_{2s} + \frac{k_c k_v (T^* - T)}{\tau_c D + 1} \quad [10]$$

hence, for small changes

$$\Delta W_2 = \frac{k_c k_v (\Delta T^* - \Delta T)}{\tau_c D + 1} \quad [11]$$

Combining Equations [6] and [11] gives

$$\Delta T = \frac{K_1 \Delta T^* + (\tau_c D + 1)(k_1 \Delta W_1 + k_2 \Delta h_1 + k_4 \Delta h_2)}{(\tau_c D + 1)(\tau D + 1) + K_1} \quad [12]$$

The value of  $K_1$  that may be employed is now limited by stability considerations because the system is described by a second-order differential equation. Examination of the characteristic equation

$$[(\tau_c D + 1)(\tau D + 1) + K_1] \Delta T = 0 \quad [13]$$

reveals that the following relationship exists between the system parameters and the desired system damping ratio  $\zeta$

$$\zeta = \frac{\tau_c + \tau}{2 \sqrt{\tau_c \tau (1 + K_1)}} \quad [14]$$

or

$$K_1 = \frac{(\tau_c + \tau)^2}{4 \zeta^2 \tau_c \tau} - 1 = \left( \frac{\tau_c + \tau}{\tau} \right)^2 \frac{1}{4 \zeta^2} - 1 \quad [15]$$

Fig. 5 shows graphically the relationships given by Equation [15]. In order to be able to employ values of  $K_1$  greater than 10 and obtain a system damping ratio of 0.7,  $\tau/\tau_c$  must be greater than 20.

Even when  $\tau/\tau_c$  is only greater than 5.0 for small changes about a condition of a high net rate of flow, the over-all system damping ratio is not appreciably different at a much lower net rate of flow. For example, if  $\tau/\tau_c = 5$  at a high flow rate and if  $K_1$  is set for a damping ratio  $\zeta = 0.5$ , namely  $K_1 \approx 6.5$ , then when the flow rate is decreased by a factor of 10,  $\tau/\tau_c$  becomes approximately 50,  $K_1$  becomes approximately 65, and the damping ratio  $\zeta$  is found from Equation [14] to be 0.44. This condition arises from the counteracting effects of increasing  $k_2$  and increasing  $\tau$  as the net rate of flow through the tank decreases.

With a high flow rate through the tank, as  $\tau/\tau_c$  approaches 1, the maximum value of  $K_1$  approaches 3 and the beneficial steady-state effects of having large values of  $K_1$  are not possible (i.e.,

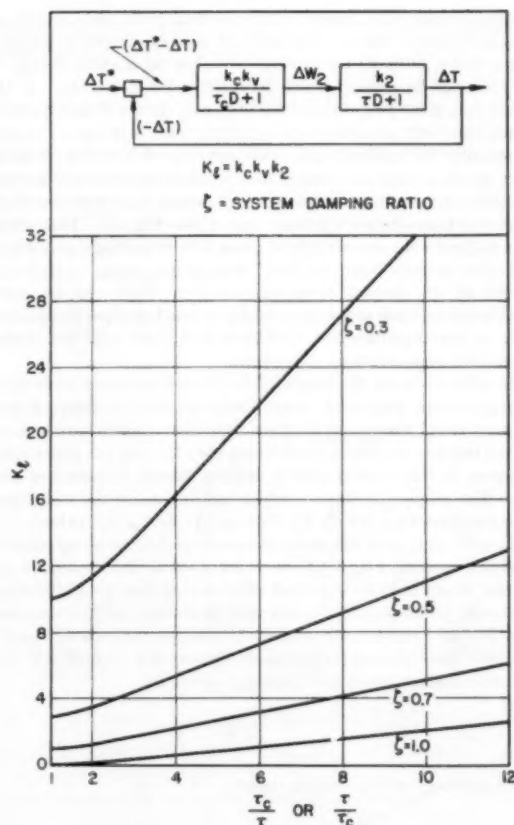


FIG. 5 GRAPH OF  $K_1$  AS A FUNCTION OF  $\tau/\tau_c$  AND  $\zeta$

large offset will occur). However, the dynamic characteristics of the closed loop do not change appreciably with wide variations in net flow through the tank until  $\tau/\tau_c$  approaches 1 when the net rate of flow is low. When the controller lag exceeds the process lag at low tank-flow rates, it tends to predominate over the process lag at all flow rates because both  $K_1$  and  $\tau$  are inversely proportional to the flow rate, and the variation of  $K_1$  due to changing from low to high flow rates through the tank begins to show a marked increase in system damping ratio at high flow rates. Having a small ratio of process time constant to controller time constant might occur when the mixing is accomplished in a very small tank. It is also true that small amounts of delay (dead time) may become significant when the mixing time constant is small. This effect will not be considered here, although the graphical methods to be discussed later can handle it readily.

The results of the discussion of the previous few paragraphs also apply to cases where the single lag may be at some part of the closed loop other than the controller, but the lag effect must be cascaded so that it does not interact with the process lag.

#### REGULATION WITH A NONLINEAR VALVE

The large variation of loop gain with net rate of flow through the tank suggests using a nonlinear control valve to counteract this variation. Nichols and Ziegler (1)<sup>2</sup> have presented an excellent qualitative discussion of many of the factors which ex-

<sup>2</sup> Numbers in parentheses refer to the Bibliography at the end of the paper.

perience shows to be important in considering the use of nonlinear characteristics. The problem at hand seems to be one of employing a valve, with its connecting lines, having a gain (change in flow/change in stroke) which increases with flow rate. If the valve gain were proportional to flow rate, then a simple proportional controller adjusted to have a minimum satisfactory degree of stability for small changes at low net rates of flow still would be very stable at high net rates of flow because the process time constant also decreases with increasing net rate of flow, with the result that  $\tau_p/\tau$  becomes much greater than 1 (see Fig. 5). This condition indicates the desirability of using a valve having a gain which increases as more than the first power of flow rate. A tentative choice of the desired valve characteristic often can be made readily on the basis of the linearized (for small changes) analysis as long as nonlinearities like hysteresis and dead zone are absent from the components of the system.

In order to study the performance of such a system when large changes occur, graphical, analog, or numerical techniques may be employed. Graphical analyses have been chosen here because of the relative simplicity of showing step by step on paper what happens in this system after a sudden change in cold-flow rate  $W_1$ . The graphical solutions which follow employ the techniques developed by Paynter (2, 3), Carlson (4), and many others.

In order first to demonstrate the use of slope-line integration on a simple system, Fig. 6 has been prepared to determine the response that would be expected when a very fast (negligible-lag) controller and a linear valve are used to control outflow temperature  $T$  after a sudden, factor-of-10 increase in cold rate of flow  $W_1$  occurs. The equation for the small temperature change  $\Delta T$  that occurs in a short interval of time  $\Delta t$  is given by

$$\Delta T = \frac{\Delta t}{\gamma V C_h} [(W_1 h_1 - W_1 C_h T)_{av} + (W_2 h_2 - W_2 C_h T)_{av}] \dots [16]$$

and the rate of flow of hot fluid  $W_2$  is given by Equation (7); hence

$$W_2 h_2 = W_2 h_2 + k_p k_v h_2 (T^* - T) \dots [17]$$

If the controller regulates outflow temperature  $T$  to within a few per cent of  $T^*$ , the following approximate equation for  $W_2 C_h T$  may be used

$$W_2 C_h T = W_2 C_h T^* + k_p k_v C_h T^* (T^* - T) \dots [18]$$

In addition to serving as a means of demonstrating slope-line integration, Fig. 6 shows that the system does not tend to oscillate when a large disturbance in  $W_1$  occurs, and this solution is in substantial agreement with the tentative conclusions that might be drawn from the solution that was obtained for small disturbances.

In choosing a nonlinear valve to operate with a controller having a lag equal to the process lag at a low net rate of flow through the tank, it is possible to use an exponential valve having a gain which increases by more than the first power of flow rate. When the net rate of flow increases by a factor of 10,  $\tau_p/\tau$  becomes 10, and from Fig. 5, the value of  $K_1$  for  $\zeta = 0.5$  is approximately 3.7 times as large as when  $\tau_p/\tau$  is 1 at low net rate of flow. Since the process gain varies inversely with net rate of flow, the valve gain should increase by 37 when the flow rate is increased by a factor of 10. An exponential valve that closely approximates such requirements is described by the following equation

$$W_2 = W_{2i} [0.75 + 0.25 e^{\lambda(X - X_i)}] \dots [19]$$

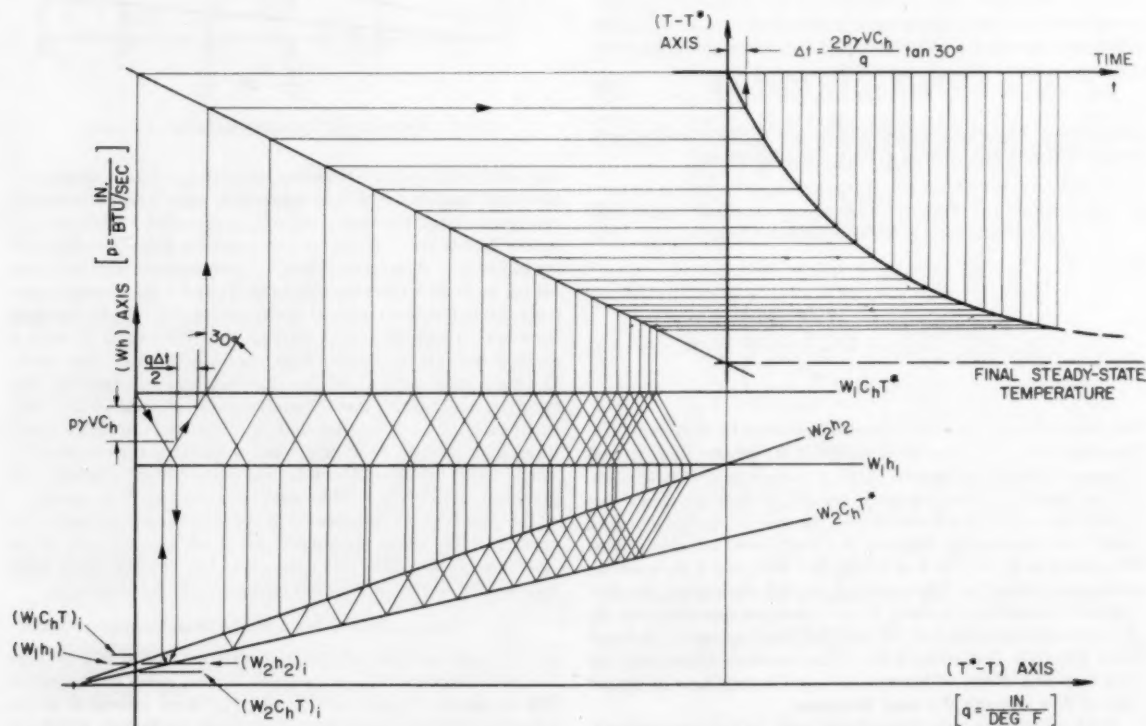


FIG. 6 GRAPHICAL SOLUTION USING SLOPE-LINE INTEGRATION TO DETERMINE RESPONSE OF SYSTEM HAVING A CONTROLLER WITH NEGLIGIBLE LAG. DISTURBANCE IS A SUDDEN FACTOR-OF-10 INCREASE IN  $W_1$

The gain of this valve at any given rate of flow is given by

$$k_v = \frac{\partial W_2}{\partial (X - X_i)} = 0.25 W_{2i} \lambda e^{\lambda(X - X_i)} \quad [20]$$

At the low flow rate,  $W_2 = W_{2i}$ ,  $X = X_i$ , and

$$k_v = 0.25 W_{2i} \lambda \quad [21]$$

At the high flow rate,  $W_2 = 10 W_{2i}$ ; therefore

$$0.25 e^{\lambda(X - X_i)} = 9.25$$

or

$$e^{\lambda(X - X_i)} = 37 \quad [22]$$

and

$$k_v = (37)(0.25) W_{2i} \lambda \quad [23]$$

The loop gain  $K_l$  at low rate of flow is given by

$$K_l = k_v k_c = \frac{(h_2 - C_h T^*) k_c (0.25) W_{2i} \lambda}{C_h (W_{1i} + W_{2i})} \quad [24]$$

The use of an exponential valve may be illustrated by considering a blending process with hot-flow enthalpy  $h_2$  equal to twice the cold-flow enthalpy

$$h_2 = 2h_1 = 1000 \text{ Btu/lb-deg F} \quad [25]$$

The specific heat of the mixture in the tank is 1.0 Btu/lb-deg F, and the weight rate of flow of cold fluid is initially equal to twice the weight rate of flow of hot fluid

$$W_{1i} = 2W_{2i} = 0.2 \text{ lb/sec} \quad [26]$$

and the system is in a steady state with the temperature of the mixture equal to a steady value that is found from the steady-flow energy equation and continuity equation to be

$$T_i = \frac{2h_2}{3C_h} = \frac{2000}{3} = 667 \text{ F} \quad [27]$$

This value also may be the desired value of the temperature

$$T^* = T_i \quad [28]$$

From Equation [27]

$$C_h T^* = \frac{2h_2}{3} \text{ and } (h_2 - C_h T^*) = \frac{h_2}{3}$$

From Equation [26]

$$(W_{1i} + W_{2i}) = 3W_{2i} = \frac{3}{2W_{1i}}$$

The expression for  $K_l$  now becomes

$$K_l = \frac{h_2 k_c \lambda}{36 C_h} = 27.7 k_c \lambda \quad [29]$$

In order to have  $K_l = 3.0$  at the initial flow-rate condition

$$k_c \lambda = \frac{3}{27.7} = 0.108 \quad [30]$$

The value of  $k_c$  probably will be determined by a number of practical factors. For simplicity, when  $k_c$  equals 0.1, then  $\lambda = 1.08$ , and for a tenfold increase in flow rate, the increase in valve stroke is found to be

$$X - X_i = \frac{\ln 37.0}{1.08} = \frac{3.62}{1.08} = 3.35 \text{ in.} \quad [31]$$

Equation [16] also applies to this system. The equation giving

the small change in valve opening  $\Delta(X - X_i)$  that occurs during a short interval of time  $\Delta t$  is

$$\Delta(X - X_i) = \frac{\Delta t}{\tau_v} \left[ k_c (T^* - T)_{av} - (X - X_i)_{av} \right] \quad [32]$$

The quantities  $W_2 h_2$  and  $W_2 C_h T^*$  are obtained as before by multiplying  $W_2$  by  $h_2$  and  $C_h T^*$ , respectively.

The beginning of a graphical solution based on Equations [16], [19], and [32] is shown in Fig. 7 for the condition when  $W_1$  is

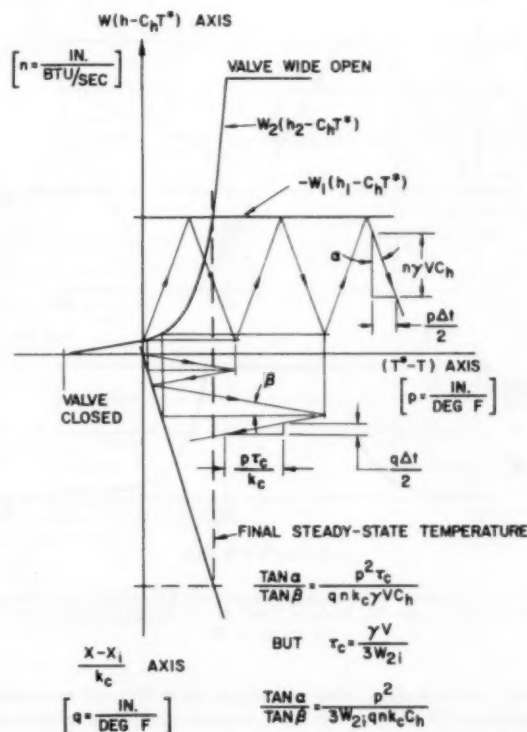


FIG. 7 BEGINNING OF APPROXIMATE GRAPHICAL DETERMINATION OF RESPONSE WHEN CONTROLLER HAS SINGLE LAG. DISTURBANCE IS A SUDDEN FACTOR-OF-10 INCREASE IN  $W_1$

suddenly increased by a factor of 10. Fig. 8 gives the partial result of this graphical solution with the output temperature  $T$  and the rate of flow  $W_2$  shown as functions of time after the disturbance in  $W_1$ . The serious drop in temperature  $T$  during the initial part of the response is caused largely by the controller lag which does not allow the controller to open the valve quickly enough to counteract the very great cooling effect of the suddenly increased rate of flow of cold fluid. The drop in temperature  $T$  would be even more serious if a factor-of-2 extra capacity had not been provided in the control valve. The effect of the large drop in  $T$  is so serious that it is advisable to determine

$$W_1(h_1 - C_h T) \text{ and } W_2(h_2 - C_h T)$$

by using  $T$  rather than the simplified scheme of substituting  $T^*$  for  $T$ . The large variation in  $T$  has been taken into account for the determination of  $W_1 C_h T$  and  $W_2 C_h T$  in the graphical solution shown in Fig. 9.

The variables  $T$  and  $W_2$  are plotted in Fig. 10 as functions of

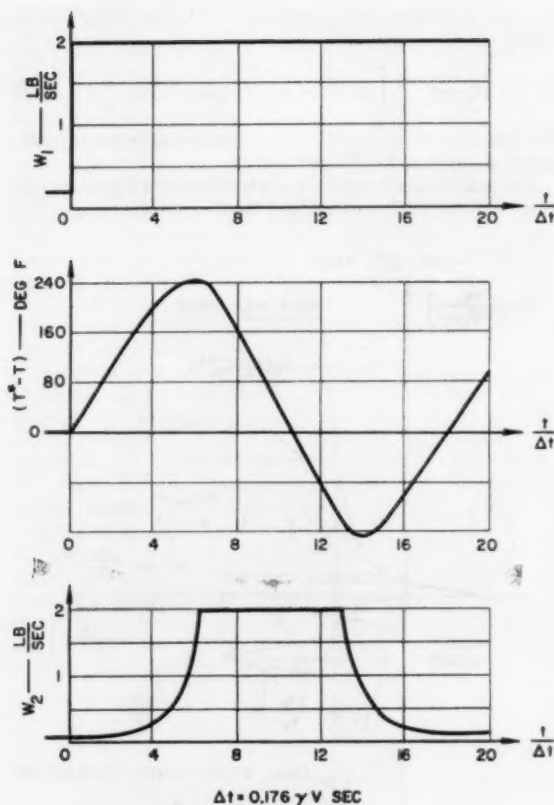


FIG. 8 PARTIAL RESULT OF APPROXIMATE GRAPHICAL SOLUTION. GRAPH OF  $T$  AND  $W_2$  VERSUS TIME AFTER SUDDEN FACTOR-OF-10 INCREASE IN  $W_1$

time after a sudden factor-of-10 increase in  $W_1$ . Of particular significance is the fact that the approximate graphical solution of Fig. 7 gives a misleading result with respect to maximum transient values of  $T$  and  $W_2$ , with respect to the rate of decay of the transient oscillation of these variables, and with respect to the final steady values of  $T$  and  $W_2$ . The main reason for the great difference between the results of the graphical solutions of Figs. 7 and 9 lies in the important stabilizing effect of the transient variation of  $T$  in the process. The result of the graphical solution of Fig. 9 is in good agreement with the result that would be expected on the basis of the linearized analysis.

The graphical techniques may be applied readily to systems having hysteresis, dead zone, or pure delay. It is very difficult to generalize the solutions that are obtained when nonlinear effects are present, and no attempt is made to do so here. Nichols and Ziegler (1) noted that a somewhat different nonlinear valve characteristic would be required if a 10-to-1 change in cold-flow enthalpy were to occur instead of the cold-flow-rate disturbance. Each situation must be considered on its own merits. A large amount of general information is usually available from a linearized analysis based on small changes of all variables.

No attempt is made to discuss the problems associated with obtaining the desired valve characteristics. Recognition must be made of the fact that the characteristics discussed here must include the resistance effects in the lines installed with the valve (1, 5).

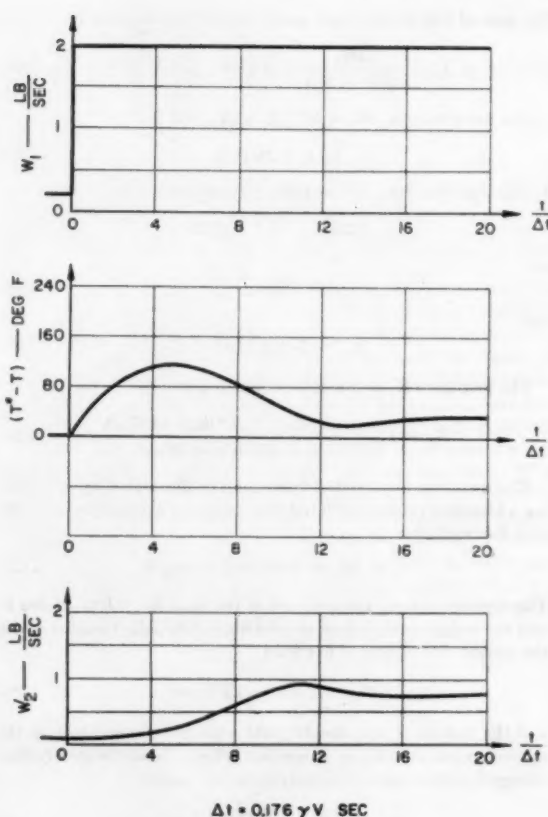


FIG. 10 RESULT OF MORE ACCURATE GRAPHICAL SOLUTION. GRAPH OF  $T$  AND  $W_2$  VERSUS TIME AFTER SUDDEN FACTOR-OF-10 INCREASE IN  $W_1$

#### CONCLUSIONS

A linear valve characteristic is shown to be adequate for use with a proportional controller on a simple blending process as long as the lag in the controller is less than one fifth of the process lag for small changes about the maximum process net rate of flow. As the controller time constant increases to the time constant of the process at high net rate of flow, the loop gain of the system is limited to relatively small values; then, large steady-state errors would be expected with load changes. However, reset (integral) control with a fixed integrating time constant might be incorporated easily to eliminate steady-state errors because the system gain varies inversely with the process time constant, leaving a nearly fixed over-all system characteristic.

However, when the process time constant is smaller than the controller time constant for small changes near a condition of low net rate of flow, then a nonlinear valve with an exponential flow versus stroke characteristic offers distinct advantages as long as the only load disturbance is in the flow rate of cold fluid  $W_1$ . A linearized analysis based on small changes of all variables proved to be very helpful in gaining an understanding of this system. Graphical analysis is shown to be an effective means of studying system behavior when large disturbances occur.

#### ACKNOWLEDGMENT

The author wishes to express his gratitude to the Control Valve Committee of the Instruments and Regulators Division of the

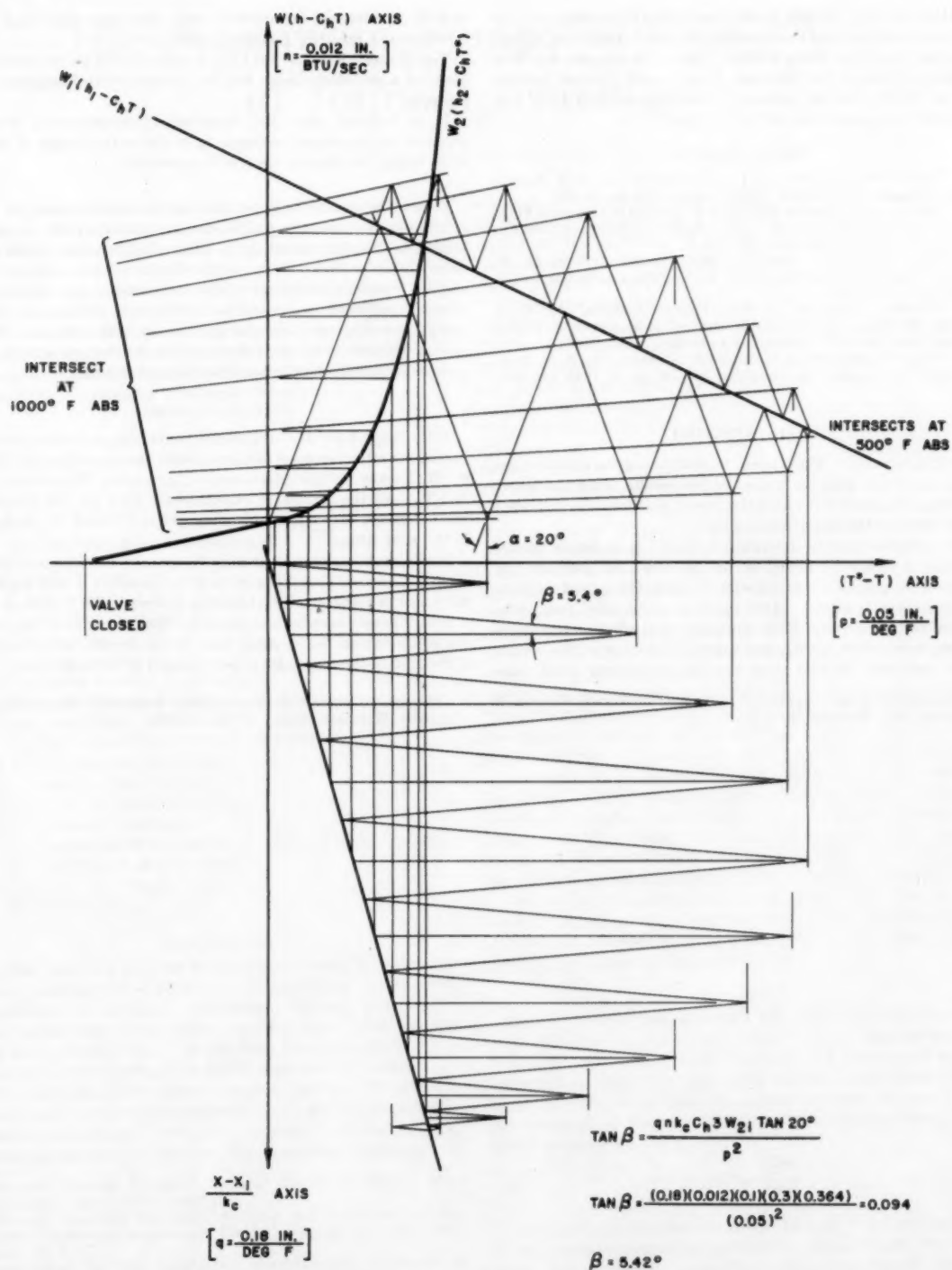


FIG. 9 MORE ACCURATE DETERMINATION OF RESPONSE WHEN CONTROLLER HAS A SINGLE LAG. DISTURBANCE IS A SUDDEN FACTOR-OF-10 INCREASE IN  $W_1$

ASME for the opportunity to take part in the Symposium and for the encouragement and constructive comments that were offered when this paper was being written. Special thanks are due Miss Constance Boyd of the Dynamic Analysis and Control Laboratory at M.I.T., for the assistance that was received from that Laboratory in preparation of the final draft.

#### BIBLIOGRAPHY

- 1 "Valve Characteristics and Process Control," by N. B. Nichols and J. G. Ziegler, *Instruments*, vol. 22, no. 1, 1949, pp. 75-81.
- 2 "Methods and Results From M.I.T. Studies in Unsteady Flow, Part 2," by H. M. Paynter, *Journal of the Boston Society of Civil Engineers*, vol. 39, no. 2, 1952, pp. 120-165.
- 3 "How to Analyze Control Systems Graphically," by H. M. Paynter, *Control Engineering*, vol. 2, no. 2, 1955, pp. 30-35; vol. 2, no. 2, 1955, pp. 72-78.
- 4 "Transient Solutions for Time-Variant Systems," by R. S. Carlson, MS thesis, Department of Mechanical Engineering, Massachusetts Institute of Technology, Cambridge, Mass., 1954.
- 5 "Valve Characteristics in Automatic Control," by S. D. Ross, *Industrial and Engineering Chemistry*, vol. 38, no. 9, 1946, pp. 878-884.

#### Discussion

R. P. BIGLIANO.<sup>3</sup> The author, in illustrating the effectiveness of the graphical analysis, compares the results using the slope-line integration technique with the "result that would be expected on the basis of the linearized analysis."

For a process such as described, it should be a simple matter to build a hydraulic model of the process and compare the results of the graphical solution with the actual measured response of the hydraulic model. This method would offer more substantial verification and should illustrate what effects nonuniform density, nonperfect mixing, and valve piping have on the results of the analysis. Should these have a pronounced effect, con-

<sup>3</sup> Research Engineer—Applied Physics, E. I. du Pont de Nemours & Company, Inc., Wilmington, Del.

trolled experiments undoubtedly will show how they may be incorporated into the graphical solution.

The ultimate goal for this kind of work should be the development of a practical design tool for process-control engineers in industry.

It is believed that the foregoing recommendation would enhance the graphical technique in so far as the design of optimum industrial process controls is concerned.

N. B. NICHOLS.<sup>4</sup> It is noted that the author comes to the conclusion that no one nonlinear-valve characteristic is satisfactory or desirable for all of the kinds of load changes which can occur in his process. Perhaps one should not lose sight of the smaller transient deviations of the tank temperature which are, of course, achieved by increase in the volume of the tank, all other things including the controller gain being held constant. This arises, of course, because of the fact that the time constant of the process is directly proportional to the tank volume.

#### AUTHOR'S CLOSURE

With respect to Mr. Bigliano's comments, an experimental mixing chamber has been designed under the supervision of Prof. F. D. Ezekiel in the Mechanical Engineering Department at M.I.T., and the results of experimental work on the dynamic characteristics of a simple blending process should be available in the near future.

Mr. Nichols' suggestion of using larger tank volumes to achieve smaller transient deviations of tank temperature is well made if the speed of response of the blending process under control is not a critical factor, because increasing the time constant of the process also increases the response time of the process under control if the gain of the controller is not changed at the same time.

<sup>4</sup> Manager, Commercial Engineering, Raytheon Manufacturing Company, Waltham, Mass. Mem. ASME.

# The Maximum Temperature Profile in Journal Bearings

By O. PINKUS<sup>1</sup> AND B. STERNLICHT<sup>2</sup>

An expression for the circumferential temperature distribution in the mid-section of a journal bearing is derived which in implicit form presents temperature as a function of angle, with bearing geometry and operating conditions as parameters. This relation is obtained from an analysis of the energy balance between shear losses and heat storage in a hydrodynamic journal bearing under the assumption that no heat is lost to the surroundings. A discussion is given on how to locate the maximum temperature in bearings of common design.

## NOMENCLATURE

The following nomenclature is used in the paper:

- $C$  = radial clearance, in.
- $D$  = shaft diameter, in.
- $J$  = mechanical heat equivalent,  $778 \frac{\text{ft-lb}}{\text{Btu}}$
- $N$  = shaft speed, rpm
- $P$  = bearing load, psi
- $Q$  = oil flow, cu in. per min
- $R$  = shaft radius, in.
- $T$  = temperature, deg F
- $U$  = linear velocity, in. per min
- $W$  = power loss, in-lb/min
- $e$  = eccentricity, in.
- $n = e/C$ , eccentricity ratio, dimensionless
- $x, y, z$  = rectangular co-ordinates
- $C_p$  = specific heat, Btu/in.<sup>3</sup> deg F
- $T_0$  = inlet oil temperature, deg F
- $\alpha, \beta, \gamma$  = viscosity constants
- $\theta$  = angle measured from line of centers (see Fig. 1), radians
- $\theta_0$  = position of oil inlet, radians
- $\mu$  = viscosity,  $\frac{\text{lb-min}}{\text{in.}^2}$

## INTRODUCTION

In the extensive field of lubrication research an important quantity was heretofore unfortunately neglected—the maximum temperature in bearings. Curiously, the temperature rise, outlet minus inlet temperature, received more attention than peak temperatures, but it is the local temperature that is of importance if the bearing is to fail because of overheating.

Obviously one of the reasons for this neglect is the difficulty of arriving at mathematical expressions for the temperature distribution in bearings. Such a distribution is a function of all bearing parameters as well as the operating conditions. As

<sup>1</sup> Journal Bearing Specialist, General Electric Company, West Lynn, Mass. Assoc. Mem. ASME.

<sup>2</sup> Bearing Analysis Specialist, Bearing and Lubricant Center, General Engineering Laboratory, General Electric Company, Schenectady, N. Y.

Contributed by the Lubrication Activity and presented at the Diamond Jubilee Annual Meeting, Chicago, Ill., November 13–18, 1955, of THE AMERICAN SOCIETY OF MECHANICAL ENGINEERS.

NOTE: Statements and opinions advanced in papers are to be understood as individual expressions of their authors and not those of the Society. Manuscript received at ASME Headquarters, February 4, 1955. Paper No. 55—A-212.

shown in this paper an accurate analysis requires also an a priori knowledge of the pressure profile in a given bearing. But no analytical expressions for a two-dimensional pressure distribution exist, and thus the job of obtaining temperature profiles is prejudged from the outset.

There have been several attempts to obtain a relation between angular position and temperature. Hagg (1)<sup>3</sup> and Vogelpohl (2) derived expressions for the temperature distribution which contain the local velocity. This makes the expressions of limited use, as the velocity is unknown and it is a part of the difficult analytical job to handle this velocity in an exact manner. Wilcock and Rosenblatt (3) estimated temperature rises over certain portions of the bearing using rather wide finite spaces of bearing surface. A continuous relationship between angular position and temperature alone was still wanting.

This paper is concerned primarily with maximum temperatures in journal bearings. The maximum temperature in any well-aligned bearing occurs somewhere along the circumferential center line which is also the line of symmetry for the axial pressure distribution. In this central infinitesimal strip oil flows in the circumferential direction and thus a one-dimensional pressure distribution suffices to obtain expressions for oil flow. There is no analytical expression for the central circumferential pressure profile in finite bearings and Sommerfeld's solution was here used as an approximation. Clearly the values of the pressure profile in finite bearings will be lower than those given by the Sommerfeld expression but as mentioned in the Analysis this is offset by the neglected heat transfer, which surely exists in finite bearings. In this infinitesimal central strip a heat balance was set up which in integrated form yields the temperature as a function of angular position from which the maximum temperature can be determined. The analysis here presented can, of course, be refined in the future when analytical expressions for the pressure distribution in finite bearings become available.

The central circumferential temperature profile also can be used to obtain a fair approximation to the two-dimensional temperature plateau by fitting parabolic or sinusoidal curves through the values of the given profile.

## ANALYSIS

One of the basic assumptions in this work is that all the power is dissipated in the oil film in the form of heat. This assumption is a fairly valid one for larger bearings, such as are used in turbines and motors, after they have reached steady-state conditions. In differential form the relation between the power loss in a bearing and the heat storage in the oil flowing through the clearance space is

$$C_p Q dT = \frac{dW}{12 J} \dots \dots \dots [1]$$

Since a relation is desired between the angle  $\theta$  and temperature  $T$ , all quantities have to be expressed in terms of these two variables. The quantities involved are the power loss  $W$  and oil flow  $Q$  which in turn contain the film thickness  $h$  and viscosity  $\mu$ . The film thickness  $h$  can be written as

<sup>3</sup> Numbers in parentheses refer to the Bibliography at the end of the paper.

$$h = C(1 + n \cos \theta) \dots \dots \dots [2]$$

with the geometry of the bearing given in Fig. 1. The viscosity  $\mu$  can be expressed in one of several analytical forms none of which is perfect but accurate enough for a given range of operation. The form chosen here is (5)

$$\mu = \frac{\gamma}{1 + \alpha T + \beta T^2} \dots \dots \dots [3]$$

where the coefficients  $\alpha$ ,  $\beta$ ,  $\gamma$  can be calculated from any three points for a given lubricant.

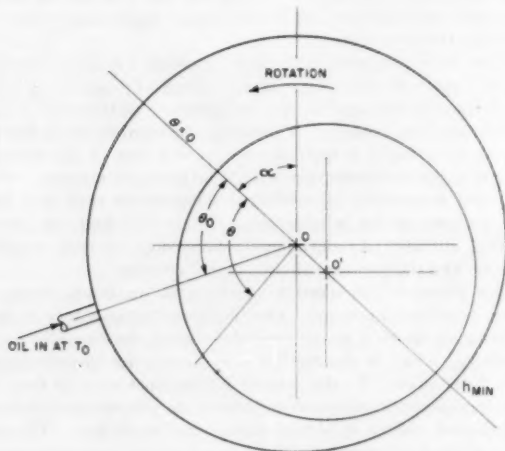


FIG. 1

Using now for oil flow the expression

$$Q = \frac{Uh}{2} - \frac{h^3}{12\mu} \frac{\partial p}{\partial x} \dots \dots \dots [4]$$

and for power loss

$$\begin{aligned} dW &= \mu A U \left. \frac{du}{dy} \right|_{y=0} \\ &= \mu R d\theta U \left[ \frac{U}{h} + \frac{h}{2\mu} \frac{\partial p}{\partial x} \right] \dots \dots \dots [5] \end{aligned}$$

This neglects flow work, the magnitude of which is small in most journal bearings.

$$u = U \left( \frac{h-y}{h} \right) - y \left( \frac{h-y}{2\mu} \right) \frac{\partial p}{\partial x} \dots \dots \dots [6]$$

where

Equation [1] is then transformed into

$$\begin{aligned} C_p dT \left[ \frac{Uh}{2} - \frac{h^3}{12\mu} \frac{dp}{dx} \right] &= \frac{\mu R U d\theta}{12J} \left[ \frac{U}{h} + \frac{h}{2\mu} \frac{dp}{dx} \right] \\ &= \frac{\mu U^2 R}{12hJ} d\theta + \frac{UR}{24J} h \frac{dp}{dx} d\theta \dots \dots \dots [7] \end{aligned}$$

$$\left[ \frac{Uh}{2} - \frac{h^3}{12\mu} \frac{dp}{dx} \right] \frac{dT}{\mu} = \frac{U^2 R}{12C_p h J} d\theta + \frac{UR}{24J C_p \mu} h \frac{dp}{dx} d\theta \dots \dots [8]$$

Substituting Equation [3] in [8]

$$\int_{T_s}^T (1 + \alpha T + \beta T^2) dT = \frac{U^2 R \gamma}{12 C_p J} \int_{\theta_s}^{\theta} \frac{d\theta}{h \left( \frac{Uh}{2} - \frac{h^3}{12\mu} \frac{dp}{dx} \right)} +$$

$$\frac{UR\gamma}{24JC_p} \int_{\theta_s}^{\theta} \frac{h^3 \frac{dp}{dx} d\theta}{\mu h \left( \frac{Uh}{2} - \frac{h^3}{12\mu} \frac{dp}{dx} \right)} \dots \dots \dots [9]$$

(Continued)

Equation [9] contains  $dp/dx$  for which no analytical expression exists for finite bearings. Using Sommerfeld's expression for the pressure distribution in an infinitely long bearing tends to yield lower shear losses and higher flows which would result in lower-temperature rises. However, this is offset by the axial heat conduction and the flow work which surely exists in finite bearings.

Since continuity demands

$$\frac{dQ}{dx} = 0$$

we have

$$\frac{d}{dx} \left( \frac{h^3}{\mu} \frac{dp}{dx} \right) = 6U \frac{dh}{dx}$$

Integrating

$$\frac{dp}{dx} = \frac{6\mu U}{h^2} - \frac{C'}{h^3}$$

we obtain

$$\frac{dp}{d\theta} = \frac{6\mu UR}{C^2} \frac{1}{(1 + n \cos \theta)^2} - \frac{C'}{C(1 + n \cos \theta)^3}$$

with

$$p = p_0 \text{ at } \theta = 0 \text{ and } \theta = 2\pi$$

Integration of this equation with the given limits as performed by Sommerfeld yields

$$p - p_0 = \frac{6n\mu UR}{C^2(2 + n^2)} \left[ \frac{(2 + n \cos \theta) \sin \theta}{(1 + n \cos \theta)^2} \right] \dots \dots [10]$$

differentiating  $p$  with respect to  $\theta$ , and replacing  $d\theta$  by  $dx/R$

$$\frac{dp}{dx} = \frac{6n\mu U}{C^2(2 + n^2)} \frac{(1 + n \cos \theta)^2 [(2 + n \cos \theta) - n \sin^2 \theta] + 2n \sin^2 \theta [(2 + n \cos \theta)(1 + n \cos \theta)]}{(1 + n \cos \theta)^4} \dots \dots [11]$$

Substituting Equations [3] and [11] in the first right-hand integral of Equation [9] and going through a series of manipulations given in the Appendix we obtain

$$\int_{\theta_s}^{\theta} \frac{d\theta}{h \left( \frac{Uh}{2} - \frac{h^3}{12\mu} \frac{dp}{dx} \right)} = \frac{1}{UC^2} \left( \frac{2 + n^2}{1 - n^2} \right) \int_{\theta_s}^{\theta} \frac{d\theta}{1 + n \cos \theta} \dots [12]$$

Substituting Equations [3] and [11] in the second right-hand integral of Equation [9]

$$\begin{aligned} \int_{\theta_s}^{\theta} \frac{h^3 \frac{dp}{dx} d\theta}{\mu h \left( \frac{Uh}{2} - \frac{h^3}{12\mu} \frac{dp}{dx} \right)} &= \frac{1}{UC^2} \left( \frac{2 + n^2}{1 - n^2} \right) \int_{\theta_s}^{\theta} \frac{h^3 \frac{dp}{dx} d\theta}{1 + n \cos \theta} \\ &= \frac{6n}{(1 - n^2)} \left( \frac{\mu}{C^2} \right) \int_{\theta_s}^{\theta} \frac{(2 + n^2) \cos \theta + 3n}{(1 + n \cos \theta)^2} d\theta \dots [13] \end{aligned}$$

Integral [12] is a common integral, and Integral [13] may be integrated by letting

$$(1 + n \cos \theta) = \frac{1 - n^2}{1 - n \cos \phi}$$

The integral of [12] is

$$\frac{2(2+n^2)}{UC(1-n^2)^{3/2}} \left[ \tan^{-1} \left( \frac{\sqrt{1-n^2} \tan \theta/2}{1+n} \right) - \tan^{-1} \left( \frac{\sqrt{1-n^2} \tan \theta_0/2}{1+n} \right) \right] \dots [14]$$

The integral of [13] is

$$\frac{6n}{(1-n^2)^{1/2}} \left( \frac{\mu}{C^2} \right) [n\phi + 2 \sin \phi] \left\{ \begin{array}{l} \phi = \cos^{-1} \frac{n + \cos \theta}{1 + n \cos \theta} \\ \phi_0 = \cos^{-1} \frac{n + \cos \theta_0}{1 + n \cos \theta_0} \end{array} \right\} \dots [15]$$

The complete solution using Equations [9], [14], and [15] is

$$\frac{UR\gamma}{2C_p J C^2 (1-n^2)^{3/2}} \left\{ \left( \frac{2+n^2}{3} \right) \left[ \tan^{-1} \left( \frac{\sqrt{1-n^2} \tan \theta/2}{1+n} \right) - \tan^{-1} \left( \frac{\sqrt{1-n^2} \tan \theta_0/2}{1+n} \right) \right] + \left( \frac{n^2}{2} \right) \left[ \cos^{-1} \left( \frac{n + \cos \theta}{1 + n \cos \theta} \right) - \cos^{-1} \left( \frac{n + \cos \theta_0}{1 + n \cos \theta_0} \right) \right] + n \left[ \sin \cos^{-1} \left( \frac{n + \cos \theta}{1 + n \cos \theta} \right) - \sin \cos^{-1} \left( \frac{n + \cos \theta_0}{1 + n \cos \theta_0} \right) \right] \right\} = \left( T + \frac{\alpha T^3}{2} + \frac{\beta T^3}{3} \right) - \left( T_0 + \frac{\alpha T_0^3}{2} + \frac{\beta T_0^3}{3} \right) \dots [16]$$

Equation [16] may be written in a simplified functional form as follows

$$\frac{3K}{(1-n^2)^{3/2}} [f(\theta) - f(\theta_0)] = g(T) - g(T_0) \dots [17]$$

where

$$K = \frac{UR\gamma}{6C_p J C^2}$$

$$f(\theta) = \left( \frac{2+n^2}{3} \right) \tan^{-1} \left( \frac{\sqrt{1-n^2} \tan \theta/2}{1+n} \right) + \frac{n^2}{2} \cos^{-1} \left( \frac{n + \cos \theta}{1 + n \cos \theta} \right) + n \sin \cos^{-1} \left( \frac{n + \cos \theta}{1 + n \cos \theta} \right)$$

$$g(T) = T + \frac{\alpha T^3}{2} + \frac{\beta T^3}{3}$$

Since Equation [17] is implicit in both  $\theta$  and  $T$ , where  $g(T)$  is a cubic, a graphical method has to be devised to obtain  $T$  as a function of  $\theta$ . With a given oil, the values of  $\alpha$  and  $\beta$  are known and so a general relation of  $g(T)$  versus  $T$  is plotted. Then for any given condition,  $g(T)$  can be calculated and the value of  $T$  picked off from the plot.

#### DISCUSSION

Equation [16] is plotted and compared in Fig. 2 for a particular case of a 13-in-diam bearing running at 3600 rpm and an attitude angle of 18 deg. The curves show that it is not until the eccentricity reaches a value of about 0.6 that an appreciable rise in temperature takes place along the bearing. It is interesting to note that this is also an eccentricity value at which the power losses begin to deviate appreciably from Petroff's expression.

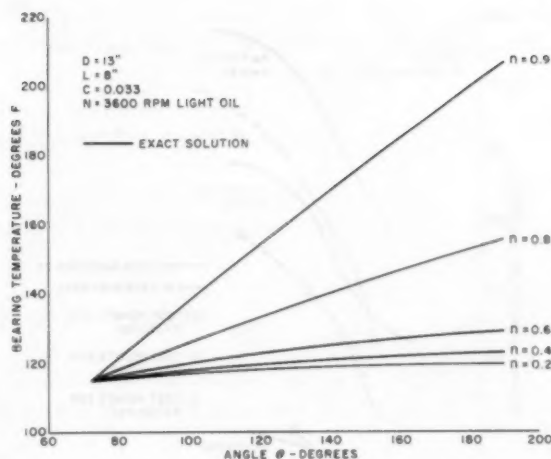


FIG. 2

The point of feeding the oil into the bearing  $\theta_0$  was left in the analysis as a parameter. It is of some interest to note the effect of shifting the inlet-oil groove on the temperature profile. Fig. 3 gives a qualitative picture of one such case. The dotted lines are the result of assuming that the inlet-oil groove is placed at  $\theta_0 = 72$  deg in all cases. The solid lines are the result of shifting the inlet-oil hole as follows

n	Shift, deg
0.9	0
0.8	9
0.6	25
0.4	37
0.2	47

From Fig. 3 it is seen that the percentage error increases with the shift but that a 10-deg shift ( $n = 0.8$ ) has only a small effect on the magnitude of the temperatures.

Some comparisons with test results are shown in Figs. 3 and 4. Considering the inaccuracies involved in determining bearing eccentricity from actual tests, the comparison between the purely theoretical prediction and experimental results seems good indeed. Some of the discrepancy in the upper curve in

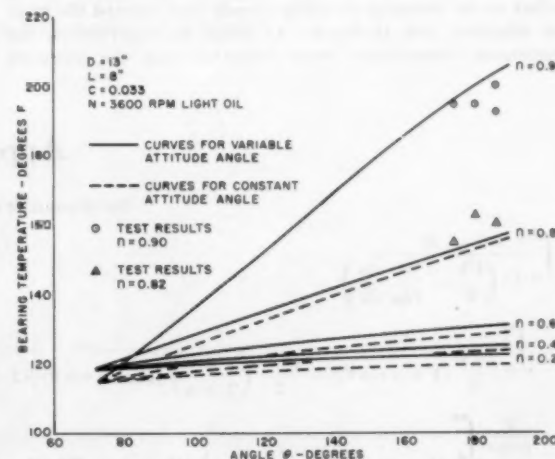


FIG. 3

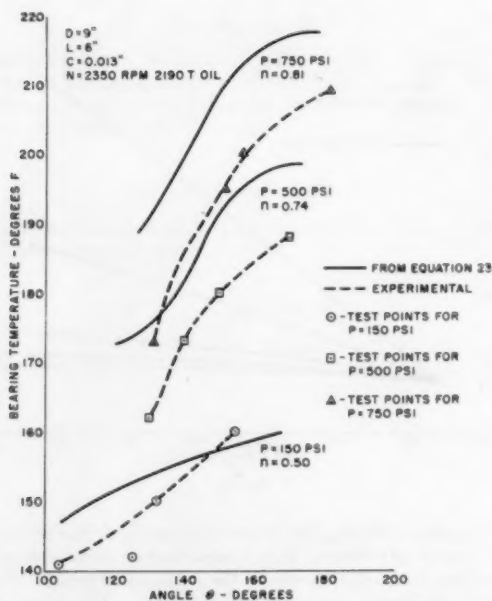


FIG. 4

Fig. 4 can be explained by the fact that the bearing used had two axial grooves at the horizontal split with a very gradual blend of groove and bearing surface and the angular span was not quite known. Thus the location of  $\theta_0$  was a matter of judgment and could easily be in error by 5 deg or more.

Equation [16] gives the maximum temperature at each axial span of a circular bearing. An item of primary interest is the maximum of these maxima, or the over-all maximum temperature in the oil film. The answer to this question will depend on the geometry of the bearing and the lubricating method. If the bearing is of the kind shown in Fig. 5(a), then the maximum temperature will occur just before  $\theta_0$ ; i.e., the oil will continue to absorb heat over a span of  $2\pi$  radians. If, as is more common, the bearing is designed as Fig. 5(b) with oil fed at both ends of the horizontal split, then the maximum temperature will occur before  $\theta_0 + \pi$ . Since cold oil enters at  $\theta_0 + \pi$ , this has a cooling effect on the incoming oil which extends back toward the point of minimum film thickness. As found by experiments, the maximum temperatures occur somewhat past the minimum

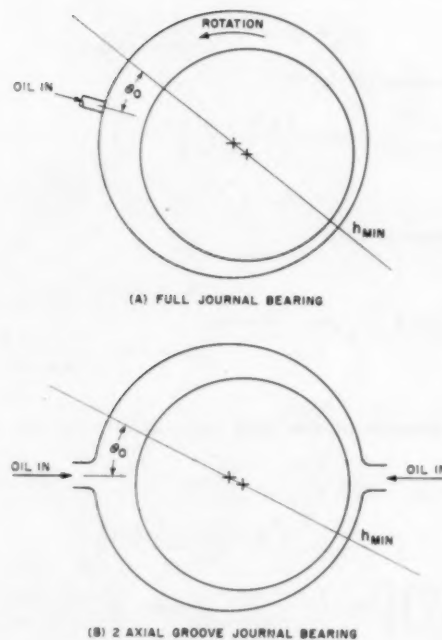


FIG. 5

film thickness. This point also happens to be the upper limit of the validity of Equation [16] as beyond the minimum film thickness the oil film becomes discontinuous and the pressures do not follow the negative values predicted by Sommerfeld's solution.

## BIBLIOGRAPHY

- 1 "Heat Effects in Lubricating Films," by A. C. Hagg, *JOURNAL OF APPLIED MECHANICS*, Trans. ASME, vol. 66, 1944, pp. A-72-A-76.
- 2 "Beitraege zur Kenntnis der Gleitlagerreibung," by G. Vogel-pohl, *VDI-Forschungsheft* 386, 1937; *Oel u. Kohle* 14, 991, 1938.
- 3 "Oil Flow, Key Factor in Sleeve-Bearing Performance," by D. F. Wilcock and M. Rosenblatt, *Trans. ASME*, vol. 74, 1952, pp. 849-866.
- 4 "On the Hydrodynamic Theory of Lubrication," by A. Sommerfeld, *Zeitschrift für Mathematik und Physik*, Band 50, 1904.
- 5 "Lubricant Testing," by E. G. Ellis, Scientific Publication, 1953, p. 45.
- 6 "Friction in the Machine and the Effect of the Lubricant," by N. Petroff, *Engineering Journal*, 1883, No. 1, 2, 4.

## Appendix

## DEVELOPMENT OF EQUATION [9]

$$\begin{aligned}
 & \int_{\theta_0}^{\theta} \frac{d\theta}{h^3 \left( \frac{Uh}{2} - \frac{h^3}{12\mu} \frac{dp}{dx} \right)} \\
 &= \int_{\theta_0}^{\theta} \frac{UCr^2}{2(1+n \cos \theta)^2} - \frac{UCr^2}{2} \left( \frac{n}{2+n} \right) \frac{d\theta}{\{(1+n \cos \theta)^2[(2+n \cos \theta) \cos \theta - n \sin^2 \theta] + 2n \sin^2 \theta[(2+n \cos \theta)(1+n \cos \theta)]\}} \\
 &= \frac{2}{UCr^2} \int_{\theta_0}^{\theta} \frac{d\theta}{[1+n \cos \theta]^2 - \left( \frac{n}{2+n} \right) \{(1+n \cos \theta)^2[(2+n \cos \theta) \cos \theta - n \sin^2 \theta] + 2n \sin^2 \theta[(2+n \cos \theta)(1+n \cos \theta)]\}}
 \end{aligned}$$

$$\begin{aligned}
&= \int_{\theta_0}^{\theta} \frac{d\theta}{(1+n \cos \theta)^2 - \frac{n}{2+n^2} \{ (1+n \cos \theta)^2 [(2+n \cos \theta) \cos \theta - n \sin^2 \theta] + 2n \sin^2 \theta (1+n \cos \theta) + 2n \sin^2 \theta (1+n \cos \theta)^2 \}} \\
&= \int_{\theta_0}^{\theta} \frac{d\theta}{(1+n \cos \theta)^2 - \frac{n}{2+n^2} \{ (1+n \cos \theta)^2 [(2+n \cos \theta) \cos \theta + n \sin^2 \theta] + 2n \sin^2 \theta (1+\cos \theta) \}} \\
&= \int_{\theta_0}^{\theta} \frac{d\theta}{(1+n \cos \theta)^2 - \left( \frac{n}{2+n^2} \right) \{ (1+n \cos \theta)^2 [2 \cos \theta + n \cos^2 \theta + n \sin^2 \theta] + 2n \sin^2 \theta (1+n \cos \theta) \}} \\
&= \int_{\theta_0}^{\theta} \frac{d\theta}{(1+n \cos \theta)^2 - \frac{n}{2+n^2} \{ (1+n \cos \theta)^2 (n+2 \cos \theta) + 2n \sin^2 \theta (1+n \cos \theta) \}} \\
&= \int_{\theta_0}^{\theta} \frac{d\theta}{(1+n \cos \theta)^2 - \frac{n}{2+n^2} \{ n(1+n \cos \theta)^2 + 2 \cos \theta (1+2n \cos \theta + n^2 \cos^2 \theta) + 2n \sin^2 \theta + 2n^2 \sin^2 \theta \cos \theta \}} \\
&= \int_{\theta_0}^{\theta} \frac{d\theta}{(1+n \cos \theta)^2 - \frac{n}{2+n^2} \{ n(1+n \cos \theta)^2 + 2 \cos \theta (1+2n \cos \theta) + 2n^2 \cos^2 \theta \cos \theta + 2n \sin^2 \theta + 2n^2 \sin^2 \theta \cos \theta \}} \\
&= \int_{\theta_0}^{\theta} \frac{d\theta}{(1+n \cos \theta)^2 - \frac{n}{2+n^2} \{ n(1+n \cos \theta)^2 + 2 \cos \theta (1+2n \cos \theta) + 2n^2 \cos \theta + 2n \sin^2 \theta \}} \\
&= \int_{\theta_0}^{\theta} \frac{d\theta}{(1+n \cos \theta)^2 - \frac{n}{2+n^2} \{ n(1+n \cos \theta)^2 + 2 \cos \theta + 2n \cos^2 \theta + 2 \cos^2 \theta + 2n^2 \cos \theta + 2n \sin^2 \theta \}} \\
&= \int_{\theta_0}^{\theta} \frac{d\theta}{(1+n \cos \theta)^2 - \left( \frac{n}{2+n^2} \right) \{ n(1+n \cos \theta)^2 + 2 \cos \theta + 2n \cos^2 \theta + 2n^2 \cos \theta + 2n \}} \\
&= \int_{\theta_0}^{\theta} \frac{d\theta}{(1+n \cos \theta)^2 - \frac{n}{2+n^2} \{ n(1+n \cos \theta)^2 + 2n(1+n \cos \theta) + 2 \cos \theta (1+n \cos \theta) \}} \\
&= \int_{\theta_0}^{\theta} \frac{d\theta}{\left[ 1 - \frac{n^2}{2+n^2} \right] (1+n \cos \theta)^2 - \frac{2n}{2+n^2} (1+n \cos \theta) (n+\cos \theta)} \\
&= \int_{\theta_0}^{\theta} \frac{d\theta}{\left[ \frac{2+n^2-n^2}{2+n^2} \right] (1+2n \cos \theta + n^2 \cos^2 \theta) - \left( \frac{2n}{2+n^2} \right) [n + (1+n^2) \cos \theta + n \cos^2 \theta]} \\
&= (2+n^2) \int_{\theta_0}^{\theta} \frac{d\theta}{(2-2n^2) + (4n-2n-2n^2) \cos \theta} \\
&= (2+n^2) \int_{\theta_0}^{\theta} \frac{d\theta}{(2-2n^2) + n(2-2n^2) \cos \theta} \\
&= \frac{1}{2} \left( \frac{2+n^2}{1-n^2} \right) \int_{\theta_0}^{\theta} \frac{d\theta}{1+n \cos \theta}
\end{aligned}$$

1. The first part of the document is a list of names and addresses.

2. The second part of the document is a list of names and addresses.

3. The third part of the document is a list of names and addresses.

4. The fourth part of the document is a list of names and addresses.

5. The fifth part of the document is a list of names and addresses.

6. The sixth part of the document is a list of names and addresses.

7. The seventh part of the document is a list of names and addresses.

8. The eighth part of the document is a list of names and addresses.

9. The ninth part of the document is a list of names and addresses.

10. The tenth part of the document is a list of names and addresses.

11. The eleventh part of the document is a list of names and addresses.

12. The twelfth part of the document is a list of names and addresses.

13. The thirteenth part of the document is a list of names and addresses.

14. The fourteenth part of the document is a list of names and addresses.

15. The fifteenth part of the document is a list of names and addresses.

16. The sixteenth part of the document is a list of names and addresses.

17. The seventeenth part of the document is a list of names and addresses.

18. The eighteenth part of the document is a list of names and addresses.

# Temperature Distribution in the Journal-Bearing Lubricant Film

BY M. B. PURVIS,<sup>1</sup> W. E. MEYER,<sup>2</sup> AND T. C. BENTON<sup>3</sup>

The equations for the adiabatic temperature distribution in the journal bearing are obtained for both the infinite bearing and the short bearing. The solutions are obtained by treating viscosity and density as functions of temperature. The solution shows that the lubricant temperature increases as it flows through the bearing and that the temperature rises as long as the film remains continuous. Since the film becomes discontinuous shortly after the point of minimum film thickness, the point of minimum film may be taken as the point of maximum temperature. A numerical example showing comparison with experimental data is presented.

## NOMENCLATURE

The following nomenclature is used in the paper:

- $a = \frac{1+n}{1-n}$   
 $c$  = specific heat, in lb/lb deg F  
 $c_r$  = radial clearance between bearing and journal, in.  
 $D$  = diameter of journal, in.  
 $h$  = film thickness, in.  
 $h_{\min}$  = minimum film thickness, in.  
 $h_{p\max}$  = film thickness at point of maximum film pressure  
 $n$  = eccentricity ratio,  $1 - h_{\min}/c_r$   
 $p$  = pressure, psi  
 $R_j$  = radius of journal, in.  
 $T$  = temperature  
 $U$  = constant velocity of surface in the  $x$  direction, ips  
 $x, y$  = Cartesian co-ordinates referred to rectangular system;  
 $x$  is related to circumferential direction,  $y$  is related to axial direction  
 $\beta$  = temperature coefficient of viscosity, per deg F  
 $\psi, \eta$  = Lagrangian constants  
 $\theta$  = cylindrical co-ordinate measured from position opposite point of minimum film thickness  
 $\lambda$  = temperature coefficient of density, per deg F  
 $\mu$  = viscosity, lb sec/sq in.  
 $\rho$  = density, pci  
 $l$  = length of bearing, in.

## INTRODUCTION

The treatments of journal-bearing theory that have appeared to date have for the most part dealt with the isothermal lubricant film in which the lubricant is assumed to remain at its initial tem-

perature as it flows through the bearing. Thus, for example, the treatments of Reynolds, Sommerfeld, and more recently, that of Ocvirk have taken this approach.

Complementing this approach is the other limiting case of an adiabatic film in which all the frictional heat developed is assumed to be carried away by the lubricant film. The temperature rises in an element of the oil film as it flows through a bearing due to the action of the shearing and pressure forces, and the deviation of the temperature rise of the lubricant element from the adiabatic temperature rise will be a function of the heat transfer from the element due to conduction to the bearing and journal.

This paper solves the problem of the adiabatic temperature distribution in the journal bearing for the bearing of infinite length as well as for the short journal bearing in which flow resulting from the circumferential pressure gradient is assumed small compared with the flow due to journal surface velocity. Neither solution takes into account the effect of pressure on viscosity. Internal energy is assumed a function of temperature and the specific heat of the lubricant must be taken constant at the mean value for the predicted temperature rise. In both solutions the effect of temperature on viscosity and density is taken into account exactly and in the latter solution the effect of side leakage is treated.

## BASIC EQUATIONS

Cope (1)<sup>4</sup> has presented the fundamental equations defining the lubrication phenomena when all the lubricant properties are assumed variable.

Reynolds equation may be expressed as

$$\frac{\partial}{\partial x} \rho \left[ \frac{Uh}{2} - \frac{h^3}{12\mu} \frac{\partial p}{\partial x} \right] + \frac{\partial}{\partial y} \rho \left[ -\frac{h^3}{12\mu} \frac{\partial p}{\partial y} \right] = 0 \dots [1]$$

The energy equation may be expressed as

$$\begin{aligned} \rho c \left[ \left( \frac{Uh}{2} - \frac{h^3}{12\mu} \frac{\partial p}{\partial x} \right) \frac{\partial T}{\partial x} + \left( -\frac{h^3}{12\mu} \frac{\partial p}{\partial y} \right) \frac{\partial T}{\partial y} \right] \\ = \left( \frac{\mu U^2}{h} + \frac{Uh}{2} \frac{\partial p}{\partial x} \right) - \left[ \left( \frac{Uh}{2} - \frac{h^3}{12\mu} \frac{\partial p}{\partial x} \right) \frac{\partial p}{\partial x} \right. \\ \left. - \left( \frac{h^3}{12\mu} \frac{\partial p}{\partial y} \right) \frac{\partial p}{\partial y} \right] \dots [2] \end{aligned}$$

Inherent in the foregoing expressions are the assumptions of negligible weight and inertia of the lubricant, and constancy of temperature, pressure, density, and viscosity through the lubricant film. It is the assumption of constant temperature through the lubricant film which reduces the basic equations to the adiabatic solution. The internal energy is assumed to be a function of temperature and the specific heat is treated as a constant. Osterle (2, 3) also has used as an adequate representation of the variation of viscosity and density with temperature the expressions

$$\mu = \mu_0 e^{\beta T} \quad \text{and} \quad \rho = \rho_0 e^{\lambda T} \dots [3]$$

where  $\mu_0$  and  $\rho_0$  are chosen for such scales of temperature that

<sup>4</sup> Numbers in parentheses refer to the Bibliography at the end of the paper.

<sup>1</sup> Member, Technical Staff, Bell Telephone Laboratories, Whippany, N. J. Assoc. Mem. ASME.

<sup>2</sup> Professor, Engineering Research, Pennsylvania State University, University Park, Pa.

<sup>3</sup> Professor, Department of Mathematics, Pennsylvania State University, University Park, Pa.

Contributed by the Lubrication Activity and presented at the Diamond Jubilee Annual Meeting, Chicago, Ill., November 13-18, 1955, of THE AMERICAN SOCIETY OF MECHANICAL ENGINEERS.

NOTE: Statements and opinions advanced in papers are to be understood as individual expressions of their authors and not those of the Society. Manuscript received at ASME Headquarters, November 16, 1955. Paper No. 55-A-216.

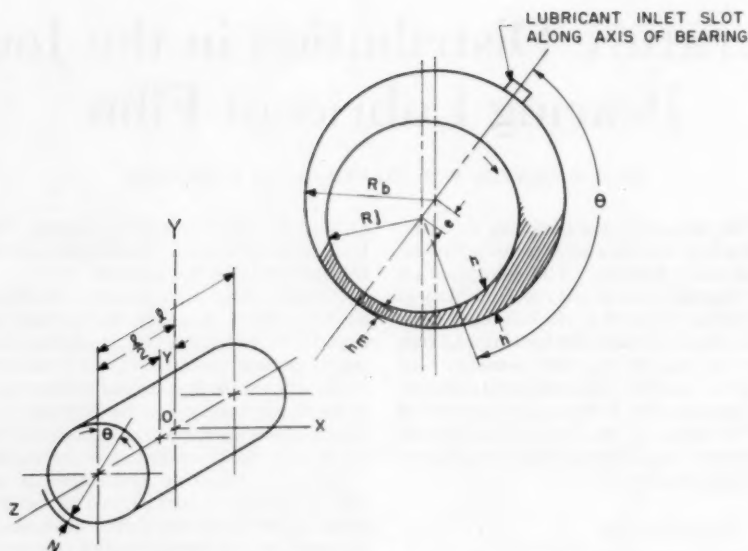


FIG. 1 FILM CONFIGURATION AND CO-ORDINATE SYSTEM

$T_0$ , the reference temperature, is zero. The effect of pressure on viscosity and density is not included in the solutions to follow. For these two simultaneous equations there are two desired solutions. These are:

- 1 The infinite-bearing solution.
- 2 The short-bearing solution.

The co-ordinate system is indicated in Fig. 1.

#### INFINITE-BEARING SOLUTION

For the infinitely long bearing, flow in the  $y$ -direction is zero, and the Reynolds equation reduces to

$$\frac{\partial}{\partial x} \left( \frac{Uh}{2} - \frac{h^3}{12\mu} \frac{\partial p}{\partial x} \right) = 0 \dots \dots \dots [4]$$

The energy equation to the same approximation becomes

$$\frac{\mu U^2}{h} + \frac{h^3}{12\mu} \left( \frac{\partial p}{\partial x} \right)^2 = \frac{\rho c U h}{2} \frac{\partial T}{\partial x} - \frac{\rho c h^3}{12\mu} \frac{\partial p}{\partial x} \frac{\partial T}{\partial x} \dots [5]$$

Solving the equations for the temperature gradient in the  $x$ -direction

$$\frac{\partial T}{\partial x} = \frac{2\mu U}{\rho c h^2 r} [1 + 3(1 - r)^2] \dots \dots \dots [6]$$

where  $r$  equals  $h_{p \max}/h$ .

For the journal bearing the following substitutions can be made

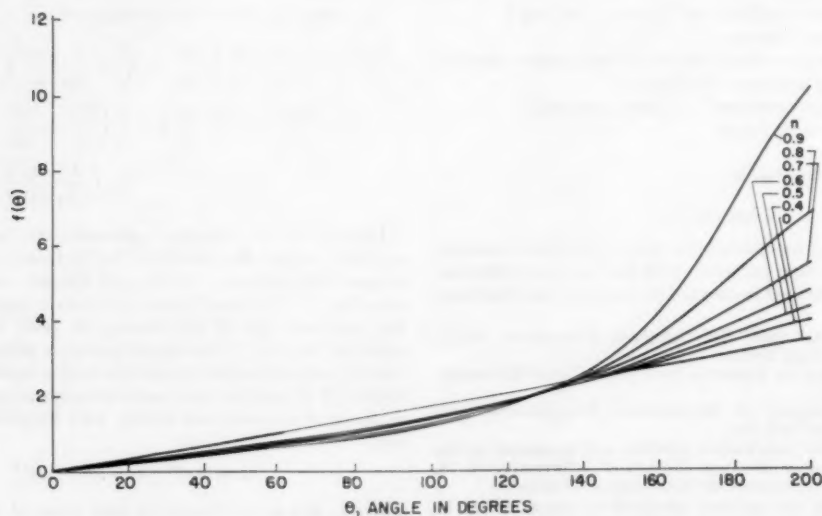


FIG. 2 GRAPH OF  $\int \frac{d\theta}{1 + n \cos \theta}$  VERSUS  $\theta$  FOR SEVERAL VALUES OF  $n$

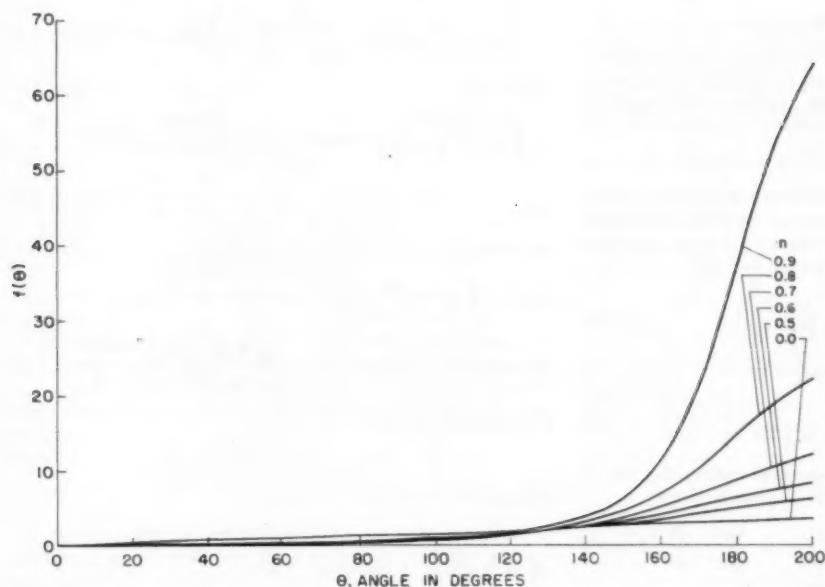
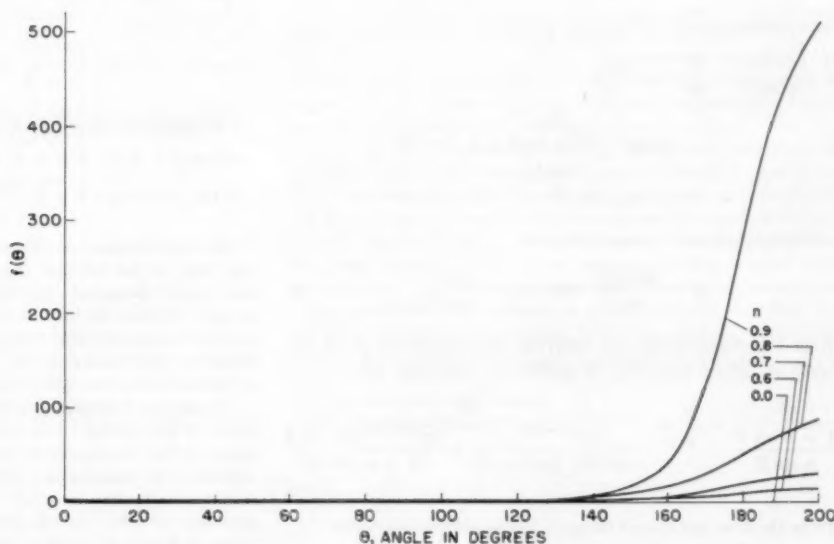


FIG. 3 GRAPH OF  $\int \frac{d\theta}{(1+n \cos \theta)^2}$  VERSUS  $\theta$  FOR SEVERAL VALUES OF  $n$

FIG. 4 GRAPH OF  $\int \frac{d\theta}{(1+n \cos \theta)^3}$  VERSUS  $\theta$  FOR SEVERAL VALUES OF  $n$



$$\left. \begin{aligned} h &= c_r(1 + n \cos \theta) \\ x &= R_i \theta \end{aligned} \right\} \dots \dots \dots [7]$$

Substitution of Equations [3] and [7] in [6] gives

$$\frac{dT}{R_i d\theta} = \frac{8U\mu_0}{c\rho_0 c_r h_{p \max} e^{(\lambda-\beta)T} (1+n \cos \theta)} - \frac{12U\mu_0}{c\rho_0 c_r^2 e^{(\lambda-\beta)T} (1+n \cos \theta)^2} + \frac{6U\mu_0 h_{p \max}}{c\rho_0 c_r e^{(\lambda-\beta)T} (1+n \cos \theta)^3} \dots \dots [8]$$

Solving for the temperature at any angle  $\theta_2$  for which the film is continuous

$$T_{\theta_2} = \frac{1}{(\lambda - \beta)} \ln [(\lambda - \beta)f(\theta) + e^{(\lambda - \beta)T_{\theta_1}}] \dots \dots [9]$$

where

$$f(\theta) = \frac{8UR_i \mu_0}{c\rho_0 c_r h_{p \max}} \int_{\theta_1}^{\theta_2} \frac{d\theta}{(1+n \cos \theta)} - \frac{12UR_i \mu_0}{c\rho_0 c_r^2} \int_{\theta_1}^{\theta_2} \frac{d\theta}{(1+n \cos \theta)^2} + \frac{6UR_i h_{p \max} \mu_0}{c\rho_0 c_r^3} \int_{\theta_1}^{\theta_2} \frac{d\theta}{(1+n \cos \theta)^3} \dots \dots [10]$$

Graphs of the integrals for several values of  $n$  are presented in Figs. 2 to 4.

## SHORT-BEARING SOLUTION

Ocvirk (4), following the method originally proposed by Michell and Cardullo, has developed a solution to the Reynolds equation which is particularly appropriate for bearings with length-to-diameter ratios of 2 or less. This solution is predicated on the assumption that the term,  $\frac{h^3}{12\mu} \frac{\partial p}{\partial x}$ , will be small compared to the term  $Uh/2$ . This solution thus includes the portion of the circumferential flow due to journal surface velocity, and neglects the portion of the flow due to circumferential pressure gradient. For this condition the Reynolds equation becomes

$$\frac{\partial}{\partial x} \left( \frac{Uh}{2} \right) = \frac{\partial}{\partial y} \left( \frac{h^3}{12\mu} \frac{\partial p}{\partial y} \right) \quad [11]$$

The energy equation to the same approximation becomes

$$\frac{\mu U^2}{h} + \frac{h^3}{12\mu} \left( \frac{\partial p}{\partial y} \right)^2 = \rho c \left( \frac{Uh}{2} \frac{\partial T}{\partial x} - \frac{h^3}{12\mu} \frac{\partial p}{\partial y} \frac{\partial T}{\partial y} \right) \quad [12]$$

Again, taking the equations simultaneously and writing the resulting equation so as to put it into the Lagrangian form

$$\frac{h}{\left( \frac{\partial h}{\partial x} \right)} \frac{\partial T}{\partial x} - y \frac{\partial T}{\partial y} = \frac{2\mu U}{\rho c} \frac{\partial h}{\partial x} + \frac{6\mu U}{\rho c h^3} \frac{\partial h}{\partial x} y^2 \quad [13]$$

Substituting into the cylindrical co-ordinate system

$$\begin{aligned} \frac{(1+n \cos \theta)}{-n \sin \theta} \frac{\partial T}{\partial \theta} - y \frac{\partial T}{\partial y} &= - \frac{2\mu_0 U R_f}{c \rho c_r^2 e^{(\lambda-\beta)T} n \sin \theta (1+n \cos \theta)} \\ &\quad - \frac{6\mu_0 U n \sin \theta y^2}{c \rho c_r^2 R_f e^{(\lambda-\beta)T} (1+n \cos \theta)^3} \quad [14] \end{aligned}$$

For the purpose of manipulation let

$$a_1 = \frac{2\mu_0 U R_f}{c \rho c_r^2} \quad \text{and} \quad a_2 = \frac{6\mu_0 U}{c \rho c_r^2 R_f} \quad [15]$$

With this substitution and applying the usual method for the Lagrange linear equation, the subsidiary equations are

$$\frac{d\theta}{1+n \cos \theta} = \frac{dy}{y} = \frac{dT}{\frac{a_1 e^{(\beta-\lambda)T}}{n \sin \theta (1+n \cos \theta)} + \frac{a_2 e^{(\beta-\lambda)T} y^2 n \sin \theta}{(1+n \cos \theta)^3}} \quad [16]$$

From the first and second terms of the subsidiary equations

$$-\frac{n \sin \theta d\theta}{1+n \cos \theta} - \frac{dy}{y} = 0 \quad [17]$$

Integrating

$$y(1+n \cos \theta) = \psi \quad y = \frac{\psi}{(1+n \cos \theta)} \quad [18]$$

From the first and third terms of the subsidiary equations

$$\begin{aligned} \frac{n \sin \theta}{1+n \cos \theta} \left[ \frac{a_1}{n \sin \theta (1+n \cos \theta)} \right. \\ \left. + \frac{a_2 y^2 n \sin \theta}{(1+n \cos \theta)^3} \right] d\theta = e^{(\lambda-\beta)T} dT \quad [19] \end{aligned}$$

Substituting for  $y$  in this equation

$$\left[ \frac{a_1}{(1+n \cos \theta)^2} + \frac{a_2 \psi^2 n^2 \sin^2 \theta}{(1+n \cos \theta)^5} \right] d\theta = e^{(\lambda-\beta)T} dT \quad [20]$$

Integrating

$$\begin{aligned} a_1 \int \frac{d\theta}{(1+n \cos \theta)^2} + a_2 \psi^2 n^2 \int \frac{\sin^2 \theta d\theta}{(1+n \cos \theta)^5} \\ = \frac{e^{(\lambda-\beta)T}}{\lambda-\beta} + \eta \quad [21] \end{aligned}$$

Substituting back for  $\psi$  and solving for  $\eta$

$$\begin{aligned} \eta = a_1 \int \frac{d\theta}{(1+n \cos \theta)^2} \\ + a_2 y^2 (1+n \cos \theta)^2 n^2 \int \frac{\sin^2 \theta d\theta}{(1+n \cos \theta)^5} - \frac{e^{(\lambda-\beta)T}}{\lambda-\beta} \quad [22] \end{aligned}$$

For a general solution

$$\varphi(\psi, \eta) = 0 \quad [23]$$

Assume the solution

$$\eta = b_1 \psi + b_2$$

where  $b_1$  and  $b_2$  are constants. Then

$$\begin{aligned} a_1 \int \frac{d\theta}{(1+n \cos \theta)^2} + a_2 y^2 n^2 (1+n \cos \theta)^2 \int \frac{\sin^2 \theta d\theta}{(1+n \cos \theta)^5} \\ - \frac{e^{(\lambda-\beta)T}}{\lambda-\beta} = b_1 y (1+n \cos \theta) + b_2 \quad [24] \end{aligned}$$

The boundary conditions are as follows:

When  $y = 0$  and  $\theta = 0$ ,  $T = T_{\theta=0}$

When  $y = 0$  and  $\theta = 0$ ,  $\frac{\partial T}{\partial y} = 0$

The first boundary condition is established from the consideration that at the inlet to the bearing the temperature may be most easily measured and thus its viscosity most easily determined. Because the inlet has been chosen to coincide with  $\theta = 0$ , and by making provision to introduce the lubricant centrally with respect to the bearing,  $y$  also becomes zero. Thus a knowledge of the inlet-lubricant temperature is necessary.

The second boundary condition is established from the symmetry of the bearing. The ordinate  $y$  is taken as zero at the mid-plane of the bearing length so that it is reasonable to assume variations in temperature will be defined in terms of distance from the center line, and that due to symmetry the variation with direction be zero. It will be noted for this boundary that the value of  $\theta$  may be taken at any  $\theta$  for which the film is assumed continuous. Thus values of 0 or  $\pi$  logically lend themselves to this boundary.

Applying the first of the boundary conditions to Equation [24]

$$\frac{e^{(\lambda-\beta)T_{\theta=0}}}{\lambda-\beta} = b_2 \quad [25]$$

Applying the second of the boundary conditions by differentiating Equation [24] with respect to  $y$

$$\begin{aligned} b_1 (1+n \cos \theta) = 2a_2 y n^2 (1+n \cos \theta)^2 \int_0^\theta \frac{\sin^2 \theta d\theta}{(1+n \cos \theta)^5} \\ - e^{(\lambda-\beta)T} \frac{\partial T}{\partial y} \quad [26] \end{aligned}$$

when

$$y = 0 \text{ and } \theta = 0, \quad \frac{\partial T}{\partial y} \text{ and } b_1 = 0 \dots \dots [27]$$

The solution then becomes

$$a_1 \int_0^\theta \frac{d\theta}{(1+n \cos \theta)^2} + a_2 y^2 n^2 (1+n \cos \theta)^2 \int_0^\theta \frac{\sin^2 \theta d\theta}{(1+n \cos \theta)^4} \\ = \frac{e^{(\beta-\lambda)T_\theta} - e^{(\beta-\lambda)T_{\theta=0}}}{\lambda - \beta} \dots \dots [28]$$

#### SPECIAL SOLUTIONS

There are three special solutions of those equations which are of interest.

The first special solution is that of the unloaded bearing. In this instance  $n = 0$ . In the infinite-bearing solution for this case  $h_{p \max}$  equals  $c_r$  since the bearing and journal operate concentrically.  $\theta$  may be taken as zero. The infinite-bearing solution then reduces to

$$T_\theta = \frac{1}{\lambda - \beta} \ln \left[ \frac{2(\lambda - \beta)UR_i \mu_{r\theta}}{c\rho c_r^2} + e^{(\lambda - \beta)T_{\theta=0}} \right] \dots [29]$$

In the short-bearing solution for this case the second term vanishes in accordance with the assumption and the solution (Equation [28]) reduces immediately to Equation [29]. This would follow since in the absence of a pressure gradient, the short bearing would have no end leakage to cause deviation from the infinite bearing. Equation [29] might be used in predicting the temperature rise for an element of lubricant flowing through a rotational viscometer.

The second special solution is that of the temperature distribution for  $\theta = \pi$ , the point of closest approach of the journal to the bearing.

For this case the short-bearing solution becomes

$$\frac{e^{(\lambda - \beta)T_\pi} - e^{(\lambda - \beta)T_{\theta=0}}}{\lambda - \beta} \\ = \frac{\mu_0 UR_i \pi}{\rho_0 c_r^2} \left[ \frac{2}{(1-n^2)^{3/2}} - 3n^2(1-n)^2 \left( \frac{y}{R_i} \right)^2 \right. \\ \left. \left( \frac{7 + 9a^2 + 9a^4 + 7a^6}{32a^3} \right) \right] \dots \dots [30]$$

At the edge of the bearing  $y = l/2$  and the expression becomes

$$\frac{e^{(\lambda - \beta)T_\pi} - e^{(\lambda - \beta)T_{\theta=0}}}{\lambda - \beta} = \frac{\mu_0 UR_i \pi}{\rho_0 c_r^2} \left[ \frac{2}{(1-n^2)^{3/2}} \right. \\ \left. - 3n^2(1-n)^2 \left( \frac{l}{D} \right)^2 \left( \frac{7 + 9a^2 + 9a^4 + 7a^6}{32a^3} \right) \right] \dots \dots [31]$$

The second term represents the variation in the edge temperature from the center-line temperature at the point of closest approach. Since the film becomes discontinuous at or shortly after the point of minimum film thickness, the expression approximates the condition at the exit of the continuous film.

Christopherson (5) states, "It is found that the exit temperature does not vary appreciably across the bearing, but it has not been found possible to demonstrate analytically that this must be the case."

Examination of Equation [31] shows that for all values of  $n$ , the second term within the expression is, at best,  $10^{-3}$  of the first term, and that the significance of the second term decreases as the value of  $n$  increases. It is for this reason that the temperature variation from the center-line value is negligible at the exit from the lubricant film.

The third special solution gives the temperature rise in a lubricant film where the viscosity and density are based, not on  $T = 0$ , but on  $T = T_{\theta=0}$ . The significance of this solution is that it shows the temperature rise in the film from the lubricant inlet point to the desired value of  $\theta$ . Then

$$\mu = \mu_{r\theta=0} e^{\beta(T - T_{\theta=0})} \text{ and } \rho = \rho_{r\theta=0} e^{\lambda(T - T_{\theta=0})}$$

The center-line temperature solution for the short bearing may then be expressed as

$$\frac{e^{(\lambda - \beta)(T_\theta - T_{\theta=0})} - e^{(\lambda - \beta)(T_{\theta=0} - T_{\theta=0})}}{\lambda - \beta} \\ = \frac{2\mu_{r\theta=0} UR_i}{\rho_{r\theta=0} c_r^2} \int_0^\theta \frac{d\theta}{(1+n \cos \theta)^2} \dots \dots [32]$$

Solving for the temperature rise

$$T_\theta - T_{\theta=0} = \frac{1}{\lambda - \beta} \ln \left[ \frac{2(\lambda - \beta)UR_i \mu_{r\theta=0}}{c\rho_{r\theta=0} c_r^2} \int_0^\theta \frac{d\theta}{(1+n \cos \theta)^2} + 1 \right] \dots \dots [33]$$

#### NUMERICAL EXAMPLE

Clayton and Wilkie (6) have devoted a portion of their experimental program to determining whether the maximum temperature at the surface of the bearing was abnormally high at the point of closest approach compared with the mean of the pressure region. Their results are presented as a series of isotherms plotted over the developed bearing surface.

To compute a temperature rise for one of their conditions of operation, it was found necessary to assume values of some of the variables involved. The specific heat was taken as 0.49 Btu/lb deg R (4570 in. lb/lb deg F); the density was assumed as 57.5 pcf (0.0333 lb/cu in.);  $\beta$  was calculated to be  $-0.0163/\text{deg F}$  from the given viscosity data. The variation of the density with temperature is neglected since the value of the density is assumed.

The minimum film thickness is given as 0.0002 in. which, for the stated diametral clearance of 0.0025 in., gives an eccentricity ratio of 0.84. The bearing load is 1500 psi at 3000 rpm. Temperature of inlet oil is 84 C (183 F) at which temperature the viscosity is  $3.84 \times 10^{-6}$  reyns.

For these conditions

$$a_1 = \frac{2\mu_{r\theta=0} UR_i}{\rho c_r^2} = 11$$

$$\int_0^\pi \frac{d\theta}{(1+n \cos \theta)^2} = 19.68 \text{ for } n = 0.84$$

Substituting into Equation [33] yields a temperature rise of 93 deg F so that  $T_\pi$  equals 276 F compared with 232 F observed.

At 4000 rpm with the same oil-inlet temperature,  $T_\pi$  is estimated by similar calculation to be 290 F compared with 250 F observed.

The higher value of temperature predicted by Equation [33] is not unreasonable since there are the factors of heat loss and thermal recirculation within the bearing which will reduce the maximum temperature from that predicted. The data of Clayton and Wilkie clearly show the existence of a thermal sink near the oil inlet in their bearing.

#### CONCLUSIONS

This paper has shown that the adiabatic solution for the short

journal bearing can be used, where the physical properties of the lubricant are defined or can be reasonably estimated, to predict the limiting temperature that can occur in the lubricant film of a journal bearing.

The film is shown to reach its maximum temperature when it becomes discontinuous, and since this point of discontinuity occurs shortly after the point of closest approach, the maximum film temperature may be assumed for all practical purposes to occur at the point of minimum film thickness.

Because of the high oil-flow rates used in modern bearing practice, the possibility of bearing failure exists where the criterion of performance is based on a bulk oil temperature from the bearing. There have been many cases (7) in which poorly placed thermometers have failed to indicate a significant rise in temperature during failure of the bearing. This can occur when the small amount of hot oil issuing from the lubricant film is diluted in the excess oil so that the temperature of the oil mixture leaving the bearing is well within the safe operational limits. The maximum film temperature estimated by the equations of the paper rather than the oil-discharge temperature is a truer value of the critical temperature for the conditions of operation in bearing performance.

#### BIBLIOGRAPHY

- 1 "The Hydrodynamical Theory of Film Lubrication," by W. F. Cope, Proceedings of the Royal Society of London, England, vol. 197, 1949, p. 201.
- 2 "On the Solution of the Reynolds Equation for Slider-Bearing Lubrication IV: Effect of Temperature on Viscosity," by F. Osterle, A. Charnes, and E. Saibel, Trans. ASME, vol. 75, 1953, pp. 1117-1123.
- 3 "On the Solution of the Reynolds Equation for Slider-Bearing Lubrication VI: The Parallel-Surface Slider Bearing Without Side Leakage," by F. Osterle, A. Charnes, and E. Saibel, Trans. ASME, vol. 75, 1953, pp. 1133-1136.
- 4 "Short-Bearing Approximation for Full Journal Bearings," by F. W. Oevirk, NACA TN 2808, October, 1952.
- 5 "A New Mathematical Method for the Solution of Film Lubrication Problems," by D. G. Christopherson, Proceedings of The Institution of Mechanical Engineers, London, England vol. 146, 1941, p. 126.
- 6 "Temperature Distribution in the Bush of a Journal Bearing," by D. Clayton and M. J. Wilkie, *Engineering*, vol. 166, 1948, p. 49.
- 7 "Journal Bearing Oil Film Temperature Measured System," Bureau of Ships Journal, vol. 3, no. 2, June, 1954, p. 39.

#### Discussion

J. A. COLE.<sup>\*</sup> The center-line temperature distribution for a narrow bearing, given in Equation [33] of the paper, may be deduced more simply as follows, using the same notation as in the paper:

Consider a segmental element of clearance space subtending  $d\theta$

<sup>\*</sup> Department of Scientific and Industrial Research, Mechanics Engineering Research Laboratory, Lubrication and Wear Division, Thorntonhall, Glasgow, Scotland.

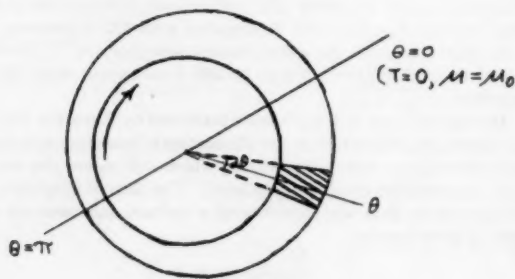


Fig. 5

in Fig. 5 of this discussion. Assuming that simple shear predominates and that pressure gradients are relatively small

$$\begin{aligned}\text{Energy input} &= \mu \left( \frac{du}{dz} \right)^2 \quad \text{per unit volume} \\ &= \mu \left( \frac{U}{h} \right)^2 b h R d\theta\end{aligned}$$

Energy loss due to oil flow into and out of the element and to the presence of circumferential-temperature gradient, again assuming linear velocity gradient across film =  $\frac{1}{2} U b h p c dT$ .

In the absence of heat loss by conduction, these quantities must be equal under steady-state conditions

$$\frac{U b h p c dT}{2} = \frac{\mu U^2 b R d\theta}{h}$$

Writing

$$\begin{aligned}\mu &= \mu_0 e^{\beta T} \\ \rho &= \rho_0 e^{\lambda T} \\ h &= c_r (1 + n \cos \theta)\end{aligned}$$

$$a_1 = \frac{2\mu_0 U R}{c \rho_0 c_r^2}$$

then

$$e^{(\lambda - \beta) T} dT = \frac{a_1 d\theta}{(1 + n \cos \theta)^2}$$

Integrating from  $\theta = 0, T = 0$  to  $\theta, T$

$$\left[ \frac{e^{(\lambda - \beta) T}}{\lambda - \beta} \right]_0^T = a_1 \left[ \frac{\gamma - n \sin \gamma}{(1 - n^2)^{3/2}} \right]_0^\gamma$$

using Sommerfeld substitution

$$1 + n \cos \theta = \frac{1 - n^2}{1 - n \cos \gamma}$$

so temperature rise

$$T = \frac{1}{\lambda - \beta} \log_e \left[ \frac{2(\lambda - \beta) U R \mu_0 (\gamma - n \sin \gamma)}{c \rho_0 c_r^2 (1 - n^2)^{3/2}} + 1 \right]$$

at position  $\theta$  (or  $\gamma$ ), equivalent to Equation [33] of the paper.

At minimum film thickness position  $\theta$  and  $\gamma = \pi$

$$T = \frac{1}{\lambda - \beta} \log_e \left[ \frac{2\pi(\lambda - \beta) U R \mu_0}{c \rho_0 c_r^2 (1 - n^2)^{3/2}} + 1 \right]$$

The authors' comparison with some experimental results obtained by Clayton and Wilkie has been elaborated in Fig. 6 herewith. The discrepancies are seen to be considerable, and the theoretical temperature rise at the minimum film-thickness position is more than 80 per cent too great, although from the designer's point of view this factor of safety may be satisfactory. The theoretical curve continues to rise (shown dashed) in the divergent part of the film, but this is unacceptable on account of film rupture.

It is implicit in the analysis that the heated oil remaining in the clearance space is cooled to the common inlet temperature on mixing with the incoming oil supply. However, calculations using Clayton and Wilkie's data for oil flow and temperatures do not give a heat balance here, showing that heat conduction plays a part.

In an analysis of temperature effects, it is desirable to deduce not only the maximum temperature, but also the effect of temperature variation on load capacity and friction calculated using

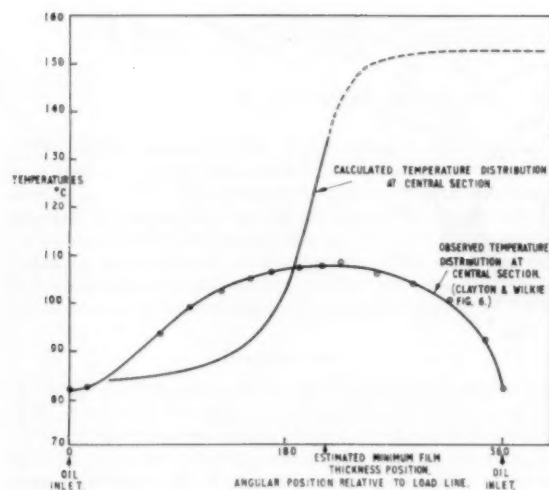


FIG. 6

constant-viscosity theory. With narrow bearing theory, the friction torque arises from simple shear only and is

$$M = \frac{lR^2U}{c_r} \int \frac{\mu}{1 + n \cos \theta} d\theta$$

$$= \frac{lR^2U}{c_r \sqrt{1 - n^2}} \int \mu d\gamma$$

using the Sommerfeld substitution.

Values of  $M$  can be calculated for the previously quoted experimental conditions of Clayton and Wilkie. Since film extent and temperature conditions in the divergent film are uncertain, the limits of the integral are taken from 0 to  $\pi$  for comparison purposes.

With constant viscosity, using the value  $\mu = 1.9 \times 10^{-6}$  reyns corresponding to the observed crown temperature 108 C,  $M = 4.8$  lb-in.

With variable viscosity deduced from the observed center-line temperature distribution,  $M = 11.4$  lb-in.

With variable viscosity according to Equation [33], using graphical integration,  $M = 5.8$  lb-in.

Thus the theory overestimates temperature rise and underestimates friction. It is at first surprising that the "observed" friction is highest, but this is probably a consequence of the limits of integration. In practice, calculations tend to overestimate friction torque because a complete  $2\pi$  film is assumed.

The application of Equation [29] of the paper giving the temperature distribution for concentric operation to the rotating-cylinder viscometer seems doubtful. The outflow is theoretically zero and is very small in practice, so that the adiabatic solution gives an ever-increasing temperature as the oil circulates circumferentially. The alternative limiting solution, in which the heat generated is assumed to be lost entirely by thermal conduction, seems preferable, and is supported by experimental evidence.<sup>6</sup>

The authors' concluding remarks on the differences likely to occur at high oil-flow rates between oil outlet and maximum film temperatures are important. The use of high oil-supply pressure and inlet grooving does not lead to efficient cooling of high-speed bearings since the excess oil flow leaves the bearing almost im-

mediately and provides cooling only by mixing with the hydrodynamic outflow. There is a need for research into the whole question of the removal of frictional heat from high-speed bearings.

OSCAR PINKUS.<sup>7</sup> A constructive step has been taken by the authors in the complex and neglected field of temperature distribution in journal bearings. The basic approach and mathematical skill are to be commended. Most of all, it is of great interest to have results for both the infinitely short and infinitely long bearings as these delineate the boundaries of finite bearings. There are, however, shortcomings in the presentation which impair the practical significance of the solution.

In the past, most expressions on temperature profiles suffered from the ballast of unknown parameters. The present solution on the infinitely long bearing also contains such an unknown quantity,  $h_p$  max. Admittedly, this value can be calculated by setting Sommerfeld's pressure gradient equal to zero and solving for  $\theta$  corresponding to  $p_{max}$ . This, however, can be done only by graphical means.

The second more serious objection regards the authors' treatment of the value of  $\theta_1$ , the point of admittance of the lubricant. They assume this point to be at  $\theta = 0$  but this is just one case out of an infinite number of other possibilities. It would be a rare coincidence indeed if the inlet-oil hole in practical bearings were to lie on the line of centers. Then too, even if such were the case, the original value of  $\theta_1 = 0$  could not possibly remain a constant for all the various eccentricity ratios considered. In a circular bearing, for example, a change from  $n = 0.2$  to  $n = 0.8$  involves a shift of attitude angle of nearly 40 deg; thus, if at  $n = 0.2$ ,  $\theta_1$  was at  $\theta = 0$ , at  $n = 0.8$ , the value of  $\theta_1$  will be 40 deg. While the values of  $\theta_1$  were left arbitrary in the solution of the infinitely long bearing, a rigid value of  $\theta_1 = 0$  was built in the solutions for the infinitely short bearing. This makes the solution of limited use in practical cases where  $\theta_1$  may start out with any value and can vary over almost 90 deg from its original value, depending on the eccentricities involved. For the same reason the plots of Figs. 2, 3, and 4 are valid only when one imagines the position of  $\theta_1$  shifted with each eccentricity ratio by the proper values of attitude angle.

#### AUTHORS' CLOSURE

The authors appreciate the discussions by Messrs. Cole and Pinkus. Mr. Cole's simplified development of the equation for temperature distribution complements nicely the more fundamental step-by-step reduction of Cope's basic equations given in the paper. Fig. 6 emphasizes the manner in which the solution lags the observed bearing temperature over most of the "on" side of the bearing while overshooting at the position of minimum film thickness to give a conservative solution. Part of the difference in shape between the solution curve and the observed bearing-temperature curve can be ascribed to the exponential function assumed to represent viscosity and density and part can be assigned to conduction effects peculiar to the experimental bearing. Mr. Cole's expansion into the subject of friction and load capacity is a welcome extension of this paper.

The authors appreciate Mr. Pinkus' comments. They are, of course, well aware of the limitations of the present solutions obtained. The paper seeks to present a solution to a classical problem which represents the limiting case rather than attempting to achieve a working equation for precisely predicting temperature rise. One would expect to find, however, that other predictions of temperature rise would fall below the outer bounds defined by the two solutions.

<sup>6</sup> "Experiments With a Rotating Cylinder Viscometer at High Shear Rates," by J. A. Cole, R. E. Petersen, and H. W. Emmons, NACA TN 3382, 1955.

<sup>7</sup> Bearing Development Engineer, Bearing and Lubricant Unit, Thomson Laboratory, General Electric Company, Lynn, Mass. Assoc. Mem. ASME.

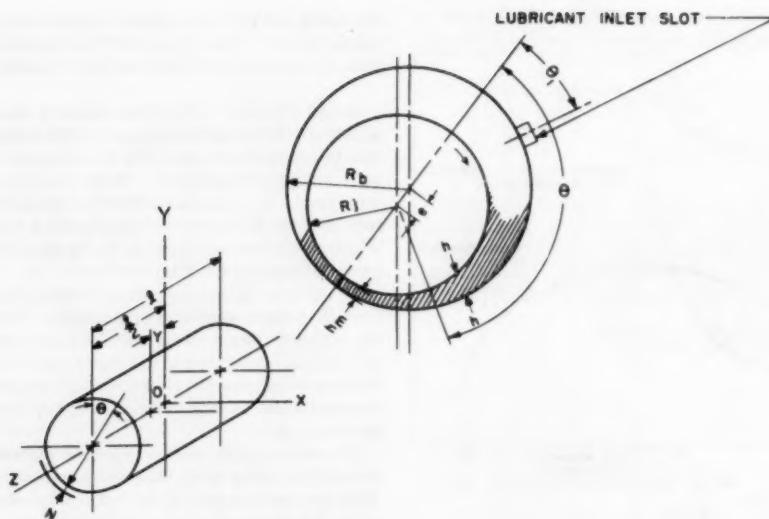


FIG. 1 (revised) FILM CONFIGURATION AND CO-ORDINATE SYSTEM

The limitations of the infinite bearing solution have been pointed up many times in the past. We merely present the solution as a matter of record; where the solution has not previously appeared, it now does. The authors, however, determined  $hp_{max}$  for one of the series of tests which they performed. Subsequent analysis of the temperature distribution measured in the lubricant film compared to the analysis achieved with the infinite bearing-temperature distribution expression clearly showed the latter to be of no practical use in predicting the former, and the authors do not recommend it for such design application.

In regard to the second objection regarding the treatment of  $\theta_1$ , the point of introduction of the lubricant inlet, the authors express their appreciation in having this limitation called to the readers' attention. This limitation can be removed by introducing  $\theta_1$  as the lubricant inlet position (see Fig. 1 revised). The first boundary condition of the solution is then revised so that when

$$Y = 0 \text{ and } \theta = \theta_1, \quad T = T_{\theta_1}$$

The requirement of the knowledge of the lubricant inlet temperature is thus retained, but the location of the inlet port is immediately generalized. The solution then becomes (Equation [28] revised)

$$a_1 \int_{\theta_1}^{\theta} \frac{d\theta}{(1 + n \cos \theta)^2} + a_2 y^2 n^2 (1 + n \cos \theta)^2$$

$$\int_{\theta_1}^{\theta} \frac{\sin^2 \theta d\theta}{(1 + n \cos \theta)^2} = \frac{e^{(\beta-\lambda)T_{\theta}} - e^{(\beta-\lambda)T(\theta=\theta_1)}}{\lambda - \beta}$$

Equation [10] of the paper may be used as it stands where  $\theta_1$  is defined as indicated above. The authors would not anticipate anyone familiar with the field having difficulty in handling the interpretation of Figs. 2, 3, and 4. For the sake of completeness the

$$\int \frac{\sin^2 \theta d\theta}{(1 + n \cos \theta)^2}$$

is given in Fig. 7.

$$\int \frac{\sin^2 \theta d\theta}{(1 + n \cos \theta)^2} = \frac{4 \tan^2 \frac{\theta}{2} + 12 \tan^4 \frac{\theta}{2} + (12 - 9a^2) \tan^6 \frac{\theta}{2}}{3a^2 (a^2 + \tan^2 \frac{\theta}{2})^3}$$

$$+ \frac{7 \tan^2 \frac{\theta}{2} + (15 - 9a^2 - 7a^4) \tan^4 \frac{\theta}{2}}{10a^4 (a^2 + \tan^2 \frac{\theta}{2})^4}$$

$$+ \frac{(7 - 9a^2 - 9a^4 - 7a^6) \tan^6 \frac{\theta}{2}}{12a^6 (a^2 + \tan^2 \frac{\theta}{2})^5}$$

$$- \frac{(7 + 9a^2 + 9a^4 + 7a^6) [\alpha^2 \tan^2 \frac{\theta}{2} - a \tan^4 \frac{\theta}{2} - (a^2 + \tan^2 \frac{\theta}{2})^2 \tan^{-1} \frac{\tan \frac{\theta}{2}}{\alpha}]}{32a^4 (a^2 + \tan^2 \frac{\theta}{2})^3}$$

FIG. 7  $\int \frac{\sin^2 \theta d\theta}{(1 + n \cos \theta)^2}$

# The Spring-Supported Thrust Bearing<sup>1</sup>

By FLETCHER OSTERLE<sup>2</sup> AND EDWARD SAIBEL,<sup>3</sup> PITTSBURGH, PA.

The slider bearing with the bearing a flexible plate mounted on springs is analyzed for its load-carrying characteristics. The deflection of the plate under load is found to create a wedge effect in the lubricant film which acts in conjunction with the wedge due to the inclination of the slider in producing a load capacity. The effect of the deflection of the bearing plate on the load capacity can be significant as is illustrated by a numerical example.

## INTRODUCTION

FOR effective load-carrying characteristics, thrust bearings rely on the formation of a wedge-shaped oil film between the slider and the bearing. This is commonly accomplished by an inclined slider moving over a rigid bearing. However, in some applications the bearing is a flexible plate mounted on an elastic foundation (springs).<sup>4</sup> Under load the plate will deform producing a wedge effect in the lubricant film which should affect the load capacity. A quantitative analysis of the influence of this wedge effect on the load capacity of the bearing does not seem to appear anywhere in the literature. It is the purpose of this paper to make such an analysis for the case where the wedge produced by the deformation of the bearing is small compared to that due to the inclination of the slider.

## BASIC EQUATIONS

The slider-bearing configuration to be investigated is as shown in Fig. 1. An inclined slider moves with a certain velocity over a flexible bearing plate mounted on springs. The pressure in the viscous lubricant drawn between slider and bearing by the motion is governed by the Reynolds equation which, if side flow is neglected, can be written

$$\frac{d}{dx} \left( h^3 \frac{dp}{dx} \right) = -6\mu U \frac{dh}{dx} \quad [1]$$

where  $p$  is the lubricant pressure,  $\mu$  is the lubricant viscosity, and the rest of the notation is as illustrated in Fig. 1. Integrating Equation [1] once we have

$$\frac{dp}{dx} = -6\mu U \left( \frac{1}{h^2} - \frac{h_m}{h^3} \right) \quad [2]$$

where  $h_m$  is the constant of integration. The boundary conditions on this equation are that  $p = 0$  at  $x = 0$  and  $x = B$ .

Equation [2] is difficult to solve since it is actually implicit in the pressure as can be seen from the fact that the bearing deflec-

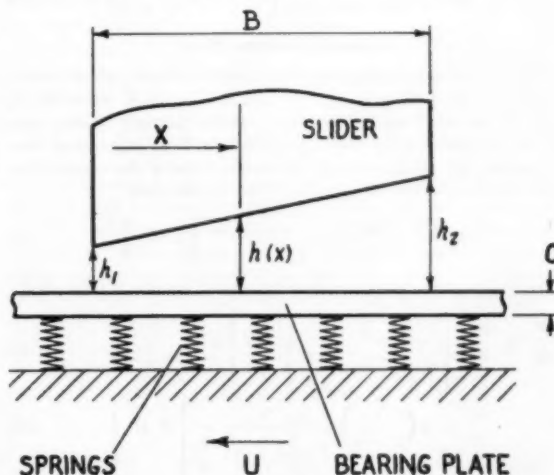


Fig. 1

tion which contributes to the film thickness is a function of the pressure. For a rigid bearing, however, the film thickness is not a function of the pressure and this case can be solved readily. In this paper a solution for the flexible bearing will be obtained by starting with the solution for a rigid bearing and computing a "correction." This correction will be small since we are restricting ourselves to the case where the effect of plate deformation is small.

## RIGID-BEARING CASE

For a slider-bearing with the bearing rigid, the film-thickness variation is given by

$$h_0 = h_1 \left[ 1 + (r-1) \frac{x}{B} \right] \quad [3]$$

where  $h_1$  is the minimum film thickness,  $B$  the slider length, and  $r$  the inlet-to-outlet film-thickness ratio  $h_2/h_1$ . The zero subscript will be used to denote the fact that the bearing is being considered rigid. For this case Equation [2] takes the form

$$\frac{dp_0}{dx} = -6\mu U \left( \frac{1}{h_0^2} - \frac{h_{m0}}{h_0^3} \right) \quad [4]$$

and is readily integrated to give

$$p_0 = \frac{6\mu U}{Bh_1^2} \left( \frac{r-1}{r+1} \right) \frac{x(B-x)}{\left[ 1 + (r-1) \frac{x}{B} \right]^2} \quad [5]$$

for the pressure distribution. In this equation the new integration constant and  $h_m$  have been evaluated by the boundary conditions that  $p = 0$  at  $x = 0$  and  $x = B$ . For future reference

$$h_{m0} = h_1 \frac{2r}{r+1} \quad [6]$$

The load capacity per unit slider width defined by

<sup>1</sup> The work underlying this paper was supported in part by the Office of Ordnance Research, U. S. Army.

<sup>2</sup> Associate Professor of Mechanical Engineering, Carnegie Institute of Technology. Assoc. Mem. ASME.

<sup>3</sup> Professor of Mechanics, Department of Mathematics, Carnegie Institute of Technology. Mem. ASME.

<sup>4</sup> "Analysis and Lubrication of Bearings," by M. C. Shaw and E. F. Macks, McGraw-Hill Book Company, Inc., New York, N. Y., 1949, pp. 321-322.

Contributed by the Lubrication Activity and presented at the Diamond Jubilee Annual Meeting, Chicago, Ill., November 13-18, 1955, of THE AMERICAN SOCIETY OF MECHANICAL ENGINEERS.

NOTE: Statements and opinions advanced in papers are to be understood as individual expressions of their authors and not those of the Society. Manuscript received at ASME Headquarters, October 7, 1955. Paper No. 55-A-195.

$$w_0 \equiv \int_0^B p_0 dx \dots \dots \dots [7]$$

is readily shown to be

$$w_0 = \frac{6\mu UB^2}{h_1^3} \frac{1}{(r-1)^2} \left[ \ln r - 2 \left( \frac{r-1}{r+1} \right) \right] \dots \dots [8]$$

#### FLEXIBLE-BEARING CASE

Now, for the slider-bearing with a flexible bearing plate we will write  $h = h_0 + H$ ,  $p = p_0 + P$ , and  $w = w_0 + W$  where  $H$ ,  $P$ , and  $W$  are small quantities which correct the rigid-bearing case to the flexible-bearing case. Substituting these expressions into Equation [2], taking account of the smallness of the corrections, and subtracting from Equation [4] we are left with

$$\frac{dP}{dx} = \frac{6\mu U}{h_0^3} \left\{ H \left[ 2 - 3 \frac{h_{m0}}{h_0} \right] + H_m \right\} \dots \dots \dots [9]$$

Substituting Equations [3] and [6] into Equation [9] we obtain

$$\frac{dP}{dx} = \frac{6\mu U}{h_1^3} \frac{1}{\left[ 1 + (r-1) \frac{x}{B} \right]^3} \left\{ H \left[ 2 - 6 \left( \frac{r}{r+1} \right) \frac{1}{1 + (r-1) \frac{x}{B}} \right] + H_m \right\} \dots \dots [10]$$

as the equation relating the corrections. The film-thickness correction  $H$  is nothing more than the deflection of the bearing plate due to the pressure distribution  $p_0$  and can be found readily by a separate analysis. Equation [10] will then yield (upon integration) the pressure correction  $P$  and by an integration of  $P$  over the slider length the load-capacity correction  $W$  can be found.

To determine the deflection of the bearing plate it will be necessary to consider the supporting springs to act as an elastic foundation with a certain modulus  $k$  defined as a vertical force exerted by the foundation per unit area of the plate for a unit deflection of the plate. The configuration of the bearing-plate deflection is shown in Fig. 2. To find  $H$  we must first find  $y$  the deflection of the plate from its original unloaded position. In general, this deflection can be written

$$y(x) = \int_0^B i(x, s) p_0(s) ds \dots \dots \dots [11]$$

where  $i(x, s)$  is an influence function giving the deflection at  $x$  due to a unit load at  $s$ . This influence function is given in<sup>4</sup>

$$i(x, s) = \frac{\beta}{2k} e^{-\beta|s-x|} [\cos \beta|s-x| + \sin \beta|s-x|] \dots [12]$$

with  $\beta^4 = k/4D$  where  $D$  is the flexural rigidity of the plate per unit width given by  $D = Ec^3/12(1-\nu^2)$ . In this expression  $E$  is the modulus of elasticity,  $\nu$  is Poisson's ratio, and  $c$  the plate thickness.

Since by previous restrictions  $y$  must be extremely small, the quantity  $\beta$  will be taken to be very small. By expanding the influence function into a power series in  $\beta$  and neglecting higher-order terms we obtain the following simplified expression for it

$$i(x, s) = \frac{\beta}{2k} [1 - \beta^2(s-x)^2] \dots \dots \dots [13]$$

Substituting Equations [13] and [5] into Equation [11] and integrating, we obtain the following for the plate deflection

<sup>4</sup> "Strength of Materials, Part II," by S. Timoshenko, D. Van Nostrand Company, Inc., New York, N. Y., 1940, p. 4.

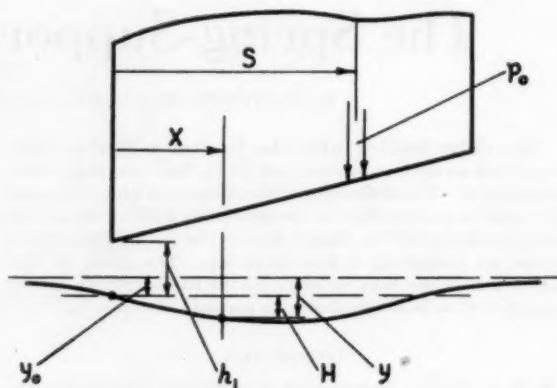


FIG. 2

$$y = \frac{3\beta\mu U}{kBh_1^3} \left( \frac{r-1}{r+1} \right) \{ [BI_{13} - I_{22} - \beta^2(BI_{33} - I_{44}) + 2\beta^2[BI_{22} - I_{33}]x + \beta^2[I_{22} - BI_{13}]x^2] \} \dots [14]$$

where

$$I_{mn} \equiv \int_0^B \frac{s^m}{\left[ 1 + (r-1) \frac{s}{B} \right]^n} ds \dots \dots \dots [15]$$

The deflection  $y_0$  shown in Fig. 2 is the foregoing expression with  $x$  set equal to zero. Subtracting  $y_0$  from  $y$  to obtain  $H$  we have

$$H = \frac{3\beta^3\mu U}{kBh_1^3} \left( \frac{r-1}{r+1} \right) (A_1x + A_2x^2) \dots \dots [16]$$

where  $A_1 = 2(BI_{22} - I_{33})$  and  $A_2 = (I_{22} - BI_{13})$ .

Thus the film-thickness correction has been determined. It now remains to substitute this into Equation [10] and integrate to obtain the pressure correction. When this is carried out we obtain

$$P = \frac{36\mu^2\beta^3U^2}{kB^2h_1^4} \frac{r^2(r-1)}{(r+1)^2} \left[ 2A_1(I_{03}J_{13} - I_{13}J_{03}) - 6A_1 \frac{r}{r+1} (I_{03}J_{14} - I_{14}J_{03}) + 2A_2(I_{03}J_{23} - I_{23}J_{03}) - 6A_2 \frac{r}{r+1} (I_{03}J_{24} - I_{24}J_{03}) \right] \dots [17]$$

where the  $J$ 's are indefinite integrals defined by

$$J_{mn} \equiv \int_0^x \frac{s^m}{\left[ 1 + (r-1) \frac{s}{B} \right]^n} ds \dots \dots \dots [18]$$

The new integration constant and  $H_m$  have been evaluated by the boundary conditions that  $P = 0$  at  $x = 0$  and  $x = B$ .

The load-capacity correction can then be determined by performing the following integration

$$W \equiv \int_0^B P dx$$

This theory will now be illustrated by a numerical example.

#### NUMERICAL EXAMPLE

Consider a 2-in-long slider moving with a velocity of 320 ips

over an infinitely long bearing plate with a flexural rigidity per unit width of  $6.25 \times 10^6$  lb-in.<sup>2</sup> supported by springs which effect a foundation modulus of 40,000 psi. The lubricant has a viscosity of 5 microrayn, the minimum film thickness is 0.001 in., and the film-thickness ratio is 2.

If the bearing were rigid, the load capacity per unit slider width would be 1017 lb as determined by Equation [8] and the pressure midway along the slider (at  $x = 1$ ) would be 711 psi as determined by Equation [5]. By the methods of this paper the pressure midway along the slider taking bearing flexibility into account works out to be 662 psi, a decrease of about 7 per cent over the rigid-bearing case. The load capacity works out to be 979 lb, a decrease of about 4 per cent.

Thus it appears that using such a flexible bearing plate mounted on springs does not produce a favorable effect on the load capacity.

## Discussion

S. E. WEIDLER.<sup>6</sup> The authors' series of papers on lubrication in the aggregate is indeed a worthy contribution to the literature. The least of their rightful claims is that their series has renewed interest and activity in the field of lubrication analysis.

The main objection of the writer stems from the title of the authors' paper in that they imply their solution is applicable to all classes of spring-mounted thrust bearings.

Classification of a spring-mounted bearing may be determined by answering the following questions: Is the runner (slider) flexible or rigid? Is the stator pad (bearing plate) flexible or rigid? Are the springs mounted behind the runner, or behind the stator pad? At zero static load, does either the runner or the stator pad have other than zero slope? Is either bearing member segmented? Thus, aside from any consideration of whether or not any particular class represents a practical bearing, there are at least 32 classes of spring-mounted bearings. To at least one of these classes, as exemplified by the G-E thrust-bearing application to hydraulic turbine-driven generators, the authors' solution does not apply. This bearing consists of a flat rigid runner, with springs nestled under segmented, flexible stator pads.

Thus the writer not only would like to comment on the authors' paper, but also relate his experiences relative to the G-E thrust bearing.

If the authors' bearing is to have any practicality, the saw-tooth runner must have at least two teeth so that equilibrium on the bearing plate is automatically satisfied. However, in all probability the number of teeth in the runner will have to be greater than two, say six or eight. According to the numerical values of the authors, the plate rigidity of  $6.25 \times 10^6$  lb-in. and a spring constant of 4000 psi yields a  $\beta$ -parameter value of approximately 0.11 in.<sup>-1</sup>; i.e., it will take 9 in. of plate width (in direction of runner motion) before the effect of unit pressure on deflection has decayed by some 63 per cent. Thus the deflection curve for a practical bearing may be quite different from that stipulated by the authors. This bearing has other interesting problems. Presumably the bearing-plate deflections would lag behind the taper lands on the runner during transient motion. Is this phase lag appreciable at steady state?

In the paper it does not follow that since  $y$  is small,  $\beta$  is small. Next, the writer is not sure that the pressure correction at the midway point is any measure of the load-capacity correction for the following reason: Equation [17] of the paper is the first step in an iteration process to an analytical solution. Hence local pressure corrections are likely to be in considerable error. On the other hand, if Equation [17] is integrated over the area, the

load-capacity correction calculated may be sufficiently accurate. Lastly, why is the outlet-film thickness maintained constant between the rigid-bearing plate and flexible bearing-plate case? Why not keep the inlet-film thickness constant? Or why not match the average distortion with the rigid-plate film thickness? Each of these criteria will give different results for the load-capacity correction.

With regard to the G-E thrust bearing, the writer originally made a rather naive attempt at a quasianalytical solution of the following equation

$$D \frac{d^2 h}{dx^2} + k \frac{dh}{dx} - \frac{6U\rho\nu}{h^3} - \frac{C_1\nu}{h^3} = 0 \dots\dots [19]$$

which represents a combination of the once-integrated Reynolds equation and a once-differentiated equation for the deflections of an infinite strip on an elastic foundation. This sixth-order ( $C_1$  is an arbitrary constant of integration) differential equation along with the zero moment, shear, and fluid-pressure conditions on a finite-width, one-dimensional bearing leads to a trivial solution if linearized.

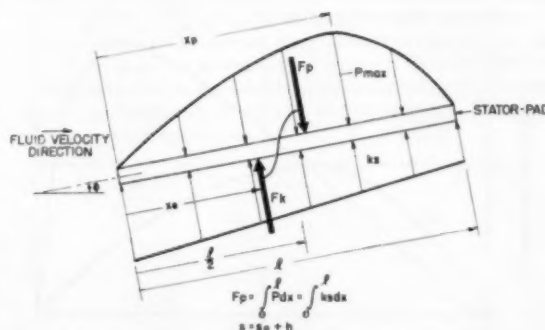


FIG. 3 ONE-DIMENSIONAL, RIGID STATOR-PAD THRUST-BEARING PRESSURE DISTRIBUTION

Upon reflection, with the physical picture of Fig. 3 of this discussion, it can be concluded that the rigid stator pad on an elastic foundation has only a trivial solution available. As demonstrated by Norton,<sup>7</sup> the physically useful fluid-pressure distribution has the characteristic that the position of the maximum pressure occurs downstream of the stator-pad mid-point; i.e.,  $l/2 \leq x_p \leq l$  according to the angular position  $\phi$ . Further, the magnitude of the maximum pressure is a function of  $\phi$ . If the fluid pressure has only one maximum, then the center of fluid pressure will be located somewhere near the position of this maximum pressure. The viscous fluid requires a positive angular position  $\phi$  to develop fluid pressure resulting in a foundation-pressure distribution like that illustrated in Fig. 3. If the elastic foundation can exert only compression on the surface of the stator pad, the position of the foundation center of pressure has the range  $0 \leq x_p \leq l/2$ . Thus an unbalanced couple is produced tending to restore the stator-pad angular position  $\phi$  to zero. The couple arm is zero when  $\phi$  is zero. If the stator pad is made slightly flexible, the fluid center of pressure will be moved downstream further from the mid-point and the foundation center of pressure will be moved toward the mid-point with a resultant couple arm of much the same magnitude as in the rigid stator-pad case. If now, the stator pad is passed to the zero-rigidity case, then the equilibrium conditions become completely impossible.

The next question is: What conditions are necessary for a non-

<sup>6</sup> Engineering Analyst, Analytical Engineering Section, General Electric Company, Schenectady, N. Y. Assoc. Mem. ASME.

<sup>7</sup> "Lubrication," by A. E. Norton, McGraw-Hill Book Company, Inc., New York, N. Y., first edition, 1942, p. 72.

trivial solution? Considering the once-integrated Reynolds equation in a slightly different form

$$\frac{dp}{dx} = \frac{6\nu}{h^3} \left( U\rho - \frac{2m}{h} \right) \quad [20]$$

it is seen that density, a function of temperature (pressure effects on density and viscosity are negligible), will shift the position of the maximum pressure; but its effect on load capacity as shown by Raimondi and Boyd<sup>8</sup> is only on the order of 10 per cent. However, kinematic viscosity, with its usual variation of 75 per cent as a function of temperature, along with density variation, might prove sufficient for a nontrivial solution. This, of course, ignores the obvious changes in boundary conditions or in mechanical parameters such as plate thickness that may be made to establish conditions for nontrivial solutions.

The writer set up the elasticity equation, Reynolds equation, and fluid-energy equation, including effects of variable density and viscosity, along with the appropriate boundary conditions on the IBM-CPC. A pressure distribution corresponding to usual bearing loads was assumed, such as  $P_1$  in Fig. 4, herewith.

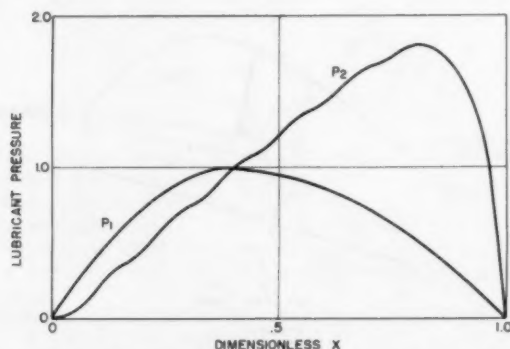


FIG. 4 ONE-DIMENSIONAL, FLEXIBLE STATOR-PAD THRUST-BEARING PRESSURE ITERATIONS

From this, deflections and hence film thicknesses were calculated. With these film thicknesses and the assumed pressure distribution, the temperature distribution can be calculated. Finally, a new pressure distribution  $P_2$  in Fig. 4 is calculated. The process is indicated in Fig. 5(a). As the process is continued, the calculated stator-pad deflections yield an average negative  $\phi$  so that the inlet-to-outlet film-thickness ratio is less than 1. Then, of course, an unrealistic pressure distribution would be calculated. Superimposed on these distributions are oscillations of half wave length corresponding to increment size as illustrated in Fig. 4.

These oscillations are due partly to the fact that conditions at any particular iteration do not satisfy both the Reynolds equation and energy equation simultaneously. Further, the space derivatives of pressure, as predicted by Reynolds equation, are extremely sensitive to film-thickness changes and hence to calculation of stator-pad deflections.

Pressure distributions other than  $P_1$  were assumed, all yielding similar results and all yielding more violent oscillations with successive iterations. However, if an inlet pressure of the same magnitude as the expected average pressure is assumed, these oscillations at least seem to remain constant in magnitude though the "average" pressure distribution will vary between successive iterations.

<sup>8</sup> "The Influence of Surface Profile on the Load Capacity of Thrust Bearings With Centrally Pivoted Pads," by A. A. Raimondi and J. Boyd, Trans. ASME, vol. 77, 1955, pp. 321-330.

The massive changes between pressure distributions, illustrated in Fig. 4, can be reduced by averaging the calculated pressure distribution with the previous pressure distribution, i.e., by using a damping factor of  $1/2$ . The oscillations can be safely muted by iterating between the fluid-energy equation and the Reynolds equation several times for a given film-thickness distribution. This iteration scheme, as illustrated in Fig. 5(b) of this discussion, was used successfully with an inlet pressure ap-

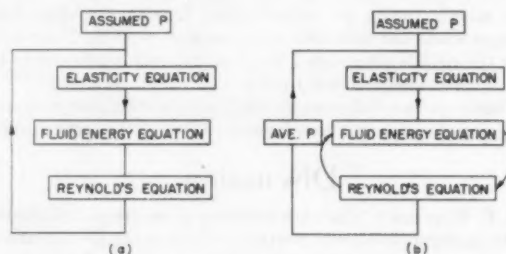


FIG. 5 ONE-DIMENSIONAL, FLEXIBLE STATOR-PAD ITERATION SCHEMES

proximately equal to the expected average pressure and again the pressure distribution moved inexorably to the condition where the angle  $\phi$  was negative for most of the flexible stator pad. However, the number of iterations needed to reach this condition was more than double that for the zero inlet-pressure case. Thus it seems that a larger inlet pressure (such that, for example, the viscous effects are masked) is needed for a nontrivial solution.

The purpose of this last part of the discussion was (1) to indicate that a successful iteration method was used to search for a nontrivial pressure distribution; and (2) that only a trivial pressure distribution was found for the flexible stator-pad spring-mounted bearing even though an appreciable inlet-oil pressure was finally allowed.

Further confirmation of these views was obtained as a result of calculations carried out on taper-land bearings. In each case for the flat-taper lands, pressure distributions were as characterized by Norton<sup>7</sup> although the temperature rise through the bearing approximated actual values. For a parabolic-crown profile superimposed on the taper land, the maximum pressure is not only increased, but its position is shifted upstream toward the inlet edge as suggested by Raimondi and Boyd.<sup>8</sup> Conversely, if the profile is concave (but  $\phi$  positive everywhere), the maximum pressure should be decreased and its position shifted downstream away from the inlet edge. This last profile corresponds roughly to what might be expected in flexible-pad spring-mounted bearings.

At the risk of smiting the brow of the applied mathematician, the writer states that the experiences as just related do constitute an informal proof that only trivial solutions are available for the one-dimensional G-E thrust bearing. For if one considers a pressure and temperature distribution that satisfies the three governing equations simultaneously and a pressure and temperature distribution which is being iterated upon, the differences between these two sets of distributions are disturbances. If the disturbances build up without limit, as they did in the cases just related, then the system is unstable. On the other hand, if the system is stable, then the disturbances should decay; and certainly thrust bearings in actual machines are stable systems.

Thus it is seen that the theory is not sufficiently complete for analysis of the G-E thrust bearing. For instance, there are at least two other promising effects not included so far: (1) Side-

leakage; i.e., the actual bearing is a two-dimensional problem. (2) Effective pad width; i.e., perhaps the effective pressure distribution extends only over a portion of the pad and in this manner equilibrium is attained. The effects of side-leakage are twofold: It reduces the average pressure of the pressure distribution for the one-dimensional case, and it shifts the maximum pressure toward the inlet edge. Stable solutions for the two-dimensional case can be searched for, quite conveniently, on large computers such as the IBM-704. If, in this case, only a trivial solution is available, then the writer would be tempted to say that item (2) is the usual condition of the flexible, spring-mounted, stator-pad bearing.

#### AUTHORS' CLOSURE

The authors would like to thank Mr. Weidler for his very interesting discussion. He is perfectly correct when he points out that our analysis does not apply to all spring-supported thrust bearings and in particular to the G-E thrust bearing which he describes. Our purpose in this paper was to shed some light on the relative importance of a film-wedge developed by elastic deformation to the built-in film-wedge and to this end we chose a configuration which would show up the difference and lend itself to analytic treatment. In addition to being thus restricted to a specific type of spring-supported bearing our analysis is further limited, as Mr. Weidler points out, by the fact that we essentially assume that successive sliders are infinitely far apart. The fact that they are not would certainly exert a quantitative change in the results. This may well be a direction in which further work should be done.

Mr. Weidler's questions in paragraph six call for detailed answers:

- (a) Our way of making  $y$  small was to make  $\beta$  small.
- (b) A calculation of the load-capacity correction, while not made in the earlier version of the paper, is made in this final version.
- (c) We purposely compared the nonrigid bearing with the rigid bearing on the basis of the same minimum film-thickness, feeling that this was a reasonable thing to do. Of course other bases of comparison would yield different results. However, since we intended to consider only one case it seemed most important to choose the one in which a physical limitation would not be violated.

In the early version of the paper which Mr. Weidler saw, we limited ourselves to finding the pressure specifically at the center only because we did not have computing facilities available. Later we worked out the total load-carrying capacity. These calculations were quite laborious. Since that time we have made calculations on an IBM 650 for another situation, that of a rigid slider on an elastic bearing plate. We were able to get the pressure distribution and the total load. We found a most interesting situation. In the region of the fluid exit, the effect of the elasticity of the surface was to increase the pressure but this soon changed to a decrease as one moved toward the inlet. The net effect was a decrease in the total load-carrying capacity. Again in this problem the minimum film thickness was kept constant. We plan to report on this work shortly.



# Instrumentation for Steam-Consumption Tests on Medium Steam Turbine-Generator Sets

By D. E. KIMBALL,<sup>1</sup> WEST LYNN, MASS.

In a 1954 paper (1)<sup>2</sup> we presented various measures of the uncertainties of the data of precision steam-consumption tests on medium-sized steam turbine-generator sets, deriving them from the over-all results of the tests and from comparisons of duplicate instruments used in them. In the present paper we describe briefly the instruments and their calibrations, and we present typical calibration corrections. The instruments and their calibrations have been used for many years. Most comparisons presented here demonstrate that instruments of high precision have small calibration corrections which are significant and that most corrections do not change significantly. They also show that these instruments can be relied upon in very precise turbine steam-consumption tests

## INTRODUCTION

IN our 1954 paper (1) we presented various measures of the uncertainties of the data of precision steam-consumption tests on 22 medium-sized turbine-generator sets rated 2500 to 18,750 kw. These tests were made in accordance with the ASME Power Test Code for Steam Turbines or associated codes. These measures were derived from comparing the over-all results of these tests. Also, we presented the uncertainties of their flows, powers, and steam conditions, as derived from comparisons of data from duplicate instruments. It is the purpose of the present paper to present brief descriptions of the instrumentation used in these tests, typical calibrations of them, and brief descriptions of the facilities for the calibrations.

## GENERAL

None of these testing methods is novel; all have been in use for many years. Many have been described in much greater detail in references listed at the end of the paper and are still in use with only minor modification.

Most steam-rate runs are 1 hr long, heat-rate runs about 2 hr. Usually the load and most of the test conditions have been held quite constant for 15 min or more before readings are started; and we continue to take readings until careful observation of the important readings indicates that the data have been constant for a test period of the proper length.

Wattmeters and flow-nozzle differentials often fluctuate somewhat more than other instruments. Hence we read them every

minute, thus getting a great many readings. Condensate is weighed as 5-min tankfuls, unless 3 or 4-min ones will nearly fill the tanks. We read steam conditions and most other data every 5 min.

In this paper we present typical instances of two or more calibrations of the same instruments. Some instruments show much less uncertainty from their calibrations than we found in our 1954 paper (1) by the analysis of test data from duplicate instruments; this is as expected. Other instances show the opposite; this is not surprising, since the instances are selected at random, whereas the 1954 paper presented uncertainties derived from many tests.

## WEIGHED FLOW

Our 1954 paper concludes that 0.12 per cent is the uncertainty of the throttle flows of the factory steam-consumption tests, as measured by weighing the condensate.

For these tests, we weigh the condensate in two tanks on carefully calibrated scales for precise, equal, alternate periods of 3, 4, or 5 min.

There are four sets of tanks and scales: two of 3400 lb capacity each, for tests with maximum flows of 68,000 lb/hr or less; and two 10,000-lb tanks for flows up to 200,000 lb/hr. The 10,000-lb scales have 2000-lb dials and four 2000-lb drop weights. Before and after each test, the scales are completely calibrated.

The scales are overhauled annually to correct minor maladjustments. After overhaul, each scale must pass an acceptance calibration. For this, each scale is fully loaded and unloaded three times in 200-lb steps, with the requirement that at no point may the total spread of the six readings exceed 0.04 per cent of the scale capacity.

Fig. 1 presents one set of before-test and after-test calibrations of the 10,000-lb tanks. It shows the "up" cycle, the only one used for a test. For the two scales, it shows about 1 lb as the root-mean-square value of the differences between the individual

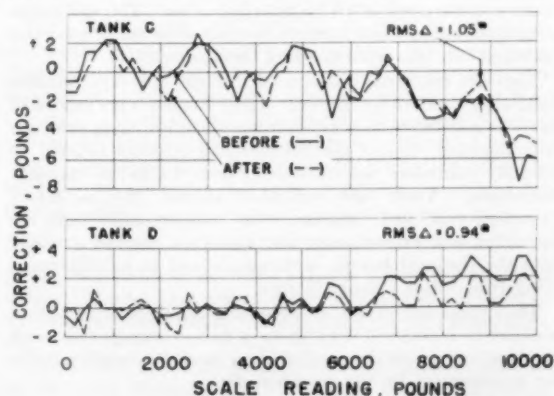


FIG. 1 CALIBRATION CORRECTIONS OF 10,000-LB SCALES BEFORE AND AFTER STEAM-CONSUMPTION TESTS

<sup>1</sup> Supervisor, Turbine Thermodynamic Development Engineering, Medium Steam Turbine Department, General Electric Company. Mem. ASME.

<sup>2</sup> Numbers in parentheses refer to the Bibliography at the end of the paper.

Contributed by the Power Test Codes Committee and presented at the Diamond Jubilee Annual Meeting, Chicago, Ill., November 13-18, 1955, of THE AMERICAN SOCIETY OF MECHANICAL ENGINEERS.

NOTE: Statements and opinions advanced in papers are to be understood as individual expressions of their authors and not those of the Society. Manuscript received at ASME Headquarters, October 14, 1955. Paper No. 55-A-206.

readings of the two calibrations; this corresponds to differences of 0.02 per cent at an average tankful of 5000 lb, or an uncertainty of about 0.01 per cent in the average flow of two tanks, as caused by the differences between the two calibrations. This accounts for a very small part of the 0.12 per cent uncertainty of weighed flow.

The weighing cycle is controlled by two timing devices for each tank. One device for each tank times its filling period very precisely; the other prints the tare and full weights, and actuates the dump valve. All four devices are driven by a constant-frequency source which is checked against the Arlington radio time signals.

This weighing equipment is completely automatic. However, throughout each test, we have a trained operator present to make certain that the cycling is correct and that the inlet and dump valves are drop-tight. Also, he performs certain refinements of the measurements: He gently adds a 10-lb weight on the scale platform before the tare reading is taken, to make certain that all readings are "up" readings; and he reads and records the full and tare readings with considerably greater accuracy than the printer records them. Also, he reads and records the instant of the shifting of the inlet valves to the nearest half second.

Weighing the condensate is a direct means of measuring steam consumption. But to make it precise, we prevent all leakages out of the system or into it, or measure them carefully after reducing them as much as possible.

#### POWER

The uncertainty of the measurement of the generator output of these tests is 0.10 per cent.

For most factory tests, the generator output is measured on four wattmeters, two duplicating each other in each of two phases, in the two-wattmeter method; each meter has its own instrument transformers. For tests in the owners' plants, the generator neutral is often grounded; hence there we usually use six wattmeters, two in each of the three phases; often both wattmeters in a specific phase use the same instrument transformers.

These wattmeters have been built for extra precision and reliability, they have been selected carefully, and reserved for this work. Their springs are carefully aged. Their scales are precisely graduated.

Before and after each test, they are carefully calibrated in General Electric's Measurements Laboratory at West Lynn, Mass. This calibration includes a-c readings of each meter at the power factor, voltage, and frequency for the specific generator to be tested and at each of 50 values of current input to the meter over the range which the tests may cover. This calibration obtains its voltages and currents from a special motor generator set whose only load is the meters of these calibrations.

Each test wattmeter is compared with one of several portable laboratory standard wattmeters. These standards are calibrated monthly and before each steam-rate calibration, using precision potentiometers against d-c voltages and currents referred to carefully maintained and calibrated standard cells and standard resistances. These are calibrated against the laboratory "standard volt" and "standard ohm" whose temperatures are controlled with extreme care, and which are checked annually with the National Bureau of Standards and in an interworks comparison within General Electric.

The voltage and current for calibrating the laboratory standard wattmeters is obtained from banks of Edison storage cells, with precision voltage dividers and resistors to obtain values suitable for measurement by the potentiometers.

Fig. 2 presents typical wattmeter calibrations. It shows the before-test and after-test calibrations of four of the six watt-

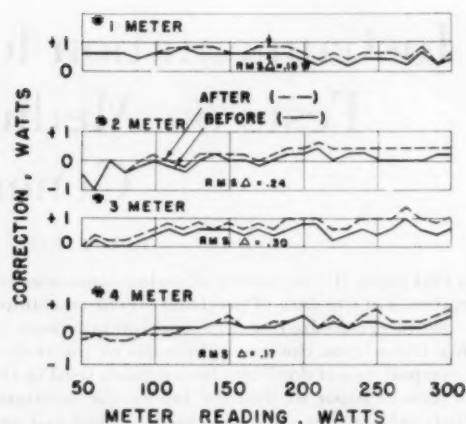


FIG. 2 CALIBRATION CORRECTIONS OF TEST WATTMETERS BEFORE AND AFTER STEAM-CONSUMPTION TESTS IN THE OWNER'S PLANT

meters used in one test in the owner's plant. It shows no calibration correction of more than 1 watt on a 300-watt scale. Also, the root-mean-square differences between the individual before-test and after-test corrections for the various instruments vary from 0.16 to 0.30 watt; this corresponds to differences of 0.12 per cent, and could cause an uncertainty of 0.03 per cent in the average power measured by six wattmeters, as caused by the differences between the two calibrations. This accounts for only one tenth of the 0.10 per cent uncertainty of generator output.

Before and after each steam-rate test, each test current transformer is calibrated against one of three specially designed and carefully built multitap laboratory standard transformers. For calibration, each test transformer has the actual meters and leads to be used in the turbine test as the burden of its secondary winding or it has the equivalent burden; the calibration is made at the frequency of the test and at several currents over the test range.

Each laboratory standard transformer has its windings and core so arranged that its losses are very small and are little affected by operating conditions; also, it can be calibrated against itself. In the calibration of the test transformer, the primaries of the test and standard transformers are connected in series. Their secondaries are connected in opposition to each other in such a way that a variable inductance can measure the phase angle between the transformers and can compensate for it; and a galvanometer and a slide-wire resistor can measure the difference between the nominal ratio and true ratio of the two transformers. Checks among the laboratory standard transformers separate their effects from the test transformer effects. This arrangement avoids the inaccuracies which might be caused by having to measure the high primary and low secondary currents directly; and it allows a galvanometer with a specific accuracy to determine the transformer's true ratio much more accurately by measuring the difference than it could measure the ratio directly. The potential transformers are calibrated similarly.

For the calibration of either CT or PT, the primary current or voltage is obtained from special motor-generator sets with filters and regulators to obtain suitable input.

Fig. 3 presents the before-test and after-test calibrations of a current and a potential transformer. It shows that their true ratios differ only a few tenths of a per cent from their nominal ratios, when used with small burdens as in these steam-consumption tests. And the differences between before-test and after-test calibrations are barely perceptible.

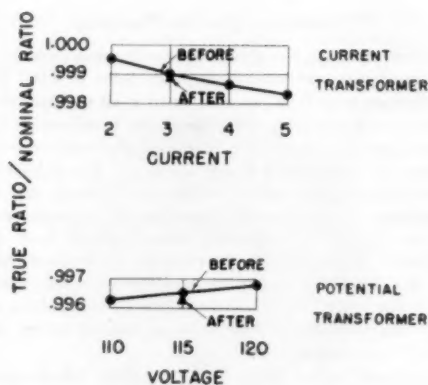


FIG. 3 CALIBRATION CORRECTIONS OF TEST INSTRUMENT TRANSFORMERS, BEFORE AND AFTER STEAM-CONSUMPTION TESTS IN THE OWNER'S PLANT

#### TEMPERATURE

The uncertainty of the initial temperature measurements of these tests is 0.3 F. This corresponds to 0.02 per cent in the overall performance of condensing tests, 0.03 per cent noncondensing.

Each of the principal steam temperatures of these tests is measured on two carefully made chromel-constantan thermocouples immersed 6 in. in close-fitting ASME-type finned wells in the low-velocity steam-inlet and noncondensing exhaust pipes. These use thermocouples, methods, and calibration facilities developed by Buckland, Stack, and Alford (2). The thermocouple voltages are measured on two portable precision potentiometers, each with its own set of auxiliaries, including precision light-beam galvanometer, transfer switch, and water-ice bath for the cold junctions. Each potentiometer is connected to one thermocouple measuring each temperature.

Fig. 4 is a photograph of a thermocouple. Its 12-in.-long stainless-steel sheath projects about 6 in. from its well; a flexible cable covers the rest of the high-temperature part of it. Except for its copper terminals, the rest of it is covered by a kinkproof rubber covering.

When first made, and before and after each test, each thermocouple is calibrated in three electrically heated baths, one each

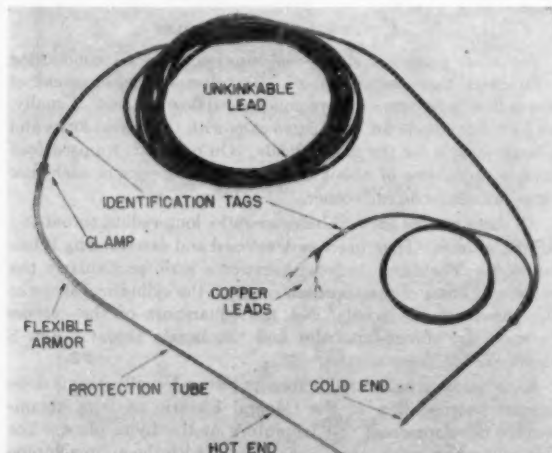


FIG. 4 PRECISION THERMOCOUPLE FOR TURBINE STEAM-CONSUMPTION TESTS

at 449.4 F and 621.3 F, the freezing points of tin and lead, respectively, and one at the sulphur-vapor point, which the atmospheric pressure can cause to vary from 831 to 834 F. These baths and their furnaces were designed and constructed carefully for these calibrations. They are loaded with charges of tin, lead, or sulphur certified by the National Bureau of Standards. They are checked for contamination against a platinum-resistance thermometer. The baths and the resistance thermometer are checked annually by the National Bureau of Standards and by interworks comparisons within General Electric. Contamination of the tin and lead baths can be detected readily by noting a small gradually accelerated drop of temperature during the freezing part of any precision calibration instead of a constant temperature then. The sulphur-vapor bath is relatively unaffected by contamination.

The calibration of each thermocouple includes precise readings with 6 in. immersion in the tin and lead baths and at immersions of every inch from 4 to 10 in. in the sulphur-vapor bath. For tests at temperatures significantly above the sulphur-vapor point, the thermocouples are calibrated by comparing them with the platinum-resistance thermometer in a copper block inside a similar electric furnace.

Our standards require that for precision temperature measurements, a thermocouple must have less than 0.6 deg F variation in its calibration among the various immersions between 5 and 10 in., inclusive, in the sulphur-vapor bath.

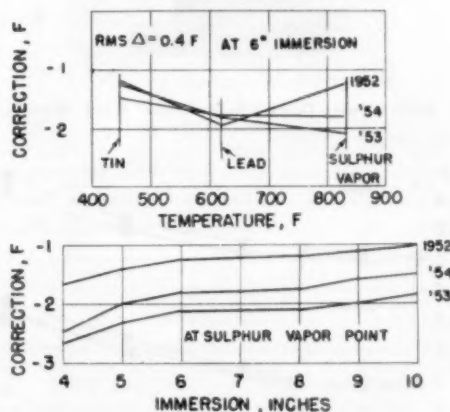


FIG. 5 CALIBRATION CORRECTIONS OF A PRECISION THERMOCOUPLE

For a typical precision thermocouple, Fig. 5 presents the calibration corrections from three calibrations a year apart. This shows corrections of 3 deg F or less. The 0.4 deg F root-mean-square change between successive calibrations at 6 in. immersion corresponds to a difference of 0.03 per cent in over-all turbine performance and could cause an uncertainty of 0.02 per cent in over-all performance as accounted for by the differences between two successive calibration corrections of each of two thermocouples.

#### INITIAL PRESSURE

The uncertainty of the initial pressure measurement of these tests is 0.32 psi. This corresponds to 0.007 per cent in the overall efficiency of condensing turbines, 0.045 per cent noncondensing.

On each test, the turbine initial pressure and adjacent pressures are measured on piston-type dead-weight gages of laboratory accuracy. Noncondensing exhaust pressures above 35 psig are read on two or more such gages. Fig. 6 shows one of these gages

with weight for reading a pressure of 1100 lb. These gages have piston areas of 0.125 sq in. Their weights are standardized to limits such that the error of the total of weights will not exceed 0.05 per cent of the reading for pressures above 50 psig. The weights are suitable for reading pressures up to 1000 psig to the nearest 0.1 psi.

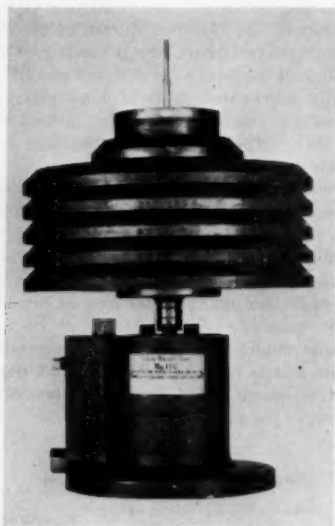


FIG. 6 PISTON-TYPE DEAD-WEIGHT GAGE WITH WEIGHTS FOR MEASURING 1100 PSIG

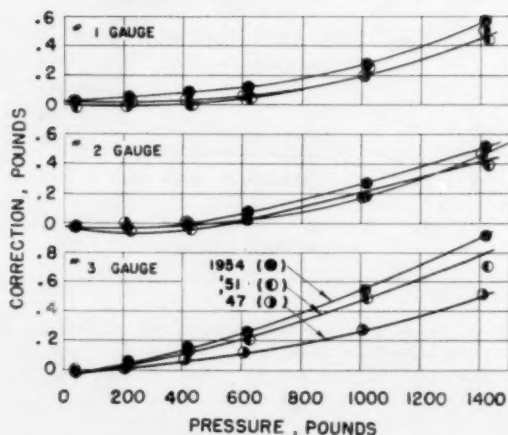


FIG. 7 CALIBRATION CORRECTIONS OF DEAD-WEIGHT GAGES

Periodically, and also before certain tests, each gage is calibrated against a still more precise laboratory standard dead-weight gage tester with carefully standardized calibrating weights.

Fig. 7 presents plots of the corrections from three calibrations on each of three typical gages over a 7-year period. It will be noted that no calibration correction exceeds 1.0 psi even at 1400 psig, that the corrections are approximately 0.0005 times the pressure, and that the test points for each individual calibration lie within 0.01 psi of a smooth line. The 0.1-psi scatter of the corrections of the various calibrations of a gage corresponds to an uncertainty of 0.001 per cent in over-all performance of a turbine.

#### CONDENSING EXHAUST PRESSURE

The uncertainty of the exhaust-pressure measurement of our factory condensing steam-consumption tests is 0.017 in. Hg. This corresponds to 0.08 per cent in over-all turbine efficiency.

For factory condensing tests, the steam is exhausted through an exhaust adapter about 4 ft long with the same cross section and shape as the exhaust-flange opening. The exhaust static pressure is measured in four carefully made holes in the walls of these adapters, two being well spaced in the upstream wall, two in the downstream, and all being about halfway down through the adapter. Each hole is observed by an engineer to make certain that its edges are square and free of burrs; each is at least two diameters long. For the larger Lynn turbines, we also measure the pressure in two or more basket tubes, such as described in reference (3).

Each exhaust vacuum is read on a precision low-pressure manometer. These have  $\frac{1}{8}$ -in-ID precision glass tubing, engraved scales, and riders with verniers and with gage lines behind and in front of the meniscus. Each manometer is connected to its pressure hole by translucent plastic tubing to detect any condensate in the connection. However, practically all condensation in the connection is prevented by venting atmospheric air into the lines through a 0.03-in-diam hole briefly before each reading.

We read the atmospheric pressure in the test building on a precision mercury-in-glass barometer with  $\frac{1}{8}$ -in-ID glass. This is calibrated against a similar barometer in the River Works' Thomson Laboratory and they are checked occasionally against barometers at a weather observatory.

Before each test, we read each manometer carefully at maximum vacuum with no load on the generator. By this check, we detect and correct any leaky manometer connections and any other unsatisfactory conditions in the system for measuring exhaust pressure.

The exhaust-pressure instrumentation for tests in the owners' plants is the same as in the factory except for the pressure holes. The exhaust flange usually extends inward from the walls of the exhaust connection, causing the passage area of the exhaust connection to exceed the flange opening and disturbing flow along the walls. Thus we cannot use adapter pressures as at the factory. Hence in many field tests, the exhaust pressure is measured mostly in about four or more basket tubes mounted in the plane of the exhaust flange and distributed uniformly over the passage.

#### CONDENSATE-FLOW NOZZLES

For most precision steam-consumption tests on condensing turbines in their owner's plant, the principal measurement of steam flow is by one or more condensate-flow nozzles. Usually, we have one nozzle for one or two runs with the lowest loads and a larger nozzle for the higher loads. On one test, we used four nozzles, using two of about the same size in series in each flow range, as checks on each other.

All these nozzles are low-diameter-ratio, long-radius, throat-tap ASME nozzles. Their use was developed and described by Buckland (4). They are made with extreme care, particularly the shape and finish of the approach contour, the cylindrical shape of the throat of the nozzle, and the squareness of the corners between the throat-tap holes and the nozzle throat. Fig. 8 shows one of these nozzles.

Each nozzle is calibrated before its tests. Usually, this is done against weighed flow in the General Electric medium steam-turbine developmental test laboratory at the Lynn plant. For this calibration, each nozzle is assembled with the approach pipe and resistance straightener which are to be used in the tests. At times, we calibrate two nozzles in series; thus we have three

measurements of flow for each calibration point; this allows us to detect any point whose discharge coefficients may be less reliable than the coefficients of the other points.

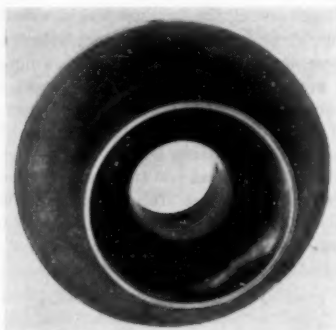


FIG. 8 ASME-TYPE LONG-RADIUS, LOW-RATIO FLOW NOZZLE WITH THROAT TAPS—VIEW AT ENTRANCE

These nozzles are used with differential pressures between 4 and 36 in. of water-covered mercury. These differentials are measured on high-pressure precision manometers; these have riders with verniers and with gage lines behind and in front of the meniscus, precision-engraved scales, verniers, and precision  $\frac{1}{16}$ -in-ID tubing.

Fig. 9 presents the discharge coefficients from two calibrations on each of three of these nozzles, each of which was used in steam-consumption tests on one or more turbine-generator sets in their

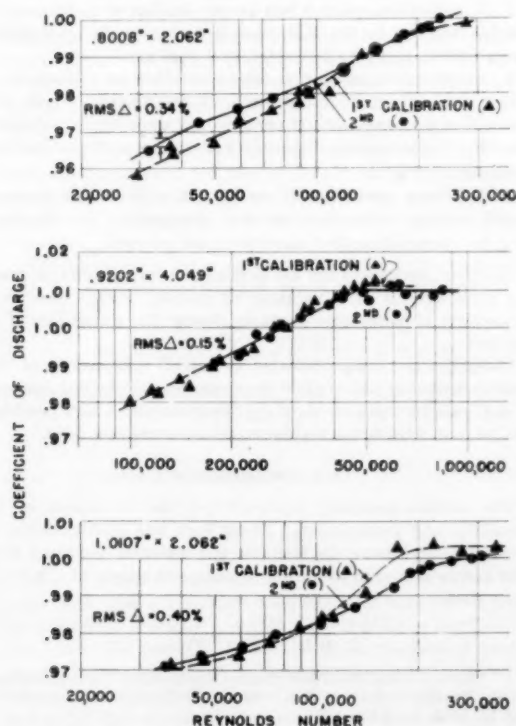


FIG. 9 CONDENSATE-FLOW NOZZLES—DISCHARGE COEFFICIENTS FROM TWO CALIBRATIONS ON EACH OF THE THREE NOZZLES

owner's plant. The three nozzles have root-mean-square differences of 0.40, 0.15, and 0.34 per cent between the individual calibration points of one calibration on a nozzle and the line of the other calibration of that nozzle. The root-mean-square value of these differences is 0.32 per cent. The analysis in the Appendix notes that the uncertainty to be charged to the test use and the calibration use of a once-calibrated test instrument is about 0.91 times the difference between two calibrations. Thus these differences correspond to an uncertainty of 0.29 per cent in the condensate flow of a turbine as measured by one of these nozzles if calibrated only once, as usual.

#### STEAM-FLOW NOZZLES

Our 1954 paper (1) notes that we use a low-diameter-ratio, long-radius, throat-tap ASME steam-flow nozzle in the inlet line of each factory steam-consumption test, using it as a check on the weighed condensate flow. That paper describes their installation. These nozzles are made to the same design and manufacturing methods as the nozzles just described for measuring condensate flow, but these are considerably larger because the specific volume of the steam is several times that of the condensate.

The steam-flow nozzles are not calibrated for each test, although Moss and Johnson (5) carefully calibrated this type of nozzle when developing their use for measuring steam flow. Also, some nozzles have been used for several of these tests.

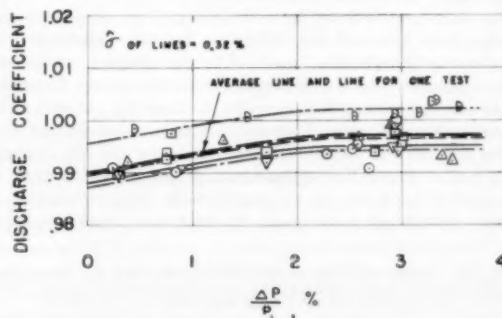


FIG. 10 STEAM-FLOW NOZZLES—APPARENT DISCHARGE COEFFICIENTS FROM INDIVIDUAL RUNS OF FIVE FACTORY STEAM-RATE TESTS, ALL USING THE SAME FLOW NOZZLE

Fig. 10 presents the discharge coefficients of one flow nozzle as derived from the weighed condensate flow of each of the individual runs of five factory turbine steam-rate tests. This figure shows a line for each of four of these tests and an average line which coincides with the line for the fifth test. The line for each test fits its points quite well even though all five lines have exactly the shape which we derived from 13 tests using six such nozzles. The standard deviation of the lines for the five tests from the average line is 0.32 per cent. When from this we remove 0.12 per cent, the uncertainty of our weighed flows, as the square root of the difference of the squares, we obtain 0.30 per cent as a measure of the uncertainty of one of these nozzles each time it is used. In our 1954 paper we derived 0.20 per cent as the corresponding figure derived from using five of these nozzles in two to five tests each; and we derived 0.35 per cent as the uncertainty for measuring flow by an uncalibrated steam-flow nozzle.

#### STATION INSTRUMENTS

In each steam-consumption test in an owner's plant, we read some of the more important types of data from the station instruments, in addition to the test instruments. Comparisons

of these data with the data from our precision test instruments serve as a measure of the uncertainty of the station instruments and also as calibrations of the station instruments at least as of the period near the tests.

Table 1 presents the comparisons of station-instrument data with precision-test instrument data from the four field tests whose results were presented in our 1954 paper (1).

TABLE 1 COMPARISON OF DATA BY STATION AND PRECISION-TEST INSTRUMENTATION FOR STEAM-CONSUMPTION TESTS ON FOUR MEDIUM STEAM TURBINE-GENERATOR SETS IN THEIR OWNERS' PLANTS

Field test no.	Generator output: Test minus station, per cent		Throttle flow: Test minus station per cent	
	Average	Root mean square	Average	RMS
1.....	-2.7	3.0	.....	.....
2.....	-1.7	4.2	-0.3 <sup>a</sup>	0.5 <sup>a</sup>
3.....	-0.3	0.4	-0.9 <sup>b</sup>	1.3 <sup>b</sup>
4.....	-4.7	5.0	.....	.....
Average (or RMS).....	-2.4	3.6	-0.6	1.0

<sup>a</sup> Referred to station condensate-flowmeter.

<sup>b</sup> Referred to station steam-flowmeter.

For the generator output of the four tests, it shows that we read an average of 2.4 per cent less power by the precision-test wattmeters than by the station watt-hour meters. And the root-mean-square value of the differences between the instruments is 3.6 per cent for the individual runs.

For their throttle flows, the table shows 1.3 per cent as the root-mean-square value of the difference for the individual runs between the throttle flow measured by the precision condensate-flow nozzle and that derived from the station steam flowmeter, in the one test with such data. Also, it shows 0.5 per cent as the corresponding difference between the station condensate flowmeter and the test condensate-flow nozzle, for the one test with such data. These flow differences are much smaller than indicated by much of our experience with data obtained from station flowmeters. On about 30 large steam turbines, Kratz

TABLE 2 COMPARISON OF THROTTLE FLOWS BY PRECISION AND STATION EQUIPMENT FOR STEAM-CONSUMPTION TESTS ON LARGE STEAM TURBINE-GENERATOR SETS

Author	Station meter	Quantity of tests	Flow: test minus station, per cent	
			Avg	RMS
Pollock.....	Condensate	32	+0.2	1.8
Pollock.....	Steam	32	+1.3	2.1
Kratz.....	Condensate	21	-0.1	2.1
Kratz.....	Steam	28	+0.7	1.6

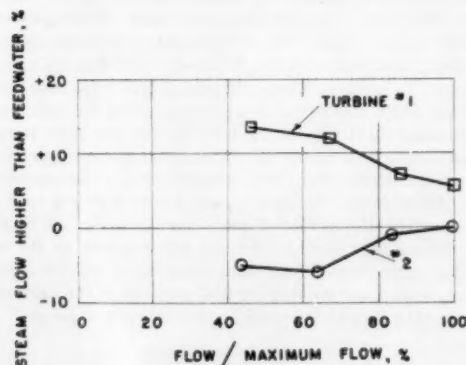


FIG. 11 STATION FLOWMETERS—COMPARISON OF STEAM FLOWMETERS AND FEEDWATER-FLOWMETERS FOR TWO DUPLICATE TURBINES

(3) and Pollock (6), presented plots which are summarized in Table 2. These show about 2 per cent as the root-mean-square difference between station flow nozzles or orifices and precision-test flow nozzles or weighed flows for individual turbines. The algebraic averages among the turbines was significantly smaller.

Further, Fig. 11 presents the differences between the station steam flowmeter and the station feedwater flowmeter on each of two medium steam turbines. These differences are between data which were taken after the calibration corrections were applied to the meters but not the orifices or nozzles. Each turbine has 5 per cent more discrepancy between its meters at half flow than at maximum flow. And one turbine never had differences less than 5 per cent. Yet these are from data that were carefully read and that were checked from time to time by our engineer. These differences are of about the same order as we often encounter in data taken on station instruments.

### CONCLUSIONS

In this paper we present several typical instances of two or more calibrations of the same instruments. These serve to show the order of magnitude of the calibration corrections and the differences between successive calibrations. In general, the uncertainties derived here from successive calibrations are usually a small fraction of the uncertainties derived in our 1954 paper (1) from the use of duplicate instruments in turbine tests; this is as expected.

Many of the calibrations presented here have such small corrections as to seem almost negligible. However, even these are essential for precision tests, for these reasons in addition to the obvious reduction in uncertainty by applying some corrections:

1 A calibration before a test assures us that an instrument is suitable for use in the test, and it measures the calibration corrections to apply to the instrument readings.

2 An after-test calibration determines that an instrument is still suitable for use and determines the amount which the corrections may have shifted permanently since before the tests, if at all. It also tends to divide the uncertainty of the calibration corrections by  $\sqrt{2}$ .

3 For some new types of equipment, such as new thermocouple metals, calibrations assist in determining the standard data to which calibration corrections are referred.

However, we believe our use of duplicate instruments for reading most data is very valuable in making certain that each instrument is performing properly during the actual period of the test.

Finally, these comparisons of successive calibrations of the same instruments and our last year's analysis of the test readings of duplicate instruments show that instruments of high precision can be used reliably for turbine steam-consumption tests.

### ACKNOWLEDGMENTS

The author gratefully acknowledges the assistance of his associates and predecessors. Their work has been essential in developing and using the facilities and methods described here. The author has been in partial or complete charge of this work since 1940.

### BIBLIOGRAPHY

- "Accuracy and Results of Steam-Consumption Tests on Medium Steam Turbine-Generator Sets," by D. E. Kimball, Trans. ASME, vol. 77, 1955, pp. 1355-1367.
- "Temperature: Its Measurement and Control in Science and Industry," by B. O. Buckland, Stack, and Alford, Reinhold Publishing Corporation, New York, N. Y., 1941, p. 884.

3 "Experience in Testing Large Steam Turbine-Generators in Central Stations," by E. M. Krata, Trans. ASME, vol. 77, 1955, pp. 1369-1374.

4 "Fluid-Meter Nozzles," by B. O. Buckland, Trans. ASME, vol. 56, 1934, p. 827.

5 "A System for the Measurement of Steam With Flow Nozzles for Turbine Performance Tests," by S. A. Moss and W. W. Johnson, Trans. ASME, vol. 55, 1933, p. 145.

6 "Testing Large Steam Turbines With Weighing Tanks," by W. A. Pollock, Trans. ASME, vol. 75, 1953, p. 89.

## Appendix

### UNCERTAINTIES AS DETERMINED FROM CALIBRATIONS

We wish to determine what uncertainty in test data to charge to a test instrument, based on the root-mean-square difference between successive calibrations on the same test instrument.

It is in order to assume that most of this difference,  $\Delta$ , is caused by the test instrument. Suppose that the uncertainty of the test instrument itself whenever it is being used is only twice the uncertainty of the rest of the calibration setup. We can remove the uncertainty of the rest of the setup as the square root of the difference of the squares. Then we have the uncertainty of the test instrument, as used during a test, as  $\sqrt{2^2/\sqrt{2^2 + 1^2}}$  or 0.895, or, say, 0.90 times the total uncertainty of a single calibration, or to 0.63  $\Delta$ .

If we have before-test and after-test calibrations, we may use their average for calculating test results. The uncertainty of this average of two calibrations can be estimated as  $1.00 \Delta / (\sqrt{2} \cdot \sqrt{2})$  or 0.50  $\Delta$ .

In each steam-consumption test, each instrument is read ten or more times on each of three or more runs. This reduces the uncertainty of those types of test instruments for which much of the calibration uncertainty may occur in reading the test instrument. This tends toward making the uncertainty of the test use of the test instrument somewhat less than the calibration uncertainty of the instrument itself, say, to 0.90 times it, or to 0.57 times the difference between two calibrations.

We will not distinguish between the accuracy with which calibration personnel and test personnel read a test instrument; presumably, calibration personnel read more carefully, but we have test-directing engineers observing the test readings for accuracy.

We can combine the uncertainties from one or two calibrations with the uncertainty from the use of the test instrument in a test, getting

$$\epsilon_1 = \sqrt{(0.57 \Delta)^2 + (0.71 \Delta)^2} = 0.91 \Delta$$

for a once-calibrated instrument, and

$$\epsilon_2 = \sqrt{(0.57 \Delta)^2 + (0.5 \Delta)^2} = 0.76 \Delta$$

for a twice-calibrated instrument.

## Discussion

N. R. DEMING.<sup>3</sup> In presenting this description of test instruments and their calibrations the author has summarized for the electric-utility industry a wealth of testing "know how" accumulated over the years by his company in conducting precision economy tests on steam turbine-generator sets. Although he refers to tests on medium-sized units, most of the instruments and techniques described are equally applicable to tests on the

largest central-station units. With the increasing amount of attention being given to the thermal performance of units this paper will be received with much interest.

According to the author's 1954 paper (author's reference 1), most of the tests referred to were conducted to obtain engineering data. The same instruments, with exception of the weigh tanks, however, were used in those tests required by the turbine purchaser. Thus use of the instruments described in this paper is not limited to the laboratory but extends to operating power plants when precision tests are desired.

Since the paper is sponsored by the ASME Power Test Codes Committee, it has been suggested that it would be appropriate to compare the instruments and methods described therein with those specified by the ASME Test Code for Steam Turbines. A general observation is that most of the instruments used by the author are mentioned either in the code or in the supplements on instruments and apparatus but that in many cases the author has established additional or more exacting standards of design specification and performance not covered by the code. A few examples will illustrate.

**Weighed Flow.** Two of the most important parts of water weighing are the accuracy of the scales and the measurement of the time intervals for each tank. The code states that weighing scales shall be checked prior to the test and caused to weigh with an accuracy within 2 in 1000. The author indicates that his scales are more accurate than this without calibration and that after the calibration is taken into account the remaining uncertainty is only 1 in 10,000.

With respect to measurement of the time interval the code requires that the time of diversion of water flow from one tank to another shall be determined to within 2 sec. The author has found that a trained operator can read this time to the nearest half second when automatic equipment is employed to do the switching.

**Power.** Apparently it is not so easy to meet the code requirements with respect to the magnitude of the permissible wattmeter calibrations. The great majority of the differences in the author's Fig. 2, and also the root-mean-square values lie within a range of 0.1 per cent of full scale reading. There are several points where the difference is greater, but less than 0.3 per cent, the value at which the code requires further comparisons or even test rejection.

**Temperature.** The author's choice of 6-in. immersion for thermocouples coincides with the recommendation in the code.

Chromel-constantan for thermocouples is not one of the pairs of metals suggested by the code, but no doubt one reason for the use of these two materials is the much greater emf they will generate. This amounts to about 70 per cent more than for the chromel-alumel combination and 40 per cent more than for the iron-constantan combination at the level of modern throttle temperatures. Of course this reduces the uncertainty in the temperature measurement.

It is interesting to note that in the code the use of standard melting points as a means of calibration is specifically not recommended for test-code accuracies, the reason given being difficulty in manipulation.

**Pressures.** The test code deals at length with pressure-measuring instruments and test connections. However, no limits on the magnitude of dead-weight gage calibrations or on the variation between successive calibrations are given.

The author's instruments for measuring exhaust pressure conform with the code with respect to inside diameter of glass tubes and the use of verniers.

**Flow Nozzles.** The code places the limit of possible error in flow measurement by either a flow nozzle or a thin-plate orifice at  $\pm 1.50$  per cent and  $\pm 1.25$  per cent for steam and water, respec-

<sup>3</sup> Design Engineer, Steam Engineering Department, Westinghouse Electric Corporation, Philadelphia, Pa. Mem. ASME.

tively. No distinction is made as to type of primary element and no mention is made of calibrations.

The author does not say what methods, if any, are used to minimize the amount of pulsations of the mercury in the manometers used to measure the pressure drop across a flow nozzle. The code does prohibit attempts to reduce pulsations by damping means. However, solenoid-operated valves are currently being used in some tests to stop the pulsations completely at precisely measured time intervals to allow the observer to take careful readings.

*Station Instruments.* The author points out the uncertainty to be expected in the use of station instruments. Evidently greater errors can be expected in the measurement of power than in flow measurement. The errors are greater for steam flow than for condensate flow and greater when station meters are used rather than test manometers.

It may be that the Power Test Codes Committee will want to consider review of the code and make revisions to reflect current practice in running precision tests.

W. A. POLLOCK.<sup>4</sup> This paper presents a very good outline of the steps which are necessary to obtain the desired reliability and accuracy from instruments used in turbine tests.

The author reports the percentages of uncertainty of measurements of flow, power, temperature, initial pressure, exhaust pressure, and the corresponding effect on over-all turbine efficiency.

It is quite evident that he is well aware of the difficulty of obtaining a close approach to so-called absolute accuracy. He

<sup>4</sup> Technical Engineer of Power Plants, Wisconsin Electric Power Company, Milwaukee, Wis. Mem. ASME.

describes the painstaking efforts that are made to insure precise measurement. He appreciates that to gather doubtful data is a waste of time and expense when positive methods can be used.

We are reminded that instruments of a high quality are essential, first to obtain the best accuracy, and then to retain this accuracy as long as possible. A high degree of accuracy is essential not only in tests to determine if the turbine meets its guaranteed heat rate, but also in those conducted later to determine the possible need for turbine maintenance.

Instrumentation for daily turbine operation requires ruggedness and reliability with some sacrifice of accuracy, but for testing a turbine accuracy should come first, within practical limitations, of course.

The most important measurements are those of input flow and output power. Measurement of condensate flow by weighing tanks is more accurate than by flow nozzles and their use in owner plants should be encouraged wherever possible.

#### AUTHOR'S CLOSURE

The author wishes to thank Messrs. Deming and Pollock for their comments. Mr. Deming's comparisons of the accuracies of these tests with those in the ASME code are quite interesting.

In answer to Mr. Deming's inquiry, the flow-nozzle manometer connections were open during each test run, with no dampers or quick-closing valves.

Mr. Deming comments that apparently station instruments are less accurate for measuring power than flow; this is true in the data in Table 1. On the other hand, the data in Fig. 11 are typical of what we often find in flow measurements by station instruments.

# Procedures for Testing Large Steam Turbine-Generators in Central Stations

By E. M. KRATZ<sup>1</sup> AND J. C. WESTCOTT,<sup>2</sup> SCHENECTADY, N. Y.

The instrumentation and procedures required to run a reliable performance test on a large steam turbine-generator require careful and detailed planning. The location of the measurements for the test of a turbine-generator with a typical feedwater cycle and the type of instruments and their application is described. The accuracy of measuring the performance is evaluated from an analysis of the probable errors in measuring flows, temperatures, pressures, and generator load. The probable errors determined by this method are compared to the consistency of data that has been obtained on turbine performance tests and to performance measured by more than one method.

## INTRODUCTION

PERFORMANCE tests of large steam turbine-generators must of necessity be run in the central station after the unit is in service. The experience of the authors' company in the participation in a large number of these tests has been reported previously.<sup>3</sup> This paper will describe the calibration and application of the instruments used and the testing procedure required to measure the performance of large steam turbine-generators accurately. An evaluation of the expected accuracy of the measured performance also will be made from an analysis of the expected errors in the measurements. The expected accuracy obtained by the analysis will be compared to the consistency of data from repeat or check points on the same unit, comparison of performance measured by more than one independent means, and comparison of tests on duplicate units.

## FLOW MEASUREMENTS

Fig. 1 is a schematic diagram of a typical reheat turbine and feedwater cycle showing the location of instrumentation used for a performance test. This diagram does not show the connections to auxiliary equipment such as evaporators, steam air heaters, and condensate storage or surge tanks. It is desirable to run performance tests with this equipment out of service to reduce the number of measurements and possibilities of testing errors. All connections between such equipment and the test piping must be positively isolated by either closing two valves with an open drain between them, a blank flange, or one valve and an open-end pipe. Miscellaneous piping within the cycle,

such as steam-line drains to the condenser or drain tank, and heater-drain by-passes are not shown on the diagram. These lines also must be positively isolated as just described to insure that no steam or water is flowing in them. Feedwater-heater vents are shut off where possible during the test. Where this cannot be done, they are throttled down and the high-pressure heaters vented to atmosphere so that the amount of steam flow can be observed and held to a minimum. Low-pressure heaters usually must be vented to the condenser during the test to prevent them from becoming airbound and inoperative. These vents are throttled down the maximum amount that will still permit proper operation of the feedwater heaters.

It is impractical to provide reliable calibrated instrumentation to measure directly throttle or reheat steam flow, since it is not practical to provide for inspection and cleaning of flow nozzles installed in high-pressure piping. Neither are there facilities available for calibration under operating conditions. The throttle flow is therefore obtained from a measurement of condensate or boiler feedwater flow.

Two calibrated flow nozzles are used to measure the condensate flow to the deaerator. One of these is selected to give a pressure drop of about 40 in. Hg at the maximum test load. This nozzle will have a deflection of only about 10 in. Hg at half load, and a smaller nozzle sized to give about 40-in-Hg pressure drop at half load is used for the tests at low loads. Prior to the test each nozzle in its section of pipe with flow straighteners is calibrated in a laboratory against weighed or volume-measured flow.<sup>3</sup> The upstream section of the pipe with a flow straightener is 20 pipe diameters long and the downstream section is 10 diameters long. These pipe and nozzle assemblies are then installed in the station just before the performance tests are to be run to assure cleanliness and good condition of the nozzle at the time of test.

The pressure drop across the nozzle is measured with two manometers connected to two independent pairs of upstream and downstream pressure taps. The connecting lines slope downward from the pressure taps to the manometers. If this cannot be accomplished, the highest point in the line must be vented to eliminate air pockets. Precautions also must be taken to assure that the lines to the upstream and downstream taps are at the same temperature. A relatively small difference in the temperature of the two lines can cause an appreciable error, especially if the vertical distance between the nozzle and manometers is large. If the two nozzles are installed in parallel with each other, or with a station run of pipe, two closed valves with an open drain between them must be provided in the lines not in use to be sure that all of the condensate flow is measured.

At this location in the cycle the calibrated nozzle measures the turbine-exhaust flow and the total of the extraction flows to the three low-pressure heaters after corrections are made for the change in level in the hot well and gland-seal tank, condensate-pump leakage, the drain from the air-ejector condenser to the hot well and the net sealing-water leakage into or out of the boiler feed pumps. This net leakage is determined from the measured difference between the sealing flow to and from the pumps.

<sup>1</sup> Supervisor, Turbine Performance Engineering, General Electric Company. Mem. ASME.

<sup>2</sup> Engineer, Large Steam Turbine-Generator Department, General Electric Company. Assoc. Mem. ASME.

<sup>3</sup> "Experience in Testing Large Steam Turbine-Generators in Central Stations," by E. M. Kratz, ASME Paper No. 54-A-258.

Contributed by the Power Test Codes Committee and presented at the Diamond Jubilee Annual Meeting, Chicago, Ill., November 13-18, 1955, of THE AMERICAN SOCIETY OF MECHANICAL ENGINEERS.

NOTE: Statements and opinions advanced in papers are to be understood as individual expressions of their authors and not those of the Society. Manuscript received at ASME Headquarters, November 18, 1955. This paper was not preprinted.

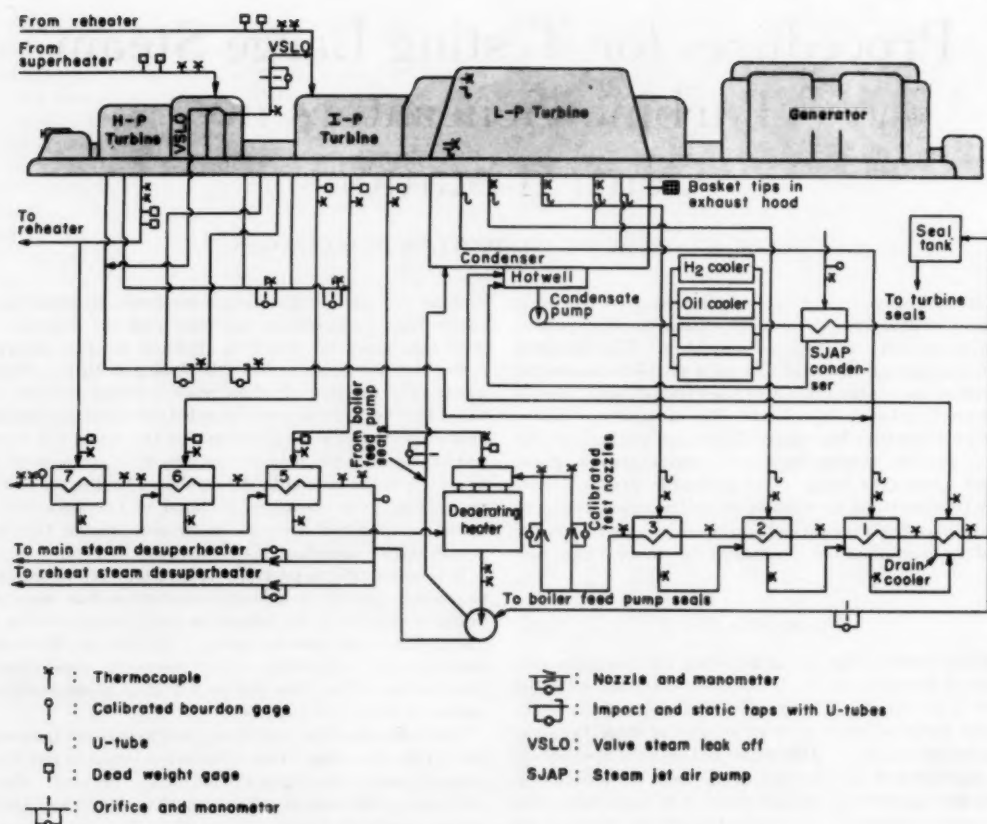


FIG. 1 DIAGRAM OF CYCLE AND LOCATION OF INSTRUMENTS

These sealing flows are measured with sharp-edged orifices built and installed to ASME test code specifications and with mercury manometers.

When the calibrated nozzles are located in the condensate line to the deaerator, as shown in Fig. 1, very rapid fluctuations in the condensate flow are usually dampened out in the low-pressure feedwater heaters and leakage from the condensate to the steam side of the low-pressure heaters will not cause an error in the measured flow to the deaerator. However, the water temperature and therefore the Reynolds number may be higher than can be obtained with calibrating equipment available. Therefore it must be assumed that the flow coefficient of the nozzle and pipe section is a function of the Reynolds number only and is constant after turbulent-flow conditions are obtained. An alternate location of the flow nozzle is in the condensate line to the low-pressure heater, provided it can be established that no low-pressure feedwater-heater leakage exists.

Where wet steam is extracted from the turbine to a low-pressure heater from which the drain is pumped back into the condensate line, the test nozzle must be installed downstream from the return point or else the drain flow from the heater must be measured accurately with a calibrated nozzle or orifice. A heat balance to calculate the extraction flow to a heater obtaining steam from a wet turbine stage may be in error. The enthalpy of the steam to the heater cannot be measured and is usually estimated from the turbine expansion line determined by the test data. However, the expansion line represents the average

enthalpy of the steam in the turbine. Since a large amount of excess moisture, as much as one per cent of the throttle flow,<sup>4</sup> may be extracted with the steam, failure to obtain a measurement of the drain flow from this heater will result in too low a measured throttle flow.

The extraction flows to the three high-pressure heaters and to the deaerating heater are obtained from heat balances on the high-pressure heaters and a heat balance and flow balance around the deaerator which require temperature and pressure measurements as shown in Fig. 1. The flow from the boiler-feed-pump discharge to the throttle and reheat-steam desuperheaters is measured with uncalibrated flow nozzles or orifices and mercury manometers. The desuperheating flow is seldom more than three per cent of the throttle flow so that the accuracy obtained from an uncalibrated nozzle is satisfactory as long as the nozzle installation and differential measurement are adequate and the nozzle is known to be in good condition. The leakage flow from the boiler feed pumps and the change in level in the deaerator storage tank also are measured. The four high-pressure extraction flows are therefore the only unknown quantities and are obtained from a simultaneous solution of the four heat balances and flow balance.

The turbine shaft-end-packing leakages to the number five heater and the control-valve leakage to the intermediate-pressure

<sup>4</sup> "Operating Characteristics of the 100,000-Kw Essex Turbine Generator," by Stanford Neal and V. S. Renton, *Trans. ASME*, vol. 72, 1950, p. 267.

section are measured with sharp-edged orifices and mercury manometers. The shaft-end-packing leakages and the control-valve leakages to the number one heater are measured with pitot tubes and mercury U-tube manometers.

A study of Fig. 1 will reveal that, from the individual flows measured as just described, the throttle and reheat flows can be determined by a flow balance.

An analysis of the various items involved in obtaining throttle and reheat flows as outlined indicates a "probable error" of 0.26 per cent. In this paper the term probable error is used to indicate root-mean-square error. About 68 per cent of a large group of tests will be in error less than the probable error and about 32 per cent will be in error greater than the probable error. Kimball<sup>3</sup> gives a good discussion of the theory of errors as applied to the subject of turbine testing. The various items making up the 0.26 per cent are discussed in the following paragraphs.

The probable error of the flow coefficient of the calibrated flow nozzle and pipe section is 0.17 per cent. This is based upon the calibration data shown in Fig. 2 for eight flow nozzle and pipe sections. Each pipe has four static-pressure taps located one diameter upstream of the nozzle flange as shown in Fig. 3 and the nozzle has four static taps located in the throat. Differentials are read on each of the four pairs of taps during calibra-

tion. Three of the test sections were calibrated at three laboratories and four at two laboratories. Three have been calibrated twice at the same laboratory and one was calibrated three times at the same laboratory. Each point in Fig. 2 is the deviation of the average coefficient measured during one calibration of two pairs of pressure taps 180 deg apart from the average of the coefficients from all calibrations of that pipe and nozzle section.

During turbine tests, flow-nozzle differentials are read at one-minute intervals on two pairs of pressure taps 180 deg apart. An analysis of the differences between the readings obtained from these two pairs of taps on 51 test points taken at random indicates a probable error of 0.06 per cent in flow as a result of errors in measuring nozzle-pressure drop.

An additional 0.1 per cent probable error has been allowed for the station piping ahead of the test section being different from the nozzle calibration piping and for error in correcting for the expansion of the nozzle with higher temperature water.

In obtaining the error for the extraction flows to the high-pressure heaters it has been assumed that, where the instrumentation is duplicated, water temperatures are known to within 0.5 F and steam temperatures within 1.0 F. This accuracy is justified by an analysis of the temperature-measuring equipment and leads to an additional probable error of 0.10 per cent of throttle flow. Errors in other measurements contributing to throttle flow are 0.03 per cent for the measured change in water stored in the hot well and gland-seal tank, and 0.12 per cent for measurements of miscellaneous flows such as the sealing water

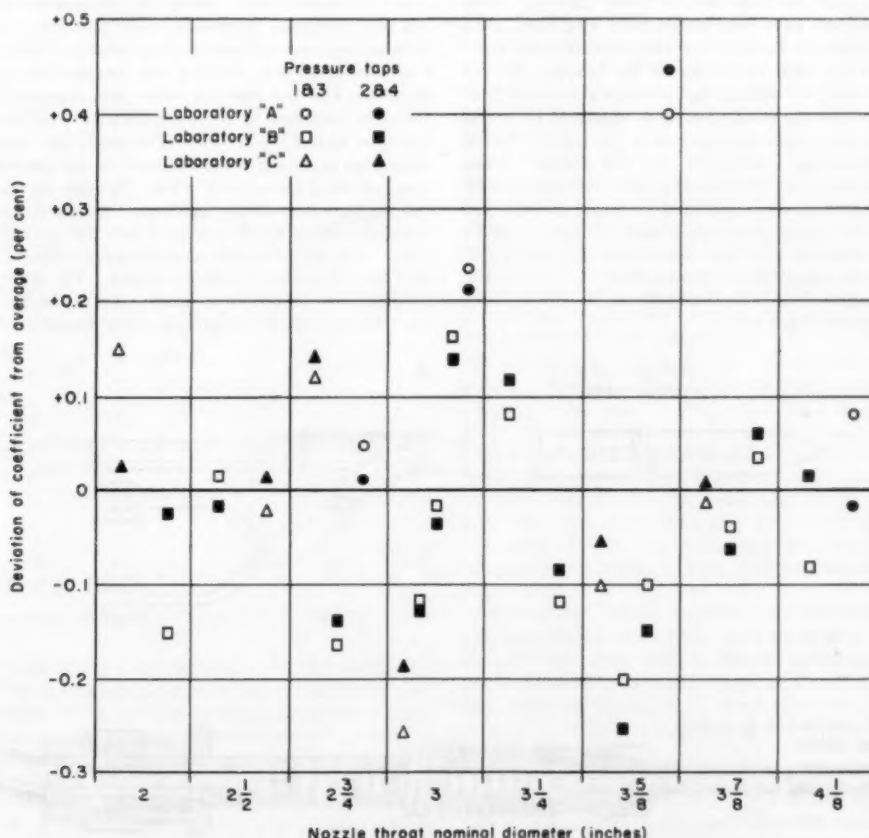


FIG. 2 CALIBRATION OF TEST FLOW NOZZLES AND PIPE SECTIONS

<sup>3</sup> "Accuracy and Results of Steam-Consumption Tests on Medium Steam Turbine-Generator Sets," by D. E. Kimball, ASME Paper No. 54-A-253.

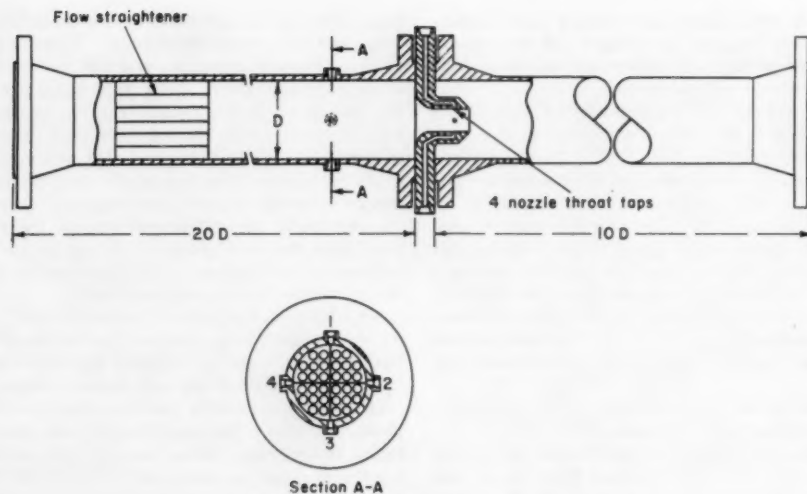


FIG. 3 TEST FLOW NOZZLE PIPE ASSEMBLY

to and from the boiler feed pumps and the drain from the air-ejector condenser to the hot well.

It has been possible to check the reliability of throttle flow obtained by the method that has been outlined. Several nonre-heat turbine-generators have been tested both with normal extraction to the feedwater heaters and with nonextraction operation. When testing with extraction to the heaters, throttle flow has been obtained by adding high-pressure extraction flows from heat balances to the condensate flow measured by a test nozzle. With nonextraction operation all of the throttle flow is condensed and measured directly by the test nozzle. When tests are run extracting and nonextracting with the same control-valve setting, the throttle flows corrected for initial pressure and temperature and the change in first-stage shell pressure should be equal. The data from the four most recent machines tested with both extraction and nonextraction operation have been analyzed. The root-mean-square of the differences between throttle flows by the two methods was 0.15 per cent.

#### TEMPERATURE MEASUREMENTS

All steam and water temperatures are measured with calibrated test thermocouples. The thermocouples are made of chromel-P and constantan wires which are continuous between the hot and cold junctions to prevent errors induced by thermal emf's from temperature differences or gradients at connections. Fig. 4 is a cross section showing the construction of the thermocouples. The hot-junction wires are supported by two-hole porcelain insulators in a  $\frac{1}{4}$ -inch-diameter stainless-steel protection tube with a  $\frac{1}{32}$ -in. wall. The protection tube prevents the wires from becoming work-hardened at the location where high-temperature gradients will occur. The hot junction is made by welding the wires together in a bead. The bead is peened in a slot in the steel plug which is welded into the end of the protection tube. A length of flexible metal armor is fastened to the  $\frac{1}{4}$ -inch steel tube to prevent work-hardening. The wires in the armor are insulated by porcelain beads. From the flexible armor to the cold junction the wires are in a cotton-and-rubber insulation.

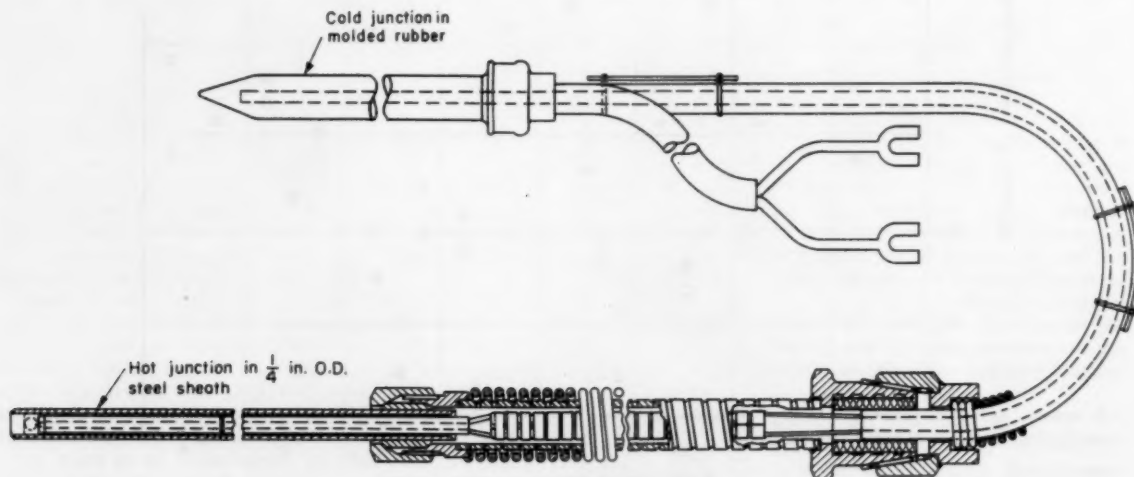


FIG. 4 THERMOCOUPLE CROSS SECTION

Two copper leads are soldered to the thermocouple wires at the cold junction which is in a molded-rubber covering. The wires, insulators, and tubing at the hot junction are cleaned carefully and baked before assembly. After the thermocouple is completed it is aged for four hours at 1200 F to minimize corrections for immersion of the hot junction in the thermocouple well.

Each completed thermocouple is calibrated at 6-inch and 12-inch immersion at temperatures of 80 F, 177 F, 430 F, 663 F, 776 F, 888 F, and 1000 F before it is used. Calibrations are made in an oil bath up to 663 F and in an electrically heated cylindrical copper block with longitudinal holes at higher temperatures. The standard of comparison is a platinum resistance thermometer which has been checked by the National Bureau of Standards and also is checked periodically at the standard freezing and vapor points. The copper block has been explored by means of differential thermocouples to determine variations in temperature between the several holes in which the test and standard instruments are inserted. There is no measurable difference between the holes at the same immersion. There is a temperature gradient of about 0.1 F per inch along the length of the block. The thermocouples to be calibrated and the standard instrument are always immersed the same distance. Each thermocouple also is calibrated before it is used for a turbine test over the range of temperature and immersion for which it will

couples. Since each instrument is checked before it is used the uncertainty of the correction should be no more than 0.2 F.

At locations in the cycle where errors in temperature have a relatively large effect on the measured turbine-generator performance the instrumentation is duplicated. For the cycle in Fig. 1 these locations are as follows:

Throttle steam to the high-pressure section.

Exhaust steam from the high-pressure section to the reheater.

The reheated steam to the intermediate-pressure section.

Boiler-feed flow from the number 6 high-pressure heater.

Condensate flow to and from the deaerator.

Boiler-feed flow to the number 5 high-pressure heater.

It is important that the physical location of the thermocouple wells be considered carefully. In condensate and feedwater lines they should be located so that water leaving the heater or after a pipe connection has a chance to mix thoroughly. The temperature of the cold reheat steam leaving the high-pressure-section exhaust also may be stratified and these wells preferably should be located after one or two elbows and approximately 15 feet from the exhaust connection. In any case, the best location for the wells is dependent upon the length of pipe needed to obtain complete mixing and the heat loss from the pipe. Extraction steam temperatures should be measured near the turbine and near the feedwater heaters to obtain the heat loss unless the lines are very short. Heater drains are measured between the heater and its drain-control valve. The temperature of shaft-packing leakages from the turbine must be measured to account properly for the work done by this steam. Temperature measurements are shown at the exhaust of the intermediate-pressure section. These readings are not necessary to determine the heat rate of the unit; however, they are of value to determine the condition of the intermediate-pressure section by the enthalpy-drop method.

It is estimated that water temperatures are measured with an accuracy of 0.5 F and steam temperatures to 1.0 F where the instrumentation is duplicated. The thermocouples are read with precision potentiometers and separate light-beam galvanometers. The cold junctions are immersed in an ice-water bath. The smallest division on the potentiometer dial is 0.01 mv and the reading can be estimated to  $\pm 0.001$  mv which represents about 0.03 F when using chromel-P-constantan thermocouples. The potentiometers are calibrated to 0.05 mv or 0.15 F. Each thermocouple is read every five minutes for a two-hour test period. When in use the thermocouple hot junction is at the bottom of the well. If the well extends inside the pipe wall several inches and the pipe and well are insulated properly, the bottom of the well and thermocouple hot junction are very close to the fluid temperature. It is estimated that this error will be no more than 0.2 F with water and 0.5 F with steam. The probable errors in turbine heat rate resulting from errors in measuring throttle, high-pressure-section exhaust, and reheat temperatures are 0.06 per cent, 0.05 per cent, and 0.04 per cent, respectively.

In small lines such as valve-stem leakoffs and sealing water to and from pumps where wells would cause an appreciable restriction, thermocouples may be peened in the pipe wall. Where proper precautions are taken to prevent heat loss from the pipes and along the thermocouple wires adjacent to the hot junction these measurements will be correct within a few degrees.

#### PRESSURE MEASUREMENTS

The pressure measurements at the throttle and exhaust of the high-pressure section and at the inlet to the intermediate-pressure section are duplicated. These pressures and all other pressures above about 35 psia are measured with deadweight gages.<sup>4</sup> It

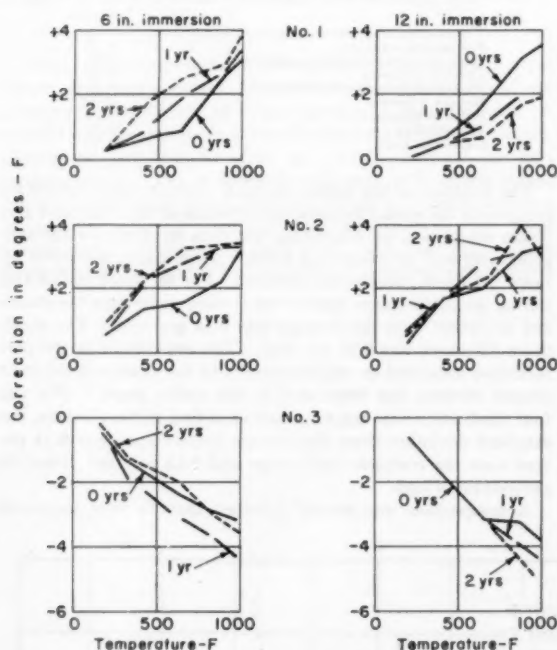


FIG. 5 CALIBRATION RECORD FOR THREE TYPICAL THERMOCOUPLE

be used. A record of the calibrations of each thermocouple is kept in order that those with the least change in calibration with use and immersion can be used for the most important temperature measurements. In Fig. 5 the calibration record is shown for three typical thermocouples over a two-year period of time. A check of the records of 30 thermocouples used on performance tests gives an average change in calibrations at 430 F, 663 F, 888 F, and 1000 F of 0.5, 0.7, 0.7, and 0.5 deg, respectively, at six inches immersion over a two-year period. At 80 and 177 F the change in correction was less than 0.2 F for all 30 thermo-

is important that the connecting lines between the pressure tap and the gage be known to be filled with water and that the proper correction is made for the weight of the water column. With the exception of the turbine-exhaust pressure, all pressures below 35 psia are measured with mercury U-tubes. The pressure lines to the mercury U-tubes are purged with air, since at low-pressure levels uncertainties in the correction for water legs may cause significant errors in the pressure reading. Since the change in water enthalpy with pressure is small, condensate and feedwater pressures are measured with calibrated Bourdon gages. The deadweight gages are checked periodically against a gage which has been calibrated by the National Bureau of Standards. The error in reading throttle, high-pressure exhaust, and reheat pressure is less than 0.1 per cent of the pressure which corresponds to errors in turbine heat rate of 0.01 per cent for throttle pressure, 0.01 per cent for high-pressure exhaust pressure, and 0.01 per cent for reheat pressure.

The turbine-exhaust pressure is measured with mercury absolute gages connected to basket tips located at the exhaust flange. The construction and characteristics of the basket tips are described elsewhere.<sup>3</sup> The error in exhaust pressure is 0.02 in. Hg. The resulting error in heat rate is dependent upon the load and exhaust pressure. Near rated load and at exhaust pressures of 1.0 to 1.5 in. Hg the error in heat rate is approximately 0.04 per cent.

#### LOAD MEASUREMENT

The generator output is measured by the three-wattmeter method. Where bushing current transformers are supplied with the generator, these are calibrated prior to the test with the secondary burden of the test instruments and leads. Three test potential transformers are connected from line to the generator neutral. The potential transformers also are calibrated before the test with the burden of the test instruments and leads. The output of the generator is read by three indicating wattmeters or watthour meters. Where indicating wattmeters are used, each instrument is read at one-minute intervals over the two-hour test period. Indicating ammeters and voltmeters also are connected to the test secondary circuits and read at five minute intervals. No other wiring or instruments are connected to either the current or potential transformers. When watthour meters are used the load is obtained by counting the revolutions of the meter disk.<sup>3</sup> With this arrangement checking the load-measuring setup is simple and direct. The total output is obtained from three single-phase load measurements which usually are very nearly equal. The wattmeters or watthour meters and voltmeters and ammeters are calibrated in the laboratory before and after the test. The indicating wattmeters are calibrated after each test point with portable d-c calibrating equipment.

The calibration data on the current and potential transformers are certified to be correct to within 0.1 per cent and are expected to be better than 0.05 per cent. The indicating wattmeters have 120 scale divisions. Each of the meters is read at one-minute intervals during the two-hour test period. On 12 one-hour runs taken at random from tests on three different turbine-generators the average of the indicated readings taken on the odd minutes

agreed with that taken on the even minutes within 0.036 per cent. The wattmeter deflections on these runs were from 37 to 83 per cent of full scale. We have assumed that the probable reading error is 0.05 per cent when the data takers are properly trained and that the over-all uncertainty of the generator-output measurement is 0.2 per cent when using indicating wattmeters.

In the previous paper<sup>3</sup> the comparison between load measurements with watthour meters and indicating wattmeters was given as 0.15 per cent. Additional data have been obtained, and on a total of 52 test points from three turbine performance tests the average difference between the two methods was 0.06 per cent. From these data we have concluded that watthour meters are satisfactory for measuring generator output by counting revolutions of the meter disk where proper measures are taken to eliminate friction and heating effects as outlined previously.<sup>3</sup>

#### PROBABLE OVER-ALL ACCURACY

The combined error in over-all turbine performance tests made with the instrumentation which has been described is 0.34 per cent, which is obtained as the square root of the summation of the square of the probable errors from the measurements given in Table 1.

TABLE 1 ERRORS IN TURBINE PERFORMANCE TESTS

	Per cent
Throttle temperature	0.06
Reheat temperature	0.05
High-pressure exhaust temperature	0.04
Throttle pressure	0.01
High-pressure exhaust pressure	0.01
Reheat pressure	0.01
Exhaust pressure	0.04
Throttle flow	0.26
Generator load	0.20

The accuracy of the testing methods also can be evaluated by comparing the spread between check points at the same load and steam conditions, by comparing test data on duplicate turbine-generators and by comparing turbine performance measured by more than one independent method. For 58 check points run during the performance tests of ten turbine-generators the standard deviation from the average was 0.14 per cent. The maximum difference was 0.25 per cent. The consistency of the performance measured on duplicate units in the same and different central stations was illustrated in the earlier paper.<sup>3</sup> For the four duplicate reheat machines tested at four power stations, the standard deviation from the average performance was 0.34 per cent over the complete load range and 0.15 per cent above 60 per cent rated load.

A comparison was shown<sup>3</sup> between throttle flow measured

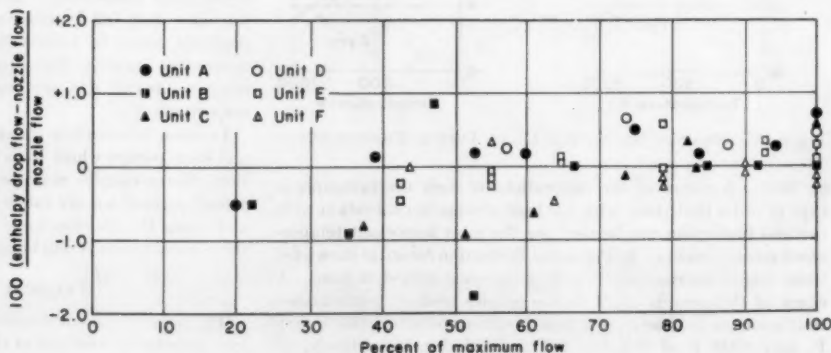


FIG. 6 COMPARISON OF THROTTLE FLOW BY ENTHALPY DROP AND BY NOZZLES

by enthalpy drop and load on noncondensing sections of cross-compound turbine-generator units and the same flow based upon a calibrated flow nozzle. Fig. 6 shows these data with the addition of the same type of information from tests of three additional turbines. Throttle flow calculated from enthalpy-drop measurements averaged 0.01 per cent higher than the throttle flow from nozzle or orifice measurements and the maximum difference was 1.9 per cent. The root-mean-square of the differences between throttle flow from the two methods of measurement is 0.47 per cent. From 60 per cent to 100 per cent of maximum flow the largest difference was 0.6 per cent and the root-mean-square of the differences was 0.32 per cent.

From an analysis of the measurements used to obtain throttle flow from a condensate-nozzle measurement a probable error of 0.26 per cent was derived which would result in an error for throttle flow by enthalpy and load measurements of

$$\sqrt{(0.47^2 + 0.26^2)} = 0.39 \text{ per cent}$$

However, from considering the errors previously derived for temperature, pressure, and generator-output measurements, the uncertainty of throttle flow calculated from enthalpy drop is 0.56 per cent. These data indicate that the uncertainty in throttle flow from condensate flow or throttle and exhaust-temperature errors is considerably less than expected from an analysis of the individual instrument and reading errors.

#### STATION INSTRUMENTS

When measuring turbine performance with station instruments, obtaining a reliable throttle flow and generator load are of primary importance as when running an accurate test. A reliable flow measurement is usually the most difficult to obtain. Station primary-flow elements are usually designed for low-pressure drops. This is desirable as it reduces throttling losses, but as a consequence the magnitude of errors in flow measurement is increased. Errors from transmitters, recorders, and integrators can be reduced by calibrating them carefully. These errors may be eliminated by connecting a test manometer to the

primary element which has been done on a large number of turbine-generator performance tests. Forty per cent of the checks of steam and water flows calculated from differential measurements across station primary elements differed from the same flows as established by carefully calibrated test instruments by more than 1.0 per cent.

One of the most common causes of incorrect load readings is neglecting the voltage drop in the secondary leads from the potential transformers to the watt-hour meter. This is frequently in the order of 1.0 per cent and is in the direction to make the indicated load too low. In one installation this correction was over 2.0 per cent. The voltage drop can be calculated readily from the design current used by the meters in the circuit if the length and size of the wires from the PT's to the watt-hour meter are known. Large distances between the PT's and meters and high power-consuming devices such as voltage-regulator coils in the metering circuit have frequently explained apparently poor turbine-generator performance.

#### CONCLUSIONS

When measuring the performance of a large turbine-generator, errors in throttle flow and load are the most significant. This is true for both highly accurate tests and for data obtained from station instruments. For a test run with the best instrumentation and with careful attention to testing procedures, flow and load measurements contribute over 90 per cent of the probable error in the results.

When they are made carefully, other measurements contribute a small amount of error to the measurement of the over-all turbine performance. Other than the best method, however, cannot be justified. For example, increasing the uncertainty in throttle temperatures from 1.0 to 5.0 F would increase the probable error in heat rate from 0.34 to 0.45 per cent. Accurate pressure and temperature measurements are also of value in checking the condition of the turbine by enthalpy-drop measurements and accurate pressure measurements can be used to check the testing procedures.



# A Practical Application of Uncertainty Calculations to Measured Data

By L. W. THRASHER<sup>1</sup> AND R. C. BINDER<sup>2</sup>

In order to answer questions as to the reliability of measurements, it is desirable to classify two types of measurements: (a) The multiple sample, and (b) the single sample. The case for multiple-sample measurement is well established, whereas the case for single sample has not been established. It is proposed that the tester estimate his error—the uncertainty interval—and give odds that the error would be less than the uncertainty interval if the measurement were repeated a large number of times. A numerical example is presented.

## INTRODUCTION

QUESTIONS arise frequently as to the reliability of the results of equipment performance. In order to answer these questions, it appears desirable to classify two types of measurement, the multiple sample and the single sample. In multiple-sample measurement all readings are taken enough times using enough observers and enough different instruments so that the reliability of the results can be investigated by statistical relations. In single-sample measurement the readings are made only once so that the reliability of the results is not found by repetition.

Methods for the treatment of multiple-sample measurement are available in the publications of the American Society for Testing Materials.<sup>3</sup> The case for single-sample measurement has not been so well established. Kline and McClintock<sup>4</sup> made some proposals for single-sample measurement which look very promising. The following discussion supplements the work of Kline and McClintock.

Although multiple-sample measurements are desirable, time and cost considerations often restrict the tester to single-sample measurements. Thus it would be helpful if measures of reliability for single-sample measurements could be established.

## DEFINITIONS AND METHOD

To avoid confusion, the definition of several terms should be reviewed. The difference between the true value of a quantity and a single observed or measured value of the quantity is the "error" of the measurement. The accuracy of a measurement is indicated by the size of the error; an accurate measurement has a small error, whereas an inaccurate measurement has a large error. The "precision" of a measurement is indicated by how sharply or

clearly the experimental result is defined. Note that a precise measurement is not necessarily accurate. Since the true value is seldom known, the error is usually estimated. The estimate of what the error might be is the uncertainty of the measurement.

For the single-sample measurement it is proposed that the tester describe the uncertainty of his measurement in terms of what he believes would happen if the measurement were repeated a large number of times. In this way one can estimate his error—the uncertainty interval—and can give odds that the error would be less than the uncertainty interval if the measurement were repeated a large number of times. The reliability of a result described in this manner is indicated by the size of the uncertainty interval and the magnitude of the odds. Large odds would indicate a reliable result.

In order to understand this method more fully, it is useful to study the relationship of a priori probability, statistical probability, and betting odds.<sup>5</sup> The a priori probability or simply the probability that an event will happen is defined as the number of cases favorable to the event, divided by the total number of independent and equally likely cases that are possible. A probability of one means certainty. A probability of zero means impossibility. In actual cases the probability is always less than one. Probability may be expressed either as a fraction, as a decimal, or as a per cent. For example, probabilities of 1/2 or 0.5 or 50/100 or 50 per cent are all equivalent.

For a simple event, as the throwing of several identical dice, the total number of possible cases for the event and various probabilities can be determined by analysis. For a more complicated problem, however, say, the measurement of static pressure of water flowing in a pipe, a probability analysis would be much too complex. If results of a large number of measurements were available, a statistical analysis could be made and "statistical probabilities" could be computed for these complex cases as is done in multiple-sample measurements.

There is a simple relation between probability and odds. If the probability that the error will be less than the uncertainty interval is 95 per cent (19/20), the odds that the error will be less than the uncertainty interval are said to be 19 to 1 (19 out of 20). In reverse, if the odds are 19 to 1 (19 out of 20), the probability is 19/20 or 0.95 or 95 per cent. Thus odds are another way of expressing probability.

In a single-sample measurement, a result given as 20 psi  $\pm$  1 psi (19 to 1) means that the one making the measurement thinks that if the measurement were repeated a large number of times, the odds would be 19 to 1 or that the probability would be 95 per cent that the true value will be within the range of 20 psi  $\pm$  1 psi.

In general the method parallels the ideas used in mathematical statistics. The uncertainty interval is similar to the confidence limits of statistics, and the use of odds corresponds to the confidence level. It is to be emphasized that statistical parameters have a firm mathematical basis, whereas the terms used for single-sample measurement are only estimates based upon the experience and judgment of the observer.

<sup>5</sup> "The Science of Chance," by H. C. Levinson, Rinehart and Company, New York, N. Y., 1950.

<sup>1</sup> Research Engineer, California Research Corporation, La Habra, Calif.; formerly Research Fellow, Purdue University, W. Lafayette, Ind. Assoc. Mem. ASME.

<sup>2</sup> Professor of Mechanical Engineering, School of Mechanical Engineering, Purdue University, W. Lafayette, Ind. Mem. ASME.

<sup>3</sup> "ASTM Manual on Quality Control of Materials," second printing, May, 1951.

<sup>4</sup> "Describing Uncertainties in Single-Sample Experiments," by S. J. Kline and F. A. McClintock, *Mechanical Engineering*, vol. 75, 1953, p. 3.

Contributed by the Power Test Codes Committee and presented at the Diamond Jubilee Annual Meeting, Chicago, Ill., November 13-18, 1955, of THE AMERICAN SOCIETY OF MECHANICAL ENGINEERS.

NOTE: Statements and opinions advanced in papers are to be understood as individual expressions of their authors and not those of the Society. Manuscript received at ASME Headquarters, October 13, 1955. Paper No. 55-A-205.

## NUMERICAL EXAMPLE

A test to determine the discharge coefficient of an orifice meter will be used as a numerical example of the method. Measured quantities are: Weight of water flowing; time interval; water temperature; pressure differential across the orifice; and meter dimensions. The uncertainty intervals were chosen as follows:

$$\text{Weight (} w \text{)} 25 \pm 1/16 \text{ pounds} \dots \dots \dots \frac{\Delta w}{w} = 0.25\% \text{ (19 to 1)}$$

$$\text{Time (} t \text{)} 100 \pm 0.2 \text{ seconds} \dots \dots \dots \frac{\Delta t}{t} = 0.20\% \text{ (19 to 1)}$$

Density ( $\rho$ ) uncertainty in temperature measurement caused an uncertainty in density of water of 0.01 per cent. ....

$$\frac{\Delta \rho}{\rho} = 0.01\% \text{ (19 to 1)}$$

$$\text{Pressure differential (} h \text{)} 30 \pm 0.1 \text{ mm Hg} \dots \dots \dots \frac{\Delta h}{h} = 0.33\% \text{ (19 to 1)}$$

$$\text{Pipe diameter (} D \text{)} 0.8220 \pm 0.0001 \text{ in.} \dots \dots \dots \frac{\Delta D}{D} = 0.012\% \text{ (19 to 1)}$$

$$\text{Orifice diameter (} d \text{)} 0.1660 \pm 0.0001 \text{ in.} \dots \dots \dots \frac{\Delta d}{d} = 0.06\% \text{ (19 to 1)}$$

The orifice equation can be solved for the discharge coefficient  $C$  in the form

$$C = \theta w t^{-1} \rho^{-1/2} h^{-1/2} \phi^{1/2}$$

where  $\theta$  is a constant, and  $\phi = (d^{-4} - D^{-4})$ .

According to the square law,<sup>4</sup> the uncertainty in  $C$  is given by

$$\frac{\Delta C}{C} = \left[ \left( \frac{\partial C}{\partial w} \right)^2 \left( \frac{\Delta w}{C} \right)^2 + \left( \frac{\partial C}{\partial t} \right)^2 \left( \frac{\Delta t}{C} \right)^2 + \left( \frac{\partial C}{\partial \rho} \right)^2 \left( \frac{\Delta \rho}{C} \right)^2 + \left( \frac{\partial C}{\partial h} \right)^2 \left( \frac{\Delta h}{C} \right)^2 + \left( \frac{\partial C}{\partial \phi} \right)^2 \left( \frac{\Delta \phi}{C} \right)^2 \right]^{1/2}$$

Then

$$\frac{\Delta C}{C} = \left[ \left( \frac{\Delta w}{w} \right)^2 + \left( \frac{\Delta t}{t} \right)^2 + \left( \frac{1}{2} \frac{\Delta \rho}{\rho} \right)^2 + \left( \frac{1}{2} \frac{\Delta h}{h} \right)^2 + \left( \frac{1}{2} \frac{\Delta \phi}{\phi} \right)^2 \right]^{1/2} \dots [1]$$

$\Delta \phi / \phi$  is evaluated by the square law

$$\frac{\Delta \phi}{\phi} = \left[ \left( \frac{\partial \phi}{\partial d} \right)^2 \left( \frac{\Delta d}{\phi} \right)^2 + \left( \frac{\partial \phi}{\partial D} \right)^2 \left( \frac{\Delta D}{\phi} \right)^2 \right]^{1/2} = \frac{4}{d^{-4} - D^{-4}} \left[ d^{-8} \left( \frac{\Delta d}{d} \right)^2 + D^{-8} \left( \frac{\Delta D}{D} \right)^2 \right]^{1/2}$$

For this orifice meter  $\Delta \phi / \phi = 0.24$  per cent (19 to 1). Substituting the uncertainties into Equation [1] gives the uncertainty interval for  $C$

$$\frac{\Delta C}{C} = 0.4 \text{ per cent (19 to 1)}$$

The measured value of  $C$  is reported as  $C = 0.625 \pm 0.4$  per cent (19 to 1).

Thus the tester believes that if the measurement were repeated a large number of times by independent observers, the probability is 95 per cent that the true value of  $C$  would lie in the range  $C = 0.625 \pm 0.4$  per cent.

## DISCUSSION

The results of a multiple-sample measurement giving only the average, and the maximum and minimum values of a measured quantity would be considered incomplete because these parameters alone give little clue as to how the measured values were distributed.

In a similar way, the result of a single-sample measurement with an uncertainty interval alone might be considered incomplete because the tester gives no estimation of what he believes the distribution might be if his measurement were to be repeated many times.

In one method of reporting the reliability of a single-sample measurement, the equation called the linear law<sup>4</sup> is used. The resulting uncertainty is said to be the maximum uncertainty of the measurement. There is a question as to the meaning of this maximum uncertainty.

Suppose it is desired to measure the relation between a quantity  $y$  as a function of some quantity  $x$ . In a multiple-sample measurement, at some value  $x_1$ , values of  $y$  would be measured a large number of times and the average of the measurements  $\bar{y}_1$  would be found. For a very large number of measurements, the average  $\bar{y}_1$  might be taken as the "true" value of  $y$ . Statistical analysis of the values of  $y$  would give the standard deviation  $\sigma$  or any other parameter needed to describe fully the reliability of the measurement. This procedure repeated at  $x_2, x_3, \dots, x_n$  is illustrated graphically in Fig. 1.

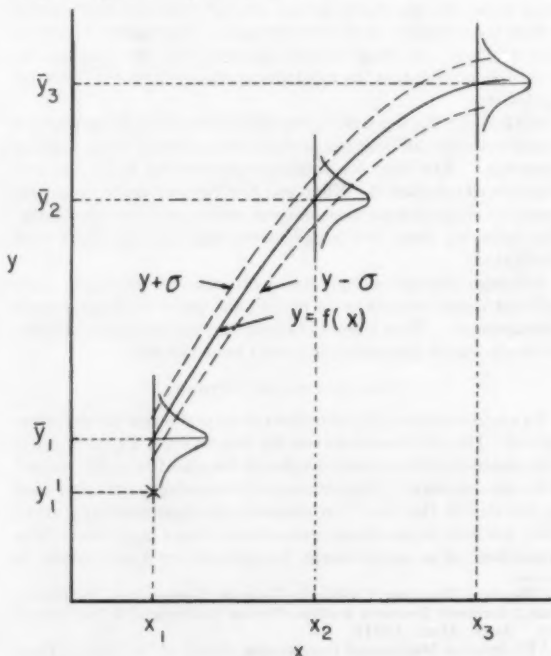


FIG. 1

For a single-sample measurement at  $x_1$ , say, some value  $y_1'$  is obtained. From the definition of the true value of  $y$  as the average of a very large number of independent measurements, it is apparent that there is no "maximum" uncertainty of  $y_1'$  because for a fixed  $x_1$ ,  $y_1'$  might be anywhere in the distribution of  $y$  about  $\bar{y}_1$ .

Because of the doubtful meaning of any maximum uncertainty for single-sample measurements, it is advantageous for the

tester to say something about what he believes the distribution would be if the measurement were repeated a large number of times. The use of odds is a method of adding this essential information.

## Discussion

S. J. KLINE.<sup>6</sup> The authors are to be congratulated for their clear presentation of an example of an uncertainty calculation. It is, of course, always agreeable to observe other workers employing the methods that one has suggested. This writer certainly agrees that a proper analysis of the uncertainty is an extremely useful tool in achieving good experimental results as well as a considerable timesaver. The following comments may be of use in adding to what has been said by the authors.

Apparently, the authors inadvertently have overlooked the paper by W. A. Wilson.<sup>7</sup> This paper, and the discussions thereto, point up very clearly the importance of the use of uncertainty analysis, in a systematic fashion, during the design stages. The importance of uncertainty analysis in the design stage cannot be overemphasized. In this writer's work, and in several other laboratories with which he is familiar, it has now become standard practice to require an analysis of uncertainty using the methods of footnote 4 of the paper as a necessary preliminary step before the prints of any experimental apparatus will be released for construction. This precaution has been found to result both in the improvement of the accuracy of experiments and in the minimization of unsatisfactory apparatus.

Another comment that might be added to the present paper concerns the general form of a nondimensional equation for calculation of the uncertainty in a result. The equation used by the authors is taken from Equation [7] of Kline and McClintock.<sup>4</sup> In its original form this equation was

$$w_R = \left[ \left( \frac{\partial R}{\partial v_1} w_1 \right)^2 + \left( \frac{\partial R}{\partial v_2} w_2 \right)^2 + \dots + \left( \frac{\partial R}{\partial v_n} w_n \right)^2 \right]^{1/2} \dots [2]$$

where  $w$  = uncertainty interval,  $R$  = result,  $R = R(v_1, v_2, \dots, v_n)$ , and  $v_1, \dots, v_n$  are in the  $n$  measured quantities. It has been found from considerable experience, that a nondimensional form of this equation is very useful because it allows all thinking to be done on a percentage basis and because in most cases although it is more complex looking it is actually simpler to use. Such a general nondimensional form can be derived as follows: Divide Equation [2] herewith, by the result being calculated,  $R$ . This gives

$$\frac{w_R}{R} = \left[ \left( \frac{\partial R}{\partial v_1} \frac{w_1}{R} \right)^2 + \left( \frac{\partial R}{\partial v_2} \frac{w_2}{R} \right)^2 + \dots + \left( \frac{\partial R}{\partial v_n} \frac{w_n}{R} \right)^2 \right]^{1/2} \dots [3]$$

Now, taking only the first term of the right-hand side of Equation [3], divide top and bottom by the variable in question  $v_1$ , yielding

$$\frac{\partial R}{\partial v_1} \frac{w_1}{R} = \frac{v_1}{R} \frac{\partial R}{\partial v_1} \frac{w_1}{v_1} = \frac{1}{R} \frac{\partial R}{\partial \ln v_1} \frac{w_1}{v_1} = \frac{\partial \ln R}{\partial \ln v_1} \frac{w_1}{v_1}$$

If similar operations are done for each term on the right-hand side of Equation [3], we obtain the desired form as

<sup>6</sup> Assistant Professor, Mechanical Engineering Division, Stanford University, Stanford, Calif. Mem. ASME.

<sup>7</sup> "Design of Power-Plant Tests to Insure Possibility of Results," by W. A. Wilson, Trans. ASME, vol. 77, 1955, pp. 405-407.

$$\frac{w_R}{R} = \left[ \left( \frac{\partial \ln R}{\partial \ln v_1} \frac{w_1}{v_1} \right)^2 + \left( \frac{\partial \ln R}{\partial \ln v_2} \frac{w_2}{v_2} \right)^2 + \dots + \left( \frac{\partial \ln R}{\partial \ln v_n} \frac{w_n}{v_n} \right)^2 \right]^{1/2} \dots [4]$$

An examination of Equations [2] and [4] of this discussion shows that  $\partial R / \partial v$  is the multiplicative factor which converts a unit uncertainty in the measured quantity into a unit uncertainty in the result, but  $\partial \ln R / \partial \ln v$  is the factor that converts a 1 per cent uncertainty in the measured quantity into a 1 per cent uncertainty in the result. The  $\partial \ln R / \partial \ln v$  is nearly always the more useful quantity.

One more comment needs to be made concerning the present paper. This relates to the matter of fixed errors and cross checks. In the first place, it needs to be repeated that the use of an uncertainty analysis alone in a single sample experiment is far from a desideratum. Inherently, a single-sample experiment is one in which the estimates of accuracy are not well established. Consequently, it is always better actually to replicate when it is feasible to do so. But if replication is impossible, then it should be recognized clearly that the accuracy situation is poor and, not only a single-sample uncertainty analysis, but also adequate cross checks such as energy balances, calibrations, and theoretical comparisons should be utilized to the greatest degree possible to ameliorate the situation. The cross checks not only provide the means for detection of really large errors, and thus yield greater accuracy, but they also provide the means for improved judgment in the future and give the strongest kind of verification of the reliability of the results.

Closely related to this problem of cross checks is the subject of fixed errors. First, we must recall that a fixed error is an error which is inherent in the means for data taking and cannot be eliminated by mere repetition. We then distinguish two cases: (a) The uncertainty intervals due to fixed errors are small compared to those due to random errors; (b) the uncertainty intervals due to fixed errors are equal to, or greater than, those due to random errors. While the writer hesitates to disagree with the authors, it is his opinion that the method they have proposed will work for case (a), but that it needs modification for case (b). Some discussion and a simple illustration will perhaps clarify this point.

If we desire to make a measurement of, say, pressure, which we intend to do with a Bourdon gage, it will not suffice simply to take ten Bourdon gages, with one observer for each gage, and then merely use the average of the resulting ten readings unless the factory or some other source has recently made a calibration of these instruments. If such calibrations had not been made, it is clear that we would get ten readings with so much scatter that simply averaging them would not provide useful data. If the instruments had been calibrated recently, we probably would have more success. Of course, the purpose of these calibrations is to eliminate the fixed error either by adjustment of the gage or by application of correction constants. Unfortunately, we do not always work with instruments that have just been calibrated, and in some cases such as very high temperatures no calibration standard is available.

There are four ways in which we can assure ourselves that the uncertainty intervals due to fixed errors are small compared to those due to random errors: (a) Use a primary-type instrument that is known to rely for its reading directly on some known physical law, such as a U-tube manometer and, in addition, make sure that no problems of sampling or response rate are important; (b) calibrate our instrument against an instrument of known greater accuracy, preferably one of a primary type; (c) replicate

the reading a great many times using not only many observers, but many fundamentally different types of instruments so that we can determine all possible fixed errors due to sampling, response, or recording; (d) calculate the fixed error by theoretical means. If the uncertainty due to fixed errors is inherently small or if we have measured the fixed error accurately enough by one of the means listed so that the uncertainty in the correction is small compared to the uncertainty due to random errors, and if we have applied this correction, then, and only then, will the mean of many readings approach the true value we are attempting to find.

It then follows immediately that if the value of the uncertainty due to fixed errors has not been or cannot be shown to be small compared to the uncertainty due to random errors then we must allow for the uncertainty due to fixed errors as well as that due to random errors in "guestimating" the total uncertainty interval in a given reading. It is therefore clear that in such cases visualization of mere repetition of the reading will not suffice and in this

sense the method suggested by the authors will be inadequate. It is to be noted that this does not invalidate their method, but it does mean that one must visualize a slightly broader class of experiments in the mental processes to be utilized in guestimating the uncertainty interval than that suggested by the present paper.

#### AUTHORS' CLOSURE

The authors thank Professor Kline for his excellent discussion of the capabilities and limitations of his method for calculating uncertainties. His remarks help clarify some of the weaker sections of his original paper.<sup>4</sup>

The authors agree that, as in the past, test instruments should be calibrated and test results should be cross-checked in order to reduce fixed errors to a minimum. An uncertainty analysis will not take the place of the usual precautions to insure accuracy in equipment test work.

# Investigation of Causes of Low Wheel-to-Rail Adhesion and Possible Methods of Improving It

By F. G. FISHER<sup>1</sup> AND R. K. ALLEN<sup>2</sup>

Wheel-to-rail adhesion is fundamental to the operation of a railroad. The potentially high tractive effort of modern diesel-electric and electric locomotives has focused attention more sharply on conditions which limit adhesion. Train stalls, rail burns, flat wheels, and damaged electric traction equipment all point to the importance of the problem. Extensive tests have yielded much information on the causes of low adhesion and methods of improving it. The results indicate that running adhesions in excess of 26 per cent can be maintained by the application of certain materials to locomotive drivers or to the rail.

## INTRODUCTION

THE ability of the diesel-electric locomotive to pull heavy loads is widely recognized; but just how much a certain locomotive can pull over a given profile, and what its speed will be, depend upon many factors. Among these, the adhesion between the locomotive wheel and the rail is of basic importance. This affects the whole railroad operating picture. There is no question but that a major improvement in wheel-to-rail adhesion would be of far-reaching importance to the railroads.

The limit of locomotive hauling capacity is determined by the friction between the wheels and the rails. Up to the present time limiting values of running adhesion have been accepted generally in railroad practice as follows: (a) Fifteen per cent of weight on drivers for greasy moist rail; (b) 20 per cent for clean dry rail; and (c) 25 per cent for clean dry rail well sanded. Although a starting adhesion limit of 30 per cent was tentatively set for locomotives with electric drive, its attainment required specially favorable conditions which could not be counted upon in day-to-day operation. The tests here described indicate the possibility of maintaining high operating adhesions, even under adverse conditions.

Stalling of trains as a result of wheel slip is costly. For example, in one case continuous stalling on a short grade with a trailing load of 8000 tons necessitated reducing the load to 7000 tons. This required an extra train every seventh day to handle the traffic. At \$2 per mile, this represented an annual increase in cost of \$20,800 for a 200-mile round trip.

The cost of extra trains, however, is only part of the expense chargeable to wheel slippage. It is also a major cause of damaged traction equipment, burnt rails, flat wheels, costly train delays, parted trains, and poor ballast and rail condition resulting from

excessive sanding. Moreover, to prevent stalling on limiting grades it is often necessary either to provide extra crews for pusher service or to add one or more units to the locomotive—units that are needed for only a small fraction of the total run.

Efforts to minimize wheel slippage have involved expensive technical skill and engineering development. Design of both mechanical and electrical locomotive parts has been improved; various gadgets have been added; and extensive tests have been conducted on sanding equipment, methods of sand application, and grade and quantity of sand. Any possibility of reducing time and maintenance expense devoted to combating wheel slip would be welcomed by the railroads. If this could be done without affecting the revenue-producing capacity of the motive power, and without introducing a disproportionate first cost, it would be especially desirable.

The combined efforts of a railroad, a locomotive builder, and a materials manufacturer have been channeled toward this end. New methods have been devised for increasing wheel-to-rail adhesion. The results will profoundly affect present locomotive operating practice as well as future motive-power design.

## LABORATORY AND INITIAL FIELD WORK

Weather was known to influence the limit of rail adhesion. Field reports indicated that adhesion was lowest when relative humidity was high, as at the onset of rain or a very light rain—particularly when a light speckled rust film formed on the rail head. Conversely, adhesion was high under dry sunny conditions.

Rust films were examined in the equipment manufacturer's laboratory. Films, from a mere trace to a deep reddish brown, were formed on a flat steel plate machined from a section of 100-lb rail. Friction coefficients were measured on these films by determining the breakaway force necessary to cause translation of the steel plate with a fixed load applied to it by a steel sphere. The results indicated that the heavier the rust film, the higher the coefficient of friction. With the heavier rust films, the steel plate began to pit, the sphere tended to rest in these pits, and friction coefficients above 40 per cent were obtained.

These results were inconclusive so the contact between a locomotive driver and the rail was examined more critically. The contact or wear band on the rail head was found to vary from practically no width for new rail to about 1 in. for badly worn rail. A similar variation was found in the wheel tread.

Calculations based on a 40-in-diam wheel with a 60,000-lb-axle load showed contact pressures from 30,000 psi up to the elastic limit of the metal, depending on the amount of wheel and rail wear. Assuming moderate wear, the range narrows to 70,000 to 100,000 psi. The contact area is 0.4 to 0.5 sq in.—nearly rectangular in shape, but with rounded corners. Its dimension across the rail head is approximately three times that along the rail.

A new laboratory device consisting of a flat steel plate and a barrel-shaped steel member was designed to simulate this condition as closely as possible. The plate was made from rail

<sup>1</sup> Assistant Mechanical Engineer, Reading Company Railroad, Reading, Pa.

<sup>2</sup> Engineer, Physics Investigations and Analysis, Locomotive and Car Equipment Laboratory, General Electric Company, Erie, Pa.

Contributed by the Railroad Division and presented at the Diamond Jubilee Annual Meeting, Chicago, Ill., November 13-18, 1955, of THE AMERICAN SOCIETY OF MECHANICAL ENGINEERS.

NOTE: Statements and opinions advanced in papers are to be understood as individual expressions of their authors and not those of the Society. Manuscript received at ASME Headquarters, August 22, 1955. Paper No. 55-A-132.

steel and left at 255 Brinell hardness. The barrel member was machined with two radii—one representing the curvature of the wheel and the other the crown of the rail. It was hardened to 300 Brinell to approximate Class "A" and "B" wheel hardnesses. The new device produced an area with a shape factor of 3 to 1, and a contact pressure of 75,000 psi, which conformed closely with actual wheel-rail contact conditions.

The new equipment was tested initially without forming any film on the plate in an effort to obtain readings representing clean wheels and rail. The results were erratic, varying from 10 to 35 per cent. Both members were cleaned with various solvents, such as alcohol and benzene, but the randomness of the readings did not improve.

After a time it was noticed that the friction coefficient was high when the plate surface could be wetted with distilled water, and low when the plate would not wet. Investigation finally disclosed that thin oil films producing boundary lubrication were influencing the results.

Prior to test, when polishing the plate to duplicate the high polish of the rail-wear band, finger marks were made on its edges. If water contacted these marks when rinsing the emery grit, the minute oil deposit in them immediately displaced the rinse-water film from the plate through surface-tension equilibrium. The plate could not then be rewetted, and the friction coefficient was low. If care was taken to prevent this, the friction coefficient was high.

Investigation showed that animal oil could spread the same creep film by surface-tension equilibrium of the water, oil, and metal interfaces. With fresh petroleum oil this action did not occur, rather the oil floated on top of the water film which continued to adhere to the metal surface. In this case friction coefficients were not as low as with animal-oil creep films.

Samples of oxidized deposits obtained from the low rail of curves, when tested, showed the same creep action as animal oil. Oxidation of the petroleum oils converted them chemically to a molecule similar to that in animal oils and capable of forming creep films. Laboratory results with several types of films, Table 1, showed that animal-oil films give rise to the worst condition. Subsequent tests showed that oxidized rail deposits fall in the same category.

TABLE 1 ADHESIONS WITH VARIOUS FILMS

(Laboratory Tests)		
Maximum contact pressure—75,000 psi		
Surface condition	Per cent static coefficient of friction	Film appearance
Surfaces—clean, wettable, and either dry or covered with distilled water. Finishes from 150 grit cloth to 400.....	30 to 35	None
Thin layer of petroleum oil deposited over plate surface.....	20	Visible
Layer of petroleum oil on plate blown very thin with compressed air.....	21	Opaque
Plate with above petroleum oil film rubbed vigorously with clean cloth. (Friction coefficient is a function of film thickness.)....	15 to 27	Invisible
Oil from fingers deposited over plate surface by direct contact.....	16 to 19	Opaque
Above film rubbed vigorously with clean cloth....	10 to 13	Invisible
Oil from fingers allowed to spread over plate surface by contact with water (creep film).....	18 to 21	Invisible

To check friction coefficients on actual rail, the laboratory equipment was modified by mounting the barrel-shaped member in a U-frame with lead weights attached. The frame contained an outrigger to which a pull scale could be attached to determine the limiting coefficient of friction, or breakaway adhesion, on a rail head. Readings were made on apparently clean rail, except in one instance as noted in Table 2. Under conditions of high relative humidity before the sun reached the rail, adhesions were low, especially if measured in the vicinity of oil deposit. Under bright sunlight the readings were high. In just a few hours readings at a given location would change from low to high values.

TABLE 2 LIMITING ADHESIONS UNDER VARIOUS TRACK CONDITIONS

Limiting adhesion factor, per cent	Track conditions	Weather
MAIN-LINE LEVEL, TANGENT TRACK		
43 to 25.....	Wettable (film free)	Cloudy, 67% RH recent rain
30 to 20.....	Not wettable	80% RH—sun just beginning to shine
BRANCH-LINE 2 PER CENT GRADE, TANGENT TRACK		
43 to 36.....	Wettable section (film free)	Cloudy overcast; 75% RH
27 to 23.....	Not wettable section	
25 to 16.....	Not wettable	Overcast; extremely low ceiling. 87% RH
BRANCH-LINE 1 PER CENT GRADE, SLIGHT CURVE, MOUNTAIN VALLEY		
27 to 17.....	Not wettable	Mountain fog; creek nearby; overcast
15 to 10.....	Measurement on wear band of a rail coated with oil deposits	

RH = relative humidity.

The next step in verification of laboratory theory was to transfer the work to the railroad. Necessary recording meters, described in detail later, were installed on a diesel-electric locomotive.

Traction-motor torque was calculated from meter readings and the motor-characteristic curve by the formula

$$T = k\phi I_a \dots \dots \dots [1]$$

where

$T$  = motor torque, ft-lb

$k$  = factor to convert electrical to mechanical units

$I_a$  = motor armature current

$\phi$  = magnetic flux (from motor-characteristic curve)

The corresponding tractive effort is

$$TE = \frac{T GR}{0.5 WD} \times \text{efficiency} \dots \dots \dots [2]$$

where

$TE$  = tractive effort, lb

$T$  = motor torque per axle, Equation [1]

$GR$  = motor-gear ratio

$WD$  = wheel diameter, ft

Adhesion then is

$$F = \frac{TE}{W} \times 100 \dots \dots \dots [3]$$

where

$F$  = adhesion factor, per cent

$W$  = weight per driving axle, lb

Thus it was possible to obtain a continuous record of adhesion being developed by the locomotive and limiting adhesion at the time of a wheel slip.

Limiting adhesion as low as 11 to 12 per cent without sand was found. In certain locations, with sanders wide open, 18.5 per cent was the limit, while in others no difficulty was experienced in obtaining 21 per cent on sand. Weather influenced the picture, with moist damp evenings giving the worst conditions. Locations which repeatedly showed low limiting adhesions and excessive wheel slip were marked on the meter tapes and revisited on foot. In virtually every case oxidized oil deposits were found on the edge of the rail. Under proper atmospheric conditions these spread a creep film out over the rail head, covering the wear band.

Oil deposits were formed principally on wide-gage rail and flattened and widened rail heads on the low rail at curves. The

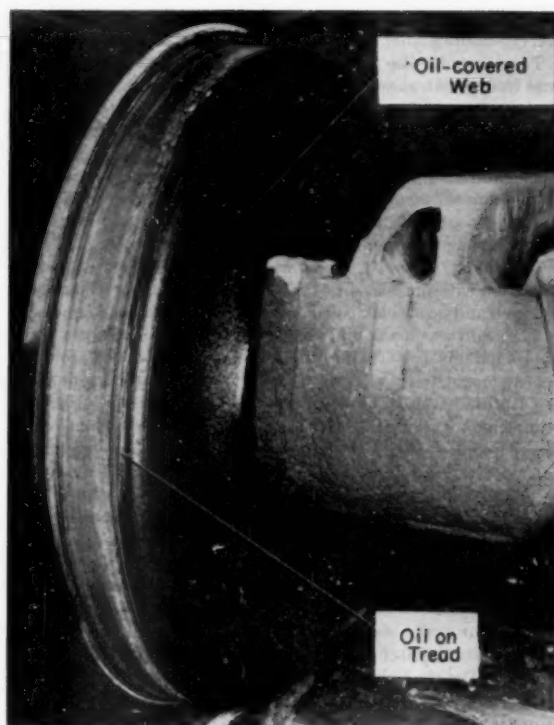


FIG. 1 FREIGHT-CAR WHEEL, SHOWING HOW OIL LEAKING FROM JOURNAL BOX SPREADS TO TREAD

outer edge of the car-wheel treads is usually coated with oil from journal-box leakage, Fig. 1. In such locations this portion of the tread contacts the outer edge of the rail and lays down an oil deposit. A similar situation occurs when crossing frogs and switch points.

Measurements at these locations showed friction coefficients as low as 10 per cent. Values varied with time and track conditions. Heavy oil deposits under conditions of high humidity gave the lowest adhesion. Continual exposure to sunlight without additional oil contamination eventually oxidized thin films until they no longer affected adhesion. Continued heavy rain also improved adhesion by exhausting the oil supply of these reservoirs. Investigation showed that removal of the oil deposits eventually led to good adhesion. It therefore remained to determine the most expeditious method of removing these deposits, together with the thin film formed from them.

#### POSSIBLE METHODS OF IMPROVING ADHESION

While the many and varied causes of locomotive wheel slip include items related to locomotive design, maintenance, and operation, others related to maintenance of way, and still others involving train dispatching and physical layout of the line, the prime cause is the contamination of the rail surface already described.

Although there may be many methods of removing this thin oil film that causes slipping, all are not equally effective or practical. In the laboratory, abrasion or polishing proved good, but it is impractical for railroad use. Early tests with flame cleaning showed it to be too slow and costly. Chemical attack on the oil film seemed most promising. Two approaches were tried, namely, rail cleaning and rail conditioning.

The first method consisted of cleaning the rail with detergents. Material used had to penetrate the film at a rate that would permit the residue to be washed off the rail in a few seconds. Many chemicals were tested, both in the laboratory and in actual service. Cleaners of the solvent type were found to be best. High alkali or acid-type cleaners, because of incomplete penetration of deposits, tend to leave a residue that made the rail more slippery.

To clean rail successfully the proper solution and correct rate of detergent application had to be determined, a source of adequate water and steam supply provided, equipment for spraying had to be assembled, and the question of whether to apply from the locomotive, the caboose, or a separate unit decided. Lack of steam supply on diesel-electric freight locomotives, as well as other considerations, pointed to the choice of a separate unit either self-propelled as shown in Fig. 2, or mounted in a specially designed railroad car.

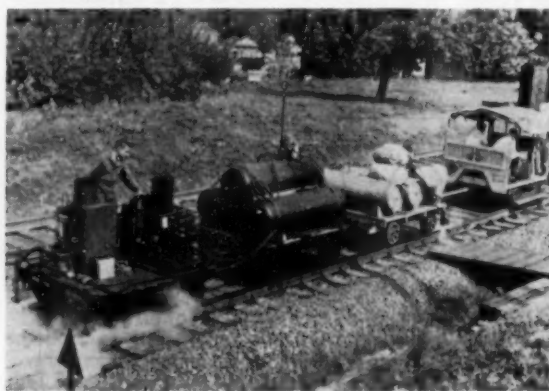


FIG. 2 EQUIPMENT USED IN 1954 RAIL-WASHING TESTS

Successful tests were conducted in 1954. This method, however, was limited to clear-weather use since the cleaner emulsified on contact with wet rail and gave negative results. Moreover, costs proved prohibitive for practical operation. This left two alternatives: (1) Concentrate on the mechanical and electrical causes of wheel slip mentioned, or (2) seek some material (other than sand) which, when applied to locomotive wheels or rails, would almost instantly neutralize the oil film. Publicizing the work already done resulted in an offer by a chemical company of some materials of its manufacture which were said to increase rail adhesion greatly. Service tests proved these to be highly successful in rail conditioning. Variations of the conditioners have been evaluated on the dynamometer test stand. The best have been set aside for further testing in actual service.

#### METHOD OF CONDUCTING FIELD TESTS

Road tests were made on two grades. The shorter, referred to as Temple Grade, is approximately 13,000 ft long. The ruling portion of 1.0 per cent is approximately 4600 ft long on a 2-deg curve. The tonnage rating of this grade is 2500 adjusted tons per diesel-electric locomotive unit. These units are 1500 or 1600 hp and have a continuous tractive-effort rating of approximately 52,500 lb. Depending upon traffic, the operation varies between two units with 5000 adjusted tons, three units with 7500 adjusted tons, and four units with 10,000 adjusted tons with two lead units and a two-unit pusher up the grade, or four units in the lead for the entire run.

Two 1600-hp road-switcher units with a rating of 5000 adjusted tons were used as test units. They were generally assigned to train RB-2, which is usually dispatched from Reading Yard at

the foot of the grade. The train has no momentum, therefore the units are soon at full load on the grade.

This railroad operates all its freight trains on an adjusted tonnage basis. That is, the actual tonnage of the train is so adjusted for rolling resistance as to require the same drawbar pull per locomotive unit regardless of the train consist.

The longer grade, referred to as Catawissa Grade, is 35 miles long with 1 mile of level tangent track near the middle. The average grade is 0.63 per cent. There are over 150 major curves, the sharpest being 12 deg 30 min. The tonnage rating on this grade is 2400 adjusted tons per locomotive unit. The usual train consists of three 1500 to 1600-hp diesel-electric units with a trailing load of 7200 adjusted tons.

Prior to each test run the wheel diameters of each locomotive unit were measured and the light weight stenciled on each car in the train was recorded, together with the load weight shown on the waybill. When no load weight was shown, it was estimated as accurately as possible. A sample tonnage log sheet is shown in the Appendix.

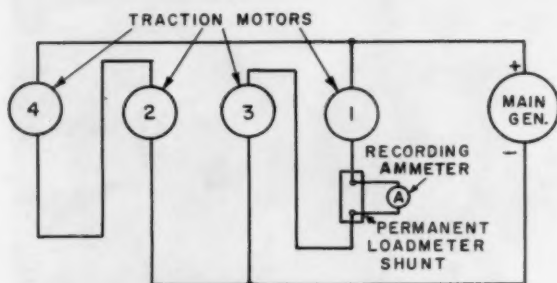


FIG. 3 CONNECTION OF AMMETER IN LEADING LOCOMOTIVE UNIT

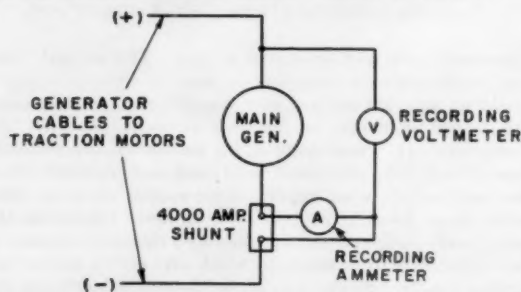


FIG. 4 CONNECTION OF DUAL METERS IN TRAILING LOCOMOTIVE UNIT

Test equipment installed on the locomotive units consisted of one single and one dual Esterline-Angus recording meters, and a transition indicator. The single instrument, an ammeter, was mounted in the cab of the leading locomotive unit and connected, as shown in Fig. 3, to record the current in No. 1 traction motor. The dual instrument was mounted in the cab of the trailing unit. The voltmeter and ammeter elements were connected as shown in Fig. 4. An indexing needle on each tape of this meter is fitted with a push button and used to record mile posts, stations, or any other landmarks needed for identification purposes. The second indexing needle on the ammeter was connected in the wheel-slip relay circuit to record wheel slips. The second needle on the voltmeter was connected across the sander circuit to record sanding operations. In addition, a transition indicator light was installed in the cab of the trailing unit. Observers in this cab kept a minute-by-minute log of motor current, speed, transition, and

other pertinent data, as shown by the sample sheet in the Appendix.

The Appendix also shows a sample ammeter tape typical of the ones from which the adhesion charts in Figs. 5 through 13 were made.

#### TEST RESULTS

The adhesion graphs shown on the accompanying charts were made from the recording ammeter tapes of the runs indicated. They were selected to show operating conditions on normal rail as compared to washed rail and conditioned rail.

*Chart No. 1 (Fig. 5).* This was chosen as typical of normal operation with untreated rail. Regular operating procedure was followed and no special instructions were given to the engineman.

The train was made up in the yard and dispatched at a point approximately 1500 ft from the foot of the grade. Hence there was no momentum to help ascend the grade. Intermittent sanding was used over the entire grade. In spite of this sanding, constant slipping occurred. By the time the locomotive had reached the center of the 2-deg curve sustained slipping required reducing the throttle twice for short intervals, as indicated by the chart.

The first impression gained from this evidence might be that tonnage ratings should be reduced. Operating experience on this grade does not bear this out. Trains are dispatched with the same adjusted tonnage, and with normal rail and weather conditions satisfactory operation is obtained. The railroad operates similar locomotive units of different makes in this service. At the consent of the manufacturers the rating for all multiple-unit operation is 52,500-lb continuous tractive effort at approximately 9 mph. For the lightest units, weighing 246,000 lb, this equals 21.3 per cent adhesion. The tape used in Fig. 5 was chosen because it represents track and weather conditions comparable to Fig. 6. It also shows that normal operating conditions could produce a stalling case, even in good weather.

*Chart No. 2 (Fig. 6).* Prior to this test the rail from Pike Street Tower to Temple Station—a distance of approximately

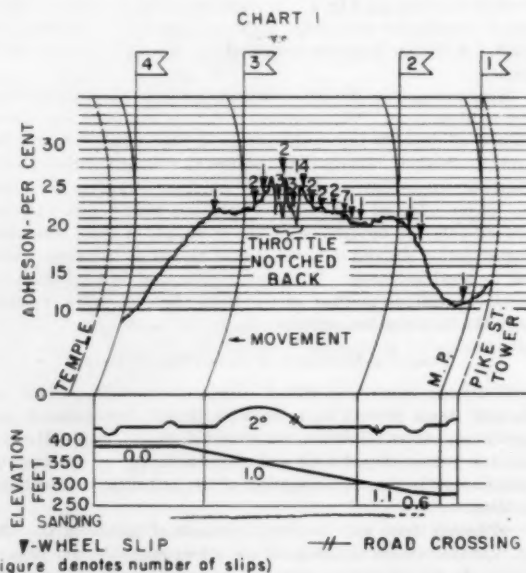


FIG. 5 ADHESION CHART OF TEST ON TEMPLE GRADE WITH UNTREATED RAIL

(Train RB-2 10/5/54; diesel units 663 and 621, 71 cars—58 loads, 13 empties—5123 adjusted tons; tonnage rating for grade, 5000 adjusted tons; weather clear).

3½ miles—was washed, using the equipment shown in Fig. 2. The engineman was instructed to use sand only if necessary to stop constant slipping.

Although this train did not start from rest at the foot of the grade (as was the case in Fig. 5) its speed through the station and yard was so restricted that the momentum to assist on the grade was no different than in Fig. 5.

The locomotive units used were approximately the same in speed-tractive effort rating as those in Fig. 5, and therefore would have practically the same hauling capacity. Nevertheless, slipping in this case was considerably less. Only sparing use of sand

was required and there was no need to reduce the throttle. The only physical difference was that the rail had been washed, using the method proved most effective by a long series of preliminary tests.

Chart No. 3 (Fig. 7). Regular operating procedures were followed in this test and no special instructions were given to the engineman.

Because of speed restrictions, trains approach this grade with a minimum of momentum. Moreover, since the grade is approximately 35 miles long, the benefit of any momentum is quickly lost.

This chart covers only about the first 40 per cent of the grade. Some of the worst spots are in the initial 5 miles, where there are 20 curves of various lengths ranging from 2 deg to 7 deg 30 min. The tape indicates over 50 slips, and intermittent sanding was used over all this section.

The next difficult section of this grade is at Frey's Curve. Here the tape indicates over 10 slips on an 11-deg 30-min curve 1200 ft long.

The last difficult area shown is through Shumans Tunnel. This is approximately 400 ft long in the center of an 11-deg 24-min curve 1200 ft long. The troublesome area extends west of the tunnel where there are two reverse curves of 6 deg for a total of 1200 ft.

At first glance this chart also seems to indicate that the tonnage rating is too high. However, it is based on tractive effort at 18 per cent adhesion, which is less than the continuous rating of the locomotive units. While not of daily occurrence, trouble on this grade is sufficiently frequent in good weather to warrant consideration of further cuts in tonnage ratings. In bad weather it is occasionally worse. The condition is aggravated by the fact that the line is single track, and is located in the mountains of East Central Pennsylvania where weather and atmospheric conditions change constantly.

Chart No. 4 (Fig. 8). Prior to this test the rail from Beaver Valley to Catawissa—a distance of 13 miles—was washed, using the equipment shown in Fig. 2. The engineman was instructed to use sand only if necessary to stop constant slipping.

This train is essentially similar to that in Fig. 7, except for slightly more tonnage. The adhesion curve, however, shows a

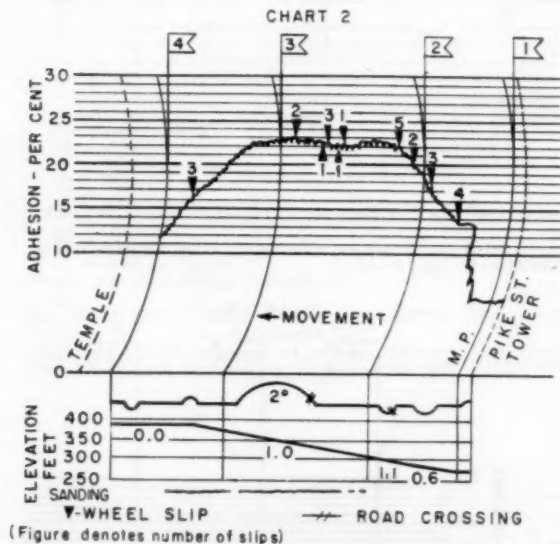


FIG. 6 ADHESION CHART OF TEST ON TEMPLE GRADE WITH WASHED RAIL  
(Train HA Extra 10/12/34; diesel units 449, 485, 483, and 481; 122 cars—117 loads, 5 empties—10,379 adjusted tons; tonnage rating for grade, 10,000 adjusted tons; weather clear.)

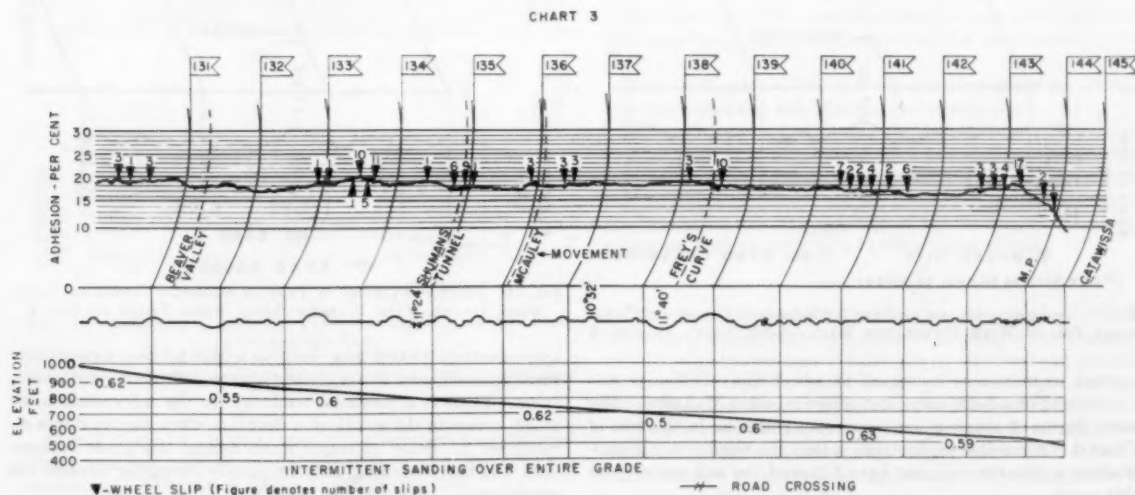


FIG. 7 ADHESION CHART OF TEST ON FIRST PORTION OF CATAWISSA GRADE WITH UNTREATED RAIL  
(Train NP-8 11/3/34; diesel units 273A, 266B, and 272A; 132 cars—114 loads, 18 empties—7281 adjusted tons; tonnage rating for grade, 7200 adjusted tons; weather clear.)

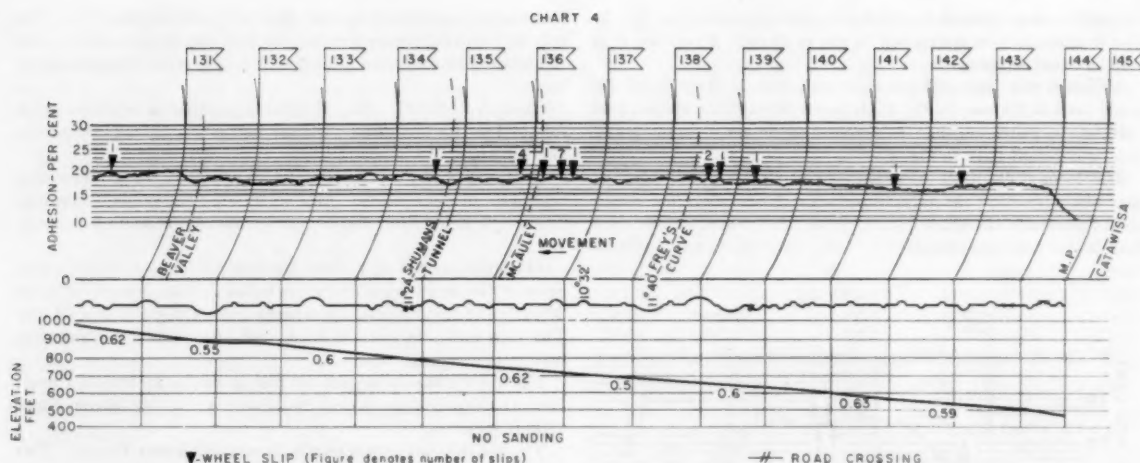


FIG. 8 ADHESION CHART OF TEST ON FIRST PORTION OF CATAWISSA GRADE WITH RAIL BETWEEN CATAWISSA AND BEAVER VALLEY WASHED

(Train NP-8 11/5/54; diesel units 273A, 266B, and 272A; 123 cars—108 loads, 15 empties—7326 adjusted tons; tonnage rating for grade 7200 adjusted tons; weather clear.)

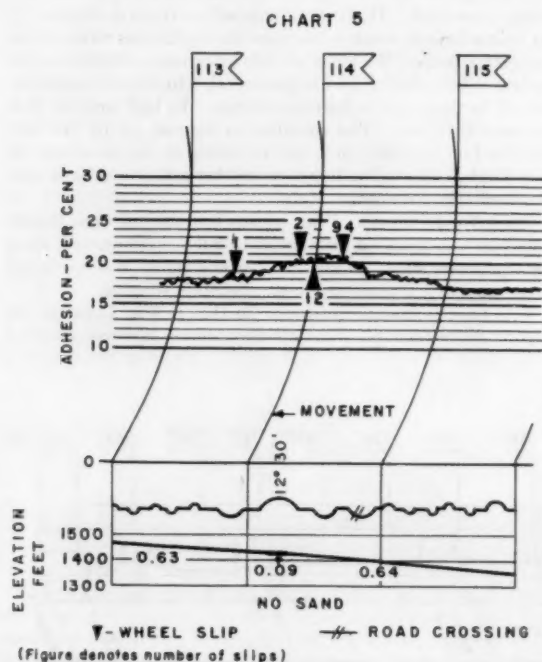


FIG. 9 ADHESION CHART OF TEST AT SHARPEST CURVE ON CATAWISSA GRADE WITH UNTREATED RAIL. SAME TRAIN AS FIG. 7

marked improvement in regard to wheel slip. Difficulty was experienced on a 7-deg curve just before reaching McAuley. The same degree of slipping was experienced here as in the test of Chart 3. A possible explanation is that the nozzles on the rail-washing apparatus may not have followed the rail properly on this curve.

Chart No. 5 (Fig. 9). This is a later portion of the same tape as Fig. 7, and shows operation through 12-deg 30-min curve east of Girard Manor where slipping was most severe. The curve is

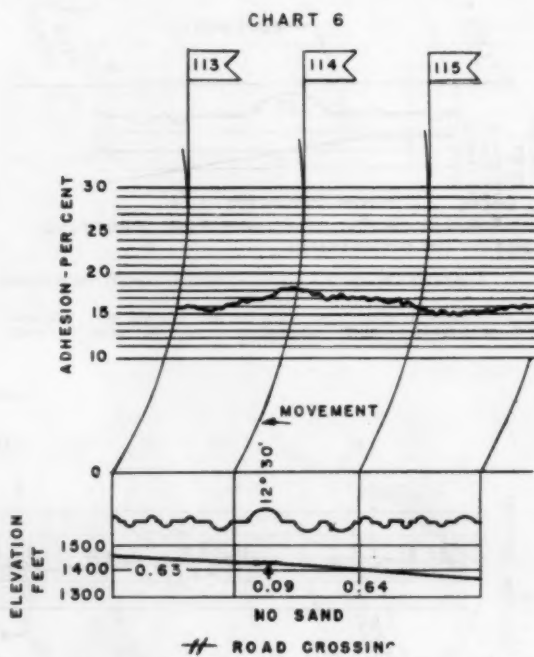


FIG. 10 ADHESION CHART OF TEST AT SHARPEST CURVE ON CATAWISSA GRADE WITH WASHED RAIL. SAME TRAIN AS FIG. 8

approximately 1500 ft long, built on a high fill over a constantly running creek, and is completely surrounded by wooded mountains. There is a continual tendency for the rail surface to be moist, except in the middle of a clear day when the sun shines directly on it. Since all major trains ascend this grade between dusk and early morning, they frequently encounter adverse rail conditions.

Chart 6 (Fig. 10). Here are shown the best results possible with rail washing—absolutely no wheel slip in the curve, without the use of sand.



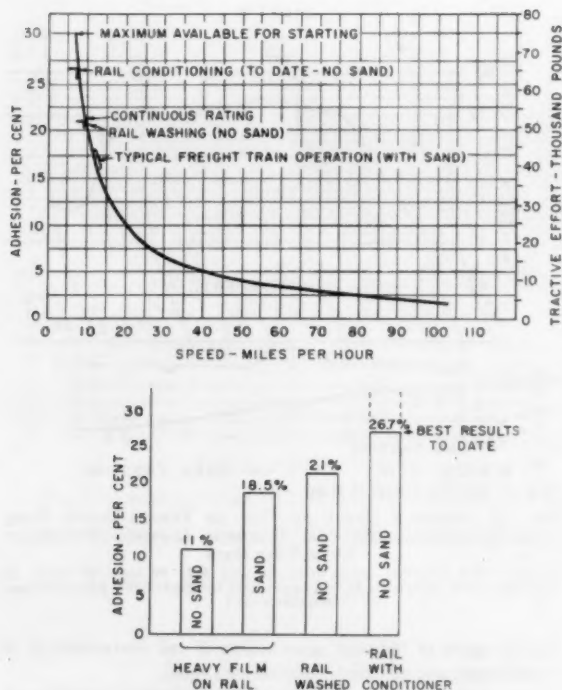


FIG. 14 RESULTS OF SERVICE TESTS WITH VARIOUS CONDITIONS OF RAIL SURFACE

2 The method of washing required for practical use proved to be costly, tedious, and complicated; requiring storage capacity for solution and water, and a means of producing hot water and steam.

3 Satisfactory results required such careful control of the working process as to practically necessitate its being made automatic.

4 Maximum adhesion resulting from careful rail washing was 21 per cent without sand (measured from traction motor torque at 9-mph train speed). Limited improvement on this value could be obtained with sand.

5 Rail washing did not remove the last vestige of oil film. Nevertheless, higher adhesions could be maintained on this thin film than on the same rail prior to washing. The use of rail washing and sand definitely improved adhesion in areas of heavy oil deposits.

In order to offset the limitations of rail washing, means were sought to improve adhesion by conditioning the rail in some manner other than by washing or sanding. Tests on a conditioning compound were begun in the Spring of 1955. Up to the date of compiling this paper the following results have been attained:

1 Improvement in adhesion with rail conditioner is much greater than with rail washing.

2 Improvement with rail conditioner as compared to normal rail conditions is exceptional.

3 Sustained adhesions have been obtained on conditioned rail as high as 26.7 per cent (measured from traction motor torque

at 5.5-mph train speed). This value has been maintained without the use of sand.

4 The precise limit of adhesion possible with rail conditioning had not been established when this paper was compiled.

The chart in Fig. 14 indicates the steps of improvement to this date, and its significance in relation to the curve of the available tractive effort of a typical diesel-electric locomotive.

#### ACKNOWLEDGMENTS

The authors desire to acknowledge the valuable assistance rendered by their associates in the preparation of this paper. They also acknowledge the assistance rendered by representatives of the following companies:

Manufacturers of equipment:

Turbo Machine Company, Lansdale, Pa.

Manufacturers of cleaners:

Dearborn Chemical Company, Chicago, Ill.

Eagle Soap and Chemical Company, Reading, Pa.

Magnus Chemical Company, Garwood, N. J.

Oakite Products Company, Inc., New York, N. Y.

Pennsylvania Salt Manufacturing Company, Philadelphia, Pa.

Manufacturers of conditioners:

National Aluminate Corporation, Chicago, Ill.

## Appendix

Return 2nd 147		DATE 5-25-55	TOTAL 16	
LOC. NO. 487-487-845			TOTAL 89	

R.R.	CAR NO.	ACTUAL POUNDS			WEIGHT REPORT (POUNDS)		
		IN. WT.	OUTWEIGHT	TOTAL	IN. WT.	OUTWEIGHT	TOTAL
AA	283	46,900	50,400	97,300	25	25	50
MW	874	42,100	67,600	109,700	25	34	59
GIN	732	44,900	74,300	119,200	25	37	62
Ed	126	64,200	87,800	152,000	30	44	74
B+D	434	32,000	72,800	104,800	25	49	74
"	041	40,000	102,000	142,000	20	51	71
NYC	861	52,500	54,100	106,600	25	27	52
NKP	502	41,200	45,100	86,300	25	22	47
Sou	723	47,400	103,800	151,200	25	56	81
B+D	135	56,700	150,400	207,100	30	75	105
CBQ	900	42,800	65,700	108,500	25	33	58
WM	394	54,100	85,100	139,200	25	57	82
B+D	631	40,800	116,300	157,100	25	58	83
"	145	37,300	102,000	139,300	25	40	65
"	713	39,400	102,400	141,800	25	55	80
"	883	39,300	115,900	155,200	25	58	83
"	104	38,200	74,400	112,600	25	47	72
"	589	38,900	128,500	167,400	25	61	86
"	301	50,400	142,800	193,200	25	71	96
"	407	38,600	103,200	141,800	25	51	76
"	258	42,200	103,900	146,100	25	52	77
"	437	38,200	88,900	127,100	25	44	69
TS	028	40,100	104,700	144,800	20	53	73
ACV	023	38,300	120,100	158,400	20	60	80
PNV	557	39,200	120,800	160,000	20	60	80
PS	093	38,800	103,000	141,800	25	54	79
B+D	037	53,100	101,600	154,700	25	71	96
"	639	38,500	104,500	143,000	25	52	77
WM	059	40,800	102,600	143,400	25	51	76
"	802	41,800	112,600	154,400	25	56	81
TOTALS		102700	2,930,100	4,222,800	740	1,464	2204

Return		TEST NO. <u>9</u>	SHEET NO. <u>2</u>				
TRAFFIC NO. <u>2nd JH7</u>		DATE <u>5-25-55</u>	PAGE <u>86</u>				
LOCK NO. <u>487-447-445</u>		NOTES <u>3</u>	TOTAL <u>89</u>				
R.R.	CAR NO.	ACTUAL WEIGHT			WEIGHT REPORT (TONS)		
		LT. WT.	COUNTERS	TOTAL	LT. WT.	COUNTERS	TOTAL
BEO	211	38,400	107,600	146,000	25	53	78
WM	710	38,000	101,700	140,700	25	51	76
BEO	859	37,800	93,300	131,100	25	46	71
"	581	40,700	101,100	141,800	25	50	75
"	076	39,400	103,600	143,000	25	51	76
"	864	38,000	116,900	154,900	25	58	83
"	026	38,900	116,300	155,200	25	58	83
"	525	38,100	108,800	146,900	25	54	79
"	322	39,900	118,000	157,900	25	60	85
WM	072	43,700	106,200	149,900	25	53	78
BEO	551	42,700	148,600	191,300	25	74	99
"	736	38,900	125,700	164,600	25	62	87
"	938	38,900	116,900	155,800	25	58	83
CZ	812	38,000	116,100	154,100	25	58	83
PRR	463	36,500	91,200	127,700	25	49	74
"	446	38,000	113,300	151,300	25	57	82
BEO	781	37,700	91,500	129,200	25	48	73
"	897	39,400	118,100	157,500	25	57	82
"	852	39,300	115,600	154,900	25	58	83
"	256	39,300	101,200	140,500	25	50	75
"	108	51,600	146,300	197,900	25	73	98
"	227	51,600	146,300	197,900	25	74	99
LN	165	39,000	123,600	162,600	25	62	87
BO	333	47,100	156,500	203,600	25	78	103
Rdg	214	38,100	123,700	161,800	25	62	87
"	328	38,000	125,600	163,600	25	63	88
"	317	38,200	125,800	164,000	25	62	87
"	532	38,000	117,600	155,600	25	59	84
"	666	39,200	126,600	165,800	25	65	89
"	377	38,000	126,600	164,600	25	61	86
TOTAL		1215,500	3,536,200	4,751,700	750	1762	2212

Return		TEST NO. <u>9 (F.G. Fisher)</u>		SHEET NO. <u>1</u>	
TRAFFIC NO. <u>2nd JH7</u>		DATE <u>5-25-55</u>		PAGE <u>487-447-445</u>	
LOCK NO. <u>3:05 PM</u>		NOTES <u>3:30 PM</u>		TOTAL <u>Sunday-Norm</u>	
C.B. Sharley		Rutland		Lewiston-Que.	
C. Spiegler (running)				Lewiston-Que.	
L. Mayer				Allen-Gadde	
TIME	WEIGHT	WHEELS	WHEELS	WHEELS	WHEELS
6:52	400	16	1	1/10	
53	400	16	1	1/10	
54	550	15	1	1/30	
55	750	14	1	1/30	
56	850	11	1	1/40	
57	1000	9	1	2/10	
58	1075	8	1	2/10	
59	1035	8	1	2/10	
7:00	1100	8	1	2/10	
101	1085	8	1	2/10	
102	1200	6.5	1	2/30	
103	1450	4	1	2/30	
104	1300	5.5	1	2/40	
105	1375	4	1	2/40	
106	1350	5	1	2/40	
107	1300	7	1	2/40	
108	1100	8	1	2/40	
109	1050	8	1	2/40	
110	950	10	1	2/40	
111	850	12	1	2/40	
112	700	16	1	2/40	
113	700	21	1	2/40	
114	500	26	3	2/40	
4 B Wheel Slips					
No Foundry					

Return		TEST NO. <u>9</u>	SHEET NO. <u>3</u>				
TRAIL NO. <u>229 JH7</u>		DATE <u>5-25-55</u>	PAGE <u>86</u>				
LOCK NO. <u>487-447-445</u>		NOTES <u>3</u>	TOTAL <u>89</u>				
R.R.	CAR NO.	ACTUAL WEIGHT			WEIGHT REPORT (TONS)		
		LT. WT.	COUNTERS	TOTAL	LT. WT.	COUNTERS	TOTAL
Rdg	794	39,200	116,200	155,400	25	58	83
	056	39,300	117,300	156,600	25	58	83
	782	38,900	115,100	154,000	25	54	79
	407	38,000	113,700	151,700	25	60	85
	279	38,900	123,800	162,700	25	61	86
	225	45,300	80,800	126,100	25	40	65
	691	38,200	E	38,200	25	E	25
	748	50,000	4,400	54,400	25	2	27
	477	38,900	129,300	168,200	25	65	90
	541	51,500	143,900	195,400	25	72	97
	002	47,400	108,800	156,200	25	54	79
	512	39,100	E	39,100	25	E	25
	213	50,100	119,300	169,400	25	59	84
	725	50,800	124,800	175,600	25	62	87
	458	39,300	119,700	159,000	25	60	85
	021	38,200	114,800	153,000	25	59	84
	130	38,100	115,300	153,400	25	58	83
	464	39,400	115,800	155,200	25	58	83
	886	38,000	112,200	150,200	25	56	81
	104	38,900	112,600	151,500	25	56	81
	039	38,100	122,200	160,300	25	61	86
	147	38,200	118,600	156,800	25	59	84
	177	38,000	122,200	160,200	25	61	86
470	38,200	114,400	152,600	25	57	82	
522	39,200	124,000	163,200	25	62	87	
212	39,000	124,800	163,800	25	63	88	
235	38,800	121,200	160,000	25	60	85	
425	48,800	E	48,800	25	E	25	
583	49,600	40,000	89,600	25	20	45	
TOTAL		1,004,400	3,882,000	4,886,400	725	1435	2160

Test #9		
5-25-55		
	Actual-lbs.	Report-Tons
Sheet #1	4,232,800	2204
Sheet #2	4,749,100	2512
Sheet #3	4,097,400	2160
	13,079,300	6876
	Tons 6,540	
Adjustment		
10 Tons/car	890	890
	7,430	7766



We have all been aware of the importance of adequate adhesion, both to traction and to braking. The following is a description of some of the adhesion tests at our laboratory and some observations made during road tests which it is believed will be in general agreement with, and supplementary to, this paper.

The adhesion tests in our laboratory were somewhat similar to the laboratory tests described in this paper in that (a) we used a large brake dynamometer and obtained values at full loads between a standard wheel and a regular section of rail, and (b) we took the wheel-tread condition into consideration as well as the rail.

The rail section was clamped in the dynamometer applying head and forced against the wheel with loads from 8000 to 28,000 lb, simulating the wheel-load range from light passenger cars to diesel-electric locomotives. Then a gradually increasing tangential force was applied until a force was reached that gave a sustained skidding between wheel and rail section, as shown by a dial indicator which measured the motion between wheel and rail in thousandths of an inch.

The rail surface was prepared by grinding to a smooth polished surface which measured 4 to 5-microinch finish on a surface profilometer. Tests were made with the rail surface clean and with the rail surface coated by a film produced by rubbing the surface with a cloth that had been used to clean a section of rail head in a main-line track. Two conditions of wheel-tread surface were used. One can be described as "rough" and the other as "polished," and both within the range of wheel-tread surfaces encountered in service.

On clean dry rail, the static adhesion was approximately the same for both rough and polished wheel treads. See Fig. 15. The addition of water had little or no effect on the rough-tread adhesion, but appreciably reduced the adhesion with the polished tread.

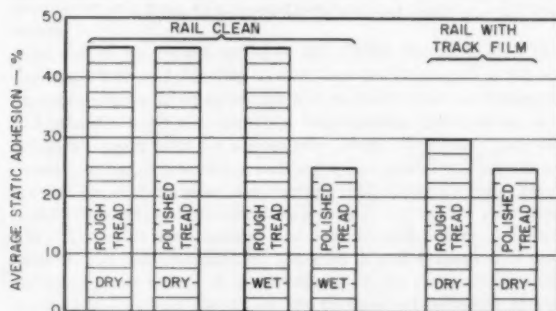


FIG. 15 AVERAGE STATIC ADHESION, 36-IN. STEEL WHEEL  
(Tests were made on a brake dynamometer with loads of 8000 to 28,000 lb applied to a standard rail section. Rail surface, 4-microinch finish; wheel-tread surface—rough, 80 microinch; polished, 5 microinch.)

On rail coated with track film, the dry-adhesion value was appreciably reduced with both the rough and the polished wheel treads. The toughness of the track film as compared with the water film is illustrated by the fact that the irregularities of the rough tread, which were apparently capable of piercing the water film, had only slightly more effect on the track film than did the polished tread.

We did not include the effect of water on the track film, as the addition of water had little or no effect under our test conditions. The film-coated rail surface was not wettable and the small amount of water used was not sufficient to remove the track film.

The percentage of static adhesion during our tests was about the same throughout the range of wheel loads from 8000 to

28,000 lb with some decrease (possibly 15 per cent) as the loads increased.

A few years ago we co-operated in some road tests on electric freight locomotives with a large Eastern railroad where the objectives were to determine the effectiveness of automatic sanding for correcting wheel slip. The tests afforded an excellent opportunity for observing variations in adhesion as the trains were heavy and almost no sand was used except as automatically applied for the few seconds required for correction at the instant the wheels started to slip.

Some of the observations we made relating to sanding during that road test may be of interest in evaluating and applying the information disclosed in this paper. We observed the following:

(a) Continuous sanding was actually needed only a small percentage of time, and usually there was considerable distance between points of slippage.

(b) Sanding could be delayed under average conditions until slippage actually started, and still correct slippage if applied quickly, before slip speed exceeded rail speed more than 1 or 2 mph. In fact, many slips were self-recoverable, without sand, until the slip speed had increased 5 to 6 mph above rail speed.

These observations would suggest that the authors might give added consideration to applying the rail conditioner automatically at the instant of wheel slip, for the general condition, and apply it continuously only when the necessity was indicated by frequent recurrence of slippage. This method has been found to reduce greatly the amount of sand required, and it is presumed could be even more beneficial from a cost standpoint in the saving of chemical.

Does this rail conditioner have any chemical effect detrimental to locomotive or track parts? Is there any effect on signals?

#### AUTHORS' CLOSURE

Both Mr. Tack and Mr. Wilson point out the tremendous importance of adhesion to braking. This is especially true in high-speed passenger and commuter service where equipment design has been limited by the adhesion available. Our investigation was conducted under motoring conditions because we were specially set up to make these measurements. Some measurements, made during electric braking, showed that adhesion limits were roughly the same as for motoring and that the phenomenon was basically the same under motoring or braking, with due allowance for such side effects as weight shift and speed.

Mr. Tack describes the use of a continually dragging clasp brake on the wheel tread to improve adhesion. As he points out, the Brown-Boveri Company of Switzerland has had such good success with their antislip brake design that its application is universal on some European railroads. The abrasion, and consequent heating, destroys the thin films present on the locomotive driving wheels, roughens the surfaces, and provides wear particles which help overcome the track film. This method, when used to overcome a locomotive wheel slip, will permit maintaining about 90 per cent of the normal tractive effort while correcting a wheel slip, in contrast to "power-removal" systems which unload the locomotive from about 50 to 100 per cent for two seconds or longer until the slip is corrected.

The effect of abrasion from tread brakes, however, is greatly lessened in areas of heavy track film. These oil reservoirs and neighboring thin films are the underlying cause of loss of adhesion. A direct attack on these sources is a strike at the cause of low adhesion and will produce the most pronounced effect in correcting it.

The tests which Mr. Wilson describes indicate an effect of surface roughness on filmed and wet rail in contrast to little effect on clean dry rail (45 per cent adhesion). This can be

accounted for by the "Weld-Interlock" Theory\* of friction which has strong acceptance at present for explaining metal-to-metal friction forces.

If the wheel and rail surfaces had a perfect finish (no asperities on either surface), the peak contact pressure would be in the elastic range and could be determined from the Hertz equations for elastic deformation. For average wheel and rail wear the value would be approximately 75,000 psi. The thin films would generally support this pressure and virtually no "cold weld" would occur. Likewise there would be no asperities, so that no interlocking would occur. The friction coefficient would be virtually zero.

This never actually occurs in practice and there are always asperities. The wheel-rail contact is formed on these asperities. The contact pressures on these microscopic areas are above the plastic flow point of the wheel and rail steel so that flow takes place until enough asperities are engaged to form sufficient area to support the wheel load. As the asperities flow to form the supporting contact area, there is a disturbance of any films that might be present. If these films are fractured, cold weld occurs. The friction will increase as the percentage of contact area in cold weld increases.

As the surface finish becomes rougher, the asperities become higher. In forming the contact area they undergo greater deformation and probably are better able to fracture the films than smoother surfaces thus affording a higher percentage of cold weld. Unfortunately, locomotive and car wheels tend to acquire a high polish under rolling conditions which, as pointed out, may be as smooth as four to five microinches. The advantages of tread brake application in increasing the potential cold-weld area under filmed rail conditions is apparent.

Mr. Wilson mentions that in past tests poor adhesion areas

\* "Metallic Friction and Lubrication by Laminar Solids," by E. Koenigsburg and V. R. Johnson, *Mechanical Engineering*, vol. 77, 1955, p. 142.

were localized and that many slips were self-correcting under five mph slip speed. We concur in this most heartily. In fact, slips or wheel walks of two or three mph are quite frequent and may account for 90 per cent of all slips under the worst rail conditions. Usually they are self-correcting. If wheel-slip relays which unload the engine have too sensitive a setting, they are a real detriment and cause needless loss of momentum by detecting these slight self-correcting wheel walks.

Extremely poor adhesion areas are localized, usually being confined to wide-gage track on curves, to switches, and to cross-overs where heavy oil reservoirs are present to continually supply the films.

In answer to Mr. Wilson's questions, the signalling was monitored on track where the chemicals were tested. No loss of shunt was recorded during these tests. The chemical did not exhibit a corrosive effect on the rail other than to leave it clean so that initial rusting was accelerated during a rain.

As mentioned several times, the basic difficulty underlying poor adhesion is the excessive accumulation of heavy oil reservoirs with their consequent films as a result of journal oil losses. Whatever the railroads can do in the way of preventive or corrective maintenance to counteract these reservoirs will pay the greatest dividends in overcoming low adhesion. Correct gaging, better oil seals and oil applicators, and control of overoiling will help immeasurably.

Where high adhesions are required, a direct attack on the reservoir and films is the surest method. If the chemists provide a commercial means of accomplishing this, it will still be wise to continue with the preventive maintenance outlined above.

The authors' purpose will be accomplished if at some future time it is possible for a superintendent to operate his division at a given level of adhesion with complete confidence that his rail and equipment is good for that amount and that his operation will not bog down because of the caprice of nature

# First Commercial Supercritical-Pressure Steam-Electric Generating Unit for Philo Plant

By S. N. FIALA,<sup>1</sup> NEW YORK, N. Y.

The commercial success of higher pressures, higher temperatures, reheat, larger units, and single-boiler, single-turbine unit designs has given customers of the utility industry cheap electric power. The Philo project reflects efforts to continue this trend by opening up new avenues of approach. The engineering, design, manufacturing, construction, and operating experience on the 120,000-kw steam-electric generating unit operating at 4500 psi, 1150 F initial temperature with double reheat (first, at 1050 F and, second, at 1000 F) should provide the know-how to create units of still greater economy within the next decade.

## INTRODUCTION

IT IS generally recognized that the commercial success of higher pressures, higher temperatures, reheat, larger units, and single-boiler, single-turbine unit designs has been the most substantial factor in the availability of cheap electric power to the customers of the utility industry. Combined with progress in developing efficient techniques of design, construction, operation, generation, and transmission, the resulting economies provide an incentive to continue the search for further improvements.

In one of his recent speeches Mr. Philip Sporn<sup>2</sup> said, "The American Gas and Electric System has been engaged in a continuous program of co-operation and research with the designers and manufacturers of generation, transmission, distribution, and utilization equipment for almost fifty years. Our basic aim—to pioneer, to break new trails, and to sponsor new developments in production, transmission, distribution, and utilization—has been pushed forward with accelerating emphasis during the past decade. That this development has been carried out on a sound basis is well demonstrated by the growth and expansion of our system, by our record of improvement in the economy of mass generation of electric energy, by the efficiency of operation of our extensive integrated system and the low-cost electric service this has given our communities, and by the financial health of our operations."

There is a definite relationship between operating temperature of a cycle and optimum pressure of the cycle. Metallurgy has progressed to the point where temperatures can now be utilized which make attractive the use of steam pressures above the critical pressure of water. At 1150 F steam temperature in the ultimate sizes feasible, the optimum cycle economy can be obtained

with steam pressure of approximately 4500 psi. In the light of this and our judgment that future metallurgical progress will permit a continued increase in maximum steam temperature, it was deemed imperative to obtain experience in the operation of supercritical steam generators and turbines. Such experience would provide a base for designs of the most economical arrangement of the units which will be installed during the next decade.

To gain this experience, The Babcock & Wilcox Company and the General Electric Company co-operated with the American Gas and Electric Service Corporation in extensive preliminary studies and later in the design and construction of a prototype unit at the Philo Plant of the Ohio Power Company, a member of the American Gas and Electric System. The early stages of work on this unit were described in an article in *Electrical World*, June 29, 1953. The Philo Plant was chosen as the location for this unit because of its central location and the impending retirement of Unit 1, a 40,000-kw reheat machine which had been installed in 1923. The full 125,000-kw capacity of the new unit, to be called Philo Unit 6, is fitted into a space only slightly larger than that made available by the removal of the 40,000-kw machine.

## CYCLE SELECTION

When operating pressure in the steam cycle is raised above the present maximum standard, in the range of 2500 psi, it becomes impractical to design natural-circulation boilers. Natural circulation cannot be used above 3206 psia because no difference in densities corresponding to the vapor and liquid phases of the fluid exists which could be used to induce circulation. Above 3206 psia, there is only a single homogeneous phase at any temperature.

As density of steam approaches that of water, pumping to induce circulation is required. Once the need of forced circulation is established, then its use may be exploited to obtain the maximum benefit at a minimum incremental cost.

To design a steam generator to operate above the critical pressure Babcock & Wilcox has developed its "Universal Pressure" design. This is a once-through-type steam generator in which circulation is provided by action of the feed pumps and the relatively large pressure drop through the unit.

Thermodynamic studies indicate that for each throttle steam temperature there is a corresponding throttle pressure which gives the maximum cycle efficiency. This is apparently true, both on an ideal basis and on a practical basis where turbine efficiencies are included. The optimum pressures of the actual cycles are somewhat lower than for the ideal cycles because of the effect of decreasing turbine efficiency with decreasing volume flow. This phenomenon of optimum operating pressures has not been experienced in the past because standard practice has always limited pressures for mechanical reasons below those pressures which would be optimum for the temperatures used. It was decided that 1150 F represented the maximum temperature that could be achieved with presently available materials. In this design, we wished to use the maximum combination of tem-

<sup>1</sup> Chief Engineer, American Gas and Electric Service Corporation. Mem. ASME.

<sup>2</sup> President, American Gas and Electric Service Corporation. Contributed by the Power Division and presented at the Diamond Jubilee Annual Meeting, Chicago, Ill., November 13-18, 1955, of THE AMERICAN SOCIETY OF MECHANICAL ENGINEERS.

NOTE: Statements and opinions advanced in papers are to be understood as individual expressions of their authors and not those of the Society. Manuscript received at ASME Headquarters, September 7, 1955. Paper No. 55-A-137.

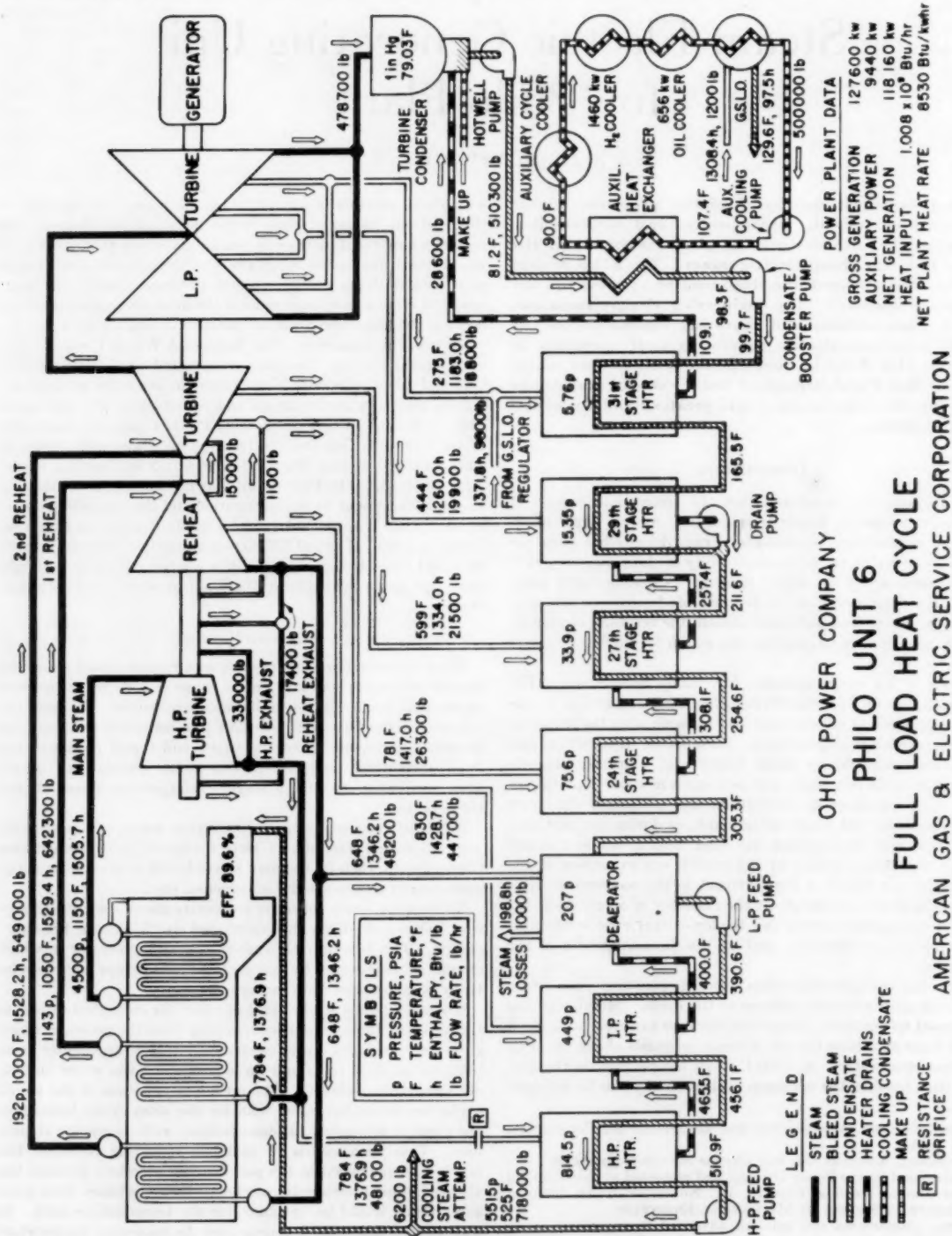


Fig. 1

OHIO POWER COMPANY  
**PHILO UNIT 6**  
**FULL LOAD HEAT CYCLE**  
 AMERICAN GAS & ELECTRIC SERVICE CORPORATION

perature and pressure justifiable, since the basic premise of the project was the close relation and interdependence of the two. An operating pressure of 4500 psi was then selected not only because of its apparent optimum relation to 1150 F but also because it gives operating pressures in the feedwater-heater lines, boiler, and steam lines which are within the limits of presently established codes.

In this particular decision and throughout the design of the unit as a whole we have attempted to meet the letter of the applicable codes. In many instances, this has called for excessively conservative design conditions which we feel ultimately could be somewhat modified. The Boiler Code, for instance, calls for feedwater shutoff valves to be designed for 20 per cent in excess of design pressure at a temperature corresponding to design saturation temperature in the boiler. Attempting to interpret this requirement literally, we have called for 706 F (the critical temperature of water) as the design temperature for the two big feedwater shutoff valves, even though the maximum conceivable temperature that could reach these valves by action of the feedwater heaters is approximately 575 F.

Reheat at 1150 F was initially included in design considerations to obtain the gain in cycle performance associated with reheat. Preliminary discussions with the turbine manufacturer indicated that there would be considerably more difficulty in designing a reheat stage to handle steam at approximately 1000 psi and 1150 F than at 4500 psi and 1150 F. This problem arises from the larger volumes that have to be handled at the lower pressures and the resulting higher bucket stresses. 1050 F seemed to be more reasonable for the reheat temperature although it reduced the cycle efficiency somewhat. This increment of efficiency was recovered, however, by the use of a second reheat which becomes feasible at the high initial pressure of the cycle. The second reheat temperature of 1000 F was chosen to limit design difficulties on the first stage of the turbine following this reheat and to retain approximately 1 1/4 per cent moisture in the exhaust of the turbine at full load. Pressures for the two reheat points were selected on the basis of optimum cycle efficiency as well as on the optimum boiler reheat-inlet temperatures.

Realizing the developmental nature of this unit, its size was not selected on the usual basis. On the one hand, the unit had to be kept relatively small so that experience could be obtained with a moderate investment; on the other hand, the unit had to be large enough to be a true prototype of future machines and to have steam-volume flows which could be utilized at reasonably high efficiencies in the early stages of the turbine. A rating of 125,000 kw appeared to be a good balance between these effects and was selected for this machine. During all design work, decisions as to possible courses of action were guided by the desire to make this a true prototype of a larger unit having a capacity more suitable for our system.

With the main and reheat steam conditions and unit size selected, a detailed heat balance was laid out. Studies indicated the optimum feedwater temperature to be about 565 F with the reheat pressures which were selected. Feedwater temperature to the boiler in this cycle has been limited, however, to 525 F by introducing an artificial pressure drop in the extraction line to the highest pressure heater. The maximum feedwater temperature of 525 F was selected so that the transition zone between the waterlike phase and the steamlike phase of the fluid would be located in a low-temperature low-heat-input section in the steam generator. Feedwater enters the steam generator by flowing through the three cyclones and some of their associated walls in series. Consequently, there is a certain unavoidable heat input before the water is carried to a relatively low-temperature zone in the rear of the steam generator. This heat input established the feedwater-temperature limit.

The restriction introduced in the extraction line of the top heater can be changed and the top heater has been designed so that it can operate at the full 565 F feedwater temperature. This will be one of the many things to be tried out when the unit actually goes into operation. It may develop, however, that it is absolutely necessary to keep the unstable transition zone in areas of low-heat input if deposits are to be avoided.

To limit oxygen in the feedwater as much as possible and thus to prevent oxide build-up, a high-quality deaerator has been included in the cycle. The location of the feed pumps normally would be directly under the deaerator to handle the smallest possible volume of fluid. Our investigations indicated that conventional feedwater-heater designs could not be adapted for the 5500-psi feedwater pressure required and the time schedule did not permit research and development of special designs. Therefore the pumps were split into two sections, with the high-pressure feedwater heaters intermediate, operating at 2100 psi.

The arrangement of the heat balance was completed by the inclusion of other conventional items such as hydrogen coolers, oil coolers, and the GSLO condenser in the condensate cycle. The final heat balance is shown in Fig. 1, giving a heat rate of 8530 Btu per kw-hr.

#### GENERAL ARRANGEMENT

The general arrangement of Unit 6 in the plant is shown in plan and section in Figs. 2 and 3, respectively.

The steam generator and its auxiliaries are located in the area formerly occupied by three 600-psi standard boilers and one reheat boiler which served Unit 1. The only major structural changes required in the boiler room were the raising of the roof in the area immediately above the steam-generator proper, the strengthening of columns carrying the steam generator, air heater, and new stack, and the erection of the new coal bunkers. These coal bunkers were located over the front end of the steam generator for easy access to the cyclones and to the existing coal-handling system. A new pit was opened in the basement floor below elevation 708 ft 0 in. to accommodate the slag tank and its removal equipment.

Unit 1 turbine was carried across the north half of the mouth of a 70-ft-diam  $\times$  6-ft-thick caisson. This caisson extends from elevation 708 ft 0 in. down to bedrock at approximately elevation 637 ft 0 in. Since the circulating-water tunnel into this pit which had served the old unit was adequate for the new unit without increasing tunnel velocities excessively, it was decided to utilize the pit with a minimum amount of change. The center line of the pit was maintained as the dividing line between the new Unit 6 and the old Unit 2, so that, should it at some time in the future seem desirable, a new unit of the opposite hand could be located in place of Unit 2.

The caisson was, therefore, removed to levels somewhat below 708 ft so that a heavy beam could be thrown across the pit, slightly to the north of the center line. The mean free span of this beam is approximately 66 ft. It is 7 ft 3 in. wide and 13 ft 6 in. deep with generous haunches at each end. The beam is tied back with cross members to the semicircle of the caisson and this combined structure forms a base for the conventional-type turbine foundation which rises from the basement elevation of 708 ft 0 in. to the turbine floor at 735 ft 0 in.

Adjacent to the turbine a portion of an open pit along the north end of the plant which had housed the plant machine shop was framed over to provide space for the control room. A small extension beyond the existing turbine-room wall was made to house the exciter and to provide space to pull the generator rotor. A small crane was provided in this area to handle the exciter and the generator rotor.

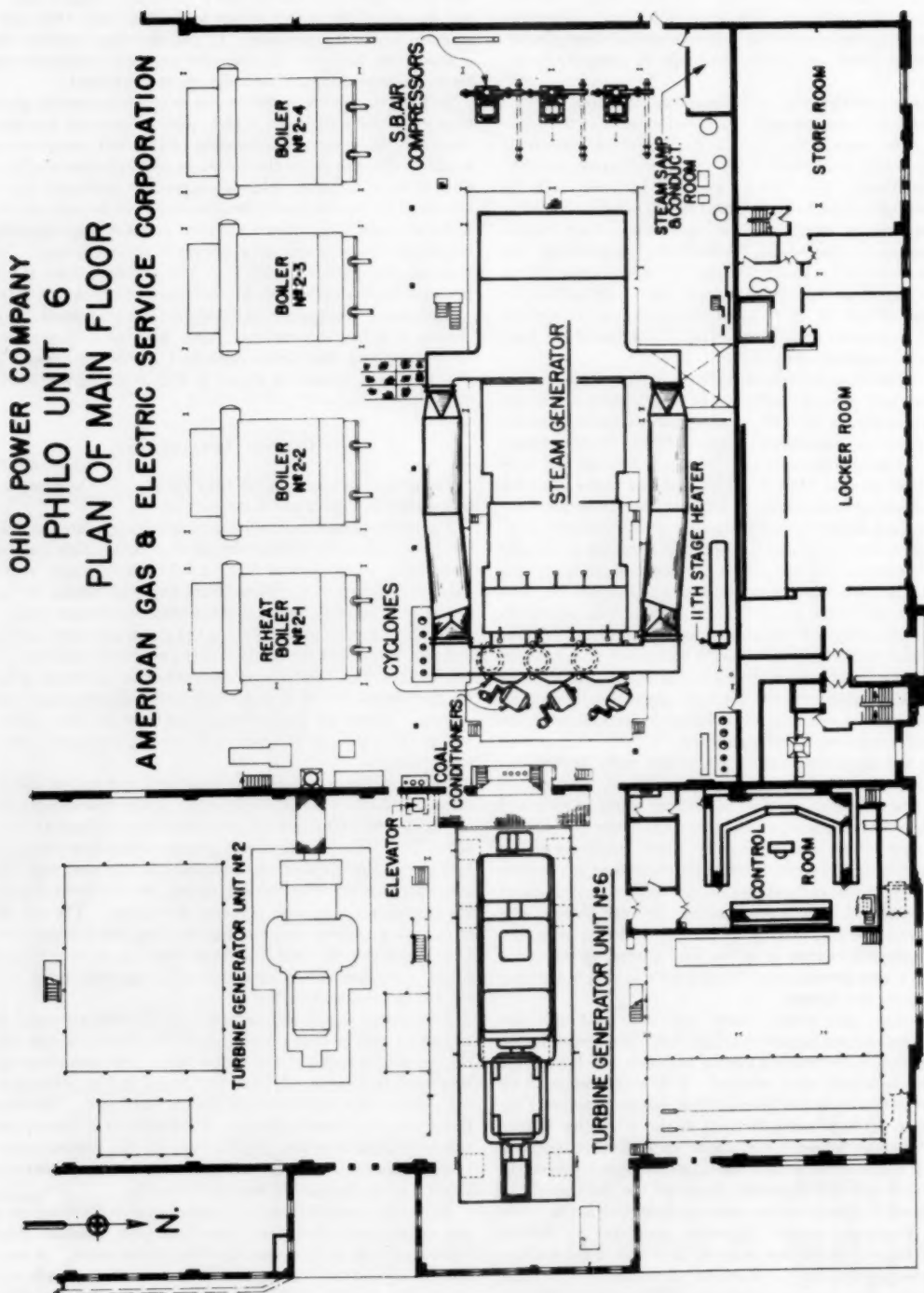


FIG. 2

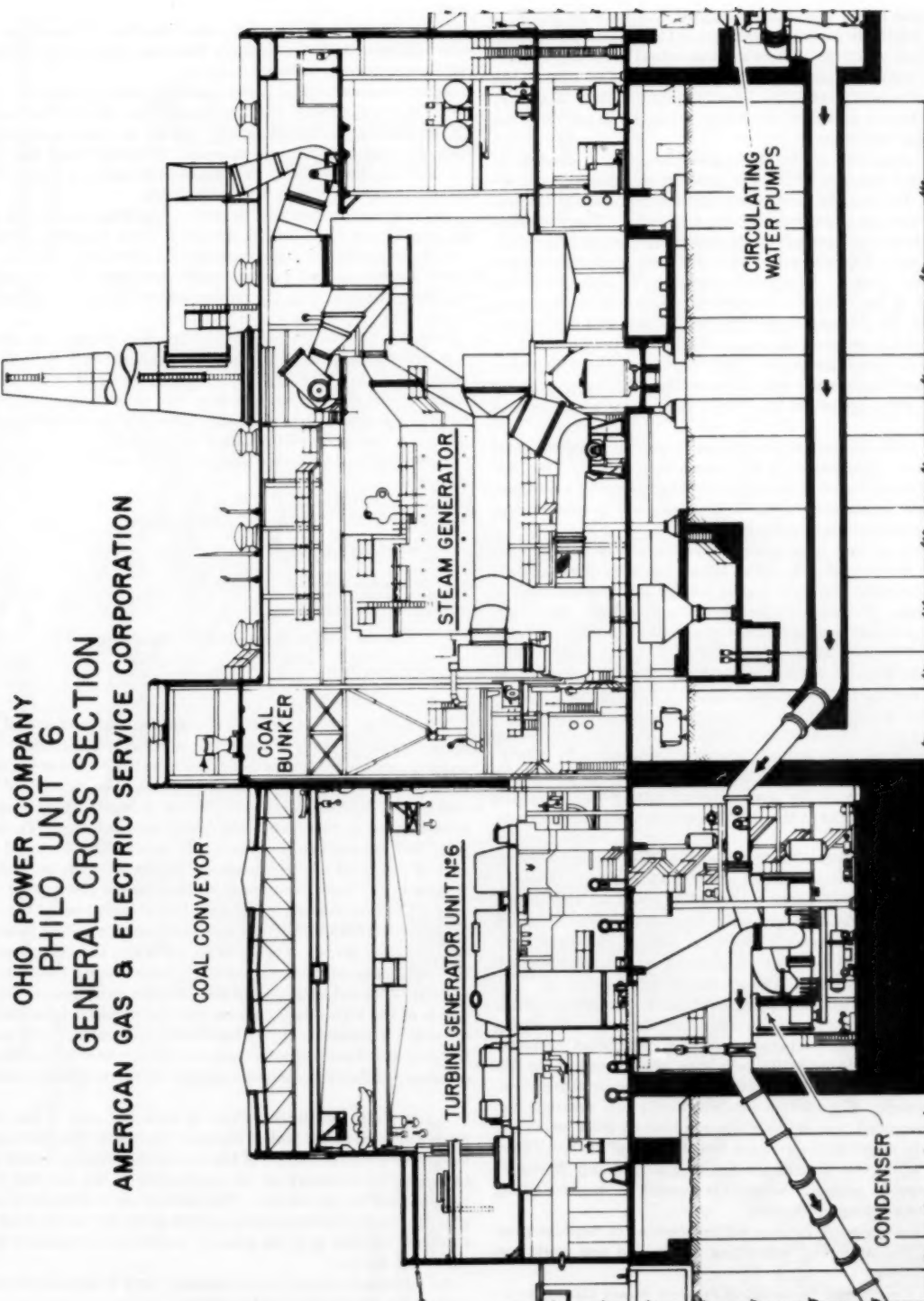


Fig. 3

### THE STEAM GENERATOR

The Philo steam generator,<sup>1</sup> designed and built by B&W, is rated at 675,000 lb per hr at 4500 psi and 1150 F with a feedwater temperature of 525 F. There are two reheat sections; the first will raise 655,000 lb per hr at 1225 psi from 800 F to 1050 F; the second will raise 520,000 lb per hr at 185 psi from 630 F to 1000 F. The unit has an estimated capability of 740,000 lb per hr at the main steam conditions.

The arrangement of the steam generator, Fig. 4, consists of cyclone-fired furnaces in front of pendant superheaters and reheaters. The walls of the cyclones and the front wall of the primary furnace are cooled by incoming feedwater. The transition from water to steam occurs in the primary superheater in the coolest gas zone. The remainder of the wall and pendant surface is superheater surface. The final superheater is arranged across the width of the furnace. The convection pass is divided by a baffle with the primary superheater on one side and the two reheat sections in series on the other. Gas flow is proportioned by dampers at the outlet of each side. By control of firing rate, main steam temperature will be controlled and, by positioning these dampers, one of the two reheat temperatures will be controlled.

The superheater surface is arranged to provide adequate fluid temperature equalization at the superheater outlet. The four pipes conveying steam to the turbine inlet originate at a common point in the superheater header so that they will be subjected to only small differences in temperature.

To eliminate any temperature difference at the turbine, the exit from the first reheater outlet header has been made a single line of adequate length to insure mixing and equalization of temperature. The second reheater has four outlets. These are piped to give best mixing and are protected against severe temperature differences by an attenuator.

To avoid slagging conditions in the pendant and convection sections, flue-gas recirculation is employed to limit gas temperature. Flue gas taken from the convection-pass outlet at 800 F is mixed with hot gas at 3000 F from the primary furnace to reduce gas temperatures entering the pendant sections to 1900 F, which is below the ash-fusion temperature. The design of the recirculating gas ports for most effective mixing was developed on a pilot-scale model at the B&W Research Center at Alliance, Ohio.

The steam generator is equipped with a B&W tubular-type air heater. Based on experience at the Philo Plant and elsewhere, the cold-end section of this air heater will be equipped with Corten tubes. Corten exhibits a greater resistance to corrosive attack from the sulphur compounds present in the flue gas of the high-sulphur coal burned at Philo. Experience indicates that the life of Corten is about 2 to 2½ times that of mild steel.

Because of the high-sulphur content of the coal (4 to 5 per cent), measures have been taken to avoid fouling the air heater during periods when inlet-air temperature would drop the stack gas below its dew point. Steam-heating coils have been placed in the discharge duct of the forced-draft fan to raise air temperature whenever necessary. Combustion air, which will also ventilate the plant, is supplied from outside through heating coils which are designed to maintain a minimum temperature of 70 F. These, together with a rise through the fan of approximately 25 deg F, should provide adequate safeguards against air-heater fouling and serious corrosion difficulties.

The steam-generator furnace will be operated at negative pressure. In the interest of expediting design and test work, our

usual pressurized operating procedure was abandoned on this one unit.

Coal will be handled by the present facilities at the plant. A new bunker of 1100-ton capacity has been erected and will provide approximately a 24-hr storage.

Since measurement of performance is vital on this unit, coal to the unit will be weighed three times (1) on the main belt scale; (2) on the unit's own belt scale; and (3) on a strain-gage-type scale in series with the second scale. This third scale has been included to provide actual experience with this type scale. Mechanical sampling of coal will be employed.

A direct-fired system will be used. Coal from the bunker will be crushed en route to the cyclones. One hammer-mill-type crusher of 50-tons-per-hour capacity will serve each cyclone. A B&W apron-type feeder with variable speed control will convey coal from the bunker to the crusher and will control coal flow to the cyclone.

Primary air from the forced-draft fan at a temperature of 685 F joins the coal stream from the feeder and carries it through the crusher and into the cyclone. Tempering air is available to maintain the coal-air mixture at a safe temperature. A small flow of cool air is introduced at the inlet end of the feeder to maintain a dry atmosphere within its sealed casing.

Table 1 gives an average analysis of the coal to be burned in this unit.

TABLE 1 COAL ANALYSIS

Moisture, per cent.....	10
Ash, per cent.....	16
Volatile, per cent.....	35
Fixed carbon, per cent.....	39
Heating value, Btu per lb.....	10,500
Sulphur, per cent.....	4.
Ash-fusion temperatures (reducing atmosphere)	
Initial deformation, deg F.....	2130
Fusion, deg F.....	2290
Fluid, deg F.....	2425

The primary burner, centrally located at the inlet end of the cyclone furnace, imparts a whirling motion to the crushed coal and primary-air mixture, which distributes the coal over the slag-covered surface of the cylindrical furnace. The velocity of the coal and air stream entering the burner is regulated by a cantilever damper to maintain a high tangential velocity. To complete the combustion, secondary air, constituting 75 to 80 per cent of the total air, is introduced tangentially to the cyclone furnace in the same direction of rotation as the primary air and coal. The high velocity produces a helical path toward the rear of the cyclone where the gas reverses direction before entering the discharge throat. Owing to its viscosity, the movement of the molten slag on the surface of the furnace is much less than the velocity of the entering air, and this provides an intense scrubbing action of the high-velocity air on the coal particles imbedded in the slag. This results in very high combustion rates. The quantity and distribution of secondary air are regulated by cantilever dampers which also maintain a smooth entrance of high-velocity air.

Tertiary air, constituting three to eight per cent of the total air, is admitted at the central region of the primary burner to prevent excessive recirculation of fine coal in the primary burner and to supply the necessary air for combustion of fine material that gets into the burner vortex. The tertiary air is introduced tangentially to a cylindrical housing which gives the air the same direction of rotation as in the primary burner and is regulated by a cantilever damper.

An automatic retractable oil-lighting torch is installed in each cyclone for establishing coal ignition.

Molten slag tapped from the cyclones passes to the floor of the

<sup>1</sup> "First Commercial Supercritical-Pressure Steam Generator for Philo Plant," by W. H. Rowand and A. M. Frendberg, published in this issue, pp. 409-416.

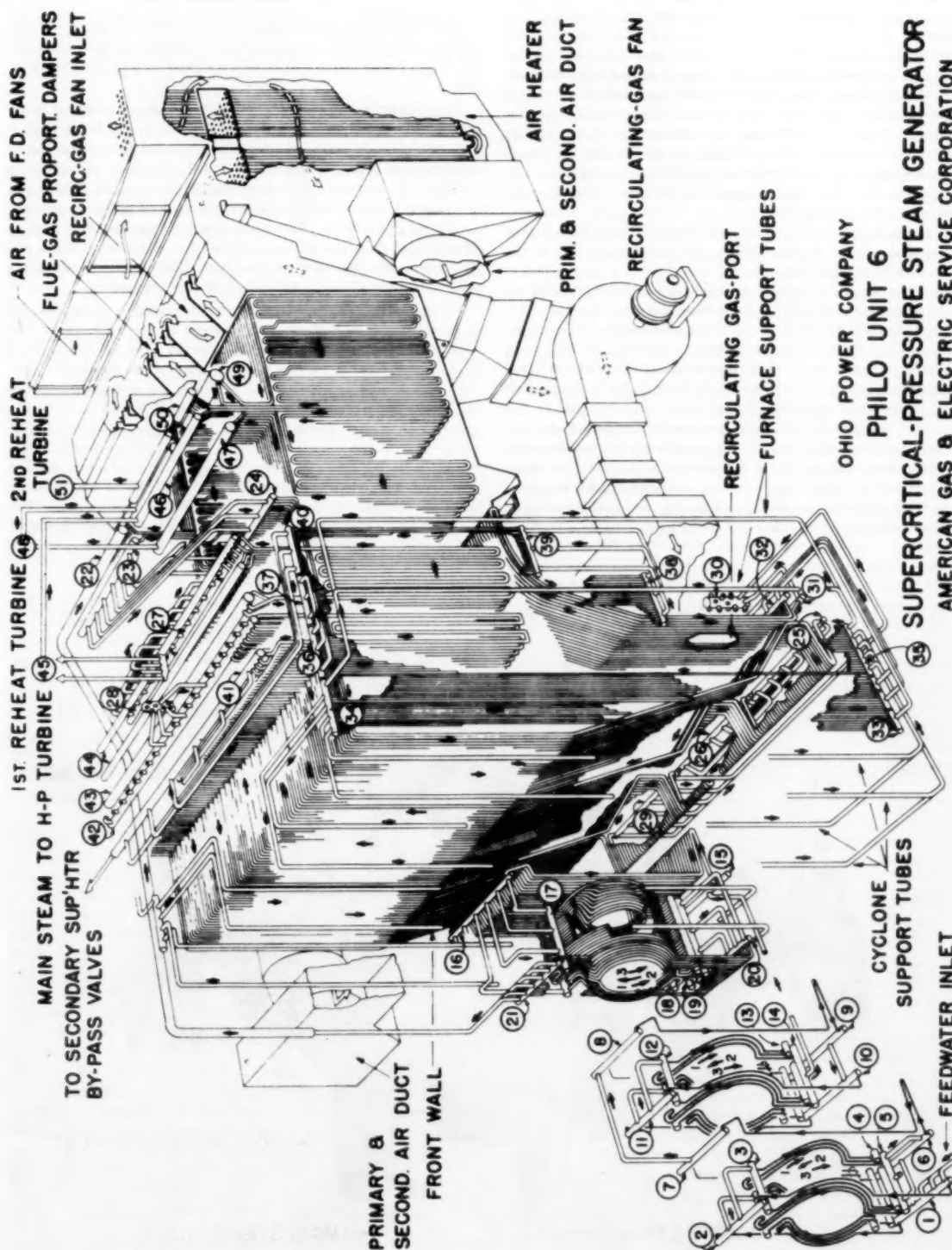


Fig. 4

primary furnace and then to a water-filled slag tank. From this tank, slag will be pumped to the existing ash pit in the rear of the plant.

The cyclone furnace is a very effective dust collector and for this reason no special dust-removal equipment has been provided.

The steam generator is equipped with 45 slag blowers. Twenty-four of these are fully retractable and are located in the convection pass. The others will clean the walls of the secondary furnace. All slag blowers will be driven by air motors. To limit condensate make-up, air will be used as the blowing medium. A blowing procedure has been designed to produce a minimum upset in steam temperatures.

Two centrifugal double-width, double-inlet, forced-draft fans with special airfoil blading will supply combustion air to the cyclones at 51 in.  $H_2O$  pressure.

The selection and design of fans suitable for the conditions encountered in gas recirculation were considered to be of primary importance. The fans finally selected were two overhung single-inlet centrifugal fans. It was originally planned to utilize an ID-type fan for this service but because of some initial operating difficulties experienced with this type fan on another type unit in similar but less severe conditions, this was abandoned. To avoid the exposure of a large-diameter shaft to the hot gas and to eliminate some shaft sealing, responsible for the trouble with the other fans, the overhung design was selected. Provisions have been made to test these fans at rated speed and temperature. This will be accomplished by running the fan at rated speed and recirculating air, allowing the input energy to be converted to heat.

#### THE TURBINE-GENERATOR

The turbine-generator utilized to convert the energy of the high-pressure high-temperature steam in this cycle into kilowatt-hours has been designed and built by the General Electric Company.

This 3600-rpm tandem-compound double-flow turbine is rated 125,000 kw at initial steam flow of 675,000 lb per hr at 1150 F and 4500 psi. At full load, steam is expanded from these initial conditions to 1225 psi and 800 F in a double-shell high-pressure turbine. The steam is then reheated in the boiler to 1050 F and expanded through the first reheat turbine to an exhaust condition of 185 psi and 630 F. The steam is again reheated, this time to 1000 F, and then passed through the second reheat turbine and the double-flow low-pressure turbine. The double-flow turbine is equipped with 26-in. long buckets in the last stage.

All four of these turbine sections are arranged in tandem on the same shaft. The high-pressure turbine is carried between the Nos. 1 and 2 bearings with steam entering adjacent to the No. 2 bearing and flowing toward the front end of the machine. The first and second reheat-turbine sections are arranged between the Nos. 3 and 4 bearings with the first reheat steam entering the middle section and flowing forward toward the front end before exhausting to the second reheater. Second reheat steam enters the same middle belt and flows through the second reheat section and then through a crossover to the double-flow low-pressure section. The double-flow section is carried between bearings Nos. 5 and 6. The high-pressure turbine is shown in section in Fig. 5.

The turbine, from the first reheat point on, is a conventional

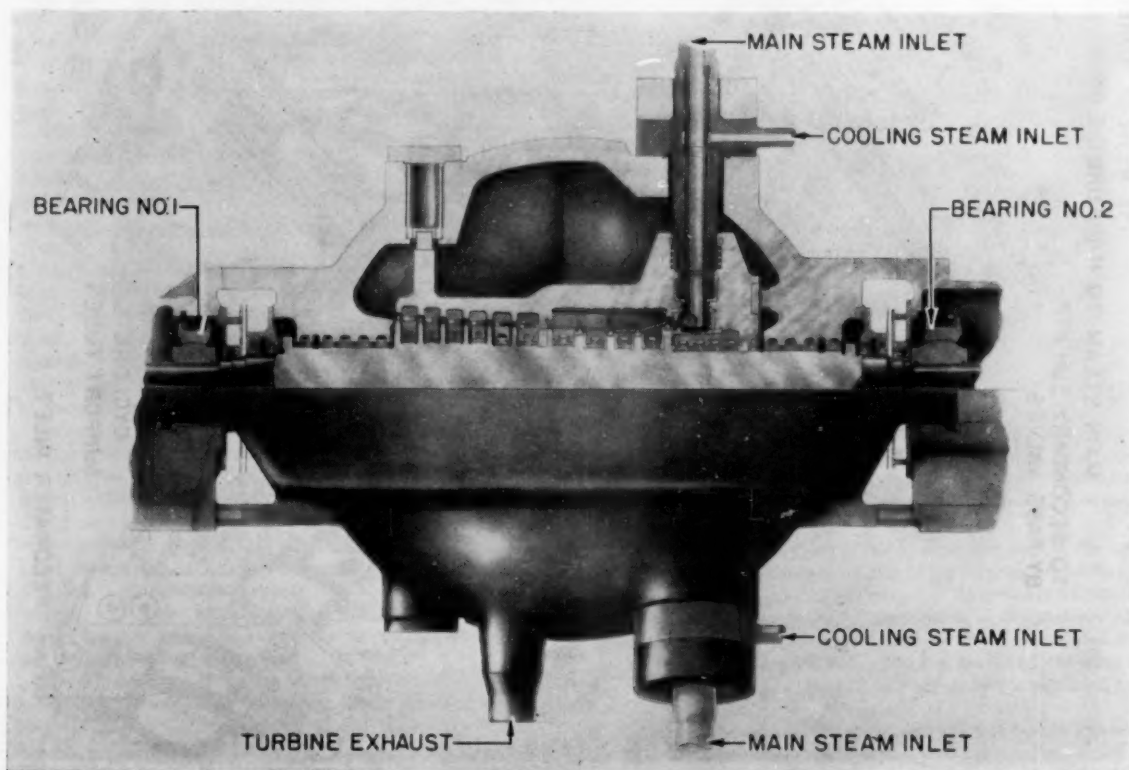


FIG. 5 OHIO POWER COMPANY, PHILO UNIT 6, SUPERCRITICAL-PRESSURE TURBINE, AMERICAN GAS & ELECTRIC SERVICE CORPORATION

arrangement similar to many machines which General Electric has built. The high-pressure high-temperature turbine, however, represents many new concepts. Designing for the high pressure is not so difficult as for the high temperature. Pressure parts tend to be relatively small because of the low specific volume of the steam being handled (about 0.19 cu ft per lb). In so far as possible, optimum pressure shapes, that is, spherical and cylindrical, were used. The outer shell of the high-pressure turbine, for instance, is a perfect sphere except for the supporting horns, shell joints, steam inlets, and exhaust pipes.

The initial concept of handling the high temperatures was to use massive stainless-steel inner shell sections in the high-pressure turbine. Because of the difficulty of providing adequate bolting materials, these shells might have been in a barrel arrangement with assembly of the rotor and the diaphragms from one end. This concept was unattractive for several reasons:

- 1 The high cost.
- 2 The difficulty of getting sound stainless-steel forgings or castings.
- 3 The difficulties which were, at that time, being experienced with the lack of dimensional stability of stainless-steel inner shells.
- 4 The additional effort associated with maintaining a machine with a barrel-type inner shell.

For these reasons, among others, the General Electric Company suggested that steam cooling of the inlet steam pipes, first-stage-nozzle assemblies, inner shell, and high-pressure packing be utilized. Also, it was suggested that the rotor be cooled on the first few stages, if necessary. With this cooling, the requirements for stainless steel could be limited to the inlet pipes, first-stage-nozzle assembly, the first three diaphragms, shell bolts, buckets, and minor trim. The remainder of the machine, the inner shell, the turbine rotor, etc., could then be made of a ferritic material operating at reasonable temperatures. This cooling-steam arrangement presented not only a highly satisfactory solution for the design of this machine but also pointed the way toward future designs for even higher temperatures. The complete description of the manner in which this steam is circulated to cool the machine is given in a companion paper by Messrs. Elston and Sheppard.<sup>4</sup>

It was generally felt that experience should be obtained not only on the cooling-steam arrangement of the shells and diaphragms but also in the use of both ferritic and austenitic rotors. The ferritic rotor would operate with cooling steam passing over the first several wheels, while the austenitic rotor could operate without cooling steam on the wheels. Tests were run as to the better manner in which to obtain an austenitic rotor, either by the use of a solid austenitic forging from front standard to coupling or by the fabrication of a welded rotor with an austenitic center section and ferritic ends. The latter is still under development so that two completely interchangeable rotors have been manufactured, i.e., one, entirely ferritic, and the other, entirely austenitic. Two conditions of cooling are planned, i.e., one, with the austenitic rotor and shell cooling alone; the other, with ferritic rotor and both shell and rotor cooling.

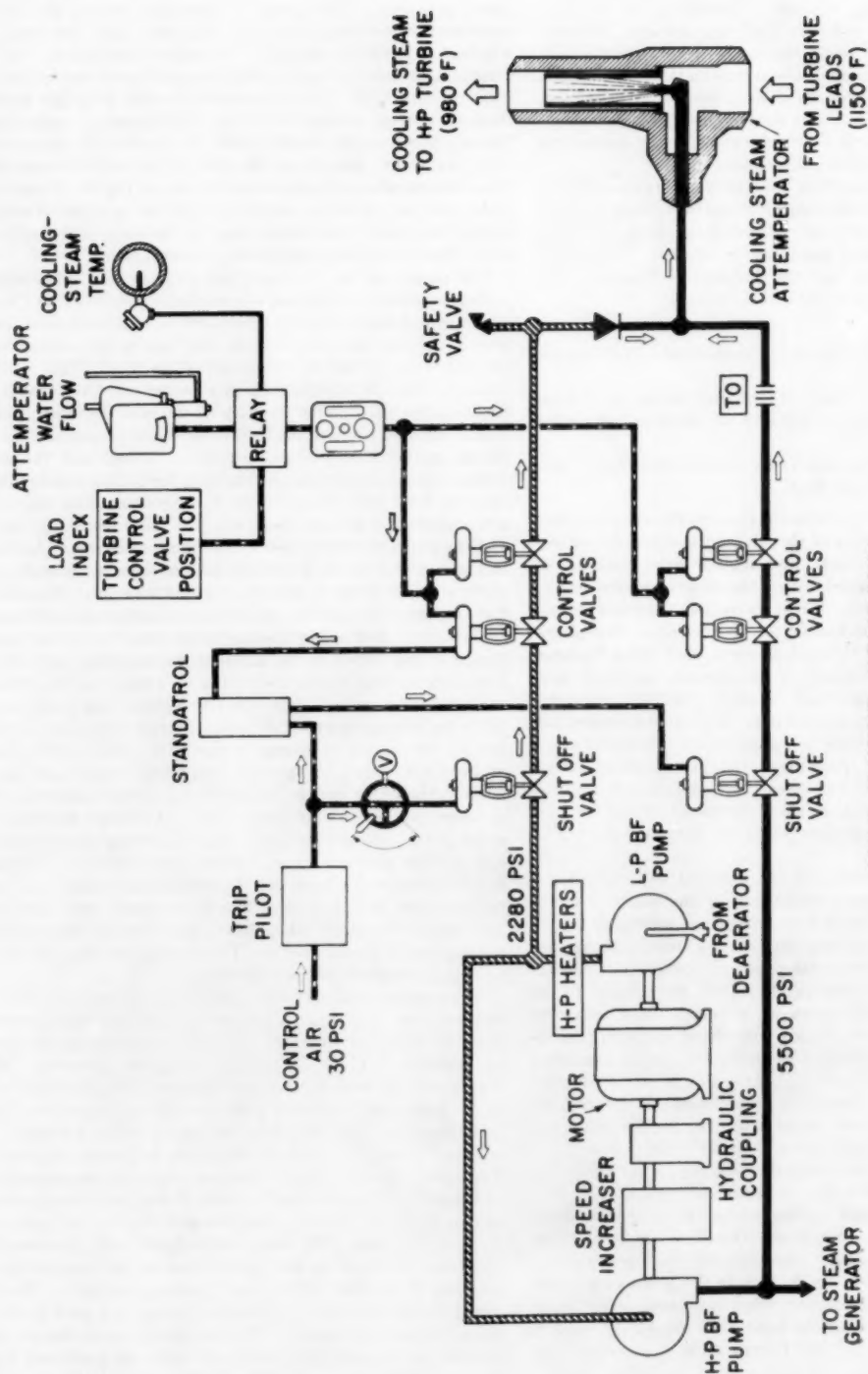
To accomplish this steam cooling, an exterior source of steam at approximately 980 F is required. Obtaining this steam presented a real problem because in one case the cooling-steam flow required is about 40,000 lb per hr and, in the other case, about 100,000 lb per hr. In both cases, there is a small reduction in over-all cycle efficiency since the basic 4500 psi, 1150 F cycle is being diluted by a 3800 psi, 980 F cycle (first-stage pressure at

which steam enters the machine). At first it was suggested that the cooling steam be taken from an intermediate header in the steam generator. This proved impossible because of the requirement of meeting the two differing flow rates, the higher of which would tend to starve the secondary superheater. In the arrangement finally adopted, steam from the four steam leads at 4500 psi and 1150 F is attemperated to 980 F before flowing through resistance orifices to the cooling-steam connections. These orifices are in parallel with the first-stage nozzles and therefore always proportion the flow to the total throttle flow. The attemperator and controls are shown in Fig. 6. These controls must be extremely reliable so that the machine is neither chilled nor overheated and so that, in the event of trip-out, the water flow is positively shut off to prevent flooding.

The piping for the cooling steam and the four main-turbine leads is drained by a common motor-operated drain valve. Good attemperator control is particularly difficult since the steam pressure in the four main steam leads, and thus in the cooling-steam attemperator, is directly proportional to load. This relation exists because the machine is a single-valve machine; that is, all four valves work together discharging steam at the same pressure to the turbine. At full load, 5500-psi water is available to discharge against 4500-psi steam pressure. At half load, the steam pressure drops to 2250 psi and the main feedwater pressure drops only to 4700 psi. To alleviate this problem, two sources of attemperating water are used; one, the main feedwater header, and the other, the low-pressure feed-pump discharge. As shown in Fig. 6, a stop valve, located in each of these water lines, positively shuts off the flow when the turbine trips out. Main steam flow, measured by turbine control-valve position and attemperator flow, both modified by cooling-steam temperature, act to position first two valves in the 2200-psi line until the load reaches such a point that this pressure can no longer supply sufficient attemperating water. Valves in the 5500-psi line then open to carry the attemperator to full load. Shutoff valves are provided in each line in case of leakage in one or the other of the control stations not in use. A separate temperature trip is provided to trip out the whole unit in the event that the cooling-steam temperature goes excessively high or low. A strainer has been provided in the cooling-steam line after the attemperator to prevent any foreign particles from entering the machine. Extensive instrumentation has been incorporated in the machine to detect temperatures in various locations in the inner and outer shells and around the nozzle assemblies to gage the effectiveness of the cooling-steam arrangements. These temperatures will be recorded continuously in the control room.

The primary controls for this machine are similar to those of a conventional machine. All functions are remotely controlled from the main control room. The four stop valves are tripped by solenoid or by action of the emergency governor. These valves may be individually closed for test during full-load operation. Each control valve is positioned by an hydraulic cylinder and these, too, may be closed during operation for test. The stop valves are backseating so that there will be no stem leakage. The control valves, being positioning, cannot be backseating and, therefore, have three leakoffs: One, at the first reheat pressure; one, at the second reheat pressure; and the last, at 1 psig to the steam-sealing line. Provisions have been made periodically to condense and weigh the first leakoff from the first control valve as a means of checking on stem and bushing clearance. We have found that the reduction in the stem leakage is a good measure of the reduction in clearance. The two first reheat-intercept valves and the two second reheat-intercept valves are positioned by the pre-emergency governor. Reheat stop valves in the second reheat line are tripped shut by the emergency governor. No reheat stop valves are provided in the first reheat line because the po-

<sup>4</sup> "First Commercial Supercritical-Pressure Steam Turbine—for Philo Plant," by C. W. Elston and R. Sheppard, published in this issue, pp. 417-426.



OHIO POWER COMPANY  
PHILO UNIT 6  
TURBINE COOLING-STEAM ATTEMP.-WATER CONTROL  
AMERICAN GAS & ELECTRIC SERVICE CORPORATION

Fig. 6

tential overspeed of the machine due to failure of first intercept valves is not serious. The lubricating system utilizes a single oil cooler which is supplied with condensate-quality water from the closed turbine-auxiliary cooling system.

The only important variation from standard control practice is that an initial pressure governor has been provided, not only to act as an overriding control to maintain pressure above a certain level but, if desired, to act as the sole pressure regulator on the system. Thus the control valves may be positioned either by the initial pressure governor or by the regular speed governor. A turbine by-pass pressure regulator also is provided to control pressure during the starting cycle.

The shafts of the machine are steam sealed. The steam-seal regulator draws its supply of pegging steam from the by-pass system which will be pressurized both during start-up and shortly after a trip-out. During the short interval after trip-out while the superheater by-pass valve is opening, we expect the shafts to be sealed by the steam escaping from the first and second reheaters. Very careful attention has been given to the design of controls which guarantee that the steam-seal-regulator pegging valve cannot open unless there is slightly superheated steam available. This assures that the regulator cannot pass water to the turbine seals when starting up with the by-pass system still filled with relatively cold water.

Four main steam leads, each 7.70-in. OD  $\times$  4.25-in. ID of Type 347 stainless steel, connect to four stop valves located under the front of the machine. Each stop valve serves its own control valve. The whole assembly of stop and control valves is mounted on a rigid frame which is hung on rod hangers. The control gear for the control valves is mounted in a box within the body of this frame so that only a reach rod coming down from the front standard is necessary to position the individual pilots of each control-valve mechanism. Steam flows from the control valves through four leads which loop under the turbine-foundation arch and up to the high-pressure shell. Steam exhausts from the high-pressure turbine through two 12-in. lines to the first reheater. First reheat steam returns through two 12-in. lines, one each to the two first reheat intercept valves mounted on the upper shell of the first reheat turbine. Exhaust from the first reheat turbine returns to the second reheater through two 18-in. lines. Second reheat steam at 1000 F leaves the reheater through four 16-in. lines which connect into two 18-in. lines just before the second reheat stop and intercept valves. One pair of these valves is located on each side of the stop-and-control-valve assembly. Platforms serve the whole area for ease of maintenance. The second reheat intercept valves are angled out to give a minimum pressure drop and discharge downward into two 20-in. lines which pass under the turbine arch and into the lower shell of the second reheat turbine. All low points in these lines are drained by air or motor-operated drain valves connected to the drip leg of the condenser.

The 3600-rpm generator is rated 156,250 kva at 15 kv, 0.80 pf, 0.5 scr, and 300 psi  $H_2$  pressure. A 600-kw gear-driven exciter operating at 900 rpm and 250 volts supplies excitation current.

In selecting this generator, it was realized that machine ratings will continue increasing at least to the point where forced-cooling arrangements will prove economical and that we should, therefore, have some operating experience with this type of cooling. The machine, therefore, has forced cooling of both the rotor and stator. Two pressure systems are used. One is a low-pressure system for ventilating the rotor and stator core. The other is a high-pressure system for ventilating the stator windings. Gas for rotor cooling flows through the rotor and stator core and back to an axial-flow fan. Discharge from this fan flows to the two turbine-end coolers and repeats the cycle.

A high-pressure centrifugal blower, located on the outboard

end of the rotor, pumps gas through the outboard coolers and then through a header and flexible-hose system to each of the stator coils. Warm gas is returned from the turbine end of the machine to close the cycle. Present state of development of blowers required that the fan providing stator-coil ventilation be of centrifugal design, larger in diameter than the inside diameter of the stator. This meant that the blower had to be either designed for disassembly or located on the outboard end. The latter arrangement was chosen so that the blower could be an integral part of the rotor. This blower and the generator bushings could not be located at the same end of the generator because of the interference between the taps leading to the bushings and the header and connecting tubes of the high-pressure ventilating system. The generator bushings were, therefore, moved to the turbine end of the generator. This is not the better arrangement because of the complications of generator leads and hydrogen-cooler piping under the generator but was accepted on this machine with the assurance that on subsequent machines axial-flow blowers of suitable head would be developed so that the blower could be located on the turbine end of the rotor.

The generator bushings are hydrogen-cooled. On the inside of the copper cylinder, which forms the conducting part of the bushing, is a tube of insulating material which will conduct hydrogen from the high-pressure system into the bushing and discharge against the walls of the cylinder before returning to a lower-pressure area. At 30-psi hydrogen pressure the bushings will carry 8000 amp.

Hydrogen seals for the shaft will utilize the conventional vacuum system where gas-free oil is injected between floating rings to form the shaft seal. Oil-drain lines from the generator bearings are trapped through a vented detrainment section to preclude the possibility of hydrogen returning to the main oil tank in the event of shaft-seal leakage.

#### FEEDWATER CONDITIONING

At the outset it was recognized that almost perfect control of feedwater conditions was essential to the successful operation of this unit. Initial concepts of the means and quality of this control were outlined and then largely substantiated by personal observation of German experience with Benson boilers at subcritical pressure by comprehensive tests carried out on a small supercritical-pressure steam generator at the B&W Research Center at Alliance, Ohio, and by several test programs carried out at various locations on our system.

The first criterion of adequate water quality is that dissolved solids must be kept very low since any solids carried into the steam generator will be either deposited in the transition zone or carried by the steam into the turbine. Owing to the lack of data on the solubility of various solids in steam, it is possible to conjecture that the presence of solids in the feedwater might result in a greater problem of turbine deposition than steam-generator deposition. It was learned that this apparently is the case in the German experience.

The second criterion of quality requires reduction to a minimum of corrosion not only in the steam generator but also in the feedwater cycle. Any significant quantities of iron oxide in the feedwater would likely result in deposits within the steam generator. It was decided to limit corrosion by pH control through the addition of ammonia or a suitable amine. The control point has been set and confirmed by test at approximately 9.5. Mechanical deaeration of the highest efficiency available is utilized and various designs for equipment in the condensate cycle before the deaerator will minimize the possibility of air leakage. Consideration is being given to the addition of hydrazine as a chemical scavenging agent with a decision pending the results of

tests presently under way both on 2000-psi cycles and on the small supercritical steam generator.

In attempting to keep dissolved solids to an absolute minimum, all leakage into the cycle must be eliminated in so far as possible. The most likely source of this contamination is the condenser. As a result, condenser design is directed at obtaining the maximum possible freedom from seepage leaks. Among other arrangements, sprayed-rubber coatings are to be applied to the tube sheets to seal off the rolled tube ends. Cupronickel tubes of 70-30 composition were selected as suitable to withstand the high pH conditions on the steam side and the conditions met on the circulating-water side so as to minimize tube failures. Similarly, feedwater-heater tubes will be, for the most part, fabricated of 70-30 cupronickel.

A multipurpose demineralizer with a capacity of 100,000 lb per hr is provided. This can be operated either continuously, by-passing about 20 per cent of the condensate to maintain solids at a minimum or, during start-up or shutdown of the steam generator, to remove any solids which might wash out during these transient conditions. This latter condition of start-up and shutdown governs the capacity of the demineralizer. Although condensate from the old section of the plant will be employed as make-up to this unit, it is planned that this water will be "polished" by the demineralizer before use. In addition, filters will be included to operate with the demineralizer or singly, for by-passing condensate during normal operation or during start-up or shutdown. It has been established that filtration can effectively remove appreciable quantities of iron oxide even at low concentration levels. A test program designed to evaluate this fact quantitatively and govern the selection of suitable filter materials has been largely completed.

In all these considerations, there has been the need for information not previously available nor even previously required, such as the organic leaching from resins employed in demineralization at particularly low-concentration levels. Tests are now under way to determine the extent of this leaching. Another test has been instituted at Philo Plant to gain information on the performance of various alloy condenser tubes in a steam atmosphere approximating that on Unit 6. Three different tube metals (90-10 cupronickel, 70-30 cupronickel, and arsenical copper) are being tested in a small condenser which has been tapped into one of the existing units. A second condenser with aluminum tubes and tube sheets has been paralleled with the first to gain experience with this metal. Both steam-side and cooling-water-side experience will be obtained since the cooling water for these small test units is the same as that used for the large condensers. While this is a long-range type of test which could not be completed before tube orders had to be placed, it did serve as a helpful guide.

Particular attention has been paid to develop procedures to clean the steam generator chemically and to operate the unit initially so as to free the cycle of contamination such as the siliceous material always present after construction. These procedures have been worked out in great detail and it is our belief that they will give the expected degree of water quality.

The control conditions contemplated for successful operation although rigid are, we believe, realistic. They are as follows:

Dissolved solids less than 500 ppb (parts per billion)  
Silica as  $\text{SiO}_2$  less than 20 ppb  
Iron less than 10 ppb  
pH 9.5

To assist in maintaining these control conditions, numerous sampling connections have been provided along with suitable instrumentation in the control room, such as recorders for con-

ductivity, dissolved hydrogen, dissolved oxygen, and pH to monitor these variables continuously.

#### CONTROLS

Entirely new concepts are introduced in the control of supercritical-pressure once-through steam generators. The steam generator no longer possesses a tremendous elastic reservoir, the vaporizing saturated water, whose pressure is highly sensitive to changes in temperature. Supercritical-pressure water is a homogeneous phase whose properties such as specific volume and enthalpy continuously change from those at the feedwater conditions to those at the superheater-outlet conditions. Addition of heat makes the fluid expand in a manner similar to the expansion of a gas, not in the sudden isothermal expansion, which water experiences during evaporation. Pressure in the steam generator must be controlled, therefore, as in a typical flow process by varying either the input pressure or the outlet area. System pressure is regulated, therefore, either by variation of the feedwater pressure against an area determined by control-valve position, or by variation of turbine-control-valve area with a constant feedwater flow. Regulation of pressure by either of these flow methods leaves the outlet temperature to be controlled by variation in heat input.

Basically, the primary control functions, therefore, are:

- (a) Flow determined by turbine-control-valve position and pressure regulated by feed-pump discharge pressure.
- (b) Or flow determined by feed-pump flow and pressure regulated by turbine-control-valve position.
- (c) And superheater-outlet temperature in either case regulated by heat input to the steam generator.

Before the final control arrangements were designed, response tests were run by the Bailey Meter Company on The Babcock & Wilcox test unit. These tests indicated the complete feasibility of the basic control concepts as described.

Feedwater flow and pressure are controlled by variation of the high-pressure feed-pump speed by a hydraulic coupling. Feedwater flow from each of the two pumps is measured and totalized. Total feedwater flow is also measured by a single flowmeter at the steam-generator-inlet header. Flow is automatically balanced equally between the two pumps. The total flow signal is then balanced against an output from the main superheater-header-outlet pressure controller and the unit load, as measured by first-stage bowl pressure in the turbine or against a manual input, to give the corrected signal to position the hydraulic couplings on the feed pumps. When the total flow signal is balanced against a manual input signal selected by the operator, this manual signal becomes the single loading device for the whole unit. During this type of operation, the feedwater flow is maintained constant and the turbine valves automatically position under action of the initial pressure governor to maintain system pressure. As the control valves respond to this governor, electrical load will fluctuate. This is contrary to the usual governing procedures wherein the control valves are positioned by the operator, and so long as initial pressure and temperature remain constant, load on the unit is unchanged. It was felt that pressure control by the turbine-control valves might be somewhat faster and more flexible. And, since load variations in this central location on the AG&E system are not intolerable, it was included as an alternate means of pressure regulation.

Flow below 125,000 lb per hr through either of the pumps automatically opens the emergency leakoff valves on the pump in question. Total feedwater flow of less than 225,000 lb per hr measured on the total flowmeter, trips the unit off the line. The total flowmeter also can be used in the primary control if maintenance is required on either of the individual flowmeters. A

low superheater-outlet temperature override is provided to reduce feedwater flow in either mode of operation if superheater-outlet temperature tends to drop below 1000 F. A lockout is provided on this safety device for use during start-up.

A pressure switch acts to open the superheater by-pass valves if pressure at the platen superheater-inlet header tends to rise above the set pressure on the safety valves. The by-pass valves function, therefore, as power-relief valves to reduce the number of times the main safety valves will have to open.

Combustion control for this unit is concerned with the regulation of heat input to provide desired outlet-steam temperature. Since the ratio of heat input to pounds of water flowing is under the operator's control, the operator may select any desired outlet temperature. In other words, the steam generator does not have a limited temperature characteristic like a subcritical-pressure boiler, but an infinite combination of flows and temperatures may be attained.

Since it takes approximately two minutes for an element of water to pass through the entire length of this steam generator at full load, there is a considerable time delay between changes in firing rate and changes in outlet-steam temperature. It was decided, therefore, to take the primary temperature measurement which would indicate changes in heat input per lb of water from a zone as near the feedwater-inlet header as practicable. In passing through the boiler, the feedwater flows first through the three cyclones and their associated walls in series. The water temperature leaving the cyclones is very nearly the conversion-zone temperature of slightly above 700 F. This is a zone of temperature where shadowy discontinuities of some properties, such as specific heat, exist as reminders of the evaporative process below the critical pressure.

The conversion-zone temperature was selected as the anticipator to force the firing rate up or down during transient conditions. Subsequent response-rate tests on the small Alliance steam generator indicated the correctness of this choice. From stabilized conditions, a sudden increase in water flow with no change in firing rate caused outlet-steam temperature to rise first and then, after an appreciable interval, drop below the original conditions. The conversion-zone temperature, however, dropped immediately to a new level showing correct direction and good speed of response. The conversion-zone temperature, although not controlled at any particular level over the load range of the unit, is used as the anticipator to modify firing rate. The signal for combustion control, therefore, comes from a total-water-flow measurement, modified by conversion-zone temperature and final steam temperature.

This master combustion-control signal regulates air flow through each of the cyclones. Air flow, in turn, determines coal feed to each of the cyclones. Oxygen-analysis equipment will be used as a bias for each of the cyclones to obtain the optimum air-fuel ratio. Induced-draft-fan vane positions will be controlled by furnace draft. Recirculation gas flow will be automatically proportioned to the total air flow through the unit and corrected by gas temperature in the convection pass. This proportion may be biased by the operator who will observe slagging conditions in the pendant superheater and judge whether the gas temperature entering this zone should be increased or decreased by lowering or raising the flow of recirculating gas.

Reheat steam temperatures will be controlled by positioning gas dampers in the outlet of the convection pass. These dampers cross the back of the primary superheater pass on the left-hand side of the unit, and the reheater pass on the right-hand side. The two reheaters are in series in the gas pass so that gas-side control of both reheat temperatures would have been exceedingly difficult. The alternate possibilities were:

1 To control to whichever temperature was lower (relative to design value) and attemperate ahead of the other reheater to keep its outlet temperature down to the design value.

2 Or control to whichever temperature was higher and let the other temperature sag.

Thermodynamic studies indicated that the loss to the cycle efficiency due to attemperation was about equal to the loss due to lowering one of the reheat temperatures. The second method of control was chosen because it is less complicated. Space has been left in the cold reheat lines, however, for the subsequent inclusion of attemperators if they should prove desirable.

Since storage in the deaerator is limited to approximately 2-min flow at full load, deaerator level controls the flow from the condensate booster pumps. Hot-well level is controlled by the addition of make-up to the cycle or by the routing of condensate to storage. Automatic heater-level controls are utilized on each of the feedwater heaters.

Throughout the design of this unit, the basic AG&E concept of automatic control has been observed. All control functions are either completely automatic or are under the operator's control remotely from the central control room located on the turbine-room floor alongside the high-pressure machine. To supervise the operation of the unit, extensive instrumentation has been provided. All important functions are recorded in full view of the operator. Other functions are either indicated or provided with alarms.

To protect this unit, many interlocks and special trips are provided. Some peculiar to this unit are as follows:

1 Less than 225,000 lb per hr of feedwater flow trips unit to protect furnace tubes.

2 Extreme high or low main steam temperature trips unit to prevent over-temperature or quenching.

3 Over-all unit trip opens one superheater by-pass valve and trips off one feed pump, if both are in service, to maintain nominal circulation to cool floor tubes in primary furnace.

4 Loss of both recirculating gas fans trips unit to protect pendant superheater from excessively high gas temperature.

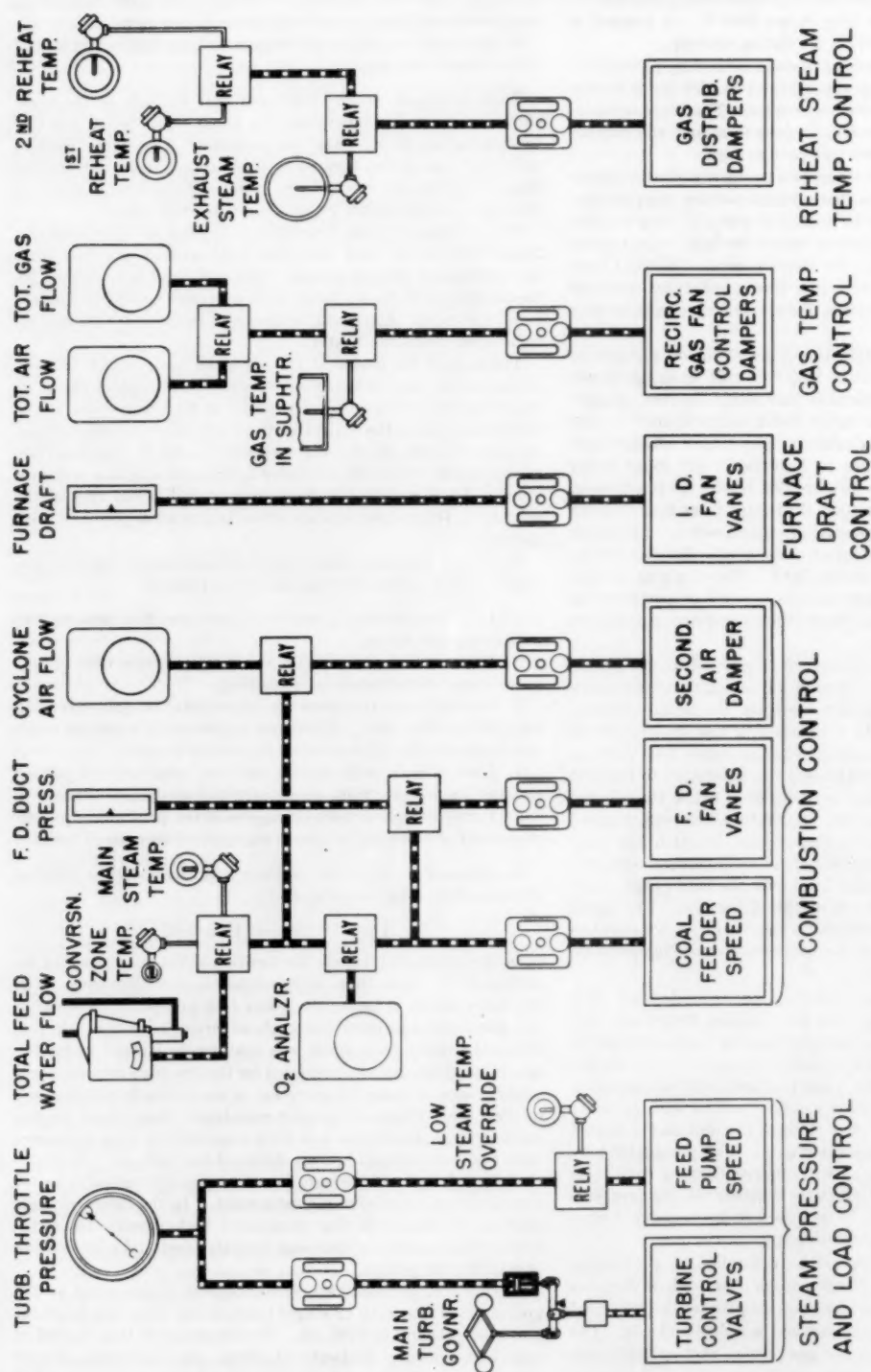
5 Extreme high or low-cooling-steam temperature trips unit to prevent overheating or quenching internal sections of turbine.

A schematic arrangement of these controls and their relation to each other is shown in Fig. 7.

#### FEED PUMPS AND HEATERS

In the design of this cycle, the location of the deaerator was determined by other than thermodynamic considerations. The deaerator serves to locate the boiler feed pumps at a somewhat higher-temperature level than might otherwise have been selected. When the boiler feed pump was tentatively located under the deaerator, designs were considered for the two high-pressure feedwater heaters suitable for operation at the full feedwater pressure of 5500 psi. Designed along conventional lines, these heaters reached large dimensions and were considerably more expensive than two conventional heaters designed for 2100 psi. Although the heat rate suffered, we were forced by this differential in heater cost to go to a split-pump arrangement. In the future, designs must be developed so that economical high-pressure feedwater heaters can be built to overcome the extra cost and complication of splitting the pumps.

In this arrangement, two constant-speed pumps rated at 924 gpm at 3550 rpm with 12 stages take suction from the deaerator and raise pressure to 2100 psi. The feedwater is then heated in two high-pressure feedwater heaters, the 16th-stage heater operating at 447 psia, and the 11th-stage heater operating at 819 psia to 510.8 F. Two variable-speed eight-stage pumps rated



OHIO POWER COMPANY

PHILO UNIT 6

## BASIC CONTROL DIAGRAM

AMERICAN GAS &amp; ELECTRIC SERVICE CORPORATION

Fig. 7

at 1027 gpm at 6500 rpm then raise the pressure to 5450 psia. Estimated efficiency of both types of pumps is 78 per cent. Feedwater is raised from 510.8 to 525 F in the variable-speed pumps.

One of the LP and one of the HP pumps have been coupled to a single motor in a tandem arrangement. One shaft end of a 4000-hp 3550-rpm induction motor is directly connected to the LP feed pump through a flexible coupling. The other end of the motor shaft is directly coupled to a fluid-drive coupling rated 3000 hp at 3550 rpm having twin oil coolers. The coupling, in turn, is connected to a step-up gear with a ratio of 1.88 to drive the HP pump at 6500 rpm. Feedwater output from the pumps is regulated by controlling speed of the HP pump. A complete speed range on the coupling has been provided for by suitably sizing the oil coolers so that the main unit can be operated at variable pressures down to the discharge pressure of the constant-speed LP pumps if such should prove feasible during operation. Over-all length of each pump unit is approximately 42 ft.

Each set of pumps is protected by a pair of emergency leakoff valves in parallel, with a combined capacity of 125,000 lb per hr at 5500-psi inlet pressure and 200-psi discharge pressure. Flashing water from these valves is carried back to a centrifugal separator and flash pot on the side of the deaerator.

The rotor of the HP pump is balanced by opposing impellers so that no balancing drum is needed. Any small unbalance will be taken by a thrust bearing. The LP pump has all stages facing in one direction. Hydraulic balance will be maintained by a balancing-drum arrangement on the discharge end.

Seals on these pumps are particularly critical. The manufacturer proposed a packingless arrangement, utilizing two floating bushings. On the LP pump, cool condensate from the condensate booster pumps at 250 psi is injected into a chamber surrounding the two floating bushings to quench flashing on the suction end of the pump. Pressure differential from 250 psi, inward to the suction pressure and outward to atmospheric pressure, spreads the two floating bushings out against ground radial sealing surfaces. At the discharge end of the pump the arrangement is similar but the seals operate against the balancing-drum leakoff which is piped to the deaerator. Floating bushings allow close clearances which will be maintained by the bushings positioning themselves to any shaft running condition.

A similar arrangement was proposed for the HP pump seals. This would have required a source of cool water at approximately 2100 psi. The only simple way to obtain this water would have been to extract the necessary amount from the discharge of the LP feed pumps and cool it sufficiently to do the required quenching. It was estimated that a total of 60 gpm, 15 gpm per seal, would have been required at approximately 150 F. This would have meant degrading roughly 6,000,000 Btu per hr from a temperature level of 375 F down to 150 F. We felt that this was an unnecessarily heavy burden on the heat rate. In the final design which was adopted the pressure is broken down to deaerator pressure in a floating-bushing arrangement. Since the water enters the pump at 510.8 F, this means that there will be some flashing. Stainless materials have been utilized in this area on the bushings and shaft sleeves to minimize damage. Outside of this leakoff is another pair of floating bushings with a cool-water injection identical to the LP pump seals. Inward flow of cool injection water from these seals will quench almost immediately the flashing of the mixture coming from the inner bushings.

Full-sized models of these shaft seals have been built and tested at full pressure, temperature, and speed by the manufacturer. Performance during these tests has been good.

Once the decision had been made to split the feed pumps into two sections each, the two HP feedwater heaters became standard heaters operating at 2100 psi.

The 11th-stage heater, drawing its extraction steam from the

HP turbine exhaust, has a nominal steam-side operating pressure of 819 psia, although its design pressure is 1300 psia, so that the throttling device in the extraction line to this heater can be removed if this proves feasible in operation. The heater was designed with a terminal-temperature difference of 10 deg F to reduce its size since low terminal-temperature difference was, in effect, being wasted by throttling in the extraction line to the heater. Duty on the heater with 510.8 F outlet temperature is 43.2 million Btu per hr. The 16th-stage heater, taking extraction from the 16th stage in the first reheat section of the turbine, has an operating pressure of 465 psia with a design pressure of 500 psia and a terminal-temperature difference of zero deg F. Duty on the heater at full load is 53.1 million Btu per hr.

Both heaters have 10 deg F drain coolers and utilize  $\frac{1}{8}$ -in.-OD 70-30 cupronickel tubes. Drains from the 11th-stage heater are dumped to the 16th-stage heater through an automatic level-control valve. The 16th-stage heater drains are dumped through automatic level-control valves to the condenser during start-up and to the deaerator when the pressure difference between the two becomes large enough to overcome a large static head existing between the two.

The 70-30 cupronickel tubes have been used in the low-pressure heaters because of the high pH value of the feedwater.

#### CONDENSER

Special condenser design has been utilized to adapt to severe conditions which this cycle imposes. The 70-30 cupronickel tubes and steel instead of Muntz-metal tube sheets have been used to minimize ammonia attack. The tube sheets inside the water box and the tube ends have been rubber coated to reduce the possibility of leakage. The air-cooler section, which is probably most vulnerable to attack, has been designed so that only a small number of tubes is used. The water-box covers have special manholes so that these tubes can be replaced without removing the entire water-box cover. Two special spray pipes have been introduced into the neck of the condenser. One discharges steam at 300 F maximum from the high-pressure flash tank, and the other spray in cool condensate to blanket this steam to prevent the heat from backing up into the turbine exhaust. Because of large movement and high temperature, a water-cooled Phillips joint was used to take the expansion of the long exhaust neck.

#### HIGH-TEMPERATURE PIPING MATERIALS

Type 347 stainless steel was selected as the most suitable material for use in fabricating the main steam lines. Other alloys were suggested but were rejected because of lack of experience with their use and their absence from existing boiler codes. We will obtain experience with one of these alloys, however, in a small test section which has been connected in parallel with the main steam lines.

Welds in the main steam lines will be made with the consumable backing-ring process. This procedure utilizes a shielded-arc to draw a gas-backed ring into the joint to form a first-pass bead completely fused with the parent metal and without any crevices. Postweld heat-treatment to 1925 F will be used. All welds will be radiographed.

#### ELECTRICAL

Unit 6 generator is tied through a 3-phase, 15,000/132,000-volt, 150,000-kva transformer to the two existing 132-kv buses at Philo. Auxiliary power at 4 kv is normally supplied to two buses by a 12,500-kva transformer tied directly to the generator leads. For start-up and emergency conditions a second auxiliary transformer supplies power to these buses directly from the main 132-kv buses. Large motors which generally are used in pairs are tied alternately to the two 4-kv bus sections. This includes the

4000-hp feed-pump motors, the largest yet built for this service, the forced and induced-draft fans, the recirculating-gas fans, condensate booster pumps, and others. Two sections of 550-volt bus are provided to service smaller auxiliaries. These buses are served by two 4-kv/550-kv, 1200-kva transformers.

#### STARTING-UP EQUIPMENT

An external recirculating system is required with a once-through-type boiler to replace the natural circulation which exists in a conventional boiler even during start-up. Cold condensate must first be circulated as the fires are started and then progressively hotter water and later steam must be disposed of until the steam at the superheater outlet is at a condition suitable for starting the main turbine. To protect cyclone and furnace-wall tubes we have adopted the basic operating maxim of not firing unless at least 225,000 lb per hr of water is circulating. This was based upon a minimum water velocity of 7 fps through the cyclone tubes. Interlocks have been provided to shut off all fires if flow should at any time drop below this minimum amount.

The recirculation system is one of the major points of difference between a conventional boiler and the once-through-type boiler. The design of this system represented one of the most challenging problems associated with the design of the unit as a whole. All equipment must be designed for completely tight shutoff against full pressure and temperature conditions. In operation, the piping and valves must withstand pressure drops from 4500 psi down to 150 psi at all temperatures between room temperature and 1150 F. In starting up and in passing through this spectrum of temperatures, the valves must pass first a waterlike phase, later steam which flashes wet and then dry again, and finally completely superheated steam. This imposes particularly severe service on these valves.

Two means of recirculation are provided: The first and main one is the turbine by-pass system which is normally used in starting and shutting down the unit; the second is the superheater by-pass system which was provided to maintain flow through the boiler in the event of unit trip out and to assist in restarting the boiler from a hot bottled condition.

The turbine by-pass system as originally conceived had an intimate relation with the turbine controls. It was intended that the turbine by-pass would open whenever the turbine throttle flow dropped below the limiting 225,000 lb per hr amount. This arrangement was out of the question, however, without keeping the whole by-pass system up to, or near, main steam temperature to prevent thermal shock to the heavy austenitic sections when the by-pass valves popped open. This constant warming was considered too costly and complicated. The turbine by-pass system is, therefore, only opened gradually under the operator's control. The function of maintaining some flow through the boiler during trip out was taken over by the superheater by-pass valve.

During the starting period, it is advisable gradually and uniformly to warm up as much of the heavy-walled pressure parts in the cycle as possible. The connection to the by-pass system was moved as close to the turbine as possible by substituting it for the above-seat drains on the turbine stop valves. The whole system, therefore, from the feedwater header through the steam generator and the four main steam leads to the stop-valve bodies is warmed during starting. Each section of pipe from a bend above the superheater-outlet header on down through the main steam leads to the stop valves and down to the recirculating system ultimately ending in the condenser is pitched downward to provide complete drainage.

Two lines from the above-seat drain taps on the two left-hand stop valves are tied together in a single line leading to one turbine by-pass stop valve. The two right-hand stop valves are

similarly tied to the other turbine by-pass stop valves. The lines leading from the individual main turbine stop valves to the two single lines leading to the by-pass stop valves are carefully located in a horizontal plane so that water cannot collect in them and then be blown from one stop-valve body into the other when the first stop valve is closed for test with load on the unit.

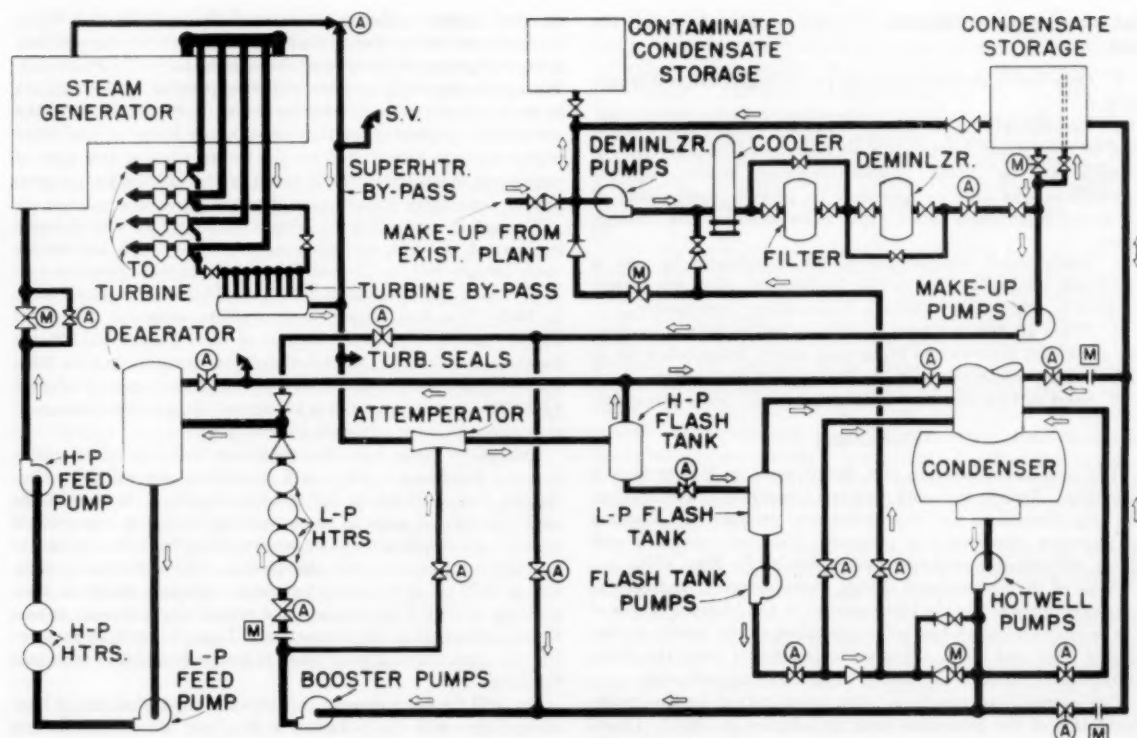
From the two by-pass stop valves, which were provided for complete tight shutoff of this system, the fluid flows into a common valve header with eight small control valves. The two stop valves and the eight control valves are operated by a common camshaft which is positioned by an oil-operated cylinder. Specially designed divergent nozzles in the throats of these valves absorb the high-pressure drop and release the steam into a large header.

The superheater by-pass system consists of two air-operated valves in parallel located above the platen superheater-inlet header. Steam in this header at full load on the unit is at 4700 psi and 900 F. These valves have a capacity of 112,500 lb per hr each. At full flow about 4500-psi pressure drop is taken in the valve and the divergent section below it. These valves are located so that the line above the seat is pitched back to the platen superheater-inlet header, and the line below the seat is pitched downward to the by-pass system. The piping immediately following the divergent section below these valves is 10-in. standard-weight pipe protected with safety valves set at 240 psi. In a full-load trip-out when the superheater by-pass valves automatically open to pass steam at 900 F, the throttling effect of dropping pressure to 150 psi cools the steam down to approximately 700 F. The thermal shock of instantly opening these valves and exposing the low-pressure parts of the breakdown system to 700 F should not be severe, especially since the piping in this area will be of ferritic material which we believe is better able to take thermal shock than austenitic.

Fourteen-inch lines connect the outlets of the turbine by-pass system and the superheater by-pass system. An attenuator is provided in this common line with adequate capacity to cool the steam to the saturation temperature corresponding to 150 psi or lower.

Originally, it had been our intention to use the deaerator as the point into which this recirculated steam would be dumped. Later in the design phase, it became increasingly apparent that soluble salts deposited in the steam generator might wash out during the starting and shutting-down procedures. To avoid contaminating the deaerator water and the top part of the condensate cycle with these salts, it was decided to purify all condensate used during the start-up or shutdown cycle before it was returned to the feedwater cycle. This is accomplished by passing all the recirculated steam-and-water mixture through two flash separators, in series, where dry and clean steam are separated by centrifugal action from the water containing any solids. The clean steam is dumped into the condenser where it is condensed and returned to the cycle. The condensate from the two flash tanks is returned either to the cycle after having been filtered and demineralized or to a dirty-water storage tank for a later cleanup. If water is being sent to the dirty-water storage tank, condensate is made up to the cycle from the main condensate storage tank. (See starting and washing diagram, Fig. 8.)

The attenuator in the recirculating line is sized so that at all times wet steam will enter the first flash-separator tank. This tank is designed to operate at 150 psi and is a cyclone-type separator. Level is maintained near the bottom of the tank by level-control valves and steam is removed from the top section of the tank through steam scrubbers and pressure-regulating valves set to maintain 150 psi to the condenser. Saturated water at 150-psi pressure drains from the high-pressure flash tank to the low-pressure flash tank which is similar in design but operates at 5-



OHIO POWER COMPANY  
PHILO UNIT 6  
STARTING AND WASHING CYCLE  
AMERICAN GAS & ELECTRIC SERVICE CORPORATION

Fig. 8

psia maximum pressure. This tank is directly connected to the steam space of the condenser. Drips from this tank are pumped to the dirty-water storage system or through the filter and demineralizer back into the main-condensate cycle. Means are provided to dump these drips directly to the condenser in the event that they are sufficiently pure.

#### STARTING PROCEDURE

Normal cold start-up of this unit will be accomplished in general in the following steps:

- 1 Close feed-pump discharge valves and start one feed pump, hot well, and condensate booster pumps.
- 2 Open turbine by-pass valves and feed-pump shutoff valve by-pass to establish flow through steam generator.
- 3 Build up pressure by throttling on turbine by-pass valves.
- 4 When steam generator is up to full pressure, open feed-pump discharge valve.
- 5 Establish 225,000-lb-per-hr flow through steam generator and put pressure control on turbine by-pass pressure regulator.
- 6 Start ID, FD, and recirculating-gas fans, and light off one cyclone.
- 7 Fire to raise fluid temperature leaving steam generator from room temperature up to approximately 900 F.

- 8 Start turbine under speed governor control.

9 Regulate firing to maintain outlet-steam temperature and load turbine with speed governor. As turbine is loaded, hold feedwater flow constant and allow turbine by-pass pressure regulator to reduce turbine by-pass flow automatically.

10 After turbine by-pass valves are fully closed, increase feedwater flow and temperature until unit is brought to full load.

In a normal shutdown, the following steps will be taken:

- 1 Reduce load and temperature on the unit until flow is 225,000 lb per hr and temperature is approximately 900 to 1000 F.
- 2 Gradually warm and then open turbine by-pass system until it is taking about 100,000 lb per hr of total 225,000-lb-per-hr flow.
- 3 Trip-off turbine and steam generator and reduce turbine by-pass flow to a value which will give an acceptable cooling rate in the steam generator and associated piping.
- 4 Circulate water until steam generator is entirely cooled.
- 5 Store steam generator full of water.

In the event of loss of electrical load or trip out of the unit by any of the relays previously described, all valves will trip shut on the turbine and one superheater by-pass valve will open to maintain some minimum flow through the steam generator. In a short time the slag and setting will have cooled and this valve will be shut. If there is any chance of restarting the unit within several hours, pressure will be maintained. If the cause of trip-

out is corrected, the following steps will be taken to restart the unit:

- 1 Open both superheater by-pass valves to give 225,000-lb-per-hr flow.
- 2 Immediately fire at one-third full-load heat input and adjust to hold steam temperature as near metal temperatures as possible at the platen superheater-outlet header. Operate recirculating-gas fans as necessary to prevent overheating of secondary superheater tubes, which have no steam flow through them.
- 3 When steam temperature at the superheater by-pass is stabilized, gradually open turbine by-pass and close superheater by-pass to establish flow through the secondary superheater.
- 4 When all flow has been transferred to the turbine by-pass, fire the steam generator to bring main steam temperature up to match metal temperatures in the front end of the turbine.
- 5 Start turbine and load as in ordinary cold-start procedure.

#### CONCLUSION

The over-all engineering and design work on this project is complete. Details are being reviewed frequently and much time is being devoted to test and operational procedures. Training of operating personnel is in progress. The construction is well along, with experimental operation scheduled for May, 1956.

Some of the accumulated design, manufacturing, and laboratory experience is already being applied in the planning stages of the production units which will be installed on the AG&E system during 1959 and 1960. Significant departures from the Philo project pressure and temperature levels are being indicated.

Our current load growth is being taken care of by the implementation of the generation program adopted in 1950.<sup>6</sup> Under this program we will have in operation by 1959 twelve 215-225 mw net capability units.

#### ACKNOWLEDGMENTS

The planning, design, construction, and operation of Philo Unit 6 call for a challenging amount of creative engineering. This effort is being carried out successfully only through the co-operation of the engineers of the companies who supply the components and the engineers of the American Gas and Electric Service Corporation who planned the project and formulated the over-all design.

We should like to conclude this paper by quoting the following from the editorial by Philip Sporn<sup>8</sup> on the philosophy of the Philo project:

"It is obvious that developments like Philo also have an important bearing on the morale of the people within the industry and those outside whom the industry is trying to attract. No people of ability, imagination, and enterprise can be expected to be attracted to any venture that is static or declining. And an industry that cannot attract its share of the young and the able cannot, over a long period of time, do anything but decline."

## Discussion

A. T. HUNTER.<sup>7</sup> We wish to compliment the authors on their

excellent papers<sup>8</sup> outlining the need for the once-through boiler in American utility work, their basic research at supercritical pressure, design considerations, and description of the Philo unit. The continuing study and investigation, paralleling as it appears to do, much of the work being carried on in connection with the commercial application of the once-through boiler in four other utility systems, augurs well for the future place of this type of equipment in satisfying the demand of the utilities for progress and for constantly reduced cost of power generation.

The authors state that the prototype unit which they describe is expected to be in operation early in 1956. The 150,000-kw once-through unit for Dayton Power & Light will operate in late 1957; that for Metropolitan Edison of 175,000-kw capacity early in 1958. The large supercritical-pressure units for Cleveland Electric and Philadelphia Electric of 250,000 and 325,000 kw capacity, respectively, are scheduled for operation in late 1958. By 1960, then, a comprehensive operating background of over 1,000,000 kw will be available to support the general commercial acceptance of these advances at that time.

Indications would point to a prediction that the bulk of utility capacity purchased as early as 5 years from now will be in sizes ranging from 200,000 to 400,000-kw capacity. In these large sizes, the over-all gains to be obtained in the use of supercritical pressure are significant and we believe will at that time be clearly justified from an economic standpoint. The supercritical pressure of 3500 psi at the present generally accepted moderate temperature of 1050 F for primary and reheat steam appears at particular advantage in this connection. This cycle will, by then, we believe, have found a solid place in our technical and economic thinking.

By 1960 the improvement in alloys and the techniques in handling them—with the reduction in their cost to be hoped for and expected as the result of their widespread use—could lead, as well, to the general use of the superpressure higher temperature cycles, with double reheat in the very large sizes.

Our compliments again to those concerned in the progressive work covered by these papers.

E. P. PARTRIDGE.<sup>9</sup> Here is creative engineering done with a deft and daring hand! Like all creative engineering, it involves calculated risks. One of these risks is that water at temperatures and pressures above the critical point may not behave chemically in a manner predictable from experience to date below 3200 psi.

If we attempt to determine how much iron oxide is dissolved in the boiler water or in the steam from a contemporary boiler operating at 2000 psi, we find ourselves struggling to measure less than 0.01 ppm. Yet when Morey and Hesselgesser,<sup>10</sup> at the Geophysical Laboratory, passed water at 15,000 psi and 932 F over iron oxide in the form of hematite ( $\text{Fe}_2\text{O}_3$ ), they found 90 ppm of iron oxide in solution in the effluent.

As we have pointed out,<sup>11</sup> this one pertinent measurement in the supercritical range suggests that enough metal oxide may go into solution in the high-temperature end of the Philo steam generator at 4500 psi and 1150 F to cause an accumulation of iron

<sup>6</sup> "The Development and Implementation of a Generation Program on the American Gas and Electric Company System," by Philip Sporn, H. A. Kammer, and S. N. Fiala, *Trans. ASME*, vol. 74, 1952, pp. 603-619.

<sup>7</sup> "Philosophy of the 4500-Psi Philo Project," by Philip Sporn, *Electrical World*, vol. 139, June 29, 1953, p. 63.

<sup>8</sup> Vice-President, Combustion Engineering, Inc., New York, N. Y. Mem. ASME.

<sup>9</sup> This discussion also includes comments on "First Commercial Supercritical-Pressure Steam Generator for Philo Plant," by W. H. Rowand and A. M. Frendberg, this issue, pp. 409-416, and "First Commercial Supercritical-Pressure Steam Turbine—Built for the Philo Plant," by C. W. Elston and R. Sheppard, this issue, pp. 417-426.

<sup>10</sup> Director, Hall Laboratories, Inc., Pittsburgh, Pa.

<sup>11</sup> "The Solubility of Some Minerals in Superheated Steam at High Pressures," by G. W. Morey and J. M. Hesselgesser, *Journal of Economic Geology*, vol. 46, 1951, pp. 821-835.

<sup>12</sup> "Water Problems in Power Generation at Supercritical Pressures—Or Through the Looking-Glass," by E. P. Partridge, *Mechanical Engineering*, vol. 77, 1955, pp. 883-885, 901.

oxide in the turbine. Will simply maintaining a pH of 9.5 in the feedwater entering the steam generator suffice to reduce to an unobjectionable level this solvent action by the supercritical fluid at the hot end? We hope so but fear not. Actual operating experience will soon begin to tell whether some other answer must be sought.

C. C. WHELCHER.<sup>12</sup> This is an excellent paper in which all of the features and design considerations for the Philo unit are combined in one presentation. Especially interesting is the discussion of the reasons for the particular choice of cycle conditions and size of the unit.

The boiler is a once-through-type steam generator in which circulation is provided by action of the feed pumps and the relatively large pressure drop through the unit. This relatively large pressure drop which yields high water velocities reduces the danger of stagnation and avoids overheating of tubes. Large pressure drop should insure adequate flow through all the various parallel-flow paths through the unit. These higher velocities increase heat-transfer rates which result in a more compact unit.

Mention is made of the special design features incorporated in the condenser to reduce the possibility of leakage into the cycle. The requirements for purity of feedwater in a supercritical cycle are comparable to those for nuclear-reactor cycles. The rubber coatings should have the added advantage of tending to reduce erosion of tubes in their inlet. Some feedwater-heater manufacturers are welding tubes to tube sheets to prevent leakage, and to make a better strength connection than possible by rolling. Since the condenser is the most likely location for contamination,

the possibility of doing the same thing in a condenser could be considered. Increased cost seems to be the main problem, since a condenser with welded, or brazed tubes, would be somewhat more costly. The temperature changes and the resultant thermal stresses which cause loosening of tubes are much greater in feedwater heaters than in a condenser. Where leakage must be kept to a minimum, welding or brazing of tubes to tube sheets is a possibility for consideration, although the problems associated with the replacement of tubes may offset the advantages of welding.

The properties of supercritical-pressure water have resulted in a somewhat unique control scheme in which the fuel-firing rate is determined by the main steam temperatures. The complexity of the system makes it necessary to have more functions trip, increasing the possibility of trip-out from malfunctioning of the controls. This, however, is the price of progress. The protection of the final superheater tubes from overtemperatures on a sudden drop from high to light load will require the careful attention of the operator, especially with regard to the control of the turbine by-pass valves. As experience is gained in the operation of this unit and applied to successive units of this type, it is possible that the degree and complexity of the control system may be somewhat reduced.

It is hoped that a companion paper will be prepared on the experience with, and performance of, the supercritical-pressure unit after the start-up has been completed.

A pioneering project such as this can be most successfully developed through the joint efforts of the utility's engineer and the equipment manufacturer. This paper indicates that this has taken place in the development of this unit. It is typical of the progress and developments in the art of steam-electric generation which has taken place to date.

<sup>12</sup> Chief Steam Engineering Division, Pacific Gas & Electric Company, San Francisco, Calif. Mem. ASME.



# First Commercial Supercritical-Pressure Steam Generator for Philo Plant

By W. H. ROWAND<sup>1</sup> AND A. M. FRENDBERG,<sup>2</sup> NEW YORK, N. Y.

From experience with the pioneer 2500-psi steam power plant of the Twin Branch Plant of the Indiana and Michigan Electric Company on the American Gas and Electric System, installed in the early 1940's, and subsequent knowledge accumulated in the field, another significant advance into pressures above the critical is now being made at the Philo Plant of the Ohio Power Company. This is the 4500-psi, 1150 F two-stage reheat unit developing approximately 125 megawatts—a joint effort of the American Gas and Electric Service Corporation, the General Electric Company, and The Babcock & Wilcox Company.

## INTRODUCTION

THE public utilities and the manufacturers who supply their equipment have co-operated in a continued effort to produce more kilowatts for less fuel. This increase in efficiency of steam power plants can best be accomplished by increasing the operating pressure and temperature (1).<sup>3</sup> Generally speaking, these advances take place in small increments. However, periodically, the accumulation of knowledge makes it possible to take a significant jump to an entirely new plateau. This was the case with the 2500-psi installation at the Twin Branch Plant of the Indiana and Michigan Electric Company on the American Gas and Electric System. Completed in the early 1940's this installation established the outposts of what could be expected from cycles operating below the critical pressure (2, 3, 4).

Sufficient knowledge has now been acquired to permit another significant jump, this time to pressures above the critical. In May, 1953, the American Gas and Electric Service Corporation entered into an agreement with the General Electric Company and The Babcock & Wilcox Company to build a 4500-psi, 1150 F, two-stage reheat unit to develop approximately 125 megawatts at the Philo Plant of the Ohio Power Company (5).

Because of the pioneering involved and the many untried features throughout the entire installation, it was decided to limit its size to as small a unit as possible, while still being commercially practical. With these conditions in mind, it was agreed that the size of the unit would be about 125 mw.

All design considerations were in accordance with existing codes of the ASME and the State of Ohio.

A steam generator for pressures above the critical presents many considerations in design, metallurgy, fabrication, and operation (6). The solution to some of these has come from the experience and research of the past. Solutions to others have come from active, continuing present-day research. Un-

doubtedly, some problems will be encountered which will have to be solved after the unit is put into operation.

## NEED FOR ONCE-THROUGH BOILER

Previous papers (6) have shown the properties of steam and water at pressures above the critical. When heat is added to water at 5000 psi, it gradually increases in volume and its enthalpy gradually increases. As the temperature is increased in the range between 700 and 800 F its volume and enthalpy both increase more rapidly, and above 800 F these properties change gradually again, Figs. 1 and 2. There is no latent heat, no saturation temperature, no boiling; instead there is a continual, gradual change of properties with only a single phase existing at any one time.

This, then, requires a different type of steam generator—a once-through steam generator where feedwater is pumped into one end of a continuous flow path, along which heat is supplied and from which superheated steam is released.

The idea of a once-through boiler is not new. The Babcock & Wilcox Company has experimented with once-through-type steam generators since 1916. The savings in steel as a result of the absence of a steam drum and the use of small-diameter tubes caused the Germans to adopt this type of unit for subcritical pressures just before the last war. There are now more than 50 of these units in Germany operating at pressures below the critical.

Fig. 3 shows a cross section of the Philo supercritical steam generator. This unit replaces and occupies the same space in the building as four boilers installed in 1923, which were among the first reheat units installed in this country. These boilers supplied a 40-mw turbine which had a heat rate of about 14,000 Btu per net kw-hr. This reduction from 14,000 to an expected 8500 Btu per kw-hr is an example of the increase in efficiency which has taken place in the field of power generation in the past 30 years.

This unit is fired by cyclone furnaces, a Babcock & Wilcox Company development, which allows complete combustion of coal in a very small volume. With this complete combustion, a small furnace can be used with gas recirculation to cool the gas and the ash particles below the slagging temperature before they reach the convection sections. The coal is burned in the cyclone furnace; the gases and the slag enter a primary furnace from which the slag is tapped into an ash tank; the gases flow into the secondary chamber where they are mixed with the recirculated gas before flowing on to and through the convection surface and through an air heater.

The feedwater enters one of the three cyclone furnaces at 525 F; travels through the cyclone furnaces and front-wall tubes of the primary furnace in series; then goes to the primary superheater where it flows through the rear part of the convection section on one side of the unit. Steam then flows through the walls of the secondary chamber, the front two banks of convection surface, and through four steam lines to the turbine. The two reheaters are in series alongside the primary superheater with gas by-pass dampers for controlling reheat temperature.

## SUPERCritical PILOT UNIT AT ALLIANCE

In the solution of the many design considerations encountered,

<sup>1</sup> Vice-President, The Babcock and Wilcox Company. Mem. ASME.  
<sup>2</sup> Chief Staff Engineer, Boiler Division, The Babcock and Wilcox Company.

<sup>3</sup> Numbers in parentheses refer to the Bibliography at the end of the paper.

Contributed by the Power Division and presented at the Diamond Jubilee Annual Meeting, Chicago, Ill., November 13-18, 1955, of THE AMERICAN SOCIETY OF MECHANICAL ENGINEERS.

NOTE: Statements and opinions advanced in papers are to be understood as individual expressions of their authors and not those of the Society. Manuscript received at ASME Headquarters, September 7, 1955. Paper No. 55-A-135.

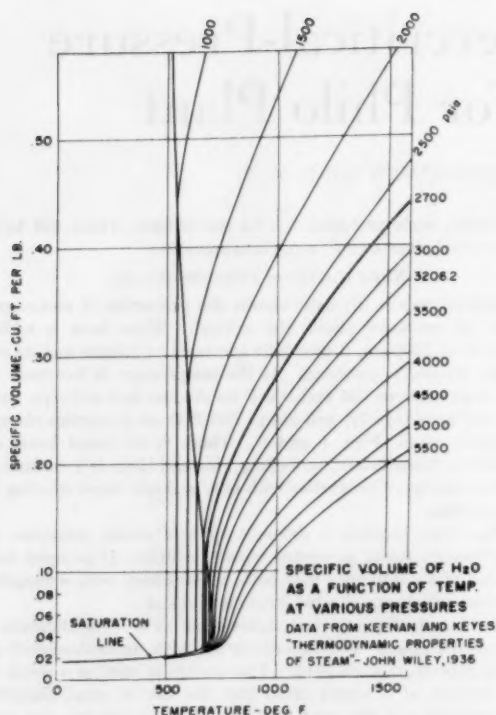


FIG. 1

much basic scientific and engineering data not heretofore available were required. The use of B&W's pilot universal pressure (6) unit at the Alliance, Ohio, Research Center was indispensable in developing this information. In 1951, when the need for a jump to supercritical-pressure operation was apparent, it was decided to build this pilot unit in order to develop in advance much of the basic design data that would be needed.

The pilot unit consists of a single tube which lines the walls of a gas-fired refractory furnace and then forms a parallel-flow convection section. The unit is adequately instrumented with thermocouples for measuring fluid temperatures, heat fluxes, and metal temperatures which could indicate the point of any internal deposit.

The pilot unit and the auxiliary system are equipped with numerous sampling points for checking water and steam analysis throughout the system.

It is furnished with the very latest equipment for water treatment and is instrumented as fully as possible for measurement and control. Fig. 4 shows a schematic arrangement of the unit and its auxiliaries with all of the points where water samples can be obtained.

The unit handles approximately 1200 lb per hr of feedwater at approximately 5000 psi and 220 F and delivers steam at 4500 psi and 900 F. It went into operation early in 1953. The initial investigations consisted of the following:

- 1 Properties of the fluid.
- 2 Pressure-drop characteristics with variations in mass flow, pressure, and temperature.
- 3 Response characteristics and the control required.
- 4 Measurement of the fluid-film heat-transfer coefficient.

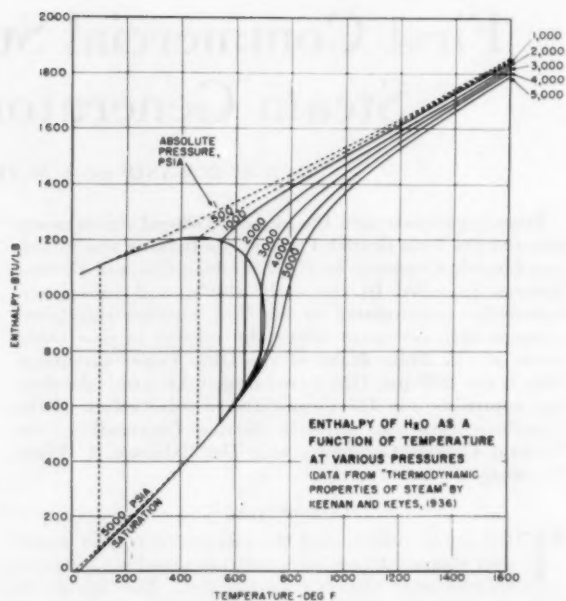


FIG. 2

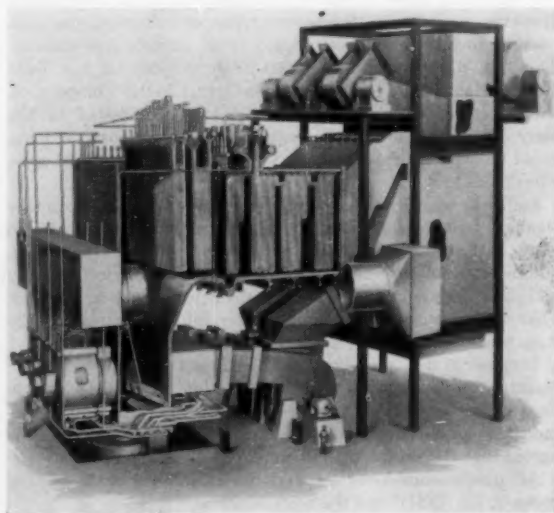


FIG. 3 THE BABCOCK AND WILCOX SUPERCRITICAL-PRESSURE STEAM GENERATOR

#### PHILO UNIT DESIGN CONSIDERATIONS

*Distribution of Heat-Absorbing Surface and Selection of Materials.* Of the 985 Btu added to each pound of the fluid in the high-pressure part of this unit, approximately 235 Btu are added to raise the feedwater from 525 F to the critical temperature 705 F, and approximately 750 Btu are added to superheat the steam above this point. This compares to approximately 705 Btu to generate steam and 370 Btu to superheat the steam in a 2000-psi 1050 F cycle with 450 F feedwater.

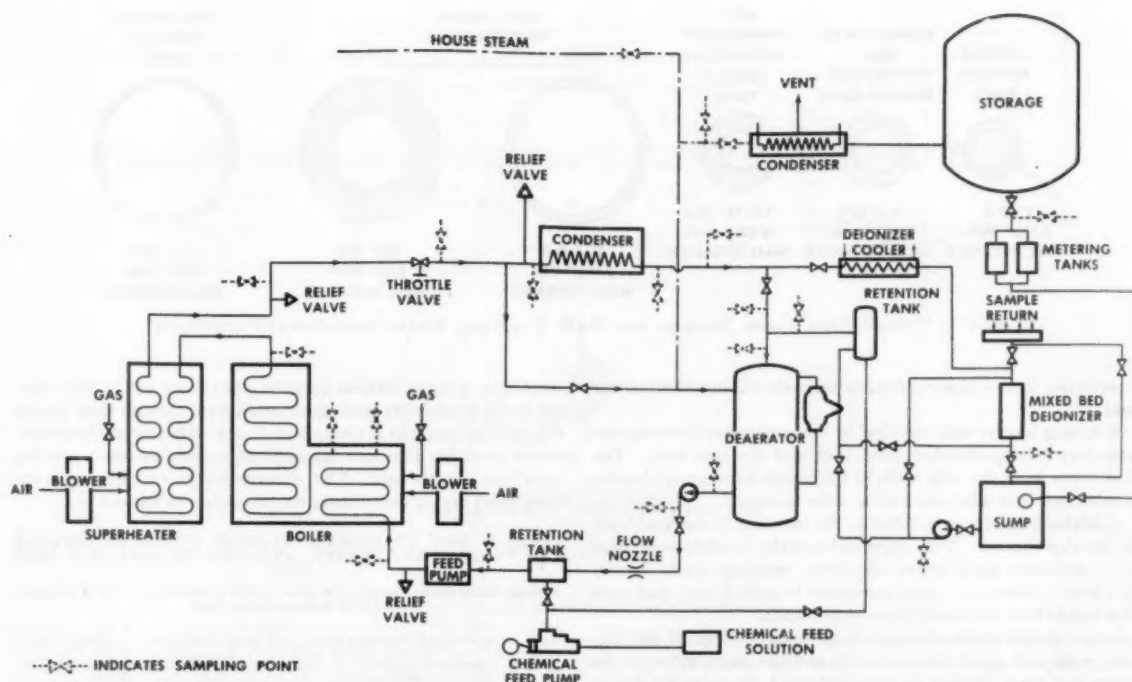


FIG. 4 SCHEMATIC CIRCUIT DIAGRAM OF ALLIANCE SUPERCRITICAL TEST SYSTEM

With this relatively small amount of heat to be added to the fluid as water, there comes the choice of arranging the circuits either so some of this heat is absorbed by the water in economizer surface or so all of it is absorbed by the water in furnace high-heat-input area. The latter condition was chosen because it gives some relief in the alloy requirements for the furnace tubes. However, it leaves the problem of getting surface equivalent to economizer surface with low enough receiving temperature to efficiently cool the gas below 800 F entering the air heater.

To accomplish this the primary superheater with a fluid-inlet temperature of 700 F is located on one side of the rear part of the convection pass with the low-pressure reheater having an inlet steam temperature of 630 F on the other side.

Since such a high percentage of heat goes into superheating, it is necessary to form the entire secondary mixing chamber enclosure of superheater surface. The use of steam-cooled furnace surface in high-duty power boilers has generally been avoided in the past because of the possibility of excessive thermal stresses in the tubes resulting from a high temperature differential around the circumference of the tubes. The thickness of the tubes required for this pressure, when placed in the high-heat-input zones, further accentuated the problem. However, this high pressure also helps to overcome these difficulties since the steam-film conductance is high and it is practical to use a high pressure drop, giving steam-mass flows of over 2,000,000 lb per sq ft-hr.

In selecting the alloys for this surface, there were areas where the ferritic croloys appeared to be border line from the standpoint of oxidation, and the use of austenitic steel was considered. Since its thermal conductance is much lower, the metal temperature increases and although the allowable stress is higher, there is no appreciable reduction in wall thickness. Because the coefficient of expansion of the austenitic alloy is greater, the thermal stress which could cause fatigue failure is higher. The solution

used was to alter the design to remain within the use limit of ferritic alloys.

Table 1 shows the distribution of steel and alloys in the pressure parts for the Philo unit. Fig. 5 shows typical cross sections for tubing in various parts of the unit.

TABLE 1 PROPORTION OF STEEL AND ALLOY IN PRESSURE PARTS FOR B&amp;W UNIVERSAL PRESSURE STEAM GENERATOR FOR PHILO PLANT

	Pounds	Per cent of total
Steel	627033	37.90
Carbon moly	145539	8.80
Croloy 1/2	32383	1.95
Croloy 1	253448	15.30
Croloy 1 1/4	121414	7.35
Croloy 2 1/4	267099	16.10
Croloy 3M	19600	1.20
Croloy 9M	27000	1.60
Croloy 18-8	161273	9.80
	1654780	100.00

*Temperature Equalization in Circuits.* When steam or water is heated in parallel-flow paths any unbalance in heat absorption will result in temperature differences between tubes. To prevent this temperature difference from being cumulative through the unit, considerable thought was given to equalizing the fluid temperature at points along the flow path.

Usually, where connections were required between circuits, six connecting tubes were used. Fluid from 80 to 120 heat-absorbing tubes was brought into six connecting tubes resulting in some degree of mixing.

These six connectors were crossed over between the cyclone furnaces in such a way that the fluid from the rear of one cyclone furnace went to the front of the next cyclone furnace and so forth. Therefore any unbalance in heat input in one cyclone furnace will be offset in the next one.

The connection from the last cyclone furnace to the primary

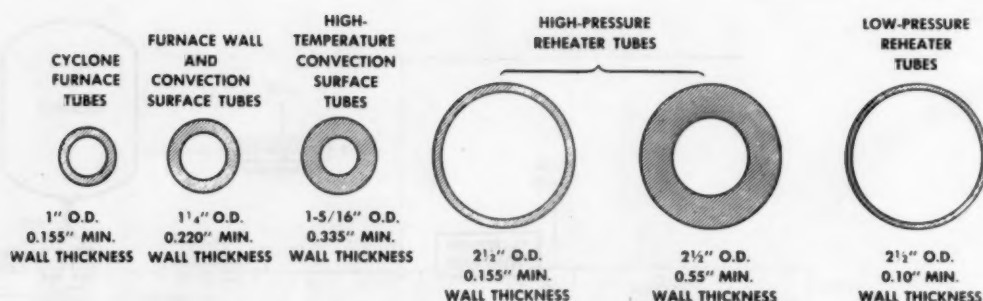


FIG. 5 TYPICAL TUBE CROSS SECTIONS FOR B&W UNIVERSAL STEAM GENERATOR AT PHILO PLANT

superheater in one pipe resulted in intimate mixing of all of the fluid.

A mixing header was installed in the connectors between the secondary mixing-chamber front wall and the rear wall. The connectors from the side walls to the platen superheater header were crossed over to opposite sides of the furnace.

A mixing header was installed at the entrance to the final bank of the superheater. Two superheater-outlet headers were used with alternate superheater elements entering each header and with steam-outlet pipes connected in such a way that each pipe would have the same temperature steam.

Major temperature differentials between sections of the furnace walls will occur because some sections have water in the tubes and other sections have superheated steam in the tubes. Smaller temperature differentials will occur as a result of unequal heat absorption in adjacent tubes in the same section. Because of these temperature differentials, consideration of supports, tie bars, and sealing at corners, was important. Considerable thought had to be given to the arrangement of flow paths to keep these temperature differentials to a minimum.

**Feedwater Conditioning.** In a once-through steam generator any material entering with the feedwater must either be deposited in the unit or leave with the steam. The early German once-through units operating at subcritical pressures encountered trouble because of dissolved solids and corrosive gases in the feedwater. However, the more recent units in Germany have been operating without trouble from either source.

Nevertheless, because of the lack of knowledge of precise limits on feedwater conditions for once-through boilers, in general, and particularly for a once-through unit operating above the critical pressure, an extensive program was carried out on the Alliance Research Center pilot unit to investigate the limits of feedwater conditioning.

The initial phase of the water-treatment investigation consisted of short-time runs to establish the conditions which would be necessary for a successful long-time run. It soon became apparent that iron pickup in the preboiler equipment—one of the major feedwater problems in the operation of high-pressure central-station subcritical-pressure boilers—was also a limiting factor in supercritical-pressure once-through units. Investigation of the limit for the amount of iron which could be tolerated in the feedwater showed that approximately 0.01 ppm was the limit. It was found possible to control the amount of iron pickup in the entire cycle by controlling the feedwater pH through the addition of ammonia or volatile amines. Dissolved solids in the feedwater were maintained at very low levels by the prevention of feedwater contamination, addition of only the highest quality make-up and by-pass demineralization of a part or all of the condensate.

After the limits for control had been established during these

short runs, a run of 4000-hr duration was carried out to determine the boiler availability with these conditions. At no time during this 4000-hr run was it possible to detect with any of the instruments available that any appreciable deposition was occurring anywhere in the unit. The average water conditions at the boiler inlet during this 4000-hr run are shown in Table 2.

TABLE 2 B&W UNIVERSAL PRESSURE STEAM GENERATOR FOR PHILO PLANT—WATER ANALYSIS ON ALLIANCE TEST UNIT

Average water conditions at boiler inlet of 4500-lb test unit at B&W Research Center during 4000-hr run:

pH.....	9.55
Dissolved oxygen, ppm.....	0.005
Total dissolved solids, ppm.....	0.21
Iron as Fe, ppm.....	0.011
Silica as SiO <sub>2</sub> , ppm.....	0.041
Ammonia as NH <sub>3</sub> , ppm.....	3.0
Major solids constituents were:	Present in trace amounts were:
Silicon	Copper
Iron	Calcium
Sodium	Magnesium
Sulphates	Chlorides

Early in 1955 the outlet of the original test unit was connected to another single tube in a separate gas-fired furnace arranged so the steam temperature could be raised to 1150 F. The reason for testing at 1150 F with tubing of the same alloys as used in the Philo unit was to determine if the treating chemicals, such as ammonia, would have any adverse effect on the alloys at this higher temperature, and also to determine the stability of the chemicals at 1150 F. A 2000-hr test run using the same feedwater conditions as in the foregoing 4000-hr run has shown that the higher temperature has no ill effects.

Investigations in operating plants have shown that the limit set for iron in the feedwater can be obtained on a full-scale unit. Also in a commercial plant it should be possible to maintain lower values for silica and total dissolved solids than those maintained during the test run.

Additional tests are being conducted to study the use of hydrazine as an oxygen scavenger, particularly with reference to the optimum point in the cycle for its addition, optimum concentration, and the best means for controlling its addition.

**Heat-Transfer Rates at Supercritical Pressure.** No published heat-transfer data exist for steam at supercritical pressures flowing through a tube. Very limited data had previously been obtained above the critical pressure but with steam flowing in an annular space and at much lower Reynolds numbers than used in the universal pressure steam generator. Therefore an electrically heated test section was installed at the discharge of the pilot unit where fluid could be supplied at temperatures from 220 to 1000 F at pressures up to 5000 psi in order to secure heat-transfer data for use in the design of the Philo unit. This test section consisted of a horizontal 6-ft-long section of Type 304 tubing, 0.300 in. ID and 0.540 in. OD. Thermocouple wells

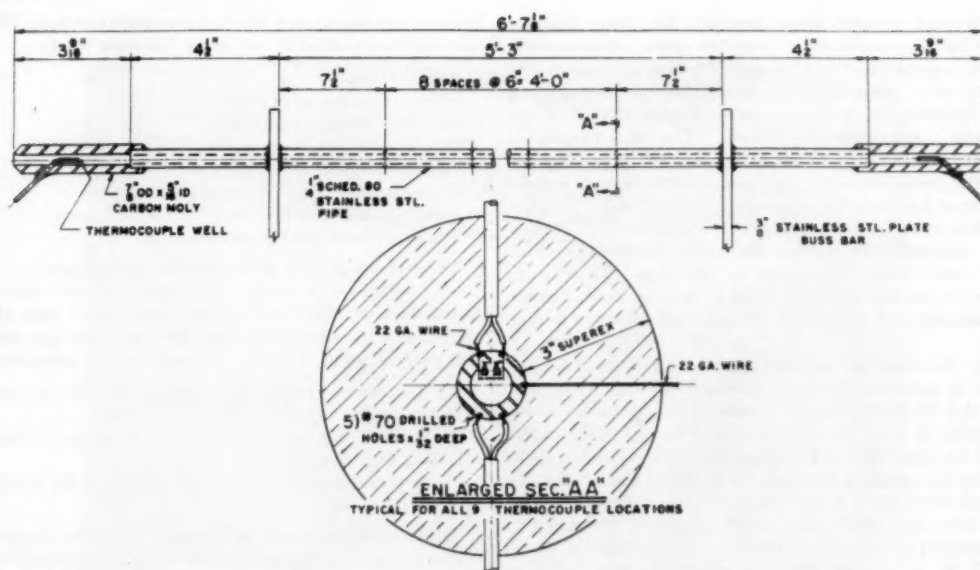


FIG. 6 DETAIL OF HEAT-TRANSFER TEST SECTION

were installed at each end of the tube and a pressure gage connected to a point slightly upstream of the test section. Power was supplied to the tube from three 40-kva transformers. The central 4 ft of the test section was equipped with a pair of thermocouples and a voltage tap spaced every 6 in. It was thus possible to obtain two outside-tube temperatures at each of nine locations and to determine the voltage drop across each 6-in. section of the tube. The test section was insulated with 3 in. of Superex which was wrapped with asbestos tape and aluminum foil. Four sets of surface and depth thermocouples were installed in the insulation along the length of the tube in order to determine the magnitude of the radially outward heat flow.

Fig. 6 shows the detail of the test section.

Fluid flow and heat input could be measured with an accuracy of  $\pm 1/2$  per cent.

Data were obtained at various flow rates, temperatures, and pressures at heat fluxes from 150,000 to 600,000 Btu per sq ft-hr based on inside diameter of the tube. Film conductances proved to be higher than those based on a McAdams correlation (7) particularly in the temperature range of 800 to 1000 F. A future paper will report on the results of these tests in detail.

The Philo unit was designed on the basis of the McAdams correlation, leaving the difference between this and the test data as "safety factor."

**Gas-Flow Study.** To determine the best shape for the mixing chamber and the best arrangement for introducing the recirculated gas to give good mixing and to obtain even gas-flow distribution over the convection surface, a  $1/8$ -scale model (6) was built and tested at the Alliance Research Center. Gas was fired in the air duct to the cyclone furnaces to give 1000 F air temperature while room air was used for recirculated gas. This combination of 1000 F air and room air gave approximately the same density ratio as that for the gases in the actual universal pressure steam generator. Several different arrangements were tested before the final design was established for the Philo unit.

#### FABRICATION AND ERECTION

The development of the universal pressure steam generator presented many interesting problems and opportunities in fabri-

cation and examination of tubing, particularly in the alloy grades, welding, cleanliness, and shop assembly of large components to simplify field erection.

**Fabrication of Tubing.** The confidence with which this project has been undertaken is based on the long-term experience which we have had in the metallurgy and fabrication of high-pressure, high-temperature alloy tubing. Considerable alloy experience has been accumulated in the Alliance Research Center, at the Tubular Products Division Works in Beaver Falls, and in long-time operation of alloy tubing in a great range of central-station installations.

One problem of particular importance in the building of the universal pressure steam generator arises from the fact that in a forced-flow steam generator it is essential to have approximately equal flow areas in all parallel circuits to insure flow stability. With the help of the Tubular Products Division an investigation was conducted to determine if commercial manufacturing tolerances for tube thickness would cause an undue variation of the inside diameter of these heavy-wall small-diameter tubes. It was concluded that tubing fabricated to commercial tolerances will be acceptable in view of the rigid control and inspection techniques employed throughout the manufacturing process.

To insure soundness of the heavy-wall tubing, every foot of tubing fabricated for the high-pressure portion of the unit was examined by the supersonic reflectoscope.

Fabrication of the tubing into component parts required many special precautions. For example, in making tube bends, it was essential that flow areas were not reduced materially. To insure that this was accomplished steel balls of prescribed diameters were passed through the bends after shop fabrication. The need to maintain uniform internal flow areas also precluded the standard practice of welding tubes with the use of a backing ring. After considerable investigation, the shielded, inert-gas, metallic arc-welding procedure, without the use of a backing ring, was selected.

**Shop Assembly.** In the assembly of modern boilers a careful economic investigation is made to determine the balance between large-scale shop assembly of components and piecemeal field erection which will give the lowest installed cost.

The universal pressure steam generator has many features which make large-scale shop assembly quite advantageous. The use of a great many small-diameter tubes with a high percentage of alloy tubes requiring stress-relieving after welding makes it advantageous to shop assemble components which can be put into a stress-relieving furnace. The total number of welds were reduced by welding tubes directly to the headers without the usual stubs on the headers. All of this reduces the amount of field welding required.

Each flow circuit makes a convenient component for shop assembly complete with support and guide attachments which could be very accurately aligned in the shop. These components were assembled and shipped in frames which protect against misalignment or damage to the small-diameter flexible tubes.

Another advantage of maximum shop assembly is the degree of control it permits over internal cleanliness and inspection. The fact that the wall thickness of most of the headers and connecting tubes in this unit is about equal to the inside radius precluded the possibility of providing standard inspection openings. Shop procedures were employed to insure that all component parts were clean upon completion of fabrication. All openings were then sealed with tight caps which are removed during erection just before field closure of the opening.

Figs. 7, 8, 9, and 10 show various shop-assembled components.

#### INSTRUMENTATION FOR INITIAL OPERATION

When starting up a unit such as this, there is a need for more instruments than usual to provide a continual guide to the operators and to provide a source of information to confirm the design. The Philo unit will have one 12-point temperature recorder indicating fluid temperatures to show the operator the

temperature rise in each circuit throughout the unit. Temperatures will be recorded at each of the following points:

- Feedwater inlet.
- Inlet to primary superheater.
- Outlet of primary superheater.
- Outlet of steam-mixing header at furnace rear wall.
- Inlet at each side of platen superheater.
- Outlet at each side of platen superheater.
- Inlet to final superheater bank after steam mixer.
- Final superheater outlet on each side.

There also will be a 160-point selective temperature recorder having 8 banks of 20 points. The first bank will indicate additional fluid temperatures to show temperature rises along the fluid-flow path in smaller increments than those just mentioned. The remaining 140 points will be used for such indications as:

- 1 Temperature unbalance among each of the six connectors between circuits at various points in the unit.
- 2 Temperature unbalance among 20 adjacent tubes in a high-heat-input wall section.
- 3 Temperature unbalance among tubes of the pendant convection superheaters.

All of these are to be permanently installed thermocouples connected to panel-board instruments. In addition, there will be some temporary thermocouples as required for establishing operating procedures.

Permanent sampling points for water and steam are provided at five points throughout the unit. A change in analysis from point to point would provide an indication of internal deposition and its location. From these five points it should be possible to establish where samples need be taken for continuous water-conditioning control.

These permanently installed test points should be sufficient

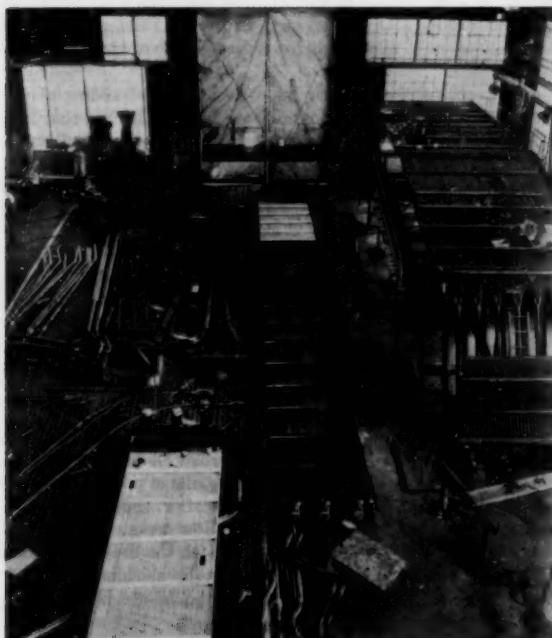


FIG. 7 PART OF FURNACE SIDE WALL, SHOP-ASSEMBLED, READY FOR SHIPMENT

(This assembly is approximately 55 ft long  $\times$  5 ft 6 in. wide. The light-colored section is the shop studded area.)

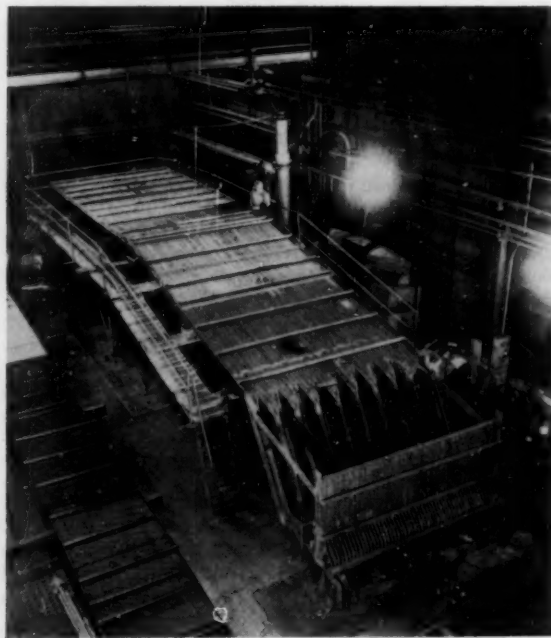


FIG. 8 PART OF FURNACE FRONT WALL AND SCREEN BEING ASSEMBLED IN SHOP

(The assembly frame which was made of pipes and plates welded together was not attached physically to the tube assembly at any point.)

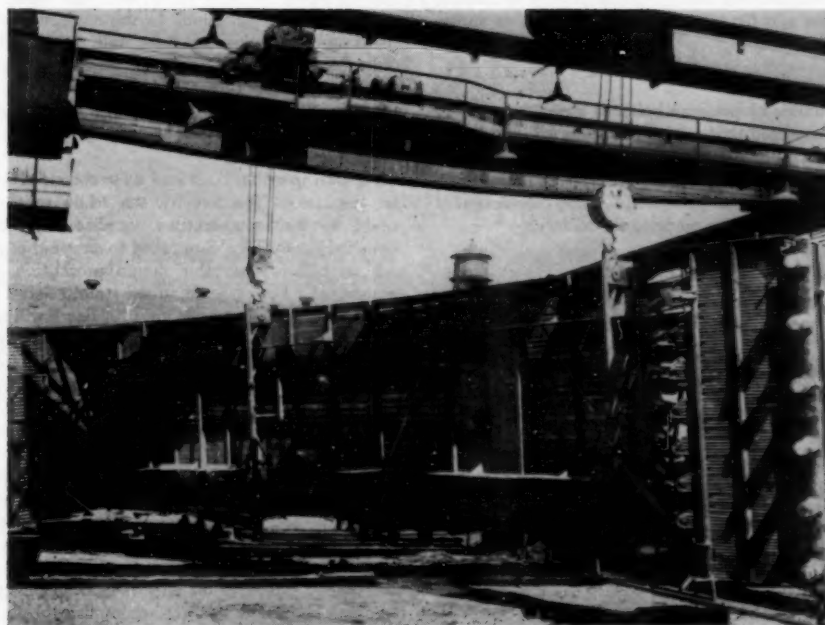


FIG. 9 THE SAME SECTION AS THAT SHOWN IN FIG. 8 ON ITS WAY FROM SHOP TO STRESS-RELIEVING FURNACE



FIG. 10 SECTION OF PRIMARY FURNACE FRONT WALL PARTLY ASSEMBLED IN SHOP  
(In the foreground is the floor of the unit. In the center of the picture are the tubes bent to form the cyclone-furnace throat.)

for operating guides. These, together with the usual portable test equipment, should provide plenty of information to confirm the design conditions and for use in the design of future supercritical-pressure units.

#### CONCLUSION

Erection of the universal pressure boiler is well along at the Philo Plant. It is expected that initial operation will take place sometime early in 1956. A complete program of testing is planned for the unit to study all of the special design characteristics under full-scale commercial operation. Upon completion of these tests further reports will be made to the society.

#### BIBLIOGRAPHY

- 1 "Principles of Boiler Design for High Steam Temperatures," by G. W. Kessler, Trans. ASME, vol. 77, 1955, pp. 919-926.
- 2 "Natural-Circulation Test Results on the 2500-Psi Twin Branch Boiler," by W. H. Rowand and T. B. Allardice, Trans. ASME, vol. 66, 1944, pp. 17-21 (published in special pamphlet section under "Furnace Performance Factors").
- 3 "Operating History of the 2500-Psi Twin Branch Plant," by Philip Sporn and E. G. Bailey, Trans. ASME, vol. 66, 1944, pp. 1-16 (published in special pamphlet section under "Furnace Performance Factors").
- 4 "Distribution of Heat Absorption and Factors Affecting Performance of Twin Branch 2500-Psi Boiler," by F. G. Ely and L. B. Schueler, Trans. ASME, vol. 66, 1944, pp. 23-32 (published in special pamphlet section under "Furnace Performance Factors").
- 5 "A New Power Generation Milestone," by Philip Sporn, *Electrical World*, vol. 139, June 29, 1953, pp. 72-76, 138, and 140.
- 6 "Developing the First Commercial Supercritical Steam Generator," by W. H. Rowand, *Power*, vol. 98, September, 1954, pp. 73-80.
- 7 "Heat Transfer to Superheated Steam at High Pressures," by W. H. McAdams, W. E. Kennel, and J. N. Addoms, Trans. ASME, vol. 72, 1950, pp. 421-428.

#### Discussion

A. R. WEISMANTLE.<sup>4</sup> At the writer's company, we have been actively working on the development of a pilot plant and on supercritical steam-generator designs, and thus fully understand

<sup>4</sup> Assistant Manager, Steam Department, Foster Wheeler Corporation, New York, N. Y. Mem. ASME.

and appreciate the difficulties which had to be faced and overcome in order to bring forth the Philo steam generator. We extend our congratulations to the engineers of the several co-operating companies involved and, in addition, particularly commend the authors for their very clear exposition of these accomplishments. But, of course, we and other engineers in the industry all realize the tremendous impetus given this whole development by the bold pioneering spirit and vision of Mr. Philip Sporn.

Our own investigations lead us to concur substantially with all the conclusions reached by the Philo unit designers. With regard to fluid-temperature equalization, the authors have described the extreme care taken to assure this on the Philo unit, and we believe that this design precaution cannot be over-emphasized. For example, in the stainless-steel outlet section an excess metal temperature of only 200 deg F will reduce the ASME criterion for metal specification from safe service to an operating expectancy of 1000 hr to rupture. The principle of frequent mixing and redistribution of the fluid was found necessary for the successful operation of subcritical once-through units in Europe, and it is even more essential for supercritical steam conditions.

The proportioning of the metals and the great number of different types used for the Philo unit, as shown by Table I of the paper, indicate the extreme care used by the designers to minimize cost. The unexpectedly small amount of stainless steel is a measure of the success of the gas-recirculation principle in shifting thermal duty into the low heat-input convection zone. The authors indicate the difficulty for effective arrangement of tail-end surfaces, but show how this was accomplished by a parallel arrangement of primary superheater and low-pressure reheater. It is expected that the substantial gains possible from more effective low-temperature heat recovery at the steam generator will warrant further development in this direction.

The authors point out the necessity for placing steam-cooled surfaces in the radiant zone, but from their description one obtains the impression that they are doing this with some degree of hesitancy. From our experience with almost 1000 radiant-superheater and reheater installations during the past 30 years, including the first 1000 F job at Atlantic City for Mr. Sporn's company, we can assure them that, with proper design, this part of the unit will be all right.

# First Commercial Supercritical-Pressure Steam Turbine—Built for the Philo Plant

By C. W. ELSTON<sup>1</sup> AND R. SHEPPARD,<sup>2</sup> SCHENECTADY, N. Y.

This paper describes the essential design features of a 125,000-kw, 3600-rpm, tandem-compound, double-flow steam turbine designed for steam conditions of 4500 psig, 1150 F initial temperature, 1050 F at the first reheat, and 1000 F at the second reheat. The engineering objectives, problems, and solutions are emphasized more than the description of design details.

## INTRODUCTION

THE latest major advance in maximum steam-turbine initial pressure took place in 1941 when the 76,000-kw unit at the Twin Branch Station of the Indiana & Michigan Electric Company went into service at 2300 psig. Although at the time this was approximately twice the maximum pressure previously utilized, pressures of this order of magnitude are in common use today.

Maximum initial temperatures, on the other hand, have progressed more steadily: 900 F in 1936, 950 F in 1938, 1000 F in 1947, 1050 F in 1948, and 1100 F in 1953. A temperature of 1050 F is used extensively today, reflecting the limit of applicability of ferritic materials for piping and pressure vessels. The use of 1100 F is increasing, but no significant trend has developed.

The development of the 125,000-kw unit for the Philo Plant of the Ohio Power Company, designed for steam conditions of 4500 psig, 1150 F initial temperature, 1050 F at the first reheat, and 1000 F at the second reheat, is another milestone of progress in the development of more economical electric power production through higher initial steam conditions.

From the turbine designer's point of view, the step to these steam conditions represents a step twice as great as any previously taken because the doubling of throttle pressure is combined with a 50-deg-F increase in initial temperature. Hence certain traditional steam-turbine design concepts were abandoned in favor of a fresh approach, and it was deemed desirable by all concerned to obtain operating experience on a power system with a unit of moderate size, small enough to be prudent yet large enough to make the experience gained applicable to future turbines of much larger rating with reasonable extrapolation.

This supercritical-pressure turbine, although designed for commercial service on a power system, from the designer's point of view has been approached basically as a large developmental unit. In some instances, for example maximum rotor temperature, we have deliberately accepted conditions more severe than neces-

sary in order to obtain engineering knowledge applicable to even further advances in the future. The operation of such a prototype will provide experience with new approaches to the problems of higher pressures and temperatures.

The relatively low allowable stresses of ferritic steels above 1050 F compel the use of austenitic steels. As utilized in some previous turbine designs, austenitic castings and forgings with relatively thick sections have demonstrated extreme susceptibility to thermal distortion due to the combined characteristics of lower heat conductivity, higher coefficient of expansion, and lower elastic limit. In the Philo design, the wall thicknesses of the austenitic-steel parts have been made as small as possible by the application of such design concepts as:

(a) Steam cooling—accomplished by surrounding all austenitic parts inside the turbine with a thin thermal insulating metallic liner and circulating cooling steam at almost full pressure between this liner and the more massive ferritic sections which are maintained at lower temperature and which carry the main portion of the pressure load. The resulting small pressure load allows the use of thin-walled austenitic nozzle boxes and steam inlets with low-temperature gradients and reduced susceptibility to distortion.

(b) Individual control-valve bodies of small diameter and consequently thinner walls.

(c) Multiple steam pipes—the number of main steam pipes from the boiler is increased to four with individual turbine stop valves placed in each line permitting small valve bodies and pipe of reduced wall thickness.

(d) Simple throttling control with full 360-deg arc admission to the first-stage nozzle.

These design concepts and other unique features soon to be proved by actual operating experience in the Philo development turbine may point the way to even higher pressures and temperatures and make possible the use of substantially reduced amounts of austenitic materials.

## THERMODYNAMICS

The practical thermodynamic gains resulting from higher initial pressures and temperatures have been presented by J. E. Downs.<sup>3</sup> As indicated by Downs' general study, the 125,000-kw rating of the Philo unit is too small to take full advantage of the thermodynamic gain possible with initial steam pressure of 4500 psig. The detailed heat-balance diagram is shown in a companion paper,<sup>4</sup> by S. N. Fiala, with a net turbine heat rate of 7380 Btu/kwhr at 1 in. Hg abs exhaust pressure which represents about a 4.5 per cent gain relative to a turbine of the same type and rating as the Philo unit, but with the steam conditions of the most recent additions to the American Gas & Electric system, 2000 psig, 1050 F initial and reheat temperatures. This gain would increase to

<sup>3</sup> "Margins for Improvement of the Steam Cycle," by J. E. Downs, ASME Paper No. 55-SA-76.

<sup>4</sup> "First Commercial Supercritical Pressure Steam-Electric Generating Unit for Philo Plant," by S. N. Fiala, published in this issue, pp. 399-407.

<sup>1</sup> Manager—Turbine Engineering, Large Steam Turbine-Generator Department, General Electric Company. Mem. ASME.

<sup>2</sup> Supervisor—Turbine Product Engineering, Large Steam Turbine-Generator Department, General Electric Company. Mem. ASME.

Contributed by the Power Division and presented at the Diamond Jubilee Annual Meeting, Chicago, Ill., November 13-18, 1955, of THE AMERICAN SOCIETY OF MECHANICAL ENGINEERS.

NOTE: Statements and opinions advanced in papers are to be understood as individual expressions of their authors and not those of the Society. Manuscript received at ASME Headquarters, September 13, 1955. Paper No. 55-A-159.

approximately 6.0 per cent on turbines of 400,000-kw rating, which would be large enough to use 4500 psig or higher initial pressure effectively. Although by normal standards a 125,000-kw unit cannot be considered small, the first-stage buckets are only about  $\frac{3}{8}$  in. long at these high pressures. With these small flow passages, the leakage areas with practical running clearances between the stationary and rotating parts have a significant effect on efficiency.

In the thermodynamic and aerodynamic design of this turbine, we have not contemplated any new phenomena occurring in steam expanding from supercritical pressure at the inlet of the turbine. The properties of supercritical-pressure, superheated steam have been assumed to be a continuous function of pressure as given in Keenan and Keyes, Steam Table.<sup>5</sup>

#### TURBINE ARRANGEMENT

The cross section of the entire turbine is shown in Fig. 1. The 4500 psig, 1150 F initial steam enters the high-pressure turbine section through four nozzle boxes and expands through 11 stages toward the front standard to the first reheat pressure, exhausting at about 1250 psig, 800 F. The steam is then reheated to 1050 F, entering the center of the intermediate section through two intercept valves located on the upper half of the turbine casing. The steam entering the inner shell from the intercept valves expands through nine stages toward the middle standard exhausting to the second reheater at approximately 207 psig, 660 F. It should be noted that all steam pressures and temperatures stated here and elsewhere are design values at maximum design throttle flow. The steam from the second reheater at 1000 F re-enters the intermediate turbine through two bottom-inlet pipes, passes through eight single-flow stages to the crossover, and then expands to the condenser through the double-flow, low-pressure turbine section having 26-in. last-stage buckets.

By this arrangement, the new problems associated with the 4500 psig, 1150 F steam are confined to the relatively small, separate high-pressure section. The remainder of the turbine with an opposed-flow, intermediate section, and followed by a double-flow low-pressure section, is a relatively standard arrangement with which considerable successful experience has been obtained. Except for features of the latter portion of the turbine that are unique to the over-all system, the discussion of design details will be confined to those of the high-pressure turbine section.

<sup>5</sup> "Thermodynamic Properties of Steam," by J. H. Keenan and F. G. Keyes, John Wiley & Sons, Inc., New York, N. Y., first edition, 1936 (latest printing, March, 1944).

#### HIGH-PRESSURE TURBINE SECTION

The cast-ferritic outer casing of the high-pressure section (Fig. 2) is essentially spherical in shape because, in addition to this being a logical design to enclose the inner casing and the horizontal flange bolts, it also minimizes stress in the casing and its flange bolting. The pressure between the inner and outer casing is first-reheat pressure. The inner casing, cast of the same chrome-moly-vanadium ferritic steel, is shielded from temperatures above about 1000 F by the use of thin-wall austenitic steel (Type 347) liners. Cooling steam taken from the main steam lines and desuperheated to 960 F, enters the flanges of the four steam inlets and is circulated in the space between the austenitic liners and the ferritic inner casing. The temperature of the inner casing which carries the major portion of the pressure load is maintained within approximately 5 deg F of cooling-steam temperature. The details of the cooling system will be described later.

Each of the four main steam inlets feeds a separate austenitic nozzle box through a slip joint. The nozzle boxes are positioned in the inner casing by a key arrangement which permits free relative expansion. At maximum flow the design pressure in the nozzle boxes is 4320 psig with 3790 psig in the first-stage shell and the space surrounding the nozzle boxes. The 530-psi maximum pressure differential permits the forged nozzle boxes to be designed with relatively thin walls that will heat and cool uniformly with low thermal stresses. Because the initial steam flow is controlled by throttling, the pressure stresses in the nozzle boxes decrease with flow. A conventional partial arc admission would impose about 2500 to 3000 psi differential on the nozzle boxes, requiring much heavier walls and associated parts.

The welded diaphragms containing the nozzles of the second, third, fourth, and fifth stages are stacked and hooked together axially, but individually centered in the inner casing. This novel arrangement provides an articulated structure, free to expand, which isolates the inner casing from the high-temperature steam in the steam path. From this point on, the turbine stage construction is essentially the same as currently being used in many other turbines built by the authors' company.

#### HIGH-PRESSURE ROTORS

The high-pressure turbine-casing system, the diaphragms, and packings are designed to accommodate three types of rotors, two of which have been manufactured; i.e., (a) an all-austenitic rotor, and (b) a steam-cooled ferritic rotor.

The austenitic rotor will be installed initially to gain experience,

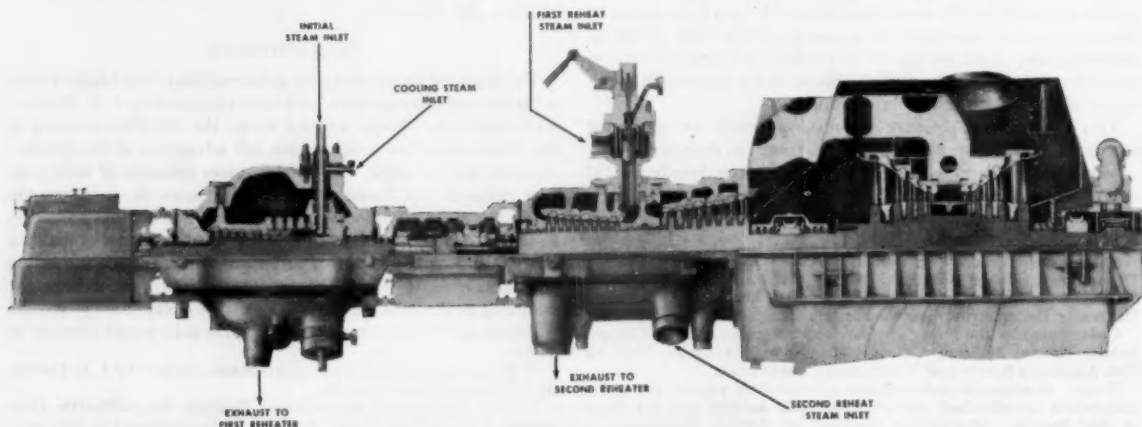


FIG. 1 QUARTER SECTION OF ENTIRE TURBINE

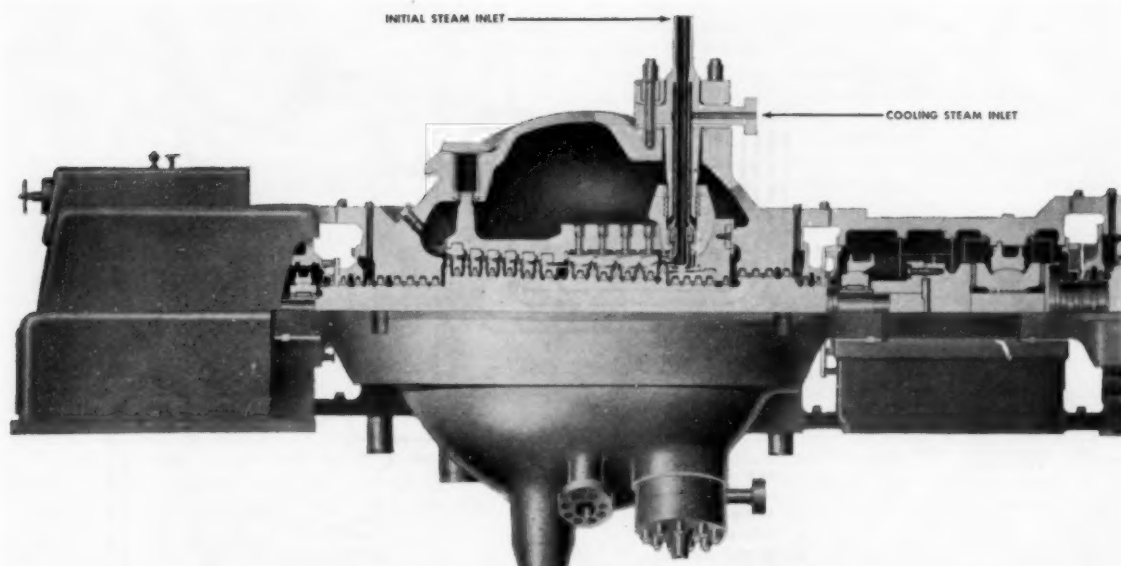


FIG. 2 QUARTER SECTION OF THE HIGH-PRESSURE SECTION OF TURBINE

particularly with regard to its behavior during starting and rapid load changes. The rotor cooling system intended only for the ferritic rotor will be put in service with the austenitic rotor and temperature-measuring devices will be installed to explore the effectiveness of the rotor cooling scheme. If the austenitic rotor is found to have unsatisfactory stability or other undesirable operating characteristics, this preliminary performance data on the rotor cooling system will enable the introduction of the ferritic rotor with reasonable assurance that the temperatures are within permissible limits.

The austenitic rotor is machined from a solid forging of Type 347 steel. Since the alloyed 12 per cent chromium buckets installed on this rotor have a different thermal-expansion coefficient, the multiple-hook dovetails have been designed so that full contact between all hooks will occur only at the normal operating temperature. Previous operating experience with an austenitic journal supported on a tin-base, babbitt-lined sleeve bearing demonstrated poor journal performance in the form of rapid cutting and scoring of the journals, possibly because of the relatively low yield strength of the austenitic material. Satisfactory operation was obtained by shrinking ferritic forged sleeves over the journals; therefore this feature is being applied to this austenitic rotor.

The second rotor manufactured for this turbine will be a completely ferritic rotor of the 1 Cr,  $1\frac{1}{4}$  Mo,  $\frac{1}{4}$  V alloy used for many years by the company for turbine construction. Because of the high operating temperature of this unit, however, it will be necessary to utilize cooling of the first few stages to maintain a maximum rotor temperature of 1025 F at which adequate safety factors on high-temperature strength can be maintained. This is the first time, to the authors' knowledge, that this type of rotor cooling has been employed in a steam turbine. Thermocouples placed in the steam space adjacent to the rotor will be used to monitor the operation of the rotor cooling system.

Because the high-pressure turbine rotor is relatively very light in weight, it was not possible to design the journal bearings with sufficient loading to assure avoidance of whipping instability without using an untried length-diameter ratio. For this reason

the bearings of the high-pressure section are designed as pivoted-shoe type to provide maximum assurance of bearing stability.

#### STEAM-FLOW DIAGRAM

A schematic flow diagram including the various control valves is given in Fig. 3.

Steam from the boiler reaches the turbine through four separate main steam pipes. Each main steam line has a separate stop valve (1) and a separate control valve (2) located external to the turbine and just below the turbine-room floor. The four control valves are operated by their individual operating cylinders under the control of conventional starting handwheel and speed governor and an initial pressure regulator. The control valves all lift simultaneously, resulting in simple throttling control feeding the full 360-deg arc of first-stage nozzles, as discussed previously.

To enable the stop valves to be constructed with the greatest possible simplicity and ruggedness, no internal by-pass is used. Steam pressure is equalized across the stop valve with the control valves shut by means of a small separately positioned external by-pass valve (5) permitting the 4500-psi pressure to be built up gradually over 5 to 10 min to warm the control-valve bodies and associated piping. Once the pressure is equalized, all four stop valves are opened wide at once.

When starting the cold boiler, the stop valves are closed, and the boiler feed pump builds up full water pressure against the closed stop valves, and one or more of the multiple pressure-reducing valves (7) of Fig. 3 are opened so as to throttle 4500-psi water in the amount of about 225,000 lb/hr to the deaerator. Fire is established in the boiler, the temperature is raised slowly, and the pressure-reducing valves (7) are opened gradually by means of a pressure regulator so as to maintain substantially constant flow through the boiler and recirculating system. The steam is desuperheated after throttling through the reducing valves before entering the deaerator. The pressure-reducing valves (7) must handle the 225,000 lb/hr recirculation flow from conditions of 60 F water to as high as 1150 F superheated steam. When the temperature of the steam reaches about 900 F, the

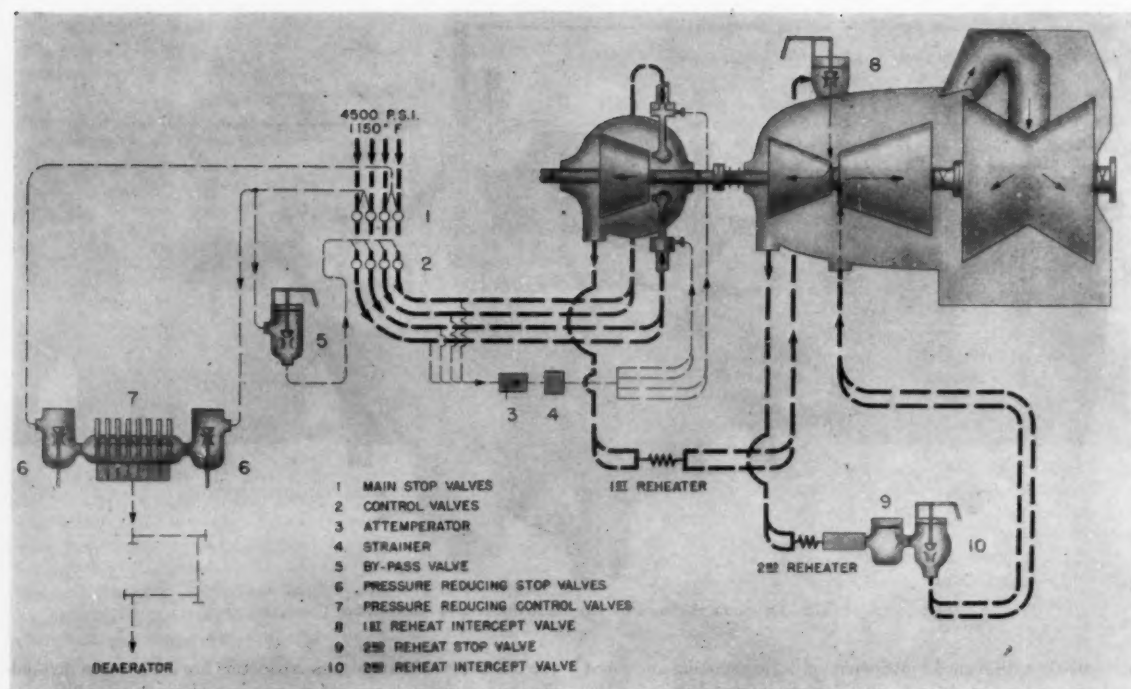


FIG. 3 SCHEMATIC STEAM-FLOW DIAGRAM

main stop valves (1) are opened, and the turbine is made ready to roll. The control valves (2) are positioned by hydraulic relays under control of a starting handwheel so as to control speed by hand while coming up to synchronous speed. After the unit is synchronized, the pressure-reducing valves are gradually closed automatically by the pressure regulator as the main control valves (2) are opened. Stop valves (6) in the pressure-reducing lines are closed automatically by the same pressure regulator and operating mechanism simply to prevent any 4500-psi steam leakage from the stem packings of pressure-reducing valves which could not be stem-sealed.

As the control valves are opened and the boiler firing rate is increased, the pressure in the four nozzle groups increases in proportion to increase in steam flow to the turbine.

#### INTERNAL COOLING ARRANGEMENT OF THE HIGH-PRESSURE TURBINE SECTION

Before leaving the diagram in Fig. 3, attention is called to the four pipes that take steam from the main steam lines between the control valves (2) and the nozzle boxes. For shell cooling only approximately 60,000 lb/hr of steam at full load is metered through orifices at the four main steam-inlet flanges and is desuperheated at (3) under control of a tempera-

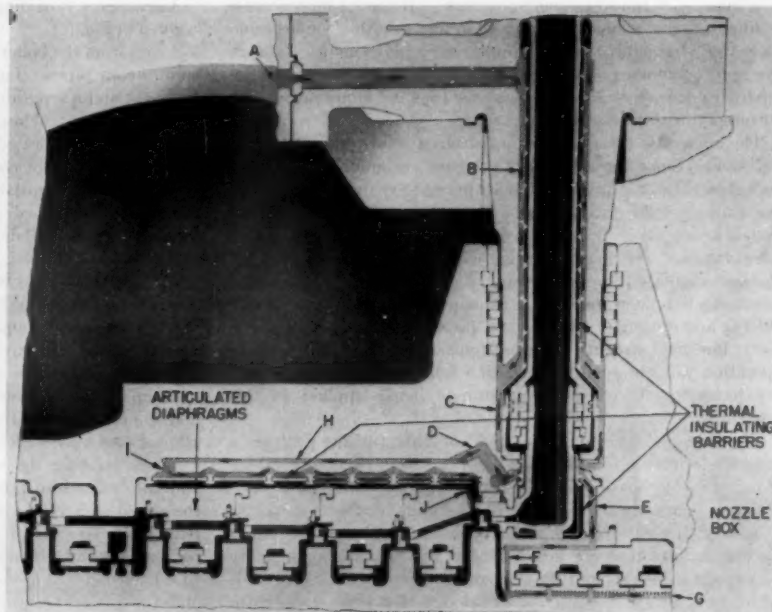


FIG. 4 ENLARGED CROSS SECTION SHOWING PATH OF COOLING STEAM WITHOUT ROTOR COOLING

ture-sensing element so as to supply steam at 960 F through four entry points at the inlet flanges to the high-pressure section.

The construction details in the region of the main steam inlets, first-stage nozzle, and the cylindrical portion of the inner casing

surrounding the first four diaphragms are shown in Fig. 4. The cooling steam which enters at the flange of each of the main steam inlets flows radially inward to the region of the first-stage nozzles along path *A-B-C* where it divides into two paths. One path *E-F-G* is around the first-stage-nozzle boxes and out through the inner rings of the high-pressure packing. This provides for moderate temperature at the high-pressure packing. The second path *D-H-I-J* is down along the horizontal flange to the fifth-stage diaphragm whence the cooling steam flows in a zig-zag fashion between the inner casing and the thin liners back to the first-stage shell. Restricting orifices are provided at *A*, *D* and *E* to insure proper distribution of the cooling steam in their respective channels. It should be noted that the austenitic parts exposed to 1150 F steam are separated from the cooling steam by a metallic, thermal-insulating barrier. In this manner practically all of the steady-state temperature gradients occur in the lowly stressed thermal barriers instead of in the more highly stressed austenitic parts. The pressure in the cooling-steam space is maintained slightly higher than that at the discharge of the first stage by the pressure drop across orifices at *A*, *D*, and *E*.

With rotor cooling, the system is modified as shown in Fig. 5. The total cooling-steam flow is increased to 100,000 lb/hr by enlarging the orifices at *A*. This additional flow supplies the

conditions are the piping and valves, the high-pressure rotor, and the first-stage buckets, and each of these involves problems peculiar to each application. In the selection of materials for the piping and valves, the major problem is to insure that the material is not only reasonably weldable, but also that the resulting welds will give reliable operation without suffering embrittlement or cracking. Selection of a rotor material requires specifying a material which can be supplied in the relatively large forgings required for the high-pressure rotor without introducing an undue number of unsolved problems at the steel mill. In addition, the rotor material must be such that reasonable assurance of heat stability at the operating temperatures can be obtained. Steels for high-temperature buckets should have, in addition to the required high-temperature strength, such desirable properties as a reasonable degree of damping, machinability, and sufficient workability to permit riveting the tenons which secure the bucket covers.

After considering several of the superalloys developed for gas turbines and jet-engine applications, it was decided to build the piping and valves out of Type 347 (18 Cr, 10 Ni, 1 Cb) materials. Although it might have been desirable to obtain operating experience with applicable superalloys, they were not utilized for this application primarily because it was felt that extensive welding

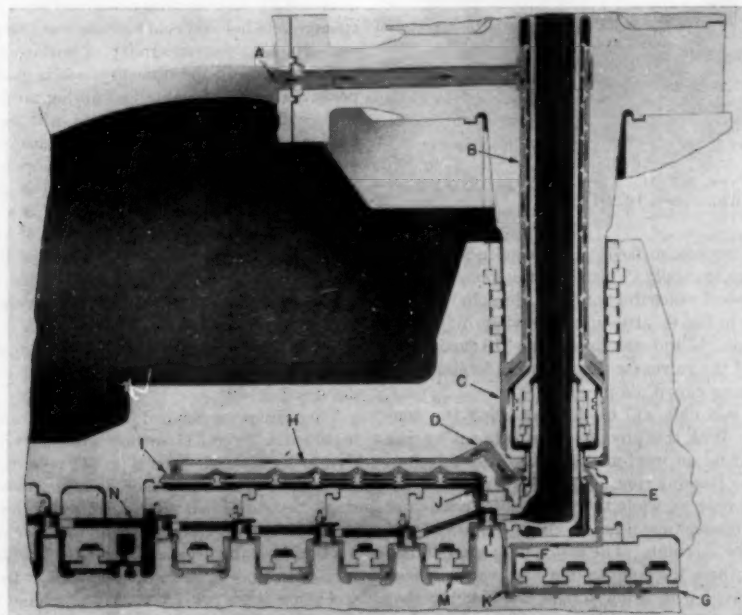


FIG. 5 ENLARGED CROSS SECTION SHOWING PATH OF COOLING STEAM WITH ROTOR COOLING

diaphragm-packing leakage along path *K-L-M-N* by appropriate enlargement of orifices at *E*. Leakage control is employed at both the admission and discharge sides of the buckets to minimize the mixing of rotor-cooling steam with the main flow in the steam path.

#### HIGH-TEMPERATURE MATERIALS

In the design of this unit to meet the throttle conditions of 4500 psig, 1150 F, considerable thought was given to the selection of the materials exposed to this combination of high pressure and high temperature. The major components exposed to these

investigations coupled with relatively long-time laboratory exposure of such weldments to steam-turbine temperatures should be on hand before predicating the operation of even this developmental unit on the use of these superalloys. It is recognized that both welding difficulties and operating troubles due to weld cracking and embrittlement have occurred in past applications of the Type 347 steels, but it was felt that with the rather considerable investigations being conducted by the entire industry, these problems would be solved satisfactorily.

The Type 347 piping was made as pierced seamless-steel tubing with 0.060 in. being removed from the pipe wall on both the inner

and outer surfaces to eliminate any surface defects which might occur during the piercing and rolling operations. This piping was then subjected to the usual visual inspection coupled with physical tests, with flattening rings and etch rings being removed from each pipe length. In addition, the piping was ultrasonically inspected using a shear wave traveling circumferentially in the pipe, a longitudinal wave traveling radially be-

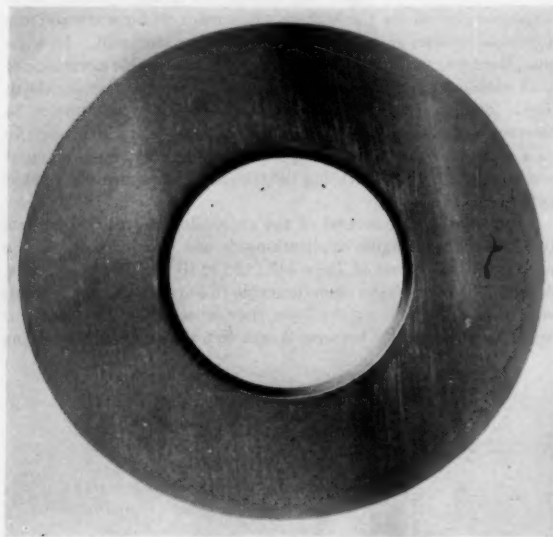


FIG. 6 SECTION OF TYPE 347 MAIN STEAM PIPE. DEFECT AT RIGHT ( $6\frac{3}{4}$  IN. OD)

tween the inner and outer wall surfaces, and a longitudinal wave traveling axially through the wall. This inspection revealed that one pipe length had a defect which did not break through to either wall surface as is shown in Fig. 6. Because of previous difficulties with the welding of Type 347 and stabilized Type 316 castings, it was decided to make all the valves for this unit from forgings, the control valve bodies being closed die forgings.

All the welding on this unit will be done utilizing the consumable backing ring. With this process, the small backing ring which is used is melted by an inert-gas first pass resulting in a weld with effectively no backing ring. The next few passes are laid in by the inert-gas process, while the major outer portion of the weld is finished by manual metal-arc welding. Two types of electrodes will be used for this unit. The first type is a low-ferrite Type 347 electrode in which the composition has been balanced to give both a sound weld with a low ferrite content, together with assurance against sigma embrittlement during long-time high-temperature operation. This electrode requires a 1925 F postweld treatment in order to furnish not only a full stress relief but also either to put the small ferrite content into solution or to spheroidize it so that no sigma embrittlement will occur later. The second electrode to be used is the 16-8-2 (16 Cr, 8 Ni, 2 Mo) recently developed by The Babcock & Wilcox Company. In both field and laboratory investigations, this electrode has produced sound welds, and it is planned that this 16-8-2 electrode be used for the welds which must be made at the station. The decision regarding postweld heat-treatment of the 16-8-2 weldments is awaiting the results of current laboratory investigations. However, the piping welds made in the fabricator's shop will utilize the low-ferrite Type 347 electrode with the 1925 F postweld treatment being performed in heat-treating furnaces. Com-

parative experience will be obtained on these two approaches to the austenitic welding problem.

In the design of the rotor for the high-pressure section, several lines of attack were adopted since no design could be developed which did not introduce either design or operating problems on which significant operating experience was unavailable. As stated previously, it was intended that three high-pressure rotors would be constructed, each one involving either new rotor materials or manufacturing processes, or else the utilization of new design concepts. The first rotor would be constructed of Type 347 steel since considerable experience was already available on the production of forgings of this alloy approximating the sizes required for this application. Thermal stability, however, is the major question regarding the use of a Type 347 rotor. Relative to ferritic steels previously used for turbine rotors, this steel has lower yield strength, higher coefficient of thermal expansion, and lower thermal conductivity. Because an austenitic steel does not undergo a transformation, heterogeneity of these and other properties may be a factor. Such instability difficulties were encountered in the heat-indication tests of the forging at both the steel mill and in our factory, but it was not possible to ascertain definitely whether this was a true heat instability, or a transient runout caused by the method of heating (by radiation) in the heat-indication lathe. Since satisfactory results could be obtained by slow heating rates, and since the difference between steady-state hot and cold runouts was acceptable, it appears most probable that nonuniformity of surface emissivity may be the primary cause of the difficulty. It is expected that satisfactory performance will be obtained during normal operation since the surface heat-transfer coefficients will be greatly improved in both magnitude and uniformity when operating in high-density steam. Accordingly, the Type 347 forging was processed through production up to the final machining stage. At this point the rotor was returned to the steel mill for a final high-temperature heat-treatment to insure the removal of any stresses induced by the machining operations. It was then returned to the turbine factory, finish-machined, heat-indication tested, bucketed, spin tested and will be shipped with the turbine for the initial operation of this unit.

The ferritic (1 Cr,  $1\frac{1}{4}$  Mo,  $\frac{1}{4}$  V) alloy rotor built for this unit involves no new problems except rotor cooling, which has been discussed previously.

The third rotor planned for this unit would be a composite rotor in which a Type 347 section will be welded directly to ferritic Cr-Mo-V sections. The type 347 section will be limited to only the high-temperature stages, and the welds would be placed at the stage beyond which the ferritic alloys are satisfactory. These welds between the austenitic and ferritic rotor sections would be made using a high-nickel electrode on which considerable laboratory experience is currently available. In particular, austenitic-to-ferritic welds using this electrode have been made in pipes of 16-in. OD with approximately 3-in. wall, and these welds have been subjected to approximately 300 cycles between 300 and 1100 F with no cracking whatsoever occurring. The development of this composite rotor includes making a full-size prototype weldment which can be cycled between 300 and 1200 F, with superposed vibration stresses simulating rotor operation, to insure that a weldment of satisfactory long-time reliability can be obtained. Because of some initial welding difficulties which occurred on this prototype, the construction of this composite rotor has been delayed considerably beyond the original planned date of completion.

The higher-temperature buckets for this unit are to be made of an alloyed 12 per cent chromium steel (12 Cr, 1 Mo, 1 W,  $\frac{1}{4}$  V). Considerable operating experience is available on this particular bucket alloy, and with careful design its high-temperature strength is satisfactory for this application.

For the bolting, steels and design practices on which considerable experience is already available will be used. The bolting for the austenitic parts will utilize a hot-cold worked alloy of 19 Cr, 12 Ni, 3 W, 1 Cb, which has been in operation for 8 years with excellent operating reliability. This alloy has sufficient high-temperature strength at the operating conditions so that no cooling will be required. The ferritic parts will utilize a 12 per cent chromium bolting alloy similar to that of the high-temperature buckets. It will be necessary, however, that slight steam cooling be utilized on five of the inner-casing flange bolts on each side of the turbine and this design practice has been successfully employed in many machines constructed over the past five years. The steam at 900 F for cooling these bolts is bled from a lower stage in the high-pressure turbine section, and is circulated between the bolt shank and the flange hole, passing in series from one bolt to the next and then discharged into the 1250 psig area between the inner and outer shells.

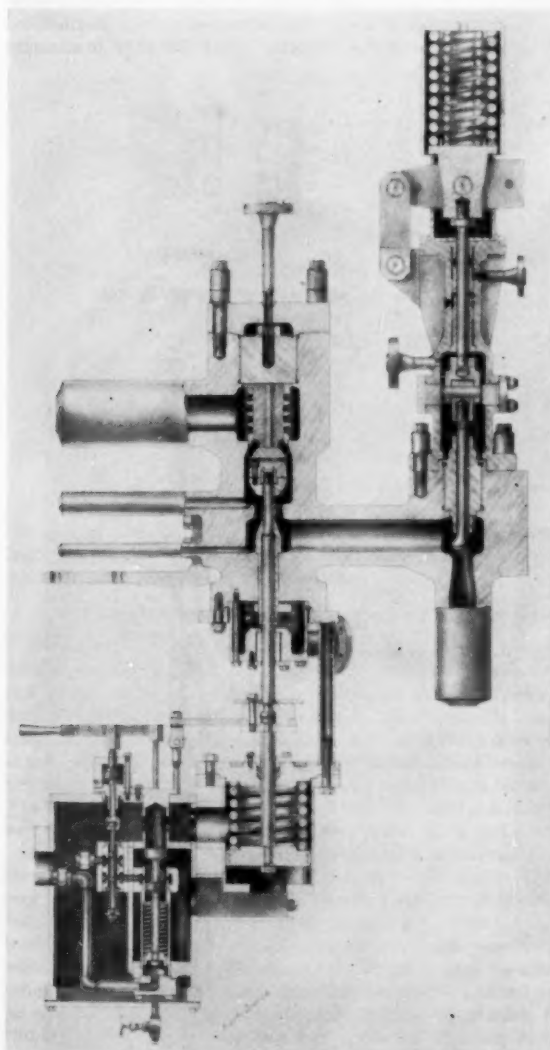


FIG. 7 CROSS SECTION OF STOP VALVE AND COMPANION CONTROL VALVE

#### VALVE DESIGN

A cross section of one of the four sets of stop valves and control valves is illustrated in Fig. 7 with the stop valve on the left and control valve on the right. In order to minimize the body diameter and hence the wall thickness, the strainer assembly is located above the valve disk instead of around it as is our usual practice. A feature of both the 4500-lb stop valves and the control valves is the use of a threaded plug which takes the pressure drop from 4500 psig to 1250 psig at maximum load, and to vacuum at starting, thus reducing materially the pressure load for which the stop-valve cover flange must be designed and correspondingly reduce the load on the outer bonnet flange of the control valves. A leakoff between the threaded plug and the outer cover or bonnet is connected to the high-pressure turbine section exhaust pressure. A similar-type plug design has been in successful turbine valve service for about 15 years. The stop valves are stem-sealed and hence are designed with large clearances since they normally are either fully shut or fully open. Hard-surface facing is applied to the contact surfaces of valve disks and seating surfaces and no removable valve seats are employed. Spirally wound austenitic gaskets with asbestos filling are employed at all 1150 F flange points of the valves and other pipe flanges. This gasket has been in highly successful use for 2 years at 1100 F and on many 1050 F applications for much longer periods of time.

The operating mechanism includes a provision for valve testing which permits one control valve and its companion stop valve to be closed while the turbine is carrying full load. By this means the freedom of the valves to close in case of emergency can be assured. This operation may be remotely performed from a central control room or at the valve location. This routine test operation can be performed with only about 6 per cent reduction in load momentarily, owing to the fact that the four take-off lines feeding the cooling-steam system are sized sufficiently large and connected together to act as equalizers to feed the otherwise idled nozzle box. All oil-operating cylinders are in fully enclosed housings to minimize fire hazard.

A cross section of one of the two 1250-psig intercept valves is shown in Fig. 8. The valve disk is of the fully balanced type with solid piston rings surrounded by a surface-hardened, pressure-balancing cylinder and external by-pass similar in construction to that used successfully for many years. The oil operating cylinders are located at the floor line on either side of the turbine in fully guarded enclosures consistent with the usual fireproofing practices employed in the design of turbines built by the authors' company. One of the two intercepting valves can be alternately closed daily under full load to exercise it and test its freedom to close. A 0.8 per cent reduction in terminal speed on loss of maximum load is made possible by locating these valves on the casing instead of placing them as close as practical in the steam lines external to the turbine.

The 207-psig intercept valves are of the angle-body type illustrated in Fig. 9 and are similar in construction to the high-pressure intercept valves with the oil-operated cylinders in fully guarded enclosures. The intercept valves are all controlled by the same pre-emergency governor, which is actually a speed governor set to start the intercept valves closed at 101 per cent speed and to have them fully closed at 105 per cent speed.

A careful study of the overspeed potential in the two reheaters showed that failure of the 1250-psig intercept valves to close on loss of maximum load would result in an overspeed of about 120 per cent rated speed and therefore no reheat stop valves are required for this reheater. However, the overspeed which would result from failure of the 207-psig intercept valves on loss of maximum load would be appreciably higher and therefore reheat stop

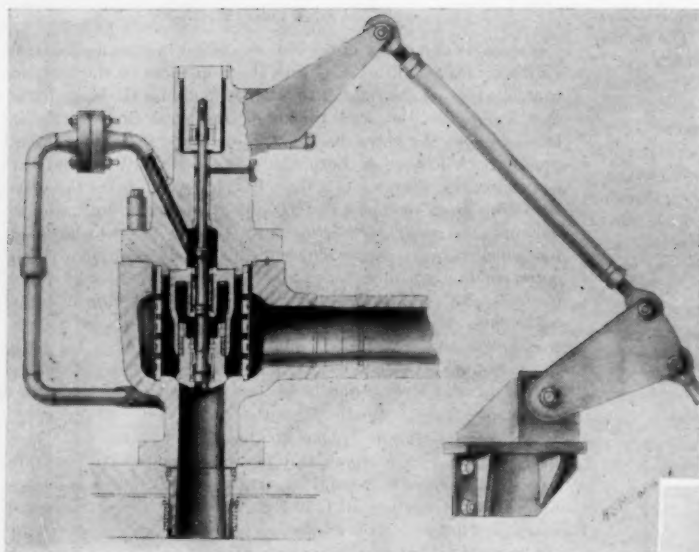


FIG. 8 CROSS SECTION OF 1250-PSIG INTERCEPT VALVE

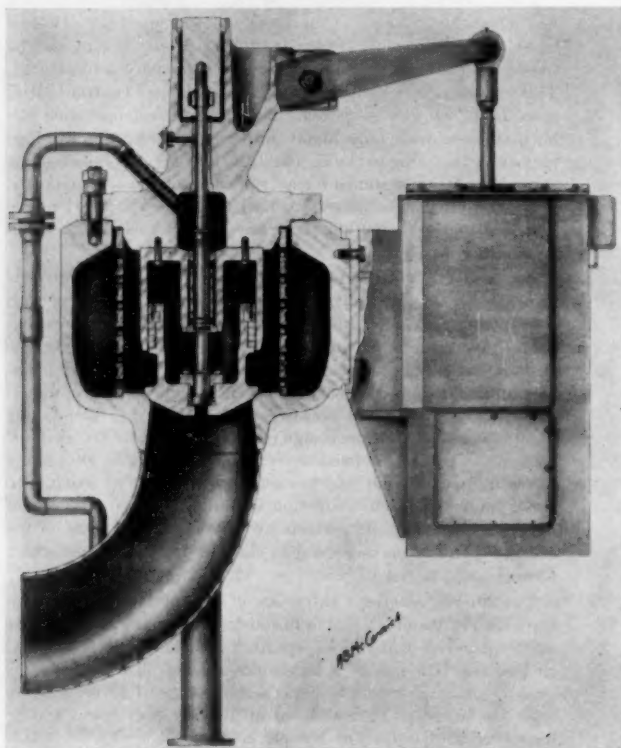


FIG. 9 CROSS SECTION OF 207-PSIG INTERCEPT VALVE

valves are provided in the low-pressure reheater lines. It is expected that the overspeed potential of the high-pressure reheater on larger turbines will be higher than it is on this unit and therefore we would expect to supply reheat stop valves on both reheaters on most double-reheat machines.

The overspeed which would result if both sets of intercept valves failed on loss of maximum load is quite appreciably over 120 per cent. Since maloperation of the single pre-emergency governor could cause such a failure, the control mechanism for the high-pressure intercept valves are tripped directly by the turbine emergency governor.

A cross section of one of the two stop valves and one of the eight pressure-reducing valves in the by-pass system is shown in Fig. 10. The multiple reducing valves are operated in sequence from a camshaft which is initial-pressure controlled. The multivalve design was chosen in order to favor the noise problem. Easily removable hard-surfaced valve seats are provided anticipating frequent replacement due to the unpredictable erosion problem. Valve-stem packings are close-clearance soft rings of graphited asbestos reinforced with nickel alloy, to minimize

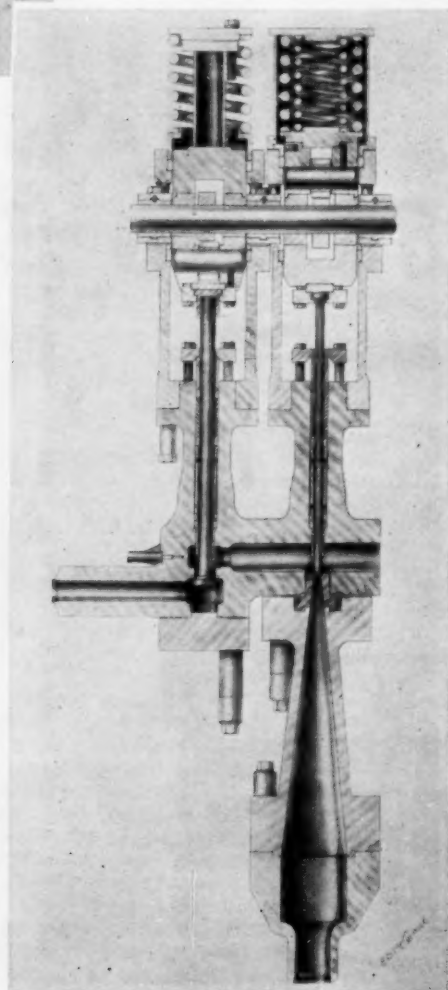


FIG. 10 CROSS SECTION OF STOP VALVE AND PRESSURE-REDUCING VALVE IN THE BY-PASS SYSTEM

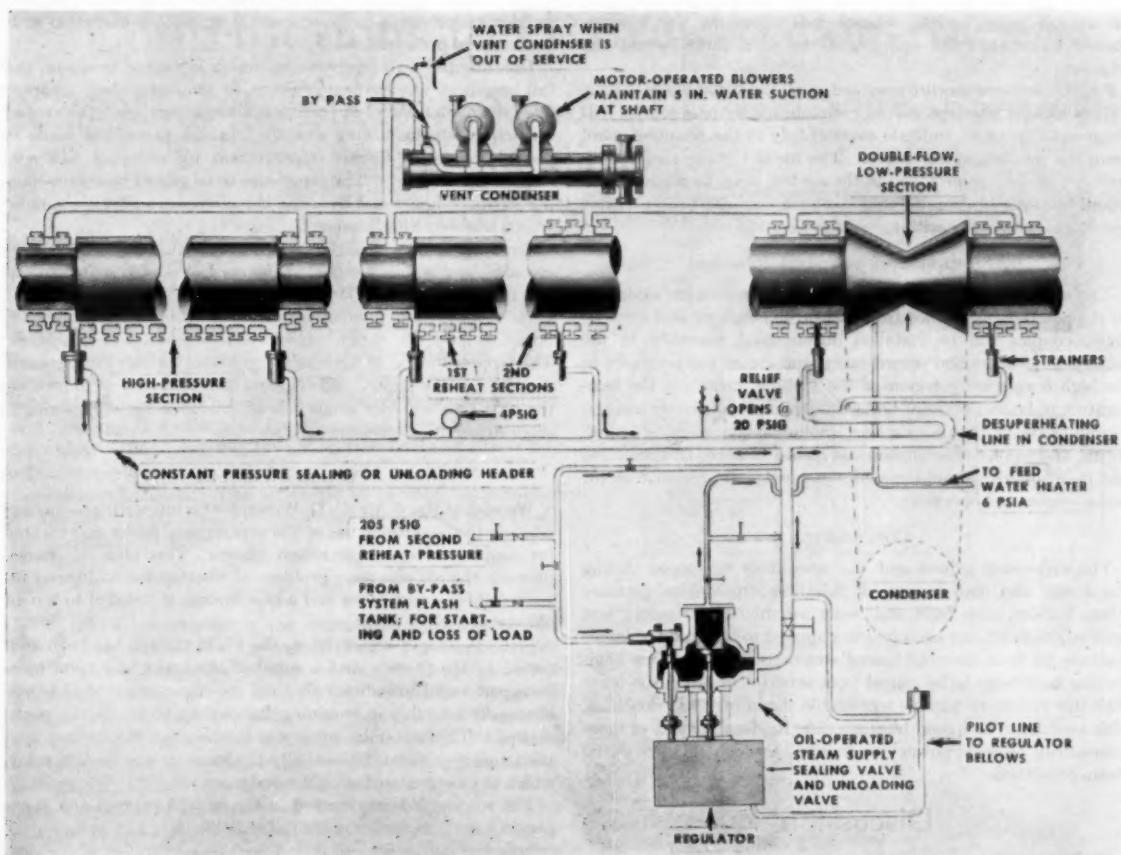


FIG. 11 SCHEMATIC DIAGRAM OF PACKING, STEAM-SEALING SYSTEM

the leakage when handling 4500-lb water. Pressure is removed from the packing glands by closure of the stop valves upstream when the reducing valves are out of action.

#### STEAM-SEAL SYSTEM AT TURBINE-SHAFT PACKINGS

All shaft packings are of the labyrinth type with steam from a 4.0-psig constant-pressure header supplying all glands from standstill to full load, thus permitting full vacuum to be established with turbine on the  $2\frac{1}{2}$  rpm turning gear. This system is illustrated in Fig. 11. To prevent leakage into the turbine room, a slight vacuum of about 5 to 10 in. of water is maintained between the two outer labyrinth rings by means of a motor-driven blower. The steam is condensed in a shell and tube-type vent condenser and the air is discharged outside the station through a vent pipe.

An oil-operated combination steam-sealing and unloading regulator valve maintains exactly 4 psig at each of the glands with any excess of steam from the high-pressure packings not needed by the low-pressure turbine packings discharged through the unloading valve to a lower-stage pressure of the low-pressure turbine section. The temperature of the steam feeding the low-temperature packings of the double-flow section is reduced to saturation temperature, approximately 212 F, by passing it through a simple desuperheating loop consisting of about 30 ft of bare pipe in the condenser neck prior to its reaching the shaft-packing boxes. The vent condenser is in the condensate system and provision is made to by-pass the vent condenser in the water

circuit in the event of tube leakage. While the faulty tube is being plugged, the two centrifugal blowers are designed to handle both steam and air when assisted by the temporary water spray if the by-pass valve is opened to remove the resistance of the vent condenser. This steam-seal system is typical of many in service for the past 5 years.

#### PROTECTIVE FEATURES

The quantity of 960 F cooling steam is substantial and if the temperature of this steam increases or decreases suddenly from its normal value it is potentially able to impose quite drastic cooling or heating with consequent thermal stresses. For this reason the control system provides for an alarm at temperatures 60 deg F higher or lower than normal, and for tripping of the control valves at 100 deg F higher or lower than normal.

The trip controllers on the control-room panel will indicate continuously the cooling-steam temperature. In addition to the temperature trip and alarm features, provision is made to trip the water control valve in the desuperheater automatically whenever the turbine main-steam flow is shut off.

A similar temperature alarm-and-trip system is provided to warn the operators and trip the turbine valves if the main 1150 F steam temperature in one of the supply lines to the stop valves varies beyond set limits of 1250 F maximum and 850 F minimum.

The following provisions are included to trip the turbine valves in case of low vacuum; thrust failure, overspeed, or generator

differential relay action. Signal indications in the remote-control room alert the operator as to what fault caused the tripping.

Position transmitters are provided on all the turbine stop valves, control valves, intercept valves, recirculating by-pass valves, and steam-seal valves to indicate continuously in the remote-control room the position of all valves. The usual turbine supervisory instruments also are provided in the control room to measure and record bearing vibration, differential expansions, shaft eccentricity, speed, and camshaft position.

#### INSTRUMENTATION FOR DATA PURPOSES

The high-pressure turbine section with its austenitic rotor will be shipped fully assembled from the turbine factory and some 60 thermocouples will be installed during final assembly at the factory to measure and record metal and steam temperatures in the high-temperature region of the turbine, including the temperature of horizontal joint bolts, flanges, inner and outer casings, as well as steam in various stages, cooling steam, packing leakoff steam, and so on. The continuous record of these temperatures and their analysis should provide very valuable information for both designer and operator.

#### CONCLUSION

The experience gained and the new ideas developed during the design and manufacture of this first supercritical-pressure steam turbine, now built and being assembled for factory test prior to shipment, are already being applied to the study of larger turbines for even more advanced steam conditions. New engineering knowledge to be gained from actual operating experience with this prototype turbine will enable the industry to continue, with confidence and good business risk, its development of more economical electric power production through higher initial steam conditions.

### Discussion

C. D. WILSON.\* This excellent paper describes and illustrates an actual machine with solutions to many of the design

problems involved in building a steam turbine for operation with supercritical pressures.

Isolating the high temperature, which is needed to obtain the full benefit of supercritical pressure, in small chambers separate from the main body of the casing is always desirable. The novel method of steam cooling described in the paper has made it possible to obtain further improvement by reducing wall sections to a minimum. The experience to be gained by steam-cooling ferritic spindles and by using the alternate austenitic spindle will be watched with interest.

Studies we have made of steam cycles utilizing supercritical steam pressures, have indicated the need of double reheat to obtain maximum gain. They also have indicated that the optimum value of first reheat pressure is not too far removed from the inlet pressure used on many present-day single-reheat machines. This appears to be in agreement with the turbine arrangement described in the paper, and suggests the possibility of improving the heat rate on older single reheat machines by superposing a small supercritical-pressure turbine.

#### AUTHORS' CLOSURE

We wish to thank Mr. C. D. Wilson for his interesting comments relating to the possible use of the supercritical boiler and turbine for topping older single reheat plants. This idea, of course, presents the old economic problem of whether the additional investment for a new boiler and a new turbine is justified to top an old steam turbine plant.

Since the paper was written, the Philo turbine has been spin tested in the factory and a number of checks and tests have been performed to indicate that the cooling steam system is mechanically effective in confining the cooling steam in the paths desired. The austenitic rotor was used during the factory spin tests and it performed essentially the same as any ferritic rotor, which is most reassuring to the designers.

The turbine is being erected in the field at present and is expected to go into service in the fall of 1956.

\* Engineer, Allis-Chalmers Manufacturing Company, Milwaukee, Wis. Mem. ASME.

# Contributions to Hydraulic Control—7

## Analysis of the Effects of Nonlinearity in a Valve-Controlled Hydraulic Drive

By E. I. REEVES,<sup>1</sup> CAMBRIDGE, MASS.

A method is developed for analyzing the performance of a valve-controlled hydraulic drive consisting of a closed-center four-way valve, hydraulic motor, and mechanical load. This analysis facilitates the determination of the amplitude and phase of the fundamental component of load velocity in response to sinusoidal valve-spool motion and includes the effects of three sources of nonlinear performance: The pressure-flow characteristics of the valve, orifice-type hydraulic leakage, and nonlinear speed-dependent friction. The analysis is verified by analog-computer results and experimental data from an actual valve-controlled drive.

### INTRODUCTION

**D**URING recent years, the demand for high-performance servomechanisms to control large inertial loads has accelerated the development of fluid-power-control techniques. Although the use of a valve-controlled hydraulic drive in a wide variety of systems has indicated certain advantages of this form of fluid control, serious difficulty has been encountered in applications where extremely high performance is required. A major portion of this trouble arises from inadequate knowledge of the nature and effect of nonlinear phenomena inherent in the valve-controlled drive. The analysis given in this paper was developed in an effort to supply a more complete description of these nonlinear attributes.

In the simplest form, the valve-controlled hydraulic drive consists of a four-way flow valve, a hydromechanical transducer (ram or rotary hydraulic motor), and a mechanical load. The input to the system is valve-spool position, and the output is load velocity. Discussion here is confined to a four-way valve of the closed-center variety, and the notation used is shown in Fig. 1. The transducer and load portion of the system are shown in Fig. 2. The sources of nonlinearity to be investigated are three; namely, the pressure-flow characteristics of the valve, orifice-type hydraulic leakage across the valve-output lines, and coulomb friction in the load.

The plan of attack is based on the frequency-response method of analysis. This analytical technique may be generalized to include nonlinear system elements by defining the frequency response or "describing function" of a nonlinear element as the amplitude ratio and phase shift between the input and the fundamental component of the output. The describing function is, therefore, a linear approximation to the description of the nonlinear element and differs from the more common incremental

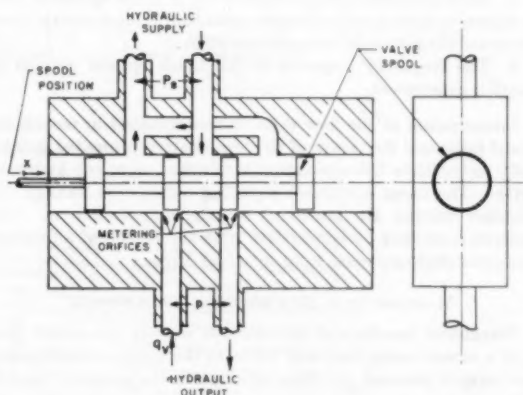


FIG. 1 THE FLOW VALVE

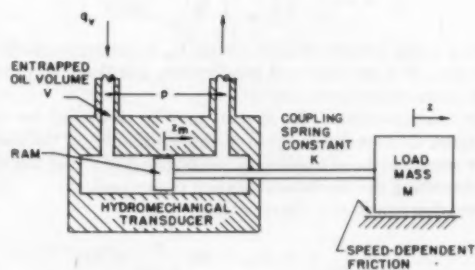


FIG. 2 TRANSDUCER AND LOAD PORTION OF THE DRIVE

or small-variation linear approximation in that the describing function is dependent on signal amplitude as well as frequency. The describing function of the nonlinear portion of a closed-loop system may be combined with the frequency response of the remainder of the system, and thus permit treatment of the entire system by conventional analytical techniques in order to evaluate the frequency response and stability margin of the system. In particular, periodic behavior or "hunting" may be predicted with reasonable accuracy.<sup>2,3</sup> The purpose of this paper is the development of a method<sup>4</sup> for determining the describing function of a valve-controlled hydraulic drive. The computation of

<sup>1</sup> Research Engineer, Dynamic Analysis & Control Laboratory, Massachusetts Institute of Technology.

Contributed by the Machine Design Division and presented at the Diamond Jubilee Spring Meeting, Baltimore, Md., April 18-21, 1955, of THE AMERICAN SOCIETY OF MECHANICAL ENGINEERS.

NOTE: Statements and opinions advanced in papers are to be understood as individual expressions of their authors and not those of the Society. Manuscript received at ASME Headquarters, December 30, 1954. Paper No. 55-8-9.

<sup>2</sup> "A Frequency Response Method for Analyzing and Synthesizing Contactor Servomechanisms," by R. J. Kochenburger, part 1, Trans. AIEE, vol. 69, 1950, pp. 270-284.

<sup>3</sup> "Sinusoidal Analysis of Feedback-Control Systems Containing Nonlinear Elements," by E. C. Johnson, Jr., part 2, Trans. AIEE, vol. 71, 1952, pp. 169-181.

<sup>4</sup> "Evaluation of the Effects of Nonlinearity in a Valve-Controlled Hydraulic Drive," by E. I. Reeves, SM thesis, Department of Electrical Engineering, Massachusetts Institute of Technology, Cambridge, Mass., January, 1954.

describing functions that include possible parameter ranges for the drive and incorporation of these describing functions in the analysis of closed-loop systems are left for future study.

Determination of the describing function of the drive is accomplished in three steps:

1 A mathematical description of the system is formulated and presented as a block diagram, thus allowing the isolation of the nonlinear portions of the system as unidirectional blocks, each giving an output which is uniquely determined by the present value of the input or inputs.

2 Each nonlinear block is replaced by a linear operation that is chosen so as to give an output equal to the fundamental component of the output of the nonlinear block.

3 The frequency response of the linear system derived in step 2 is determined.

Linearization of the flow valve is accomplished in nondimensional form, and the results of the linearization presented graphically to facilitate the application of this analysis to any hydraulic drive. The linear operations replacing orifice-type leakage and coulomb friction are presented by algebraic equations. The analysis is verified by comparison with the results of an analog-computer study and data from an actual drive.

#### MATHEMATICAL DESCRIPTION OF THE SYSTEM

Blackburn<sup>4</sup> has derived the equation relating the output flow  $q_v$  of a closed-center four-way valve to the spool displacement  $x$  and output pressure  $p$ . This equation in the notation used in this paper is

$$q_v = \alpha C_v \sqrt{\left(\frac{GP_s}{\rho}\right)} \sqrt{\left(1 - \frac{xp}{|x|P_s}\right)} \quad [1]$$

where  $\alpha$  is the peripheral port width,  $C_v$  is the orifice discharge coefficient,  $G$  is gravitational acceleration,  $\rho$  is the fluid density, and  $P_s$  is the supply pressure.

The load portion of the system may be described by three equations, the first developed from flow continuity for the volume under compression on one side of the transducer  $V$  and the other two describing the mechanical portion of the load.

From flow continuity, the equation

$$q_v = \frac{V}{2\beta} \dot{p} + H_1 p + H_2 \frac{p}{\sqrt{|p|}} + A \dot{z}_m \quad [2]$$

may be derived where  $\beta$  is the fluid bulk modulus,  $H_1$  is the laminar leakage coefficient,  $H_2$  is the orifice-type leakage coefficient,  $A$  is the ram area, and  $z_m$  is the ram position.

The equations describing the mechanical portion of the system are

$$pA = K(z_m - z) \quad [3]$$

and

$$pA = M\ddot{z} + F_1\dot{z} + F_2 \frac{\dot{z}}{|\dot{z}|} \quad [4]$$

where  $K$  is the spring constant of the mechanical coupling between ram and load,  $M$  is load mass,  $F_1$  is the viscous-damping coefficient,  $z$  is load position, and  $F_2$  is the value of coulomb friction assumed to be independent of the magnitude of load velocity but always in opposition to motion. Inherent in the derivation of Equations [1], [2], [3], and [4] are the assumptions of incompressible fluid flow, negligible ram mass, negligible friction

at the ram, and constant volume of oil under compression. These assumptions were made in an effort to simplify the presentation in this paper and are valid for the systems used to verify the analysis.

Ram velocity  $\dot{z}_m$  may be eliminated from Equations [2] and [3], giving

$$q_v = \left(\frac{V}{2\beta} + \frac{A^2}{K}\right) \dot{p} + H_1 p + H_2 \frac{p}{\sqrt{|p|}} + A \dot{z} \quad [5]$$

thus reducing to two in number the equations describing the load. Equations [1], [4], and [5], which completely describe the system, may be represented by the block diagram in Fig. 3, where each nonlinear operation is represented by a function generator. The input-output characteristic of function generator No. 1 is given by Equation [1]. Function generator No. 2 produces  $H_2$  times the odd-function square root of the pressure  $p$ , and function generator No. 3 generates plus  $F_2$  for positive  $\dot{z}$  and minus  $F_2$  for negative  $\dot{z}$ .

#### LINEARIZATION OF THE FLOW VALVE

The linear equivalent of the flow valve may be derived by computing the fundamental component of  $q_v$  when  $x$  and  $p$  are assumed to be sinusoidal; that is

$$x = X \sin \omega t \quad [6]$$

and

$$p = P \sin (\omega t + \phi_p) \quad [7]$$

where the higher frequency harmonic content of  $p$  is neglected. Since  $p$  has a period  $2\pi/\omega$  and the argument of the square root involving  $p$  in Equation [1] shifts definition every  $2\pi/\omega$  seconds, the square root has a period  $\pi/\omega$  and consequently possesses an average value and even harmonics only. Expansion of the square root in Fourier series yields

$$\sqrt{\left(1 - \frac{xp}{|x|P_s}\right)} = [S_0 + S_2 \sin (2\omega t + \phi_2) + S_4 \sin (4\omega t + \phi_4) + \dots] \quad [8]$$

If the expansion of Equation [8] is substituted into Equation [1]

$$\begin{aligned} q_v &= \alpha C_v \sqrt{\left(\frac{GP_s}{\rho}\right)} X \sin \omega t [S_0 + S_2 \sin (2\omega t + \phi_2) + \dots] \\ &= \alpha C_v \sqrt{\left(\frac{GP_s}{\rho}\right)} X \left[ S_0 \sin \omega t + \frac{S_2}{2} \cos (\omega t + \phi_2) \right. \\ &\quad \left. + \frac{S_4}{2} \cos (3\omega t + \phi_2) + \dots \right] \quad [9] \end{aligned}$$

the fundamental component of  $q_v$  is seen to involve  $X$ ,  $S_0$ ,  $S_2$ , and  $\phi_2$ . The coefficients  $S_0$ ,  $S_2$ , and  $\phi_2$  are functions of  $P/P_s$  and  $\phi_p$  and may be computed by conventional Fourier-expansion techniques.<sup>5</sup> The integrals involved are elliptic in form and were evaluated during this study by numerical techniques.

If the higher-frequency harmonics of  $q_v$  are neglected,  $q_v$  may be specified by a fundamental component amplitude  $Q_v$  and phase  $\phi_v$ ; that is

$$q_v = Q_v \sin (\omega t + \phi_v) \quad [10]$$

With the application of certain trigonometric identities to the

<sup>4</sup> "Contributions to Hydraulic Control—3, Pressure-Flow Relationship for 4-Way Valves," by J. F. Blackburn, Trans. ASME, vol. 74, 1953, pp. 1163-1170.

<sup>5</sup> "Mathematical and Physical Principles of Engineering Analysis," by W. C. Johnson, McGraw-Hill Book Company, Inc., New York, N. Y., 1944, Chapter 10.

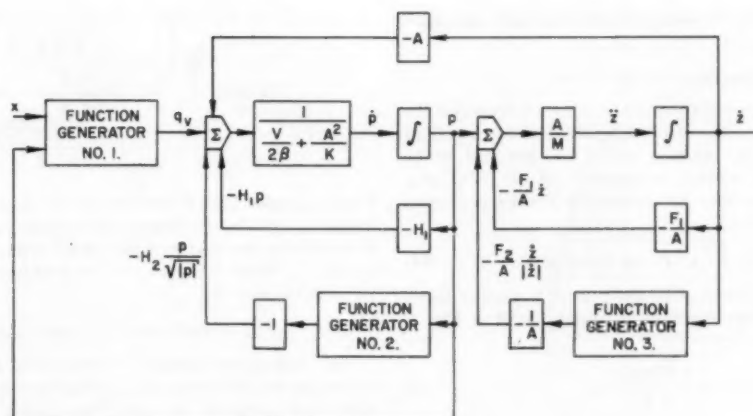
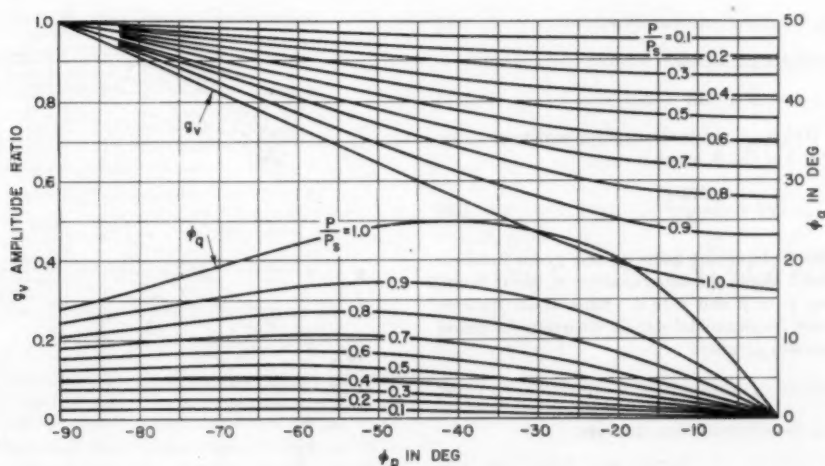


FIG. 3 BLOCK DIAGRAM OF THE SYSTEM

FIG. 4 VALVE GAIN  $g_v$  AND  $\phi_q$  VERSUS  $\phi_p$  AND  $P/P_s$ 

right side of Equation [9],  $Q_v$  may be given by

$$Q_v = aC_v \sqrt{\left(\frac{GP_s}{\rho}\right) X} \sqrt{\left[\left(S_0 - \frac{S_2}{2} \sin \phi_2\right)^2 + \left(\frac{S_2}{2} \cos \phi_2\right)^2\right]} \dots [11]$$

and the normalized valve gain  $g_v$  defined by

$$g_v = \frac{Q_v}{aC_v \sqrt{\left(\frac{GP_s}{\rho}\right) X}} = \sqrt{\left[\left(S_0 - \frac{S_2}{2} \sin \phi_2\right)^2 + \left(\frac{S_2}{2} \cos \phi_2\right)^2\right]} \dots [12]$$

The phase of  $q_v$  is

$$\phi_q = \tan^{-1} \frac{\frac{S_2}{2} \cos \phi_2}{S_0 - \frac{S_2}{2} \sin \phi_2} \dots [13]$$

Equations [12] and [13] are plotted in Fig. 4 as the normalized valve gain  $g_v$  and  $\phi_q$  versus  $\phi_p$ , parametric with respect to  $P/P_s$ . The curves of  $\phi_q$  versus  $\phi_p$  are skew symmetric about  $\phi_p = 0$  and the curves of  $g_v$  versus  $\phi_p$  are symmetric about  $\phi_p = 0$ . The flow valve, therefore, is visualized as a gain and phase shift between  $x$  and  $q_v$ . The dependence of the gain and phase shift on pressure amplitude and phase is given by Fig. 4.

Use of the curves of Fig. 4 is based on knowledge of the load gain and phase shift between  $q_v$  and  $p$  and between  $p$  and  $z$  at particular values of  $\omega$  and  $P$ . If the phase shift between  $q_v$  and  $p$ , that is,  $\phi_q - \phi_p$ , is known for a particular frequency and value of  $P$ , the actual values of  $\phi_p$  and  $\phi_q$  may be found by plotting the locus of  $\phi_q - \phi_p$  on Fig. 4. The intersection of this line with the appropriate  $P/P_s$  curve gives the value of  $\phi_p$  and  $\phi_q$ . Knowledge of  $\phi_p$  and  $P/P_s$  determines the value of valve gain from the second set of curves in Fig. 4. The load gain between  $p$  and  $q_v$  coupled with the known value of  $P$  determines the value of  $Q_v$  and, consequently, the value of  $X$ . Knowledge of the gain and phase shift between  $p$  and  $z$  allows the determination of the magnitude and phase of  $z$ . In the following

section, a method is given for computing the load gain and phase shift.

#### LINEARIZATION OF THE LOAD

Linearization of the load portion of the system is based on the determination of the fundamental components of the functions  $H_2[p/\sqrt{|p|}]$  and  $F_2(z/|z|)$  when  $p$  and  $z$  are assumed to be sinusoidal. The fundamental component of  $H_2[p/\sqrt{|p|}]$ , which is termed  $h_2$  here, may be derived by Fourier expansion techniques and is given by

$$h_2 = 1.113 H_2 \sqrt{P} \sin(\omega t + \phi_p) \dots [14]$$

Dividing Equation [14] by  $p$  gives the gain of the linear transmission  $g_h$  used to replace function generator No. 2 of Fig. 3, that is

$$g_h = \frac{1.113 H_2}{\sqrt{P}} \dots [15]$$

The fundamental component of  $F_2(z/|z|)$  may be computed in similar fashion and is found to be

$$f_2 = 1.273 F_2 \sin(\omega t + \phi_z) \dots [16]$$

where  $\phi_z$  is the phase of  $z$  in the assumed relation

$$z = \dot{Z} \sin(\omega t + \phi_z) \dots [17]$$

Dividing Equation [16] by  $z$  yields the replacement gain  $g_f$  for function generator No. 3 of Fig. 3, which is

$$g_f = \frac{1.273 F_2}{\dot{Z}} \dots [18]$$

Substitution of the replacement gains  $g_h$  and  $g_f$  for function generators Nos. 2 and 3 allows the determination of linear transfer functions relating  $q_s$  to  $p$  and  $p$  to  $z$ . Since these transfer functions are valid only for sinusoidal signals, time differentiation is replaced by the operator  $j\omega$  where

$$j = \sqrt{-1} \dots [19]$$

With the  $j\omega$  notation, these transfer functions are

$$\frac{p}{q_s} = \frac{\left[ \frac{F_1 + g_f}{(H_1 + g_h)(F_1 + g_f) + A^2} \right] \left[ \frac{M}{(F_1 + g_f)j\omega + 1} \right]}{\frac{M \left( \frac{V}{2\beta} + \frac{A^2}{K} \right)}{(H_1 + g_h)(F_1 + g_f) + A^2} (j\omega)^2} \dots [20]$$

$$+ \frac{M(H_1 + g_h) + \left( \frac{V}{2\beta} + \frac{A^2}{K} \right) (F_1 + g_f)}{(H_1 + g_h)(F_1 + g_f) + A^2} j\omega + 1$$

and

$$\frac{\dot{z}}{p} = \frac{\frac{A}{F_1 + g_f}}{\frac{M}{F_1 + g_f} j\omega + 1} \dots [21]$$

Evaluation of the gain and phase shift between  $q_s$  and  $p$  from Equation [20] requires that the values of  $g_h$  and  $g_f$  be known. Since  $g_h$  and  $g_f$  are functions of  $P$  and  $\dot{Z}$ , respectively, commensurate values of  $P$  and  $\dot{Z}$  must be found before Equation [20] can be evaluated. Computation of  $P$  and  $\dot{Z}$  may be accomplished by combining Equations [18] and [21] and solving for  $P$

$$P = \dot{Z} \sqrt{\frac{\left[ \frac{M}{F_1 + \frac{1.273 F_2}{\dot{Z}}} \omega \right]^2 + 1}{\frac{A}{F_1 + \frac{1.273 F_2}{\dot{Z}}}}} \dots [22]$$

From Equation [22],  $P$  may be plotted against  $\dot{Z}$  for a particular frequency and the resulting commensurate values of  $P$  and  $\dot{Z}$  used in evaluating the load gain and phase shift from Equations [20] and [21]. These data may then be used in the way prescribed in the previous section.

#### EXPERIMENTAL VERIFICATION

The analysis presented in the preceding sections was verified by comparing the results obtained using this analytical technique with those achieved by use of an analog computer and data from an actual hydraulic drive. The curves given in Figs. 5 and 6 show typical comparison between the analysis and computer

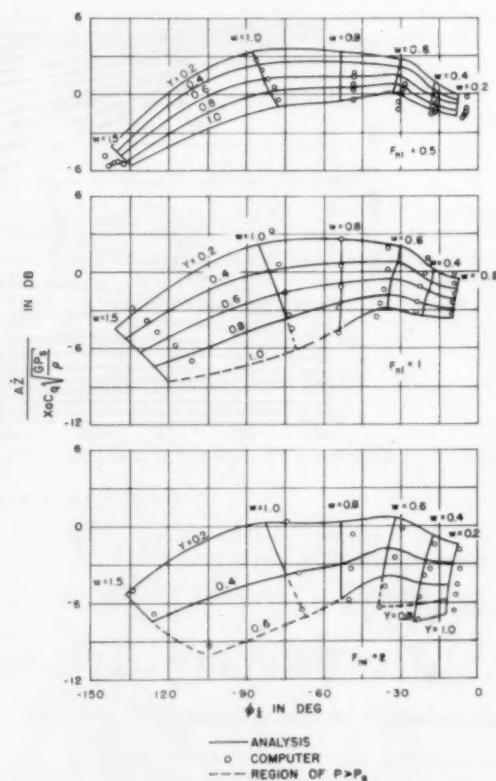


FIG. 5 SYSTEM GAIN VERSUS PHASE (LINEAR LOAD)

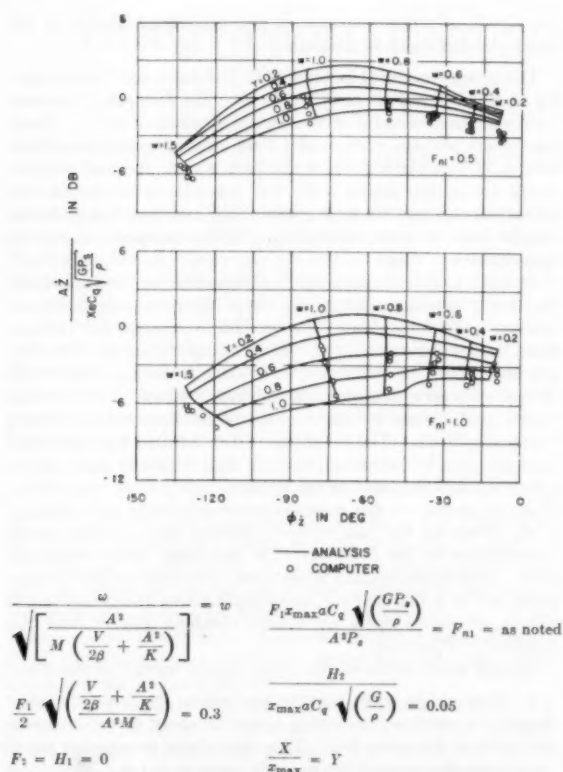


FIG. 6 SYSTEM GAIN VERSUS PHASE (NONLINEAR LOAD)

results for five sets of system parameters. These data are plotted as system relative gain versus system phase shift parametric with respect to frequency and amplitude of the valve-pool motion. The values of system parameters are given in the figure captions, and the quantity  $x_{\max}$  is defined as the maximum value of spool displacement.

Comparison of the analytical results with data obtained using an actual drive is presented in Fig. 7 and is plotted as system gain and phase shift versus  $x/x_{\max}$  parametric with respect to frequency. The drive from which the data were obtained utilized a rotary piston-type motor, and consequently, the mechanical-load parameters are given in terms of angular velocity in the associated figure caption.

The comparisons given in Figs. 5, 6, and 7 show that the analysis predicts trends in system performance but degenerates in accuracy as the level of nonlinearity increases or as the input-signal level decreases. Inaccuracy in the predicted values of gain and phase shift must be attributed to two causes; namely, the neglect of the harmonic content of signals which do contain distortion and may become badly distorted at low signal level, and the inaccuracy of representation of the actual drive by the mathematics given in the second section. The latter difficulty is not characteristic of the computer results but appears at several points in the analysis of the actual drive. In the analysis of the actual drive, the inaccuracies stem from the assumptions of closed-center valve characteristics and zero variation in the value of  $F_2$  with load motion. An actual valve may possess appreciable deviation from closed-center characteristics because of radial clearance and rounding of land and port edges. In gen-

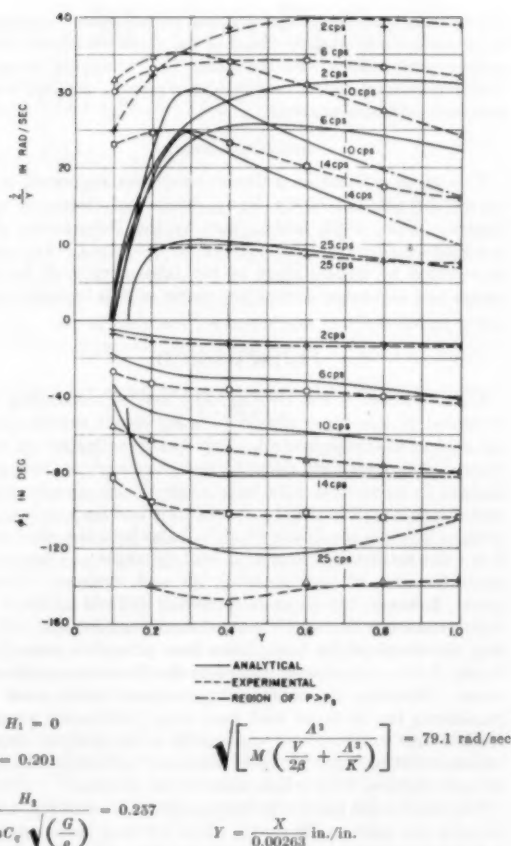


FIG. 7 COMPARISON OF EXPERIMENTAL AND ANALYTICAL DESCRIBING FUNCTIONS

eral, the friction level will tend to decrease with increasing load velocity. Nevertheless, the comparison given in Fig. 7 is considered adequate for lack of more accurate representation of the component parts of the system.

### CONCLUSIONS

From the comparisons just made, the following conclusions may be drawn concerning the adequacy of the analytical technique for predicting system performance:

- 1 The analysis will predict trends in system performance and will give quantitative results of restricted accuracy.
- 2 The accuracy of the results decreases with increasing nonlinearity level and decreasing signal level.
- 3 Although the accuracy of predicted results for the systems analyzed in the previous section is sufficient for engineering purposes, that is, consistent with the ability to measure system parameters, the number of systems that have been analyzed is insufficient to permit the numerical specification of analytical accuracy.

In conclusion, the fact is emphasized that the analysis presented here is an attempt to produce a linearization technique that includes the effects of nonlinear phenomena. As with most first attempts, the analysis may prove too cumbersome to be of practical advantage. However, the application of the analysis

to a sufficient number of systems may permit general statements to be made concerning the effects of the various nonlinearities on system performance. Furthermore, the principles presented here may be used and/or modified by others to formulate a more adequate method of analysis.

#### ACKNOWLEDGMENT

This paper is based on a thesis<sup>4</sup> which was supported in part by the Department of the Navy, Bureau of Ordnance, under Contract NOrd 9661, and in part by the Department of the Air Force, under Contract No. AF 33(616)-2263. The author is indebted to the members of the laboratory staff for their advice and assistance during the course of this investigation.

### Discussion

M. S. FEDER.<sup>7</sup> The development and substantiating data presented in this paper should be a significant contribution to the field of hydraulic control. Previous investigators on valve-controlled systems have either limited their work to incremental changes in valve motion or have neglected oil compliance and load dynamics. The paper presents a method for handling large changes in valve amplitude which includes both the effect of the flow-valve nonlinearity as well as load dynamics and thereby extends the area of understanding for such systems. Unfortunately, however, the paper is somewhat difficult to follow partially because it deals with several nonlinearities, and it is felt that the development might have been presented with greater clarity if the analysis were limited to the flow-valve nonlinearity alone. However, the added complications, which arise from considering the nonlinear load, have some justification when it is realized that experimental verification of an analysis omitting coulomb friction could probably not have been obtained because of static friction in hydraulic motor-drive systems.

The heart of the paper is presented in the curves of Fig. 4 which describe the valve nonlinearity. It is felt that these curves are sufficiently general and useful to warrant more detailed explanation on their application than was given in the paper. In this connection, the following method for using Fig. 4 was worked out for the simple case of a valve driving a linear load:

- 1 For a range of frequencies  $W$  determine the phase shift  $\phi_e - \phi_s$  between load pressure  $P$ , and flow  $q_s$ . For the case of a linear load the phase shift can be determined directly from the transfer function relating these variables.

- 2 Similarly, determine the gain and phase between flow and load velocity from the transfer function relating these variables.

- 3 Choose a value of  $P/P_s$ , and determine values of  $\phi_e$ ,  $\phi_s$ , and  $q_s$  from Fig. 4.

- 4 The over-all phase and gain can be determined by adding

<sup>7</sup> Sperry Gyroscope Company, Division of The Sperry Corporation, Great Neck, N. Y.

the nonlinear phase and gain of the valve from step 3 to the linear phase and gain of the load.

The process outlined in steps 1 to 4 should then be repeated for a range of values of  $P/P_s$ , to give the frequency response curves of the system for several constant values of  $P/P_s$ . These results are perhaps more useful than constant valve-amplitude curves, in that for a given closed-loop system the load requirements are usually spelled out. For example, in the simple case of pure inertia load the load accelerations and therefore pressures usually can be specified from over-all system-performance requirements.

In order to reduce the constant  $P/P_s$  curves to constant valve-amplitude curves considerable cross-plotting and calculation are required. First the calculations leading to constant  $P/P_s$  curves must be nondimensionalized. Then actual values of valve displacement can be determined for each frequency, and  $P/P_s$  curves of valve displacement against frequency for several values of  $P/P_s$  can be constructed and cross-plotted at constant valve amplitude. The amplitude ratio between the valve and load can then be computed, and the final results of gain against frequency superimposed on the frequency plots at constant  $P/P_s$ . The intersection of the constant valve-amplitude and constant  $P/P_s$  curves for the gain versus frequency plot specifies similar intersections on the  $P/P_s$  curves in the phase versus frequency plot. Tedious calculation is required to reduce the data to this form, and it is felt that for many applications an equally useful picture of system operation can be obtained quickly from the constant  $P/P_s$  curves.

Several other points in the paper appear worthy of comment.

- 1 It should be noted that the analysis on the flow-valve nonlinearity is restricted to cases of operation about zero valve opening (refer to Equation [6]). This simplifying assumption somewhat limits the scope of the paper to position servos. The writer has had occasion to deal with a velocity-control system, and in this case both analysis and data showed the valve nonlinearity to be much more pronounced at high flow rates than at zero flow. In fact, data on a complex multiloop servo system indicated that, for large valve openings, system performance was predominantly determined by the valve nonlinearity.

- 2 With regard to Fig. 7 the discrepancies in the data at low frequencies can come either from hydraulic-motor or servo-valve friction. Rotary hydraulic motors require values of  $P/P_s$  as high as 0.3 to start them. Presumably the friction factor in Fig. 7 includes this effect.

- 3 The analysis neglects the effects of flow forces on the servo valve. Dynamic flow forces acting on servo valves have been a source of difficulty. On some systems instability traced to dynamic-flow forces has been experienced, and it has been found that both the nature of the load, and the valve and torque-motor configuration affect the instability. The flow-force phenomena are not yet clearly understood and further investigation would be a worthwhile objective of future research.

# Integration of Steam and Hydro Power in Northern California

By WALTER DREYER,<sup>1</sup> SAN FRANCISCO, CALIF.

The paper reviews the history of installations and integration of steam and hydro power in northern California. The functions of steam-generated power are outlined and the economics of mingled hydro and steam demonstrated for several assumed conditions. The importance of making effective all of the installed or dependable capacity without duplicating installations is emphasized and illustrated by a graphic example. The paper concludes with a brief discussion of reserve capacity in a mingled power system and with some thoughts about the role of future nuclear plants.

## INTRODUCTION

IT WAS in the area served by Pacific Gas and Electric Company in northern California that the connecting together of steam and hydro power plants first took place some 57 years ago. In 1898 two remote and widely separated hydro plants, Folsom and Colgate, were connected at Sacramento, and in the following year the two hydro plants were tied with the local steam plant. This event gave birth to the interconnected hydro-steam power systems we know today.

This tying together of hydro and steam plants demonstrated for the first time the principles that (1) advantage could be taken of the diversity which exists in stream flow at different hydroelectric plants; (2) a steam reserve could furnish continuity in hydroelectric service, and (3) pooling of a regional demand, varying daily, seasonally, geographically, and with character of use, could result in economy because of the greater number of hours a given plant could be operated effectively.

Interconnection of steam and hydro plants at Sacramento was followed in 1902 by interconnection at Oakland of the Colgate and Electra hydro plants and the steam plants of the San Francisco Bay area. Large scale hydro-steam interconnection thereby became established.

The territory now served by Pacific Gas and Electric Company consists of 46 of California's 58 counties, has an area of 89,000 square miles, and a population of nearly six million. The 1955 peak demand on the system exceeded 3.8 million kilowatts. During 1954 some 16 billion kilowatt-hours of energy were delivered to consumers: 3.1 billion for domestic use, 7.2 billion for commercial and industrial use, 3.0 billion for agriculture, and 2.7 billion for resale, railway, and other purposes.

The company's power-production system presently consists of thirteen steam-electric plants having an aggregate capacity of 2,866,000 kw and fifty-eight hydroelectric plants with a total capacity of 1,440,000 kw, a total of 4,306,000 kw in plants owned by the company. In addition to its own generation it takes into its system some 500,000 kw of hydroelectric power generated by other agencies.

<sup>1</sup> Vice-President and Chief Engineer, Pacific Gas and Electric Company.

Contributed by the Power Division and presented at the Spring Meeting, Portland, Ore., March 18-21, 1956, of THE AMERICAN SOCIETY OF MECHANICAL ENGINEERS.

NOTE: Statements and opinions advanced in papers are to be understood as individual expressions of their authors and not those of the Society. Manuscript received at ASME Headquarters, January 4, 1956. Paper No. 56-S-8.

The magnitude of the loads served in the area during the period 1915-1955 is shown graphically in Fig. 1. Three curves are shown, the total annual energy, the total energy supplied by hydroelectric plants, and the annual peak loads since the systems serving the area became integrated in 1930. The record of the capacity of hydroelectric and steam plants installed in the area is shown in graphic form in Fig. 2.

## FUNCTIONS OF STEAM-GENERATED POWER IN "MINGLED POWER" SYSTEM

In 1926 the late A. H. Markwart, then Vice-President in Charge of Engineering of Pacific Gas and Electric Company, presented before the Society a paper entitled "Aspects of Steam Power in Relation to a Hydro Supply." In this paper he set forth in simple terms the functions of steam plants operating in conjunction with a hydroelectric system, to be:

- 1 To effect the best system economy.
- 2 For stand-by at important load centers.
- 3 For meeting the seasonal hydro deficiency during the short water period on nonregulated streams.
- 4 For meeting the dry-year hydro-energy deficiency.

These functions still hold for an area favored with potential hydroelectric power adequate to meet all increasing power demands. Where the hydro resource is not adequate to do this, power generated by thermal means obviously must be provided as well.

As far as possible steam plants should be located at important load centers so they can serve all of the aforesaid purposes. Being located at load centers, generating units also can be designed to assist in regulating incoming transmission lines, thereby reducing or perhaps eliminating the cost of synchronous condensers which otherwise would have to be provided at the termini of the lines from the hydro plants.

An integrated system composed of a number of interconnected hydro and steam plants requires the minimum amount of steam capacity to be installed for the purposes of replacing the deficiencies in hydroelectric energy in dry years, and in the dry months of normal water years. Except for run-of-river plants without forebays, or plants located at storage dams where the head may be reduced, the full capacity of the hydro should remain available to meet peak demands, but the dry-period energy deficiency must be met with steam-generated power. All hydroelectric plants are not deficient in energy, or not deficient to the same degree, at the same time; consequently, the same steam plants can be used to make up the deficiency of one hydro supply at one period and of another supply at another period. Without such integration and interconnection each hydro supply must have its own dry-year steam support.

In such an integrated system, co-ordination of storage reservoir operations, some of which may be cyclic as well as seasonal, will allow the maximum amount of available hydro power to be utilized during periods of normal or of heavy runoff. A saving of fuel will result thereby because the steam plants are not required to generate as much energy.

Somewhat conversely, the steam plants in such a system can at

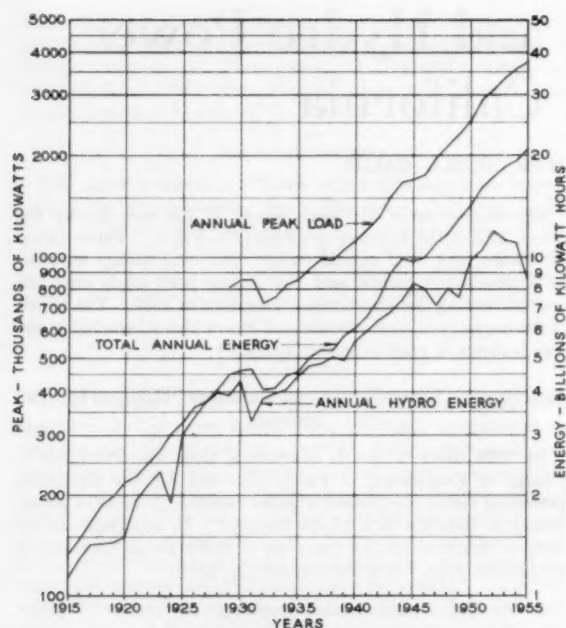


FIG. 1 LOADS IN AREA SERVED BY PACIFIC GAS AND ELECTRIC COMPANY DURING PERIOD 1915-1955

times operate at a high rate in order to allow water to be held back in reservoirs to meet demands during more critical periods. Where a power plant is located at a reservoir, head on the turbines will be maintained and more of the plant capacity will be effective. Or if the reservoir stores water for a chain of plants, their capacities will be made more effective because additional water will be available when needed. The net effect in either case is to maintain a maximum amount of effective hydro capacity and thereby keep to a minimum the total amount of capacity required to be installed on the system.

#### ECONOMICS OF MINGLED POWER

In a region with hydroelectric resources any program for expansion of generating facilities to meet expected new loads requires consideration of steam-electric plants, hydroelectric plants, or a combination of both. Unless the region is favored with an abundant supply of very cheap fuel or with a large potential of unusually low-cost hydroelectric power, it generally will be found that a combination of steam and hydro plants will provide the additional power for the lowest cost. The most economical combination will depend on the configuration of the load curve, cost of the generating plants and related transmission facilities, and the price of fuel.

The load curve for the territory served by Pacific Gas and Electric Company is used herein to illustrate the problem. The load has a high degree of diversity, with substantially equal peak demands in the summer (July and August) and in the winter (December). The average annual load factor is about 63 per cent. The actual load curve for the summer peak day, August 3, 1955, and a curve for a typical winter day having the same maximum as the day in July, are shown in Fig. 3. The summer peak, due in large part to irrigation pumping and air conditioning, occurs in the morning or early afternoon and is well sustained, while the winter peak occurs in the evening and is of short duration. There are many days in July and August when the

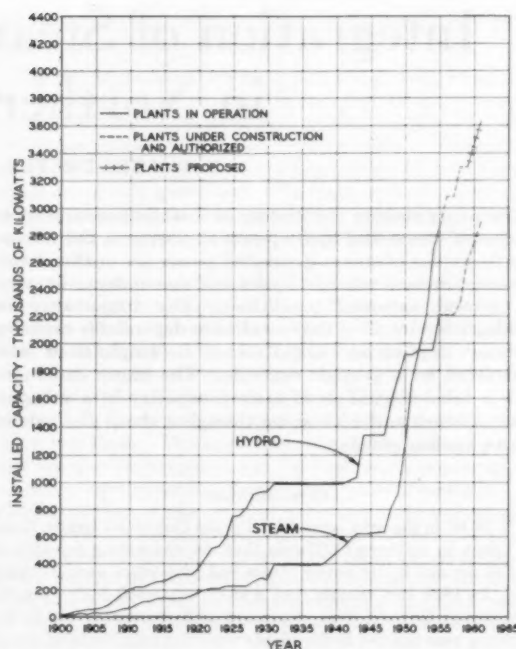


FIG. 2 INSTALLED CAPACITY OF HYDROELECTRIC AND STEAM-ELECTRIC PLANTS IN SERVICE AREA OF PACIFIC GAS AND ELECTRIC COMPANY

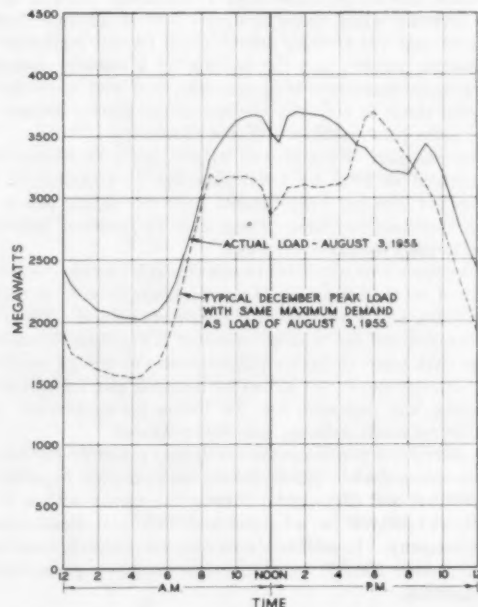


FIG. 3 TYPICAL SUMMER AND WINTER MAXIMUM LOADS ON PACIFIC GAS AND ELECTRIC COMPANY SYSTEM

load approaches the maximum, but the winter peak may occur on one of a few dark days in December.

The annual load, integrated by hours and plotted as a "kilowatt-kilowatt-hour curve" with per cent of yearly peak as ordi-

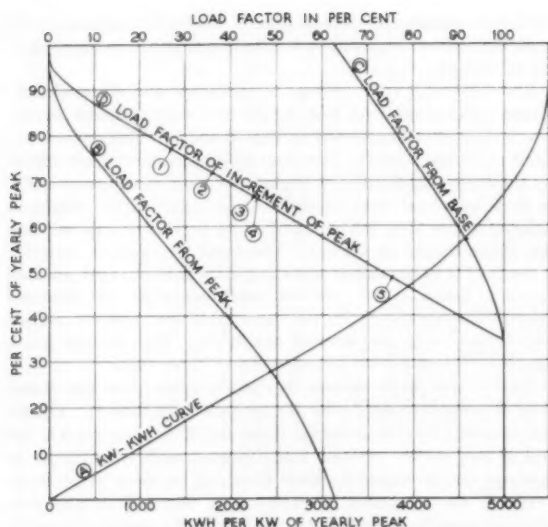


FIG. 4 RELATION OF KILOWATT DEMAND TO ANNUAL ENERGY IN POWER LOAD OF NORTHERN AND CENTRAL CALIFORNIA

nates and kilowatt hours per kilowatt of yearly peak as abscissas, is shown as curve A in Fig. 4. This chart also includes curve B showing the load factor from peak, curve C the load factor from base, and curve D the load factor at any point on the basic kilowatt-kilowatthour curve. This annual load curve is used herein solely to illustrate the principles of the economic problem. Similar curves, but plotted for each month of the year, are used in detailed planning studies, because the characteristics of the load and the amount of hydro power available vary considerably at different times of the year.

The unit cost of producing power and bringing it to some load center or main substation will vary with the capital and annual costs of the production and related transmission facilities, the cost of fuel, and with the capacity factor at which these facilities will be required to operate. The relation between unit costs and capacity factors is shown graphically for typical steam and hydro plants by a number of curves in Fig. 5. This chart includes one group of curves showing the cost of steam-generated power delivered at transmission voltage to a nearby load center for six different prices of fuel; i.e., 15¢, 20¢, 25¢, 30¢, 35¢, and 40¢ per million Btu. Investment in the steam plant and related transmission facilities was assumed to be \$160 per kilowatt; annual fixed costs with private financing on a tax-paying basis were assumed to be 15 per cent of capital costs; no-load fuel was taken at 10 million Btu per kilowatt per annum, and running fuel estimated on the basis of 10,000 Btu per kw-hr delivered at load center. These figures are reasonably in line with present-day conditions and costs.

There also are two curves showing the unit cost of hydroelectric power from assumed plants delivered to the same load center. One of these curves is typical of postwar California plants; the other is based on an estimate of the average unit cost of power from undeveloped resources of the Columbia River in the Pacific Northwest, assuming that such plants were constructed and operated under the private-enterprise system, with the full cost of the reservoirs charged to power. Investment in the hydroelectric facilities, transmission lines, and terminal substations was assumed to vary with the average annual capacity factor for which the development would be designed.

For the typical postwar California plant the costs used were

\$500 per kw for 100 per cent capacity factor and \$300 per kw for 36 per cent capacity factor. Such reduction in average unit cost would result inherently with larger installations, because the cost of increasing the capacity of water-conveyance facilities and electric generating and transmission facilities are incremental costs which generally do not affect the basic investment in water-storage facilities, diversion dams, buildings, and the like. Furthermore, unless storage reservoirs adequate to regulate stream flow under all conditions are provided, which is seldom if ever justified, the larger installation would make it possible to utilize more water during periods of high runoff and the plant would therefore produce more energy.

The curve based on Columbia River possibilities assumes unit costs of \$420 per kw for 100 per cent and \$270 for 36 per cent capacity factor. These unit figures are derived from published figures of the cost of some 5 million kilowatts of undeveloped prime power, assuming the full cost of the reservoirs charged to power. Annual costs for the hydro facilities in both cases were taken at 11 per cent of the capital costs, again reflecting private financing on a tax-paying basis, in order to provide a true comparison with the cost of generating power in privately financed steam plants. Taxes on privately financed power plants currently average between 5 and 6 per cent of capital costs.

In the example in Fig. 5 it will be noted that the average cost of the hydroelectric power is shown to be less than the cost of steam-electric power at some average annual capacity factor, even with exceedingly cheap fuel. The curve shows the assumed California hydro to be more economic for all capacity factors with fuel at about 32¢ per million Btu; for capacity factors less than 92 per cent with fuel at 30¢ per million Btu; for capacity factors less than 45 per cent with fuel at 25¢; for capacity factors less than

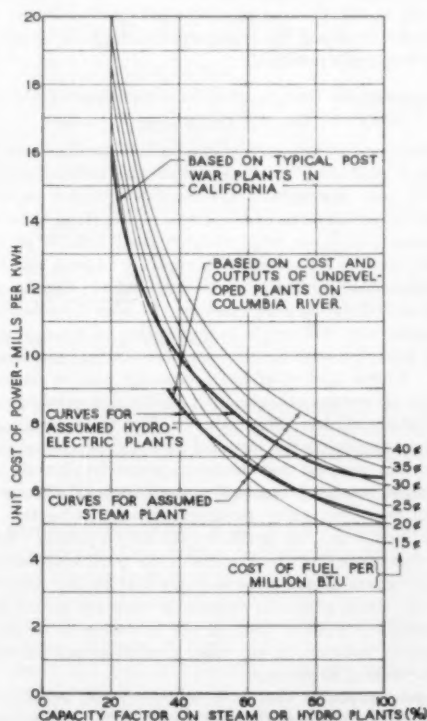


FIG. 5 UNIT COST OF POWER FROM TYPICAL STEAM-ELECTRIC AND HYDROELECTRIC PLANTS ON BASIS OF PRIVATE FINANCING

36 per cent with fuel at 20¢, and for capacity factors less than 27 per cent with fuel as low as 15¢ per million Btu.

The curve based on Columbia River costs shows hydro to be more economic for all capacity factors with fuel at 22¢ per million Btu; for capacity factors less than 75 per cent with fuel at 20¢; and for capacity factors below 46 per cent with fuel as low as 15¢ per million Btu.

These findings make it clear that for the conditions shown by these examples, a combination of hydro and steam can be made to produce power more economically than either an all-steam system or an all-hydro system. As stated before, curve D in Fig. 4 shows the load factor of the load at any point. On this curve have been marked points 1, 2, and 3 below which load factors the assumed California hydro power is cheaper than steam for fuel prices of 15¢, 20¢, and 25¢ per million Btu, respectively. Points marked 4 and 5 show load factors below which the assumed Columbia River plants would produce power for less cost than steam plants with fuel, respectively, at 15¢ and 20¢ per million Btu. It will be noted that points 1, 2, and 3 are fairly close together, indicating that for the California case it would be prudent to plan the hydroelectric development with a large installation which would operate at relatively low capacity factors, thereby obtaining more total energy from the hydro potential and the maximum saving per kilowatt-hour over equivalent steam-generated power.

The foregoing example illustrates the basic principles of the economics of mingled power. It shows that a combination of low-capacity factor hydro, i.e., "peaking hydro" and "higher than system load factor" steam, can produce economic results. It also shows that in planning hydroelectric development it may be shortsighted to keep capital costs down by designing the facilities for high load factor operation. If reasonably possible, and not too costly, the way should be left open for future expansion in order to obtain the maximum benefit from development of the hydroelectric potential.

#### ALL INSTALLED OR DEPENDABLE CAPACITY SHOULD BE EFFECTIVE AT TIME OF SYSTEM PEAK DEMANDS

If system reserves are considered a separate problem, maximum economy of production will be achieved with utilization at times of system peak demands of (1) the full installed capacity of steam-electric plants and hydroelectric plants other than run-of-river plants and those with variable head located at storage reservoirs, (2) the full dependable capacity of such run-of-river and variable-head hydroelectric plants, and (3) the dependable capacity available from other sources. To plan the power system in any other way will result in duplication of some amount of installed capacity, with its attendant continuing burden of fixed charges. Unless such duplicated capacity can be useful as a reserve for short-time outages or to facilitate scheduling of overhaul, it usually will have little value to offset these charges.

In order to make the full installed (or full dependable) capacity effective, it is essential that the hydro plants be planned so they can generate enough power under conditions of adverse water supply to meet the energy requirements of that portion of the peak load assigned to be carried by the hydro plants. And it is equally important that the amount of the peak load assigned to the hydro plants must not be so large that in dry years it will require the steam plants to operate at capacity factors beyond their reasonable ability; that is, not in excess of 90 per cent, preferably 85 per cent, in any month, or at an annual capacity factor in excess of 80 per cent.

It is quite probable that with adverse water conditions the total supply of hydroelectric energy will be 25 per cent or more below the amount normally available. For some plants the reduction will be even greater. The system must be planned to

meet such situations, and any general academic economic study must be modified to include the criteria mentioned in the preceding paragraph.

The division of load between hydroelectric and steam-electric plants under conditions with ample and with deficient stream flow is illustrated graphically in Figs. 6 and 7. These charts use Pacific Gas and Electric Company kilowatt-kilowatt-hour curves for the peak-load months of August and December, respectively, to show how load must be assigned to typical hydro plants in order to utilize their full capacity in dry periods as well as when the water supply is normal. The total steam-plant capacity is assumed to be capable of operating at up to 85 per cent monthly capacity factor under adverse conditions. In the example shown, this capacity factor in August is 77 per cent for normal and 85 per cent for adverse conditions. The corresponding figures for December are 46 per cent and 72 per cent.

Run-of-river plants necessarily operate as base-load plants and their capacity is reduced when stream flow is diminished. Operation of plants located at storage dams and of plants located at the end of long water conduits and equipped with surge tanks or forebays can be varied to allow their full capacity to be made available for a number of hours each day. With adequate afterbay capacity provided, it is possible in dry periods to operate such plants so all available water can be used to run the plant at full capacity during peak loads, and shut them down or at least back them down during off-peak hours, thereby making their output most effective and, if properly planned, their capacity fully useful in meeting peak demands.

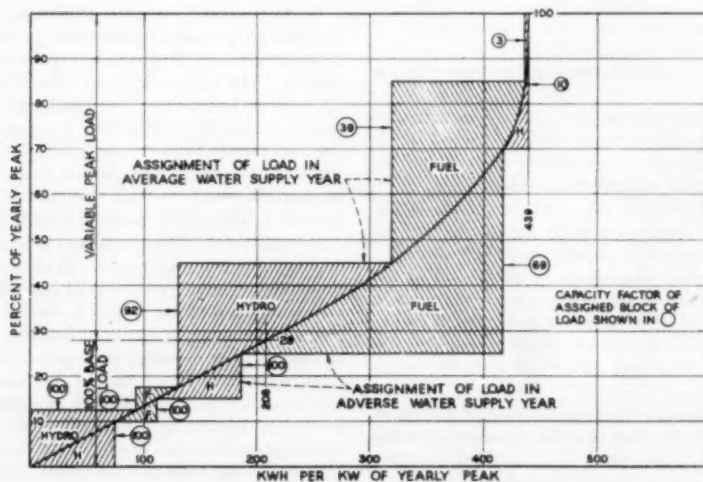
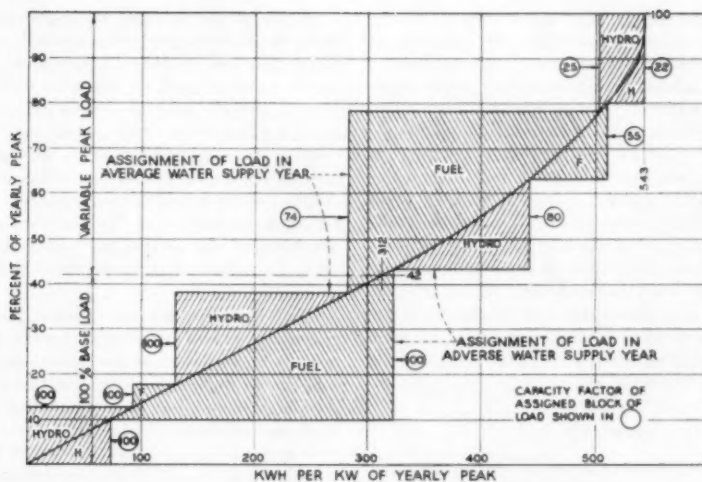
Hydroelectric plants on the Pacific Gas and Electric Company system have long been planned so all of their available capacity is useful under the load curve. As a result of this planning, the effective capacity of its own hydro plants at the time of the winter peak load is 1,279,000 kw with normal water supply and 1,246,000 kw with adverse water supply, the reduction of 33,000 kw occurring at older stream-flow plants operating without regulating forebays, and at plants located at storage dams. Corresponding figures at the time of the summer peak are 1,313,000 and 1,226,000, a reduction of 87,000 kw under adverse conditions.

Figs. 6 and 7 show how all available hydroelectric capacity (except run-of-river and variable-head plants) can be made effective by changing the assignment of load to be carried as the available energy varies with changes in water supply. This has the important economic effect of making it unnecessary to increase the capacity of the steam plants in order to make up the energy deficiency of the hydro. All that is necessary is to operate the steam plants at higher capacity factor in dry years than in normal water years.

Under the aforesaid method of system planning, there is no duplication of capacity and the total installed capacity of the hydroelectric and steam-electric plants is kept to a minimum. Hydro plants, including transmission to load centers, may well cost from \$300 to \$500 per kw, with corresponding fixed annual costs of \$33 to \$55 per kw year. Steam plants, with appurtenant transmission, will run around \$160 per kw and fixed annual costs, excluding cost of running fuel, will run around \$24 per kw year. It is obvious that mingled power systems should be planned to avoid rendering hydroelectric capacity ineffective in dry years, thereby making it unnecessary to "double up" on installed capacity. Such planning makes it possible to save capital and annual costs of the order which is described in the foregoing.

#### CONSIDERATION OF RESERVES IN A MINGLED POWER SYSTEM

Reserves in capacity and in energy are required for several purposes, including the following:



- 1 Rolling reserve immediately available to meet changes in local or system interruptions.
- 2 Reserve for overhaul of generating equipment.
- 3 Reserve for outages not planned or scheduled.
- 4 Reserve for load growth in excess of estimates.

Generating capacity in an amount not less than the sum of (1) the capacity required to meet load changes without impairing frequency and (2) the capacity of the greatest single risk of sudden outage, should be rolling at all times, even at the peak period. This rolling reserve should be able immediately to replace the loss of capacity due to failure of a generating unit or a transmission circuit. Hydroelectric plants, particularly those of the impulse type, are better-suited for this than steam plants.

Overhaul of equipment may require capacity to be out of service for considerable periods of time, usually longer periods for thermal than for hydro plants. However, the annual peak demands on a system generally occur during definite periods

which are of limited duration; consequently a large amount of the needed overhaul can be done, without impairing reserves, during periods when maximum demands are well below the annual peak.

## SOME THOUGHTS ABOUT FUTURE THERMAL PLANTS

The practical motive power of today's thermal power plants is the internal-combustion engine or the gas turbine for small plants, and the steam turbine for large plants. It will not be long, however, before consideration also must be given to nuclear power plants as a means of complementing the hydro system. Extraordinary progress is being made in developing nuclear power plants and they may become economic sooner than we have believed possible.

Recent reports indicate that the unit capital cost of nuclear plants will be relatively high, but that fuel costs are likely to be low. These facts indicate that nuclear power plants will be most economic when operating at high capacity factor. When

their ability to operate successfully has been demonstrated and the cost of the power they generate under different conditions of operation has become established, an analysis similar to the one included herein can be broadened to include nuclear power plants with conventional steam and hydro plants.

As of today, it appears that when nuclear power plants become competitive economically they will fit very well into existing integrated power systems, whether they be all-steam or a combination of hydro and steam. If, as now appears, nuclear power plants will be most economic under base-load operation, they will supplant conventional-type plants now operating on base, and these supplanted conventional-type plants will operate at lower capacity factor to meet the low load-factor segments of the load. There is nothing new about this. It is the procedure which long has been followed when new and more efficient steam capacity was installed, either on all-steam systems or on mingled power systems made up of hydro and steam plants.

## Discussion

I. A. WINTER.<sup>2</sup> The integration of steam and hydro power, as presented in this paper, is a well-established practice and has proved to represent the most economical use of natural resources comprising fossil fuels and falling water. The factual data presented in the paper are of considerable interest as it is not the general practice of contributors to present a detailed analysis of their systems, which may be of considerable value to planners in other regions. The charts and graphs presented are unique in this respect.

The historical note concerning the inception of the interconnected hydro and steam-power systems as we know them today is of interest as it is indicative of the pioneering spirit which has been manifested in the development of industries and natural resources in the Great Pacific West. The utility engineers in that region are known for their bold approach to the many problems with which they have been confronted and have so ably solved.

The development of hydroelectric power at economical sites is an essential measure in the conservation of our natural resources. The integration of hydro and fossil-fuel power in an electric-utility distribution system parallels in significance the use of falling water as a continuing resource integrated with fossil fuels which are expendable.

Studies of the development of the uses of electric energy in metropolitan areas points up the fact that the expansion in its use is creating a transportation problem. The problem resulting from this situation can be appreciated by determining the transportation facilities required to deliver coal to a modern high-capacity station. This suggests the necessity for early development of the transportation of pulverized coal by pipe lines. Sufficient development work has been achieved in this field to demonstrate that such systems are feasible, both from an operating standpoint and financially.

<sup>2</sup> Consulting Engineer, Denver, Colo.

Studies of the enlarged steam-generating stations being projected in the immediate future also indicate that water for condensation purposes presents a major problem. In many instances, stored water released by the generation of hydroelectric power may provide the necessary source for a continuing supply of condensing water for a thermal power plant. Some magnitude of this problem may be understood by noting that steam plants frequently require an amount of cooling water equivalent to a hydroplant of the same kilowatt capacity where the heads developed are comparatively great. To the credit of a hydroelectric storage development also accrues the conservation of water for domestic and commercial purposes, flood protection, navigation, and irrigation.

Mention has been made frequently of a possible conflict between nuclear and other forms of power plants. The writer sees no basis for such fears as the indications are that hydro power will supplement nuclear power in the future in the same manner it now supplements fossil-fuel generation. Hydro power may be used most effectively in the production of the components of nuclear power as is now being done in the Pacific Northwest. This co-ordination will permit the development of hydro installations having lower than normal plant factors, since it would be possible to adjust the production of nuclear components in accordance with availability of the energy.

During the early period in the development of the modern type of hydroelectric power installations, plants having a load factor of 70 to 80 per cent were considered necessary to be economically feasible. The broad interconnection of utilities systems as practiced today has made it possible to develop plants having load factors of from 30 to 40 per cent, with equivalent economy. Since the fixed charges for a hydroelectric plant are assured throughout its useful life, such developments will be attractive investments comparable with fossil or nuclear plants because of the uncertain variable in the cost of expendable fuels in the future.

Perhaps too much emphasis has been placed upon the so-called development of prime power. It does not appear logical that a profitable generation period of 20 years should be reduced because the records indicate, or it may be assumed, that a period of 1 or 2 years of subnormal stream flow would make it necessary to curtail the delivery of energy in certain areas. It is believed that a more realistic approach to the problem is justifiable, whereby the maximum over-all economy of production may be achieved. Such consideration appears fair since the utility customer can not assure its supplier that it will be able to take its normal demand throughout the years of its contract. The planning of hydro developments should reflect this consideration.

A large field for the co-ordination of nuclear and hydro power is presented in isolated areas where fossil fuels are not available. Most areas have potential sites for the development of hydroelectric power in a much broader sense than these areas may possess fossil fuels. It is therefore very likely that the trend in the future development of hydro power may be closely affiliated with the perfection of nuclear power plants.



